NIST
PUBLICATIONS

NBS SPECIAL PUBLICATION 665

U.S. DEPARTMENT OF COMMERCE/National Bureau of Standards

Wind and Seismic Effects

Proceedings of the Twelfth Joint UJNR Panel Conference

NATIONAL BUREAU OF STANDARDS

The National Bureau of Standards[1] was established by an act of Congress on March 3, 1901. The Bureau's overall goal is to strengthen and advance the Nation's science and technology and facilitate their effective application for public benefit. To this end, the Bureau conducts research and provides: (1) a basis for the Nation's physical measurement system, (2) scientific and technological services for industry and government, (3) a technical basis for equity in trade, and (4) technical services to promote public safety. The Bureau's technical work is performed by the National Measurement Laboratory, the National Engineering Laboratory, and the Institute for Computer Sciences and Technology.

THE NATIONAL MEASUREMENT LABORATORY provides the national system of physical and chemical and materials measurement; coordinates the system with measurement systems of other nations and furnishes essential services leading to accurate and uniform physical and chemical measurement throughout the Nation's scientific community, industry, and commerce; conducts materials research leading to improved methods of measurement, standards, and data on the properties of materials needed by industry, commerce, educational institutions, and Government; provides advisory and research services to other Government agencies; develops, produces, and distributes Standard Reference Materials; and provides calibration services. The Laboratory consists of the following centers:

Absolute Physical Quantities[2] — Radiation Research — Chemical Physics — Analytical Chemistry — Materials Science

THE NATIONAL ENGINEERING LABORATORY provides technology and technical services to the public and private sectors to address national needs and to solve national problems; conducts research in engineering and applied science in support of these efforts; builds and maintains competence in the necessary disciplines required to carry out this research and technical service; develops engineering data and measurement capabilities; provides engineering measurement traceability services; develops test methods and proposes engineering standards and code changes; develops and proposes new engineering practices; and develops and improves mechanisms to transfer results of its research to the ultimate user. The Laboratory consists of the following centers:

Applied Mathematics — Electronics and Electrical Engineering[2] — Manufacturing Engineering — Building Technology — Fire Research — Chemical Engineering[2]

THE INSTITUTE FOR COMPUTER SCIENCES AND TECHNOLOGY conducts research and provides scientific and technical services to aid Federal agencies in the selection, acquisition, application, and use of computer technology to improve effectiveness and economy in Government operations in accordance with Public Law 89-306 (40 U.S.C. 759), relevant Executive Orders, and other directives; carries out this mission by managing the Federal Information Processing Standards Program, developing Federal ADP standards guidelines, and managing Federal participation in ADP voluntary standardization activities; provides scientific and technological advisory services and assistance to Federal agencies; and provides the technical foundation for computer-related policies of the Federal Government. The Institute consists of the following centers:

Programming Science and Technology — Computer Systems Engineering.

[1]Headquarters and Laboratories at Gaithersburg, MD, unless otherwise noted; mailing address Washington, DC 20234.
[2]Some divisions within the center are located at Boulder, CO 80303.

Wind and Seismic Effects

Proceedings of the 12th Joint
Panel Conference of the U.S.-Japan
Cooperative Program in
Natural Resources

May 19-23, 1980
National Bureau of Standards
Gaithersburg, MD

E.V. Leyendecker and R.M. Chung, Editors
Center for Building Technology
National Engineering Laboratory
National Bureau of Standards
Washington, DC 20234

PREFACE

The Twelfth Joint Meeting of the U.S. - Japan Panel on Wind and

Seismic Effects was held in Gaithersburg, Maryland on May 19-23, 1980.

This panel is a part of the U.S. - Japanese Cooperative Program in Natural

Resources (UJNR). The UJNR was established in 1964 by the U.S. - Japan

Cabinet-level Committee on Trade and Economic Affairs. The purpose of

the UJNR is to exchange scientific and technology information which will

be mutually beneficial to the economics and welfare of both countries.

These proceedings include the program, the formal resolutions, and

the technical papers presented at the Joint Meeting. The texts of the

papers have been edited for obvious errors and clarity.

It should be noted that throughout the proceedings certain commer-

cial equipment, instruments or materials are identified in order to

specify adequately experimental procedure. In no case does such inden-

tication imply recommendation or endorsement by the National Bureau of

Standards, nor does it imply that the material or equipment identified

is necessarily the best for the purpose.

Preparation of the proceedings was partially supported by funds

from the National Science Foundation.

H. S. Lew, Secretary
U.S. Panel on Wind and
Seismic Effects

ABSTRACT

The Twelfth Joint Meeting of the U.S.-Japan Panel on Wind and
Seismic Effects was held in Gaithersburg, Maryland on May 19-23, 1980.
The proceedings of the Joint Meeting include the program, the formal
resolutions, the Task Committee Reports, and the technical papers. The
subjects covered in the papers include: (1) the characterization of
seismic ground motion, (2) the characterization of natural wind and extreme
wind records, (3) structural response to earthquake loading, (4) storm
surge and tsunamis, (5) recent developments in seismic design criteria,
(6) technical cooperation with developing countries, (7) earthquake hazard
mitigation, and (8) structural response to wind loading.

SI CONVERSION UNITS

In view of the present accepted practice for wind and seismic technology, common units of measurements were used throughout this publication. In recognition of the position of the United States as a signatory to the General Conference on Weights and Measures, which gave official status to the International System of Units (SI) in 1960, the table below is presented to facilitate conversion to SI Units. Readers interested in making further use of the coherent system of SI units are referred to: NBS SP 330, 1977 Edition, The International System of Units; and ASTM Standard for Metric Practice.

TABLE OF CONVERSION FACTORS TO SI UNITS

	Customary Units	International (SI) UNIT	Conversion Approximate
Length	inch (in)	meter (m)[a]	1 in = 0.0254 m*
	foot (ft)	meter (m)	1 ft = 0.3048 m*
Force	pound (lbf)	newton (N)	1 lbf = 4.48 N
	kilogram (kgf)	newton (N)	1 kgf = 9.807 N
Pressure or Stress	pound per square inch (psi)	newton/per square meter	1 psi = 6895 N/m^2
	kip per square inch (ksi)	newton per square meter	1 ksi = 6895 x 10^3 N/m^2
Energy	inch·pound (in-lbf)	joule (J)	1 in·lbf = 0.1130 J
	foot·pound (ft-lbf)	joule (J)	1 ft·lbf = 1.3558 J
Torque or Bending Moment	pound·inch	newton-meter (N·m)	1 lbf·in = 0.1130 N·m
	pound·foot (lbf-ft)	newton-meter (N·m)	1 lbf·ft = 1.3558 N·m
Weight	pound (lb)	kilogram (kg)	1 lb = 0.4536 kg
Unit Weight	pound per cubic foot (pcf)	kilogram per cubic meter (kg/m^3)	1 pcf = 16.018 kg/m^3
Velocity	foot per second (ft/sec)	meter per second (m/s)	1 ft/s = 0.3048 m/s
Acceleration	foot per second square (ft/s^2)	meter per second square (m/s^2)	1 ft/s^2 = 0.3048 m/s^2

---

[a] Meter may be subdivided. A centimeter (cm) is 1/100 m and a millimeter (mm) is 1/1000 m.

* Exactly

CONTENTS

Themes and Technical Papers

Theme I: CHARACTERIZATION OF SEISMIC GROUND MOTION

Theme II: CHARACTERIZATION OF NATURAL WIND AND EXTREME WIND RECORDS

Theme III: STRUCTURAL RESPONSE TO EARTHQUAKE LOADING

PROGRAM OF THE TWELFTH JOINT MEETING
OF THE
U.S.-JAPAN PANEL ON WIND AND SEISMIC EFFECTS
MAY 19-22, 1980
AT THE
NATIONAL BUREAU OF STANDARDS
GAITHERSBURG, MARYLAND

MONDAY — May 19 OPENING SESSION

10:00 a.m.   Call to order by Dr. H. S. Lew, Secretary, U.S. Panel

Remarks by Dr. Thomas A. Dillon, Deputy Director, National Bureau of Standards

Remarks by Mr. Hiroyoshi Kurihara, Counselor, Embassy of Japan

Remarks by Dr. Edward O. Pfrang, Chairman, U.S. Panel

Remarks by Mr. Yoshijiro Sakagami, Chairman, Japanese Panel

10:30 a.m.   Introduction of U.S. Panel Members by U.S. Chairman and Japan Panel Members by Japanese Chairman

10:45 a.m.   Election of Conference Chairman

10:50 a.m.   Adoption of Agenda

 1:00 p.m.   Dense Instruments Array Program of the Public Works Research Institute for Observing Strong Earthquake Motion -- Y. Sakagami, T. Okubo, T. Iwasaki, K. Kawashima

 1:30 p.m.   Recent Strong-Motion Results from Imperial Valley Earthquake, October 15, 1979 -- J. R. Filson

 2:00 p.m.   Three-Dimensional Synthethic Accelerograms for Design Earthquake Ground Motion -- M. Watabe

 2:20 p.m.   Study of Short and Long Period Dynamic Ground Characteristics in the Sendai District -- M. Watabe, Y. Kitagawa

 2:40 p.m.   Discussion

 3:20 p.m.   Hurricane Wind Speeds in the United States -- M. E. Batts, L. R. Russell, E. Simiu

 3:50 p.m.   A Statistical Result on Maximum Surface Winds Surrounding Typhoons -- S. Fujiwhara, I. Subbaramayya

 4:10 p.m.   Surface Winds from Hurricane Frederic: An Engineering Viewpoint -- T. Reinhold

 4:30 p.m.   Hurricanes David and Frederic 1979 -- C. Barrientos

 4:50 p.m.   Discussion

| 5:00 p.m. | Task Committee Meetings |

                            A.   Strong-Motion Instrumentation Arrays and Data
                            B.   Large-Scale Testing Program
                            C.   Repair and Retrofit of Existing Structures
                            H.   Soil Behavior and Stability during Earthquakes

| 6:00 | Adjourn |

TUESDAY   –   May 20

9:00 a.m.	Seismic Response of Floating Offshore Structures -- H. Tsuchida, S. Iai, S. Noda
9:30 a.m.	Critical Excitation of Structures -- R. F. Drenick, G. Bagchi
10:00 a.m.	Dynamic Test of Three-Story Reinforced Concrete Structure -- K. Ohtani
10:20 a.m.	Buckling Analysis of Buried Pipelines under Seismic Loads -- C. C. Chen, T. Ariman, L. H. N. Lee
10:40 a.m.	Discussion
11:10 a.m.	Shaking Table Tests of Earth Retaining Structures on Improved Grounds -- S. Noda, S. Kitazawa, H. Tsuchida
11:30 a.m.	Full-Scale Experimental Study on Aseismic Performance of Medium-Rise Reinforced Concrete Wall Structure -- M. Hirosawa, T. Goto, H. Hiraishi, and M. Yoshimura
11:50 a.m.	Discussion
1:00 p.m.	Soil Dynamics - State of the Art, 1980 -- W. F. Marcuson III, A. G. Franklin, P. F. Hadala
1:20 p.m.	Dynamic Analysis of Sheet Pile Foundation -- T. Asama, Y. Shioi, M. Okahara, Y. Mitsuie
1:40 p.m.	Dynamic Behavior of Multicolumn Foundation with Inclined Piles during Earthquake -- T. Asama, Y. Shioi, H. Asaruma, Y. Mitsuie
2:00 p.m.	Analysis of Liquefaction Potential of Sands on Level Ground During Earthquakes Using Cyclic Strain Controlled Tests -- F. Y. Yokel, R. M. Chung, R. Dobry, and R. S. Ladd
2:20 p.m.	The Participation Factor of Horizontal Force Applied to Pile Foundations -- Y. Sugimura, M. Watabe
2:40 p.m.	Discussion
3:20 p.m.	Operational Model for Forecasting Storm Surges in NOAA -- C. Barrientos
3:40 p.m.	Storm Surge Prevention Around the River Mouths in Japan -- H. Hashimoto
4:00 p.m.	Discussion

4:10 p.m.   Task Committee Meetings

                    D. Structural Performance Evaluation
                    E. Land Use Programs for Controlling Natural Hazard Effects
                    F. Disaster Prevention Methods for Lifeline Systems
                    G. High Winds (Extreme Winds and Structural Response)
                    H. Soil Behavior and Stability During Earthquakes
                    I. Storm Surge and Tsunami

5:00 p.m.   Adjourn

WEDNESDAY –   May 21

9:00 a.m.   New Structural Design Enforcement for Building Structures -- K. Nakano,
                    M. Watabe

9:30 a.m.   Impact of Draft Highway Bridge Seismic Design Guidelines -- J. D. Cooper,
                    R. L. Mayes, R. L. Sharpe

10:00 a.m.   New Specifications for Earthquake-Resistant Design of Highway Bridges in
                    Japan -- E. Kuribayashi, T. Iwasaki, O. Ueda

10:40 a.m.   Single-Story Residential Masonry Construction in Uniform Building Code
                    Seismic Zone – Tentative Recommendations -- R. J. Morony

11:00 a.m.   Discusion

11:20 a.m.   Earthquake Disaster Preparedness Program of Lima, Peru -- M. Watabe

11:50 a.m.   Discussion

1:30 p.m.   Fundamental Factors in Optimizing Earthquake Disaster Mitigation
                    Investment -- Y. Sakagami, E. Kuribayashi, O. Ueda, and T. Tazaki

2:00 p.m.   Wood Sheathed Diaphragms as Lateral Force Resisting Elements -- E. Zacher

2:30 p.m.   A Proposed Method for the Evaluation of Aseismic Performance of Existing
                    Timber Dwellings -- T. Murota, H. Okada

2:50 p.m.   An Evaluation Method on Aseismicity of Earth Structures (Road
                    Embankments) -- T. Fujii, Y. Sasaki

3:10 p.m.   Discussion

3:50 p.m.   Tour of The National Bureau of Standards

5:00 p.m.   Adjourn

THURSDAY –   May 22

9:00 a.m.   Wind-Induced Vibration of Truss Members of the Commodore Barry Bridge --
                    G. F. Fox

9:30 a.m.   Calculation of the Gust Responses of Long-Span Bridges (II) -- N. Narita,
                    H. Sato

10:00 a.m.   Active Turbulence Generator for Wind Tunnel Study of Bridge Aerodynamic
                    Stability -- R. J. Cermak, B. Bienkiewicz, J. Peterka

10:30 a.m.   Discussion

11:10 a.m.	Report on the U.S.-Japan Cooperative Research Program on Large-Scale Testing --
11:35 a.m.	Report on the U.S.-Japan Cooperative Research Program in Earthquake Engineering on Repair and Retrofit Buildings and Lifelines --

Task Committee Reports

1:30 p.m.	A.	Strong-Motion Instrumentation Arrays and Data
1:40 p.m.	B.	Large-Scale Testing Programs
1:50 p.m.	C.	Repair and Retrofit of Existing Structures
2:00 p.m.	D.	Evaluation of Performance of Structures
2:10 p.m.	E.	Land Use Programs for Controlling Natural Hazard Effects
2:30 p.m.	F.	Disaster Prevention Methods for Lifeline Systems
2:40 p.m.	G.	Extreme Winds and Structural Response
2:50 p.m.	H.	Soil Behavior and Stability During Earthquakes
3:00 p.m.	I.	Storm Surge and Tsunami

3:30 p.m.	Adoption of Formal Resolutions
4:00 p.m.	Adjourn

MEMBERSHIP LIST

1980

Dr. Edward O. Pfrang
Chairman
Chief, Structures and Materials Division
Center for Building Technology, NEL
National Bureau of Standards
Washington, DC   20234
(301) 921-2196

Dr. H. S. Lew
Secretariat
Leader, Construction Safety
Structures and Materials Division
Center for Building Technology, NEL
Washington, DC   20234
(301) 921-2647

Dr. S. T. Algermissen
Office of Earthquake Studies
Denver Federal Center
Branch of Earthquake Tectonics, USGS
Stop 978, Box 25046
Denver, CO   80225
(303) 234-4014

Dr. Celso Barrientos
Research Meteorologist
National Oceanic and Atmospheric
  Administration
8060 13th Street
Silver Spring, MD   20910
(301) 427-7613

Mr. Billy Bohannan
Assistant Director
Wood Engineering Research
Forest Products Laboratory, USDA
P.O. Box 5130
Madison, WI   53705
(608) 257-2211

Dr. Roger D. Borcherdt
Chief, Branch of Ground Motion
  and Faulting
Office of Earthquake Studies, USGS
345 Middlefield Road
Menlo Park, CA   94025
(415) 323-8111

Dr. A. Gerald Brady
Physical Scientist
Office of Earthquake Studies, USGS
345 Middlefield Road
Menlo Park, CA   94025
(415) 323-8111

Mr. James D. Cooper
Structures and Applied Mechanics Division
Federal Highway Administration
Office of Research HRS-11
Washington, DC   20590
(202) 557-4315

Mr. Jerry Dodd
Bureau of Reclamation
P.O. Box 25007
Denver Federal Center
Denver, CO   80225
(303) 234-3089

Mr. G. Robert Fuller
Architectural and Engineering Division
Department of Housing and Urban Development
Washington, DC   20411
(202) 755-5924

Dr. Michael P. Gaus
Division of Problem-Focused Research
  Applications
National Science Foundation
1800 G Street, NW
Washington, DC   20550
(202) 632-5700

Mr. John J. Healy
Chief, Research and Development Office
Department of the Army
DAEN-RDM
Washington, DC   20314
(202) 272-0260

Dr. William B. Joyner
Office of Earthquake Studies
Branch of Ground Motion and Faulting, USGS
345 Middlefield Road
Menlo Park, CA   94025
(415) 323-8111

Mr. John W. Kaufman
Atmospheric Sciences Division
National Aeronautics and Space Administration
Marshall Space Flight Center, AL   35812
(205) 453-3104

Mr. James Lander
National Oceanic & Atmospheric Administration
Environmental Data Service
National Geophysical and Solar-Terrestrial
  Data Center
Boulder, CO   80302
FTS 323-6474 or (303) 449-1000, ext. 6474

Dr. E. V. Leyendecker
Leader, Earthquake Hazards Reduction
  Group
Structures and Materials Division
Center for Building Technology, NEL
National Bureau of Standards
Washington, DC   20234

Dr. Shih C. Liu
Program Manager
Division of Problem-Focused Research
  Applications
National Science Foundation
Washington, DC   20550
(202) 632-5700

Dr. Richard D. McConnell
Office of Construction
Veterans Administration
811 Vermont Avenue, NW
Washington, DC   20420
(202) 389-3103

Dr. William F. Marcuson, III
Research Civil Engineer, WES-SH
Waterways Experiment Station,
  Corps of Engineers
P.O. Box 631
Vicksburg, MS   39180
FTS 542-2234 or 636-3111, ext. 2234

Dr. Richard D. Marshall
Leader, Structural Engineering
Structures and Materials Division
Center for Building Technology, NEL
National Bureau of Standards
Washington, DC   20234
(301) 921-3471

Mr. John F. Meehan
Department of General Services
Office of Architectural Construction
Sacramento, CA   95805
(916) 445-8730

Mr. Howard L. Metcalf
Deputy Director for Construction
  Standards and Design
Office of the Assistant Secretary
  of Defense
(MRA&L) Room 3E763
The Pentagon
Washington, DC   20301
(202) 695-2713

Dr. John B. Scalzi
Program Manager, Division of Problem-
  Focused Research Applications
National Science Foundation
1800 G Street, NW
Washington, DC   20550
(202) 632-0648

Mr. Charles Scheffey
Director, Office of Research
Federal Highway Administration
Department of Transportation
Washington, DC   20590
(202) 357-5754

Mr. Lawrence C. Shao
Assistant Director for General Reactor
  Safety Research
Nuclear Regulatory Commission
Washington, DC   20555
(301) 427-4442

Dr. Warren A. Shaw
Head, Civil Engineering Department
Civil Engineering Laboratory
Naval Construction Battalion Center
Port Hueneme, CA   93043
(805) 982-5407

Dr. Charles C. Thiel
Assistant Associate Director for Mitigation
  and Research
Federal Emergency Management Agency
Washington, DC   20472
(202) 653-7860

Alternates:

Mr. Michael Changery
National Climatic Center
Federal Building
Asheville, NC   28787
(704) 258-2850, ext. 217

Dr. Jerry Harbour
Site Safety Research Branch
Office of Site Safety Research Branch
Nuclear Regulatory Commission
Washington, DC   20555
(301) 427-4370

Dr. R. B. Matthiesen
Research Civil Engineer
Branch of Seismic Engineering, USGS
345 Middlefield Road
Menlo Park, CA   94025

Mr. Ronald J. Morony
Program Manager
Building Technology Research Staff
Department of Housing and Urban
  Development
Washington, DC   20410
(202) 755-0640

Mr. Drew A. Tiedemann
Bureau of Reclamation
Engineering and Research Center
Denver Federal Center
Denver, CO   80225
(303) 234-3029

Mr. Yoshiziro Sakagami
Chairman
Director General, Public Works
  Research Institute
Ministry of Construction
Asahi 1-banchi, Toyosato-machi,
  Tsukuba-gun
Ibaraki-ken 305, Tokyo

Dr. Ryuichi Iida
Secretariat
Director, Planning and Research
  Administration Department
Public Works Research Institute
Ministry of Construction
Asahi 1-banchi, Toyosato-machi,
  Tsukuba-gun
Ibaraki-ken 305, Tokyo

Mr. Tatsuo Asama
Director, Structure and Bridge Department
Public Works Research Institute
Ministry of Construction
Asahi 1-banchi, Toyosato-machi,
  Tsukuba-gun
Ibaraki-ken 305, Tokyo

Dr. Nozomu Den
Head, Seismology and Volcanology Division
Meteorological Research Institute (MRI)
Japan Meteorological Agency (JMA)
1-1, Nagamine, Yatabe-machi, Tsukuba-gun
Ibaraki-ken 305, Tokyo

Mr. Shigemi Fjuiwhara
Head, Typhoon Research Division
Meteorological Research Institute (MRI)
Japan Meteorological Agency (JMA)
1-1, Nagamine, Yatabe-machi, Tsukuba-gun
Ibaraki-ken 305, Tokyo

Dr. Yoshimi Goda
Director, Marine Hydrodynamics Division
Port and Harbour Research Institute
Ministry of Transport
3-1-1, Nagese, Yokosuka-shi,
  Kanagawa-ken 239, Tokyo

Mr. Hiroshi Hashimoto
Head, Coastal Engineering Division
River Department
Public Works Research Institute
Ministry of Construction
Asahi 1-banchi, Toyosato-machi,
  Tsukuba-gun
Ibaraki-ken 305, Tokyo

Dr. Sadaiku Hattori
Chief, Seismology Section
International Institute of Seismology and
  Earthquake Engineering (I.I.S.E.E.)
Building Research Institute
Ministry of Construction
Tatehara 1-banchi, Oh-ho-machi, Tsukuba-gun
Ibaraki-ken 305, Tokyo

Mr. Masaya Hirosawa
Chief Researcher
Building Research Institute
Ministry of Construction
Tagehara 1-banchi, Oh-ho-machi, Tsukuba-gun
Ibaraki-ken 305, Tokyo

Mr. Toshio Iwasaki
Head, Ground Vibration Division
Earthquake Disaster Prevention Department
Public Works Research Institute
Ministry of Construction
Asahi 1-banchi, Toyosato-machi, Tsukuba-gun
Ibaraki-ken 305, Tokyo

Mr. Motoo Kobayashi
Head, The First Geographic Division
Geographical Survey Institute
Ministry of Construction
Kitazato 1-banchi, Yatabe-machi, Tsukuba-gun
Ibaraki-ken 305, Tokyo

Mr. Eiichi Kuribayashi
Director, Earthquake Disaster
  Prevention Department
Public Works Research Institute
Ministry of Construction
Asahi 1-banchi, Toyosato-machi, Tsukuba-gun
Ibaraki-ken 305, Tokyo

Mr. Tatsuro Murota
Chief, Building Aerodynamics Section
Structure Engineering Division
Building Research Institute
Ministry of Construction
Tatehara 1-banchi, Oh-ho-machi, Tsukuba-gun
Ibaraki-ken 305, Tokyo

Dr. Keikichi Naito
Head, Meteorological Satellite Division
Meteorological Research Institute (MRI)
Japan Meteorological Agency (JMA)
1-1, Nagamine, Yatabe-machi, Tsukuba-gun
Ibaraki-ken 305, Tokyo

Dr. Kiyoshi Nakano
Director, Building Research Institute
Ministry of Construction
Tatehara 1-banchi, Oh-ho-machi,
  Tsukuba-gun
Ibaraki-ken 305, Tokyo

Dr. Nobuyuki Narita
Head, Structure Division
Structure and Bridge Department
Public Works Research Institute
Ministry of Construction
Asahi 1-banchi, Toyosato-machi,
  Tsukuba-gun
Ibaraki-ken 305, Tokyo

Mr. Setsuo Noda
Chief, Earthquake Disaster Prevention
  Laboratory
Structure Division
Port and Harbour Research Institute
Ministry of Transport
3-1-3 Nagase, Yokosuka-shi,
  Kanagawa-ken 239

Dr. Tadayoshi Okubo
Deputy Director-General
Public Works Research Institute
Ministry of Construction
Asahi 1-banchi, Toyosato-machi,
  Tsukuba-gun
Ibaraki-ken 305, Tokyo

Mr. Keiichi Ohtani
Chief, Earthquake Engineering Laboratory
Second Research Division
National Research Center for Disaster
  Prevention
Science and Technology Agency
3-1, Tennodai, Sakura-mura, Niihari-gun,
  Ibaraki-ken 305, Tokyo

Mr. Michio Ohtsuka
Acting Director, International Institute
  of Seismology and Earthquake Engineering
  (I.I.S.E.E.)
Building Research Institute
Ministry of Construction
Tatehara 1-banchi, Oh-ho-machi,
  Tsukuba-gun,
Ibaraki-ken 305, Tokyo

Mr. Yasushi Sasaki
Head, Soil Dynamics Division
Construction Method and Equipment Department
Public Works Research Institute
Ministry of Construction
Asahi 1-banchi, Toyosato-machi, Tsukuba-gun
Ibaraki-ken 305, Tokyo

Mr. Yukitake Shioi
Head, Foundation Engineering Division
Structure and Bridge Department
Public Works Research Institute
Ministry of Construction
Asahi 1-banchi, Toyosato-machi, Tsukuba-gun
Ibaraki-ken 305, Tokyo

Mr. Hiroshi Takahashi
Head, Second Research Division
National Research Center for Disaster
  Prevention
Science and Technology Agency
3-1, Tennodai, Sakura-mura, Niihari-gun
Ibaraki-ken 305, Tokyo

Mr. Hajime Tsuchida
Chief, Earthquake Resistant Structures
  Laboratory
Structure Division
Port and Harbour Research Institute
Ministry of Transport
3-1-1, Nagase, Yokosuka-shi,
  Kanagawa-ken 239, Tokyo

Mr. Osamu Ueda
Head, Earthquake Engineering Division
Earthquake Disaster Prevention Department
Public Works Research Institute
Ministry of Construction
Asahi 1-banchi, Toyosato-machi, Tsukuba-gun
Ibaraki-ken 305, Tokyo

Dr. Makoto Watabe
Head, Structure Division
Building Research Institute
Ministry of Construction
Tatehara 1-banchi, Oh-ho-machi, Tsukuba-gun
Ibaraki-ken 305, Tokyo

RESOLUTIONS OF THE TWELFTH JOINT MEETING

U.S.-JAPAN PANEL ON WIND AND SEISMIC EFFECTS

U.J.N.R.

May 19 - 22, 1980

Washington, DC U.S.A.

The following resolutions for future activities of this Panel are hereby proposed (adopted):

1. The Twelfth Joint Meeting was an extremely valuable exchange of technical information which was beneficial to both countries. In view of the importance of the cooperative programs on the subject of wind and seismic effects, the continuation of Joint Panel Meetings is considered essential.

2. The exchange of technical information, research data, the promotion of joint research programs including the exchange of personnel, and the use of available facilities should be strengthened.

3. In order to facilitate the activities of the Task Committees, the nomination of Task Committee vice-chairmen and expansion of the task committee membership is encouraged.

    To expand the activities of the Task Committee G, it is proposed that the name of the Task Committee be revised to "Wind Characteristics and Structural Response," and to include additional members.

4. The Panel on Wind and Seismic Effects recognizes the accomplishments of the U.S.-Japan Cooperative Program on Large Scale Testing. This Panel will consider at an early date, possible endorsement of the Program upon review of the proposals of both sides.

    Close working relationships should be maintained between the Panel and the Joint Coordinating Group of the Large Scale Testing Program. This should include notification of proposed research and change in direction and a periodic review of the progress of the Program.

5. The Panel on Wind and Seismic Effects recognizes the importance of the U.S.-Japan Cooperative Program on Repair and Retrofit of Buildings and Lifeline. It recommends expended implementation of the program through this Panel. The Panel urges that the program coordination of both sides shall maintain close working relationships with this Panel and the Secretariats of both sides shall be kept informed of all correspondence.

6. Recognizing that wind and seismic disaster mitigation plans benefit disaster-prone countries worldwide, that many developing countries suffer from natural disasters such as extreme winds and earthquakes, and that both the United States and Japan have been involved in international technical cooperation programs, both sides of this Panel should give consideration to conduct coordinated projects for the aid of developing countries and to maintain exchange of available technical information.

7. The date and location of the Thirteenth Joint Meeting of the Panel on Wind and Seismic Effects will be May 1981 at Tsukuba Science City, Japan. Specific dates and itinerary will be proposed by the Japanese Panel with concurrence by the U.S. Panel.

DENSE INSTRUMENT ARRAY PROGRAM OF THE PUBLIC WORKS
RESEARCH INSTITUTE FOR OBSERVING STRONG EARTHQUAKE-MOTION

by

Yoshiziro Sakagami

Tadayoshi Okubo

Toshio Iwasaki

Kazuhiko Kawashima

ABSTRACT

Based upon the knowledge accumulated from past strong-motion observations, it is widely recognized that short period ground motions are significantly dependent on source characteristics, path conditions between the source and the observation station, local geological and topological conditions. In order to investigate these effects, normal strong-motion observations performed at individual sites are not enough, and installation of dense instrument arrays are considered necessary.

Solving these important earthquake engineering problems, the Public Works Research Institute intends to press for research funds to further the dense instrument array program at ten locations. To prepare for these observations, the Public Works Research Institute installed a simple extended array consisting of four strong-motion accelerographs as a pilot station at Ashitaka Area, Shizuoka Prefecture, to begin the investigation of local soil condition effects on strong ground motions. A local laboratory array installed at the Public Works Research Institute is also being employed for this purpose.

This report briefly summarizes the dense instrument array program of the Public Works Research Institute and details the preliminary pilot array observations at PWRI in Tsukuba Science City and at Ashitaka Area, Shizuoka Prefecture.

\

In the earthquake engineering field, strong motion observations have been made in an effort to collect the actual data of seismic responses of structures and subsurface ground nearby so that improved seismic design procedures for various kinds of structures can be achieved from analysis of the recorded responses. Observations have mainly concentrated on acceleration measurements. In Japan strong-motion observation began around 1955. They were activated following the Niigata-Earthquake in 1964 in recognition of the importance of strong-motion records for analyzing earthquake damage. Currently more than a thousand strong-motion accelerographs have been installed which cover the whole of Japan.

As far back as 1934 observations began in Japan using elementary arrays of several instruments extending unilaterally in the vertical direction. Practical observations using elemental arrays began after 1959, and now the number of observatory points has reached about one hundred. The purpose of these observations has been the analysis of structural response and soil-structure interaction, while some of them have been installed for the analysis of source mechanism, wave propagation, and local site effects.

Based on the knowledge accumulated from past strong motion observations, it is widely recognized that the characteristics of ground motions, especially ground motions of short period, are strongly dependent on source characteristics, path conditions between the source and the observation station, local geological and topological conditions. It is also recognized that in order to investigate these effects, normal strong motion observations performed widely at the present are not enough, and that the installation of dense arrays are necessary.

Based on this historical background, the Executive Committee of the International Association for Earthquake Engineering, meeting on January 14, 1977 in India on the occasion of the Sixth World Conference on Earthquake Engineering, decided to hold an International Workshop on Strong-Motion Earthquake Instrument Arrays under the sponsorship of UNESCO. The International Association of Seismology and Physics of the Earth's Interior (IASPEI) joined this effort as a member of International Workshop on Strong-Motion Earthquake Instrument Arrays.

The International Workshop was held at Honolulu, Hawaii in May 1978 with participants from sixteen countries. In Japan, before holding of the workshop, another workshop on

Strong-Motion Earthquake Instrument Arrays was organized by the Steering Committee of Earthquake Engineering, Japan Science Council, to prepare a Japanese master plan of array observation. This Japanese workshop has continued to serve in the forming of Japanese plans and coordinating proposals from participating organizations.

The international workshop recommended the formation of an International Strong-Motion Arrays Council to facilitate the establishment of strong-motion earthquake instrument arrays. Based on a careful examination of the potential for the occurence of large earthquakes in 10 years, 28 locations were selected as favorable array locations. Of the 28 locations selected, six have been designated as high priority sites. These sites were judged to have an especially high probability of yielding useful data. Among the 28 locations, Eastern Tohoku, Suruga Bay-Izu, and Western Chubu areas were included, and the Suruga Bay-Izu area was designated as one of the six high priority sites.

The international workshop also recommended typical array configurations based on the fault model, such as strike slip fault, subduction thrust fault, and dip slip fault for analysis of source mechanism and wave propagation, and on topological and geological conditions for analysis of local site conditions. The establishment and maintenance of mobil strong-motion instrument array capable of making source mechanism wave propagation, and local effects measurements was also recommended for deployment immediately after the occurence of major earthquakes to record aftershocks.

Following the recommendations of the international workshop, a program of deployment of strong-motion earthquake instrument arrays in Japan is now being developed by the Japanese workshop. The program recommends three items, i.e., (a) development of a strong-motion earthquake instrument arrays system, (b) installation of arrays for source mechanism and path effect studies, and (c) installation of arrays for local site effects studies. It is hoped the program will be realized by both scientific and engineering groups. Participants include the: School of Engineering, University of Hokkaido, Earthquake Research Institute, University of Tokyo, School of Science and Engineering, The University of Tohoku and The University of Nagoya, Disaster Prevention Research Institute of the University of Kyoto, Public Works Experimental Station of the Hokkaido Development Bureau, Meteorological Research Institute of the Meterological Agency, National Research Center for Disaster Prevention of Science and Technology Agency, Public Works Research Institute of Ministry

of Construction, Building Research Institute of Ministry of Construction, and Port and Harbour Research Institute of Ministry of Transportation. Also, it is expected that the Japan Science Council will recommend that the Prime Minister of the Japanese Government enthusiastically promote the implementation of dense strong-motion instrumental array programs, including funding support.

THE DENSE INSTRUMENT ARRAY PROGRAM OF THE PUBLIC WORKS RESEARCH INSTITUTE

Recognizing the importance to understanding the characteristics of strong-motions in order to improve seismic design procedure, the Public Works Research Institute has conducted strong-motion observations since 1957 for bridges, dams, river dykes, estuary dams, underground shopping streets, submerged tunnels, et al., and the surrounding subsurface ground. Up to March 1980, the total number of SMAC accelerographs and electro-magnetic accelerographs reached 261 (131 observation stations) and 46 (46 observation stations, 439 channels), respectively. Measurements of underground motions also have been conducted since 1970 using down-hole accelerographs installed as deep as 120 m below the ground surface at seven locations in the bay areas, of Tokyo, Osaka, and Nagoya. A local laboratory array deploying accelerographs in horizontal and vertical directions is being equipped at the Public works Research Institute in Tsukuba Science City and is expected to begin measurement after May 1980.

A fuller understanding of the nature of strong ground motions is needed to provide answers to unsolved problems in estimating rational input ground motions to large structures such as long suspension bridges and submerged tunnels, in evaluating seismic risk to life-line network facilities, and in developing suitable seismic micro-zoning procedures applicable to earthquake disaster prevention planning.

Considering the importance of solving these problems, the Public Works Research Institute intends to press for research funds to promote dense instrument array programs at the ten locations shown in Figure 1, which will deploy at least ten strong-motion accelerographs at each location. Figure 2 shows a proposed standard array configuration. To prepare for these practical observations the Public Work Research Institute installed a simple extended array of four strong motion accelerographs at the pilot station in the Ashitaka Area, Shizuoka Prefecture. Observations to begin about May 1980.

THE LOCAL LABORATORY ARRAY AT THE PUBLIC WORKS
RESEARCH INSTITUTE IN TSUKUBA SCIENCE CITY

Location

The Public Works Research Institute in Tsukuba Science City is located approximately 60 km northeast of Tokyo as shown in Figure 3. Figure 4 shows the research facilities of the institute. Two local laboratory arrays are located at areas A and B, which are designated hereafter as A Field and B Field. At C area (designated as C Field) a strong-motion accelerograph with an autodial data transmission system is installed.

Geological conditions around the institute are almost uniform in the horizontal direction as shown in Figure 5. Alluvial sandy and silty deposits approximate thickness of 50 m, rest on a diluvial gravel formation as shown in Figure 6. Shear wave velocities of the alluvial and diluvial are approximately 250 m/sec and 400 m/sec, respectively.

Instrumentation

Figure 7 shows instrumentations at the A, B, and C Fields. In the A Field are 13 three-component accelerometers, i.e., seven on the surface, one at a depth of 2 m and 5 at a depth of 50 m, along an x-shaped configuration, with leg length 100 m. In the B-Field are 6 three-component accelerometers, i.e., one at the depth of 2 m, four at the depth of 66 m and one at the depth of 96 m, along an L-shaped configuration of short and long lengths of 50 m and 100 m, respectively (refer to Table 1). The x and L-shaped configurations are orientated along NS and EW lines, as are the sensor components. The main specifications of the accelerometers used are summarized in Table 2. Signals from each sensor are transmitted by cable placed in a duct as shown in Figure 8 to a central processing room of strong-motion earthquake records via a field station house. Figure 9 shows an aerial view of the A and B Fields.

At the C Field, an accelerometer is set on the ground surface. A self-trigger system is provided. Specifications of the accelerometer are essentially the same as those used in the A and B Fields.

At Fields A and B, signals are triggered either when maximum acceleration of vertical component exceeds 3 gals at both Fields (one of points with depth of 50 m at A Field, and

a point with depth of 96 m at B Field) or when maximum acceleration of one of two horizontal components at both points exceeds 5 gals. At C Field triggering of the records occurs when maximum acceleration of vertical component exceeds 3 gals.

Recording and Processing Systems

Signals from the sensors installed at A, B, and C Fields are recorded on a computer system magnetic tape in the following form (refer to Figure 10):

(i) Excluding 21 signals of the surface accelerometers at A Field, 36 of the total 57 signals triggered at A and B Fields are automatically digitized with a time interval of 1/100 second by an AD converter and stored on magnetic disk (maximum capacity of 64 MB) by the 80 KW core memory. Pre-event memories of 5 seconds are prepared for the 36 signals so that an entire recording of earthquakes motions can be achieved. Data stored on the magnetic disk are then compiled into a form of standard data processing of strong-motion records formulated by the Public Works Research Institute, and stored on a magnetic tape. Besides this recording system, an analog tape recording system is supplementarily provided to store 32 of the the 36 signals. This system can be used when the computer recording system is out of use.

(ii) While the 21 signals of the surface accelerometers at A-Field are also automatically digitized with a 1/100 second time interval by AD converter and stored on magnetic disk, pre-event memories are not provided. But time code simultaneity of the 21 signal group with those of the 36 signals is kept.

(iii) The accelerometer signal at C-Field is automatically digitized with a 1/100 second time interval by AD converter and stored on a digital cassette tape. A prevent memory of 10 seconds is provided. After an earthquake, the transmitter at C-Field automatically seeks, via telephone cable, an extension of the central processing room up to three times. If a connection occurs within any one of the three calls, the recorded data are transmitted to the computer system magnetic disk in the central processing room. If no connection is achieved within three calls from the transmitter, the transmitter goes into a hidden

stage of keeping the data stored on the cassette tape. In such a waiting situation, the transmission of the data from cassette tape to magnetic disk can be achieved by calling back from the central processing room to the transmitter at C-Field. A backup cassettee tape is provided to work so that signals induced by the next earthquake can be recorded even in cases when the first cassette tape is full and on hold.

In the recording system above, the computer system plays a principal role, and when the system is down, no recording of data can occur. Therefore, a float battery charger will supply system power for no less than 20 minutes if the electrical lines are knocked out.

For analyzing the recorded motions, a 192 KW core memory computer system is provided as shown in Figure 11. Data transmission from recording system to analyzing system is performed on a tape base. The system is designed to analyze not only the data from the A, B, and C Fields in Tsukuba Science City, but also the data obtained through the strong-motion observation network of the Public Works Research Institute which covers Japan.

THE SIMPLE EXTENDED ARRAY AT ASHITAKA AREA IN SHIZUOKA PREFECTURE

Location and Instrumentation

The Ashitaka Area is located between Numazu City and Fuji City in Shizuoka Prefecture facing Suruga-Bay. Figures 12 and 13 show the geological surface conditions and a cross section of the geological profile in the NS direction. The surface of the Ukishimagahara, Ashitaka Area, is covered with organic soil as deep as 15 m, and is underlaid by gravels, sandy and silty layers. The baserock of this area is tuff breccia existing approximately at a depth of 160 m below the surface at Higashi-tago-no-ura.

Figure 14 represents one of the typical soil profiles at Ukishima-gahara in the Ashitaka Area. Shear wave velocity of the subsurface material is in the range of 70 to 200 m/sec. Tuff breccia exists at a depth of approximately 35 m below the surface and has a shear wave velocity of approximately 650 m/sec at this site.

A simple extended array is being installed by the Public Works Research Institute crossing Ukishima-gahara in an almost NS direction as shown in Figure 15, which also presents a geological section obtained from boring data. Japan's most important traffic facilities, the National Highway Route 1, bi-path of Route 1, Tokaido Line (Railway) and Shinkansen (New Tokaido Railway), cross the array in an EW direction.

The array consists of five strong-motion accelerographs; four are installed already, i.e., one on a sand hill facing Suruga Bay, two on Ukishima-gahara, and one on a foot of the Ashitaka Mountain. An additional accelerograph is being installed between the Ukishima-gahara and a foot of Ashitaka Mountain. Figure 16 shows an aerial view of the array location.

On-site Accelerograph Storage Buildings

Four RC on-site buildings, as shown in Figure 17, were constructed to store the accelerographs at each location. Each accelerograph is set on a concrete footing 1.2 m in length, 12 m in width, and 0.3 m in thickness, and is isolated from the building footing as shown in Figure 18. Nine pine piles 20 cm in diameter and approximately 2 m long are attached to the bottom of the footing which supports the accelerographs to avoid the development of relative movement between the footing and the surrounding ground during earthquakes. The vertical position of the accelerographs is designed to be 35 cm higher than the surface of the concrete footing to avoid inundation of the accelergraphs in case of flooding.

Recording System

Four 3-component strong-motion accelerographs using digital cassette recording systems are employed for the array. Accelerograph specifications are summarized in Table 3. A maximum acceleration of ± 1 g can be recorded, the signals are digitized at 1/200 second time intervals, and are cassette stored. Time code generators are equipped for each recording system so that exact triggering time is recorded at the four sites. Crystal accuracy in the time code generator is approximately $\pm 10^{-6}$ (3 seconds per month). Auto adjustment of the crystal can be performed each 5 seconds using JJY signal. Time code generator error is designed to be controlled less than 10^{-3} second.

Float battery chargers supply electricity for no less than 6 hours in case of electricity breakdown.

AN EXAMPLE OF LOCAL LABORATORY ARRAY RECORDING

Both the local laboratory array at PWRI in Tsukuba Science City and the simple extended array at Ashitaka Area are scheduled to begin full observation after May 1980. Therefore no records have as yet been obtained at either array. A preliminary and limited observation has been performed since July 1979 on the local laboratory array using an auxiliary analog tape recording system, and a record induced by an earthquake of July 11, 1979, Richter Magnitude of 5.9, focal depth of 40 km, and an epicentral distance of approximately 120 km was successfully recorded.

Figure 19 represents acceleration records thus obtained at the north, east, south, and west edges of the cross at the 50 m depth. These are designated as N50, E50, S50, and W50 (refer to Figure 20). Since the temporary recording system consists of analog tape, simultaneity of time code is achieved between the records at N50 and W50, and between the records at E50 and S50 only.

Figures 21 and 22 represent power spectra of the acceleration records and displacements computed by double integration of the accelerations, respectively.

Ground strains induced by the earthquake were estimated using the displacements shown in Figure 22. An averaged ground strain between two observing points is defined as

$$
\begin{Bmatrix} \varepsilon_{Ax} \\ \varepsilon_{SH} \end{Bmatrix} = \frac{1}{L} \begin{bmatrix} 1 & 0 & -1 & 0 \\ 0 & 1 & 0 & -1 \end{bmatrix} \begin{Bmatrix} \mu_{1,i} \\ \mu_{2,i} \\ \mu_{1,j} \\ \mu_{2,j} \end{Bmatrix} \tag{1}
$$

where ε_{AK} and ε_{SH} represent averaged axial strain and shearing strain between the specified two points, respectively, and where $\mu_{1,k}$ and $\mu_{2,k}$ (k=1, j) represent ground displacement at point k in NE-SW and NW-SE directions, respectively. A parameter L is defined by a length between the two points and is given by $\sqrt{2}\, \ell$ in this case, where ℓ equals 50 m.

The displacement $\mu_{i,k}$ and $\mu_{2,k}$ (k=1, j) can be determined in the form

$$
\begin{Bmatrix} \mu_{1,i} \\ \mu_{1,j} \\ \mu_{2,i} \\ \mu_{2,j} \end{Bmatrix} = \frac{1}{\sqrt{2}} \begin{bmatrix} 1 & 1 & 0 & 0 \\ -1 & 1 & 0 & 0 \\ 0 & 0 & 1 & 1 \\ 0 & 0 & -1 & 1 \end{bmatrix} \begin{Bmatrix} \mu_{NS,i} \\ \mu_{EW,i} \\ \mu_{NS,j} \\ \mu_{EW,j} \end{Bmatrix}
\tag{2}
$$

where $\mu_{NS,k}$ and $\mu_{EW,k}$ (k=i,j) represent displacements at point k in the N-S and E-W directions, respectively.

According to Eq. (1), the averaged axial strain ε_{Ax} and shearing strain ε_{SH} were computed between N50 and W50, and between E50 and S50 as shown in Figure 23. The maximum value of both ε_{Ax} and ε_{SH} are estimated as 5×10^{-5}. One can approximate the averaged strain from displacement represented in Figure 22 assuming that the displacements on points i and j are in out of phase. Because the maximum displacements in Figure 22 are approximately 0.3 cm, the averaged strain based on the above assumption can be estimated as

$$
\varepsilon = \frac{2 \, \mu_{max}}{L} = \frac{2 \times 0.3}{\sqrt{2} \times 5.000} \approx 8.5 \times 10^{-5}
\tag{3}
$$

which is close to the strains determined by Eq. (1).

CONCLUDING REMARKS

The dense instrument array program of the Public Work Research Institute has been briefly described with emphasis on preliminary pilot array observations conducted at PWRI in Tsukuba Science City and at Ashitaka Area in Shizuoka Prefecture. The dense instrument array program has just begun in Japan, and because of the importance of investigating local effects on strong-ground motion in the earthquake engineering field, the encouragement of this program is highly recommended.

REFERENCES

[1]   International Association for Earthquake Engineering: Strong-Motion Earthquake Instrument Arrays, Proceedings of the International Workshop on Strong-Motion Earth-quake Instruments Arrays, Edited by W. D. Iwan, 1978, Honolulu, Hawaii, U.S.A.

[2]   Iwasaki, T., Wakabayashi, S. and Tatsuoka, F.: Characteristics of Underground Seismic Motions at Four Sites Around Tokyo Bay, 8th UJNR, Washington, D.C., 1976.

[3] Nakano, S. and Kitagawa, Y.: Earthquake Observation Systems In and Around Structures in Japan, 11th UJNR, Tokyo, 1979.

[4] Shizuoka Prefecture: Geology in Shizuoka Prefecture, edited by Tsuchi, R., 1974.

[5] Development Bureau of the Economic Planning Agency: Land Classification Map, No. 08, Part of Ibaragi-Prefecture, 1973.

[6] Kuribayashi, E., Tsuchida, H. and Watabe, M.: On the Maintenance of the Strong-Motion Accelerograph and the Data Processing the Records, 7th UJNR, Tokyo, 1975.

[7] Okubo, T.: Dense Instrument Array Program, Civil Engineering Journal, Vol. 22, No. 4, 1980.

Fig. 1 Proposed Location of Dense Strong-Motion Array by PWRI

SPECIAL AREA FOR REINFORCEMENT OF OBSERVATION

DESIGNATED AREA FOR OBSERVATION

NO	AREA	NO	AREA
1	OMAE-ZAKI	6	FURUKAWA
2	YAIZU	7	ODAWARA
3	NUMAZU	8	DAITO ZAKI
4	MATSUZAKI	9	TATEYAMA
5	SENDAI	10	CHOSHI
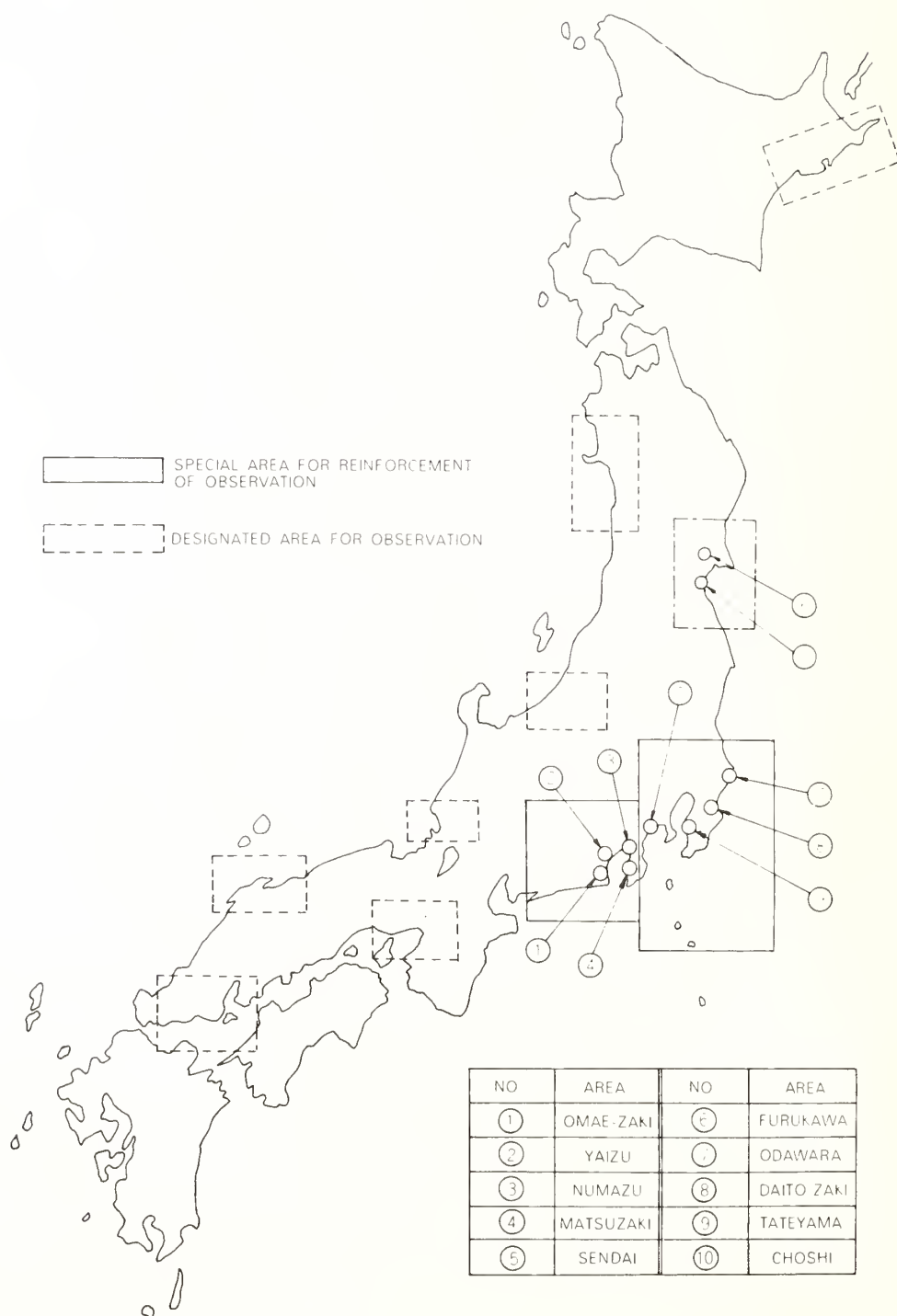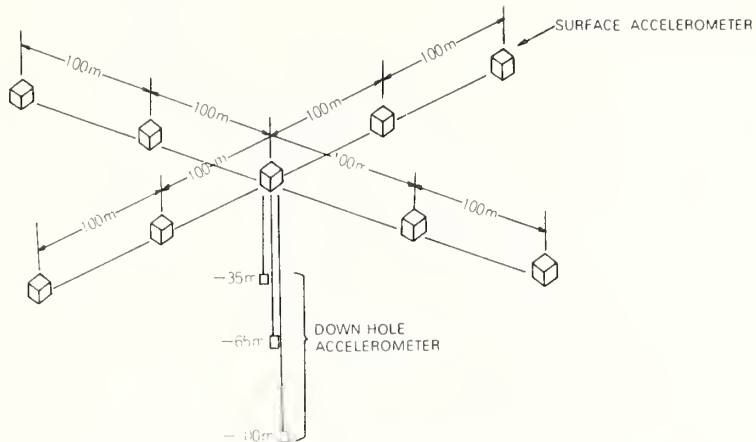
Fig. 2 Proposed Configuration of Local Laboratory Array
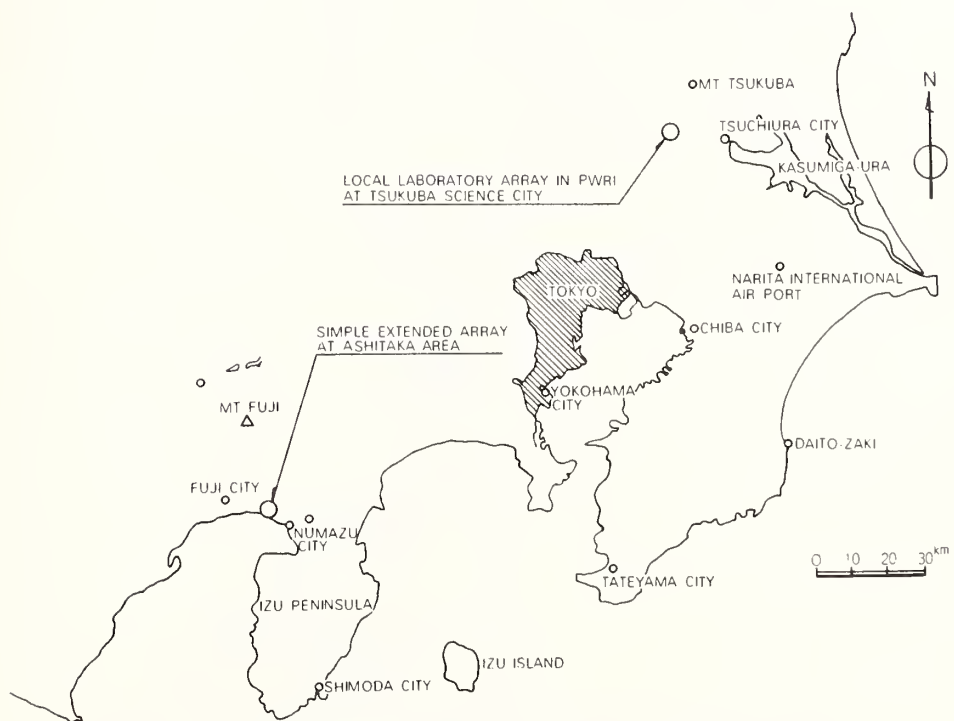
Fig. 3 Locations of Dense Strong-Motion Array by PWRI

13
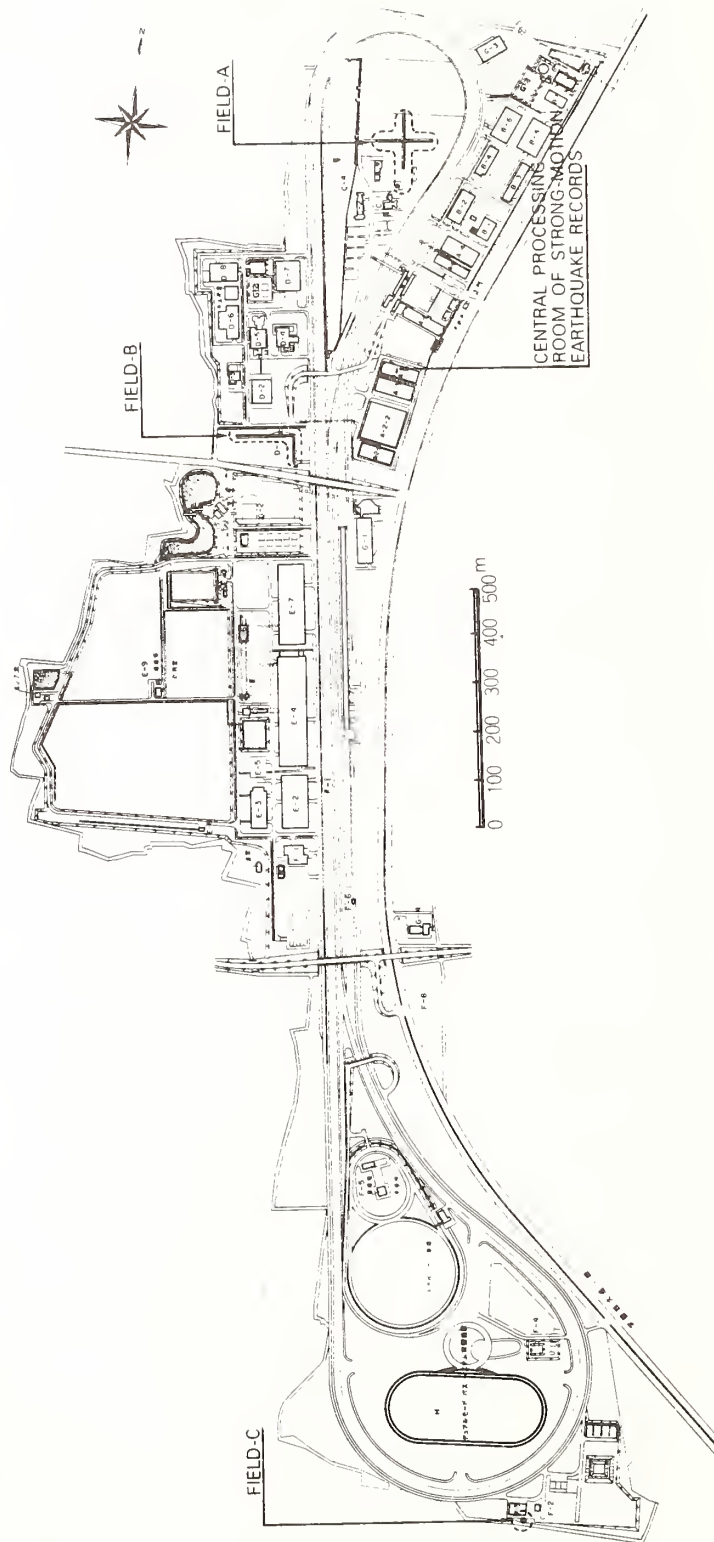
Fig. 4 Location of Local Laboratory Arrays at PWRI

14

LEGEND

SAND	LOAM	GABBRO SERIES	GNEISS
MUD	GRANITE SERIES	BLACK SCHIST	CLASTICS
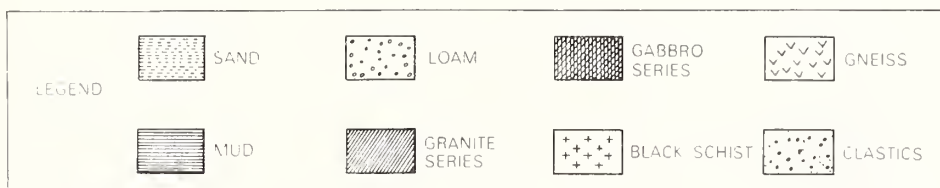
Fig. 5 Surface Geological Map Around Public Works Reserach Institute
at Tsukuba Science City (After Reference 5)
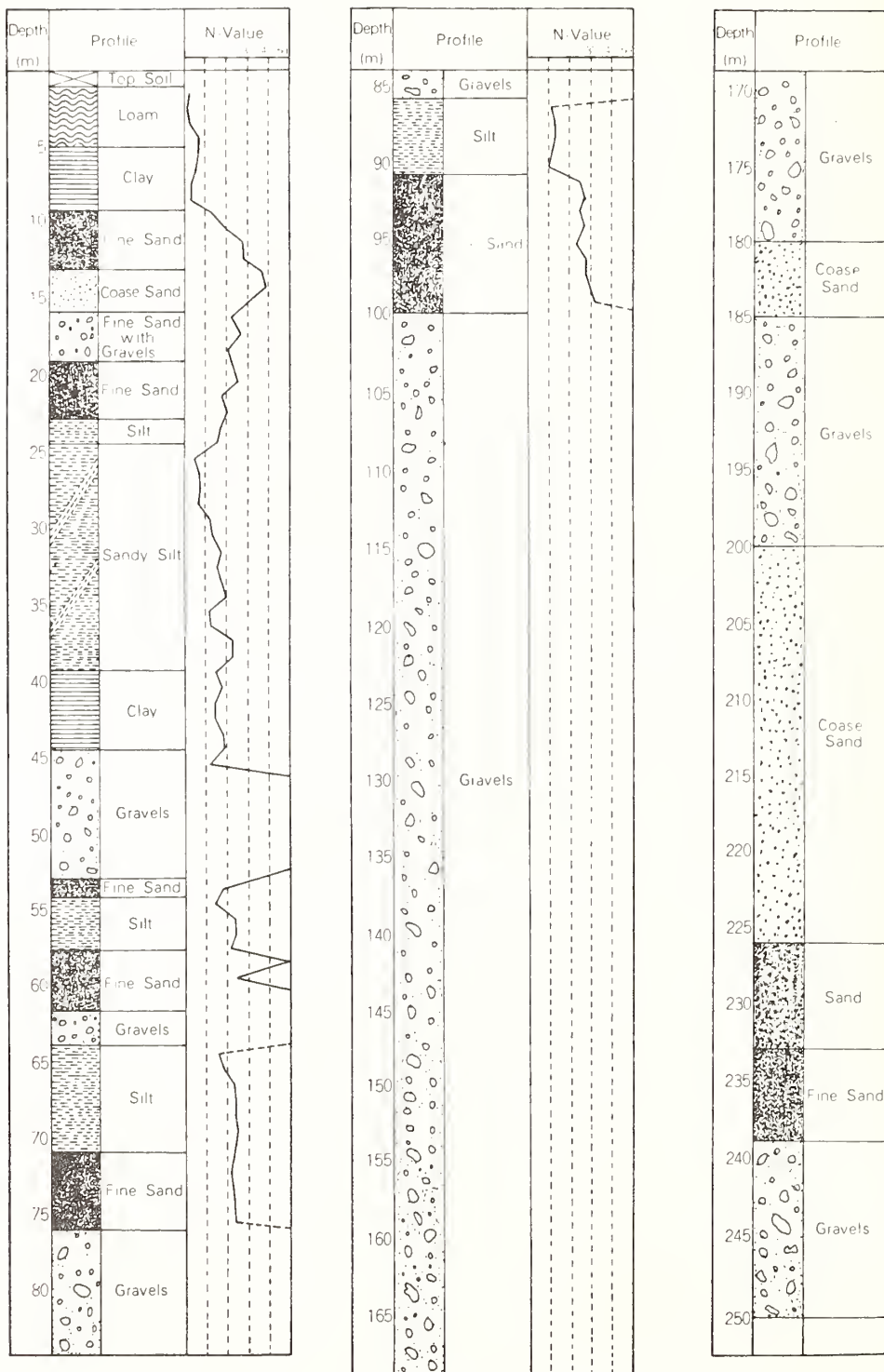
Fig. 6 Soil Profile at PWRI in Tsukuba Science City

16
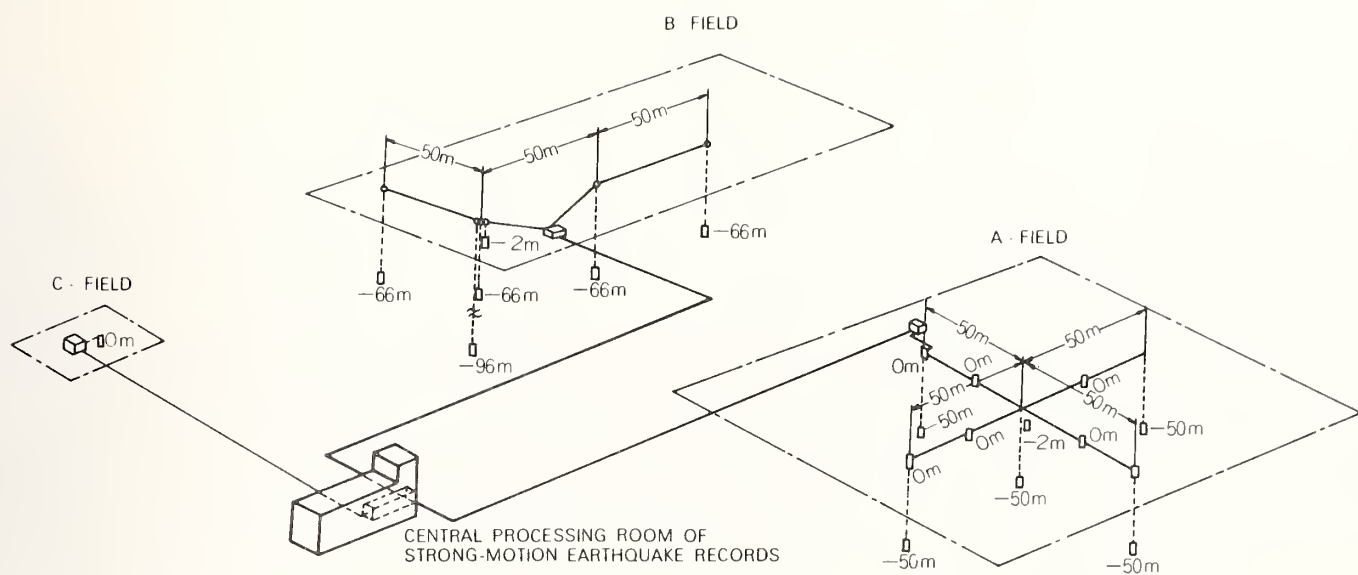
Fig. 7   Local Laboratory Arrays at PWRI

17

Table 1 Number of Accelerometer and Number of Channel
of Strong-Motion Arrays at PWRI

FIELD	DEPTH	POINTS	CHANNELS
A-FIELD	GROUND SURFACE	7	21
	-2m	1	3
	-50m	5	15
B-FIELD	-2m	1	3
	-66m	4	12
	-96m	1	3
C-FIELD	GROUND SURFACE	1	3
TOTAL		20	60

Table 2 Main Specification of Accelerometer used
by Local Laboratory Array at PWRI

Number of Component	3
Type	Velocity Feed Back
Natural Frequency	5 Hz
Frequency Range	0.1 - 50 Hz ; within 1 dB
Maximum Acceleration	$\pm$ 650 gals
Diameter, Length	ϕ 13 cm, 125 cm
Weight	50 kg

Fig. 8 A-Field of Local Laboratory Array
in PWRI at Tsukuba Science City

Fig. 9   Aerial View of Local Laboratory Arrays at PWRI
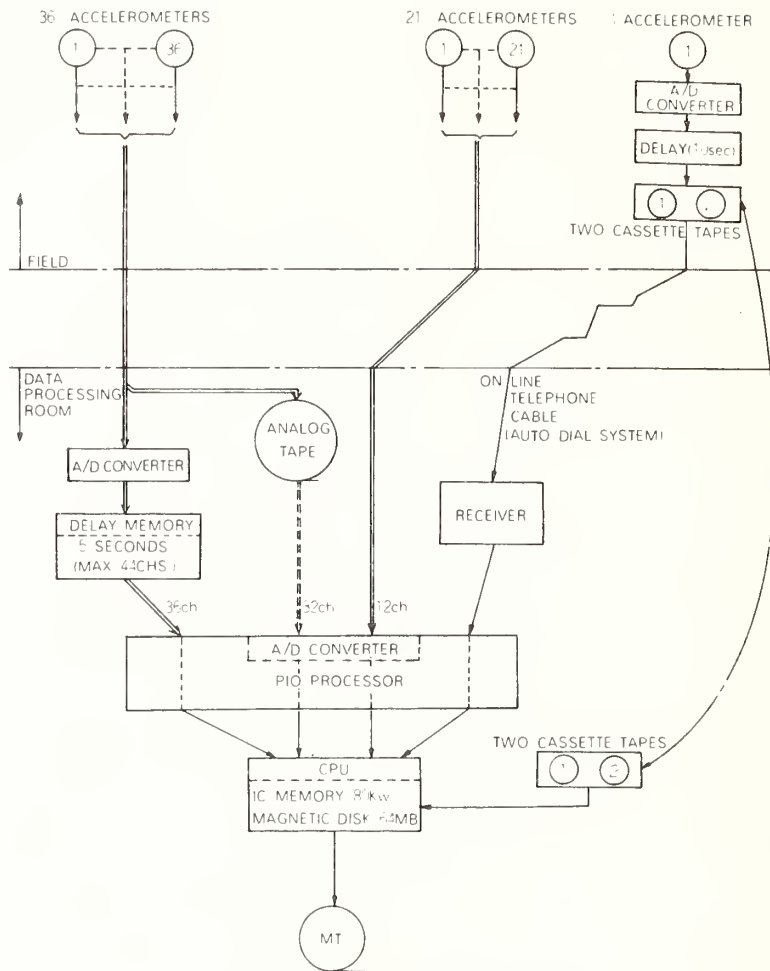
Fig. 10   Data Processing System
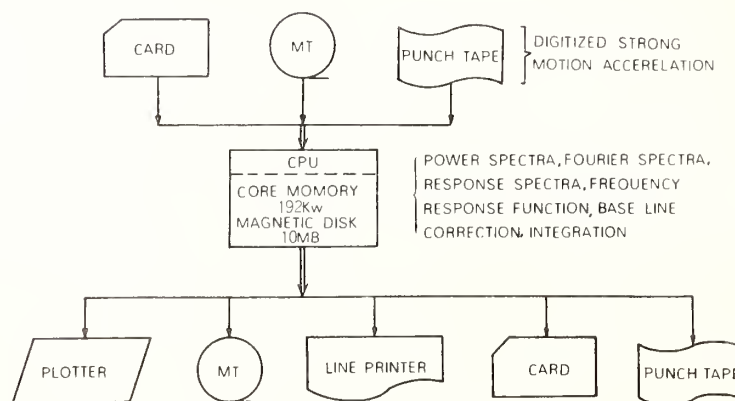
Fig. 11   Data Analyzing System

FUJI CITY

MT.ASHITAKA

UKISHIMA GRARA
(ASHITAKA AREA)

NUMAZU CITY

SIMPLE EXTENDED ARRAY

SURUGA BAY

LEGEND

GRAVAL

SAND

MUD

SAND, GRAVEL AND MUD

LOW TERRACE DEPOSIT

HIGHER TERRACE DEPOSIT

EARLY DILUVIAL DEPOSIT

VOLCANIC ASH(SHIRAHAMA GROUP etal)

VOLCANIC ASH(YUGASHIMA GROUP etal)

ANDESITE

VOLCANIC ASH AND LOAM

LAVA

LAVA

EFFUSIVE ROCK FROM OLD FUJI

BASALTIC EFFUSIVE ROCK

PUMICE FLOW

OLD LAVA OF SOMMA

BASALTIC LAVA

ANDESITE LAVA(DARUMA VOLCANO)

ANDESITE LAVA(IDA VOLCANO)

DECITE

Fig. 12 Surface Geological Map Around Ukishima-Grara,

Ashitaka Area, Shizuoka Prefecture
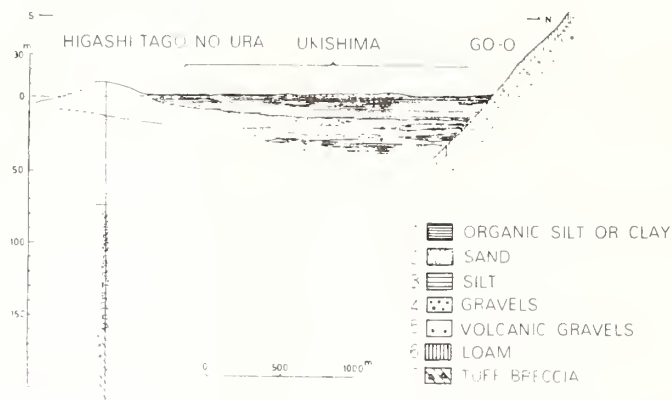
Fig. 13 Geological Condition Around Ukishima-garaha, Ashitaka Area
(After Geology in Shizuoka Prefecture edited by Tsuchi)
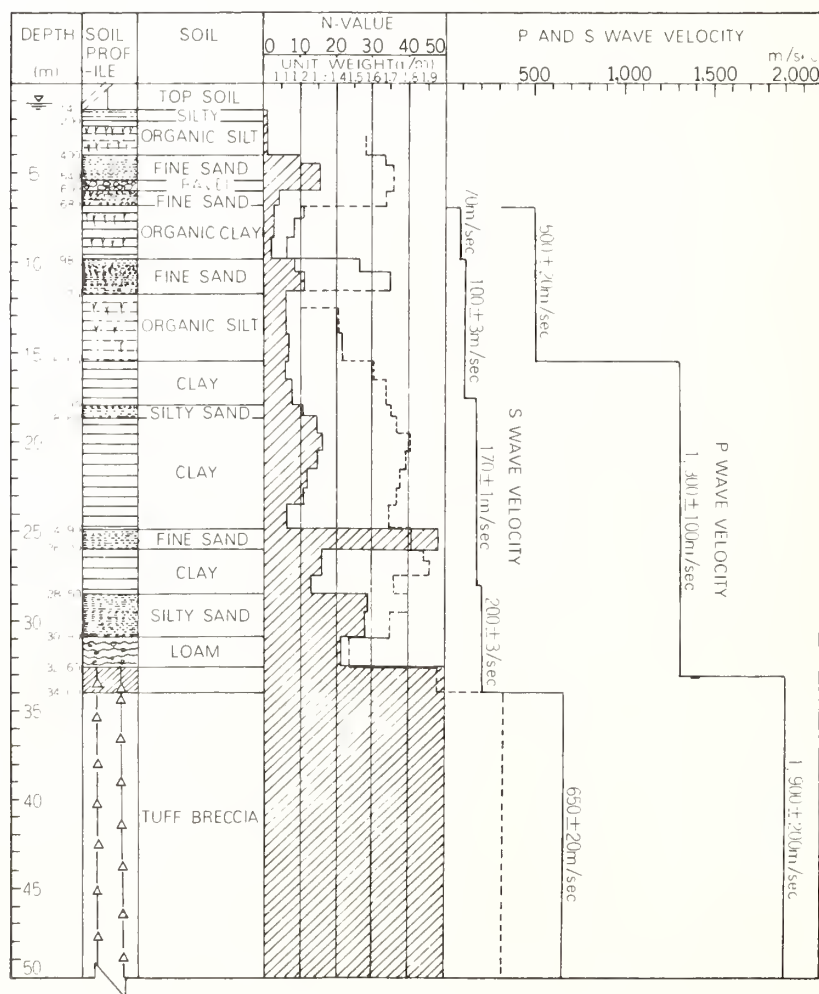
Fig. 14 Typical Soil Profile at Ukishima-gahara, Ashitaka Area
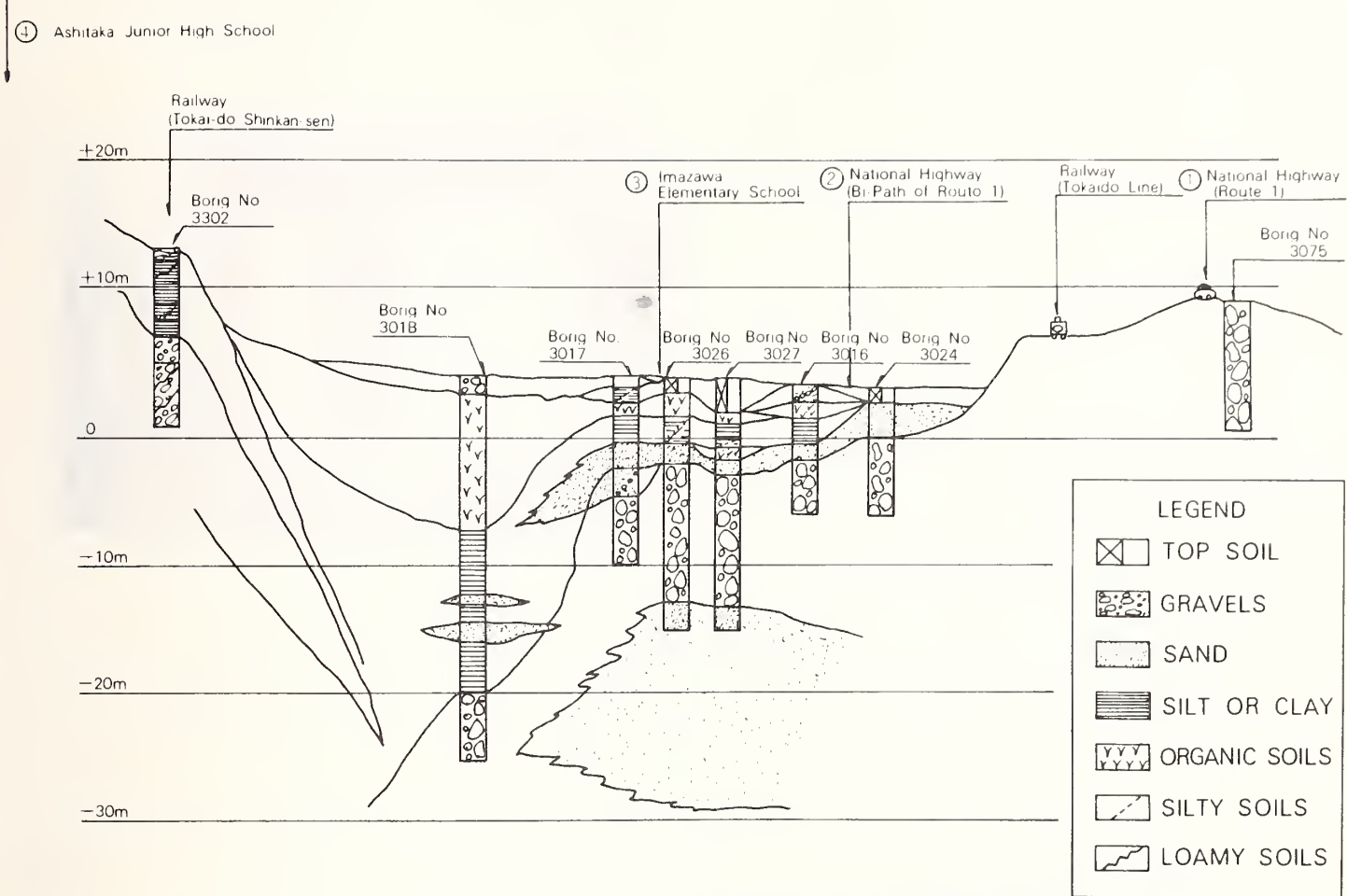
Fig. 15   Geological Condition for Simple Extended Array at Ukishima-gahara, Ashitaka Area

LEGEND

⊠ TOP SOIL
GRAVELS
SAND
SILT OR CLAY
ORGANIC SOILS
SILTY SOILS
LOAMY SOILS

Fig. 16   Aerial View of Simple Extended Array at Ukishima-gahara, Ashitaka Area

23
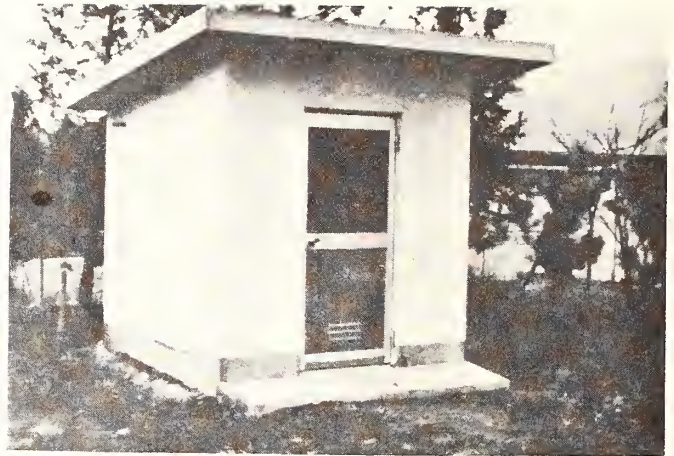
Fig. 17 On-Site Housing Storing Accelerograph
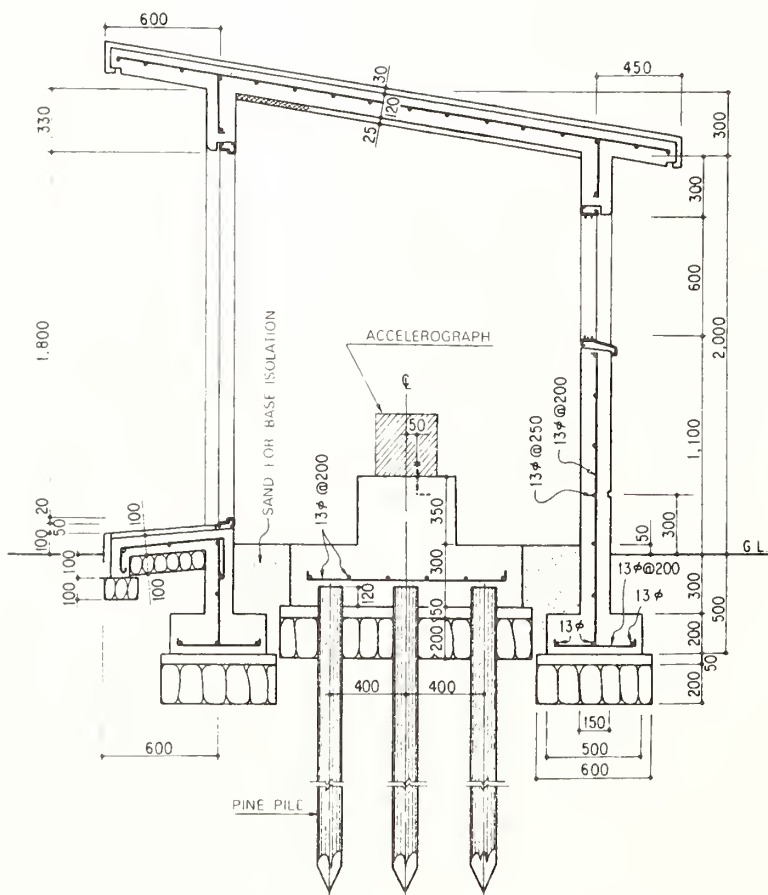
Fig. 18 On-Site Housing Storing Accelerograph

24
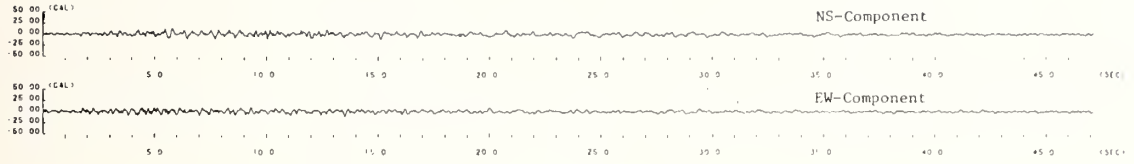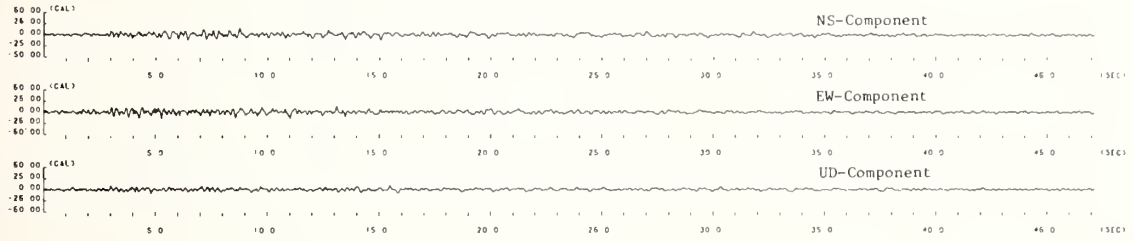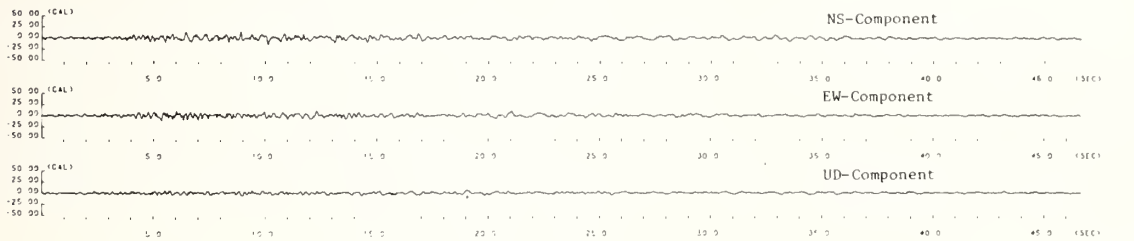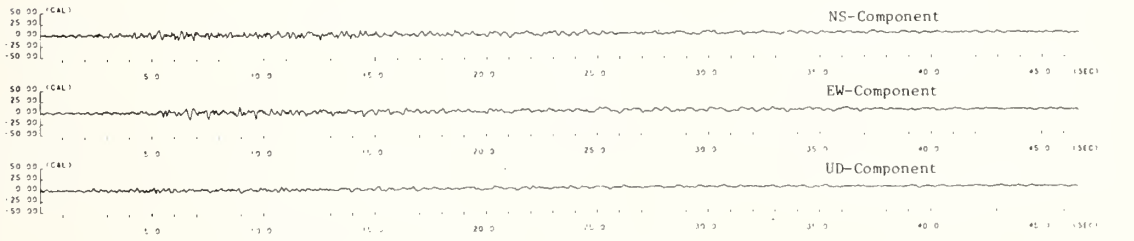
Fig. 19 Strong-Motion Accelerations Recorded at N50, S50, E50 and W50 of Local Laboratory Array of PWRI at Tsukuba Science City

Accelerometer	Type	Triaxial, Force Balance
	Full Scale Range	± 1G
	Natural Frequency	50 Hz
	Damping	70% critical
Trigger System	Sensitive Direction	Vertical
	Acceleration Set Point	0.01G
	Operation Cycle	Self-actuating for duration of earthquake, with automatic reset
Recording System	Type	Digital, phase encoded
	Number of Truck	4
	Mangetic Tape	Digital cassette tape; 2.5inch/sec.
	Frequency Response	DC – 50 Hz; –12 dB/oct
	Number of Bits	12 bits
	Dynamic Range	± 66 dB
	Sampling Rate	200 Samples/sec/channel
Power Requirements	Voltage	± 12 VDC
	Battery Charger	Float charger supplied
Time Code Generator	Accuracy of Crystal – Controlled Time	± 1 x 10^{-6}
	Auto Adjustment of Time of Crystal	Each 5 seconds by JJY Standard Time
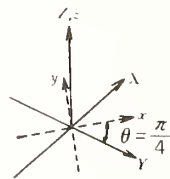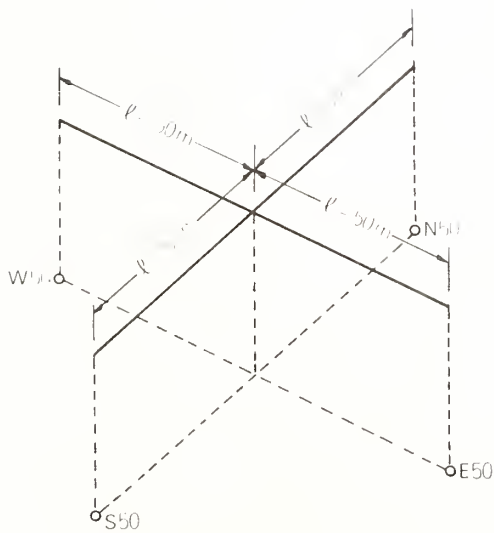
$$\begin{Bmatrix} u_x \\ u_y \\ u_z \end{Bmatrix} = \begin{bmatrix} \cos\theta & \sin\theta & 0 \\ -\sin\theta & \cos\theta & 0 \\ 0 & 0 & 1 \end{bmatrix} \begin{Bmatrix} u_x \\ u_y \\ u_z \end{Bmatrix}$$

AXIAL STRAIN BETWEEN E50 AND S50 : ε_{AX}

SHEAR STRAIN BETWEEN E50 AND S50 : ε_{SH}

$$\begin{Bmatrix} \varepsilon_{AX} \\ \varepsilon_{SH} \end{Bmatrix} = \frac{1}{\sqrt{2}\,\ell} \begin{bmatrix} 1 & 0 & -1 & 0 \\ 0 & 1 & 0 & -1 \end{bmatrix} \begin{Bmatrix} u_{x,E50} \\ u_{y,E50} \\ u_{x,S50} \\ u_{y,S50} \end{Bmatrix}$$

Fig. 20 Definition of Axial and Shear Strains Between
Two Points
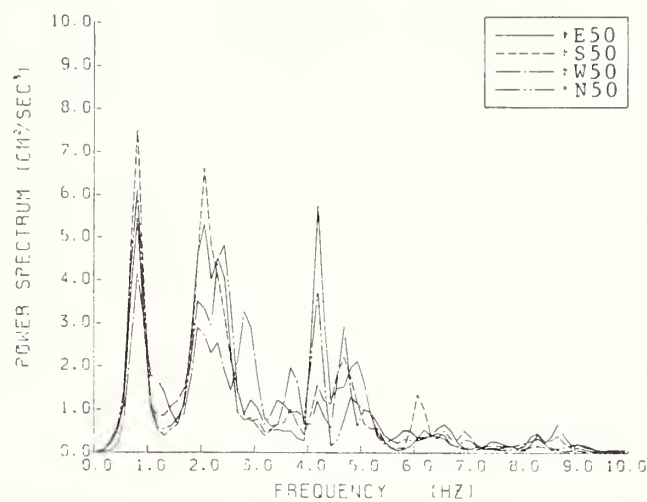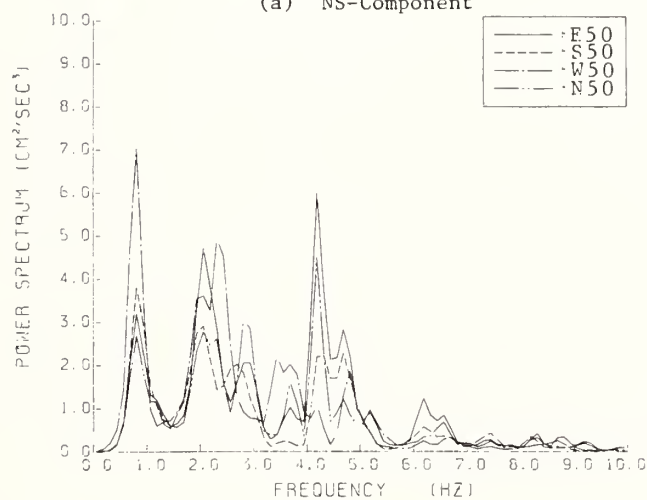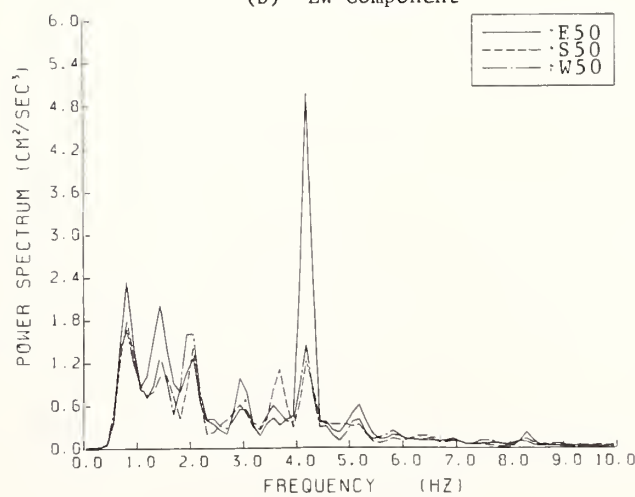
Fig. 21 Power Spectra of Acceleration Records Obtained at N50, S50, E50 and W50

27

NS-Component

EW-Component

(a) N50

NS-Component

EW-Component

UD-Component

(b) E50

NS-Component

EW-Component

UD-Component

(c) S50

NS-Component

EW-Component

UD-Component
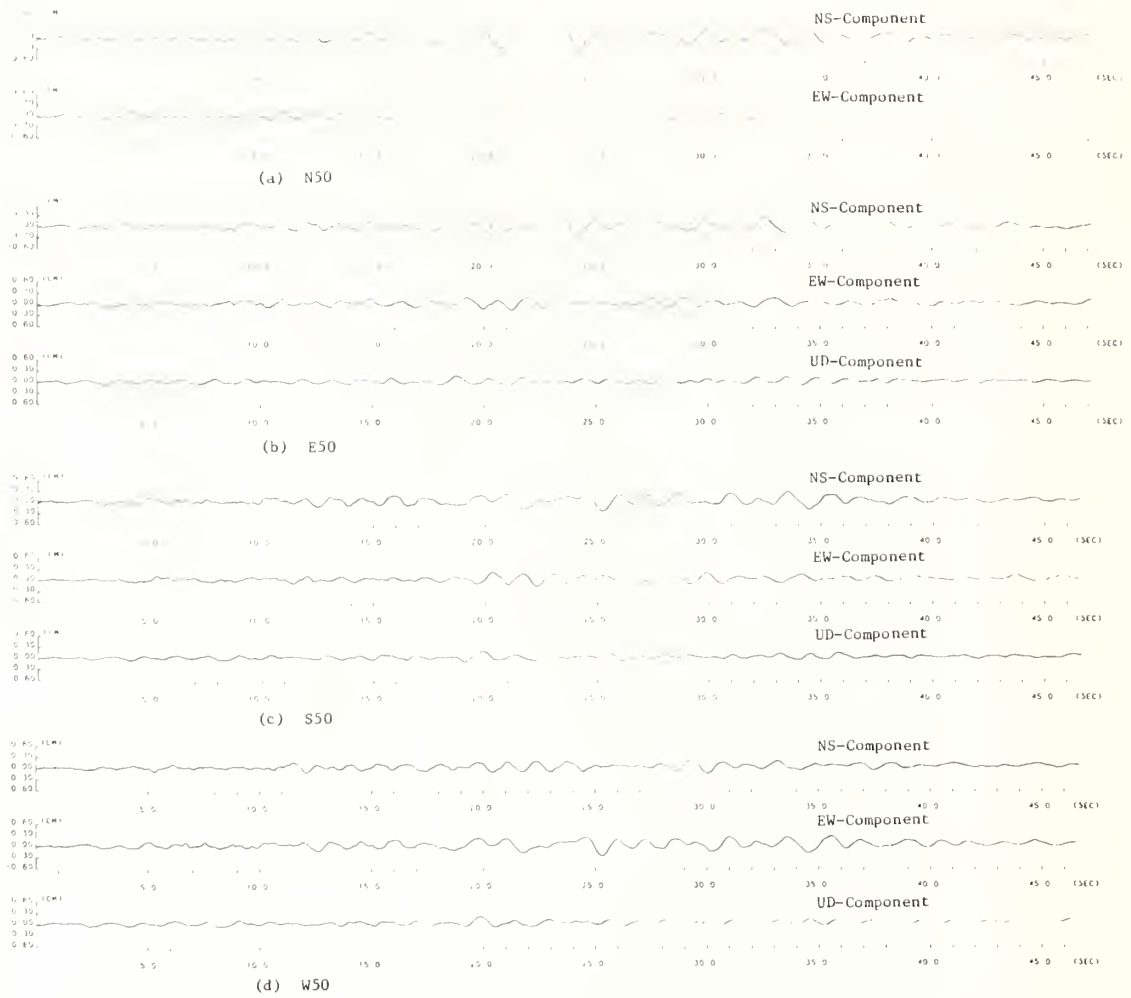
(d) W50

Fig. 22 Displacement Time History Calculated by Double Integration of Strong-Motion Acceleration Records at N50, E50, S50 and W50 of Local Laboratory Array of PWRI at Tsukuba Science City

(a) Axial Strain Between N50 and W50

(b) Shear Strain Between N50 and W50

(c) Axial Strain Between E50 and S50

(d) Shear Strain Between E50 and S50
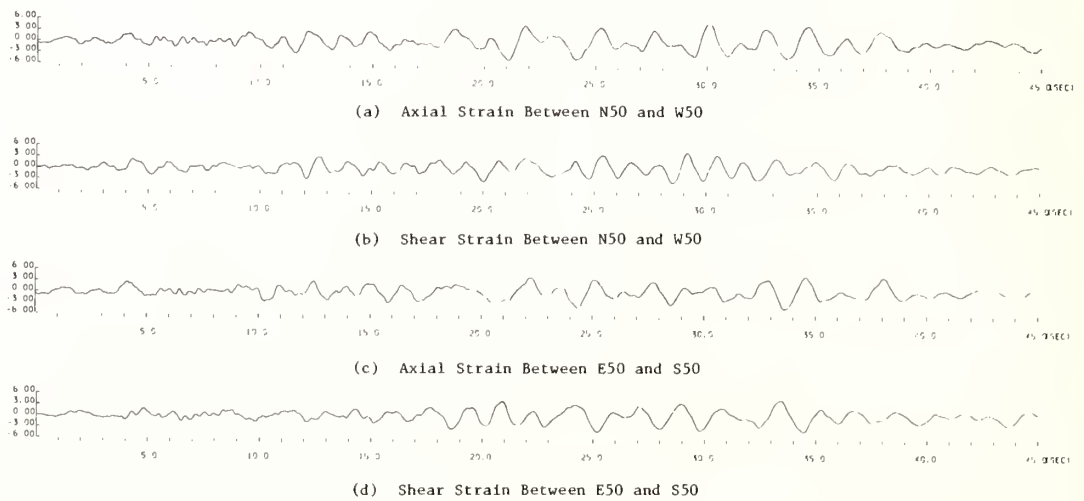
Fig. 23 Axial and Shear Strains Between Two Points

28

U.S. GEOLOGICAL SURVEY STRONG-MOTION RECORDS FROM THE IMPERIAL

VALLEY EARTHQUAKE, OCTOBER 15, 1979, PRELIMINARY SUMMARY

by
J. R. Filson

R. L. Porcella
R. B. Matthiesen (Deceased)

This report summarizes the data from near-in strong-motion accelerograph stations operated by the U.S. Geological Survey (USGS) in the Imperial Valley of California at the time of the October 15, 1979 Imperial Valley earthquake. The purpose of this report is to alert others as to the nature of the strong-motion data that is available from this event. In order to provide the information in a timely manner, the report has been limited to a summary of the data. A similar preliminary report of strong-motion data collected by the Office of Strong-Motion Studies of the California Division of Mines and Geology (CDMG) has already been issued.* A more complete report of all of the strong ground motion data is contemplated. This will require the cooperation of all of the agencies in both the U.S. and Mexico that operate strong-motion instruments in the region. A report on the processing of the data from near-in stations is in preparation.

The moderate-size (magnitude 6.4) October 15, 1979 Imperial Valley earthquake was instrumentally located on the Imperial fault approximately 25 km southeast of El Centro, California (figure 1). This location is approximately the same as that of the 1940 Imperial Valley earthquake. The following parameters are for the main shock (CIT/USGS):

Origin time: 23:16:52.4 15 OCT 79 (UTC)

Epicenter: 32.64 N, 115.33 W

Focal depth: 15 km

Magnitude: 6.4 (M_L)

The 1979 Imperial Valley earthquake triggered all of the accelerographs within about 100 km of the epicenter, and one as far away as 196 km. At this time (28 OCT 79) information is not available on all of the stations beyond 150 km. The locations of the ground motion instruments relative to the epicenter are shown in figure 1. A list of all of the

---

* Preliminary Data – Partial film records and file data – Imperial Valley Earthquake of 15 October 1979; CDMG; Sacramento, 1979.

accelerographs that are known to have been operational at the time of the earthquake and within a radius of about 150 km of the epicenter is given in table A. This list contains the station identification, an indication of the site geology, and the type and size of structure in which the instrument is housed. Most of the instruments are located in small instrument shelters or one-story buildings and are assumed to approximate a "free-field" condition. The instruments are self-contained film-recording accelerographs with a nominal upper limit on range of 1.0 g.

The data from USGS operated accelerographs are summarized in Table B and are presented in order of increasing distance of the stations from the 1940 fault trace. In addition to the distance from the fault and epicenter, the table summarizes the S-wave minus trigger times (when discernable), the peak accelerations, strong durations, and the trigger time as indicated by the WWVB time code on the record. Copies of all main-shock accelerograms from the USGS network are included in Appendix I of the complete report, but are not included in this summary version.

ACKNOWLEDGMENTS

Station Identification[1]			Epicentral[2] Distance (km)	S − t[3] Interval (sec)	WWVB[4] trigger time	Acceleration		Duration[6] > 0.1 g (sec)
No.	Name (Data Source)	Coord				Azimuth (note 5)	Maximum (g)	
5028	El Centro Sta 7 Imperial Valley Col (USGS)	32.83 W 115.50 W	26 [1]	4.6	**	230 up 140	0.52 0.65 0.36	4.9 5.5 3.7
942	El Centro Sta 6 Huston Rd (USGS)	32.84 N 115.49 W	27 [1]	5*	17:01	230 up 140	0.45 1.74 0.72	7.9 6.2 11.8
5054	Bonds Corner Hwys 98 & 115 (USGS)	32.69 N 115.34 W	6 [3]	2.4	16:57	230 up 140	0.81 0.47 0.66	13.2 12.0 13.3
958	El Centro Sta 8 95 E Cruickshank (USGS)	32.81 N 115.53 W	27 [4]	5*	17:00	230 up 140	0.50 0.55 0.64	6.9 5.8 6.9
952	El Centro Sta 5 2801 James Rd (USGS)	32.86 N 115.47 W	28 [4]	5.1	17:01	230 up 140	0.40 0.71 0.56	7.6 5.6 7.4
5165	E C Differential Array Dogwood Rd (USGS)	32.80 N 115.34 W	26 [5]	5	**	360 up 270	0.51 0.93 0.37	10.2 7.0 7.0
117	El Centro Sta 9 302 Commercial Av (USGS)	32.79 N 115.55 W	26 [6]	−	−	360 dwn 090	0.40 0.38 0.27	7.4 4.7 7.0
955	El Centro Sta 4 2905 Anderson Rd (USGS)	32.86 N 115.43 W	26 [7]	4.8*	17:01	230 up 140	0.38 0.32 0.61	6.5 6.7 6.8
5060	Brawley Airport Brawley (USGS)	32.99 N 115.51 W	42 [7]	6.3	17:03	315 up 225	0.22 0.18 0.17	2.2 5.2 1.8
5055	Holtville Post Office (USGS)	32.81 N 115.38 W	19 [8]	4.1	**	315 up 225	0.22 0.31 0.26	7.5 7.0 6.2
412	El Centro Sta 10 Community Hospital (USGS)	32.78 N 115.57 W	27 [9]	4.9	**	050 up 320	0.20 0.15 0.23	5.2 2.2 5.1
5053	Calexico Fire Station Fifth & Mary (USGS)	32.67 N 115.49 W	15 [11]	3.2	16:59	315 up 225	0.22 0.21 0.28	9.5 8.8 10.8
5058	El Centro Sta 11 McCabe School (USGS)	32.75 N 115.59 W	27 [13]	5.6	17:00	230 up 140	0.38 0.16 0.38	6.5 7.7 7.0

Table B - GROUND MOTION DATA (con't)

Station Identification[1]			Epicentral[2] Distance (km)	S – t[3] Interval (sec)	WWVB[4] trigger time	Acceleration		Duration[6] > 0.1 g (sec)
No.	Name (Data Source)	Coord				Azimuth (note 5)	Maximum (g)	
5057	El Centro Sta 3 Pine Union School (USGS)	32.89 N 115.38 W	28 [13]	5.4	**	230 up 140	0.22 0.15 0.27	6.2 5.6 6.0
5051	Parachute Test Site (USGS)	32.93 N 115.70 W	47 [15]	7.0	**	315 up 225	0.20 0.18 0.11	1.5 5.2 1.4
5115	El Centro Sta 2 Keystone Rd (USGS)	32.92 N 115.37 W	31 [16]	6	17:01	230 up 140	0.43 0.17 0.33	5.7 9.3 9.2
931	El Centro Sta 12 907 Brockman Rd (USGS)	32.72 N 115.64 W	30 [18]	5.2	17:01	230 up 140	0.11 0.08 0.15	4.9 – 3.8
5061	Calipatria Fire Sta (USGS)	33.13 N 115.52 W	57 [21]	7.4	17:06	315 up 225	0.09 0.07 0.13	– – 1 peak
5059	El Centro Sta 13 Strobel Residence (USGS)	32.71 N 115.68 W	34 [22]	5.1	17:02	230 up 140	0.15 0.06 0.12	5.0 – 2.4
5056	El Centro Sta 1 Borchard Ranches (USGS)	32.96 N 115.32 W	37 [22]	6	17:02	230 up 140	0.15 0.10 0.15	3.1 1 peak 4.8
286	Superstition Mtn USAF Camera site (USGS)	32.95 N 115.82 W	57 [26]	7.2*	17:05	135 up 045	0.21 0.09 0.12	1.1 – 0.6
5062	Salton Sea Wildlife Refuge USGS)	33.18 N 115.62 W	66 [28]	3.5*	17:11	315 up 225	0.10 0.06 0.13	1 peak – 1 peak
5052	Plaster City Storehouse (USGS)	32.79 N 115.86 W	52 [31]	5*	**	135 up 045	0.07 0.03 0.05	– – –
5066	Coachella Canal Sta 4 Siphon 15 (USGS)	33.36 N 115.59 W	84 [47]	8.5	17:11	135 up 045	0.14 0.04 0.11	0.5 – 0.3
5050	Ocotillo Wells Burro Bend Cafe (USGS)	33.14 N 116.13 W	93 [59]	7.5*	17:15	315 up 225	0.05 0.03 0.04	– – –
2316	Yuma Strand Ave (USBR/USGS)	32.73 N 114.70 W	60 [61]	*	17:11	090 up 360	0.03 0.02 0.03	– – –

No.	Station Identification[1] Name (Data Source)	Coord	Epicentral[2] Distance (km)	S - t[3] Interval (sec)	WWVB[4] trigger time	Acceleration Azimuth (note 5)	Maximum (g)	Duration[6] > 0.1 g (sec)
5065	Coachella Canal Sta 3 Siphon 24 (USGS)	33.51 N 115.77 W	105 [67]			***		
5049	Borrego Air Ranch Borrego Springs (USGS)	33.19 N 116.28 W	108 [74]	8.2	17:20	315 up 225	0.04 0.02 0.03	– – –
5064	Coachella Canal Sta 2 Demosser (USGS)	33.56 N 115.95 W	117 [79]			***		
5047	Rancho de Anza Anza Borrego Park (USGS)	33.35 N 116.40 W	127 [92]	*	17:27	135 up 045	0.03 0.02 0.02	– – –
5063	Coachella Canal Sta 1 (USGS)	33.64 N 116.08 W	131 [92]	*	17:24	135 up 045	0.02 0.02 0.03	– – –
5067	Indio So Calif Gas Co (USGS)	33.75 N 116.21 W	148 [109]			***		
5073	Cabazon Post Office (USGS)	33.92 N 116.78 W	196 [158]	*	17:55	270 up 180	0.01 0.02 0.02	– – –

[1] Ref: Western Hemisphere Strong Motion Accelerograph Station List - 1976; USGS, Open-File Report 77-374.

[2] Distance from epicenter at 32.64 N and 115.33 W. Bracketed number is distance to the nearest point on the 1940 Imperial Fault trace. Reference: Sharp, R., 1977; Open File Report 77-815; Misc Field Studies Map MF 838.

[3] S-wave minus trigger time.

    * S - t is questionable.

[4] Trigger time in minutes and seconds after 288 days (UTC) as determined from WWVB time time code. Millisecond accuracy is possible.

    ** WWVB time code not legible.

[5] Azimuthal direction of case acceleration for upward trace deflection on accelerogram (degrees clockwise from north).

    *** Accelerograph operational but did not trigger.

[6] Time span between the first and last peak greater than 0.10 g.

Figure 1. Strong-motion stations in the Imperial Valley, California.
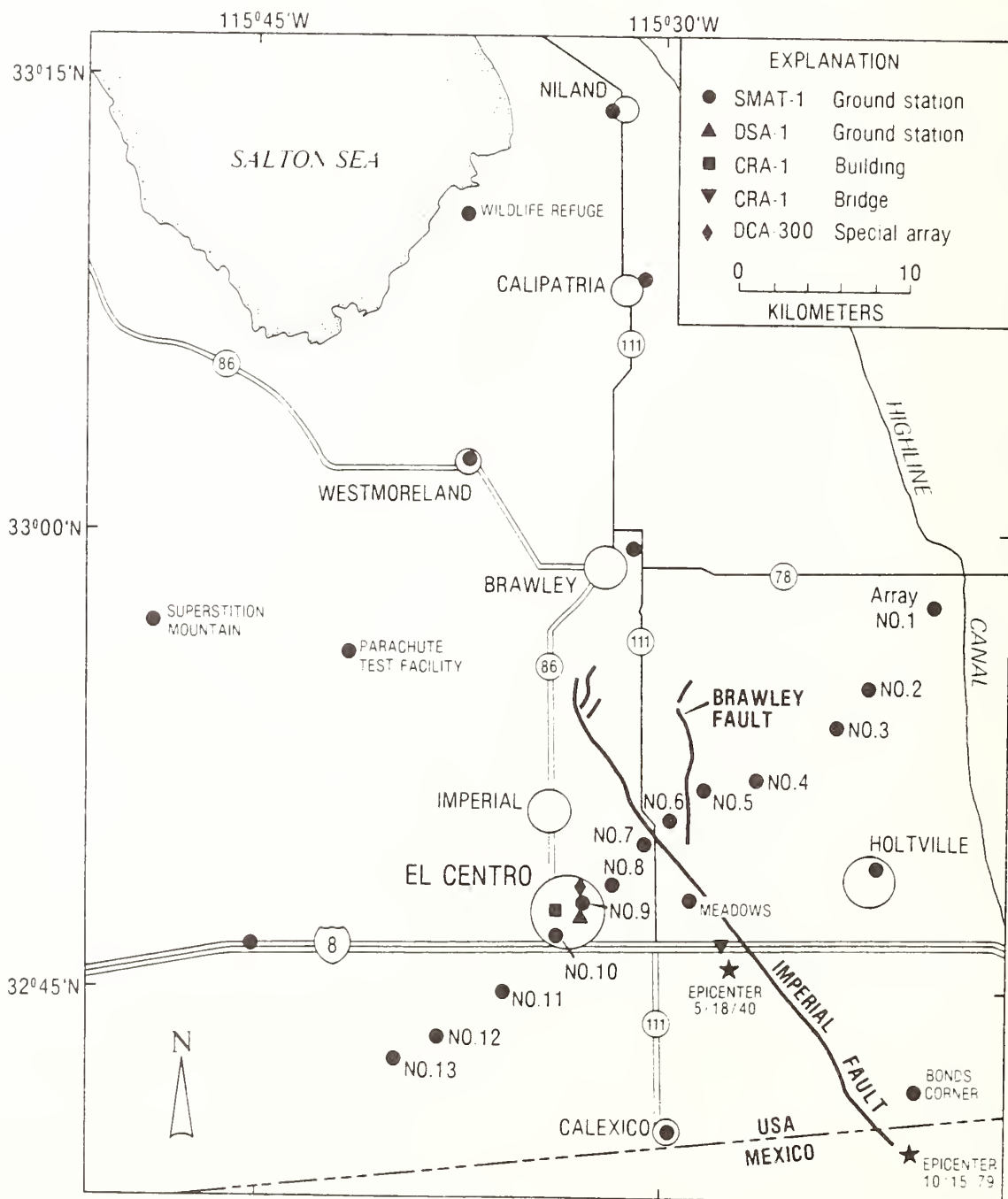
Station Identification[1]		Site geology	Structure type/size	Instrument location(s)
No	Name (Data Source) / Coord			
5054	Bonds Corner Hwys 98 & 115 — 32.69 N / 115.34 W		1-story bldg	Ground level
5049	Borrego Air Ranch Borrego Springs — 33.19 N / 116.28 W		1-story bldg	Ground level
5060	Brawley Airport Brawley — 32.99 N / 115.51 W		Inst shltr	Ground level
5073	Cabazon Post Office — 33.92 N / 116.78 W		1-story bldg	Ground level
5053	Calexico Fire Station Fifth & Mary — 32.67 N / 115.49 W		1-story bldg	Ground level
5061	Calipatria Fire Sta — 33.13 N / 115.52 W		2-story bldg	Ground level
5063	Coachella Canal Sta 1 — 33.64 N / 116.08 W		1-story bldg	Ground level
5064	Coachella Canal Sta 2 Demosser — 33.56 N / 115.95 W		1-story bldg	Ground level
5065	Coachella Canal Sta 3 Siphon 24 — 33.51 N / 115.77 W		1-story bldg	Ground level
5066	Coachella Canal Sta 4 Siphon 15 — 33.36 N / 115.59 W		1-story bldg	Ground level
5046	Collins Valley — 33.42 N / 116.47 W		Inst shltr	Ground level
5165	E C Differential Array Dogwood Rd — 32.80 N / 115.54 W		Inst shltr	Ground level, 6 instruments
464	El Centro Meadows Union School — 32.80 N / 115.47 W	Alluvium, more than 300m	1-story bldg	Ground level
5056	El Centro Sta 1 Borchard Ranches — 32.96 N / 115.32 W		Inst shltr	Ground level
5115	El Centro Sta 2 Keystone Rd — 32.92 N / 115.37 W		Inst shltr	Ground level
5057	El Centro Sta 3 Pine Union School — 32.89 N / 115.38 W		1-story bldg	Ground level
955	El Centro Sta 4 2905 Anderson Rd — 32.86 N / 115.43 W	Alluvium, more than 300m	Inst shltr	Ground level
952	El Centro Sta 5 2801 James Rd — 32.86 N / 115.47 W	Alluvium, more than 300m	Inst shltr	Ground level
942	El Centro Sta 6 Huston Rd — 32.84 N / 115.49 W	Alluvium, more than 300m	Inst shltr	Ground level
5028	El Centro Sta 7 Imperial Valley Col — 32.83 W / 115.50 W		1-story bldg	Ground level
958	El Centro Sta 8 95 E Cruickshank Rd — 32.81 N / 115.53 W	Alluvium, more than 300m	Inst shltr	Ground level
117*	El Centro Sta 9 302 Commercial Av — 32.79 N / 115.55 W	Alluvium, more than 300m	2-story bldg	Ground level

No	Station Identification[1] Name (Data Source)	Coord	Site geology	Structure type/size	Instrument location(s)
412	El Centro Sta 10 Community Hospital	32.78 N 115.57 W	Alluvium, more than 300m	1-story bldg	Ground level
5058	El Centro Sta 11 McCabe School	32.75 N 115.59 W		1-story bldg	Ground level
931	El Centro Sta 12 907 Brockman Rd	32.72 N 115.64 W		Inst shltr	Ground level
5059	El Centro Sta 13 Strobel Residence	32.71 N 115.68 W		1-story bldg	Ground level
817	Hines Pumping Plant	33.71 N 115.63 W		Gatehouse	Mid level
5055	Holtville Post Office	32.81 N 115.38 W		1-story bldg	Ground level
5067	Indio So Calif Gas Co	33.75 N 116.21 W		1-story bldg	Ground level
5050	Ocotillo Wells Burro Bend Cafe	33.14 N 116.13 W		1-story bldg	Ground level
5051	Parachute Test Site	32.93 N 115.70 W		1-story bldg	Ground level
5044	Pinon Flat Observatory	33.61 N 116.46 W		Inst shltr	Tunnel
5052	Plaster City Storehouse	32.79 N 115.86 W		1-story bldg	Ground level
5047	Rancho de Anza Anza Borrego Park	33.35 N 116.40 W		Inst shltr	Ground level
5062	Salton Sea Wildlife Refuge	33.18 N 115.62 W		1-story bldg	Ground level
286	Superstition Mtn USAF Camera site	32.95 N 115.82 W	Granite	1-story bldg	Ground level
5045	Terwilliger Valley Snodgrass Residence	33.48 N 116.59 W		Inst shltr	Ground level
2316	Yuma Strand Ave	32.73 N 114.70 W		Inst shltr	Ground level

[1] Ref: Western Hemisphere Accelerograph Station List; USGS, Open-File Rpt. 77-374.

* 1940 Strong-motion accelerogram recorded at this station. Ref: U.S. Eqks, 1940.

Table B - GROUND MOTION DATA

Station Identification[1]			Epicentral[2] Distance (km)	S - t[3] Interval (sec)	WWVB[4] trigger time	Acceleration		Duration[6] > 0.1 g (sec)
No.	Name (Data Source)	Coord				Azimuth (note 5)	Maximum (g)	
5028	El Centro Sta 7 Imperial Valley Col (USGS)	32.83 W 115.50 W	26 [1]	4.6	**	230 up 140	0.52 0.65 0.36	4.9 5.5 3.7
942	El Centro Sta 6 Huston Rd (USGS)	32.84 N 115.49 W	27 [1]	5*	17:01	230 up 140	0.45 1.74 0.72	7.9 6.2 11.8
5054	Bonds Corner Hwys 98 & 115 (USGS)	32.69 N 115.34 W	6 [3]	2.4	16:57	230 up 140	0.81 0.47 0.66	13.2 12.0 13.3
958	El Centro Sta 8 95 E Cruickshank (USGS)	32.81 N 115.53 W	27 [4]	5*	17:00	230 up 140	0.50 0.55 0.64	6.9 5.8 6.9
952	El Centro Sta 5 2801 James Rd (USGS)	32.86 N 115.47 W	28 [4]	5.1	17:01	230 up 140	0.40 0.71 0.56	7.6 5.6 7.4
5165	E C Differential Array Dogwood Rd (USGS)	32.80 N 115.34 W	26 [5]	5	**	360 up 270	0.51 0.93 0.37	10.2 7.0 7.0
117	El Centro Sta 9 302 Commercial Av (USGS)	32.79 N 115.55 W	26 [6]	–	–	360 dwn 090	0.40 0.38 0.27	7.4 4.7 7.0
955	El Centro Sta 4 2905 Anderson Rd (USGS)	32.86 N 115.43 W	26 [7]	4.8*	17:01	230 up 140	0.38 0.32 0.61	6.5 6.7 6.8
5060	Brawley Airport Brawley (USGS)	32.99 N 115.51 W	42 [7]	6.3	17:03	315 up 225	0.22 0.18 0.17	2.2 5.2 1.8
5055	Holtville Post Office (USGS)	32.81 N 115.38 W	19 [8]	4.1	**	315 up 225	0.22 0.31 0.26	7.5 7.0 6.2
412	El Centro Sta 10 Community Hospital (USGS)	32.78 N 115.57 W	27 [9]	4.9	**	050 up 320	0.20 0.15 0.23	5.2 2.2 5.1
5053	Calexico Fire Station Fifth & Mary (USGS)	32.67 N 115.49 W	15 [11]	3.2	16:59	315 up 225	0.22 0.21 0.28	9.5 8.8 10.8
5058	El Centro Sta 11 McCabe School (USGS)	32.75 N 115.59 W	27 [13]	5.6	17:00	230 up 140	0.38 0.16 0.38	6.5 7.7 7.0

Station Identification[1]			Epicentral[2] Distance (km)	S − t[3] Interval (sec)	WWVB[4] trigger time	Acceleration		Duration[6] > 0.1 g (sec)
No.	Name (Data Source)	Coord				Azimuth (note 5)	Maximum (g)	
5057	El Centro Sta 3 Pine Union School (USGS)	32.89 N 115.38 W	28 [13]	5.4	**	230 up 140	0.22 0.15 0.27	6.2 5.6 6.0
5051	Parachute Test Site (USGS)	32.93 N 115.70 W	47 [15]	7.0	**	315 up 225	0.20 0.18 0.11	1.5 5.2 1.4
5115	El Centro Sta 2 Keystone Rd (USGS)	32.92 N 115.37 W	31 [16]	6	17:01	230 up 140	0.43 0.17 0.33	5.7 9.3 9.2
931	El Centro Sta 12 907 Brockman Rd (USGS)	32.72 N 115.64 W	30 [18]	5.2	17:01	230 up 140	0.11 0.08 0.15	4.9 − 3.8
5061	Calipatria Fire Sta (USGS)	30.13 N 115.52 W	57 [21]	7.4	17:06	315 up 225	0.09 0.07 0.13	− − 1 peak
5059	El Centro Sta 13 Strobel Residence (USGS)	32.71 N 115.68 W	34 [22]	5.1	17:02	230 up 140	0.15 0.06 0.12	5.0 − 2.4
5056	El Centro Sta 1 Borchard Ranches (USGS)	32.96 N 115.32 W	37 [22]	6	17:02	230 up 140	0.15 0.10 0.15	3.1 1 peak 4.8
286	Superstition Mtn USAF Camera site (USGS)	32.95 N 115.82 W	57 [26]	7.2*	17:05	135 up 045	0.21 0.09 0.12	1.1 − 0.6
5062	Salton Sea Wildlife Refuge USGS)	33.18 N 115.62 W	66 [28]	3.5*	17:11	315 up 225	0.10 0.06 0.13	1 peak − 1 peak
5052	Plaster City Storehouse (USGS)	32.79 N 115.86 W	52 [31]	5*	**	135 up 045	0.07 0.03 0.05	− − −
5066	Coachella Canal Sta 4 Siphon 15 (USGS)	33.36 N 115.59 W	84 [47]	8.5	17:11	135 up 045	0.14 0.04 0.11	0.5 − 0.3
5050	Ocotillo Wells Burro Bend Cafe (USGS)	33.14 N 116.13 W	93 [59]	7.5*	17:15	315 up 225	0.05 0.03 0.04	− − −
2316	Yuma Strand Ave (USBR/USGS)	32.73 N 114.70 W	60 [61]	*	17:11	090 up 360	0.03 0.02 0.03	− − −

Station Identification[1]			Epicentral[2] Distance (km)	S - t[3] Interval (sec)	WWVB[4] trigger time	Acceleration		Duration[6] > 0.1 g (sec)
No.	Name (Data Source)	Coord				Azimuth (note 5)	Maximum (g)	
5065	Coachella Canal Sta 3 Siphon 24 (USGS)	33.51 N 115.77 W	105 [67]				***	
5049	Borrego Air Ranch Borrego Springs (USGS)	33.19 N 116.28 W	108 [74]	8.2	17:20	315 up 225	0.04 0.02 0.03	– – –
5064	Coachella Canal Sta 2 Demosser (USGS)	33.56 N 115.95 W	117 [79]				***	
5047	Rancho de Anza Anza Borrego Park (USGS)	33.35 N 116.40 W	127 [92]	*	17:27	135 up 045	0.03 0.02 0.02	– – –
5063	Coachella Canal Sta 1 (USGS)	33.64 N 116.08 W	131 [92]	*	17:24	135 up 045	0.02 0.02 0.03	– – –
5067	Indio So Calif Gas Co (USGS)	33.75 N 116.21 W	148 [109]				***	
5073	Cabazon Post Office (USGS)	33.92 N 116.78 W	196 [158]	*	17:55	270 up 180	0.01 0.02 0.02	– – –

[1] Ref: Western Hemisphere Strong Motion Accelerograph Station List - 1976; USGS, Open-File Report 77-374.

[2] Distance from epicenter at 32.64 N and 115.33 W. Bracketed number is distance to the nearest point on the 1940 Imperial Fault trace. Reference: Sharp, R., 1977; Open File Report 77-815; Misc Field Studies Map MF 838.

[3] S-wave minus trigger time.

   * S - t is questionable.

[4] Trigger time in minutes and seconds after 288 days (UTC) as determined from WWVB time time code. Millisecond accuracy is possible.

   ** WWVB time code not legible.

[5] Azimuthal direction of case acceleration for upward trace deflection on accelerogram (degrees clockwise from north).

   *** Accelerograph operational but did not trigger.

[6] Time span between the first and last peak greater than 0.10 g.

THREE-DIMENSIONAL SYNTHETIC ACCELEROGRAMS

FOR DESIGN EARTHQUAKE GROUND MOTIONS

by

Makoto Watabe

ABSTRACT

Three-dimensional earthquake ground motions are simulated by the use of the principal axes concept [1]. Two major procedures for mathematical modeling which simulate the three-dimensional earthquake ground motions are introduced.

The first is a completely synthetic approach, simulated by the product of a stationary random process and a deterministic intensity function in each component independent of one another. The relation between maximum response and the factors of simulated ground motions are theoretically established, and the relation is utilized for the simulation of earthquake ground motions having a pre-established response spectra.

In the second procedure, it is found that the phase angles of recorded accelerograms play an important role in determining the envelope of time history, by generating a "phase wave." The role of phase angles on the covariances of three-dimensional earthquake ground motions is also examined. Based upon the results, a set of phase angles of the three components of ground motion from a real earthquake are applied to simulate three-dimensional earthquake ground motions along principal axes, appropriate to the pre-established response spectra in each component.

INTRODUCTION

Up to the present (1980), in most cases of dynamic analyses of structural systems subjected to strong earthquake ground motions, one component of earthquake motions alone has been considered. The consideration of simultaneous response effects due to three translational components of earthquake ground motions, however, should not be neglected in the seismic design of structures, such as nuclear power plants, in which a detailed and precise seismic analysis is required.

If a very large number of recorded ground motion accelerograms were available, representative stochastic models could be established directly by statistical analyses based on these data. Unfortunately, recorded strong motion accelerograms are quite limited. Therefore, one is forced to hypothesize a model for generating simulated three-dimensional earthquake ground motions. For one such model, three-dimensional earthquake ground motions along "principal axes" have been proposed by Penzien and Watabe [1]. In these principal axes, the corresponding variances of motions have maximum, minimum, and intermediate values with zero co-variances. Utilizing this concept, three-dimensional earthquake ground motions can be simulated along three-orthogonal axes.

A general form of one-dimensional simulated ground motion can be expressed as a function of time t, such as:

$$a(t) = \zeta(t) b(t) \tag{1}$$

where $a(t)$, $\zeta(t)$ and $b(t)$ represent the simulated nonstationary ground motion, the deterministic intensity function, and the stationary random motion, respectively. Three-dimensional simulated ground motions along principal axes may be represented through the relation:

$$ax(t) = \zeta x(t)bx(t), \quad ay(t) = \zeta y(t)by(t) \quad . \quad az(t) = \zeta z(t) bz(t) \tag{2}$$

where $ax(t)$, $ay(t)$ and $az(t)$ are three components of ground motions simulated along three orthogonal coordinates and $bx(t)$, $by(t)$ and $bz(t)$ are stationary random motions stochastically uncorrelated with each other.

In this paper, spectral characteristics of simulated ground motions are represented by a pre-established response spectra. Therefore, the relation between the maximum response

values and the factors of the input process should be first established. A simple approach to estimate the maximum response subjected to nonstationary random excitation is proposed as a product of the square root of the mean square of response values and a magnification coefficient, with the constant "R" expressing the nonstationarity of the input process.

In a stochastic modeling of earthquake ground motions, such as Eq. (1), phase angles are generally considered as random values with a uniform probability distribution. However, it was found that phase spectra are important factors as well as amplitude spectra in the time domain of each sample [9]. Based on this, the effects of phase angles on the nonstationarity of time history and the covariances of three-dimensional earthquake ground motions are examined. It is one of the purposes of this paper to utilize the phase spectra of real accelerograms to simulate three-dimensional earthquake ground motions on the basis of these basic studies.

<div align="center">

SIMULATION OF THREE-DIMENSIONAL EARTHQUAKE GROUND
MOTIONS USING A COMPLETELY SYNTHETIC PROCEDURE

</div>

Relation between maximum response values and input process

The estimation procedure of the maximum of stationary random vibrations of the Gaussian process and its response has been studied by several investigators [2,3,4]. To predict the maximum response subjected to a non-stationary random ground motion with an arbitrary deterministic intensity function, a simple approach is here proposed. It is defined by the relation:

$$E\ [|J(t)|\ max]\ =\ M\ \sqrt{E\ [\overline{J^2(t)}]} \tag{3}$$

where E denotes ensemble average, $J(t)$ are response values in terms of t, and $\overline{J^2(t)}$ and M are the mean square of $J(t)$ and the magnification coefficient of $E\ [|J(t)|\ max]$ to $\sqrt{E\ [\overline{J^2(t)}]}$.

The equation of motion of a single-degree of freedom system excited by earthquake ground motions $a(t)$ can be expressed:

$$\ddot{x}(t) + 2\xi\lambda\dot{x}(t) + \lambda^2 x(t)\ =\ -a(t) \tag{4}$$

where x(t) is a relative displacement in the system having a critical damping ratio (ξ) and an undamped natural circular frequency (λ). The solution of Eq. (4) is obtained by using the Duhamel integral (with zero initial conditions):

$$J(t) = \int_{o}^{t} - h_j(t - \tau) \, a \, (\tau) \, d\tau \tag{5}$$

in which J(t) implies a relative displacement, a relative velocity or an absolute acceleration of responses, $h_j(t)$ is a unit impulse response function and τ is a dummy variable.

If a(t) is a nonstationary random process given by the product of a deterministic intensity function $\zeta(t)$ varying slowly in terms of t and a stationary random process b(t) having zero mean value, such as expressed by Eq. (1), the ensemble average of the mean square of J(t) in the duration time Td is approximated in the form [5]:

$$E \, [\overline{J^2(t)}] \doteq \overline{\zeta^2(t)} \, E \, [\overline{J_s^2 \, (t)}] \tag{6}$$

where $\overline{\zeta^2(t)}$ is the mean square of the deterministic intensity function $\zeta(t)$ and $J_s^2(t)$ is the mean square of responses $J_s(t)$ subjected only to the stationary ground motion b(t).

The stationary random process b(t) is assumed to be represented by the following relation:

$$b(t) = \sum_{j=1}^{N} A_j \cdot \cos(\omega_j t + \phi_j) \tag{7}$$

where N is the number of harmonic waves superposed, A_j is an amplitude at frequency ω_j and ϕ_j is the random phase angle with a uniform distribution of probability in the range between 0 and 2π. Therefore, through the integration of square values of $J_s(t)$ over the entire duration E $[\overline{J^2(t)}]$ can be obtained as follows:

$$E \, [\overline{J^2(t)}]_s = \sum_{j=1}^{N} \frac{1}{2} A_j^2 \cdot |H_J(i \cdot \omega_j)|^2 \cdot \gamma \tag{8}$$

in which $H_J(i \cdot \omega j)$ is the complex frequency response function of $J(t)$. λ in Eq. (8) represents the effects of transient state of response, that is 1 for $\omega j \neq \lambda$ and for $\omega j = \lambda$ is obtained as follows, by neglecting all the terms of the second order of ξ and the terms of the first order of ξ less effective than the other terms.

$$\lambda(\omega_j = \lambda) = 1 - [1 - \exp(-\xi\lambda Td)] \cdot [3 - \exp(-\xi\lambda Td)] / 2\xi\lambda Td \qquad (9)$$

Next, considering past research and the results of numerical experiments such as shown in Figure 1, the magnification coefficient M can be assumed by the following equation:

$$\log M = f_1 + f_2 / f_3 [(\log N_{eq})^{f_3} - 1] \qquad (10)$$

where Neq indicates the equivalent number of waves crossing the zero baseline to either positive or negative direction over the entire duration. It can be estimated by taking the spectral moment of response $J_s(t)$:

$$N_{eq} = Td/2\,\pi\,\sqrt{E\,[\overline{J_s^2(t)}] / E\,[\overline{\dot{J}_s^2(t)}]} \qquad (11)$$

where the dot represents differentiation with respect to time t. The coefficients f_1, f_2 and f_3 in Eq. (10) can be found to be the function of a damping ratio ξ and a nonstationarity of $a(t)$, which is represented by the ratio of total power of $a(t)$ to the one of the stationary wave expressed as $|\zeta(t)|$ max x $b(t)$ as ensemble average. This nonstationarity constant R is expressed as follows:

$$R = \int T_d\, E\,[a^2(t)]\, dt / Td \cdot |\zeta(t)|^2\, max \cdot E[b^2(t)]$$
$$= \overline{\zeta^2(t)}/|\zeta(t)|^2_{max} \qquad (12)$$

Through the rearrangement of the results of numerical experiments such as shown in Figure 2, and the trial and error procedure, the coefficients f_1, f_2, and f_3 become:

$$\left.\begin{array}{l} f_1 = 0.2 + 0.055\ \log R + 0.022R^{-0.86}\ \xi^{0.076}\ R^{-1.3} \\[6pt] f_2 = 0.12\ R^{-0.96}\ [1 - \exp(-100\xi)] \\[6pt] f_3 = R^{11\xi}[0.28 + 0.84\ \exp(-13\xi)] \end{array}\right\} \qquad (13)$$

The resulting magnification coefficients are also presented in the solid lines of Figures 1 and 2.

The relation between maximum response and amplitude Aj in Eq. (7) can be established, by substituting Eqs. (6) and (10) into Eq. (3). From the results verified by the computer simulation, it has been found that the maximum response subjected to a nonstationary ground motion can be predicted on the basis of this procedure within a 5 percent error range [5].

An example of simulation

An example of three dimensional earthquake ground motions simulated along principal axes is here introduced, in which these three components have preestablished response spectra in each component. In this procedure the amplitude spectra of stationary random motion b(t) represented by Eq. (7) are estimated as shown in the Figure 3 block chart, applying the method described above.

For this example, the parameters proposed in [7] are applied, where the velocity response spectra Sv (in cm/sec) in the horizontal component are:

$$\log S_v(m, x, T, \xi) = 0.607 m - 1.19 \log x - 1.15 + g_1(m, T) -$$
$$g_2(x, T) + g_3(\xi, T) \tag{14}$$

where m, x, T and ξ indicate magnitude of earthquake, hypocentral distance (in km), period (in sec.) and critical damping ratio, respectively. The function $g_1(m, T)$, $g_2(x, T)$ and $g_3(\xi, T)$ in Eq. (14) are defined as follows:

$$g_1(m, T) = a_1 \times [1 - (T/a_2)^{a_3}] \times [1 + T \exp(1 - a_4 T)]$$

where, $a_1 = 0.015/(m/8)^{14} + 0.055$, $a_2 = 0.045 \times 1.6^m$

$$a_3 = 1.8 \times (m/8)^{13} / [(m/8)^{13} + 0.15], \quad a_4 = 0.1/(m/8)^{15} + 0.9$$

$$g_2(x, t) = 0.25 \times x^{0.1} \times (1/\sqrt{T} - 1)$$

and, $g_3(\xi, T) = \frac{1}{2} \log [[\log_e 2.72(4\pi\eta\xi/1.78 + 1)] \times [1 - \exp(-4\pi\eta\xi)] / 4\pi\eta\xi]$ } (15)

where, $\eta = T_o/T$, $\log T_o = 0.31 m - 1.2$

The velocity response spectra defined by Eqs. (14) and (15) are derived from the results obtained through statistical analysis using 74 accelerograms recorded on rock sites in Japan [6]. The dotted lines in Reference-Figure 1 are some examples of velocity response spectra with the constant hypocentral distance 50 km for the various values of magnitude, obtained by Eqs. (14) and (15). Similar examples are shown in Reference-Figure

2 with the constant magnitude 8 for the various values of hypocentral distance. The solid lines in Reference-Figures 1 and 2 indicate the velocity response spectra obtained using the results of statistical analysis mentioned above.

The contents of this example are assumed as follows:

(i)　The magnitude of earthquake is 8 and its epicentral distance is 20 km.

(ii)　Based upon the discussions in [1] and [6], it is assumed that the major and inter-mediate principal axes are horizontal and the minor principal axis compose the vertical components of ground motions.

(iii)　The velocity response spectra with 5 percent damping by Eq. (14) are converted to pre-established response spectra in the major and intermediate principal axes by multiply-ing by 1.14 and 0.86, respectively. The above values of 1.14 and 0.86 are derived from the assumption that the energy content of earthquake ground motions can be represented by the variance of acceleration [8], the square root value of the variance can be identical to the spectral intensity, and the fact that from the results of analysis in [6] of three dimensional earthquake ground motion observations, the average ratio of the variance in the intermediate component to the one in the major component is about 0.55.

(iv)　As for the minor component, the mean ratios of the response spectra in [7] to convert horizontal components into verticals are utilized.

(v)　The shapes of deterministic intensity functions are assumed to be the ones proposed in each horizontal and vertical components in [7]. Assuming that the total time of these proposed deterministic intensity functions is 70 sec, time histories of duration 35 sec duration are generated.

Across the ensemble, only one sample is presented here. The time histories of simulated accelerograms and their velocity response spectra compared to the pre-established response spectra are shown in Figures 5 and 6, respectively. The maxima of each component and the direction of principal axes of generated three components over the entire duration are presented in Table 1. The directions are represented by the declination ψ from the pre-assumed minor axis (z) and the direction θ from the pre-assumed major axis (x) on the x - y plane as shown in Figure 4. From these results, it will be seen that the calculated response spectra agree well with the pre-established ones and the direction of each component is close to the principal axis.

SIMULATION OF THREE-DIMENSIONAL EARTHQUAKE GROUND MOTIONS
INCLUDING PHASE ANGLES OF REAL ACCELEROGRAMS

Characteristics of phase angles

Most of the recent research in the field of earthquake ground motion simulation suggests the randomness and the uniform probability distribution of phase angles in earthquake ground motions. It is also a fact, however, that the phase angle spectra of real accelerograms play an important role in determining the nonstationarity of the time history. From the results of analysis on the roles of phase angles in earthquake ground motions, it has been found that phase angles are strongly correlated to deterministic intensity functions and the shapes of response spectra [9,10]. Therefore, it may be wise to utilize positively the properties of phase angles to control envelopes of simulated accelerograms rather than to apply the synthetic random phase angles with a uniform probability distribution which may contribute little to the envelope of accelerograms. Using a set of phase angles from a real earthquake accelerogram, independent of amplitude characteristics, may be the proper procedure to realize the above idea.

Figure 7 shows the original accelerogram of Taft 1952, EW component, and a simulated one which has uniform amplitudes in each frequency component with the same set of phase angles of the original accelerograms. Let this kind of accelerogram be called as "phase wave." The phase wave is then generated in the following manner: A digitized accelerogram $a_r(t)$ due to real earthquake can be expanded into a Fourier series as follows:

$$a_r(t) = \sum_{J=0}^{N} A_j \cdot \cos(\omega_j t + \phi_j^r) \tag{16}$$

Phase wave $a_p(t)$ in Figure 7 is generated using the relation:

$$a_p(t) = P \sum_{j=1}^{N'} \cos(\omega_j t + \phi_j^r) \tag{17}$$

where P is the scaling factor of intensity, and the high frequency components in $a_r(t)$ are excluded in $a_p(t)$. It is clearly shown in Figure 7 that the envelope of the phase wave is quite similar to the original one. Therefore, this result suggests that one can simulate

the wave with arbitrary spectral amplitudes, having a similar envelope to the original one, provided that the distribution of spectral amplitudes is rather uniformly and widely scattered.

It has been pointed out by the study of Ohsaki, et al., [9] that the characteristic of nonstationarity of an earthquake ground motion can be expressed by the distribution of phase differences $\Delta\phi$, that is given by

$$\Delta\phi_j = \phi_{j+1} - \phi_j \tag{18}$$

where $\Delta\phi_j$ is defined in the range $-2\pi \leq \Delta\phi \leq 0$, and ϕ_j is the phase angle at frequency ω_j. Figures 8 and 9 show the relative frequency of phase angles and phase differences of Taft 1952-EW component in the 30 sec time duration, where high frequency components are excluded. It is seen from these figures that the distribution of phase angles is nearly uniform, while the probability distribution of phase differences has some characteristics similar to that of Gaussian. As pointed out in [9], the distribution of phase differences normalized by -2π has a quite similar feature to the envelope of time history normalized by the duration. These results suggest that it is possible to generate the nonstationary earthquake ground motions without applying deterministic intensity functions by using these characteristics of the distribution of phase differences.

For the simulation of components along principal axes, these phase angles of real accelerograms can be also applied. Provided that two components $a_k(t)$ and $a_\ell(t)$ are the components of three dimensional accelerograms along principal axes, the covariance between these components can be expressed as follows:

$$\overline{a_k(t) \cdot a_\ell(t)} = \frac{1}{2} \sum_{j=0}^{N} A_{kj} \cdot A_{\ell j} \cdot \cos(\phi_{kj} - \phi_{\ell j}) = 0, \quad k \neq \ell \tag{19}$$

The resulting equation suggests that the covariances of three dimensional accelerograms phase angles play important roles as well. Considering the fact that, in most cases, effective frequency domain in both real accelerograms and simulated ones is similar and the resultant variances defined by three-dimensional components produce a rather smooth function in terms of transforming vectors, it can be assumed that the simulated components using the phase angles of real accelerograms transformed into the

48

principal axes are already closely oriented to principal axes. The term "original" in Table 2 means the directions of principal axes of the three dimensional accelerograms Taft-1952, and El Centro-1940 from the recorded three orthogonal axes, in which the x-axis in Figure 4 corresponds to the axis of the NS component. The term "phase" in Table 2 mean the directions of principal axes of simulated three dimensional phase waves with the phase angles of real accelerograms transformed into principal axes, from simulated three orthogonal axes. In these phase waves, it is assumed that the variances of intermediate and minor components to the major component variance are 0.55 and 0.18, respectively [6]. It will be recognized in Table 2 that the directions in phase waves are very close to those of principal axes. This fact may support advantages of this procedure to generate the simulated threedimensional ground motions along principal axes.

An example of simulation

Based on the discussion above, it is possible as an example to generate simulated three-dimensional earthquake ground motions with pre-established response spectra through an iterative procedure. This example has the phase angles of Taft-1952 accelerograms transformed into the principal axes. The earthquake parameters for the pre-established response spectra are the same as those mentioned in the previous example. The results are shown in Figures 10 and 11. The resultant direction of principal axis and the maxima of simulated ground motions are presented in Table 3. It can be seen from these results that the simulated ground motion fit the pre-established response spectra very well and the direction each component is close to the principal axis. In addition, the wave forms of the simulated time histories are similar to the original ones.

CONCLUSIONS

Two major procedures for the simulation of three-dimensional earthquake ground motions which utilize the concept of the principal axes of earthquake ground motions have been introduced. One is a completely synthetic way as represented by Eq. (2), and in the other the phase angles of real accelerograms which are transformed into principal axes are utilized.

49

The relation between the maximum response and the input process factors in the former method has been established because of the importance of response spectra in engineering. This relation also can be used to predict the maximum response of a multi-storied structure and their floor responses as ensemble average [5].

The effects of phase angles on the envelope of time history and the covariances of three dimensional earthquake ground motions in the second procedure have been examined. It has been found that one can generate simulated three-dimensional earthquake ground motions along principal axes with wave forms similar to real accelerograms, using the actual sets of phase angles. On the basis of these examinations, it is concluded that for practical purposes in the seismic design of structures, the effect from vertical earthquake ground motions can not be neglected and the simulated three-dimensional earthquake ground motions calculated by the second procedure are recommended for use.

Note: A similar paper was submitted to 7th World Conference on Earthquake Engineering held in Turkey in 1980.

REFERENCES

[1] Penzien, J. and Watabe, M., 1975, "Simulation of Three-Dimensional Earthquake Ground Motions," Int. J. Earthq. Engng. Struct. Dyn., Vol. 3, pp. 365-373.

[2] Davenport, A. G., 1964, "Note on the Distribution of the Largest Value of a Random Function with Application to Gust Loading," Proc. Inst. Civ. Engng., Vol. 28, pp. 187-196.

[3] Vanmarcke, E. H., 1976, "Structural Response to Earthquakes," in Seismic Risk and Engineering Decisions, ed. C. Lomnitz and E. Rosenblueth, pp. 287-337.

[4] Iyengar, R. N. and Iyengar, S. R., 1970, "Probabilistic Response Analysis to Earthquake," ASCE, EM 3, Vol. 96, pp. 207-225.

[5] Watabe, M. and Tohdo, M., 1980, "Research on the Simulation of Three-Dimensional Earthquake Ground Motions, PART-II," Proc. 5-JEES, Tokyo, pp. 113-120.

[6] Watabe, M. and Tohdo, M., 1979, "Analyses on Various Parameters for the Simulation of Three-Dimensional Earthquake Ground Motions," Proc. 5-SMIRT, K1, Berlin, pp. 1-11.

[7] Ohsaki, Y., Watabe, M. and Tohdo, M., 1980, "Analyses on Seismic Ground Motion Parameters including Vertical Components," submitted to 7-WCEE.

[8] Arias, A., 1970, "A Measure of Earthquake Intensity," in Seismic Design for Nuclear Power Plants, ed. R. Hanson, MIT Press, pp. 438-483.

[9] Ohsaki, Y., Iwasaki, R., Ohsawa, I. and Masao, T., 1978, "A Study on Phase Characteristics of Earthquake Motions and their Application," Proc, 5-JEES, Tokyo, pp. 201-208.

[10] Kubo, T. and Suzuki, N., 1978, "An Application of Synthetic Earthquake Ground Motions to Response Analysis," Proc. 5-JEES, Tokyo, pp. 89-96.
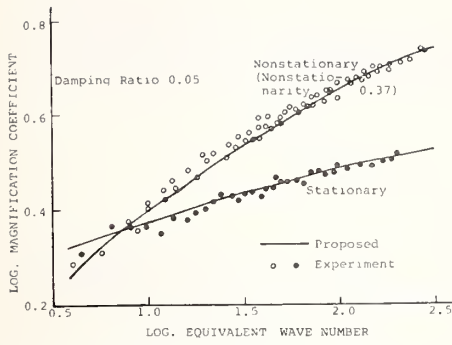
Fig.1 Relation between Magnification Coefficient and Equivalent Wave Number of Response
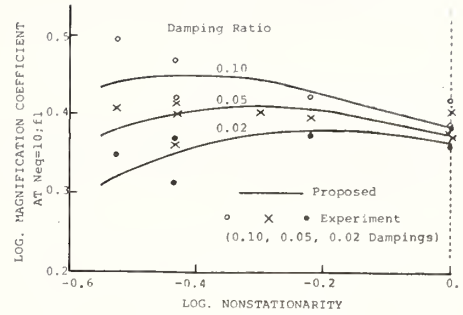
Fig.2 Relation between Magnification Coefficient and Nonstationarity of Input with the Parameter of Dampings, at Neq=10
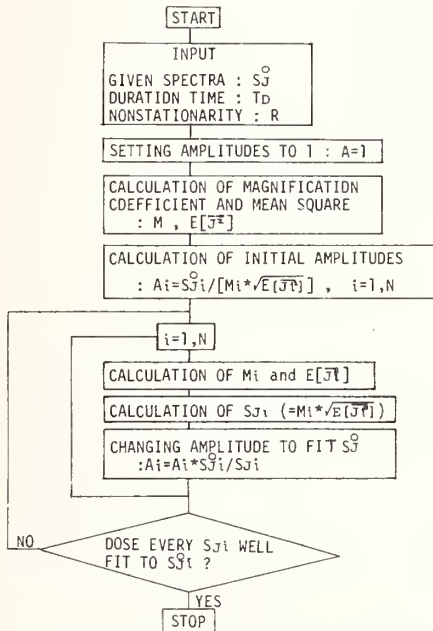
Fig.3 Block Chart for Estimation of Amplitude Spectra of Input
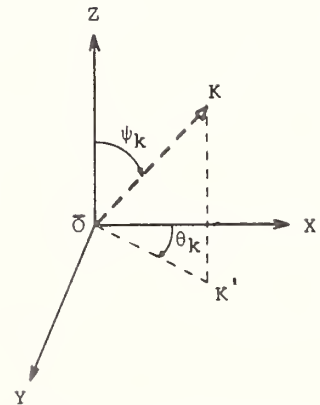
Fig.4 Principal Axis in Three Orthogonal Coordinate System
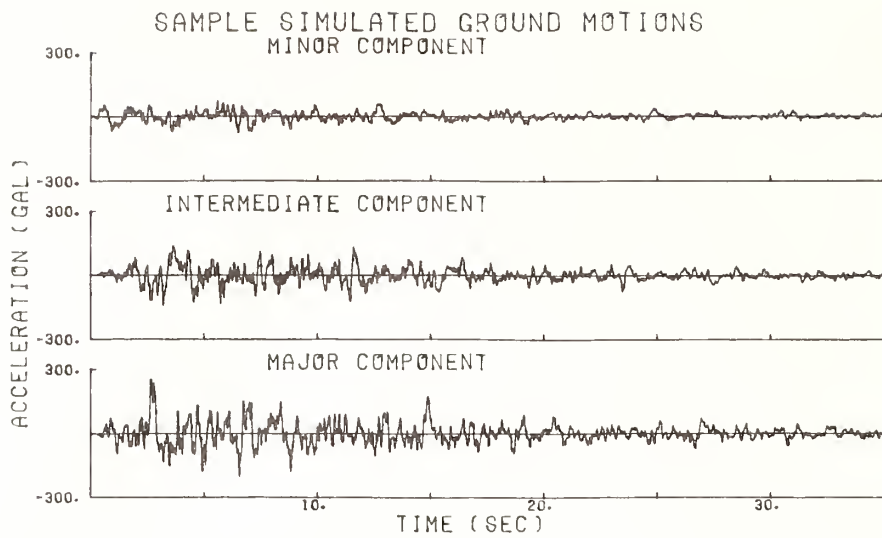
Fig.5 Time Histories of Sample Simulated Accelerograms

Table 1 Maxima and Directions
of A Sample Simulated Ground
Motion

Component		Major	Inter.	Minor
Estimated Maxima	A	230.	172.	96.
	V	38.5	28.9	18.6
Simulated Maxima	A	253.	144.	82.
	V	52.6	33.6	16.0
Direction	ψ	88.	90.	2.
	θ	- 8.	81.	24.

A ; Acceleration(gal)
V ; Velocity(kine)
ψ ,θ ; degree
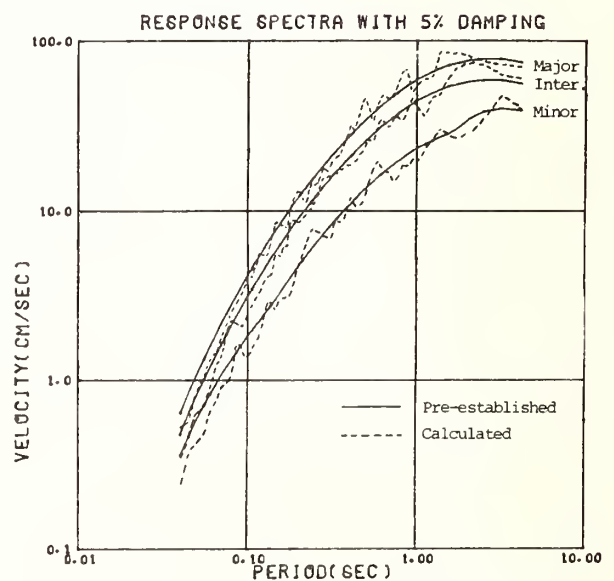
Fig.6 Pre-established Response Spectra
and Calculated Ones by Sample Simulated
Accelerograms
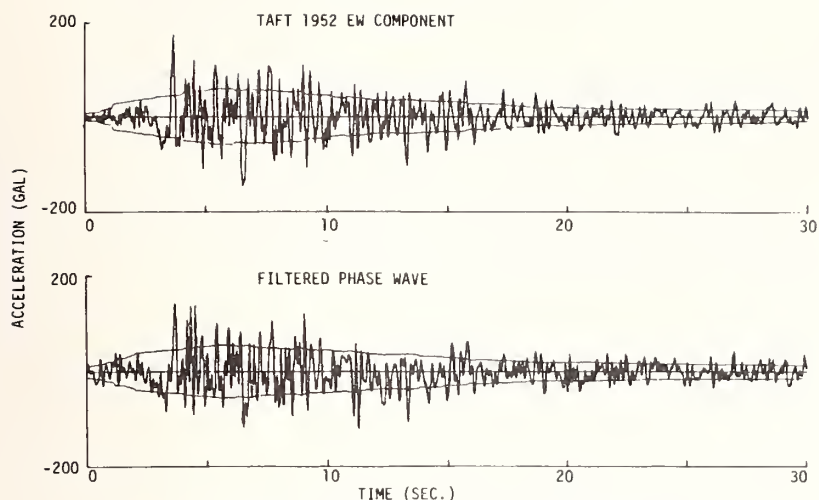
Fig.7 Original Wave (upper) and Phase
Wave (lower) of Taft 1952, EW Component
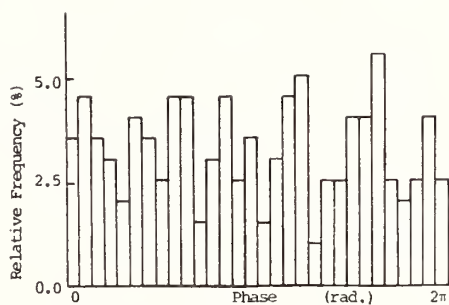
Fig.8 Relative Frequency of Phase
of Taft 1952, EW Component
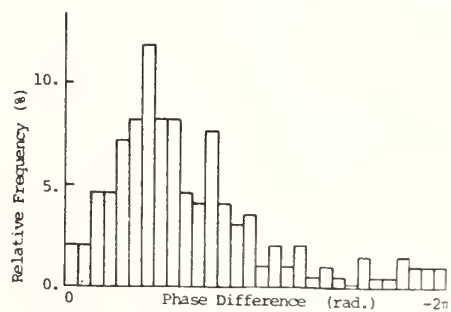
Fig.9 Relative Frequency of Phase
Difference of Taft 1952, EW Com-
ponent

Table 2 Directions of Principal
Axes of Original Waves and
Phase Waves

Record	Component	Original		Phase	
		ψ	θ	ψ	θ
Taft -1952	Major	73.	57.	88.	- 3.
	Inter.	86.	-32.	88.	87.
	Minor	18.	71.	3.	45.
El Centro -1940	Major	87.	-25.	88.	9.
	Inter.	89.	65.	89.	-81.
	Minor	4.	-43.	2.	- 2.

(degree)

53

FITTED SIMULATED GROUND MOTIONS
MINOR COMPONENT
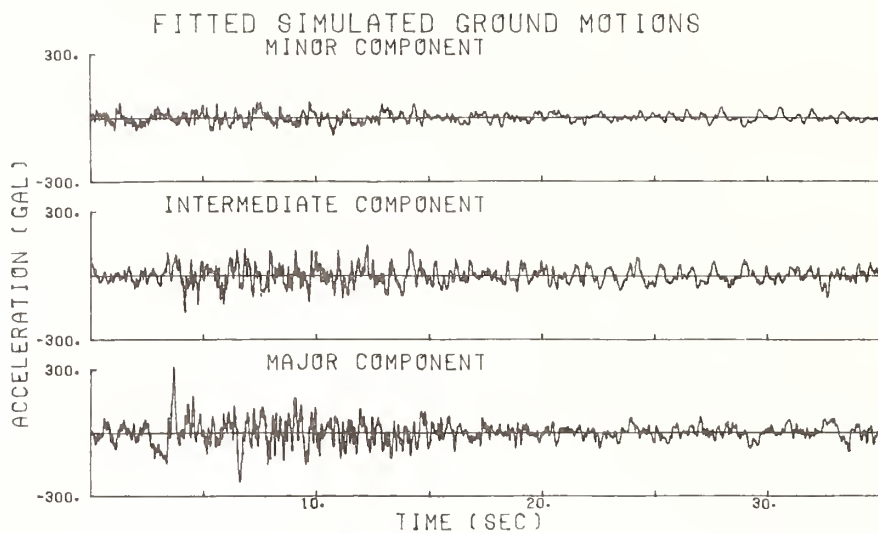
Fig.10 Time Histories of Simulated Accelerograms
by Use of Phase Angles of Taft 1952
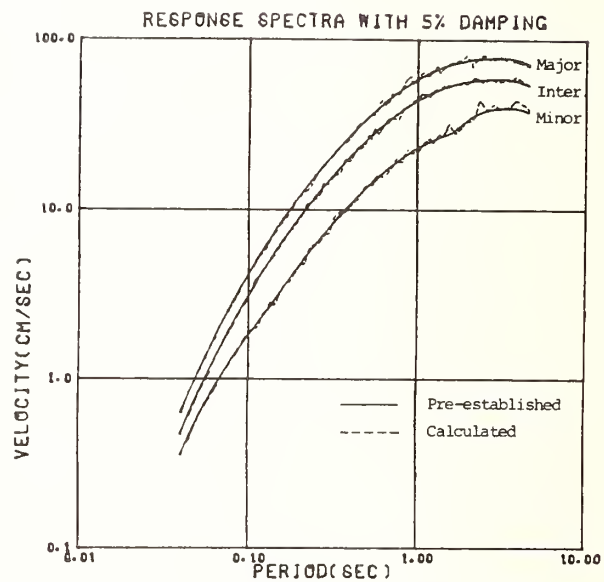
Fig.11 Pre-established Response Spectra
and Calculated Ones by Simulated Accele-
rograms through Iterative Procedure

Table 3 Maxima and Directions
of Simulated Ground Motions
by Use of Taft-1952

Component		Major	Inter.	Minor
Maxima	A	313.	172.	82.
	V	65.0	30.2	19.3
Direc-tion	ψ	86.	85.	6.
	θ	3.	-87.	55.

A ; Acceleration(gal)
V ; Velocity(kine)
ψ ,θ ; degree

54
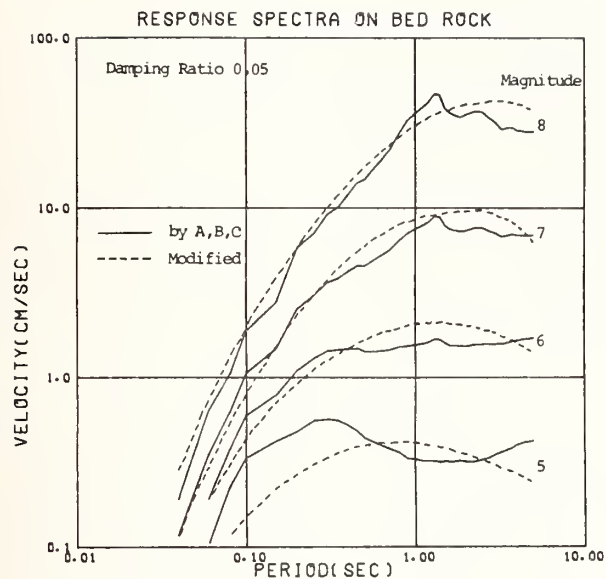
Reference-Figure 1 Velocity Response Spectra
on Rock Site at Hypocentral Distance 50km
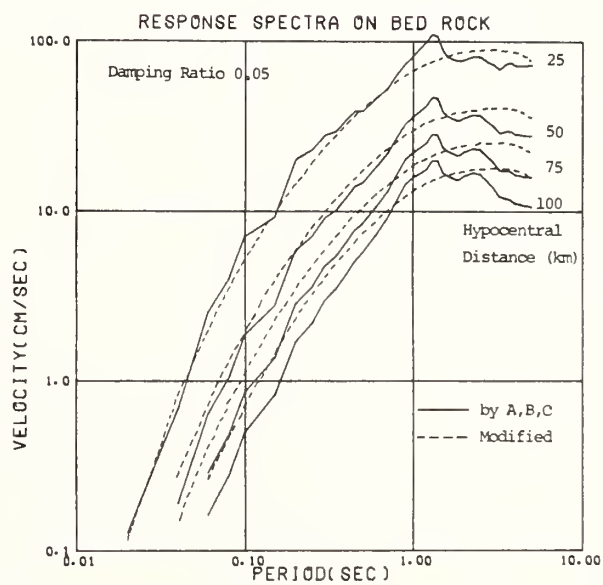
Reference-Figure 2 Velocity Response Spectra
on Rock Site at Magnitude 8

STUDY OF SHORT AND LONG PERIOD DYNAMIC GROUND

CHARACTERISTICS IN THE SENDAI DISTRICT

by

Yoshikazu Kitagawa

Makoto Watabe

ABSTRACT

The dynamic characteristics of soil-layers in a wide range of periods are investigated using the Sendai district, damaged by the 1978 Off-Miyagi Prefecture Earthquake, as an example. The deep-ground characteristics of long periods are estimated from the seismic data published by J.M.A. To estimate short period earthquake motions on the ground surface, strong motions observed in a building are analyzed considering building-subsoil interaction to produce the incident wave at the structural base rock. The seismic microzoning maps are compared to the actual building damage, and a close correlation between the two is recognized.

INTRODUCTION

One of the most important problems in the field of earthquake engineering is to predict the maximum earthquake motions in a certain place which may be defined by the seismic activity and ground characteristics. In order to clarify this more reliably, it is necessary to investigate separately each of them. Generally the ground motion in the frequency domain (G(jw)) will be expressed by the following equation,

$$G(jw) = [FS(jw) \cdot TF(jw)] \cdot ST(jw) , \tag{1}$$

where FS(jw), TF(jw) and ST(jw) represent the spectrum of the focal mechanism, the overall transmission function for the generation and propagation of earthquake waves, and the function for the wave propagation of local soil layers, respectively. The first parentheses of the equation represents the theoretical seismic records based on the focal mechanism, and the latter for the ground motion dealt with in the earthquake engineering.

The long period (10 ≥ T > 1.0 sec) which corresponds to the ground characteristics of a fairly large area is amplified by the soil layers of depth varying from a few hundred meters to 1~2 kilometers and, the short period (T ≤ 1.0 sec) corresponds to ground characteristics just beneath a construction which is affected by soil layers with a depth of less than a few hundred meters. The former represents seismic macrozoning and the latter microzoning. Using these two categories, a seismic base rock with a shear wave velocity of 2~3 km/sec, and a structural base rock with a shear wave velocity of 700 m/sec are established.

The estimates of ground characteristics in the short period range are based on the results of the analytical investigation of the damped, elastic system which is independent of frequency and microtremor measurements. The various seismic microzoning maps thus obtained are compared to the distribution of real damage to buildings.

OUTLINE OF GEOLOGICAL CONDITION

Topographical Aspects

The geological conditions of surface soil in the Sendai district are generally classified into the three areas shown in Figure 1: (1) the hilly tertiary terrain, (2) the terrace area, and (3) the alluvial plain. The oblique NE-SW line passing near the center

of the map is called the Rifu-Nagamachi tectonic line. The area west of the tectonic line is characterized by the hilly tertiary terrain and several levels of terraces. The surface deposit on this terrace is loam underlain by hard clay, gravels, pelite and shale. The hilly terrain is very hard andesite and shale, but the surface is covered with loam in several places. The aluvial plain develops east of this line and is mostly sand, silt, and gravel.

The depth of the tertiary base rock varies erratically near the tectonic line. Several areas in the plain are covered by very soft peat or mud. The soil profile and the results of seismic refraction tests by the well shooting method at representative places in the terrace and alluvial areas are shown in Figure 2.

Microtremor Measurements

The microtremors were measured at several sites shown in Figure 1 by an electromagnetic seismometer, natural period of 1.0 sec, to get the dynamic properties of soil layers [1]. The area where the measurements were performed belong to two types of geological conditions (2) and (3) mentioned above. The representative Fourier spectra of microtremors in NS and EW directions are shown in Figure 3, where sites G-06 through G-08 and sites G-17 and G-18 are on the outcrop of terrace and on the alluvial plain, respectively. Long period peaks of more than 1.0 sec reflect the deep ground characteristics, whereas short period peaks of less than 1.0 sec reflect the shallow ground ones.

Quake Degree for Deep Ground Structure

The values of the maximum displacements of NS and EW components (A_{NS} and A_{EW}, micron) observed at various stations of the Japanese Meteorological Agency are substituted in the Tsuboi's formula to get the magnitude (M) of the earthquake as the average. Under the assumption that 10^β is always regarded as the standard amplitude in the range of the long period reflecting the deep ground characteristics of a fairly large area, the following value is calculated at the J.M.A. station in the Sendai district:

$$F = \frac{1}{m} \sum_{i=1}^{m} (\sqrt{A_{NS}^2(T_i) + A_{EW}^2(T_i)} \quad / 10^\beta , \tag{2}$$

where $\beta = M - 1.73 \log\Delta + 0.83$. Δ, T_i and m denote the epicentral distance (km), the period of the phases giving the maximum displacement amplitude and the total number of the earthquake data, respectively [2]. Consequently, the value of F means the averaged amplitude at the Sendai station normalized by the standard one. Figures 4 and 5 show the F value calculated by Eq. (2) and the number of data, respectively. It is found that the degree of the quake relative to the standard one is high at the 3.0 and 5.0 sec periods, and that the data number is great at the 1.0 and 2.0 sec periods.

Setting Up of Structural Base Rock

The transfer function, which is defined by the ratio of the wave on the ground surface (Uo) to the incident wave (Uin), for the deep underground structure and for the shallow one at a representative place in the terrace near the Sendai station of J.M.A., is shown in Figure 6. The shear wave velocities V and densities ρ of the various soil-layers were determined by the seismic refraction test, the seismic data of strong motion seismographs of J.M.A., and the boring tests. As seen in Figure 6, there are some peaks which vary with the levels of the base rock but the predominant frequency between 3.0 and 4.0 Hz is common to both. This frequency also appears in the results obtained by microtremor measurements at the sites G-06 through G-08.

Consequently in this study, the structural base rock with shear wave velocity of 700 m/sec is set up to get the ground characteristics in the short period range of less than 1.0 sec. The values of shear wave velocity at intervals of 0.5' in both latitude and longitude in the Sendai district are estimated from the soil profile, results of the penetration tests, and the geological conditions. Figure 7 displays, as an example, the profile of shear wave velocity at section A-A' (line of N38°15'30") indicated in Figure 1.

SEISMIC MICROZONING

Incident Wave Motions in the Structural Base Rock

In order to estimate the earthquake motions on the ground surface, the strong motions observed at the Sendai Sumitomo Building [3] during the Off-Miyagi Prefecture Earthquake of June, 1979 (M = 7.4) were analyzed with consideration of building-subsoil interaction to get the incident wave at the structural base rock with shear wave velocity of 700 m/sec. This is an eighteen-story, steel-framed, reinforced-concrete structure with two-story

Fig.1 Geological Condition

Fig.2 Profile of Subsoil

Fig.3 Fourier Spectra
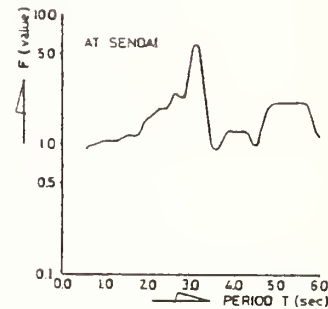
Fig.4 F-Value
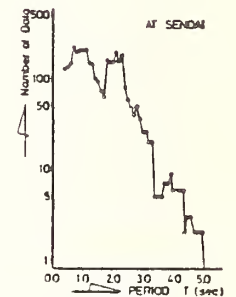
Fig.5 Number of Data
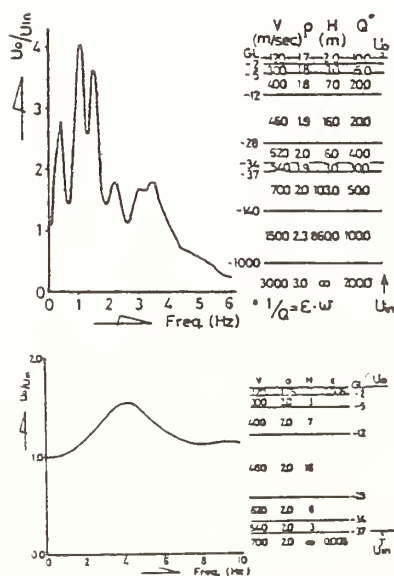
Fig.6 Transfer Function
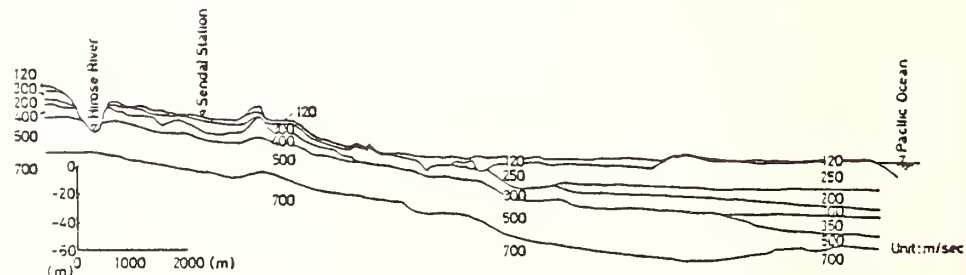
Fig.7 Profile of Shear Wave Velocity (A-A' Section)

60

basements. The plan and elevation of this building are shown in Figure 8, where the locations of strong motion accelerographs are indicated. Figure 9 shows the accelerograms recorded at the 2nd basement floor. Figure 10 displays the Fourier spectra for the accelerograms at the 18th floor, and the 2nd basement floor together with the spectral ratios between the both.

The building and subsoil were idealized as an elastic one-dimensional continuous media with some amount of damping which is independent of frequency. The parameters required in the analysis were determined from the results of the Fourier spectral ratios and seismic prospecting. The rigidities and densities of the layers representing the building and the first soil layer were modified so as to approximately satisfy the compatibility at the boundary, assuming that shear waves are propagated and reflected only in the vertical direction [4]. Figure 11 shows the observed and the calculated maximum accelerations in NS and EW directions together with the assumed shear wave velocities of this particular site. Figure 12 indicates the response acceleration spectra with damping ratio (h) of 0.05 for the observed wave at the 2nd basement floor, the calculated incident wave at structural base rock, and the calculated wave at outcropping of the 2nd basement floor level in NS and EW directions.

Using those two components at the base rock, a wave form for the major principal axis [5] was calculated and taken as the final incident wave. The direction of its axis was N18.5°E in two-dimensional space. Figure 13 shows the resultant incident wave motion at the structural base rock.

Distribution of Dynamic Characteristics of Underground Structures

The predominant period and the magnification factor are calculated at intervals of 0.5' in both latitude and longitude using Haskell's Method. The distribution maps of the predominant period and the magnification factor of the underground structure above the structural base rock are shown in Figures 14 and 15, respectively. As found from these figures, the predominant periods are around 0.2~0.3 sec in the terrace area, and 0.3~0.8 sec in the alluvial plain. Similarly, the magnification factors are about 2~3 in the former and 3~5 in the latter.
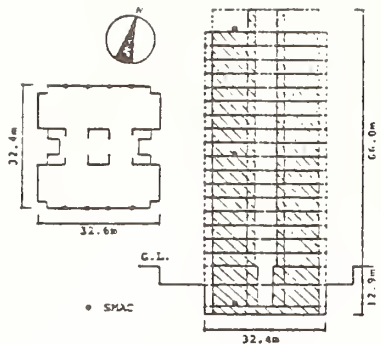
Fig.8 Plan and Section
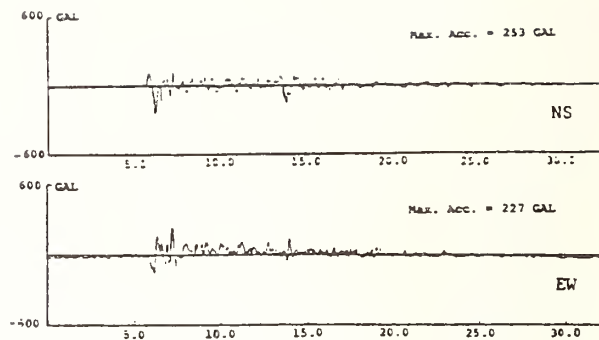
Fig.9 Accelerograms at 2nd Basement Floor
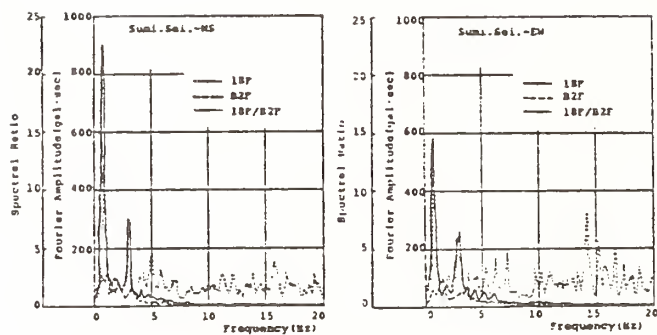
Fig.10 Fourier Spectra and Spectral Ratio
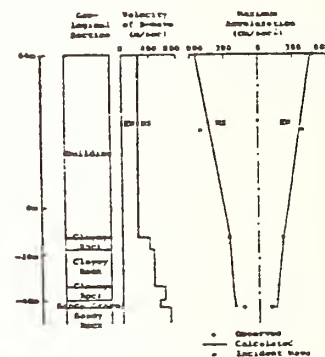
Fig.11 Max. Acceleration Values
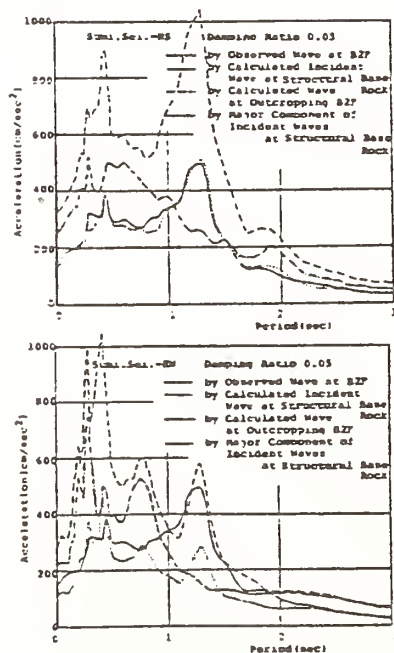
Fig.12 Response Spectra
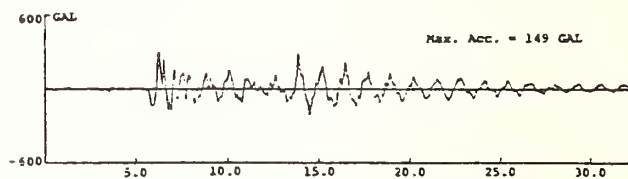
Fig.13 Final Incident Wave
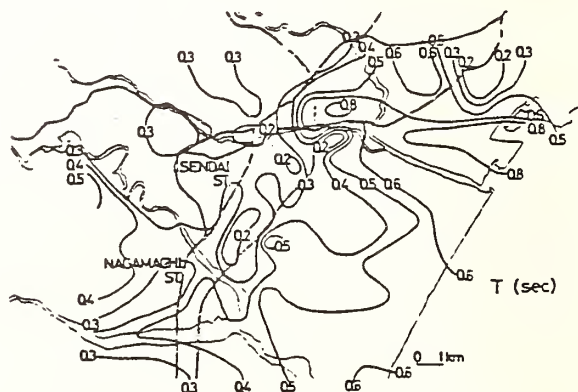
Fig.14 Distribution Map of Predominant Period

Distribution of Maximum Acceleration and Velocity

The maximum acceleration and velocity on the ground surface are calculated as the response due to the aforementioned incident wave on the structural base rock. The distribution maps of maximum acceleration and velocity are illustrated in Figures 16 and 17, where the values of contour lines are normalized by the maximum value of those maxima. As seen in these figures, the value in the alluvial plain is about 1.5 times as much as that of the several terrace levels.

COMPARISON OF STRUCTURAL DAMAGE WITH MICROZONING MAPS

Extents of Damages to Buildings

Figure 18 shows the distribution of damage to reinforced concrete buildings, steel buildings, wooden houses, and landslide areas in the Sendai district. The severe damage to reinforced concrete and to steel structures concentrated on the deluvium and the alluvial plain. Damage to wooden houses was on the alluvium and on the several terrace levels.

Three-story reinforced concrete buildings were extensively damaged by shear failure of columns in the first story. Almost all of damage to low-rise steel structures was brought about by buckling, bracing breaks, and anchoring failures. Damage to wooden houses is classified into two types: (1) damage due to ground motions on the alluvium plain and (2) damage due to terrace embankment landslides.

Comparison of Distribution of Damage with Seismic Zoning Maps

From a comparison of Figure 18 with Figure 16 or Figure 17, a close correlation between the location of severely damaged structures and the distribution of the maximum acceleration is generally apparent. It should be noted, however, that the soil is assumed to behave elastically in the foregoing analyses. In the case of severe earthquake, this will be a crude approximation and should be modified. Underground structures have been modeled by the hysteretic nonlinear systems although reliable values about the nonlinearity of soil in this district are not available. Figure 19 illustrates an example which gives the distribution of maximum accelerations obtained by such inelastic analysis where the Ramberg-Osgood hysteresis is assumed for the restoring force characteristics of soil deposits [6]. It appears that maximum accelerations tend to distribute more uniformly than those in Figure 16.
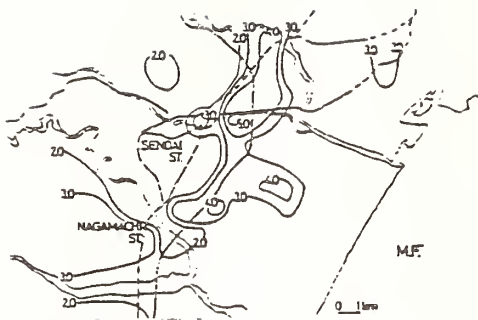
Fig.15 Distribution Map of
Magnification Factor
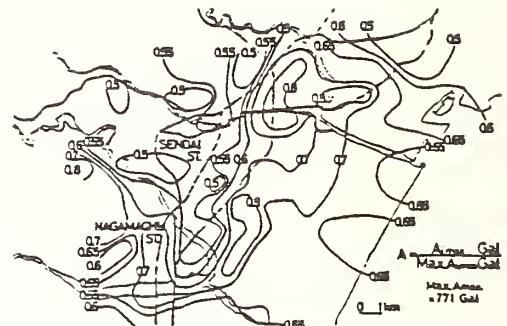
Fig.16 Distribution Map of
Max. Acceleration
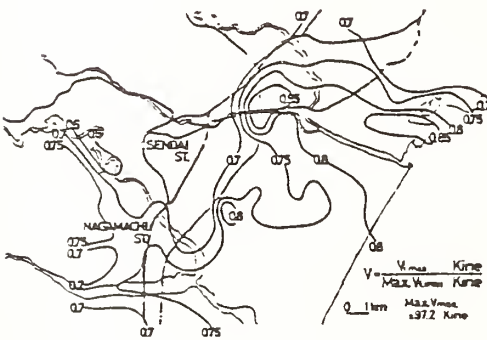
Fig.17 Distribution Map of Max.
Velocity
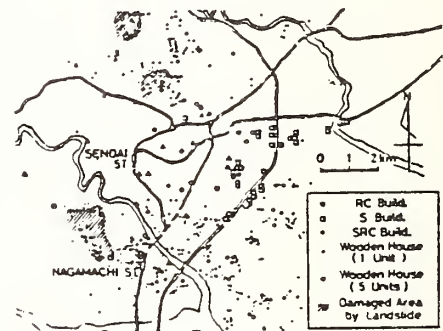
Fig.18 Distribution Map of Damage
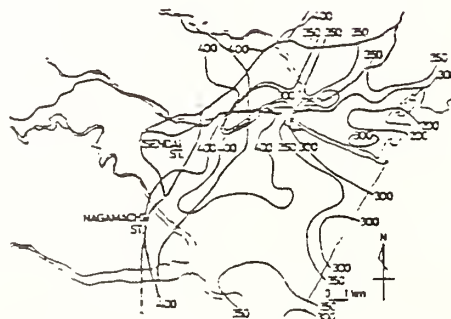
Fig.19 Distribution Map of Max. Acceleration

64

CONCLUDING REMARKS

The dynamic characteristics of underground-structures in the Sendai district have been investigated. Deep ground characteristics were estimated from the J.M.A. strong motion seismograph data, and the shallow ground characteristics were evaluated by micro-tremor measurements, boring data, penetration tests, and so on. The incident wave motion was calculated using the strong motion accelerograms recorded during the Off-Miyagi Prefecture Earthquake. The predominant periods, magnification factors, maximum accelerations, and velocities on the ground surface were computed, and the real damage to buildings compared with seismic microzoning maps. The close correlation between both is recognized. As a result, it is pointed out that the method of analytical investigation presented here is appropriate for seismic microzoning maps [7].

REFERENCES

[1] "Report on the Damage by 1978 Off-Miyagi Prefecture Earthquake (in Japanese)," Report of B.R.I., No. 86, pp. 57-81, 1979.

[2] Kitagawa, Y. and Ozaki, M., "Study on Regional Characteristics of Maximum Earthquake Motion in Japan," proc. of 5-th J.E.E., pp. 1-8, 1978.

[3] "Report on the Damage by 1978 Off-Miyagi Prefecture Earthquake (in Japanese)," Rept. of S.T.A., No. 15, pp. 58-60, 1978.

[4] Osawa, Y., Kitagawa, Y. and Ishida, K., "Response Analyses of Earthquake Motions Observed In and Around a Reinforced Concrete Building Including Building-Subsoil System," Proc. of 5-th W.C.E.E., 1973.

[5] Penzien, J. and Watabe, M., "Characteristics of Three-Dimensional Earthquake Ground Motions," Earthq. Eng. Struct. Dyn. 3, pp. 365-373, 1975.

[6]   Ohsaki, Y., Hara, A. and Kiyota, Y., "Stress-Strain Model of Soils for Seismic
      Analysis (in Japanese)," proc. of 5-th J.E.E., pp. 679-704, 1978.

[7]   Kitagawa, Y. and Matsushima, Y., "Study of Dynamic Ground Characteristics in Range
      of Short and Long Periods," Proc. of 7th W.C.E.E., 1980.

HURRICANE WIND SPEEDS IN THE UNITED STATES

by

Martin E. Batts

Larry R. Russell

Emil Simiu

INTRODUCTION

It has been previously been shown that predictions of extreme wind speeds in hurricane-prone regions cannot in general be based upon the statistical analysis of the largest annual wind speeds recorded at a given site [11, p. 84]. For this reason, estimates of extreme hurricane wind speeds at a site are commonly obtained by indirect methods [2,5,12,13] from (1) statistical information on the climatological characteristics of hurricanes, and (2) a physical model of the hurricane wind structure. The climatological characteristics of hurricanes include: (a) rate of hurricane occurrence in any given region; (b) difference between atmospheric pressures at the center and at the periphery of the storm; (c) radius of maximum wind speeds; (d) speed of storm translation (e) direction of storm motion, and (f) crossing point coordinate along the coast or on a line normal to the coast. The physical model of the hurricane wind includes assumptions on: (a) dependence of surface wind speeds upon difference between atmospheric pressures at center and periphery of the storm, radius of maximum wind speeds, speed of translation, latitude, and position of the point being considered with respect to center of the storm; (b) storm decay as the storm travels over land and its supply of energy in the form of warm moist air from the ocean surface is thus cut off; (c) reduction of wind speeds due to friction over land; and (d) ratios between wind speeds averaged over various time intervals.

Given the available statistical information on the climatological characteristics of hurricanes, probabilistic models are estimated for each of these characteristics. A large number of hurricanes is then generated by Monte Carlo simulation (random sampling) from these probabilistic models, as will be explained subsequently in the paper. The largest wind speeds occurring within each of these hurricanes at the site of concern represent the data from which the cumulative distribution function of the hurricane wind speeds at that

site is then estimated. This procedure was first developed by Russell [10], who also developed the computer program used in this work.

The purpose of this paper is to present estimates of hurricane wind speeds on the Gulf and East Coasts of the United States based on the procedure just outlined and on data taken from Ref. [4] and [5]. The probabilistic and physical models used to obtain these estimates will be described, and an analysis will be made of errors inherent in the estimates. Estimates of hurricane wind speeds in California [14] are not treated in this paper.

PROBABILISTIC MODELS

The following probabilistic models were used:

(1) The hurricane occurrence is described by a uniform Poisson process.

(2) The probability distribution of the pressure difference between center and periphery of storm, Δp_{max}, is lognormal. To eliminate values of Δp_{max} judged, in light of historical data [6], to be unrealistically high, the distribution is censored so that $\Delta p_{max} < 101.6$ mm (4.00 in) of mercury. (Note that $\Delta p_{max} = 101.6$ mm corresponds to the lowest atmospheric pressure ever recorded worldwide [15].) The effect of this censoring will be commented upon subsequently in this paper.

(3) The probability distribution of the radius of maximum wind speeds, R, is lognormal. This distribution is censored so that 8 km < R < 100 km to avoid unrealistically "tight" or "broad" storms [6].

(4) The average correlation coefficient between R and Δp_{max} is approximately -0.3 (see Ref. [6], pp. 68 and 69). All other climatological characteristics are assumed to be statistically independent.

(5) The probability distribution of the speed of translation, s, is normal. This distribution is censored so that 2 km/hr < s < 65 km/hr [6].

(6) The cumulative distribution function of the hurricane crossing point along the coast is a curve matching the historical data as recorded in Ref. [6]. Separate distribution curves are defined for entering, exiting, upcoast heading, and downcoast heading storms. The length of coast being considered for entering and exiting storms includes a 470 km segment downcoast of the location under investigation, and a 370 km segment upcoast of that location, the influence of storms not crossing these segments being

68

negligible for practical purposes. The downwind and upwind segments are unequal because, owing primarily to the presence of the translational speed of the storm, the hurricane wind structure is asymmetrical. As an example, the distribution curve assumed for entering storms affecting coastal milepost 400 n. mi, (740 km) (see Figure 1) is shown in Figure 2.

(7) The crossing points on a line normal to the coast are assumed to be uniformly distributed between 110 km and 280 km from the coast in the case of upcoast heading storms, and between 110 km and 360 km in the case of downcoast heading storms.

(8) The cumulative distribution functions of heading (direction of storm translation) for entering storms are curves matching the historical data recorded in Ref. [6]. As an example, Figure 3 shows the distribution of the storm headings about their mean value for milepost 400 n. mi. (740 km). For exiting storms, and for storms crossing a line normal to the coast, the distributions are assumed to be uniform between ± 30° of the mean. The mean values of the storm headings are obtained from the data of Refs. [4] and [6]. In all cases it was assumed that the path of the storm motion is a straight line.

<center>PHYSICAL MODELS</center>

Maximum Gradient Wind Speed

The maximum gradient wind speed can be written as:

$$V_{gx} = -\frac{Rf}{2} + \left(\frac{R}{\rho}\frac{dp}{dn}\right)^{1/2} \tag{1}$$

(see Ref. [11], p. 18), where f = Coriolis parameter, dp/dn = pressure gradient, ρ = air density, and R = radius of maximum wind speeds. It is reasonable to assume

$$\frac{dp}{dn} = \alpha\Delta p_{max} \tag{2}$$

where α is a coefficient determined empirically. It then follows from Equations 1 and 2

$$V_{gx} = K \quad \Delta p_{max} - \frac{Rf}{2} \tag{3}$$

where the notation $K = [R\,\alpha/\rho]^{1/2}$ is used. Values of K consistent with those determined empirically by the Hydrometeorological Branch (National Weather Service, National Oceanic

and Atmospheric Administration) and used in Ref. [9] vary between 6.97 m/s/mm$^{1/2}$ (77.5 mph/in$^{1/2}$) at latitude 23°N to 6.93 m/s/mm$^{1/2}$ (77.0 mph/in$^{1/2}$) at latitude 45°N. [These values may be used in conjunction with the assumption that the pressure at the periphery of the storm is p_n = 765 mm (29.77 in).]

Wind Speeds at 10 m Above the Ocean Surface

The maximum wind speed at 10 m above the ocean surface, averaged over 10-min, is assumed to be given by the empirical relation [9]

$$V(z = 10,R) = 0.865 \, V_{gx} + 0.5 \, s \tag{4}$$

Let the center of the storm be denoted by 0, and let a line OM be defined that makes an angle of 115° clockwise from the direction of motion of the storm. The 10-min wind speed at 10 m above the ocean surface at a distance r from 0 along the line OM is denoted by $V(z = 10,r)$. The ratio $V(z = 10,r)/V(z = 10,R)$, is assumed to depend on r as shown in Figure 4 [9]. Let now the angle between a line ON and line OM be denoted by θ. The 10-min wind speed $V(z = 10,r,\theta)$ at 10 m above the surface at a distance r from the storm center on line ON is a assumed to be given by the expression [9]

$$V(z = 10,r,\theta) = V(z = 10,r) - \frac{s}{2} (1 - \cos \theta) \tag{5}$$

The wind velocity vector has a component directed toward the center of the storm. The angle between that vector and the tangent to the circle centered at 0 is assumed to be between 0° and 10° in the region $0 < r < R$, between 10° to 25° in the region $R \leq r < 1.2 \, R$, and 25° in the region $r \leq 1.2 \, R$ [9].

Storm Decay

The storm decay was assumed to result from a decrease with time of the difference between pressure at the center and at the periphery of the storm, given by the following relation

$$\Delta p(t) = \Delta p_{max} - 0.02 \, [1 + \sin \phi] t \tag{6}$$

where t = travel time in hours, $\Delta p(t)$ and Δp_{max} are given in inches, and ϕ = angle between coast and storm track $(0 < \phi < 180°)$. As shown subsequently in this paper, results based

70

on this model were compared with results based on Malkin's model, which is consistent with measurements reported in Ref. [8]. This comparison appears to support validity of Eq. (6) as a conservative approximation.

Reduction of Wind Speeds Due to Friction Over Land

The factor for reducing overwater to overland surface wind speeds used in Ref. [9] is 0.78 for wind speeds over 37 m/s. In Ref. [3], the ratio $V^\ell(10)/V^w(10)$, where $V(10)$ = 10-min mean speed at 10 m above the surface, and the superscripts w and ℓ indicate "overwater" and "overland", respectively, is given as

$$\frac{V^\ell(10)}{V^w(10)} = \frac{1}{0.2\ p\ \ln \dfrac{10}{z_o}} \tag{7}$$

where the retardation factor $p = 0.83$ and the roughness length $z_o = 0.005$ m, so that $V^\ell(10)/V^w(10) = 0.79$, i.e., this ratio has almost exactly the same value as in Ref. [9]. Note that Eq. (7) is based on similarity relations applicable to storms in which the gradient wind may be regarded as geostrophic, so that its applicability to hurricane winds is uncertain, at least in the region of maximum wind speeds. In this work it was therefore assumed conservatively that $V^\ell(10)/V^w(10) = 0.85$.

Dependence of Wind Speeds Upon Averaging Time

Research results concerning the ratios of hurricane wind speeds corresponding to different averaging times do not appear to be available. In the absence of such results, it was judged reasonable to use wind speed ratios obtained for non-tropical storms by Durst which are summarirzed, e.g., in Ref. [11], p. 62. For example, the ratio between the fastest one-minute and the fastest 10-minute speed at 10 m above open terrain was assumed to be 1.18.

PROBABILITIES OF OCCURRENCE OF HURRICANE WIND SPEEDS

To estimate probabilities of occurrence of hurricane wind speeds, one thousand hurricanes were assumed to hit the area adjoining each site being investigated. (Recall that this area was defined previously in this section "Probabilistic Models," item 6 and 7.) Four categories of storms were considered: entering hurricanes (i.e., hurricanes

moving inland), exiting hurricanes (i.e., hurricanes headed toward the ocean after moving over land), upcoast heading hurricanes (i.e., hurricanes whose center remains offshore and moving upcoast), and downcoast heading hurricanes. For each location, the ratios between the number of hurricanes belonging to each of these categories and the total number of hurricanes affecting that location were estimated from the information given in Ref. [4] and [6].

The climatological data for each of the one thousand hurricanes were determined from the respective probability distributions by Monte Carlo simulation (random sampling). Associated with each hurricane is a wind field, and a set of wind speeds at the site of interest which depend upon the position of the moving hurricane center with respect to the site. These wind speeds were calculated for a sufficiently large number of such positions (6 or 7, depending on track). The largest among these speeds represents the maximum wind speed caused by the hurricane at the site. A set of one thousand such wind speeds is thus obtained, which is used as the basic set of data for the estimation of the probability of occurrence of hurricane wind speeds at the site. (This procedure was applied to estimate extreme wind speeds without regard to direction, as well as extreme wind speeds blowing in specified directions.) The wind speeds are ranked by magnitude, and the probability of occurrence of the i-th wind speed v_i, in a set of m wind speeds (m = 1,000 in the work reported herein) is obtained as follows.

Let the probability that the wind speed in any one storm is less than v be denoted by F_v. The probability that the highest wind speed V in n storms is less than v can be written as

$$P(V < v|n) = F_v^n \tag{8}$$

Let the probability that $V < v$ in τ years be denoted by $P(V < v, \tau)$. It is possible to write

$$P(V < v, \tau) = \sum_{n=0}^{\infty} P(V < v|n) P(n, \tau) \tag{9}$$

where $P(n, \tau)$ denotes the probability that n storms will occur in τ years. If a Poisson process is assumed to described $P(n, \tau)$, and if use is made of Eq. (9),

72

$$P(V < v, \tau) = \sum_{n=0}^{\infty} F_v^n \frac{(\nu\tau)^n e^{-\nu\tau}}{n!}$$

$$= e^{-\nu\tau} \sum_{n=0}^{\infty} \frac{(\nu\tau F_v)^n}{n!}$$

$$= e^{-\nu\tau} e^{\nu\tau F_v}$$

$$= e^{-\nu\tau(1-F_v)} \tag{10}$$

where ν = annual rate of occurrence of hurricanes in the area of interest for the site being considered. For $\tau = 1$, $P(V < v, \tau)$ = probability of occurrence of wind speeds less than v in any one year.

Consider now the wind speed v_i. Its probability of occurrence can be written as

$$F_{v_i} = \frac{i}{m+1} \tag{11}$$

Thus

$$P(V < v_i, 1) = e^{-\nu(1 - \frac{i}{m+1})} \tag{12}$$

The estimated mean recurrence interval of the speed v_i is then

$$N = \frac{1}{1 - e^{-\nu(1 - \frac{i}{m+1})}} \tag{13}$$

<center>NUMERICAL RESULTS</center>

Extreme Wind Speeds

Hurricane fastest-mile wind speeds at 10 m above ground over open terrain were estimated for 58 mileposts (from 150 through 3000 in increments of 50 - see Figure 1) at the coastline, and at 25 km, 50 km, 100 km and 200 km inland. The results of the calculations were smoothed as follows. For each milepost the average was calculated of the fastest-mile wind speeds at that milepost and at its two neighboring mileposts [located each at 50 n.mi. (83 km) from it]. This averaging was done, for each milepost, at the

<center>73</center>

coastline, as well as at 25 km, 50 km, 100 km, and 200 km inland. A least-squares straight line was fitted at each milepost to the five averages thus obtained. The ordinates of this line at the coastline and at 200 km inland represent the values given by the curves of Figures 5 and 6, respectively. Extreme fastest-mile speeds at distances inland of less than 200 km from the coastline may be obtained by linear interpolation between Figures 5 and 6. It is noted that the values of Figures 5 and 6 differ by at most a few percent from the corresponding unsmoothed values originally calculated for the coastline locations.

The results shown in Figures 5 and 6 represent smoothed estimates of hurricane wind speeds without regard to direction. As previously indicated, similar results were obtained for winds blowing in specified directions. As an example, estimates of coastline fastest-mile hurricane wind speeds at 10 m above ground over open terrain at milepost 600, smoothed in the same manner as the results of Figures 5 and 6, are plotted in Figure 7 as a function of direction. Similar plots for coastline locations at mileposts 150 through 2900 (in increments of 50) are included in Ref. [1].

Errors in the estimation of extreme hurricane wind speeds are dealt with in the subsequent section. It is noted here that these errors increase as the mean recurrence interval increases. Therefore, estimates of wind speeds corresponding to mean recurrence intervals exceeding 100-yr, say, may contain significant errors. Nevertheless, such estimates obtained by the rational procedure used in this paper are of interest as they provide the only available basis for assessing the validity of wind load factors currently being used for structural design purposes in hurricane-prone regions.

Probability Distributions of Hurricane Wind Speeds

The numerical results obtained from the calculations were used to estimate probability distributions of hurricane wind speeds (blowing from any direction). It was found, by using the probability plot correlation coefficient method, that in all cases the best fitting distribution for the 1-minute speeds was the Weibull distribution with tail length parameter $\gamma > 4$ (for practical purposes $\gamma = 4$ can be assumed, the differences between results based on $\gamma = 4$ and $\gamma > 4$ being negligible). As an illustration, the results obtained at milepost 450 [1-minute wind speeds at coastline over water, in knots (1 knot = 1.9 km/hr)] are plotted on Weibull (= 4) and Extreme Value Type I probability paper on Figures 8 and 9, respectively. It is seen that the results fit the Extreme Value Type I

74

distribution poorly, i.e., the results do not fit a straight line on Figure 9, as they do on Figure 8.

MIXED PROBABILITY DISTRIBUTIONS OF HURRICANE AND NON-HURRICANE WIND SPEEDS

Mixed probability distributions of hurricane and non-hurricane fastest-mile (as opposed to 1-minute) wind speeds were estimated by using the following expression:

$$P(V < v) = P_H (V_H < v) \cdot P_{NH}(V_{NH} < v) \tag{14}$$

in which $P_H (V_H < v)$ = cumulative distribution of hurricane wind speeds V_H, and $P_{NH} (V_{NH} < v)$ = cumulative distribution of non-hurricane wind speeds, V_{NH}. The distribution P_{NH} was determined as shown in this report. For the distribution P_{NH}, an Extreme Type I distribution was assumed. The parameters of P_{NH} were estimated at various locations from maximum annual wind speed data that did not include hurricane wind speeds. The results of the calculations showed that the effect of the non-hurricane winds is negligible for mean recurrence intervals of the order of 50 years or more (see Figure 10). For mean recurrence intervals of about 20 years, the estimated wind speeds that include the effect of non-hurricane winds exceed the estimated hurricane speed by about 5 percent. Note that these conclusions are not applicable north of Cape Hatteras, where non-hurricane wind may control the design at certain locations.

ESTIMATION ERRORS

The errors in the estimation of hurricane wind speeds by the procedure used in this work may be divided into four categories: (1) sampling errors, due to (a) the limited size of the data sample used in making statistical inferences on the climatological character- istics of hurricanes (in the United States these data samples correspond to lengths of record of 75 to 100 years), and (b) the limited number of hurricanes generated by the Monte Carlo simulation; (2) probabilistic modeling errors, due to the imperfect choice of the distribution functions to which the climatology data are fitted (e.g., assuming that a lognormal distribution holds when in fact a normal distribution would be more appropriate); (3) observation errors, due to the imperfect measurement or recording of the true values of the climatological characteristics; and (4) physical modeling errors, due to the imperfect

representation of the dependence of the wind speed upon the various climatological characteristics and micrometeorological parameters.

Sampling Errors

As shown in some detail in Ref. [2], the standard deviation of the errors associated with the limited size of the climatological data samples (corresponding to about 75 to 100 years of record) is of the order of 6 percent to 10 percent of the estimated wind speeds, while the standard deviation of the errors due to the limited number, m of hurricanes used in the simulation is of the order of a few percent for m $\sim$ 1,000. In some cases, say, at Jacksonville, Florida, the poorly understood and seemingly anomalous occurrence histories may lead to larger errors than are typical of the model overall. Part of the sampling errors due to the limited number of hurricanes used in the simulation is eliminated by the use of the smoothing procedure described in the preceding section.

Probabilistic Modeling Errors

To assess the effect of various probabilistic models used in the simulation, calculations were carried out at mileposts 400, 1450 and 2100 (see Figure 1) under the following assumptions:

(a) Distribution of Δp_{max} is normal. This assumption results in a decrease of the 50-yr, 100-yr, and 400-yr wind speeds with respect to the corresponding values based on the assumption of lognormality by about 5 percent, 5 percent, and 8 percent, respectively.

(b) Distribution of R is normal. This assumption results in an increase of the 50-yr, 100-yr, and 400-yr wind speeds with respect to their corresponding values based on the assumption of lognormality by about 1 percent, 2 percent, and 6 percent, respectively.

(c) Distribution of Δp_{max} and R are both normal. This assumption results in a decrease of the 50-yr, 100-yr, and 400-yr wind speeds with respect to their corresponding values based on the assumption that Δp_{max} and R are both lognormally distributed by about 3 percent, 3 percent, and 4 percent, respectively.

(d) Distribution of s is lognormal. The differences between estimates of wind speeds based on this assumption on the one hand, and on the assumption that s is normally distributed on the other hand, are negligible for practical purposes.

(e) Distribution of Δp_{max} is not censored. The censoring of the distribution of Δp_{max} ($\Delta p_{max} < 101.6$ mm) reflects the writers' belief that this upper bound is dictated by physical considerations, and that an unbounded distribution would thus be physically unrealistic. Nevertheless, calculations were carried out for five stations in which it was assumed that the lognormal distribution of Δp_{max} is unbounded. It was found that the hurricane wind speeds and their cumulative distribution functions were for practical purposes the same regardless of whether the condition $\Delta p_{max} < 101.6$ mm was assumed or not.

A final observation with regard to the choice of probabilistic models concerns the representation of the hurricane occurrences as a Poisson process. It can be shown that this model could be replaced, e.g., by a geometric probability model, without any significant effect upon the estimated results, particularly for winds with mean recurrence intervals of the order of 20 years or more.

Observation Errors

To assess the effect of possible errors in the measurement (or recording of the parameters Δp_{max} and R, calculations were carried out at mileposts 400, 1450, and 2100 (Figure 1) in which it was assumed that the mean and/or standard deviation of Δp_{max} and R are larger than those estimated from the data of Ref. [6]. Increasing both the mean and the standard deviation of Δp_{max} by a factor of 1.1 resulted in an increase in the estimated values of the 50-yr, 100-yr, and 400-yr winds of about 5 percent at milepost 400, 8 percent at milepost 1450, and 10 percent at milepost 2100. Leaving the mean unchanged and increasing the standard deviation by a factor of 1.1 resulted in an increase of the estimated speeds of the order of a few percent. The effect of increasing or decreasing the mean and/or the standard deviation of the radii of maximum wind speeds, R, by a factor as high as 1.5 was of the order of a few percent at most.

As previously indicated, the data used in this report were obtained from Ref. [6]. The estimation of hurricane wind speeds at various locations could presumably be improved by using additional sources of climatological information, e.g., those available in the archives of the Corps of Engineers. The writers believe that this is the case particularly for South Texas, Louisiana, southwest Florida and Jacksonville.

77

Note that estimated hurricane wind speeds are lower at mileposts 1000 and 1750 (Figures 1, 5, and 6) than in the regions adjacent to these mileposts. This may be due to the relation between configuration of the coast and the hurricane paths. However, it may be that hurricanes at and near these mileposts were underreported in the past. It appears therefore prudent to increase the wind speeds calculated at mileposts 1000 and 1750 by about 5 mph or 10 mph. Finally, it was found that the storm decay overland was very weak at mileposts 650 and 2250. This is due, at least in part, to the configuration of the coast at these mileposts, although the spurious occurrence of strong simulated storms may also have contributed to this result.

Physical Modeling Errors

The coefficient K in Eq. (3), the coefficient of Eq. (4), and the dependence of wind speeds upon radius represented in Figure 4, have been determined empirically by the National Weather Service on the basis of careful correlations of pressure and wind speed measurements. Clearly, the corresponding physical model of the hurricane wind field is, nevertheless, imperfect. It is the writers' belief, based, e.g., on information from Ref. [7], that the standard deviation of the errors inherent in this model is of the order of 5 percent to 10 percent.

It was noted previously that the coefficient K assumed in this work may be used in conjunction with the value p_n = 756 mm (29.77 in). To check the effect on the calculated results of the assumption p_n = 760 mm (29.92 in), calculations based on this assumption were carried out at mileposts 400, 1450, and 2100. It was found that differences between results based on p_n = 756 mm and p_n = 760 mm were of the order of 3 percent.

It was noted that results based on the model for storm decay used in this work (Eq. (6)) were compared with results based on Malkin's model, which is consistent with measurments reported in Ref. [8]. The differences between the two sets of results were in all cases small (of the order of ± 2 percent).

In estimating wind speeds over water immediately off the shoreline it was assumed that the roughness length parameters corresponds to "flow over water" conditions in all directions (this will be referred to as "surface friction hypothesis I"). In reality, each location immediately offshore is affected not only by hurricane winds which blow from the ocean (and for which the assumption that a roughness length corresponding to "flow

over open terrain" conditions may have to be used. The hypothesis that the roughness length depends upon whether the winds flow from the ocean or from land will be referred to as "surface friction hypothesis II." Whether or not "surface friction hypothesis II" is warranted is by no means always certain: indeed, near the shoreline the terrain is likely to be flooded during the occurrence of hurricanes. Nevertheless, it is of interest to check the differences between results based on surface friction hypotheses I and II. Calculations carried out at mileposts 400, 850, 1450, 2100, and 2800 showed that estimated wind speeds corresponding to hypothesis II were lower than those based on hypothesis I by an amount generally not exceeding 3 percent.

Local wind intensification due to the presence of rainbands occur at all locations south of the 30° north parallel. These intensifications might have to be accounted for by increasing the wind speeds calculated herein by as much as 10 mph (4.47 m/s) or so.

As previously noted, the physical models used in this report, and particulalry the storm decay model, provide a description of the wind field that is probably less accurate at sites located north of Cape Hatteras, N.C., (mileposts 2200 or more, see Figure 1). The numerical results obtained for these sites should therefore be viewed very cautiously.

The physical model of the hurricane wind speeds may be refined by using a detailed representation of the coastline and its adjacent bodies of water. Such refinements may result in an improvement of hurricane wind speed estimate by an amount of the order of 5 percent or so.

Additional refinements might include accounting for slower storm decay where large bodies of water are present inland, e.g., in the low-lying areas of Louisiana. Additional research is required to develop improved storm decay models in such situations.

CONCLUSIONS

In this paper, estimates are presented of hurricane wind speeds along the Gulf and East Coasts of the United States. The paper describes the sources of data, the probabilistic models for the climatological characteristics of hurricanes and the physical models for the hurricane wind speed field used in the estimations. Estimated values of fastest-mile hurricane wind speeds at 10 m above ground in open terrain at the coastline and at 200 km inland are given for various mean recurrence intervals (Figures 1, 5, and 6).

Fastest-mile wind speeds at distances inland of less than 200 km from the coastline may be obtained by linear interpolation between these values. It was found that the estimated hurricane wind speed are best fit by Weibull distributions with tail length parameters $\gamma \geq 4$, rather than, e.g., by Extreme Value Type I distributions. Estimates are given of various errors inherent in the estimated values of the hurricane wind speeds. The confidence bands for the estimates were found to be of the order of at least $\pm$ 10 percent at the 68 percent confidence level. It was also noted that, owing to the possible inapplicability of the physical models used in this work at locations north of Cape Hatteras, estimated hurricane wind speeds given for these locations should be viewed with considerable caution. In certain special cases it may be desirable to base estimates of hurricane wind speeds on more elaborate data, physical models, and representations of the coastline than those used in this work. Nevertheless, in the writers' opinion, the results presented in this paper provide a rational and consistent basis for making realistic decisions on the specification of wind speeds and load factors in hurricane-prone regions.

ACKNOWLEDGMENTS

REFERENCES

[1] Batts, M. E. et al., <u>Hurricane Wind Speeds in the Gulf and East Coasts of the United States</u>, Building Science Series Report, National Bureau of Standards, Washington, D.C., 1980.

[2] Batts, M. E., Cordes, M. R., and Simiu, E., "Sampling Errors in Estimation of Extreme Hurricane Winds," Proc. of the 3rd Engineering Mechanics Division Specialty Conference, September 17-19, 1979, Austin, Texas.

[3]   Biétry, J. Sacre, C., and Simiu, E., "Mean Wind Profiles and Change of Terrain Roughness," Journal of the Structural Division, ASCE, Vol. 104, No. ST10, October 1978, pp. 1585-1595.

[4]   Cry, G. W., Tropical Cyclones of the North Atlantic Ocean-Tracks and Frequencies of Hurricanes and Tropical Storms, 1871-1963, Technical Paper No. 55, U.S. Department of Commerce, Weather Bureau, Washington, D.C., 1965.

[5]   Gomes, L., and Vickery, B. J., On the Prediction of Tropical Cyclone Gust Speeds Along the Northern Australian Coast, Research Report R278, School of Civil Engineering, University of Sydney, February, 1976.

[6]   Ho, F. P., Schwerdt, R. W., and Goodyear, H. V., Some Climatological Characterstics of Hurricanes and Tropical Storms, Gulf and East Coasts of the United States, NOAA Technical Report NWS15, Washington, D.C. May 1975.

[7]   Holliday, C., On the Maximum Sustained Winds Occurring in Atlantic Hurricanes, Technical Memorandum No. WGTM-SR-45, U.S. Department of Commerce, Environmental Sciences Services Administration, Weather Bureau, Fort Worth, Texas, 1969.

[8]   Malkin, W., Filling and Intensity Changes in Hurricanes on Land, National Hurricane Research Project, Report No. 34, U.S. Department of Commerce, Washington, D.C., November 1959.

[9]   Revised Standard Project Hurricane Criteria for the Atlantic and Gulf Coasts of the United States, Memorandum HUR7-120, U.S. Department of Commerce, NOAA, June 1972.

[10] Russell, L. R., "Probability Distributions for Hurricane Effects," Journal of the Waterways, Harbors, and Coastal Engineering Division, ASCE, Vol. 97, No. WW1, February 1971, pp. 139-154.

[11] Simiu, E., and Scanlan, R. H., Wind Effects on Structures, Wiley-Interscience, New York, N.Y., 1978.

[12] Sklarin, J., Stochastic Analysis of Hurricane Wind Loads (Harman, T. G., and Cornell, C. A., supervisors), Report R77-2, Order No. 563, Department of Materials Science and Engineering, Massachusetts Institute of Technology, Cambridge, Massachusetts, January, 1979.

[13] Tryggvason, B. V., Surry, D., and Davenport, A. G., "Predicting Wind-Induced Reponse in Hurricane Zones," Journal of the Structural Division, ASCE, Vol. 102, No. ST12, December 1976, pp. 2333-2350.

[14] Windstorms in California, State of California, Department of Water Resources, Sacramento, California, December, 1979.

[15] Worldwide Extremes of Temperature, Precipitation and Pressure Recorded by Continental Area, ESSA/P1680032, Environmental Data Service, U.S. Department of Commerce October, 1968.

APPENDIX I - NOTATION

dp/dn = pressure gradient

f = Coriolis parameter

K = coefficient

p = retardation factor

p_n = standard pressure

$P(n,\tau)$ = probability that n storms occur in t years

$P(V < v|n)$ = probability that the wind speed V in no storms is less than v

$P(V < v/\tau)$ = probability that the wind speed V in τ years is less than v

r = distance from storm center

R = radius of maximum wind speeds

s = hurricane translational speed

t = time, in hours

V_{gx} = maximum gradient windspeed

$V(z,R)$ = maximum velocity at z meters above ground at the radius of maximum winds

$V(z,r)$ = maximum velocity at z meters above ground at the radius r from the eye

$V(z,r,\theta)$ = velocity at z meters above ground at radius, r and angle θ from OM

z = height above ground or water surface, in meters

α = coefficient

Δp_{max} = pressure drop from periphery of hurricane to its center

ρ = air density

θ = angle between lines ON and OM

ϕ = angle between storm track and coastline

ℓ = angle between storm track and coastline

Figure 1. Locator map with coastal distance intervals marked in nautical miles (1 n. mi. ≈ 1.9 km) [5].
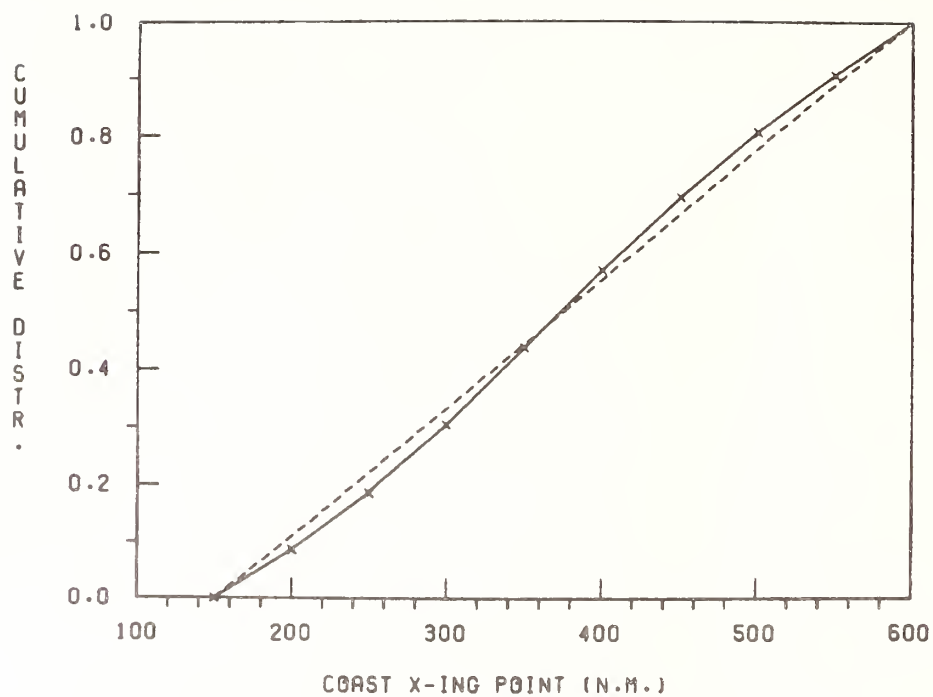
Figure 2.   Cumulative distribution function of entering hurricane crossing
point, milepost 400 n. mi. (1 n. mi. ≅ 1.9 km).
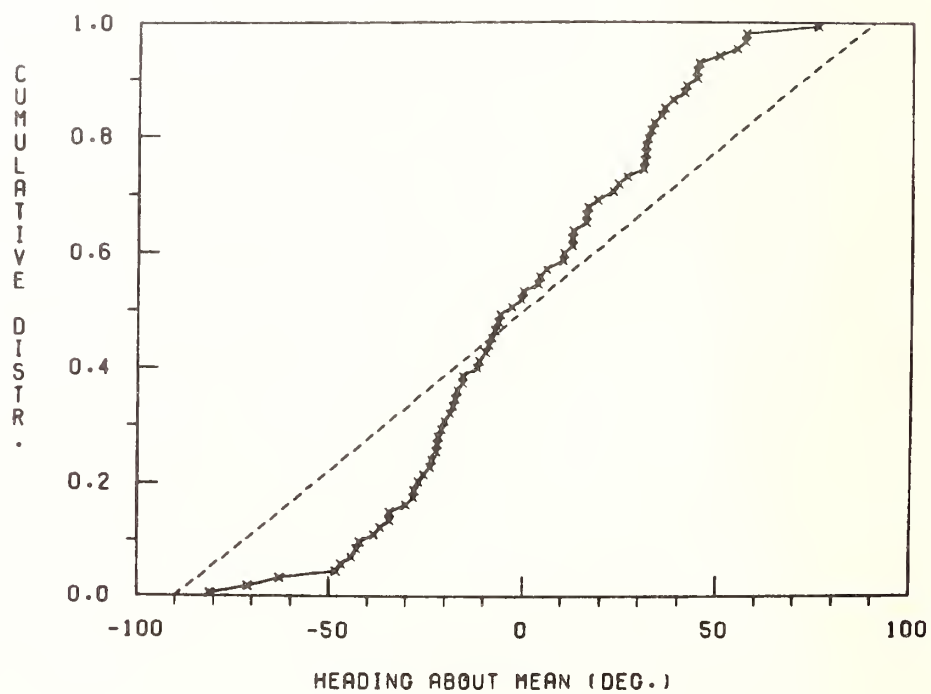
Figure 3.   Cumulative distribution function of entering storm headings about
mean, milepost 400 n. mi. (1 n. mi. ≅ 1.9).
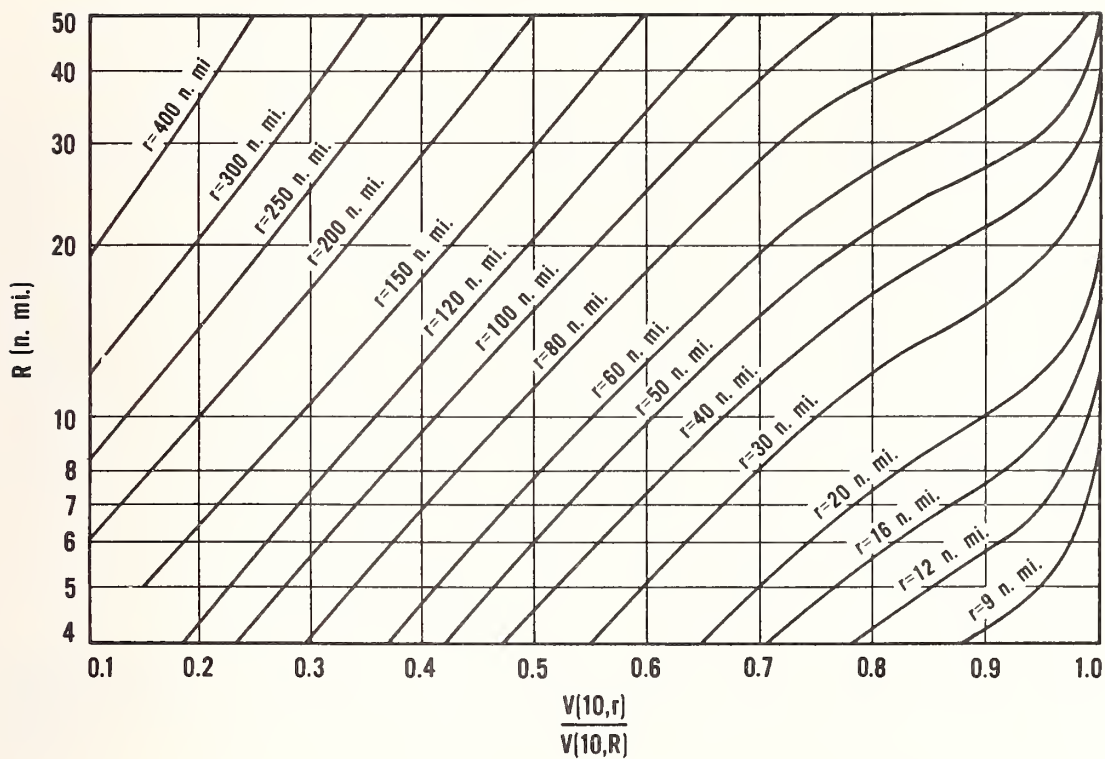
Figure 4. Ratios V(10,r)/V(10,R).
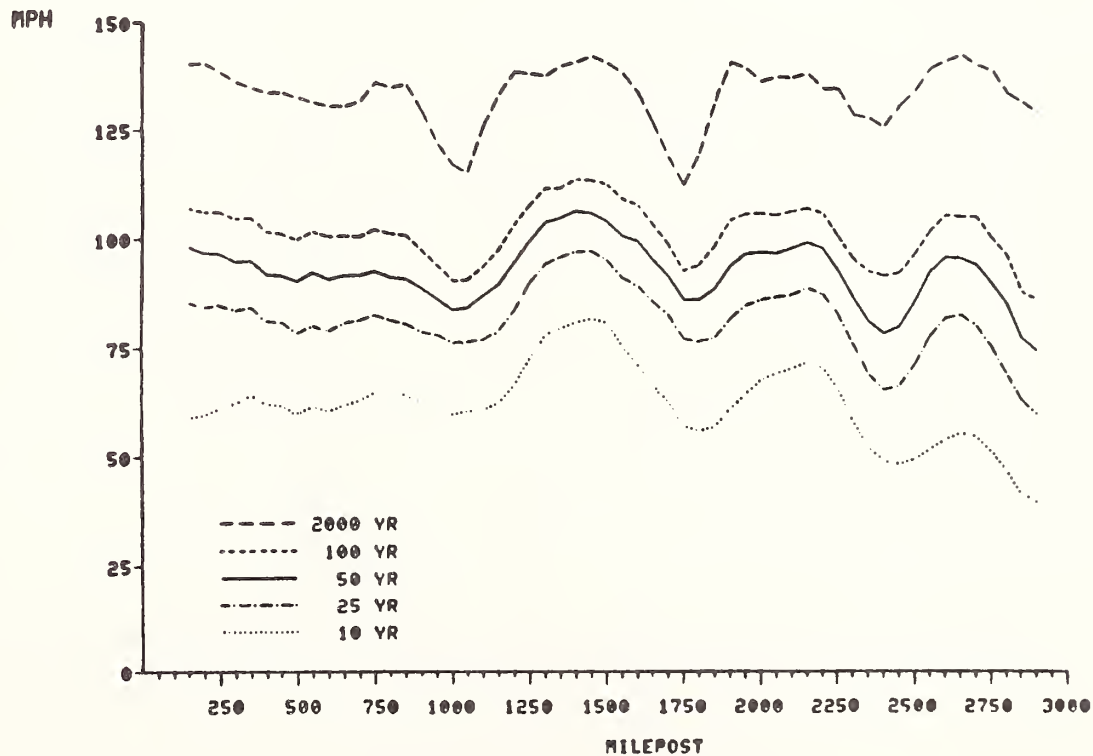
Figure 5. Estimated fastest-mile hurricane wind speeds blowing from any
direction at 10 m above ground in open terrain near the coast-
line, for various mean recurrence intervals (1 mph – 0.72 m/s).

85
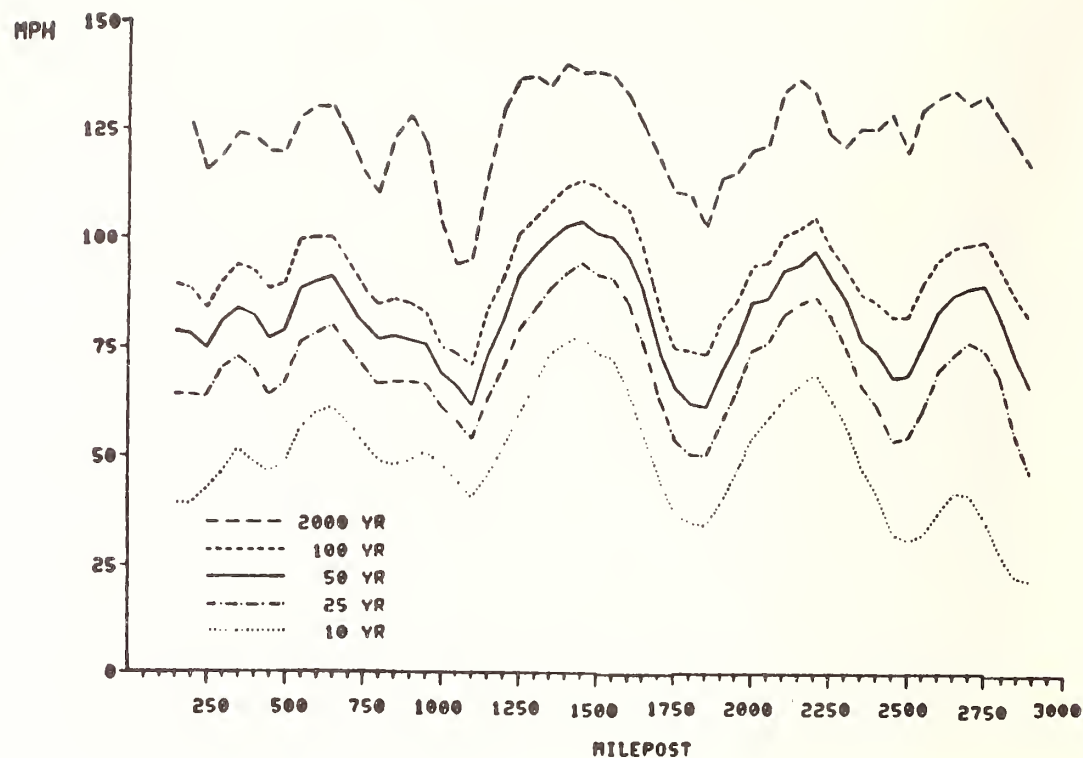
Figure 6. Estimated fastest-mile hurricane winds speeds blowing from any direction at 10 m above ground in open terrain at 200 km inland, for various mean recurrence intervals (1 mph $\simeq$ 0.72 m/s).
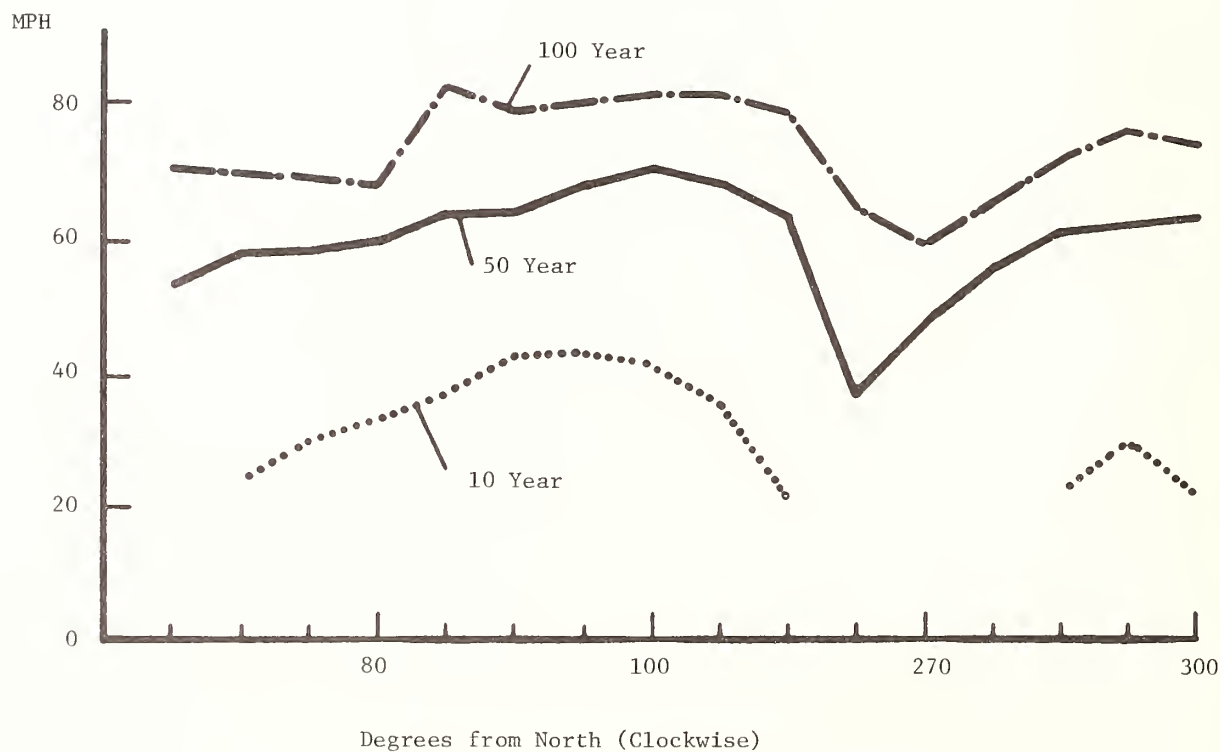
Figure 7. Estimated fastest-mile hurricane wind speeds blowing from various directions at 10 m above ground in open terrain near the coastline, for various mean recurrence intervals, milepost 600 n. mi. (1 n. mi. $\simeq$ 1.9 km; 1 mph $\simeq$ 0.72 m/s).
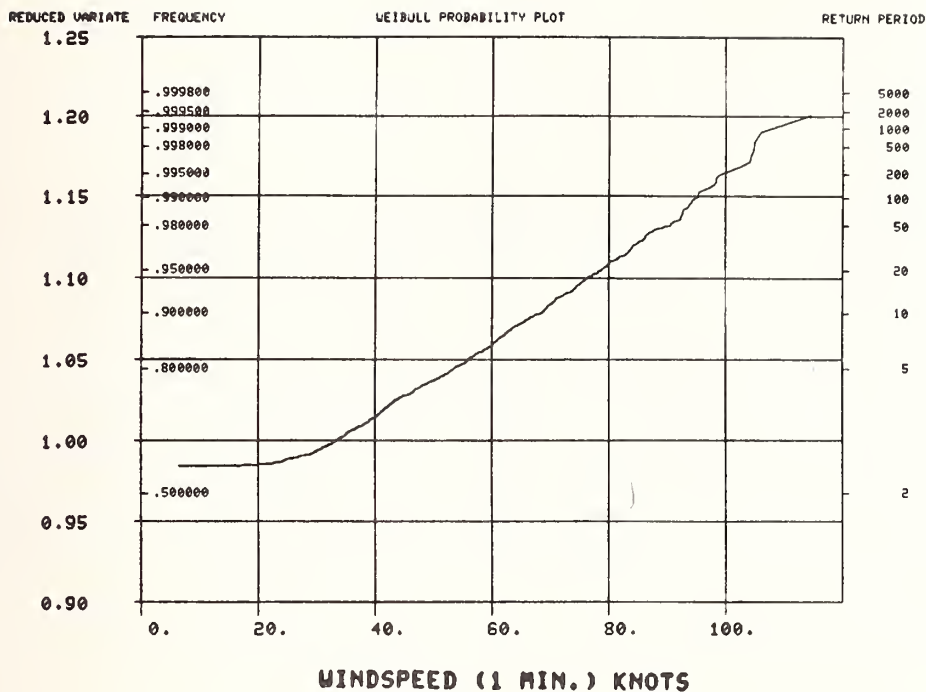
Figure 8. Weibull probability distribution plot of 1-min hurricane wind speeds, milepost 450 n. mi.
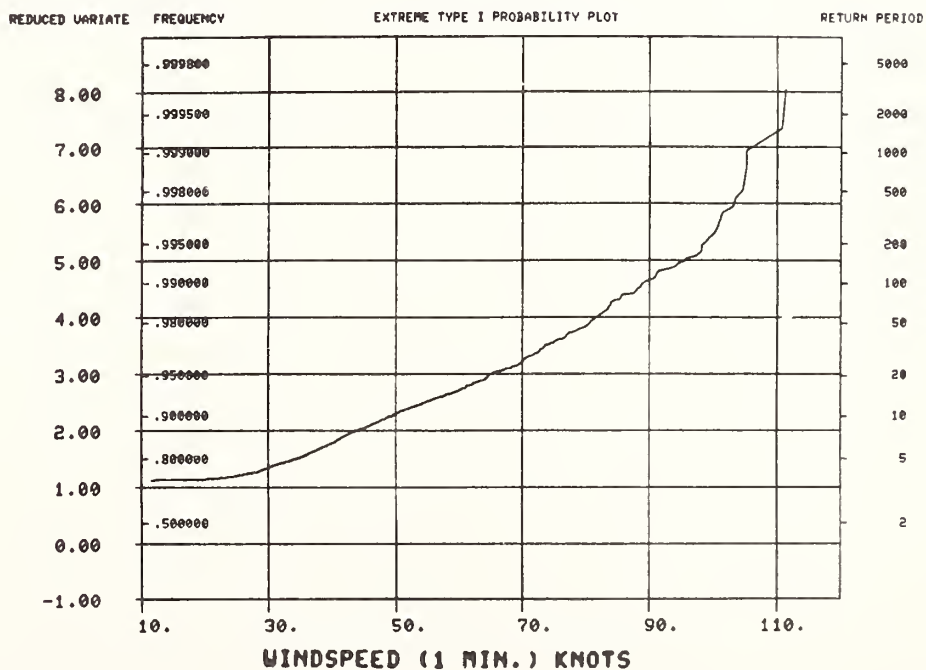
Figure 9. Extreme value Type I probability distribution plot of 1-min hurricane wind speeds, milepost 450 n. mi.
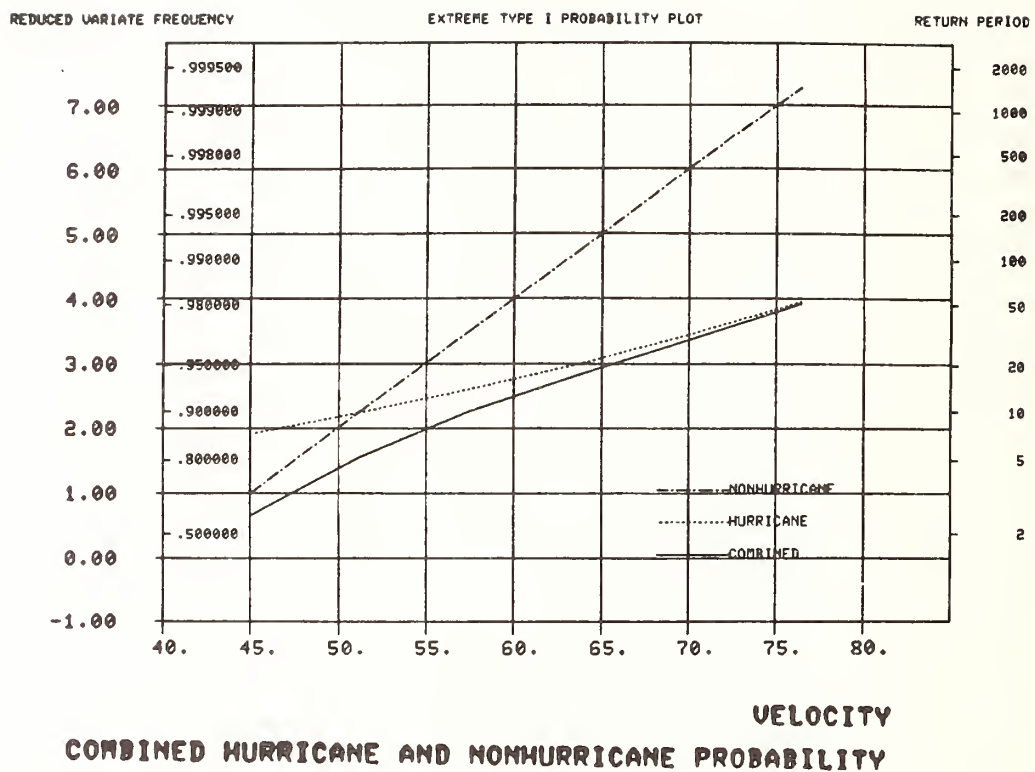
Figure 10. Extreme value Type I probability distribution of fastest-mile wind speeds.

A STATISTICAL RESULT ON MAXIMUM SURFACE WINDS SURROUNDING TYPHOONS

by

Shigemi Fujiwhara

I. Subbarramayya

ABSTRACT

Reconnaissance aircraft data from tropical storms and typhoons in the western North Pacific for the period 1974-78 were examined. Regression equations for maximum surface winds, using central pressure and the squareroot of the central pressure-depth as independent variables, were derived and compared.

INTRODUCTION

The strong wind in a tropical cyclone is the main factor that is responsible for the extensive damage caused by cyclones. The strong winds are also responsible for strong-surges which cause coastal inundations and loss of life. Therefore, accurate estimations of maximum surface winds associated with cyclones is an important problem to the tropical storm forecaster.

Horiguti (1926) suggested an empirical equation for the radial pressure profile of typhoons. Using that equation and the cyclostrophic wind assumption Takahashi (1948) showed that,

$$V_m = 4.5 \sqrt{p_n - p_o} \tag{1}$$

where, V_m is the maximum surface wind in m/sec, p_n is the peripheral pressure in mbs and p_o is the central pressure. But, earlier Takahashi (1940) obtained 5.1 for the constant on the right hand side of Eq. (1) from statistical study of observations. However, he suggested in 1948 that a value of 6 for the constant is safer. From similiar studies on hurricanes in Atlantic, Fletcher (1955) obtained the equation,

$$V_m = 16 \sqrt{p_n - p_o} \tag{2}$$

where, V_m is in kts and p_n and p_o are as in Eq. (1).

The above equations were based on very few observations in the region of strongest winds. They are primarily dependent on an extrapolation of the conditions around areas of the strongest winds.

With the advent of reconnaissance flights into tropical cyclones in the mid-1950's by the U.S. Air Force, a larger number of observations of central pressures and maximum surface winds have become available. Central pressure is obtained either directly by drop-sonde, or, by extrapolation from the temperature and height data at a 700 mb (flight) level. The surface winds, on the other hand, are estimated by comparing the state of the sea-surface with standard photographs. The individual maximum wind reports, therefore, are less accurate (Shimada, 1963) and contain subjective errors. However, reconnaisance observations are the best data available at present on maximum surface winds in tropical cylcones.

Shea and Gray (1973) examined maximum winds in relation to central pressures using aircraft observations and indicated an inverse relationship between the two.

The authors in this paper have therefore made a careful study of the relationship between V_m and p_0 using reconnaissance observations and obtained an empirical equation relating the two. There are factors other than central pressure which affect the maximum surface wind (Riehl, 1963), but those factors are of secondary importance. The authors have deliberately ignored the other factors in the present study, because, data on such parameters are less available and the future applicability of the envisaged equation would be restricted.

DATA AND ANALYSIS

The reconnaissance data for all the storms and typhoons of the western area of the North Pacific for the years 1974-78 during the typhoon season (July-November), available at the Japan Meteorological Agency, have been examined. The total number of useful observations, i.e., simultaneous central pressure and maximum surface wind, were about 510 and these are distributed approximately over the area between 10°-30°N and 110°-170°E. Though several flights may be made into a single cylcone by the Joint Typhoon Warning Center, Guam, not all are successful and a full series of observations could not be made in all the successful penetrations.

A scatter-diagram between maximum wind and central pressure was first prepared (Figure 1). The scatter is large, but the observations show a regular trend. To ascertain the nature of the trend, the total pressure range was divided into 10 mb intervals and the mean pressure and mean wind in each interval were calculated. These mean-value points show (Figure 2) a generally linear trend. Therefore, regression equations for V_m with $\sqrt{1010-p_0}$ and p_0 as independent variables have been evaluated and compared.

RESULTS AND DISCUSSION

The number of observations and the standard deviation for wind speeds in each pressure interval are presented in Table 1. The number of observations per class interval is more than 100 in weaker storms; this decreased to 5 in the extremely severe typhoon. The standard deviation of winds in each class generally increased along with the wind speed, but in

the very strong wind region, it is less than the deviation at relatively lower winds. This may be because the reconnaissance flights are less successful in very severe typhoons.

The estimated winds using Fletcher's equation have been found to be quite high compared to the observed winds. This is in conformity with the reports of other workers (Dunn and Miller, 1960). Winds estimated by the formula recommended by Takahashi show better agreement with observations, but the standard deviation of error estimates is found to be 17.87 kts.

The best-fit linear regression between V_m and $\sqrt{(1010 - p_0)}$ for the original observations is

$$V_m = 12.4 \sqrt{(1010 - p_0)} - 8.8 \tag{3}$$

where, V_m in knots and p_0 is in millibars. The standard deviation of errors of estimates of this equation is 15.87 kts. The best-fit linear equation for V_m with p_0 is

$$V_m = (1010 - p_0) + 25 \tag{4}$$

The standard deviation of errors of estimates of this equation is 15.85 kts, which is almost the same as for Eq. (3). Thus there is no statistically significant difference between the two equations, but it may be noted from Figure 2, that the mean-value points are randomly situated on either side of the straight line, while they are consistently below the curved line in the medium-wind range and above in the high-wind range. This means, Eq. (3) overestimates the intensity in the case of moderate typhoons and underestimates in the case of severe typhoons.

The weaker observed winds in very deep typhoons compared to those predicted by Eq. (4) could be partly due to the weakening of the autumn typhoons that have moved over to the Philippines and Taiwan land areas while the pressure depth is maintained by upper divergence, partly due to the recurvature of the autumn typhoons at relatively low latitudes and the subsequent structural changes in the typhoons, and partly due to the possible bias of the sampling of reconnaissance observations towards lower speeds.

It may be remembered that in either Takahashi's or Fletcher's study a linear relationship between V_m and $\sqrt{(p_n - p_0}$ had resulted only because of the cyclostrophic wind assumption they made to obtain an equation for the maximum wind from the empirical pressure

profiles. Though it appears simple reasoning that V_m^2, which is a measure of kinetic energy, may be directly proportional to the pressure depth, there are other factors like frictional force that play an important role. The actual mechanics of cyclones are quite complex and are not yet properly understood. The linear relationship between V_m and p_o, indicated above, points out the complexity of cyclone dynamics. On the other hand, it is simple to apply in forecasting operations, and is quite useful in typhoon intensity studies since p_o can be directly replaced by V_m and vice versa.

When we checked the sea surface wind data over typhoon areas which was obtained by the microwave scatterometers of Seasat, the 1978 U.S.A. experimental oceanic satellite, we found this data coincided more closely to the ship observations, but island or land observations were observed to be lower than the ship and the Seasat data because of orographic deformations.

We also found that a suitable modification of the deformations produced greater accuracy with island and land observations in comparison to sea surface winds. Observations of Takahashi's and Fletcher's papers, mentioned above, were almost all island and land data, and this kind of modification was not taken into consideration at that time.

REFERENCES

Dunn, G. E. and B. I. Miller, 1960, "Atlantic Hurricanes," Louisiana State University Press, p. 1959.

Fletcher, R. D., 1955, "Computation of Maximum Surface Winds in Hurricanes." Bull. Amer. Met. Soc., 36, 247-250.

Horiguti, Y., 1926, "On the Typhoons of the Far East." Mem. Imp. Mar. Obs., Kobe, 2, No. 3, 111-162.

Riehl, H., 1963, "Some Relationships between Wind and Thermal Structure of Steady State Hurricanes." J. Atmos. Sci., 20, 276-287.

Shea, D. J. and W. M. Gray, 1973, "The Hurricane's Inner Core Region. I. Symmetric and Asymmetric Structure." J. Atmos. Sci., 30, 1544-1564.

Shimada, K., 1963, "Some Problems in the Use of Data Obtained by Aircraft Typhoon Reconnaissance Flights." Proceedings of the Inter-Regional Seminar on Tropical Cyclones, Tokyo, Jap. Met. Agency, 307-315.

Takahashi, K., 1940, "Distribution of Various Meteorological Elements in a Typhoon." Jour. Met. Soc. Japan, 18, 125-130.

_____, 1948, "Typhoon in Japan." The Geophy. Mag., 17, No. 1-2, 1-35.

Table 1

Class Interval	1000	1000–990	990–980	980–970	970–960	960–950	950–940	940–930	930–920	920–910	910–900	900–890
No. of Obs.	47	127	115	84	39	19	31	17	8	13	7	5
S.D.	8.2	11.7	15.5	17.3	17.2	24.2	19.8	23.9	20.5	12.8	19.9	19.9

Fig. 1. Central Pressure versus Maximum Surface Wind (Scatter Diagram)

CENTRAL PRESSURE IN MBS
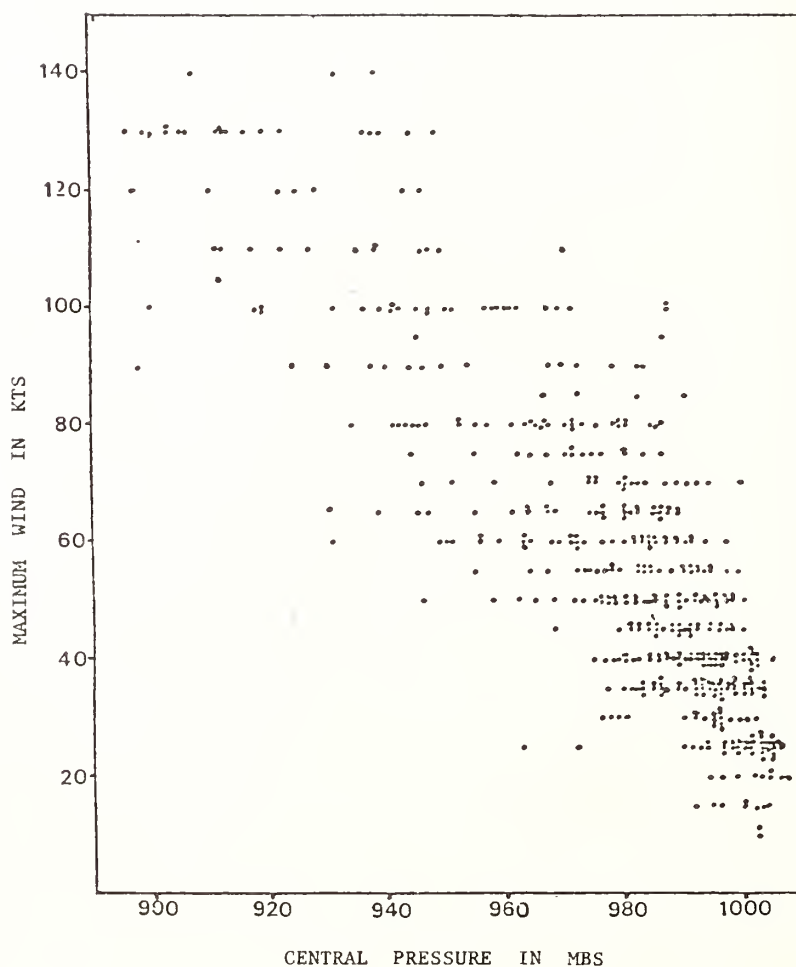
Fig. 2. Central Pressure versus Maximum Surface Wind (Statistical Curves)
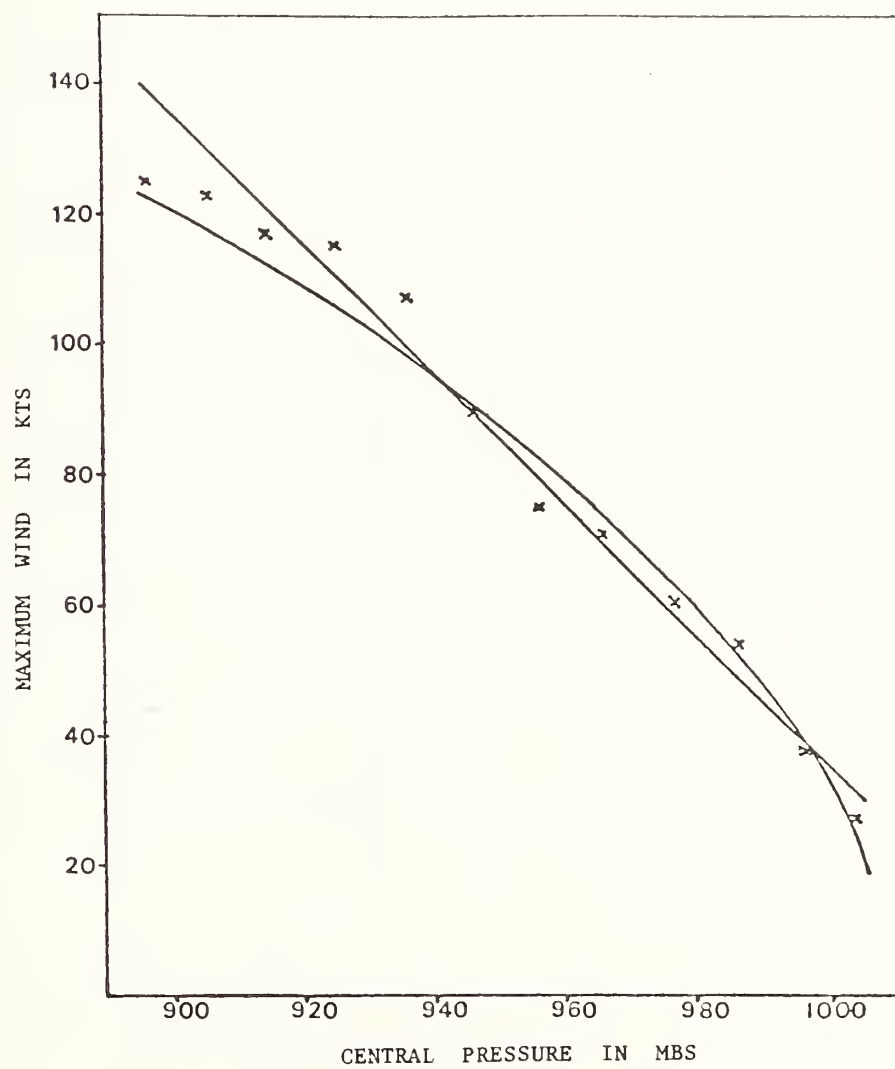
$$V_m = (1010 - p_0) + 25$$

$$V_m = 12.4\sqrt{(1010 - p_0)} - 8.8$$

SURFACE WINDS FROM HURRICANE FREDERIC:

AN ENGINEERING VIEWPOINT

by

Timothy A. Reinhold

ABSTRACT

Surface wind speed data taken during the passage of Hurricane Frederic were obtained
from ten different sites including four sites near Mobile, Alabama and six sites along the
coasts of Mississippi, Alabama and Florida. The form of the recording varies from site to
site as does the exposure, elevation and type of anemometer used. Most sites were visited
in order to estimate the type of terrain, to determine the elevation and type of
anemometer, and to note the location of any potential obstructions.

Each record is analyzed to determine peak to mean ratios between maximum gusts and 20
to 30 minute average wind speeds. These ratios compare favorably with Durst's relation-
ships between wind speeds for different averaging times using the corrections for different
elevations and types of terrain given by Simiu and Scanlan. The wind data from each site
was subsequently corrected to standard conditions, i.e. open terrain exposure at 10 meters
elevation, using the site characterization and Durst's relationships as modiifed by Simiu
and Scanlan. Consistency of different types of wind speed data is illustrated for sites
where anemometer traces were available. Future research aimed at evaluating mathematical
models of hurricane wind speeds, wind directions, and decay rates is outlined.

INTRODUCTION

On the evening of September 12, 1979, Hurricane Frederic struck the Gulf Coast of the United States between Pascagoula, Mississippi and Mobile, Alabama. Preliminary reports of the damage indicated that while significant economic losses had been suffered, structures hit by the hurricane were generally only partially demolished, expect along the shoreline where the storm surge was heaviest. Consequently, it was felt that a visit to the area for a survey of structural damage could provide information which would be useful in evaluating current building codes and construction practice.

For the evaluation of building codes and construction practice to have significant meaning, a knowledge of the wind speeds encountered is critically needed. In previous studies of hurricanes which have caused significant damage, wind speed and wind direction data have generally been quite limited and consequently estimates have been based largely on "educated guesses" or estimated from the damage. Fortunately, a large number of anemom-meters survived Hurricane Frederic and an extensive amount of data is available. Thus it is possible to produce what is perhaps the most complete description available to date of hurricane surface winds over land that is based on actual wind measurements.

The description of hurricane wind speeds and their spatial distribution which is produced by this study has several potential applications in addition to the definition of wind speeds for use in evaluating codes and building practice. A map of wind speeds during Hurricane Frederic which is based largely on observations of damage has been prepared by Fujita, Wakimoto and Stiegler [1]. The wind speeds determined from anemometer measurements will provide a check of the estimates obtained from damage observations. Also mathematical models have been developed for wind speeds associated with hurricanes and for the decay of the storm over land. Two such models have been used in programs for predicting hurricane wind speeds [2,3]. Future work is planned to evaluate the suitability of these mathematical models in describing the measured wind speeds and it is expected that it will be possible to make some estimation of the decay rate of Hurricane Frederic's winds as it moved inland.

ANEMOMETER SITES AND CONDITION OF EQUIPMENT

Wind data from Hurricane Frederic was obtained from ten sites following the storm. Four of the sites were near Mobile, Alabama and six were located along the coast between Gulfport, Mississippi and Fort Walton Beach, Florida. The locations of the sites are shown in Figure 1 together with their relation to the estimated storm track. Although none of the stations were primary National Weather Service (NWS) stations with fastest-mile recorders, four were airport locations and seven had strip chart wind recorders. A brief description of the anemometer sites listing terrain type, instrumentation, height of instrumentation and type of data available is given in Table 1. A classification of terrain types is given in Table 2.

Three of the four airport stations could easily be classified as having open exposure, type 2, conditions for the wind directions experienced during the passage of the hurricane. However, the Pensacola Naval Air Station (PNA) site was not as clean. At PNA, the anemometer was mounted on the control tower roof and experienced an open exposure for winds blowing from directions of 0 to 70 degrees and 185 to 360 degrees, measured clockwise from North. For wind directions between 75 and 180 degrees winds passed over trees which ranged from 20 to 40 feet (6-12 meters) in height and the terrain is assumed to be type 3 or similar to that over the outskirts of towns.

Terrain exposures at several other sites could not be clearly classified as fitting a specific type without any reservations. A brief discussion of the sites follows:

(a) Dauphin Island Bridge (DIB): The instrumentation is located on top of the drawbridge super structure approximately 60 feet (18 meters) above the water level. It is assumed that the exposure is type 1 (sea surface in strong winds), although Dauphin Island forms a barrier to the south and southeast on the bridge. However, because of the height of the instrumentation, the predominance of a sea exposure, particularly from the east, and the fact that the drawbridge portion is at some distance from the main body of the island or mainland, a sea exposure is considered appropriate.

(b) Gulfport Civil Defense (GCD): The instrumentation is located on a tower mounted atop a 25 to 30 foot (8 to 9 meter) building near the center of Gulfport. The strongest winds (only the peak wind speed was recorded) came from the north or northwest across a

large portion of the city. The city is not heavily built up with large buildings, and, consequently, the terrain is assumed to be similar to either the outskirts of towns or centers of towns, type 3 or type 4.

(c) Ingalls Shipbuilding (ISB): The exposure to the north and west is that of open terrain with some small bodies of water. However, there are some large warehouse-type buildings near the fire station where the anemometer was located. Winds from the south and southwest would have a sea exposure but the site was obstructed by cranes and buildings. The assumption that the terrain exposure is type 2 (open terrain) was considered to be reasonable, despite possible local effects due to neighboring buildings. During the storm, a portion of the tower above the anemometer collapsed, the direction vane was destroyed and the anemometer was tilted to the south at approximately 45 degrees. Fujita, et al. [1] also noted this damage and a picture of the anemometer is shown in their report. Wind tunnel tests on a similar anemometer tilted at 45 degrees indicated little change in the velocity measurements and consequently it is suggested that the data not be changed due to the tilt.

(d) Mobile Civil Defense (MCD): The anemometer was located two-thirds of the way up a water tower, (Figure 2) and was shielded for a number of wind directions by the tower legs, struts and center pipe. The tower was located on a rise west of the center of Mobile, about two miles into the suburbs. The city and the suburbs are heavily wooded with the trees being 30 to 50 feet tall (9 to 15 meters). Terrain type 3 or 4 was assumed.

(e) Coast Guard Cutters: The "Salvia" was moored at the Alabama State Docks and was shielded by a warehouse and a larger boat. Consequently, its wind data is highly questionable. The "White Pine" was located midstream in the south channel of the Mobile River south of Twelve Mile Island. The river banks are well forested with pine trees having an average height of 25 to 30 feet (7.5 to 9 meters). It was not possible to visit this site but a detailed report was obtained courtesy of the Quarter Master on the White Pine. This site was one of the most difficult to characterize. Information in Table 2 would lead to an assumption of category 6, pine forest, but that assumption produced wind speeds which were not consistent with any of the other data. Based partly on the results of analyzing the data using different assumptions of terrain type, it was decided to use terrain types 2 or 3.

Most of the instrumentation at the various sites received regular service by either military or NWS personnel and it can be assumed that the data are fairly accurate, indeed as accurate as the data which forms the base for extreme wind speed estimates in other parts of the United States. There are several exceptions. The anemometer at the MCD site had not been serviced for a number of years but it was removed following the storm and calibrated in the NBS wind tunnel by personnel from the Fluid Mechanics Division. Subsequently, data were corrected using the calibration curve. Also, the anemometers on the Coast Guard cutters had reportedly not been serviced since installation.

STORM TRACK

An estimate of the storm track is shown in Figure 1. The track was determined on the basis of radar pictures obtained from the Naval Weather Service at the Pensacola Naval Air Station. One of the radar pictures is shown in Figure 3. The track is similar to the one reported by Fujita, et al. [1]. It is recognized that the center of minimum pressure, the center of the region of minimum winds and the center of the rainless portion in the radar pictures may not coincide. However, in the absence of the detailed pressure and velocity information required, the center of the rainless portion of the radar picture provides a useful approximation of the location of the eye of the storm.

ANALYSIS OF WIND DATA

In order to compare the wind speed data obtained from Hurricane Frederic with design wind speeds, it is necessary to express them in the form of fastest-mile wind speeds in a standard exposure. Normally, such design wind speeds are given for open exposure conditions and a height of 30 feet (10 meters) [2,4]. Consequently, it is necessary to transform the data from the exposure and height corresponding to the actual environment of the instrument to standard exposure and height conditions, and from a mean or gust value to a fastest-mile value.

Procedures for transforming from one averaging time to another, from one terrain to another and from one elevation to another are contained in Ref. [5]. The transformation for different averaging times is based on work by Durst as modified by Simiu and Scanlan [5]. The equation is as follows:

100

$$U_t(z) = U_{3600}(z) \left[1 + \frac{0.98 \ c(t)}{\ln (z/z_o)} \right]$$
(1)

where $U_t(z)$ =   velocity for averaging time t in seconds at height z

    $U_{3600}(z)$ =   mean hourly velocity at height z

     z_o =   roughness parameter for side exposure

     $c(t)$ =   coefficient obtained from table 3, linear interpolation is allowed.

This procedure had not been verified for winds in hurricanes. Consequently, initial work was performed to check the procedure. The check was accomplished by determining peak to mean velocity ratios for 20 to 30 minute segments of the wind records from the seven anemometer sites with strip chart recordings. The peak to mean velocity ratios represent the effect of averaging time, between 2 second averages and 1200 second averages, on the peak velocity estimates. Probability distributions of the peak to mean ratios are plotted in Figure 4 for the seven sites which had strip chart records. Corresponding ratios based on Durst's work as modified by Simiu and Scanlan are plotted at the 50 percent probability level. In general, the agreement is quite good except for the data from MCD where inter-ference of the water tower may affect the data, see Figure 2. Based on this comparison, it was determined that Eq. (1) and the values of c(t) in Table 3 could be used with hurricane wind data.

Procedures for transforming wind speeds from one elevation to another and from one exposure to another are also contained in Ref. [5]. The transformations are based either on the power-law or the log-law and are designed to be used with mean hourly wind speeds. The power-law transformation requires knowledge of the power-law exponent, α, and the boundary layer height, δ, for each terrain in question. The log-law transformation requires knowledge of the roughness length parameter for each terrain. Table 2 contains values of these parameters for the various types of exposure assumed. The values are obtained largely from Tables 2.2.1 and 2.2.2 of Ref. [5] but also rely on input from Ref. [6] and [7]. Judgment was used in order to produce an even gradation of exposure types.

The log-law and power-law relationships may not apply to hurricanes, especially near the eye wall where winds are highest. Furthermore, even if they do apply there is no guarantee that the parameters developed from data for other types of storms are applicable

to hurricane winds. However, the differences between the anemometer elevations and the standard reference elevation are generally small and the approximations involved are likely to be acceptable.

Available mean, one minute average, and gust velocity data were transformed to equivalent mean, gust, and fastest-mile wind velocities for open terrain conditions at 10 meters. Initially, all data was transformed to equivalent mean hourly values. Next, the mean hourly values were transformed from the specific terrain and elevation of the instrumentation to the standard exposure conditions. Finally, the hourly values were transformed to gust and fastest-mile values of the standard exposure conditions. Consistency of the transformations was checked by recalculating the peak to mean velocity ratios for the transformed data. To obtain the peak to mean ratios, gust velocities for standard exposure conditions which were obtained from original gust velocity data were divided by corresponding mean velocity data for standard exposure conditions which were obtained from the original mean velocity readings.

Peak to mean velocity ratios for corrected data at the airport locations with the best defined exposure conditions, i.e., MOB, PRA, and EAF, are shown in Figure 5. The equivalent coefficient from Durst's relationship is also shown. Roughly eighty percent of the peak to mean ratios observed were lower than Durst's value. Figure 6 shows similar probability distributions for peak to mean velocity ratios at the other sites and clearly shows that the transformation is causing the data to collapse toward expected values for open terrain, (solid curve in Figure 5). The only curve which does not collapse well is the one corresponding to MCD data. As noted earlier, the MCD site may suffer from interference effects.

Transformations of the one minute average readings involved an additional step because the data does not represent the maximum one minute average during a certain period of time. Rather, the one minute average reading is taken at an arbitrary time, usually every hour. Consequently, a transformation which uses Eq. (1) and a c(t) corresponding to 60 seconds would be misleading since Eq. (1) refers to maximum values. A relationship between the arbitrary one minute average reading and the fastest-mile reading during that hour has been suggested by Thom [8] and is expressed as follows:

$$U_{fm} = 9.55 + 0.999 \ U_m \tag{2}$$

102

where U_{fm} = fastest-mile wind speed during an hour

U_m = one minute average reading during the same hour.

Consequently, one minute average readings were first transformed to fastest-mile wind speeds which were then transformed to mean hourly wind speeds using Eq. (1).

RESULTS OF DATA ANALYSIS

The results of the data analysis are presented in Figures 7 through 14 as fastest-mile wind speeds during hour intervals. Results are presented for 8 of the 10 sites for times between 1700 hours Greenwich mean time (GMT) on September 12 and 1500 hours GMT on September 13. Data from MCD is not presented because of the questions concerning its quality. The data from GCD consisted of a single peak wind speed observation with the corresponding wind direction.

Note that the fastest-mile wind speeds predicted from the different types of data, including one minute average readings, are quite consistent. This suggests the validity of the data analysis procedures. Different types of terrain conditions were assumed for each of the sites in order to determine the effects of overestimating or underestimating the terrain roughness. Changing the exposure type to the next rougher type could increase the fastest-mile speed from 12 to 25 percent depending on the site. However, the assumption of a terrain category other than the one chosen also resulted in a discrepancy between the fastest-mile wind speeds predicted from the gust speed on the one hand and the mean velocity data on the other hand.

FUTURE WORK

Analysis of the wind speed and direction data from Hurricane Frederic is continuing. Future work includes evaluation of the consistency of the wind speed and direction data by comparing measured values with corresponding radar pictures such as the one shown in Figure 3. A major emphasis will be placed on attempting to fit the mathematical models used in Refs. [2] and [3] to the wind and direction data. These models may provide useful tools for obtaining wind speeds between the anemometer locations and provide a basis for determining the rate of decay of the storm as it moved inland.

REFERENCES

[1] Fujita, T., Wakimoto, R., and Stiegler, D., "Mesoscale Damage Patterns of Hurricane Frederic in Relation to Enhanced SMS Imagery," Proceedings of the 19th Conference on Radar Meteorology, Miami Beach, Florida, April 15-18, 1980.

[2] Batts, M., Cordes, M., Russell, L., Shaver, J., and Simiu, E., Hurricane Wind Speeds in the United States, Building Science Series Report 124, National Bureau of Standards, Washington, D.C., May 1980.

[3] Tryggvason, B., Surry, D., and Davenport, A., "Predicting Wind-Induced Response in Hurricane Zones," Journal of the Structural Division, ASCE, Vol. 102, No. ST12, December 1976, pp. 2333-2350.

[4] "Building Code Requirements for Minimum Design Loads in Buildings and Other Structures," (ANSI A58.1-1972), American National Standards Institute, New York, 1972.

[5] Simiu, E., and Scanlan, R., Wind Effects on Structures, Wiley-Interscience, New York, N.Y., 1978.

[6] Counihan, J., "Adiabatic Atmospheric Boundary Layers: A Review and Analysis of Data from the Period 1880-1972," Atmospheric Environment, Vol. 9, 1975, pp. 871-905.

[7] Engineering Sciences Data Unit, "Characterstics of Wind Speed in the Lower Layers of the Atmosphere Near the Ground: Strong Winds (Neutral Atmosphere)," ESD Item No. 72026, London, England, November, 1972 (with Amendments A and B, October, 1974).

[8] Thom, H.C.S., "Prediction of Design and Operating Velocities for Large Steerable Radio Antennas," Large Steerable Radio Antennas - Climatological and Aerodynamic Considerations, Annuals of the New York Academy of Sciences, Vol. 116, Art. 1, pp. 90-100, New York, N.Y., 1964.

Table 1. Characteristics of Anemometer Sites

Site	Terrain Type(1)	Height of Anemometer	Type of Instrumentation	Types of Data Available		
				Strip Chart	Peak Observation	1 Minute Avg. Readings
Dauphin Island Bridge (DIB)	1	∿18m	3-cup and vane, NWS type	Yes	No	No
Eglin Air Force Base (EAF) (airport)	2	4.6m	3 blade impeller and aerovane	Yes	Yes	Yes
Gulfport Civil Defense (GCD)	3 or 4	∿27m	3-cup and vane, NWS type	No	Yes	No
Ingalls Shipbuilding (ISB)	2	∿10m	3-cup and vane, NWS type	Yes	No	No
Mobile Civil Defense (MCD)	3 or 4	∿23m	3-cup and vane, NWS type	Yes	No	No
Mobile NWS, Bates Field (MOB) (airport)	2	6.7m	3-cup and vane, NWS type	Yes	Yes	Yes
Pensacola Naval Air Station (PNA) (airport)	2 and 3(2)	∿23m	impeller and aerovane	Yes	Yes	Yes
Pensacola Regional Airport (PRA)	2	6.7m	3-cup and vane, NWS type	Yes	Yes	Yes
Coast Guard Cutter White Pine (near Twelve Mile Island)	2 or 3	∿15m above water level	impeller and aerovane	No	Yes	Yes
Coast Guard Cutter Salvia (at Alabama State Docks)	shielded	∿15m above water level	impeller and aerovane	No	No	Yes

(1) See table 2 for description of terrain type.
(2) Type 2 for wind directions 0-70 and 185-360, type 3 for wind directions 75-180.

Table 2. Velocity Profile Characteristics

Exposure Type	Type of Surface	Log-Law Surface Roughness Parameters z (m)	Power-Law Exponent α	Nominal Boundary Layer Height for Use with Power-Law δ (m)
0	Sand	.0005	.10	225
1	Sea surface (high winds)	.005	.12	250
2	Grass (open)	.05	.15	275
3	Outskirts of towns	.20	.19	340
4	Centers of towns	.40	.22	400
5	Centers of large cities	.70	.26	430
6	Pine forest	1.00	.30	460
7	Extremely high roughness	2.00	.35	500

Table 3. Coefficient c(t)

t	1	10	20	30	50	100	200	300	600	1000	3600
c(t)	3.00	2.32	2.00	1.73	1.35	1.02	0.70	0.54	0.36	0.16	0.00
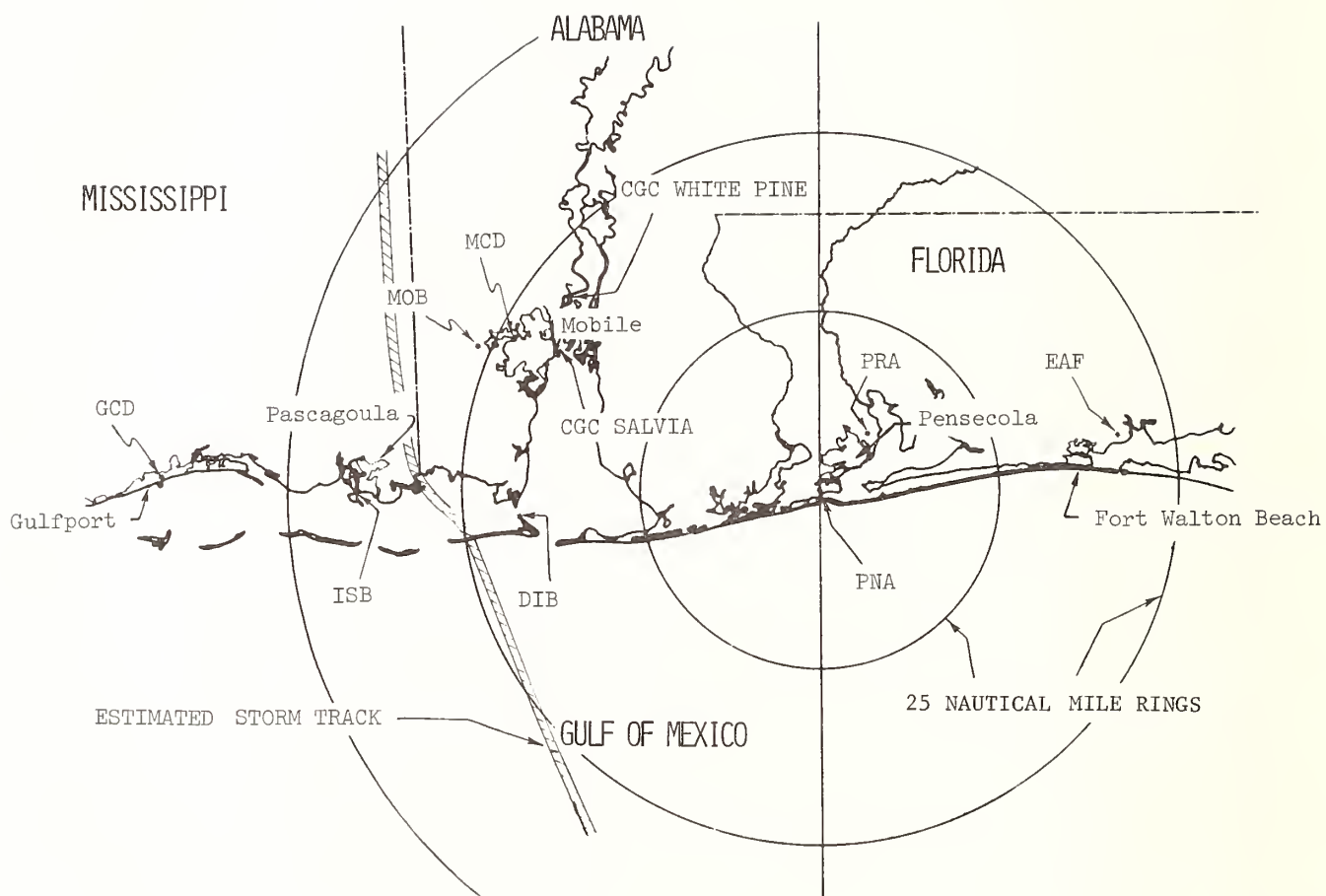
Figure 1. Map of Gulf Coast Near Mobile, Alabama Showing Anemometer Sites.

Figure 2. Anemometer Site at Mobile Civil Defense (MCD).
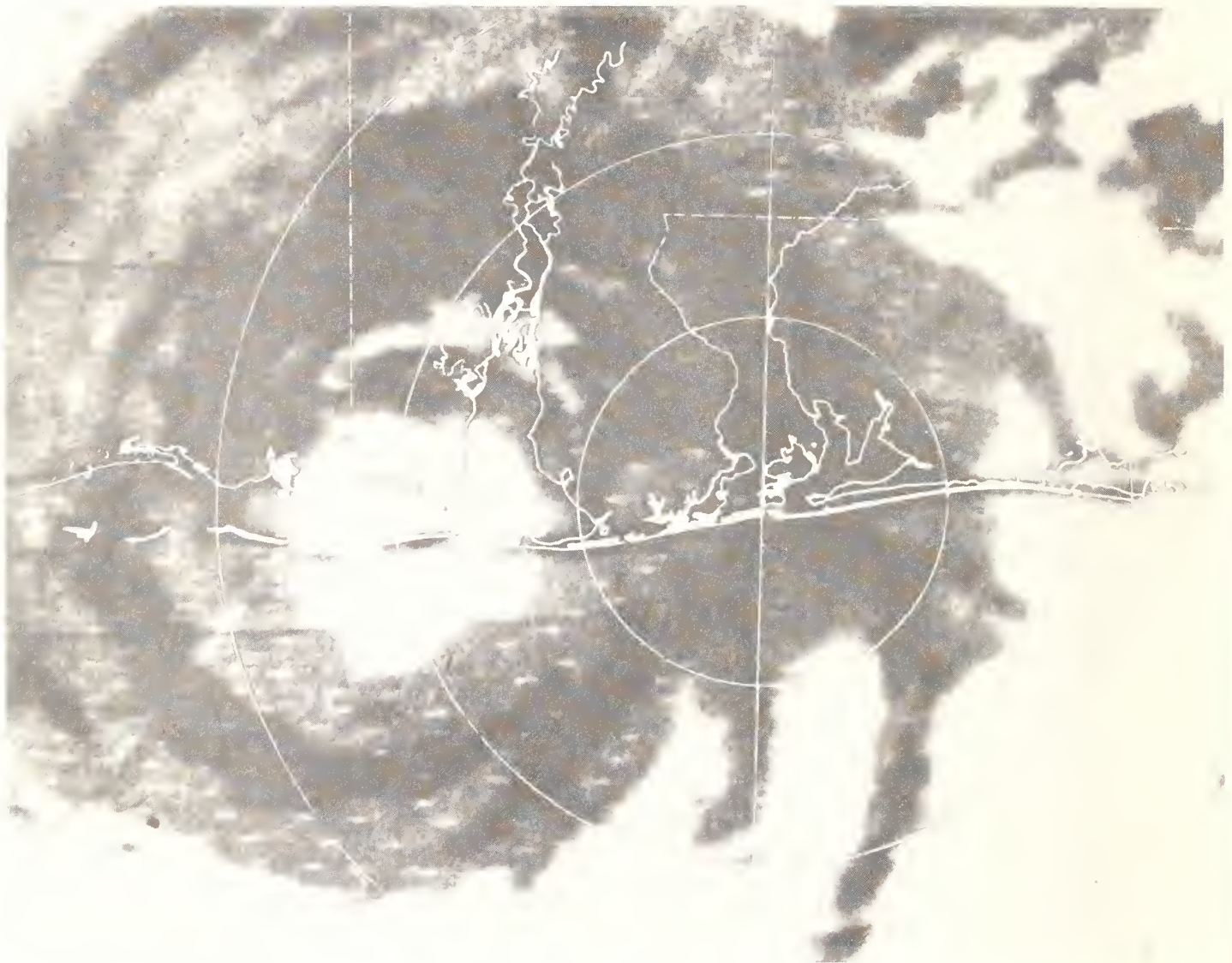
Figure 3. Radar Picture of Hurricane Frederic at 0315 GMT.
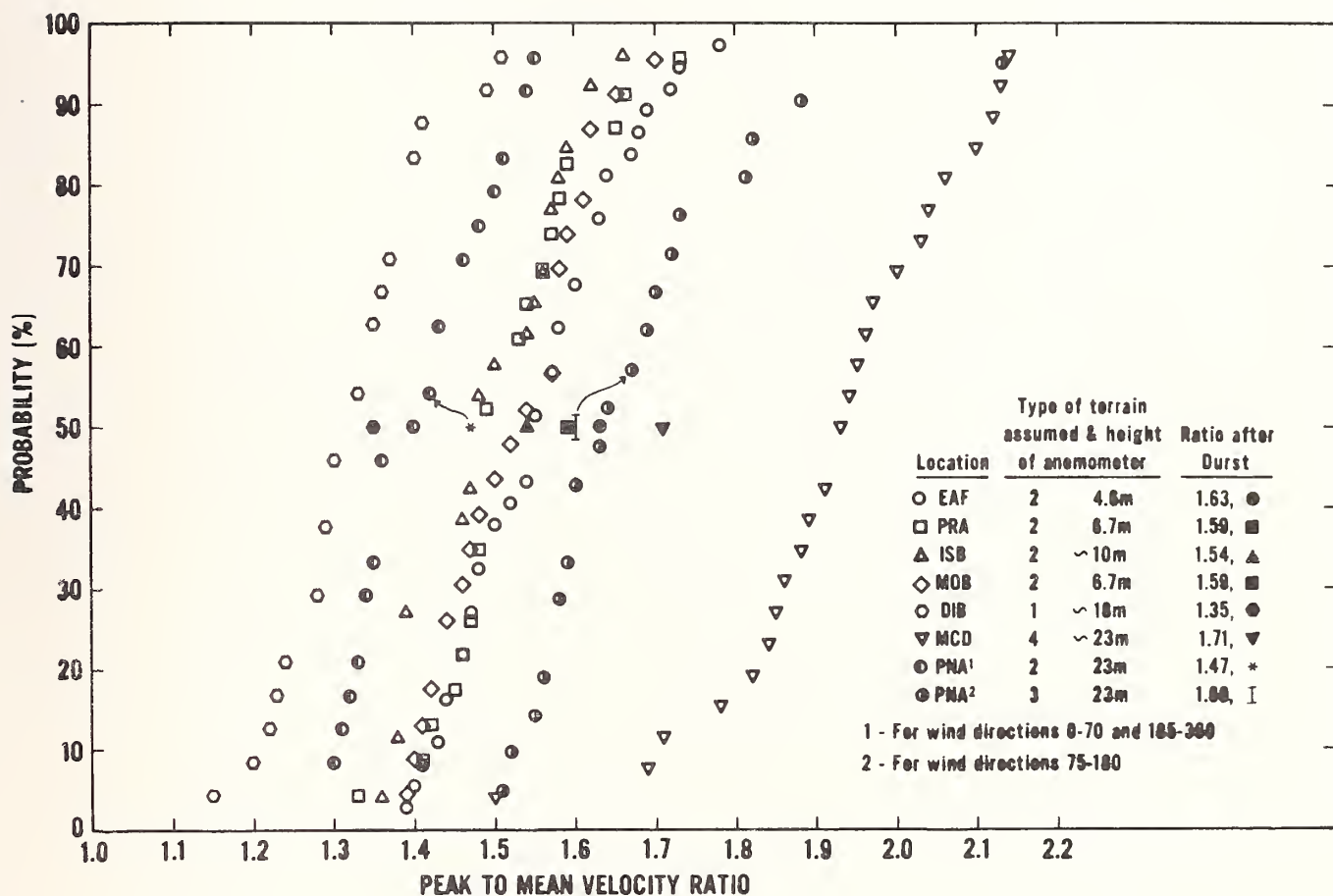
Figure 4. Probability Distributions of Peak to Mean Velocity Ratios
from Actual Data.
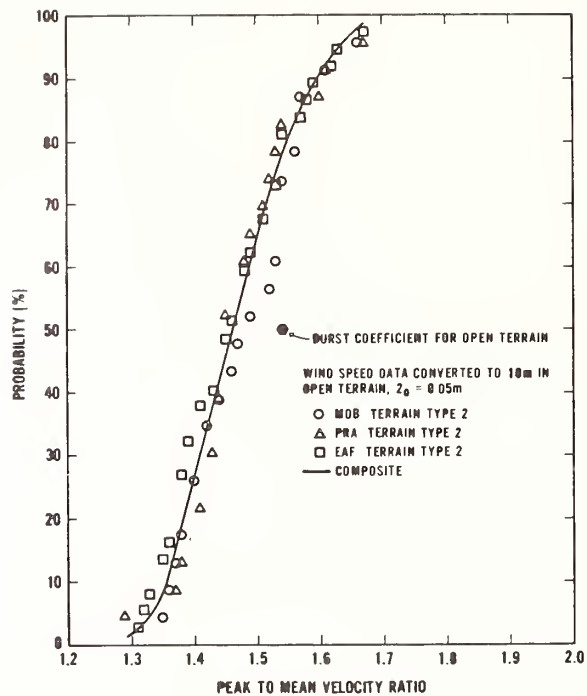
Figure 5. Probability Distributions of Peak to Mean Velocity Ratios
at Three Airport Locations – Transformed Velocities.
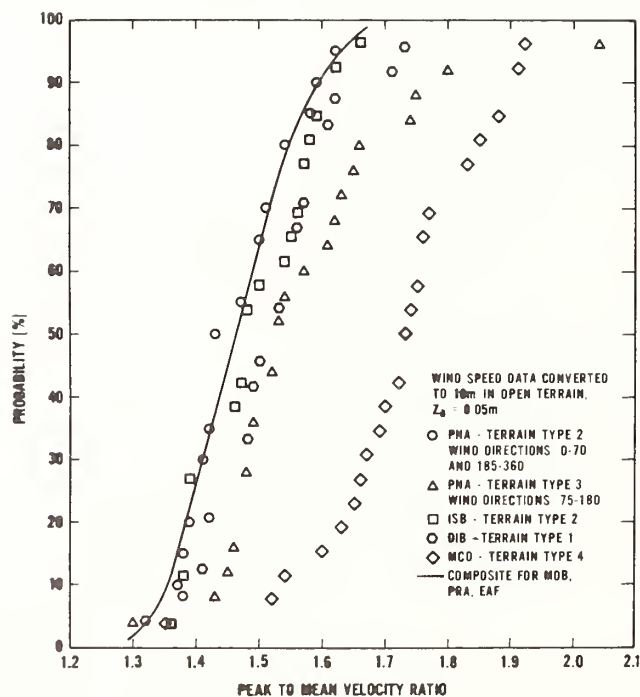
Figure 6. Probability Distributions of Peak to Mean Velocity Ratios
– Transformed Velocities.
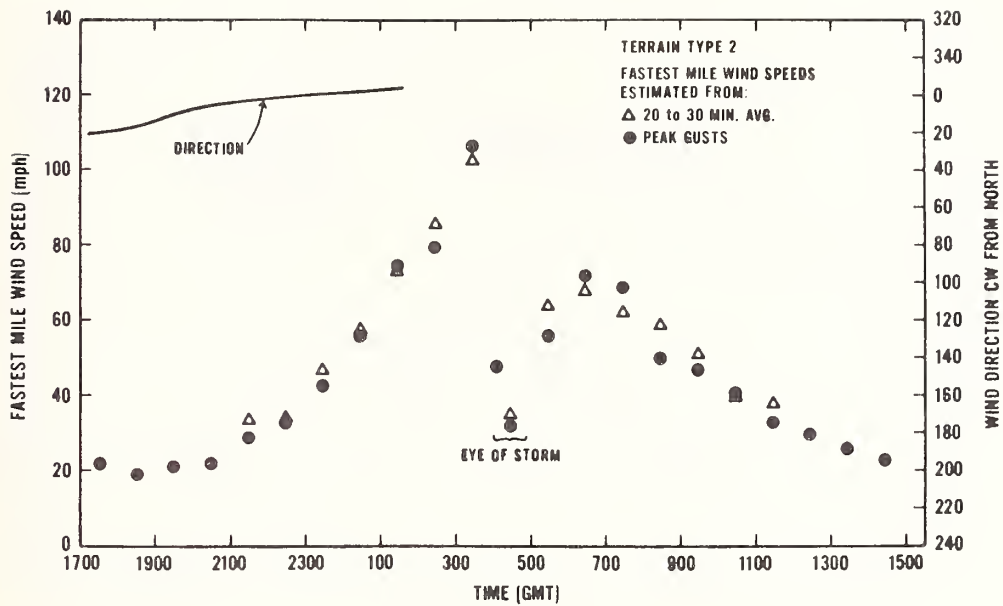
Figure 7. Maximum Fastest Mile Wind Speeds During Hour Intervals at ISB.
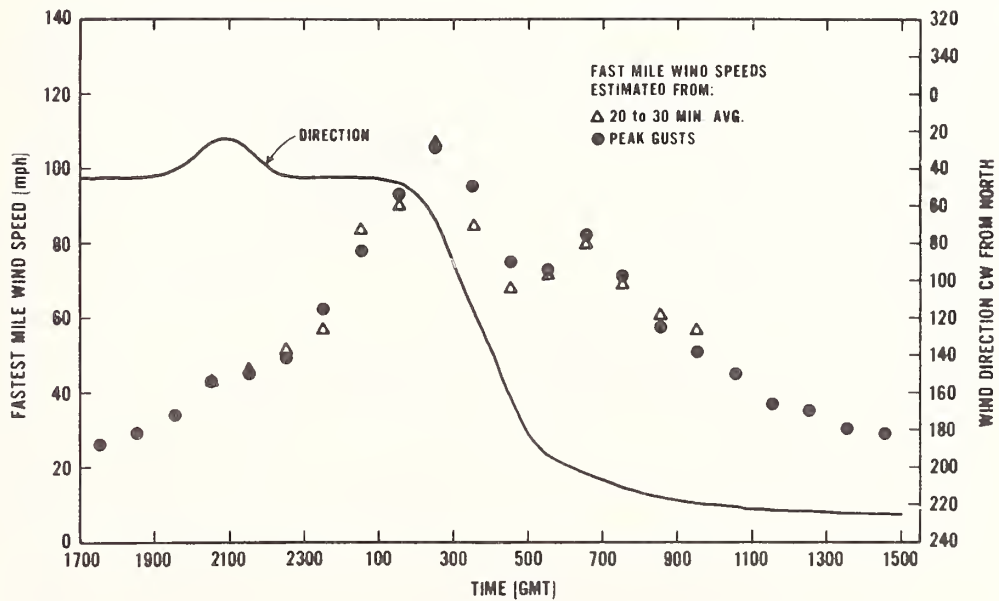
Figure 8. Maximum Fastest Mile Wind Speeds During Hour Intervals at DIB.
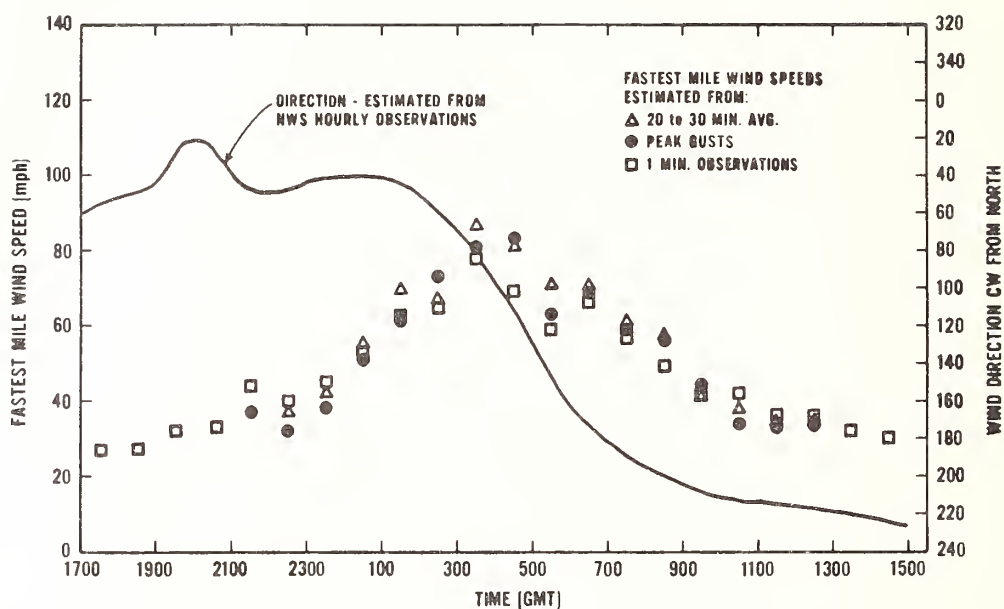
Figure 9.   Maximum Fastest Mile Wind Speeds During Hour Intervals at MOB.
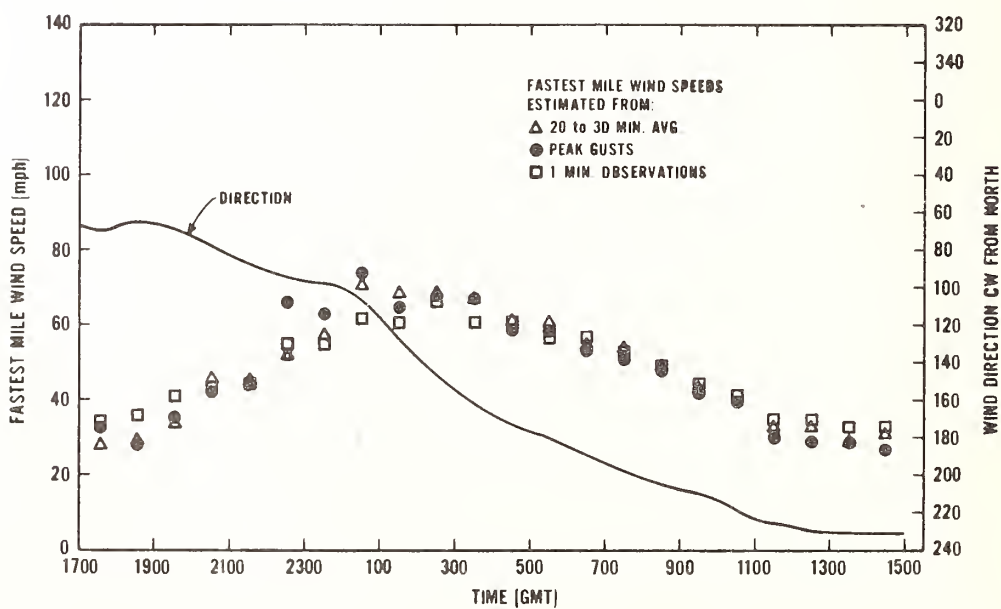
Figure 10.   Maximum Fastest Mile Wind Speeds During Hour Intervals at PNA.
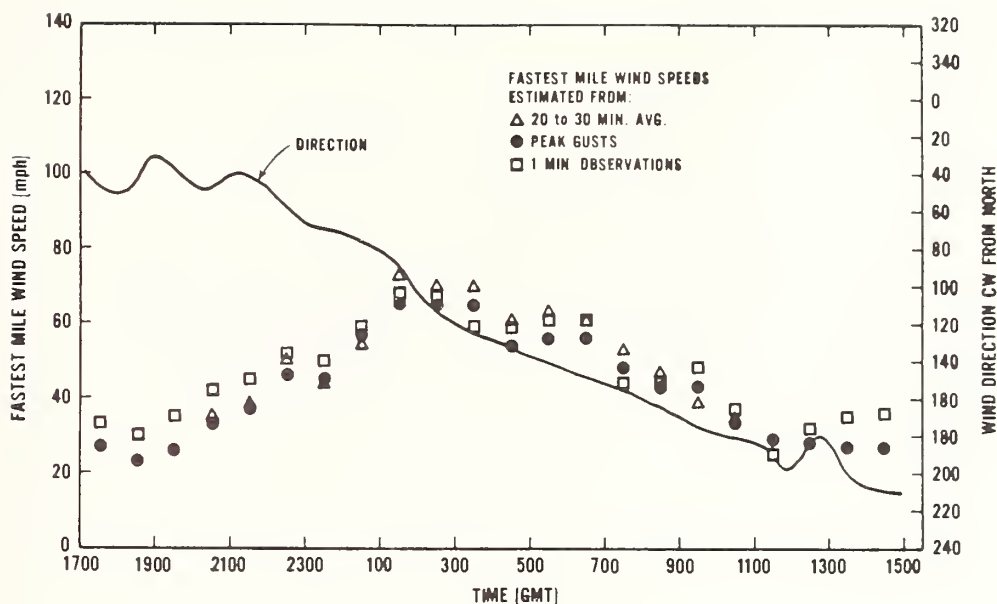
Figure 11. Maximum Fastest Mile Wind Speeds During Hour Intervals at PRA.
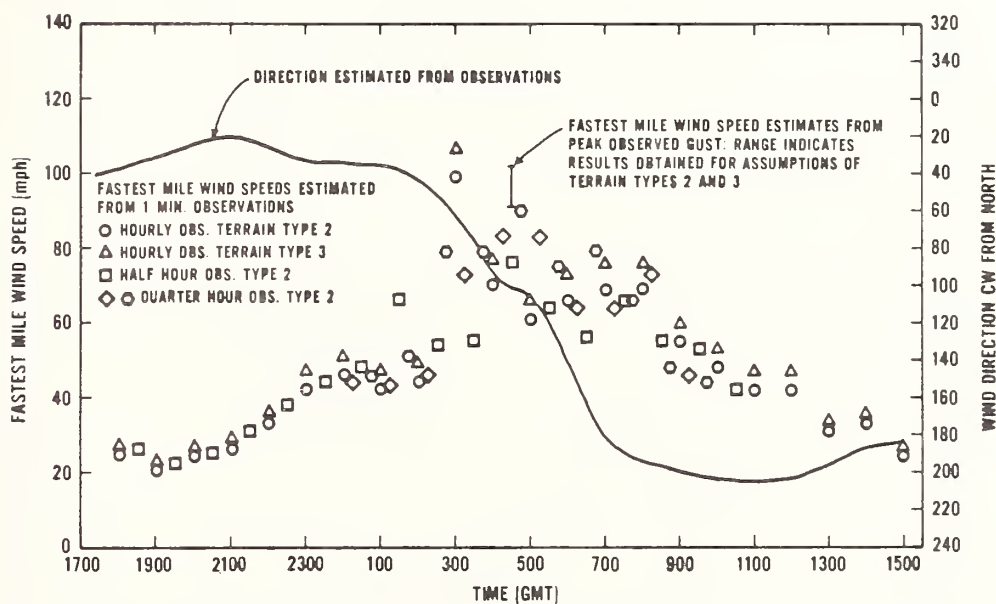
Figure 12. Hourly Fastest Mile Wind Speeds from CGC White Pine at 12 Mile Island.
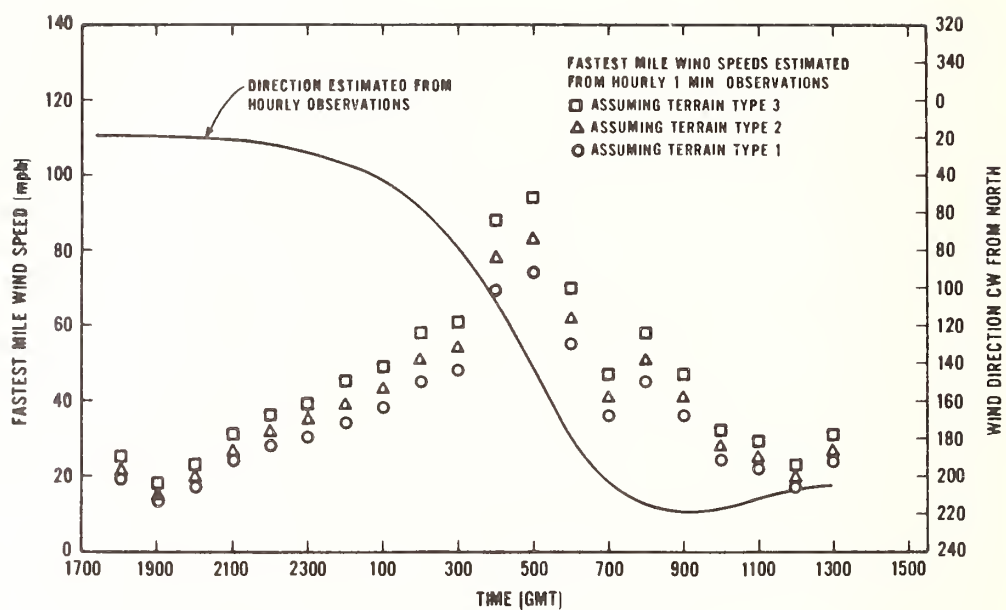
Figure 13.   Hourly Fastest Mile Wind Speeds from CGC Salvia at Alabama State Docks.
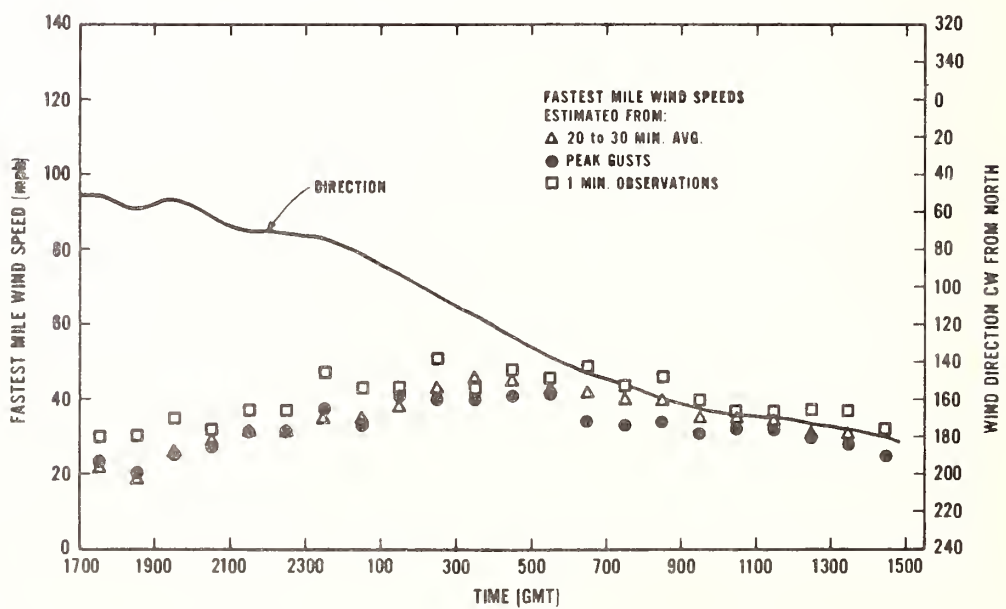
Figure 14.   Maximum Fastest Mile Wind Speeds During Hour Intervals at EAF.

114

HURRICANES DAVID AND FREDERIC 1979

by

Celso S. Barrientos

The 1979 tropical cyclone season indicated some signs of returning to a "normal" situation. These normal characteristics are lower latitude origins and tracks of tropical cyclones, more United States hurricane landfalls and more intense hurricanes hitting land areas in the Western North Atlantic. This "normal" behavior of hurricanes produced the greatest annual combined damage in the United States from tropical cyclones.

Considering equity among the sexes and human rights, 1979 was the first year male names were used for the western North Atlantic hurricanes. Female and male names were used alternatively in an alphabetical list. Although the chance for this happening is relatively small, the two most destructive hurricanes in 1979 were male--hurricanes David and Frederic.

Hurricanes David and Frederic were the strongest pair of storms to occur in the North Atlantic in a decade. In 1969, hurricanes Camile and Debie were the last two such powerful storms that roamed in these waters.

David and Frederic were like brothers--"normal" type hurricanes. Both may be regarded as Cape Verde type. The characteristics are: (1) a seed storm originating from the Cape Verde area; (2) a track of parabolic character around the periphery of the Azores-Bermuda high; (3) an intensity maintained for a long duration unless weakened by landfall; and (4) a size which expands in moving to higher latitudes, and before reaching the United States. Both hurricanes survived for more than two weeks and both caused billion-dollar damage.

David was probably the most intense hurricane of this century in the eastern Caribbean Sea area. It reached a maximum strength of 150 kt and minimum central pressure of 924 mb south of Puerto Rico on August 30, and its strength did not diminish when David struck Dominica and Santo Domingo. It was the strongest hurricane reported at Dominica since 1834 and at Santo Domingo since 1930. Fortunately, David was no longer a major hurricane when it struck the United States. The landfall was just north of Palm Beach, Florida, around mid-day September 3. The central pressure during landfall was 972 mb. Estimated maximum winds were 85 kt. There was little intensity change before the second

landfall near Savannah Beach, Georgia, approximately 24 hours later. Savannah station reported a minimum pressure of 970 mb. Since David was a big hurricane, it affected the whole east coast of the United States.

David left a death toll of 56 in the island of Dominica with 60,000 of the 80,000 residents homeless. There were seven deaths in Puerto Rico and damage estimated as 70 million dollars. The government of the Dominican Republic estimated the death toll there in excess of 1,200 with damage exceeding 1 billion U.S. dollars and 200,000 left homless. In the United States, five deaths were directly attributed to David and total damage exceeded 300 million dollars.

Frederic formed in a manner similar to David. It appeared that a second Cape Verde hurricane would shortly move through eastern Caribbean area while David was still wreaking havoc further west. Fortunately, the strength of David caused the weakening of Frederic as the warm outflowing air aloft from David descended onto Frederic and prevented development. Frederic regained strength when it reached the Gulf of Mexico. Hurricane warnings went into effect from Grand Isle, Louisiana, to Panama City, Florida, at 0930 p.m. CDT September 11.

Frederic became the first hurricane to strike Mobile, Alabama, directly since 1926. The central pressure of 946 mb and estimated maximum winds of 115 kt at landfall made Frederic the most intense hurricane of this century to affect the Mobile-Pascaguoula, Mississippi, area. The highest wind reported in the U.S. was a gust of 126 kt on the Dauphine Island, Alabama, bridge while a gust of 119 kt was observed at the Dauphine Island Sea Lab before the equipment was destroyed. The peak storm surge of 12 feet over Gulf Shores, Alabama, destroyed much of the island. Five deaths have been directly attributed to Frederic. The estimated damage is $2.3 billion. This exceeds the $2.1 billion in damage attributed to Agnes in 1972, and makes Frederic the costliest United States hurricane in history though no adjustment was made for inflation.

SEISMIC RESPONSE OF FLOATING OFFSHORE STRUCTURES

by

Hajime Tsuchida

Susumu Iai

Setsuo Noda

ABSTRACT

A study was made on the technical feasibility of a floating offshore structure from a viewpoint of seismic performance. The structure selected for the study mainly consists of a pontoon and 37 dolphins. The pontoon is 5 km in length and 0.84 km in width and it is connected to the dolphins by links and dampers. The damper has a non-linear force deformation relationship to limit the force to the dolphin below an acceptable level. For the seismic response calculation, a time history of earthquake ground motions covering a very wide period range was needed and a procedure to synthesize such a time history was developed. The seismic response to the synthesized ground motions was calculated. It was found that the structure seems to be feasible for seismic performance.

INTRODUCTION

Recently many floating offshore structures have been proposed as a fishery base, storage facility, airport, and so on. [1,2] In the case of floating offshore structures, a pontoon which may also be called a floating body is moored at a position by a chain and sinker mooring system, a tension leg mooring system, or a dolphin and link mooring system. A study was made to examine the technical feasibility of a large floating offshore structure using the dolphin and link mooring system from a viewpoint of seismic performance. In the study a method to synthesize a time history of earthquake ground motions of wide period range was developed, and an earthquake response of a sample offshore structure to the synthesized motions was calculated. This paper presents the method of synthesis and results of the response calculation.

The floating offshore structure selected as an example in the study mainly consists of a pontoon 5 km in length and 0.84 km in width in plan and 37 dolphins to which the pontoon is connected by the links. The link is connected to the pontoon through a tubular rubber fender and this system is called a damper in this paper. The damper is provided to limit a force in the link below some acceptable level.

The large mass of the pontoon and the spring effect of the damper and the dolphin form an oscillation system with a very long natural period of more than 15 seconds. As input earthquake ground motions to this structure, none of the strong-motion earthquake records available at present are appropriate because the strong-motion accelerograph can not record components of such long period with adequate accuracy. The dolphin itself is sensitive to rather short period components of earthquake ground motions. This is the reason a method to synthesize earthquake ground motions needed to be developed.

It was difficult to assess the earthquake response of the proposed floating offshore structure before the study was made, so the response calculation was computed using synthesized, earthquake ground motions. For the response calculation a number of considerations were involved in organizing the calculation system.

FLOATING OFFSHORE STRUCTURE

The plan view of the selected structure is shown in Figure 1. It consists of a pontoon of 5 km in length and 0.84 km in width and 37 dolphins. The details of the

dolphin and the damper are given in Figure 2. The damper has a non-linear force deformation relationship as can be seen in Figure 3. The damper functions in the following way. When the external forces to the pontoon are not too large, the pontoon is fixed somewhat rigidly and its oscillation is kept small. When rather large relative displacement takes place between the pontoon and the dolphin during an earthquake, the force in the link is kept below an acceptable level so that the force to dolphin is also kept below the level. The soil conditions at the structure site are considered roughly those shown in Figure 2.

When the dolphin is considered to be rigid, the total structure has a natural period of about 18 seconds for sway oscillation. The dolphin, when it is separated from the pontoon, has a natural period of about 1 second. Therefore, it was considered that, for some parts of the structure such as the link and the dolphin, both the long period components and the short period components of earthquake ground motions might be significant. Since the structure employs dampers which show distinct non-linearity, the mode superposition technique is not applicable. So, a time-history of earthquake ground motions covering a very wide period range was synthesized, and the response of the structure was calculated against the synthesized ground motions.

<center>INPUT EARTHQUAKE MOTIONS</center>

The Synthesis of Input Earthquake Motions of a Wide Period Range

Input earthquake motions are usually obtained in two ways; one is to use observed earthquake motions of which amplitude is adjusted for the condition under consideration, and the other is to simulate earthquake source mechanism and wave propagation.

Earthquake motions have been observed by different kinds of seismographs. The period band covered by a seismograph corresponds to the frequency characteristics of the instrument. For example, a SMAC-B2 accelerograph covers a period band from 0.1 second to several seconds, the one-magnification strong-motion seismograph deployed by the Japan Meteorological Agency covers a period band from one second to ten seconds, and the Lp-Lo type seismograph deployed by the Agency covers a period band from 10 seconds to 50 seconds. There is

<center>119</center>

almost no seismograph which covers a period range longer than 50 seconds. Moreover, there is no seismograph which covers a wide period range, for example a range from 0.1 second to ∞ seconds.

Theoretical seismograms are obtained using several different kinds of earthquake source mechanism and wave propagation models. Period range covered by the model depends on the complexity of the model. For example, fault models which are considered simplest [3] cover a period range from several ten seconds to ∞ seconds. Although the number of parameters required for this model is not small, most of the parameters can be obtained. There are several models which are more complex and cover a wider period range [4]. Information currently available on the earthquake source mechanism is, however, not enough to determine the parameters of these complex models.

In order to cover a wide period range from 0.1 second or short to ∞ seconds, a synthesis method of input earthquake motions of a wide period range was proposed by the authors [5]. The method is as follows: The wide period range is divided into four bands; one from 0.1 to 1-2 seconds, one from 1-2 to 6-10 seconds, one from 6-10 to 30-50 seconds, and one longer than 30-50 seconds. The borders between the bands are not sharp and they are expressed as period ranges.

The input earthquake motions are synthesized from four components of earthquake ground motions corresponding to these four period bands. The component of the period band longer than 30-50 seconds is theoretically calculated by a fault model and the other three are formed by adjusting the amplitudes of seismograms of actual earthquake motions observed by three types of seismometers. The amplitudes are adjusted according to empirical formulae on relationship among maximum recorded amplitude, magnitude, and distance to epicenter or fault plane from observation point. The empirical formulae are: the formula of surface wave magnitude [6], Tsuboi's formula [7], and Noda and Uwabe's formula [8], respectively. Each component is filtered by a corresponding band-pass filter after adjusting the amplitudes. Initial time of each component is adjusted so as the arrival times of the S waves of each component coincide. Finally, these four components are summed up to form input earthquake motions. It is believed that the earthquake ground motions synthesized in this way are reliable and achievable considering the present state-of-the-art in earthquake engineering and seismology.

Phase Delay of Input Earthquake Motion on a Base Layer

As the dolphins are located over a wide area, the time lag of seismic wave arrival among the locations of the dolphins has to be considered. In the study, seismic waves are considered to propagate in 3.5 km/s in a base layer straight from the epicenter to the structure location. The velocity 3.5 km/s is considered, in seismology, to be the velocity of S-wave propagation through the earth crust. Although actual seismic wave propagation in a base layer may be complex, this treatment of phase delay is a practical and acceptable conception in engineering practice.

Wave propagation has been observed by two of the authors using a two dimensional seismometer array which extends 2500 meters [9,10]. It is hoped that analysis of the data from this observation will provide further information.

Synthesis of Input Earthquake Motions

One earthquake considered in this study is of magnitude 8.1. Parameters of this earthquake and other data used for the synthesis are summarized on Table 1. Figure 4 shows the ground motions of four period bands and the synthesized motions. Figure 5 shows the input earthquake motions synthesized for the response analysis.

RESPONSE CALCULATION

The response calculation was made using the procedure shown in Figure 6. The surface layer overlying the design base level is idealized into a lumped mass system with non-linear springs which represent the soil stiffness, and the response of the system to the synthesized ground motions was calculated. This response was considered as input motion to the dolphins. The dolphin without the linkage to the pontoon was idealized into a lumped mass system as shown in Figure 7 and response was calculated. Stresses in the piles due to the earthquake response were next calculated. The modal analysis of the idealized system was made and the natural periods of the modes were estimated.

In the earthquake response calculation of the total structure, each dolphin was idealized into a single mass system. If each dolphin had been idealized as the model in Figure 7, the model of the total structure with 37 dolphins would have too many elements

to be accomodated in a computer of a practical, available size. For this reason the dolphin was idealized into the single mass system. The idealization was based on the result of a model analysis of the dolphin.

The mass of the idealized model representing the mass of the dolphin was connected to the pontoon with a spring which represented the force deformation relationship of the damper in Figure 3. The pontoon was assumed to have freedom of displacement in the x-axis direction (sway), in the y-axis direction (surge), and rotation about the z-axis (yaw). The model of the total structure for the response calculation is shown in Figure 8. Damping by sea water was estimated from the numerical simulation [11].

When the dolphin was idealized into the single mass system, interaction effects between the pile and the surface layer could not be taken into the response calculation. Therefore, for calculating stresses in the piles, the stresses calculated from the earth-quake response of the dolphin without linkage to the pontoon and the stresses due to the force in the link calculated in the earthquake response of the total structure were super-posed. In principle, this is not accurate; however, it may be acceptable from a practical point of view.

Accelerations, velocities, and displacements of the pontoon are shown in Figures 9, 10, and 11, respectively. Deformation and force of one of the dampers (at the connection between the No. 11 dolphin and the pontoon) are shown in Figure 12.

From this study, the floating offshore structure appears feasible from a seismic performance point of view. Further details of this study are available in separate papers [5,12].

CONCLUSIONS

(1) A procedure to synthesize the time history of earthquake ground motions covering a very wide period range was developed and presented.

(2) A procedure to calculate the earthquake response of a floating offshore structure which consists of a pontoon, dolphins, links, and dampers with non-linear force deformation relationships was organized and presented.

(3) From the response calculation, the floating offshore structure considered in this study was found to be technically feasible from a seismic performance viewpoint.

REFERENCES

[1] Kato, W., "Planning of Offshore Building-Project '76 Offshore Fishery Base," Column, No. 66, October 1977, pp. 29-36.

[2] Offshore Airport Study Group, "Floating Offshore Airport in Osaka Bay, Japan, Digest of Preliminary Engineering Study," Proceedings of the First International Conference on Offshore Airport Technology, Bethesda, Maryland, 29 April-2 May 1973, Vol. 2, pp. 43-49.

[3] Haskell, N. A., "Elastic Displacement in the Near-field of a Propagating Fault," Bulletin of the Seismological Society of America, Vol. 59, No. 2, April 1969, pp. 865-906.

[4] Wiggins, R. A., Sweet, J., and Frazier, G. A., "Seismic Risk for Offshore Structures," 10th Annual Offshore Technology Conference in Houston, 1978, pp. 529-533.

[5] Iai, S., and Tsuchida, H., "A Synthesis Method of Input Ground Motions of a Wide Period Range," Report of the Port and Harbour Research Institute, Vol. 19, No. 1, March 1980, pp. 63-96.

[6] Utsu, T., "Seismology," Kyoritsu Publisher, January 1978.

[7] Tsuboi, C., "Determination of the Gultenberg-Richter's Magnitude of Earthquakes Occurring In and Near Japan," Jishin, II, Vol. 7, No. 3, 1954, pp. 185-193.

[8] Noda, S., Uwave, T., and Chiba, T., "Relation Between Seismic Coefficient and Ground Acceleration for Gravity Quaywall," Report of the Port and Harbour Research Institute, Vol. 14, No. 4, December 1975, pp. 67-111.

[9] Hayashi, S. and Tsuchida, H., "Observation and Analysis of Ground Response in Earthquakes," Proceedings of the Sixth Joint Meeting of U.S. - Japan Panel on Wind Seismic Effects, U.S.-Japan Natural Resources Conference (UJNR), May 1974.

[10] Tsuchida, H., Kurata, E., and Hayashi, S., "Observation of Earthquake Response of Ground with Horizontal and Vertical Seismometer Arrays," Proceedings of the Sixth World Conference on Earthquake Engineering, Vol. 1, January 1977, pp. 509-514.

[11] Ueda, S. and Shiraishi, S., "On the Characteristics of Oscillations of Multi-Cylinder Floating Structure by Numerical Simulation," Technical Note of the Port and Harbour Research Institute, No. 339, July 1980 (in press).

[12] Iai, S. and Tsuchida, H., "Earthquake Response Analysis of Floating Type Structure," Technical Note of the Port and Harbour Research Institute, No. 337, July 1980 (in press).

Table.1 Procedure of synthesis of the earthquake motion of a wide period range

Period Band	Longer than 30-50 s	From 6-10 s to 30-50 s	From 1-2 s to 6-10 s	From 0.1 s to 1-2 s
Formation of seismic wave	Simulation by a fault model	Actual seismic wave observed by Lp-Lo type seismometer of J.M.A.	Actual seismic wave observed by LM_L type seismometer of J.M.A.	Actual seismic wave observed by SMAC-B2 type strong-motion accelerograph
Determination of peak value	Simulated wave itself	Formula of surface wave magnitude[6]	Tsuboi's formula[7]	Noda and Uwabe's formula[8]
Earthquake of the record wave used for the formation of the seismic wave		1977.12.24.06.02 Epicenter 39°04'N 143°38'E 0 km Magnitude 5.9 Observation station: Matsushiro		1978 Miyagi-ken Oki Earthquake 1978.06.12.17.14 Epicenter 38.09°N 142.12°E 40 km Magnitude 7.4 Ofunato
Parameters of the assumed earthquake	Fault length 120 km width 80 km dip 10° strike N40°E Dislocation 3.1 m N50°W Rise Time 9.2 s Rapture Velocity 3.0 km/s Rapture direction N50°W V_p 6.0 km/s V_s 3.5 km/s	Surface wave Magnitude $M_s = 8.2$ Epicentral Distance 155 km	Magnitude (J.M.A.) $M_J = 8.1$ Epicentral distance 155 km	Magnitude (J.M.A.) $M_J = 8.1$ Distance to the fault plane 81 km

5000 m

840 m

Pontoon
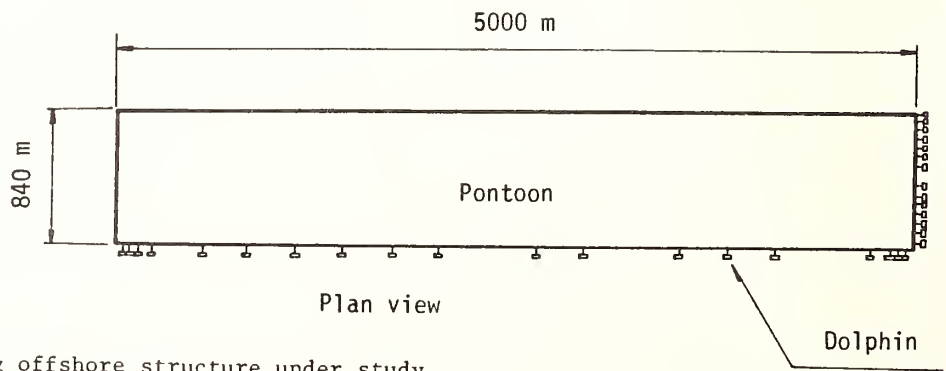
Plan view

Dolphin

Fig.1 Plan view of floating offshore structure under study
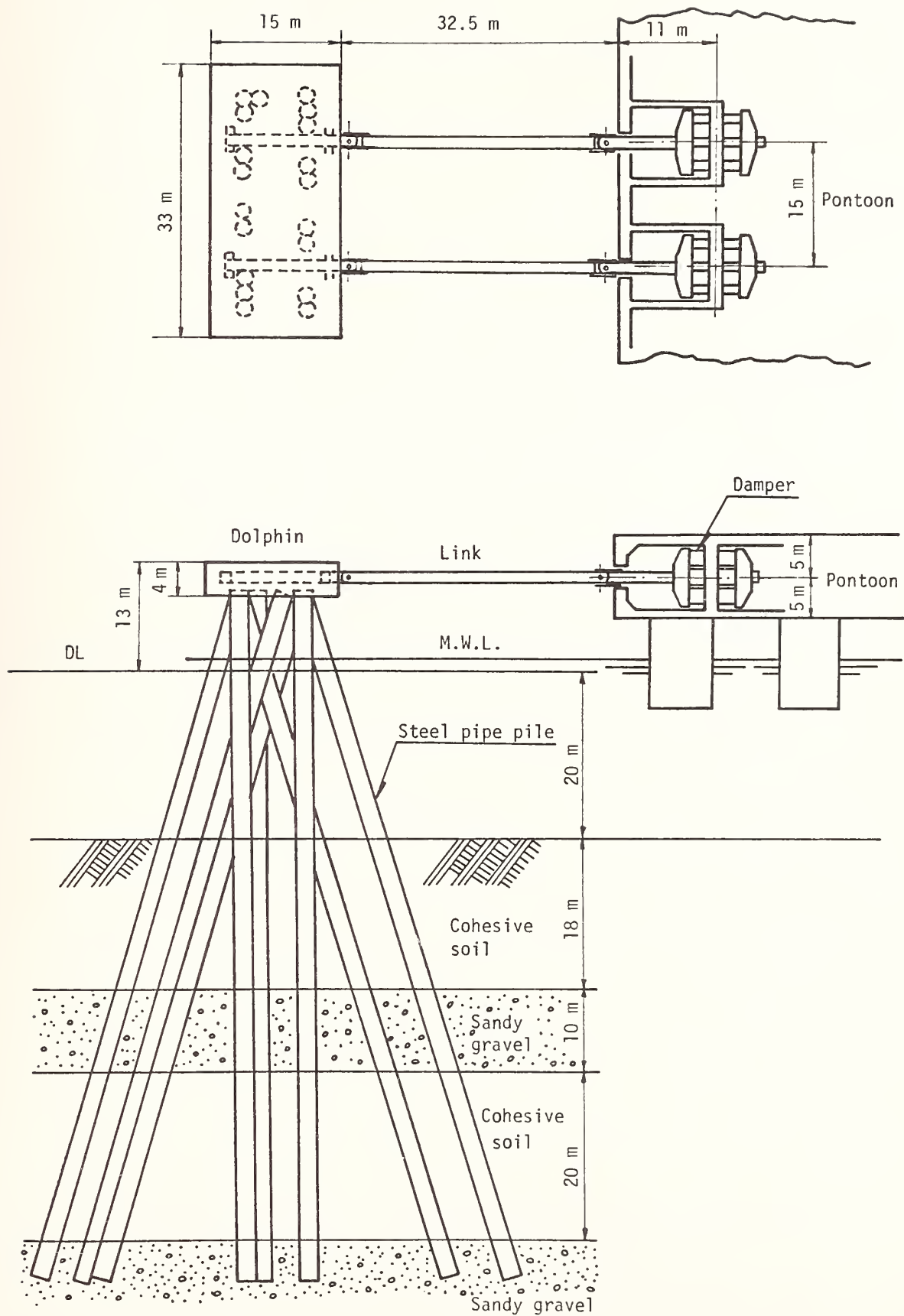
Fig.2 Dolphin and damper

125
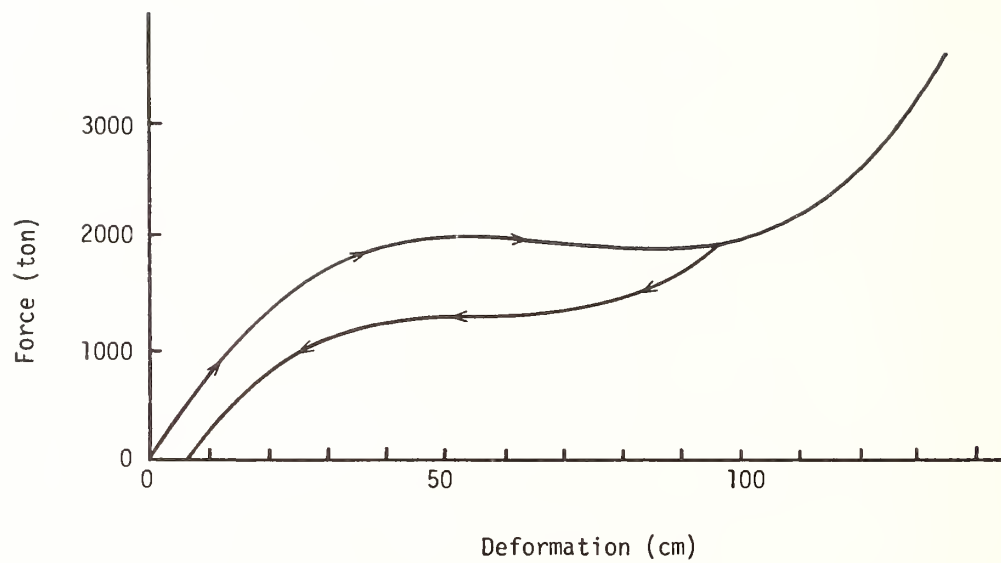
Fig.3 Load-deflection relationship of damper
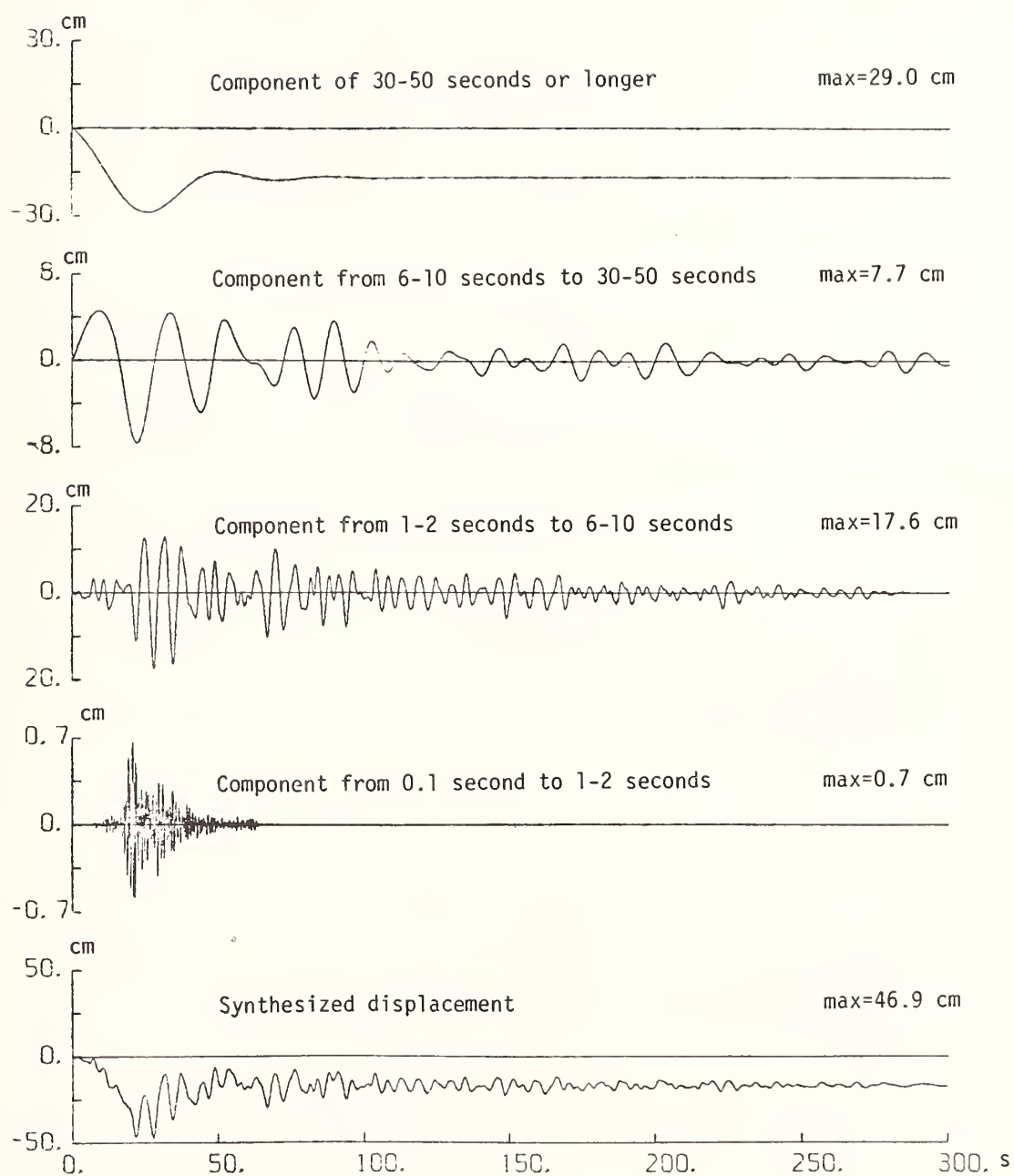
Fig.4 Ground motions for four period bands and synthesized motions
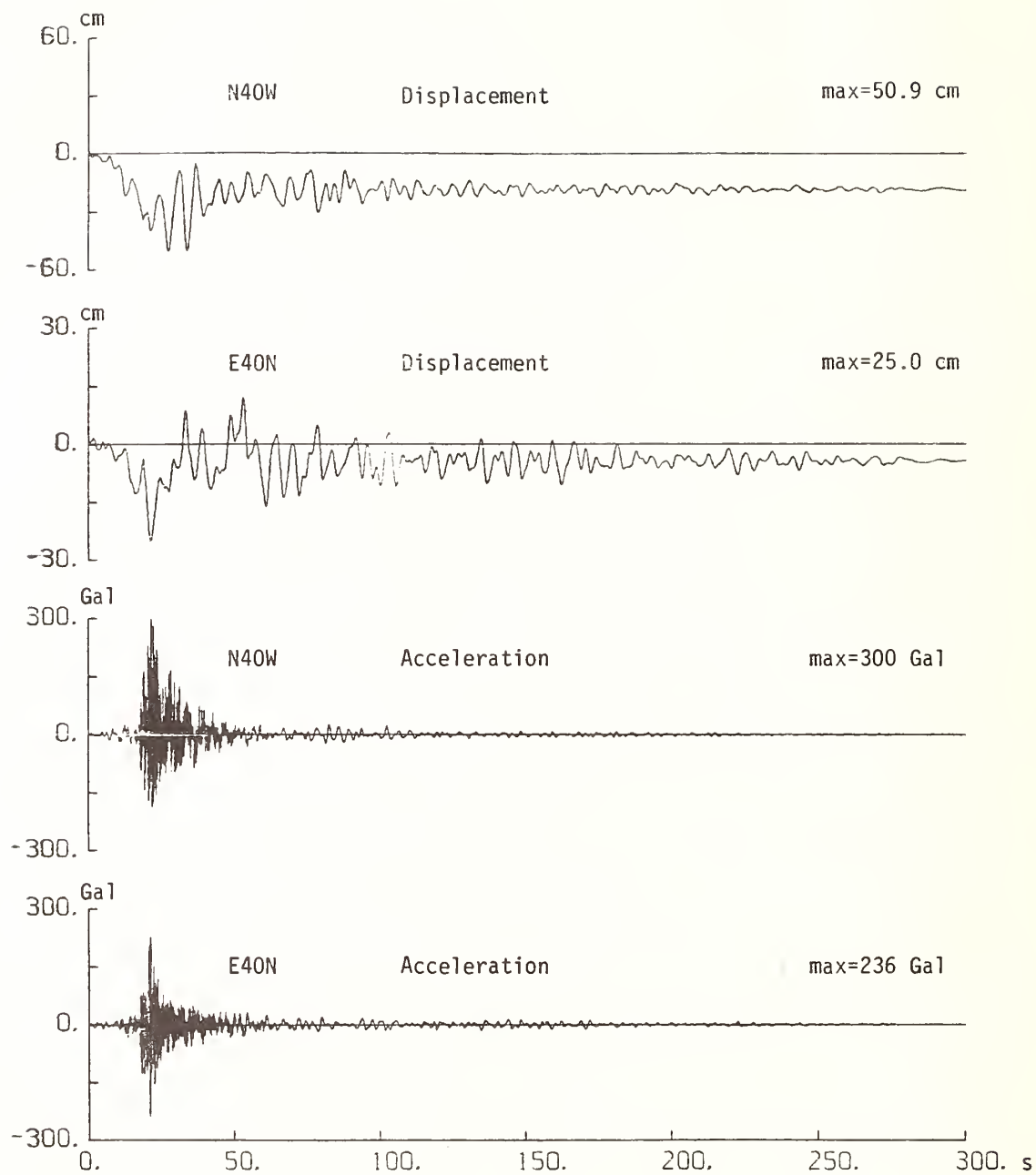
Fig.5   Input earthquake motions for reponse calculation
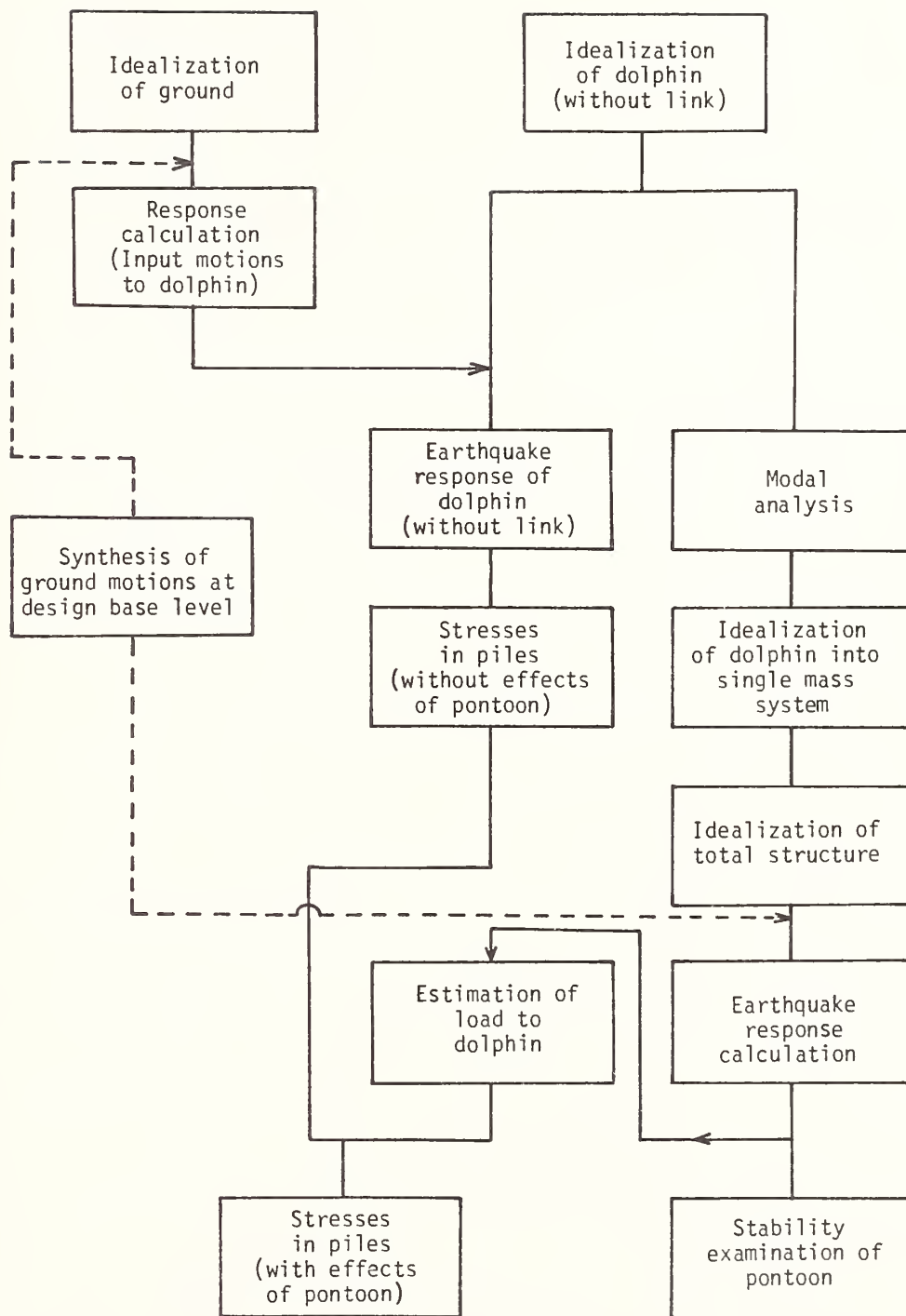
Fig.6 Flow of response calculation

Fig.7 Idealization of dolphin
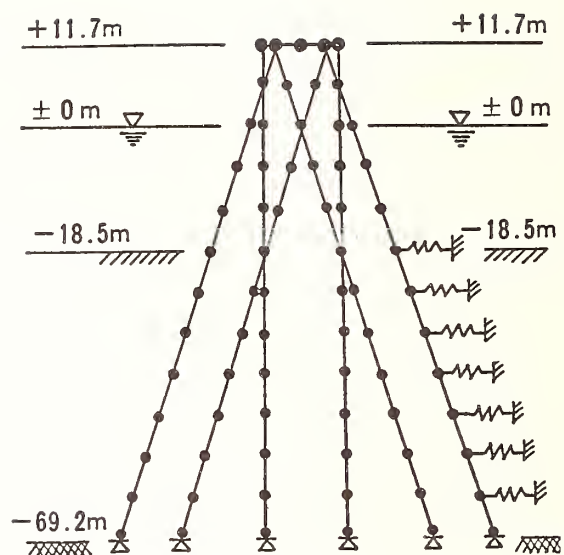
Fig. 8 Idealization of floating offshore structure under study

130
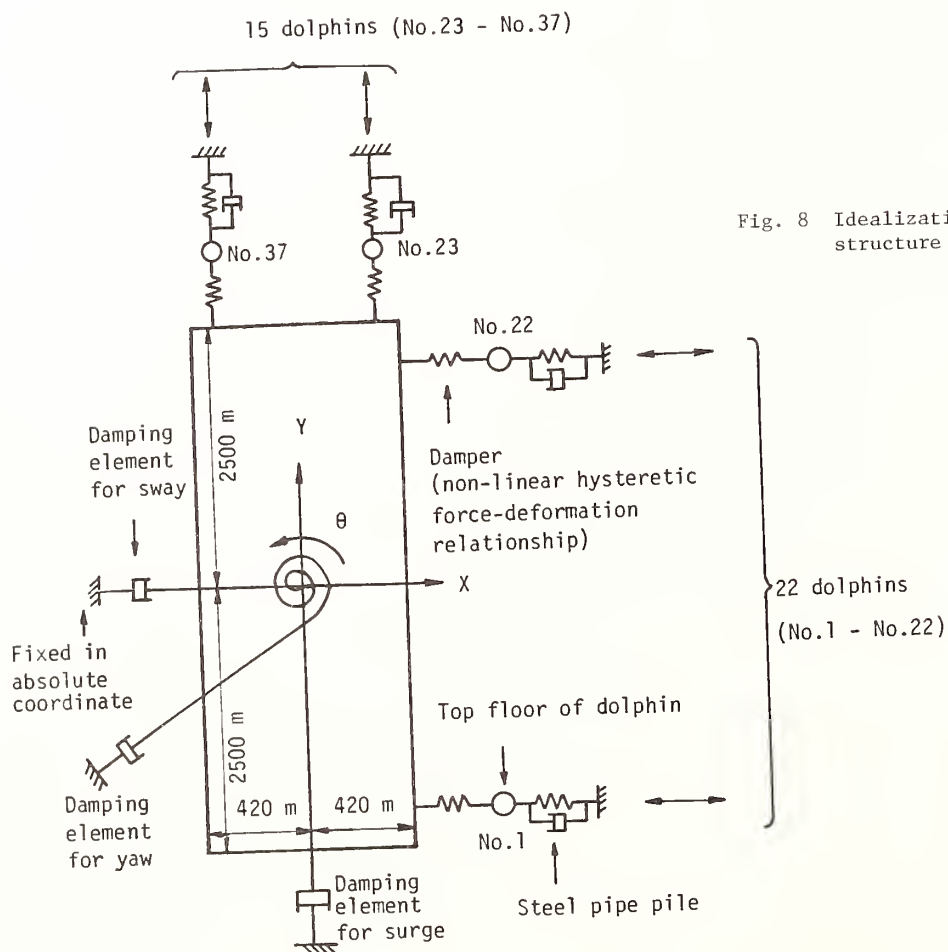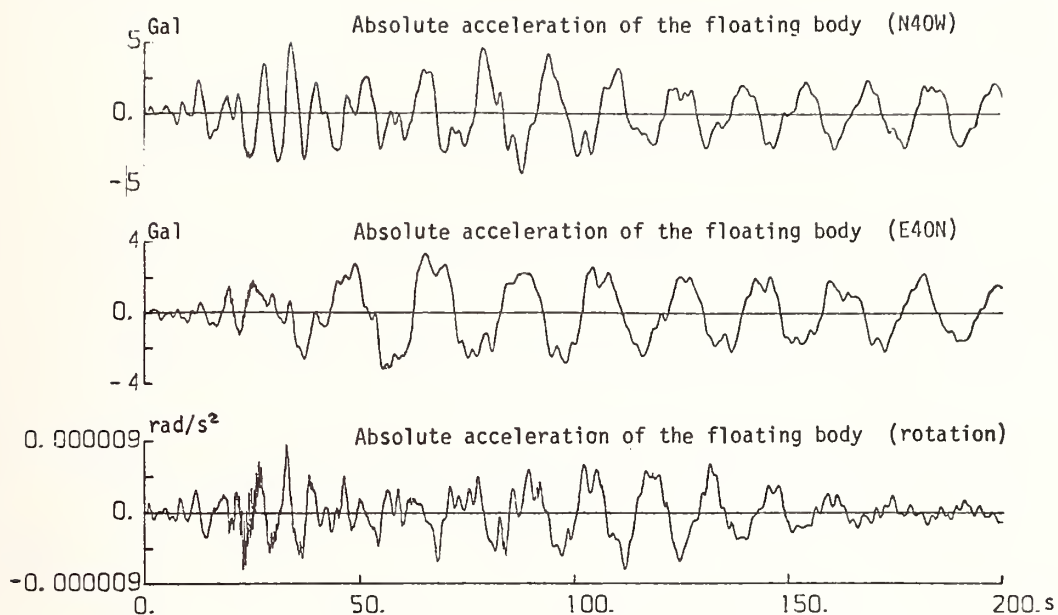
Fig.9 Acceleration response of pontoon
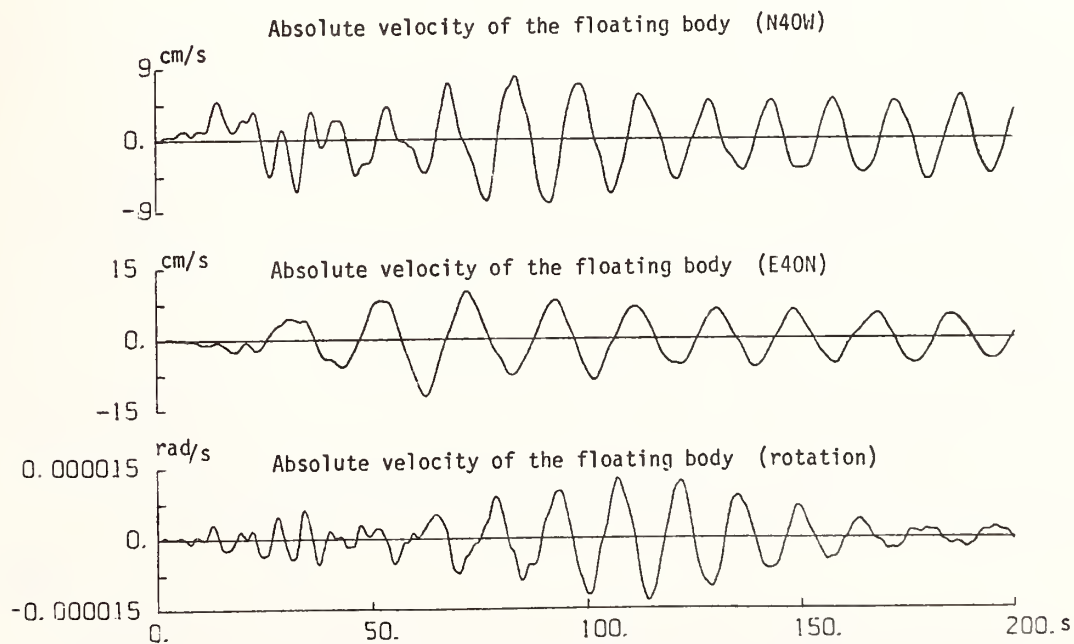
Fig.10 Velocity response of pontoon

Absolute displacement of the floating body (N40W)

Absolute displacement of the floating body (E40N)

Absolute displacement of the floating body (rotation)
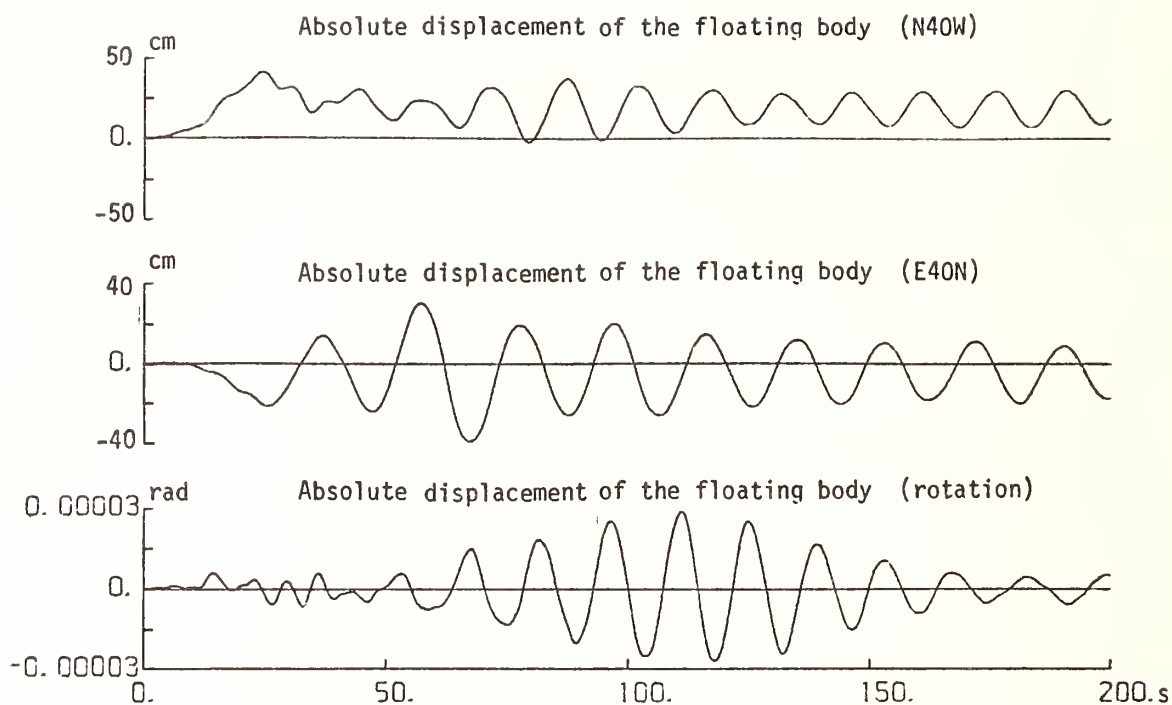
Fig.11   Displacement response of pontoon

DOLPHIN 11 (N40W direction)
Deformation of the damper

Reaction force of the damper
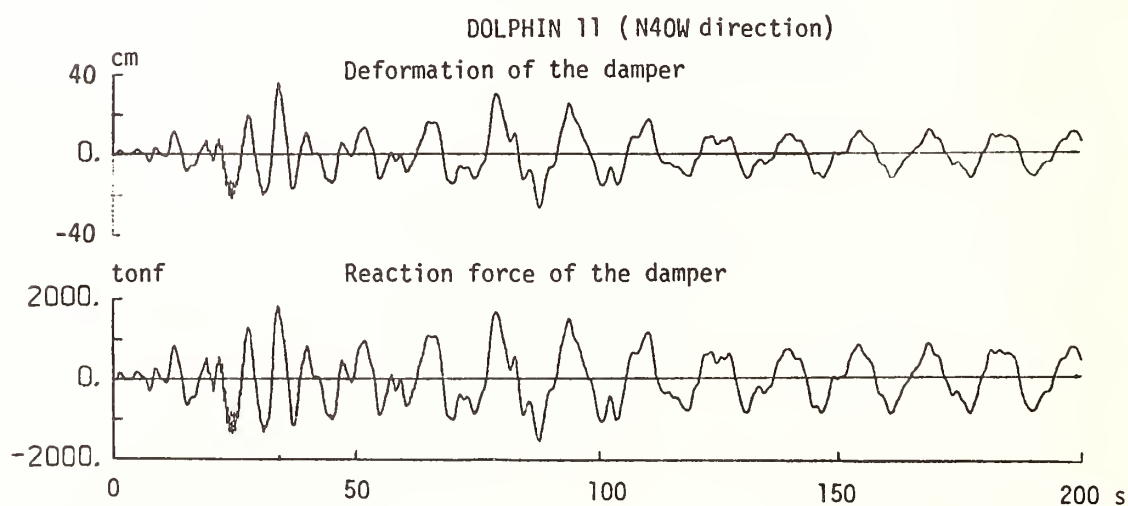
Fig.12   Deformation and reaction force of the damper (Dolphin 11)

CRITICAL EXCITATIONS OF STRUCTURES

by

R. F. Drenick

F. Novomestky

G. Bagchi

INTRODUCTION

This paper is, in a way, a progress report on the development of a new method for the assessment of structural reliability under dynamic (and notably under earthquake) loads. The main advantage of the method is that it leads to results which are valid on a rather high level of confidence. Such levels are often achieved at a price of excessive conservatism. The method avoids this by extrapolating from pertinent experience (concerning e.g., strong ground motion) to all other excitations that can realistically be expected at the site of interest. Among these excitations, it then determines those which are least favorable to the structure. The determination has some characteristics which are unusual in structural dynamics. Among them is the fact that it requires nonlinear programming methods for its solution. The procedure has been called the "critical excitation method."

The high level of assurance to which the critical excitation method aspires can be achieved by avoiding the use of information, particularly of a probabilistic kind, which is not available on a comparable level. The paper first develops the line of reasoning which indicates the need for this avoidance, then shows that the need leads to the method in a rather natural way. It proceeds to give a brief account of the problem that must be solved, and of the way in which it is being solved, as of this writing. Some typical results are quoted from a recent assessment of the earthquake resistance of a nuclear power plant in the Southeastern United States. The paper concludes with a discussion of some of the advantages and disadvantages of the method.

Most of the discussion in the paper tacitly assumes that the problem of interest is an assessment of structural reliability under dynamic loads due to strong ground motion. Similar reliability problems however are equally good candidates for the treatment by the method.

NON-ROBUSTNESS PROBLEMS

It has been pointed out in the preceding section that an assessment of the earthquake resistance of a structure should avoid information which is not available on a high confidence level, high enough at any rate to be comparable with the desired reliability of the structure. Such information is rather scant on strong ground motion. Vanmarcke [2] suggests that the following items might qualify.

(a) Duration of strong ground motion

(b) Ground motion intensity, its peak value as well as its variation with time

(c) Envelope of the amplitude spectrum

(d) Effects of macro-zone, micro-zone and site soil characteristics

(e) Effect of focal distance

To these five items, one can add a sixth, namely

(f) Bounds on the peak ground acceleration and velocity.

Some of this information is quite specific but some of it is rather qualitative (and none of it, one might note, is of a clearly probabilistic nature). One can perhaps use it to identify excitations which are patently inconsistent with all current seismic theory and experience, and which therefore are not realistic candidates for ground motions at a particular location. On the other hand it does not seem quite adequate to define those that are such candidates, let alone the probabilities of their occurrence.

It has been customary in the theoretical work in the field to supply the missing information by assumption. This is alright provided the results that are obtained in this fashion are "robust": the effect on them of variations in the assumptions must be weak. In reliability problems in general, however, results often are far from robust, and the problem of earthquake resistance appears to be no exception. One might go so far as to say that any information that can safely be supplied by assumption may be unnecessary in the first place.

134

Evidence of an analytical sort, and pointing to non-robustness, was presented in a predecessor paper [1]. It may be of interest to add here some numerical support. It bears more specifically on the non-robustness of assessments of structural earthquake resistance, relative to an almost universal assumption namely, that the ground motion during an earthquake is a sample function from a Gaussian random process. The question then is whether such assessments are affected by small variations away from the Gaussian probability measure. The answer is that they are affected, and often quite strongly so.

Figure 1 shows two pairs of probability densities. One is Gaussian. The other is Gaussian as well but only up to the points $y_0 = \pm 1.5\ \sigma$. Beyond y_0 is non-Gaussian and of a form already used in [1], namely

$$p(y) \; = \; \frac{a}{s}\left|\frac{y}{s}\right|^{m} \exp\left(\; - \; \frac{1}{r}\left|\frac{y}{s}\right|^{r}\right).$$

The parameter a is so chosen that the transitions at y_0 are continuous. The difference between the two densities are evidently small, as Figure 1 shows, no doubt too small to be detected from statistical analysis of ground motion records.

The effect of the difference can be quite large however. If the exceedance of the danger level L in Figure 1 is the assessment criterion, one finds [3] that the probabilities of such an event are

$$m = 0, \; r = 2 \; (\text{Gaussian}): \quad p = 0.020$$
$$m = 2, \; r = 2: \qquad\qquad p = 0.352$$
$$m = 0, \; r = 3: \qquad\qquad p = 0.0005$$

The assumption of a Gaussian probability measure in other words could easily have led a designer to underestimate the probability of trouble by a factor of about 17 or to overestimate it by a factor of about 40 ("easily" in the sense that he would have no way of suspecting that he had made either error).

CRITICAL EXCITATIONS

The moral of this example is that a certain caution is indicated in the assessment of structural reliability in general and of earthquake resistance in particular. By these indications information, especially of a probabilistic nature, should not be used unless

it is well documented, or else its effect on the results is demonstrably weak. The question then is how to arrive at assessments in the face of incomplete information.

The approach described in this paper is based on the idea of utilizing only information which is documented on an adequate confidence level. This information will then define a class of excitations which can realistically be expected to occur and which the structure accordingly should be able to sustain. In order to assess the reliability of the structure it is thus necessary to find those excitations in the class which induce in it the highest stresses or strains. These are then its "critical excitations." If a structure survives its critical excitations with the desired level of integrity, it will do so also with all other realistic ones. Its reliability assessment can thus be justifiably positive.

In the context of earthquake engineering, this paper more specifically considers information well enough documented if it contributes to the distinction between excitations which are realistic candidates of possible strong ground motions at a given site, and those that are not. In other words it considers only the information to be admissible which is contained in items (a) to (f) of Section 2, after having been suitably quantified. The quantification is arrived at by the following line of reasoning.

It starts with the observation that any ground motions already recorded at or near the location of interest certainly are realistic. The same can presumably be said of those recorded at locations with similar geological and seismological properties. Such records are then called the "basis excitations" for the site under consideration. In order to extrapolate from them to other not yet recorded excitations, all excitations are admitted as well which are linear combinations of the basis excitations. One notes that these combinations do share with the basis excitations many of the characteristics (a) to (f) of Section 2. They have in common with them the durations, the intensity variations with time, the amplitude spectra, and the seismological characteristics. To this extent therefore they represent current experience. However, the bounds on intensity (in whatever way the term is defined), on acceleration and on velocity must be explictly imposed.

The problem of assessing the earthquake resistance of a structure is thus reduced to that of determining its critical excitations, i.e. that of finding the linear combinations of the basis excitations which, subject to the bounds on ground motion intensity, acceleration, and velocity, achieve the largest structural response peaks.

DETERMINATION OF CRITICAL EXCITATION

The problem of determining the critical excitations of a structure is the following. It is desired to find an excitation of the form

$$x(t) = \Sigma_i \alpha_i x_i(t) \tag{1}$$

in which the sum ranges over the basis excitations $x_i(t)$. It is to be so determined that the response

$$y(t) = \Sigma_i \alpha_i y_i(t) \tag{2}$$

generated by it in a designated structural variable achieves the largest peak $\max_t y(t)$ provided that the two constraints

$$\max_t \dot{x}(t) \leq M_1, \quad \max_t \ddot{x}(t) \leq M_2 \tag{3}$$

are satisfied, as well as a third one on the "intensity" of $x(t)$. The term "intensity" is not uniquely defined. In this study it was interpreted (for sake of traditions rather than of necessity) to mean the square-integral of the ground acceleration. The third constraint thus is of the form

$$\int_0^\infty x^2(t) \, dt \leq M_o^2 \tag{4}$$

In the mathematical terminology, one would say that it is desired to find an element x, lying in the intersection of the linear manifold spanned by the basis excitations x_i with the cubes (3) and the solid ball (4), and having the property that it maximizes the peak of $y(t)$ in (2).

This is an optimization problem. There are several ways in which it can be solved. They differ chiefly in how much of the work is done analytically before numerical

137

algorithms are resorted to. The results reported below were obtained (again, for sake of tradition rather than for any other reason) by a method that starts analytically. It assumes that the time t* at which y(t) reaches its peak is known and that the problem is that of determining the coefficients α_i which achieve

$$y(t^*) = \max_\alpha \Sigma_i \alpha_i y_i(t^*) \tag{5}$$

where α stands for the vector of coefficients α_i. This problem is solved subject to the constraint (4), only. It is a least-squares problem of a rather conventional sort, with the solution

$$\alpha^* = \alpha^*(t^*) = \pm \lambda X^{-1} y (t^*) \tag{6a}$$

in which X is Gramian matrix of the accelerations $x_i(t)$, i.e., the matrix with the elements

$$x_{ij} = \int_0^\infty \ddot{x}_i(t)\ddot{x}_j(t) \, dt \tag{6b}$$

and $y(t^*)$ is the vector with the components $y_i(t^*)$. The factor λ is the Lagrange multiplier

$$\lambda = \lambda(t^*) = M_o[y^T(t^*)X^{-1} y(t^*)]^{1/2} \tag{6c}$$

in which y^T denotes the transpose of y.

This is only a partial solution, of course. For one, contrary to what has been assumed, t* is not known and for another, the constraints (3) are not observed. The determination of t* and the imposition of the constraints however can be carried out only by numerical computation. To do so, one must shorten the time interval from $(0,\infty)$ to $(0,T)$ with an appropriate T, and one must discretize the time within it to a set of N equally spaced instants t_k, k = 1,2.. N, with an appropriate N. The choice of T and N is not entirely trivial [4] but, since it is not really pertinent here, its discussion will be omitted.

In the numerical work, one can begin by deriving the preliminary solution (6) for each instant t_k, and then use it as a starting point for a nonlinear programming routine. This routine would seek the set α of coefficients which maximize the response $y(t_k)$ for

that instant and which also satisfies the constraints (3). The desired critical excitation is then the one which produces the largest among the values $y(t_k)$ determined in this fashion.

COMPUTATIONAL PRACTICE

In practice, the computational burden of executing a nonlinear programming routine at every one of several hundred time instants t_k is nearly prohibitive. To reduce it, a simpler procedure was used in the application to be described here, even though it entailed the risk of settling for a response peak that is only a local (rather than a global) maximum. Under this procedure, the maximum peak (i.e. the maximum $y(t^*)$ among the values $y(t_k)$) was first found subject to the constraint (4) only and then the constraints (3) were imposed on $y(t^*)$.

The nonlinear program routine by which this imposition was executed was the so-called penalty function method, due originally to Fiacco and McCormick [5] and later converted to a generally available computer routine by Mylander et al. [6], under the designation SUMT. In order to exploit this routine, the 2N inequality constraints (3) were first combined into one equality constant, namely

$$h = h(\alpha) = \Sigma_k \, p(x^2(t_k) - M_1^2) + \Sigma_k \, p(x^2(t_k) - M_2^2) = 0$$
$$p(z) = z^2/2 \text{ for } z \geq 0, \text{ and } p(z) = 0 \text{ for } z < 0.$$

The constraint (4) was left in its original form, i.e., as the inequality

$$g = g(\alpha) = \Sigma_k x^2(t_k) - M_0^2 \leq 0.$$

Fiacco and McCormick have shown that the constrained programming problem under study can be replaced with an unconstrained one. Its objective function is then

$$f = f(\alpha, r) = y(t^*) - r \log g + \frac{1}{r} h^2$$

and its solution approaches the desired one as $r \uparrow \infty$.

Limited computational experience as of this writing indicates that, in many cases, the nonlinear programming routine is not called at all, indicating that the constraints (3) are

subsumed under (4). In those instances in which SUMT was activated, SUMT performed reasonably well (but no better than that), perhaps justifying its reputation for slow convergence.

COMPUTATIONAL RESULTS

A small sample taken from the body of results that were obtained with this method may give an indication of its performance. The results were derived for the Sequoyah nuclear reactor which is under construction at Daisy, Tennessee. An eleven-node model of the plant was available, and so were twelve ground motion records which had been obtained at locations with geophysical properties similar to that of the Sequoyah plant. Six of these were from the U.S.A. and six from Italy. They represented the basis excitations.

The bounds on peak ground acceleration, peak ground velocity, and intensity were set at $M_1 = 0.025$ cm sec^{-1}, $M_2 = 0.346$ cm sec^{-2}, $M_0 = 0.314$ cm sec$^{3/2}$. The response peak generated in the displacement of node 1 by its critical excitation was found to be 3.646 cm. By way of comparison, the largest response peak generated by any one of the basis excitations was 2.432. The former is thus higher by a factor of 1.5 than the latter.

A typical critical excitation is plotted in Figure 2.

DISCUSSION

The critical excitation method extrapolates from existing experience, regarding strong motion at a particular location, and seeks to encompass all excitations that can realistically be expected there. It then assesses the earthquake resistance of a structure by the largest response peak generated among its variables by these excitations.

The assessments can thus be said to be based on the largest realistic response peak. A positive one is then a guarantee of adequate resistance, or at least as close to a guarantee as may be possible at present. In the example in the preceding section, for instance, it is found that there are realistic response peaks that are half again in high as those that can be derived from existing records. A comparison of the responses calculated by the critical excitation method with those obtained from the conventional response spectrum technique shows that the critical excitation method predicts somewhat higher response consistently.

140

Contrary to much current custom, no probability figures are attached to the results. Such figures, on the basis of the discussion in the second major section, cannot be relied upon and their use would degrade the confidence level of results derived by this method. In particular an argument, according to which response peaks as high as those obtained by this method are "highly unlikely," could not be pursued without a loss in the reliability of the results.

This reliability is probably the main advantage of the method over others. Its main disadvantage may be the fact that, at least in principle, a single structure has many critical excitations (one for each of its structural variables). The determination of all is clearly not practical. Computational experience however indicates that actually all need not be determined (the critical excitations for many variables are so similar that any one of them is an adequate representative of the others). However, not enough is known in either theory or practice regarding how broadly valid such representations are and how best to establish the range of their validity.

REFERENCES

[1] Drenick, R. F., "On a Class of Non-Robust Problems in Stochastic Dynamics," Stochastic Problems in Dynamics, B. L. Clarkson, ed. London: Pitman, 1977.

[2] Vanmarcke, E. H., "Structural Response to Earthquakes," Seismic Risk and Engineering Decision, C. Lomnitz and E. Rosenblueth, ed.'s New York: American Elsevier, 1976.

[3] Drenick, R. F. and Yun, C. B., Journal of the Structural Division, American Society of Civil Engineers 105, 1879-1891. Reliability of Seismic Resistance Predictions, 1979.

[4] Wang, W. Y. et al., Nuclear Engineering and Design 52 165-174. Effective Duration of Seismic Acceleration and Occurrence of Maximum Responses, 1979.

[5] Fiacco, A. V., and McCormick, G. P., 1968 Nonlinear Sequential Unconstrained Minimization Techniques, New York: Wiley, 1968.

[6] Mylander, W. C. et al., "A Guide to SUMT - Version 4," U.S. National Technical Information Service No. Ad-731-791, 1971.
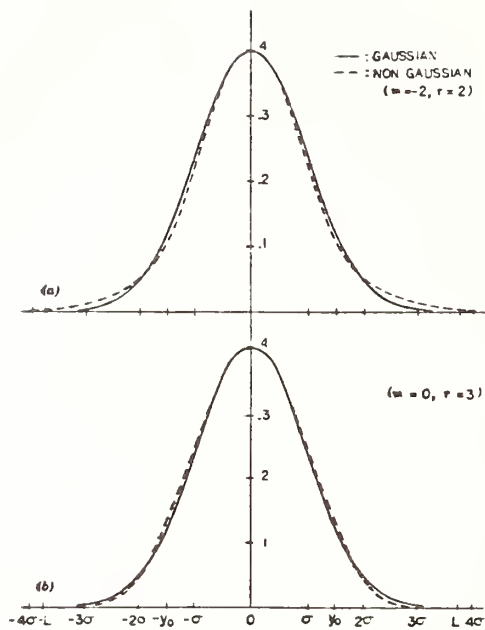
Fig. 1. Probability Density Functions
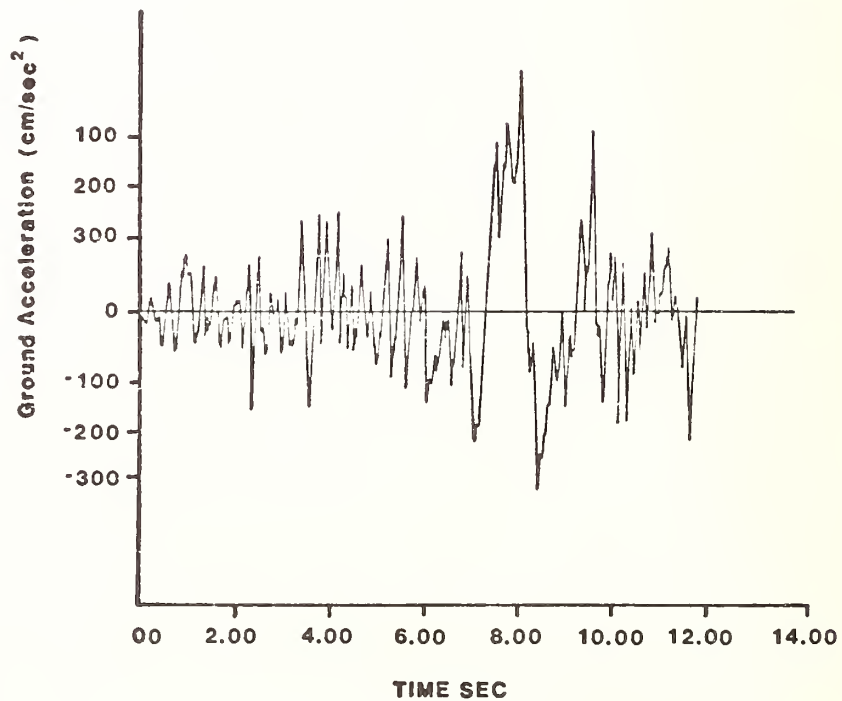
Fig. 2. Example of Critical Excitation

DYNAMIC TESTING OF A THREE-STORY REINFORCED CONCRETE STRUCTURE

by

Keiichi Ohtani

ABSTRACT

Dynamic tests using large-scale earthquake simulators are useful for confirmation of aseismic properties of reinforced concrete structures. This study presents a summary of earthquake simulator tests of a reinforced concrete structure at the Earthquake Engineering Laboratory of the National Research Center for Disaster Prevention, located at Tsukuba New Science City.

A full-size, three-story, single-bay reinforced concrete frame was built on the shaking table. The floor area of the frame was 100 m^2, the total height 10.95 m, and total weight about 285 tons. Two sets of experiments were performed. In set (Series I), only the frame was actuated, and in the other (Series II) both the frame and non-structural elements which were attached to it were actuated. The experiments were carried out in several stages of simulated and modified earthquake ground motion with an intensity sufficient to cause inelastic behavior and dynamic property changes in the frame. The dynamic behavior of the frame and the influence of the non-structural elements were investigated. In both Series I and II experiments, the change in natural frequency and the change of dynamic properties in the plastic elements were examined.

This study is a part of the U.S.-Japan Joint Earthquake Research Program.

INTRODUCTION

The best way to examine the aseismic properties of a structure is the dynamic test using the actual size structure. However, in experimental studies, test specimens are element tests or reduced scale models. It can also be noted that most tests of actual size structures are performed only in the static condition. Fortunately, the large-scale shaking table of National Research Center for Disaster Prevention has a capacity large enough to excite a model structure of up to 500 tons. Therefore, these investigations have been performed using one story, single bay reinforced concrete structure in actual size. [1]

After the 1968 Tokachi-oki Earthquake, both Japanese and American earthquake engineers saw the necessity of cooperative research projects. On August 10, 1979, the Implementing Arrangement of the U.S.-Japan Joint Earthquake Research Program was signed by the Science and Technology Agency, Ministry of Construction for Japan and the National Science Foundation for the U.S.A. One objective is to improve the aseismic properties of reinforced concrete structures. The Japanese National Research Center for Disaster Prevention has the task of producing the basic data for the pseudo-dynamic test of a seven-story reinforced concrete structure in actual size by performing an earthquake simulator test of a three-story reinforced concrete structure in actual size.

The results of experiments with a reinforced concrete structure as one of the preliminary tests of the U.S.-Japan Joint Research Program are reported here.

OUTLINE OF TEST SPECIMEN

The frame of three-story, single bay reinforced concrete was examined in this test. The test was carried in the following two cases.

(1) The frame alone (Series I).

(2) The frame with a non-structural element, a partition wall of gypsum board between the frame in the excitation direction (Series II).

Figure 1 shows the general view of test frame. Figures 2 and 3 show the setting plan of the foundation and the typical floor. Figure 4 shows the section of the excitation direction. The total height of this frame is 10.95 m, foundation girder height is 1.2 m. Story height and column height of the first floor are 3.75 m and 3.25 m, respectively.

Story height and column height of the second and third floors are 3.0 m nd 2.5 m. Frame widths are 6 m in both directions. The floor slab overhangs 2 m from the center of the column section in each direction. Each column section is 50 cm x 50 cm; floor girders in both directions are 50 cm high, 30 cm wide; and each floor beam in the tangential direction of the excitation is 45 cm x 25 cm in section. Slab thickness is 12 cm on each floor. (These sectional properties are common to each floor.) Each column footing is 3 m x 3 m in plan, 60 cm in height. The footing was fastened to the shaking table by four 2 inch steel bolts (SCM-3) at 3 or 4 positions.

This frame was designed and constructed in accordance with the Calculation Code for Reinforced Concrete Structures issued by Architectural Institute of Japan. The reinforcing steel bars used in the frame were deformed bars, SD35, having a nominal yielding stress of 3.5 t/cm^2. Concrete was a normal one with design strength of 270 kg/cm^2. However, as there was not enough time for the third floor concrete to cure after placement, high-early-strength cement was used on that level. Table 1 shows the list of the sectional properties.

A concrete weight of 2 m x 4 m x 0.5 m size is set at two places on each floor to simulate a live load. Therefore, the slab of each floor is made in consideration of a live load of 80 kg/m^2. The total weight of the frame is about 235 tons, including foundation parts. For the convenience of crack observations the surface of the frame was coated with white water paint and grid lines at intervals of 30 cm.

The experiment began about three weeks after the final concrete placement. One day before the experiment, the tested compressive strength of concrete was 260 kg/cm^2 in average value for the final concrete placement. The other concrete placements were over design strength. (Concrete was placed at four separate times.)

Series II experiments started two weeks after the Series I experiments. Repair and retrofitting work took place during this two week interval. Clear cracks which occurred in the Series I experiments were filled with epoxy resins. After they hardened, we equipped the excitation direction frame (A, B frame) with the partition wall non-structural elements. These partition walls were made of 15 mm thick gypsum board and light gauge steel attached to columns and girders. The studs were set at intervals of 90 cm with (45 x 40 x 10 x 0.6] steel. The gypsum board was fastened to both surfaces of the studs with damping

145

screws. We used this method to erect three walls on the first floor and two walls on the second and third floors. These are walls which resist fire up to three hours on the first floor and two hours on the second and third floors.

EXPERIMENTAL APPARATUS AND MEASURING EQUIPMENT

The shaking table can move in one horizontal direction by electro-hydraulic drive. It is 15 m x 15 m in size, 160 tons in weight. The maximum attainable displacement and velocity is ± 3 cm and 37 cm/sec. The table may be used on specimens weighing up to 500 tons, and may be excited to 0.55 G in acceleration with full load. The natural frequency of the system is about 20 Hz, and the operational frequency band is 0-50 Hz.

The dynamic behavior of the test frame and table can be measured in several ways: Acceleration of the table and each floor by strain gauge type acceleration pick-ups, relative displacement of each floor with ring displacement transducers, table displacement with IDS type displacement transducer located on the shaking table foundation, and wire strain gauges on the main reinforcing steel bars of each column. In Series II, we measured the strain on the gypsum board and the relative displacements between the gypsum and the concrete frame. The test data were recorded using a 64 CH digital data recorder; main data were monitored with a 14 CH analogue data recorder, and two CH pen recorders. We recorded the condition of cracks at the bottom of column on the first floor with a video recorder.

TEST SCHEDULE

Table 2 shows the test schedule. The STEP vibration uses the rectangular wave, a vibration amplitude of PP-1 mm, and a period time of 10 sec or 20 sec for the free vibration of the frame.

The SMAC-M record of the N-S component of the 1978 Off-Miyagi Pref. earthquake recorded at Tohoku University installed on the first floor was the table input for the earthquake motion test. The earthquake record was digitalized by the Building Research Institute, Ministry of Construction.

When the earthquake ground motion is simulated, because of the limitation of the 3 cm shaking table stroke, the low frequency components of the original earthquake motions

may be cut off in order to get high intensity shakes. Therefore, table inputs for the earthquake motion tests were obtained as outputs from the one-degree-of-freedom system response to the original earthquake motions. The damping constant and the natural frequency of this system is taken as $1/\sqrt{2}$ and 2 Hz respectively. In other words, this modification to the original earthquake motion was achieved using a 2 Hz high-pass filter in the acceleration. With this modification, we were able to vibrate up to about 400 gal within the 3 cm stroke limit.

TEST RESULTS

Table 3 shows the maximum acceleration responses and maximum displacements obtained. The maximum acceleration responses of Table 3 are values on the shaking table (AT), the second floor level (A2), the third floor level (A3) and the roof floor level (AR). The maximum displacements are defined as follows: DT is the relative displacement between the shaking table and its foundation; and the displacements at the first floor (D1), the second floor (D2) and the third floor (D3) are the story displacements between each floor levels. The story deflection angles between each floor level are also given in Table 3.

Test result from each series are given below.

Series I

This is the testing of the reinforced concrete frame. By microtremor measurement before the tests, the natural frequency of the frame was determined to be 2.8 Hz.

The first run of the simulated earthquake ground motion was set to produce an acceleration of 0.03 g on the shaking table. From this, a maximum acceleration on the shaking table of 36 gal and an acceleration response on the roof floor of 90 gal resulted. The story deflection angles on each floor were 1/1100 - 1/2000. Cracks were not observed on the columns and the girders. The natural frequency of the frame was 2.22 Hz after the test. An extension of the natural period of about 30 percent was observed when compared to the microtremor measurement.

The second simulated earthquake ground motion run was aimed at an acceleration of 0.15 g on the shaking table. The resultant accelerations on the shaking table and the roof floor were 140 gal and 370 gal respectively. The story deflection angle on each

floor was 1/220 - 1/480. At the bottom of column of the first floor, cracks were observed. After the test, the natural frequency of the frame was 1.28 Hz and the extension of the natural period reached to 70 percent compared to the first run result.

The third simulated earthquake ground motion test was set to produce an acceleration of 0.25 g on the shaking table. The accelerations on the shaking table and the roof floor were 220 gal and 430 gal respectively and the story deflection angle of each floor was 1/120 - 1/300. Figure 5 shows the time history. Cracks were observed at the top of column at the first floor, the girders at the second floor and even at the top of column of the third floor. Following this test, the natural frequency of the frame was found to be 1.18 Hz and an extension of the natural period to 88 percent compared to the first run result.

The fourth run of the simulated earthquake ground motion was set to produce an acceleration of 0.4 g on the shaking table. The accelerations on the shaking table were 320 gal, or 80 percent of the initial target. However, the displacement of the shaking table was 29 mm, with 30 mm the specified performance. This means that the shaking table performs as it was designed. The acceleration response on the roof floor was 500 gal and the story deflection angle of each floor reached 1/110 - 1/280. The ring type displacement transducer at the second floor that measures story deflection angles up to 1/90 was broken at its mounting part. Therefore, the actual value of the story deflection angle of the second floor could not be measured, but is assumed as almost 1/100. After the fourth run, the natural frequency was 1.14 Hz which is nearly equal to the result of the third run. From this, it could be said that the dynamic properties of the frame scarcely changed after the third run. Figures 6 and 7 show the crack behavior after the Series I tests. They show portions of the bottom of column at the first floor and the top of column of the third floor. These cracks were not serious and the members were not pushed to maximum strength. The frame shown its durability under a condition of 0.4 g earthquake motion and the design criteria of this frame is justified by these tests.

Series II

In this series, the non-structural element attached to the frame was tested. Before this vibration test, the microtremor of this frame was observed and the natural frequency estimated at 3.3 Hz. From the retrofitting of epoxy resins and the rigidity of the gypsum

148

board elements, the natural frequency of this measurement is higher than that of Series I. The damping constant of this measurement was estimated at four percent. (In the Series I tests, the damping constant was estimated at two percent.)

In the first run of the simulated earthquake ground motion, in which 0.03 g was the target acceleration at the shaking table, we obtained a 27 gal maximum acceleration on the shaking table and a 65 gal acceleration response on the roof floor. The story deflection angle of each floor was 1/2000 - 1/4500. These values were almost half those of Series I results. We estimated that the gypsum board exercised a control capacity on the displacement at the small level excitation.

From the second run in which 0.25 g was the target acceleration of the shaking table, we obtained 240 gal of the table acceleration and 350 gal of the roof acceleration. Figure 8 shows the time history. During this run, the light gauge steel, which was holding the gypsum board, was observed to move. The reason is that the carl plug, which affixed the light gauge steel to the lower surface of the girder, fell off during the acceleration. Though concrete nails are used to affix the column surfaces on the upper surfaces of the girders, a carl plug is a generally used techique on the lower surfaces of the girders. This experiment taught the following: a carl plug can resist a fairly big static load, but it is weak under a dynamic load. Then the measure to fix the girder surfaces needs important. The story deflection angle of each floor was 1/180 - 1/330 and these values increased, which proves that the gypsum boards do not contribute to reinforcement expected and that the effect of the reinforcement was lessened by the dynamic load.

In the third simulated earthquake ground motion trial in which 0.4 g was the target acceleration of the shaking table, obtained a 370 gal table acceleration and a 500 gal roof acceleration. Figure 9 shows the time history. The story deflection angles of each floor ranged from 1/130 to 1/310, and these values are approximately the same as those in the Series I frame only test. The change of the natural frequency was as follows: The natural frequency was 1.85 Hz after the first run, and the natural period increased by 80 percent compared to what it was before the experiment. The natural frequency was 1.22 Hz after the second run, and 1.19 Hz after the third. These values are approximately equal to those of Series I. In this experiment, the crack, which had been repaired in Series I, appeared again somewhat enlarged. However, no new cracks were observed.

The arrangement and analysis of the data are now under way. When it has been completed, a more detailed report will be made.

REFERENCES

[1] "Dynamic Behavior of Reinforced Concrete Frame Structures," by K. Ohtani, and C. Minowa, 11th Joint Meeting of U.S.-Japan Panel on Wind and Seismic Effects, UJNR, September, 1979.

Table 1. List of Sectional Properties

Portion	Section (cm)	Arrangement of Reinforcement		
Column	50x50	8-D22	Hoop; D10-@100	
Girder	50x30	Center	Top; 2-D22 Bottom; 2-D22	Stirrup; D10-@100
		End	Top; 4-D22 Bottom; 2-D22	
Beam	45x25	Center	Top; 2-D22 Bottom; 2-D22	Stirrup; D10-@100
		End	Top; 3-D22 Bottom; 2-D22	
Slab	12	Top; D13-@200 Bottom; D13-@200	Mesh in both axis	
Footing G.	120x50	Top; 3-D25 Bottom; 3-D25	Stirrup; D16-@200	

Table 2. Test Schedule

Series	Test No.	Input Condition
I	STEP1	Rectangular PP-1mm 0.1Hz
	RUN1	Earthquake 0.03G
	RUN2	Earthquake 0.15G
	STEP2	Rectangular PP-1mm 0.1Hz
	RUN3	Earthquake 0.25G
	STEP3	Rectangular PP-1mm 0.1Hz
	Run4	Earthquake 0.4G
	STEP4	Rectangular PP-1mm 0.1Hz
II	STEP1	Rectangular PP-1mm 0.05Hz
	RUN1	Earthquake 0.03G
	STEP2	Rectangular PP-1mm 0.1Hz
	RUN2	Earthquake 0.25G
	STEP3	Rectangular PP-1mm 0.1Hz
	RUN3	Earthquake 0.4G
	STEP4	Rectangular PP-1mm 0.1Hz

Table 3. Test Results

Series	Test No.	Maximum Acceleration (gal)				Maximum Displacement (mm) (Story Deflection Angle)			
		AT	A2	A3	AR	DT	D1	D2	D3
I	RUN1	36.3	61.3	68.3	88.6	2.34	2.77 (1/1173)	2.19 (1/1142)	1.26 (1/1984)
	RUN2	143.1	206.7	301.1	370.2	13.09	14.88 (1/218)	11.09 (1/225)	5.21 (1/480)
	RUN3	217.5	233.3	363.9	427.1	20.86	25.53 (1/127)	17.84 (1/140)	8.49 (1/294)
	RUN4	322.4	358.8	396.5	498.3	29.09	27.99 (1/116)	———	8.92 91/280)
II	RUN1	27.5	39.4	58.7	65.1	2.51	1.45 (1/2241)	1.20 (1/2083)	0.55 (1/4545)
	RUN2	235.6	259.3	359.0	374.5	19.07	17.32 (1/188)	14.10 (1/177)	7.50 (1/333)
	RUN3	369.9	432.1	473.0	498.0	28.90	25.40 (1/128)	16.24 (1/154)	7.96 (1/314)
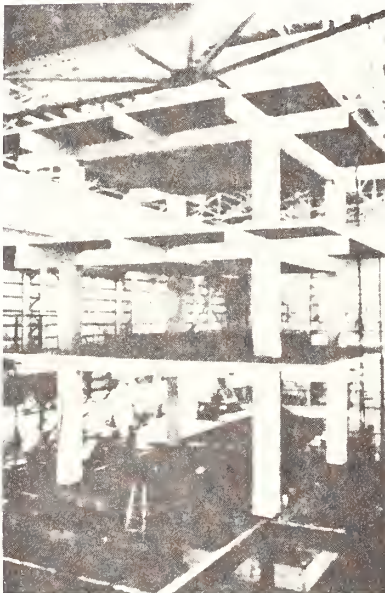
Fig. 1 General View of the Test Frame
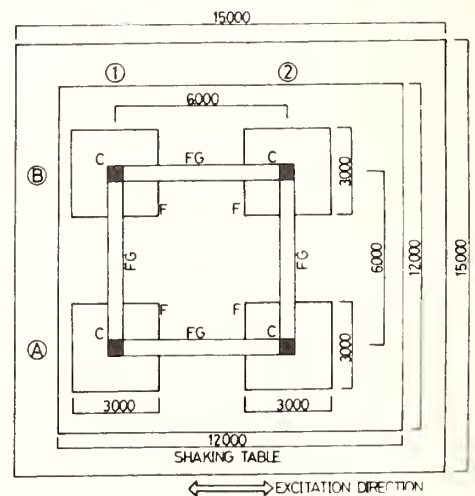
Fig. 2 Setting Plan of the Foundation
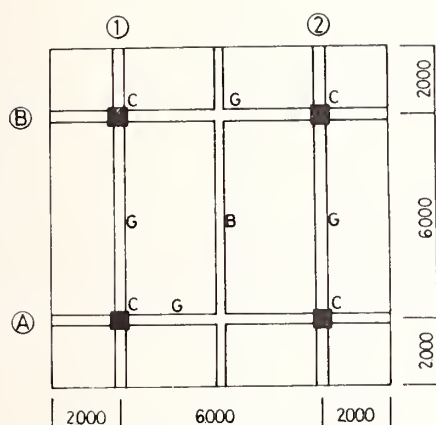
Fig. 3 Setting Plan of
the Typical Floor
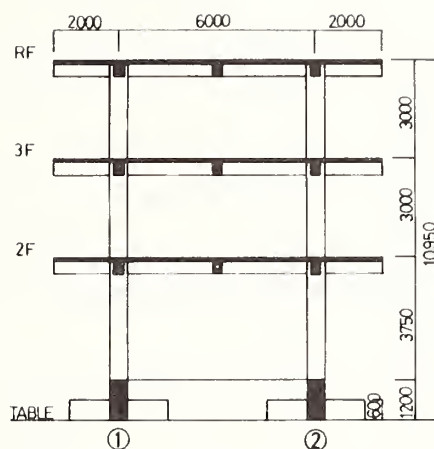
Fig. 4 Section of the Excitation Direction

Fig. 6 Crack Behavior of
the Bottom of Column
at 1st Floor

Fig. 7 Crack Behavior of
the Top of Column
at 3rd Floor
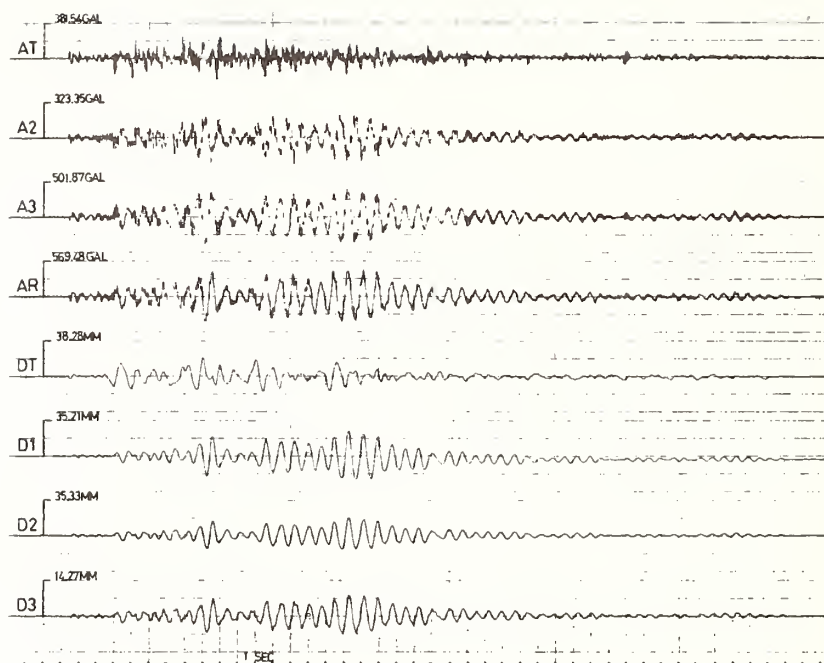
Fig. 5   Time History for the RUN3 of Series I
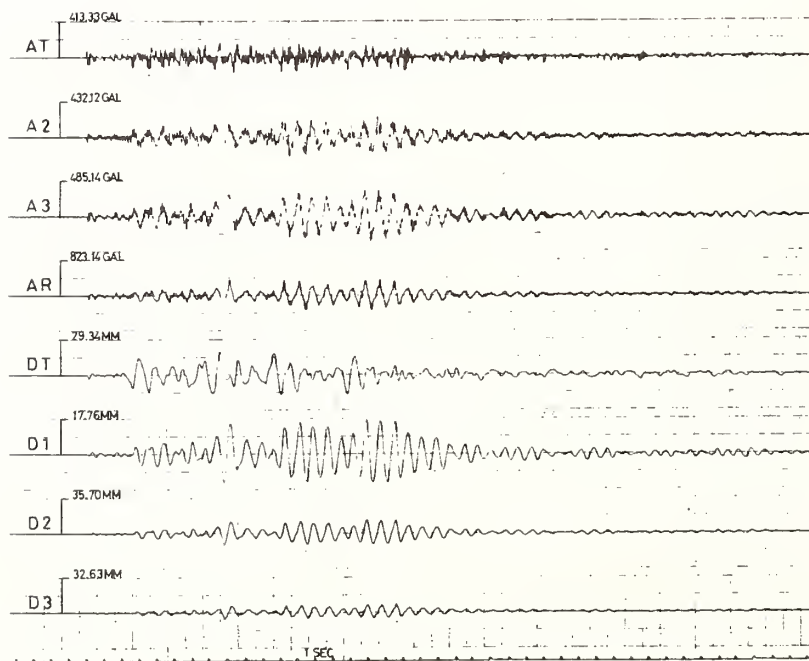
Fig. 8   Time History for the RUN2 of Series Ⅱ
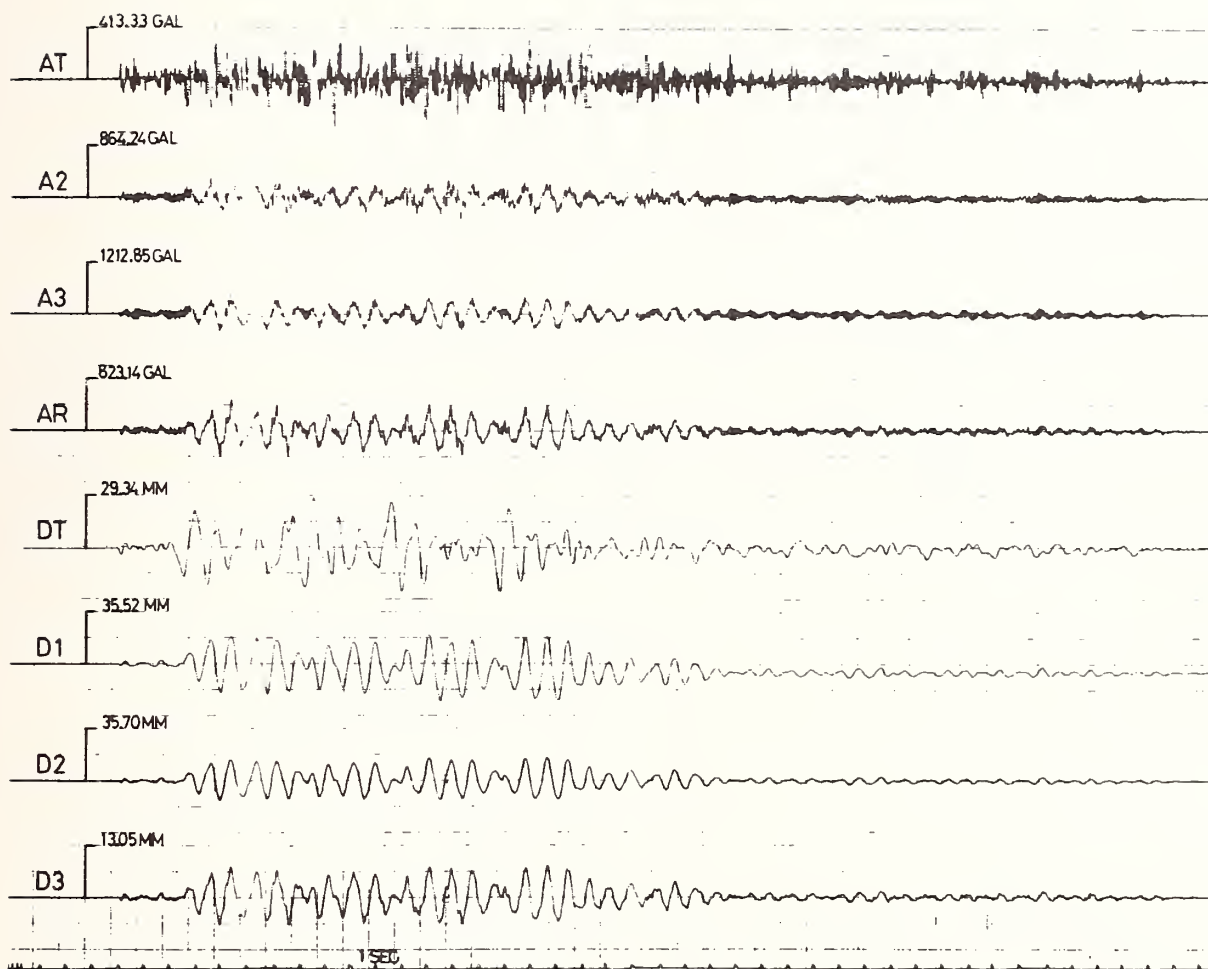
Fig. 9 Time History for the RUN3 of Series II

155

BUCKLING ANALYSIS OF BURIED PIPEINES UNDER SEISMIC LOADS

by

C. C. Chen

T. Ariman

L. H. N. Lee

ABSTRACT

The Donnell and Flügge forms of the stability equations of cylindrical shells are employed to analyze the axisymmetric, elastic quasi-static buckling of buried pipelines subject to seismic excitations. Using shell dimensions and the stiffness of the soil medium surrounding the pipe as parameters, a series of numerical results are obtained, which shows that no significant half sine wave occurring in the circumferential direction for relatively long pipes when axial buckling load reaches its minimum. It also is shown that for a given pipeline an increase in soil stiffness causes a decrease in wavelength of the critical-load instability mode and, consequently, causes an increase in axial critical load.

INTRODUCTION

Buckling failure of long buried pipelines during a severe seismic excitation has been recognized as an important problem in the pipeline industry. It has been recently attracted to the attention of earthquake engineers and researchers i.e., [1]. These studies, however, have concentrated on a long circular cylinder or tube surrounded by uniform soil medium, and subjected to uniform, static, radial pressure. Studies on the critical buckling load of buried pipelines due to axial compressive loading are rarely found in the literature. To the best of the authors' knowledge, the study on this subject was usually simplified and restricted to the model of a beam on an elastic foundation [2].

The purpose of this work is to investigate the buckling failure mode of buried pipelines under seismic excitations, using a model of a cylindrical shell surrounded by uniform springs. In the analysis, Donnell shell equations are used for quasi-shallow shells, and Flügge shell equations are employed when the shallow shell equations are not applicable. Attention is focused on the parametric studies that concern the effects on dimensions of the pipe itself as well as the stiffness of the soil medium surrounding the pipe.

FORMULATION

Consider a thin-walled circular cylindrical shell of finite length L, wall thickness h and mean radius a, with h≪a, surrounded by a uniform soil medium with extensional stiffness k, in the radial direction. On the middle surface of the cylinder, the cylindrical coordinate system x and θ is placed. Distances from the middle surface are measured by a coordinate z, positive outward. Displacement components in the x, θ and z directions are denoted by u, v and w, respectively. The cylindrical shell is considered to be subjected to edge loading and to static axial compressive loading P.

Donnell's Form of the Stability Equations

Using the stationary potential energy criterion, the nonlinear equilibrium equations of the Donnell's form are written as follows [4].

$$a\, N_{x,x} + N_{x\theta,\theta} = 0$$

$$a\, N_{x\theta,x} + N_{\theta,\theta} = 0 \tag{1}$$

$$D\nabla^4 w + \frac{1}{a} N_\theta - (N_x w_{,xx} + \frac{2}{a} N_{x\theta} w_{,x\theta} + \frac{1}{a^2} N_\theta w_{,\theta\theta}$$

$$+ kw + P\, w_{,xx} = 0$$

where N_x and N_θ are in-plane normal force intensities, $N_{x\theta}$ is in-plane shear force intensity, ∇ is the Laplace operator and $(\ )_{,x_i} = \frac{\partial}{\partial x_i} (\ )$. The linear equilibrium equations can easily be obtained by the omission of all quadratic and high-order terms in u, v, and w from Eq. (1). Introduction of the constitutive and kinematic relations to these linear equilibrium equations yields

$$a^2 u_{,xx} + \frac{1}{2}(1-\mu)u_{,\theta\theta} + \frac{1}{2}(1+\mu)a\, v_{,x\theta} + a\mu w_{,x} = 0$$

$$\frac{1}{2}(1+\mu)au_{,x\theta} + \frac{1}{2}(1-\mu)a^2 v_{,xx} + v_{,\theta\theta} + w_{,\theta} = 0 \tag{2}$$

$$D\nabla^4 w + \frac{1}{a^2} C(v_{,\theta} + w + a\mu u_{,x}) + kw + Pw_{,xx} = 0$$

In Eq. (2), μ is the Poisson's ratio and C and D are termed extensional and bending stiffness parameters, respectively, and are given by

$$C = \frac{Eh}{1 - \mu^2}$$

and $\hspace{10cm}$ (3)

$$D = \frac{Eh^3}{12(1 - \mu^2)}$$

in which E is Young's modulus.

With the aid of linear equilibrium equations given in Eq. (2), the linear stability equation of the Donnell's form can be obtained by either the adjacent-equilibrium or the minimum potential energy criterion and written in the form

$$a^2 u^*,_{xx} + \frac{1}{2}(1 - \mu)u^*,_{\theta\theta} + \frac{1}{2}(1 + \mu)a\, v^*,_{x\theta} + a\, \mu w^*,_x = 0$$

$$\frac{1}{2}(1 + \mu)a\, u^*,_{x\theta} + \frac{1}{2}(1 - \mu)a^2 v^*,_{xx} + v^*,_{\theta\theta} + w^*,_\theta = 0 \qquad (4)$$

$$D\nabla^4 w^* + \frac{1}{a^2}\, C(v^*,_\theta + w^* + a\mu\, u^*,_x) - (N_x^* w^*,_{xx} + \frac{2}{a} N_{x\theta}^* w^*,_{x\theta}$$

$$+ \frac{1}{a^2} N_\theta^* w^*,_{\theta\theta}) + kw^* + Pw^*,_{xx} = 0$$

In Eq. (4), u* v*, and w* are the displacements of the buckled shell and N_x^*, N_θ^*, and $N_{x\theta}^*$ are governed by the linear form of Eqs. (1) and can be obtained for a given edge loading condition.

It is to be noted that Eqs. (4) represent a coupled set of three equations in the variables u*, v*, w*. These equations may also be partially uncoupled and written as follows.

$$\nabla^4 u^* = \frac{-\mu}{a}\, w^*,_{xxx} + \frac{1}{a^3}\, w^*,_{x\theta\theta}$$

$$\nabla^4 v^* = \frac{-2 + \mu}{a^2}\, w^*,_{xx\theta} - \frac{1}{a^4}\, w^*,_{\theta\theta\theta} \qquad (5)$$

$$D\nabla^8 w^* + \frac{1 - \mu^2}{a^2}\, Cw^*,_{xxxx} - \nabla^4(N_x^* w^*,_{xx} + \frac{2}{a}N_{x\theta}^* w^*,_{x\theta}$$

$$+ \frac{1}{a^2}\, N_\theta^* w^*,_{\theta\theta}) + k\nabla^4 w^* + P\nabla^4 w^*,_{xx} = 0$$

Flügge's Form of the Stability Equations

In a sense, the Flügge's stability equations can be regarded as Donnell's stability equations plus a "modifying" part.

The Donnell's stability equations given in Eqs. (4) in the absence of extensional stiffness of soil medium k and axial compressive force P can be written in a matrix form as follows.

$$[L_D] \{x^*\} = \{0\} \qquad (6)$$

where $[L_D]$ and $\{x^*\}$ are a matrix differential operator and a displacement vector respectively and are given by

159

$$[L_D] = \begin{bmatrix} a^2 \dfrac{\partial^2}{\partial x^2} + \dfrac{1-\mu}{2} \dfrac{\partial^2}{\partial \theta^2} & \dfrac{1+\mu}{2} a \dfrac{\partial^2}{\partial x \partial \theta} & \mu a \dfrac{\partial}{\partial x} \\[2ex] & \dfrac{1-\mu}{2} a^2 \dfrac{\partial^2}{\partial x^2} + \dfrac{\partial^2}{\partial \theta^2} & \dfrac{\partial}{\partial \theta} \\[2ex] \text{Sym.} & & 1 + \dfrac{a^2 h^2}{12} \nabla^4 \end{bmatrix} \tag{7}$$

and

$$\{x^*\} = \begin{Bmatrix} u^* \\ v^* \\ w^* \end{Bmatrix} \tag{8}$$

The matrix differential operator according to Flügge's theory can be obtained and treated as the sum of two operators,

$$[L_F] = [L_D] + \xi [L_{MOD}] \tag{9}$$

where $[L_{MOD}]$ is a "modifying" operator and ξ is the nondimensional shell parameter defined by

$$\xi = \dfrac{h^2}{12a^2} \tag{10}$$

The modifying operator in Eq. (9) takes the form

$$[L_{MOD}] = \begin{bmatrix} \dfrac{1-\mu}{2} \dfrac{\partial^2}{\partial \theta^2} & 0 & -a^3 \dfrac{\partial^3}{\partial x^3} + \dfrac{1-\mu}{2} a \dfrac{\partial^3}{\partial x \partial \theta^2} \\[2ex] & \dfrac{3(1-\mu)}{2} a^2 \dfrac{\partial^2}{\partial x^2} & -\dfrac{3-\mu}{2} a^2 \dfrac{\partial^3}{\partial x^2 \partial \theta} \\[2ex] \text{Sym.} & & 1 + 2 \dfrac{\partial^2}{\partial \theta^2} \end{bmatrix} \tag{11}$$

Including both the soil medium effects plus the axial compressive load in Eq. (9), the matrix differential operator given in Eq. (7) becomes [3]

160

$$[L_D] = \begin{vmatrix} (1-\dfrac{P}{C})a^2 \dfrac{\partial^2}{\partial x^2} + \dfrac{1-\mu}{2} \dfrac{\partial^2}{\partial \theta^2} & \dfrac{1+\mu}{2} a \dfrac{\partial^2}{\partial x \partial \theta} & \mu a \dfrac{\mu}{\partial x} \\[2ex] & (\dfrac{1-\mu}{2} - \dfrac{P}{C})a^2 \dfrac{\partial^2}{\partial x^2} + \dfrac{\partial^2}{\partial \theta^2} & \dfrac{\partial}{\partial \theta} \\[2ex] Sym. & & (1 + \dfrac{a^2}{C}k) + \dfrac{P}{C}a^2 \dfrac{\partial^2}{\partial x^2} + \dfrac{a^2 h^2}{12} \nabla^4 \end{vmatrix} \qquad (12)$$

APPLICATIONS

In the following, parametric studies on the critical load analysis for a long simply supported cylindrical shell are considered. Since the axial buckling is the main concern in this study, only the seismically induced axial load is considered in the analysis.

Donnell's Axial Critical Load

In the absence of edge loading, the stability equation governing the deformation in the radial direction becomes

$$D\nabla^8 w^* + \frac{1-\mu^2}{a^2} Cw^*,_{xxxx} + k\nabla^4 w^* + P\nabla^4 w^*,_{xx} = 0 \qquad (13)$$

Solutions of the form

$$w^* = A \sin mx \cdot \sin n\theta \qquad (14)$$

where A is an arbitrary constant, $m = m\pi/L$, and $m,n = 1,2,3\ldots$, are seen to satisfy both the differential equation and the assumed simply supported boundary conditions. It is noted that the quantities m and n represent the number of half sine waves in the axial and circumferential directions respectively.

Substitution of Eq. (14) into Eq. (13) gives

$$P = \frac{1}{m^2}[k + D(m^2 + \frac{n^2}{a^2})^2] + \frac{C(1-\mu^2)}{a^2} \cdot \frac{m^2}{(m^2 + \frac{n^2}{a^2})^2} \qquad (15)$$

A distinct eigenvalue P corresponds to each element of the set $(\{m\} \times \{n\})$. A preliminary study in this work has shown that, when the axial compressive load P reaches its minimum,

161

the cross section remains circular. It is therefore reasonable to assume that the shell deforms in such a way that the shape is totally governed by the number of axial half sine waves. Assuming

$$w^* = A \sin \frac{m\pi x}{L} \tag{16}$$

and substituting Eq. (16) into (13), the counterpart of Eq. (15) becomes

$$P = D \frac{m^2 \pi^2}{L^2} + (k + \frac{1-\mu^2}{a^2} C) \frac{L^2}{m^2 \pi^2} \tag{17}$$

The axial critical load P_{cr} can then be obtained by minimizing Eq. (17) with respect to m as follows:

$$P_{cr} = \frac{Eh^2}{a} \left[\frac{1 + \alpha}{3(1-\mu^2)} \right]^{1/2} \tag{18}$$

where α is the nondimensional parameter,

$$\alpha = \frac{k}{(Eh/a^2)} \tag{19}$$

The number of half sine waves in the axial direction is

$$m = \left[\frac{L}{\pi} \frac{12(1-\mu^2)(1+\alpha)}{\alpha^2 h^2} \right]^{1/4} \tag{20}$$

The Batdorf parameter Z [4] is given by

$$Z = \frac{L^2}{ah} (1-\mu^2)^{1/2}. \tag{21}$$

Then, substitution of Eqs. (3) and (21) into Eqs. (17) and (20) gives

$$P = \frac{1}{2\sqrt{2}} [\frac{\pi^2}{Z} m^2 + \frac{12(1+\alpha)}{\pi^2} \cdot \frac{Z}{m^2}] \cdot P_{cr} \tag{22}$$

and

162

$$m = \frac{Z}{\pi}[12(1+\alpha)]^{1/2} \tag{23}$$

Figures 1 and 2 show the variation of critical axial load, P_{cr}, as a function of the Batdorf parameter Z for various values of m, the number of half sine waves. In Figure 1 α is zero while in Figure 2 α is unity. Similar curves for other relevant values of α would be obtained and utilized in the determination of the critical load. Therefore, this procedure could be useful in the design of buried pipelines.

Flügge's Axial Critical Load

Due to the shallowness, limitation, in the case of moderate or short cylindrical shells, Flügge's stability equations should be used rather than Donnells'.

For a simply supported shell, the displacement $\{x*\}$ has the components

$$u* = A* \sin n\theta \cos \frac{\lambda x}{a}$$

$$v* = B* \cos n\, \theta \sin \frac{\lambda x}{a} \tag{24}$$

$$w* = C* \sin n\theta \sin \frac{\lambda x}{a}$$

where A*, B*, C* are arbitrary constants and

$$\lambda = \frac{m\pi a}{L} \tag{25}$$

with m being the number of half sine waves in the axial direction of the shell. Thus Eqs. (9)-(11) yield

$$A*[\lambda^2 + \frac{1-\mu}{2} n^2(1+\xi) - \Phi\lambda^2] + B*[\frac{-1+\mu}{2}\lambda n]$$

$$+ C*[-\lambda\mu - \xi(\lambda^3 - \frac{1-\mu}{2}\lambda\, n^2)] = 0$$

$$A*[-\frac{1+\mu}{2}\lambda n] + B*[n^2 + \frac{1-\mu}{2}\lambda^2(1+3\xi) - \Phi\lambda^2] + C*[n - \frac{3+\mu}{2}\xi\lambda^2 n] = 0 \tag{26}$$

$$A*[-\lambda\mu - \xi(\lambda^3 - \frac{1-\mu}{2}\lambda n^2)] + B*[n + \frac{3-\mu}{2}\xi\lambda^2 n] + C*[1 + \xi(\lambda^4 +$$

$$2\lambda^2 n^2 + n^4 - 2n^2 + 1) + (1-\mu^2)\alpha - \Phi\lambda^2 = 0$$

where

$$\Phi = \frac{P}{C} = \frac{P(1-\mu^2)}{Eh} \qquad (27)$$

The above represents three linear equations with the buckling amplitudes A*, B*, C* as the unknowns. For a non trivial mode, the determinant of Eq. (26) must be zero. For small values of the parameters ξ and Φ, it is sufficient to retain only linear terms. Thus the determinant becomes,

$$ABC + ABc\xi - AB\lambda^2\Phi + 3AbC\xi - A\lambda^2C\Phi + aBC\xi - B\lambda^2C\Phi$$
$$+ 2DEF + 2DEf\xi + 2DeF\xi - BE^2 - 2BEe\xi - 3bE^2\xi + \lambda^2E^2\Phi - AF^2 - 2AFf\xi - aF^2\xi$$
$$+ \lambda^2F^2\Phi - DC^2 - cD^2\xi + \lambda^2D^2\Phi = 0 \qquad (28)$$

where $A = \lambda^2 + a, \quad B = n^2 + b, \quad C = 1 + (1-\mu^2)\alpha, \quad D = \frac{1+\mu}{2}\lambda n, \quad E = \lambda u, \quad F = n \qquad (29)$

with $\quad a = \frac{1-\mu}{2}n^2, \quad b = \frac{1-\mu}{2}\lambda^2, \quad c = \lambda^4 + 2\lambda^2n^2 + n^4 - 2n^2 + 1$

$$e = -\lambda(\lambda^2 - a), \quad f = \frac{3-\mu}{2}\lambda^2 n \qquad (30)$$

Solving for Φ in Eq. (28) yields

$$\Phi = \frac{R}{S} \cdot \frac{1}{\pi^2}\left(\frac{L}{ma}\right)^2 \qquad (31)$$

where $\quad R = (ABC + 2DEF - BE^2 - AF^2 - CD^2) + (ABc + 3AbC + aBC + 2DEF$

$\qquad + 2DeF - 2BFe - 3bE^2 - 2AFf - aF^2 - cD^2)\ \xi,$

$\quad S = AB + AC + BC - D^2 - E^2 - F^2 \qquad (32)$

Figures 3 and 4 give the variation of Φ which is related to the axial buckling load, as a function of the non dimensional parameter L/ma. Both figures are for a ductile iron pipe of L = 40 ft, a = 24 in, h = 0.51 in and $\xi = 3.763 \times 10^{-5}$. They differ in that the higher value of α in Figure 3 is 0.01 while in Figure 4, it is 0.5. Both figures also give the case of no soil medium around the pipe ($\alpha = 0$).

The stability of the above pipe under seismically induced axial loads can be examined using Figure 3 and 4 for selected values of L/ma (m = 1,2,3, etc.) and the corresponding values of Φ. As long as all the points for specific values of L/ma and Φ lie below the heavier dashed lines (no soil) or the solid lines (with soil) the pipe is stable. When the

axial load P and hence Φ increases, all the points move upward. As soon as any point reaches one of the curves, the pipe is in neutral equilibrium and about to buckle. Figures 3 and 4 show that the soil medium has an important effect in the critical axial load by causing an appreciable increase in P_{cr}.

REFERENCES

[1] Cheney, J. A., 1971, "Buckling of Soil-Surrounded Tubes," Journal of the Engineering Mechanics Division, ASCE, Vol. 97, No. EM4, pp. 1121-1130.

[2] Ariman, T., Muleski, G. E., 1979, "A Review of the Response of Buried Pipelines under Seismic Excitation," Lifeline Earthquake Engineering - Buried Pipelines, Seismic Risk and Instrumentation. Edited by T. Ariman, S. C. Liu and R. E. Nickell, ASME, PVP-34, pp. 1-29.

[3] Muleski, G. E., Ariman, T., and Aumen, C. P., 1979, "A Shell Model of a Buried Pipe in a Seismic Environment," J. Pres. Vessel Tech. ASME, Vol. 101, pp. 44-50.

[4] Brush, D. O. and Almroth, B. O., 1975, Buckling of Bars, Plates, and Shells, McGraw-Hill, Inc.
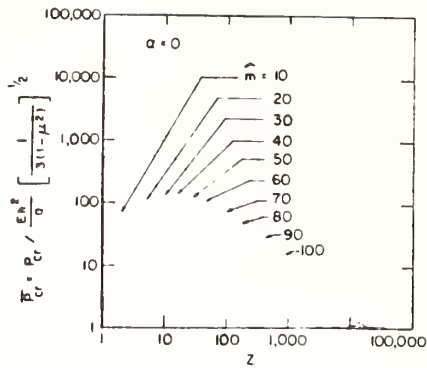
Fig. 1 Nondimensional critical axial
load $\bar{P}_{cr}$ versus Z.
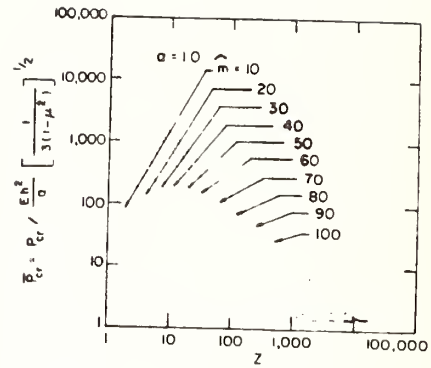
Fig. 2 Nondimensional critical
load $\bar{P}_{cr}$ versus Z.
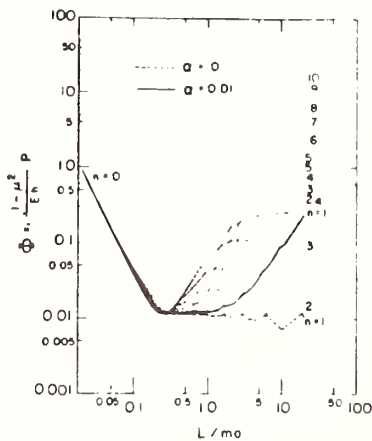
Fig. 3 Buckling diagram for axial
compression.
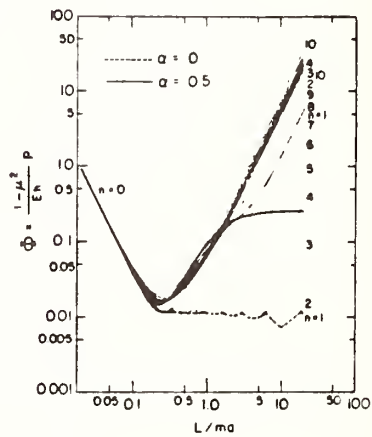
Fig. 4 Buckling diagram for axial
compression.

166

SHAKING TABLE TESTS OF EARTH RETAINING STRUCTURES ON IMPROVED GROUND

by

Setsuo Noda

Sosuke Kitazawa

Hajime Tsuchida

ABSTRACT

In coastal area land reclamation work, bulkheads are constructed around filled-in ground. In the case of gravity type bulkheads, the soft ground is improved. Instead of conventional improvement methods a Deep Mixing method (D.M. method) has been used recently.

A design procedure for these structures has been tentatively proposed. It has not been tested because the structures have yet to experience strong earthquakes. In order to improve earthquake resistant design procedures, shaking table tests are being carried out on five models of gravity bulkheads on improved ground.

This paper presents model outlines, test procedures, some experimental results, stability analyses of the present design procedure and estimates of prototype stability.

INTRODUCTION

In land reclamation work in a coastal area, the soft ground is usually improved and bulkheads are constructed around the filled-in ground. In using gravity bulkheads, the soft ground is excavated and replaced with sand of sufficient bearing capacity.

Instead of conventional ground improvement methods a Deep Mixing method (D.M. method) has been recently used in coastal work due to environmental restrictions. In the D.M. method soft clayey ground is stabilized chemically with quick lime or cement milk which is squeezed into the ground and mixed together. The strength characteristics of treated soil have been investigated in the laboratory and practical construction features are tested in the field. A design procedure for bulkheads and improved ground have been tentatively proposed. [1,2] It has not been tested because the number of these structures is limited and they have not yet experienced strong earthquakes.

In order to improve the earthquake resistant design procedure, shaking table tests are being carried out on five models of gravity bulkheads on improved ground. There are two wall types, caisson and cell; and two ground improvement types, block and pile.

This paper presents model outlines, test procedures, some experimental results, stability analyses of the present design procedure, and the estimates of prototype stability.

PURPOSES OF TEST

Much research has taken place in Japan to establish earthquake resistant design procedures for the above new soil structures. In the Ministry of Transport, a program of investigation, shown in Figure 1, is now underway. Short of a destructive test on the prototype, it is difficult to estimate soil structure stability under severe earthquake disturbance conditions accurately from only one method. Therefore, the earthquake resistant design procedure will be established by making effective use of the proven features from different models.

The model tests, now in the early stages, presented in this paper correspond to the investigations heavily outlined in Figure 1. The model tests have the following purposes:

an understanding of the differences in seismic behavior for the various improvements and wall types, the collection of data to examine the numerical simulation method, and estimates of the prototype's seismic stability.

In shaking table tests of soil structures it is often difficult to satisfy the scale effects and similitude factors. However, tests on large scale models which are regarded as small prototypes can be carried out since a shaking table with a large loading box, capable of producing large exciting forces has been constructed recently. From tests of these prototypes, differences in seismic behavior between the prototypes under varied earthquake conditions may be estimated.

A numerical simulation method will be useful in estimating behavior of the whole structure, but the method has not been completed yet. In order to examine the method and apply it to practical design work, information on dynamic soil properties and on seismic behavior is required. This information can be obtained from these model tests.

Although the models are relatively large, they are small prototypes. Therefore, taking the similitude between model and prototype into consideration as well as possible, the seismic stability of prototype is estimated from the experimental results for trial.

<center>MODELS AND TEST PROCEDURES</center>

Similitude

Since the purpose of the tests is to simultaneously obtain fundamental information from several standpoints, the model is regarded as both a small prototype and a scaled model. In determining model size and shape, the gravity type bulkhead on improved ground in the coastal area was chosen as the prototype where water depth is -20 m and soft clay extends up to -40 m.

Considering the loading box size (8m length, 4m width, and 2 m depth), 1/20 is the adopted ratio of length (Lr). Since the two kinds of silty-clay which exist off Kawasaki in Tokyo Bay (Kawasaki-A and Kawasaki-B clay) are used, the model unit weight is almost the same as that of the prototype. The acceleration on the model is also the same as that on the prototype. The ratio of cohesion of soils is 1/20, the strength of the model ground is measured by the uniaxial compression test for treated soil, and the vane test is used to measure the clayey ground.

<center>169</center>

Many variations in ground improvements are applied in practical work. For example, the soft ground may be 100 percent treated uniformly (block type), or may be treated as group piles (pile type). A wall type and a checkered pattern type are also used as variations in improvement types. In this report the block type and the pile type are modeled. In the pile type, the average strength (c_2) of composite ground is defined as follows:

$$c_2 = (1 - \beta) c_0 + \beta c_1.$$

c_0 is the cohesion of untreated soil, c_1 is the cohesion of treated soil, and β is the ratio of the cross-sectional area of treated soil to the whole one, and is called the improvement ratio. Because it is difficult to make many piles of treated soil of short diameter accurately, the strength and the diameter of treated soil and the improvement ratio do not satisfy the similitude. However, the average strength of composite ground (c_2) does satisfy the above mentioned similitude. Similitude is summarized in Table 1.

3.2 Models

Model details are shown in Table 2. Models 1 to 4 are caisson type bulkheads, and Model 5 is a cellular type bulkhead. The improved grounds are block type in Model 1 and 2, and pile type in Model 3 to Model 5. In every model, ground improvement extends to sand of sufficient bearing capacity, and that is called fixed type.

(1) Model 1 (See Figure 2)

In this model the strength of the improved ground is larger than expected, because of the difficulty in soil quality control and in the differences in curing conditions of treated soil between the model and the preliminary laboratory test. Compared to the other three caisson models, Model 1 has a wider improved ground area and a thicker gravel mound. It is judged the most resistant to earthquakes.

(2) Model 2 (See Figure 3)

Since Model 1 was strong enough in the tests, Model 2 is designed as a rather weak model. That is, the strength of treated soil is about 60 percent of Model 1 and the improved ground is smaller. Additionally, the gravel mound is 15 cm thinner and the caisson is 17 cm higher than those of Model 1.

(3) Model 3 (See Figure 4)

The improved ground consists of 99 piles of treated soil of 15 cm in diameter, and the improvement ratio is 10 percent. Pile diameter is 1.5 to 3.0 times as long as required from the similitude, but the improvement ratio is about 1/6 to 1/5 of prototype.

(4) Model 4 (See Figures 5 and 6)

Cross section and ground plane of Model 4 are shown in Figures 5 and 6, respectively. The improvement ratio is 20 percent, and the ground contains 208 piles. The improvement ratio of this model is about 1/2 to 1/3 of the prototype and resembles the prototype more than Model 3. In order to equalize the average strength of the composite grounds, the treated soil strength of Model 4 is about 1/2 that of Model 3.

(5) Model 5 (See Figure 7)

The improvement ratio is 20 percent and the bulkhead consists of three cells. The cell is 120 cm in diameter, 91.5 cm in height and 0.27 mm in thickness. It has a 6 cm wide footing but no stiffener.

Procedures for Making Models

Models are constructed right in the loading box of the shaking table. The relationship between cohesiveness and water content of untreated soil, and the relationship among the cohesion, water content, and cement content of treated soil are determined by preliminary laboratory tests. Following these findings, the prescribed amounts of clay, water, and cement are mixed and model ground of expected strength can be made. About 32 m^3 of soil is necessary to make the model ground, which must be made accurately and in a short time. Therefore, both construction procedure and soil quality is controlled carefully. Clay is mixed with water and cement by mixer (capacity: about 0.7 m^3). Clayey grounds are made with a clay of prescribed water content in each batch. Improved ground is made with a clay, water and cement. Physical properties of clay are shown in Table 3.

In the case of pile models, plastic pipes are set up and fresh treated soil is poured into them. Then, untreated soil is placed around the piles, and the plastic pipes are pulled out. The grounds are not consolidated.

Five model caissons are placed in the direction of the face line of the bulkhead. Openings of 1 to 2 cm are left between the caissons so they can move independently. Clear sand is put in as backfill, and water is poured into the loading box up to the low water level.

Shaking Conditions

The shaking table at the Port and Harbour Research Institute, Ministry of Transport, which is shown in Figure 8 is used. This is a free vibration type shaking table as illustrated in Figure 9 [3]. It generates a free vibration in one horizontal direction, which differs from the usual ground movements during earthquakes. Examples of the table and model acceleration records are shown in Figure 10. Every model is shaken 5 to 6 times with 50 to 400 gals or more of maximum acceleration. Predominant frequencies are 1 to 6 Hz, within the range of low frequencies of the design earthquake conditions; consequently the test vibrations are considered destructive. However, the number of predominant waves is only 2 to 5 which is rather few compared to the design earthquake condition.

Measurements

As shown in the model cross sections, accelerations, earth pressures, and ground strains are measured. Accelerations are measured primarily at the bottom of loading box (table acceleration), at the surface of the clayey ground, improved ground, mound, backfill sand, and at the top of caisson. Earth pressures acting from the backfill to the wall, and the pressures beneath the caisson are measured. In order to observe the occurrence of sliding failure, flexible plastic bars with strain gauges (strain meter) are buried in the ground and their bending strains are measured.

EXPERIMENTAL RESULTS

Accelerations of Ground and Wall

As acceleration examples, the first and the second peaks of several points are shown in Figure 11 and 12. In the Model 1 results shown in Figure 11, the improved ground is rather rigid and the model accelerations are amplified to less than 600 gals of the table acceleration. The caisson accelerations are not as large because the gravel mount has a shock absorbing effect against the severe disturbances. Rocking vibrations occur to the

caisson. Figure 12 shows that the improved pile ground reacts rather flexibly to large accelerations. Figures 13 and 14 show the ratios of first peak acceleration of Models 2 and 5 to that of the shaking table. The influence of average strength and the type of improved ground is found from the acceleration response.

Displacements of Wall

The horizontal displacement, settlement, and tilt of the caisson and cell walls were measured after each increment of acceleration increase. As little settlement or tilt occurred in the tests, the mounds and improved grounds are considered to have sufficent bearing capacity. However, the horizontal wall displacement does increase with the increase of table acceleration as shown in Figures 15 and 16. In Figure 15 the differences due to the variations in the models are not clear from the relationship between wall displacement and table acceleration; but as shown in Figure 16, the walls of Model 1 and Model 2 start sliding at 200 to 300 gals of acceleration on the surface of the improved ground, while the walls of Models 3, 4, and 5 are displaced by much smaller accelerations. It was observed after the tests that the pile tops of Models 3, 4, and 5 were displaced several centimeters horizontally. Consequently, it is felt that the wall displacements are caused by the pile top features. The strain meters in the ground do not indicate any signs of sliding failure.

Pressures Beneath Caisson

Dynamic pressures beneath the caissons are measured by earthpressure cells buried in the mound. Examples are shown in Figure 17, where the static pressure is assumed to be the sum of the weight of caisson and earth-pressure due to the backfill sand. The increase in dynamic pressure indicates the occurrence of rocking vibrations on the caisson.

Damage of Backfill Sand

Settlement and cracks on the surface of the backfill sand were observed after each shaking. They increase along with increases in the horizontal wall displacements and their aspects are similar to the seismic damage of gravity type bulkheads.

DISCUSSION

The purposes of these tests are to provide an understanding of the characteristics of seismic behavior and to collect the data to develop a numerical simulation method. The complete investigation cannot be reported on in this report because the numerical simulation method is still under development and the tests with the five models have just been completed. Therefore, the experimental results are compared to the results of the stability analysis using present procedure. On the other hand, the seismic stability of the prototype is estimated in consideration of the similitude.

Stability Analyses by Present Design Procedure

According to current design procedure for harbor structures [4], the stability of model walls against sliding is estimated as shown in Figure 18. Safety factors are calculated using a seismic coefficient, the ratio of maximum acceleration at the improved ground surface to the acceleration of gravity. The arrows indicate the informal cases, in which the square root is neglected since it becomes imaginary in calculating dynamic earthpressure. The face line swelling in Models 1 and 2 is considered to be caused by the sliding of the walls. Since the walls start to slide at the safety factor of about 1.0, estimates from the present design procedure do not contradict the experimental results. In Models 3 to 5, it is considered that the face line swelling is caused by the displacement of the pile tops. The swelling starts about 1.8 or less of the safety factor.

Safety factors of circular failure plotted against horizontal wall displacements are shown in Figure 19. The seismic coefficient is the ratio of table acceleration to acceleration of gravity which distributes uniformly through the model. Since the face line swellings in the block models are caused by the walls sliding on the mound, it is better to exclude them from this discussion. In Models 3 to 5 the walls start to slide at a safety factor of 2.5 or less. From observations of the improved ground, these swellings are not caused by shear failure of the treated soil but by the displacement of treated soil piles. Since rigidity and rupture strain are somewhat different between treated and untreated soils, further investigation is required despite the large circular failure safety factor.

174

Stability Prototype

The prototype is designed to a seismic coefficient of 0.2 by present design procedure. From design seismic conditions at the construction site, the maximum acceleration at the base and at the ground surface are 270 to 290 gals, and 200 to 290 gals, respectively. Predominant incident wave frequency is 0.1 to 4.0 Hz. The number of predominant waves is from 20 to 30.

Although there are some uncertainties, the particular tests are chosen as the equivalent disturbances to design seismic conditions as shown in Table 5. The number of predominant waves is somewhat less in the tests than in the design seismic condition, but it is compensated for by the somewhat larger acceleration. Also, the predominant frequencies are within the range of low frequencies, and test vibrations are in the destructive range.

When the similitude between model and prototype is regarded as satisfied, the stabilities of prototypes are estimated in Table 5. According to Table 5, sliding and wall settlement takes place to some extent but ground and bulkhead failure does not occur. Consequently, it is estimated that the prototype does not lose its function under the design seismic condition.

CONCLUDING REMARKS

In order to rationalize earthquake resistant design procedure for bulkheads on ground improved by the D.M. method, much research such as the model tests, earthquake observations, and numerical simulations have been actively pursued. This paper reports only the outline of the shaking table tests on relatively large models, hence the integration of the related research and further investigations are required.

REFERENCES

[1] Terashi, M., "Chemical Soil Stabilization Methods Applicable to Port and Harbor Construction," Proc. of 1977 Annual Research Presentations of Port and Harbor Research Institute, pp. 63-100, December 1977.

[2] Nakamura, R., "Deep Mixing Method by Cement Slurry - (I) and (II)," Umetate to Shunsetsu, No. 78, pp. 33-55, 1977 and No. 79, pp. 23-38, 1978.

[3] Chiba, T. and Noda, S., "On the Free Vibration Type Shaking Table," Proc. of 34th Annual Convention, Japan Society of Civil Engineers, Vol. 1, pp. 426-427, 1979.

[4] The Japan Port and Harbor Association, "Engineering Requirements on Port and Harbor Facilities and Its Application," March 1979.

Table 1 Similitude

Parameters	Symbols	Ratios
Length	L_r	$L_r = L_m/L_p \equiv 1/20$
Unit Weight	γ_r	$\gamma_r = \gamma_m/\gamma_p \equiv 1$
Acceleration	α_r	$\alpha_r = \alpha_m/\alpha_p = L_r/T_r^2 \equiv 1$
Time	T_r	$T_r = T_m/T_p = L_r^{1/2} = 1/4.47$
Weight, Force	W_r	$W_r = W_m/W_p = \gamma_r L_r^3 = 1/20^3$
Cohesion	C_r	$C_r = C_m/C_p = W_r/L_r^2 = \gamma_r L_r = 1/20$
Angle of Internal Friction	ϕ_r	$\phi = \phi_m/\phi_p = 1$

m : Model, p : Prototype, r : Ratio of Model to Prototype

Table 2 Model Details

		Model 1	Model 2	Model 3	Model 4	Model 5
Wall Type		Caisson	Caisson	Caisson	Caisson	Cell
Ground	Type	Block	Block	Pile	Pile	Pile
Improvement	Improvement Ratio (%)	100	100	10	20	20
Wall	Height (cm)	85	102	85	85	91.5
	Width (cm)	55	55	55	55	120
	Backfill Sand (cm)	115	115	115	115	115
Layer	Mound (cm)	40	25	40	40	16
Thickness	Ground (cm)	100	100	100	100	100
	Sand (cm)	20	10	10	10	10
Water Depth (cm)		–	–80.0	–87.5	–87.5	–87.5
Clay Used		Kawasaki–A	Kawasaki–A	Kawasaki–B	Kawasaki–B	Kawasaki–B
Clayey	Water Content W (%)	90	90	100	105	105
Ground	Cohesion C_o (kg/cm^2)	0.0104	0.0113	0.0160	0.0160	0.0140
	Water Content W_1 (%)	200	200	200	200	200
Treated Soil	Cement Content A_w (%)	10	8	15	11	11
	Cohesion C_1 (kg/cm^2)	0.635	0.370	1.640	1.018	0.843
Composite Ground	Cohesion C_2 (kg/cm^2)	(0.635)	(0.370)	0.178	0.216	0.180

Table 3 Physical Properties of Clay

		Kawasaki-A	Kawasaki-B
Specific Gravity of Solid G_s		2.69	2.64
Consistency	Liquid Limit W_L (%)	68.8	84.2
	Plastic Limit W_P (%)	33.3	34.5
	Plasticity Index I_P	35.5	49.7
Grain Size Distribution	Gravel (%)	0	0
	Sand (%)	6.8	4.4
	Silt (%)	47.1	38.6
	Clay (%)	46.1	57.0

Table 4 Specifications of Shaking Table

Max. Horizontal Acceleration	1.2 G (Full Loading)
Max. Horizontal Displacement	± 90 mm
Max. Horizontal Velocity	102 cm/sec
Frequency	0.8 ~ 4.4 Hz (Full Loading)
Loading Capacity	130 tf
Loading Box	Length 8 m × Width 4 m × Hight 2 m

Table 5 Estimated Behaviour of Prototype

	Design Seismic Condition	Model 1	Model 2	Model 3	Model 4	Model 5
Max. Acceleration of Ground (gal)	200 ~ 290	612	429	283	250	196
Max. Acceleration of Base (gal)	270 ~ 290	562	372	462	457	474
Predominant Frequency (Hz)	0.1 ~ 4.0	0.52	0.74	0.48	0.41	0.34
Number of Predominant Waves	20 ~ 30	4	3	2	2	2
Max. Acceleration of Wall (gal)	–	571	348	297	212	214
Horizontal Displacement of Wall (cm)	–	58	38	76	44	52
Settlement of Wall (cm)	–	22	–	36	6	2

Fig.1 Flow Chart of Development of Earthquake Resistant Design Procedure for Bulkheads on Improved Ground (Ministry of Transport)
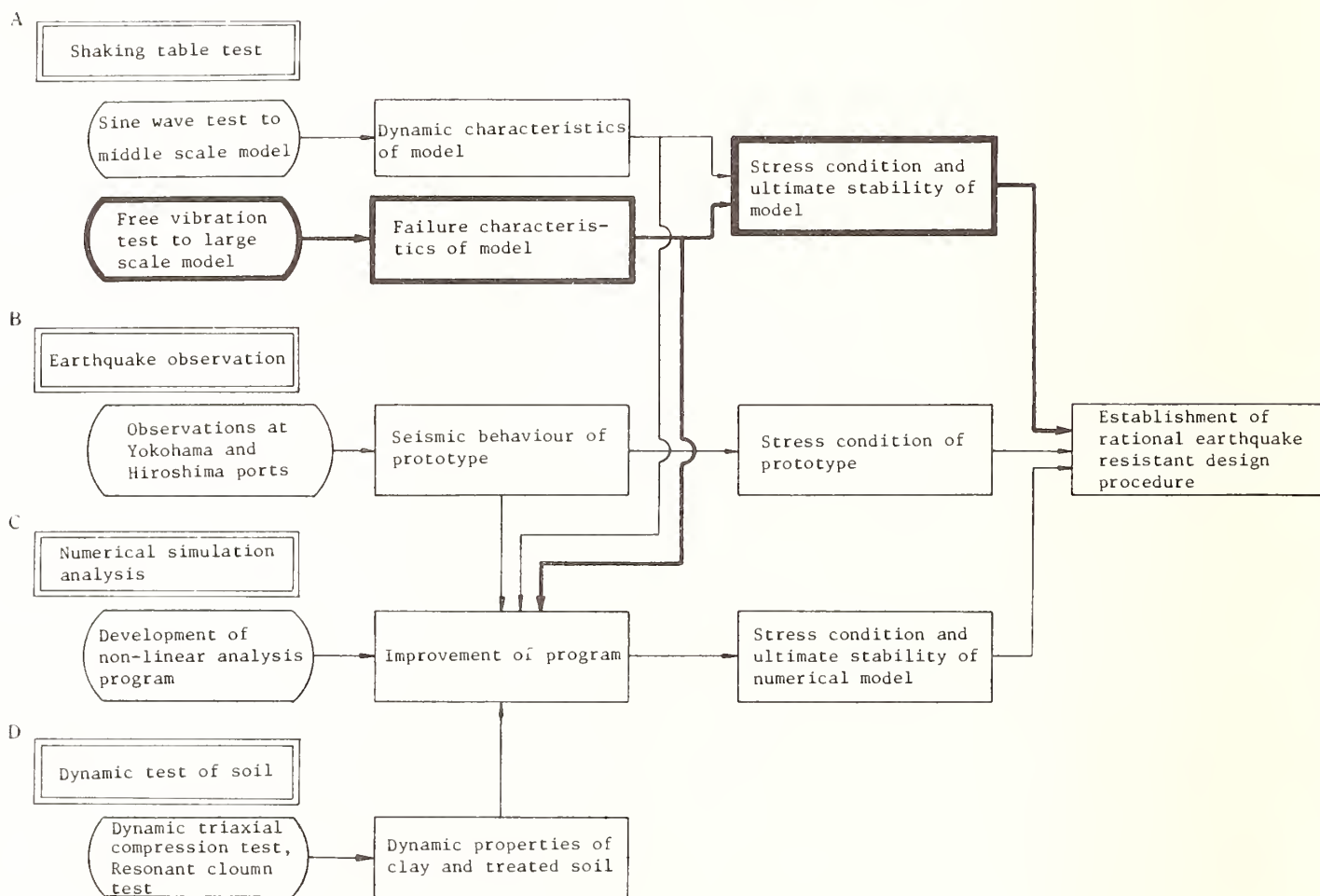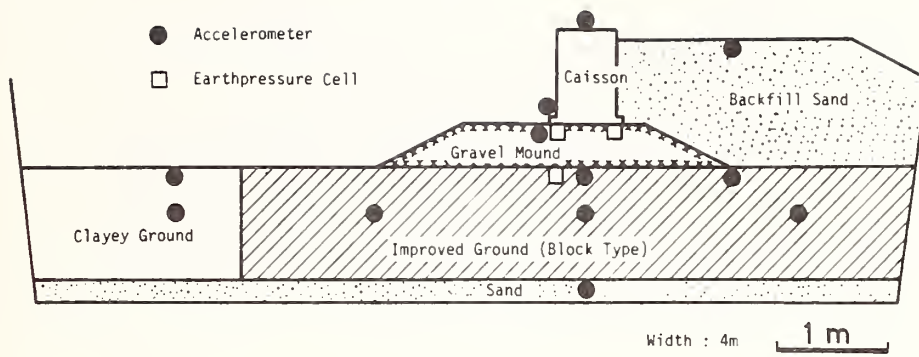
Fig.2 Cross Section of Model 1
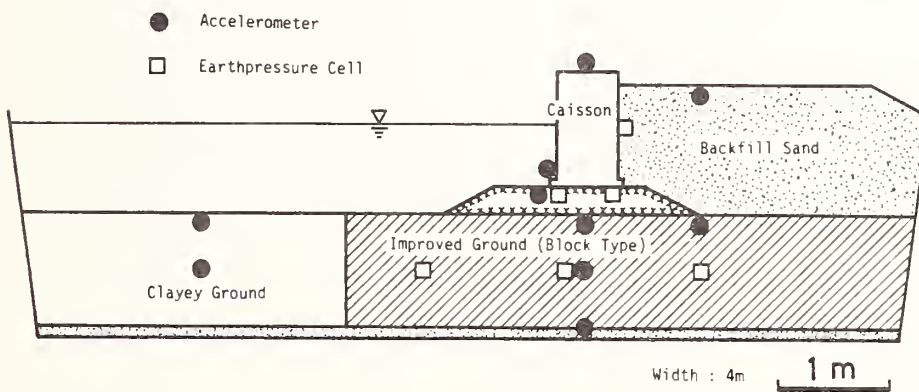
Fig.3 Cross Section of Model 2
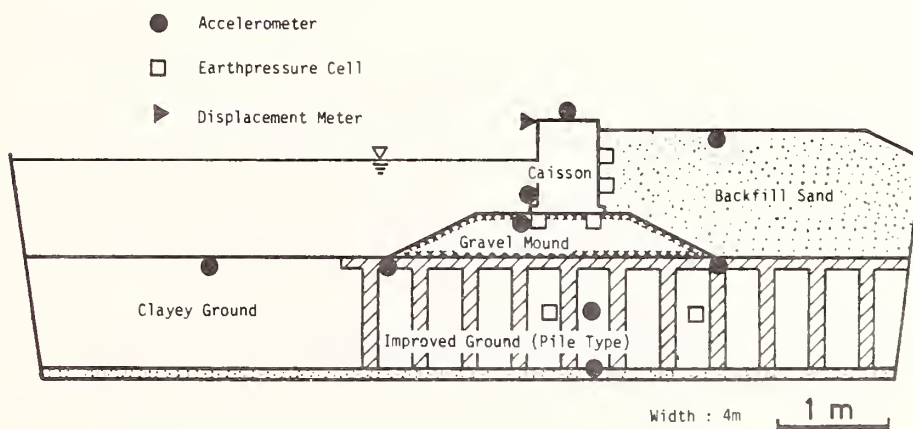
Fig.4 Cross Section of Model 3

179
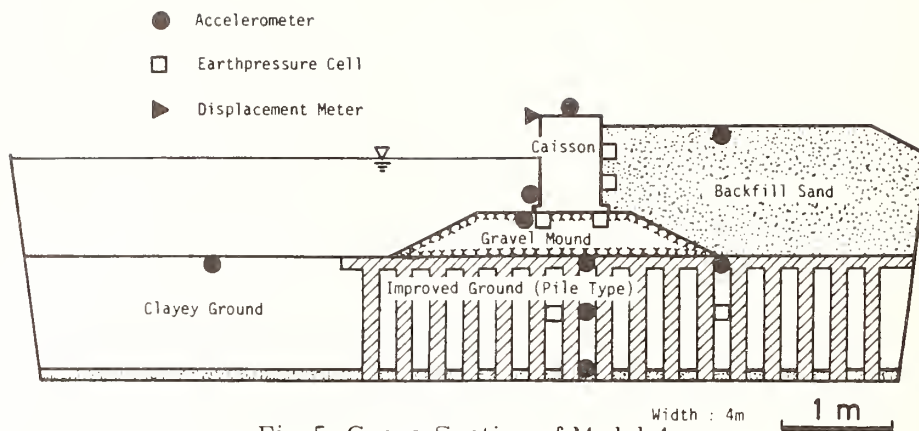
Fig.5 Cross Section of Model 4
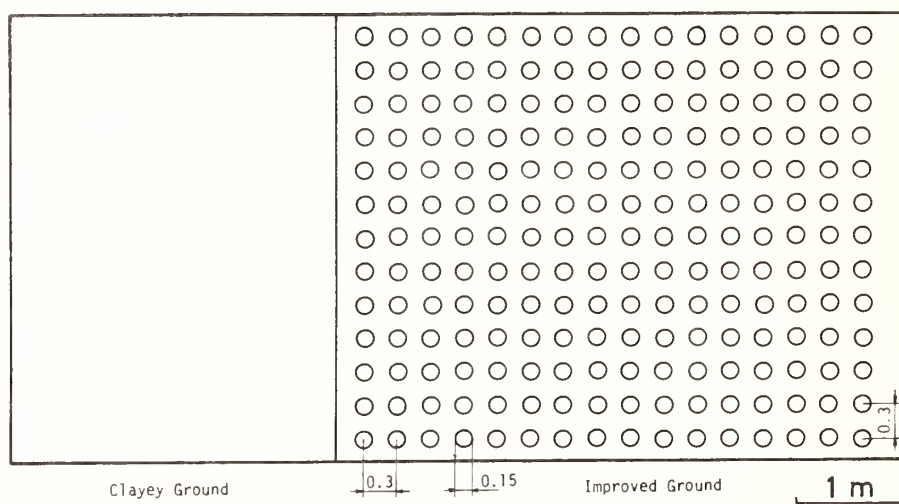
Fig.6 Plane of ground (Model 4)
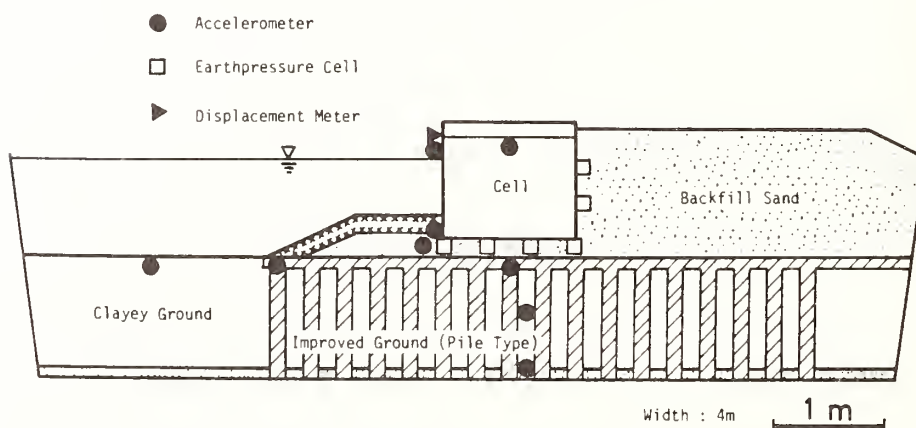
Fig.7 Cross Section of Model 5

Fig.8 Free Vibration Type Shaking Table

Spring
Oil Pressure Piston

Wall

Rail   Wheel

Foundation
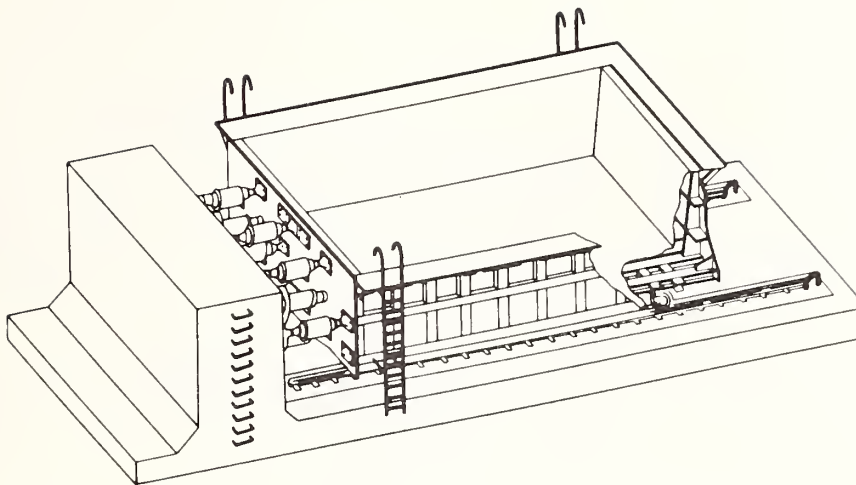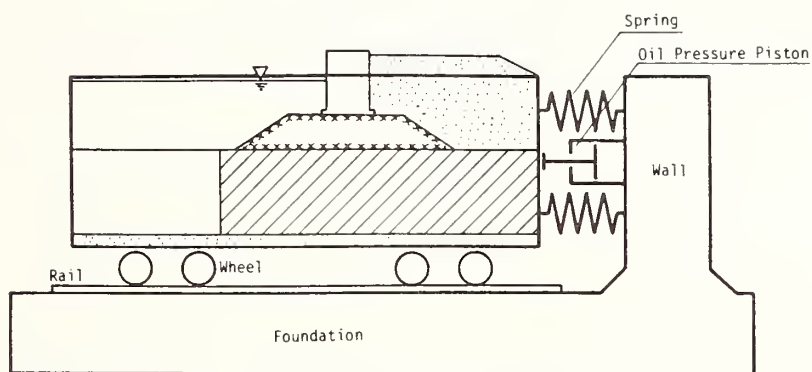
Fig.9 Mechanism of Shaking Table

gal   Model 4
400.
0.   Top of Caisson
-400.
400.
0.   Surface of Improved Ground
-400.
400.
0   Shaking Table
-400.
0.0   0.5   1.0   1.5
sec
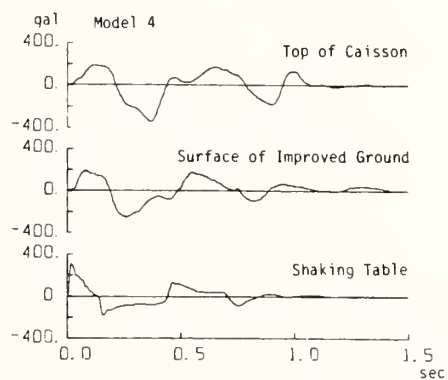
Fig.10 Acceleration Records
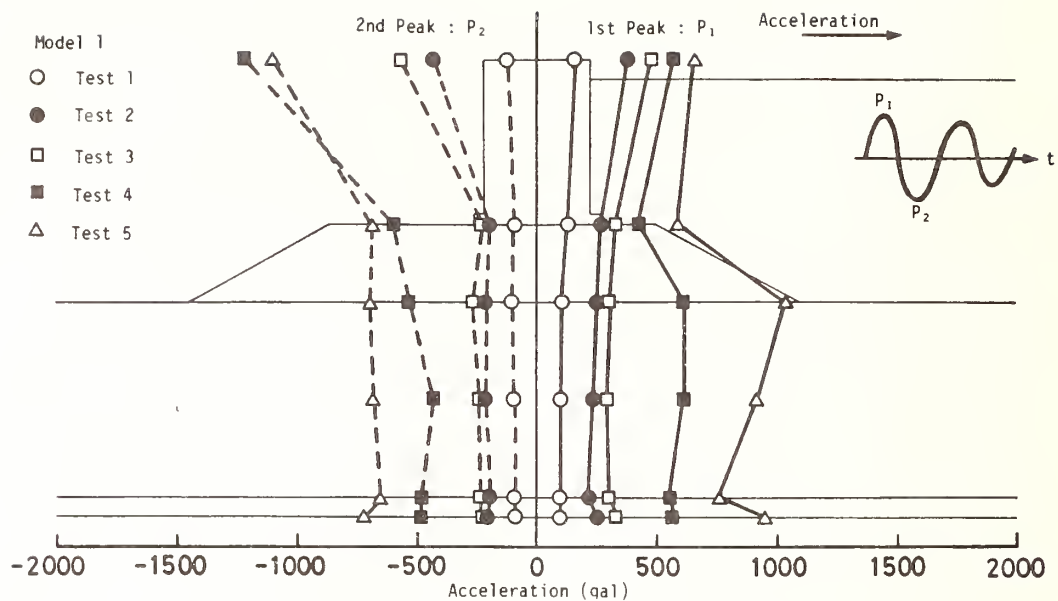
Fig.11 1st and 2nd Peak Accelerations (Model 1)
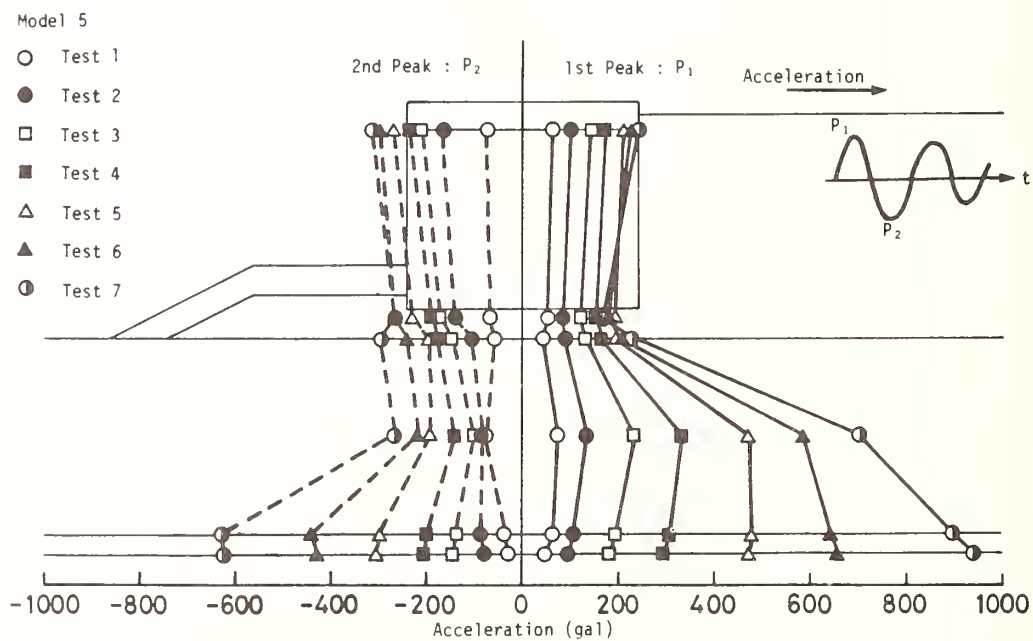
Fig.12 1st and 2nd Peak Accelerations (Model 5)
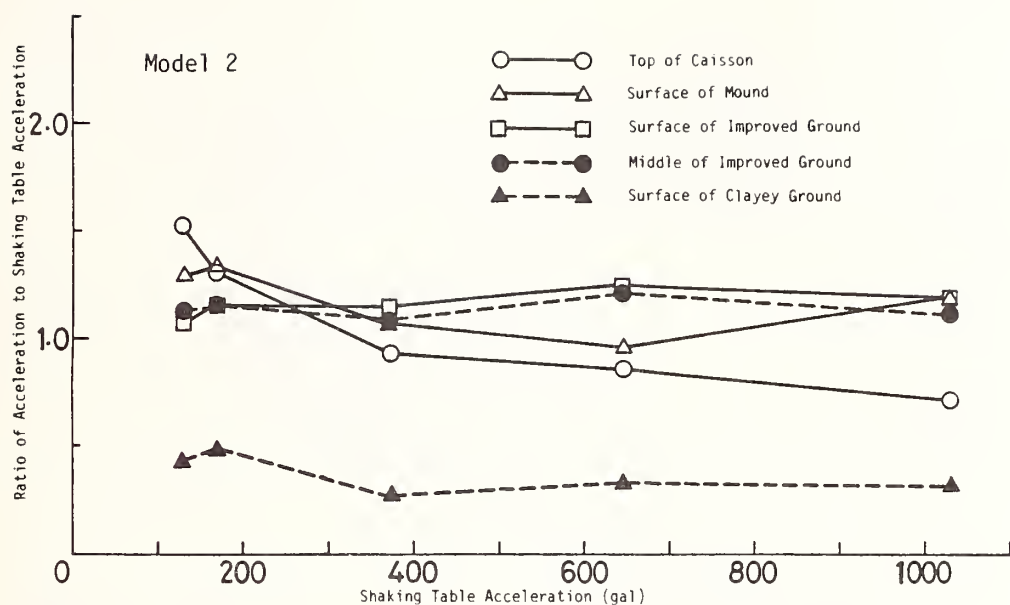
Fig.13 Ratio of Acceleration to Shaking Table Acceleration
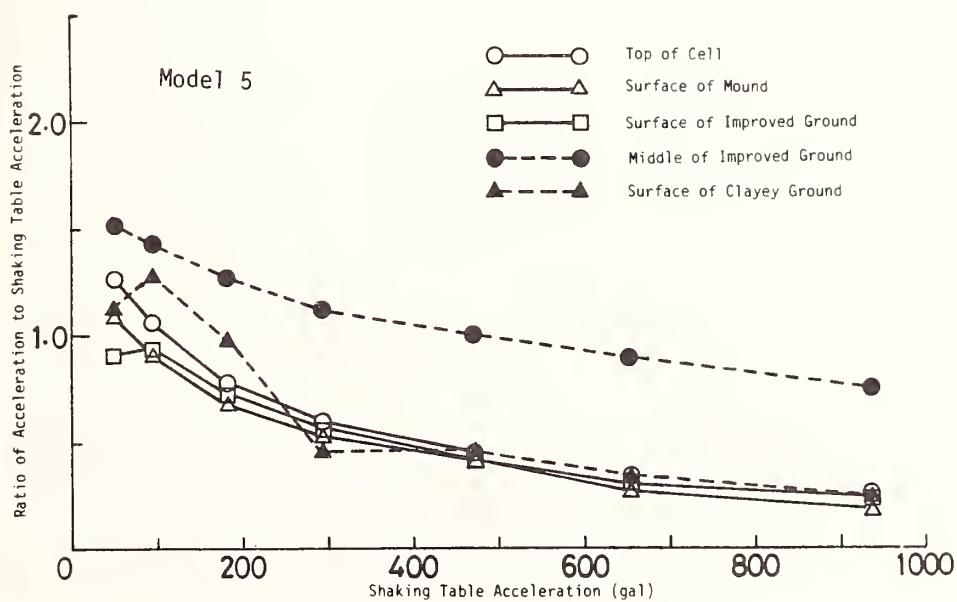
Fig.14 Ratio of Acceleration to Shaking Table Acceleration
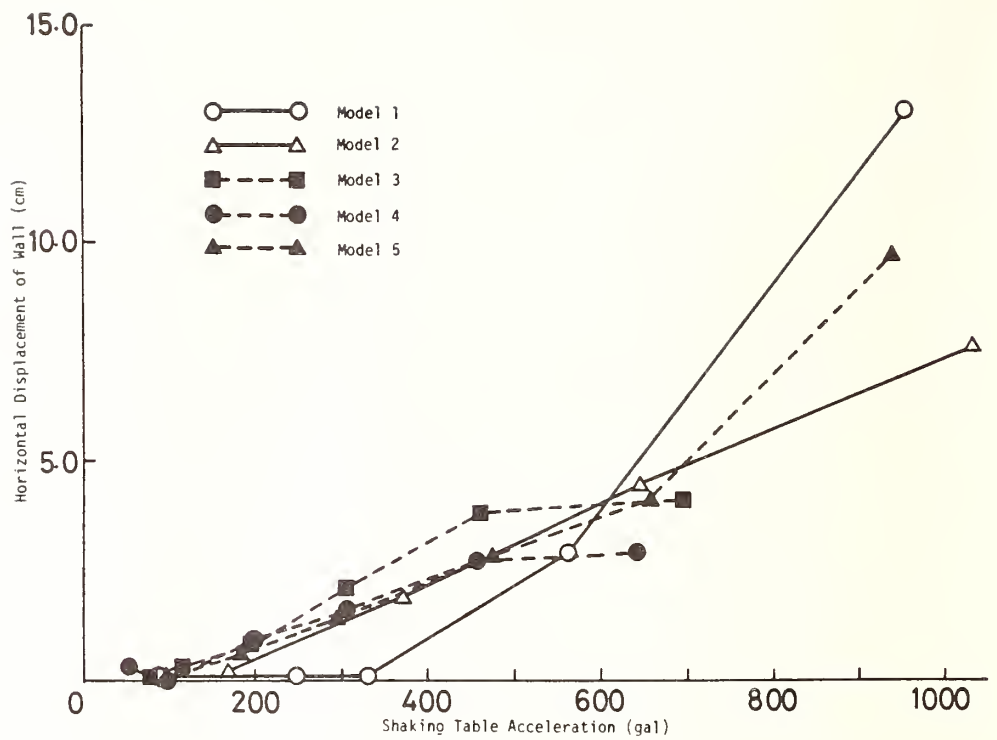
Fig.15 Horizontal Displacement of Wall to Shaking Table Acceleration
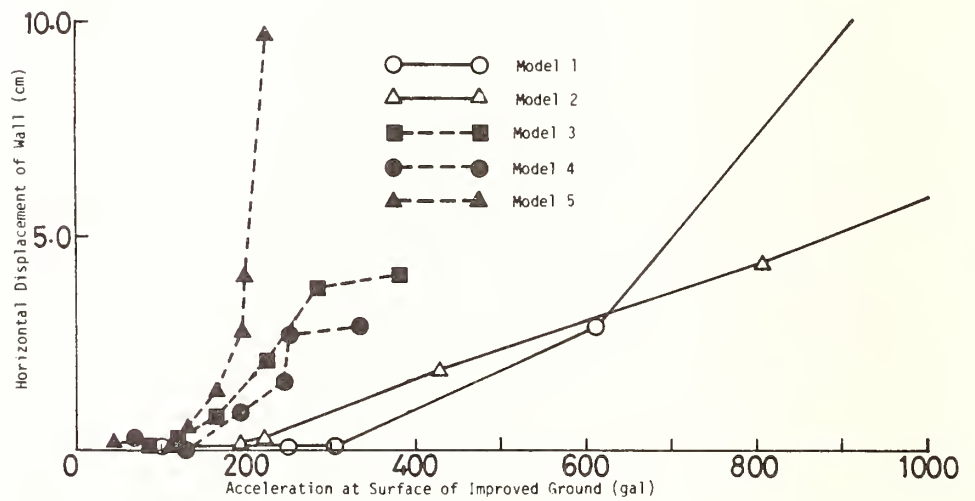
Fig.16 Horizontal Displacement of Wall to Acceleration at
Surface of Improved Ground
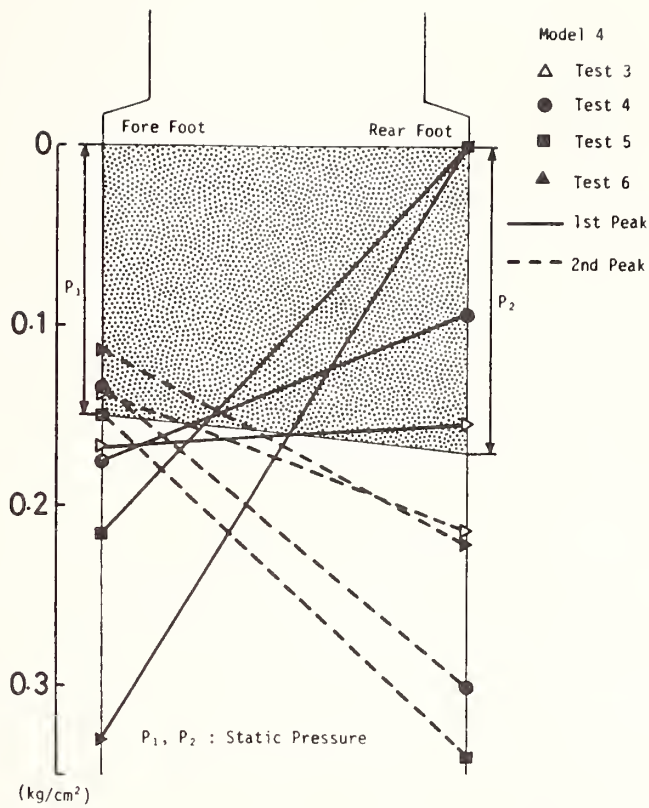
Fig.17 Dynamic Pressure beneath Caisson
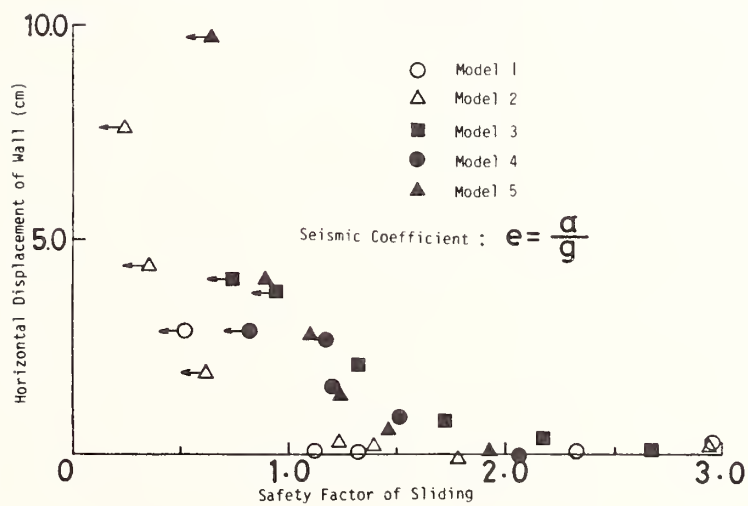
Fig.18 Horizontal Displacement of Wall to Safety Factor of Sliding
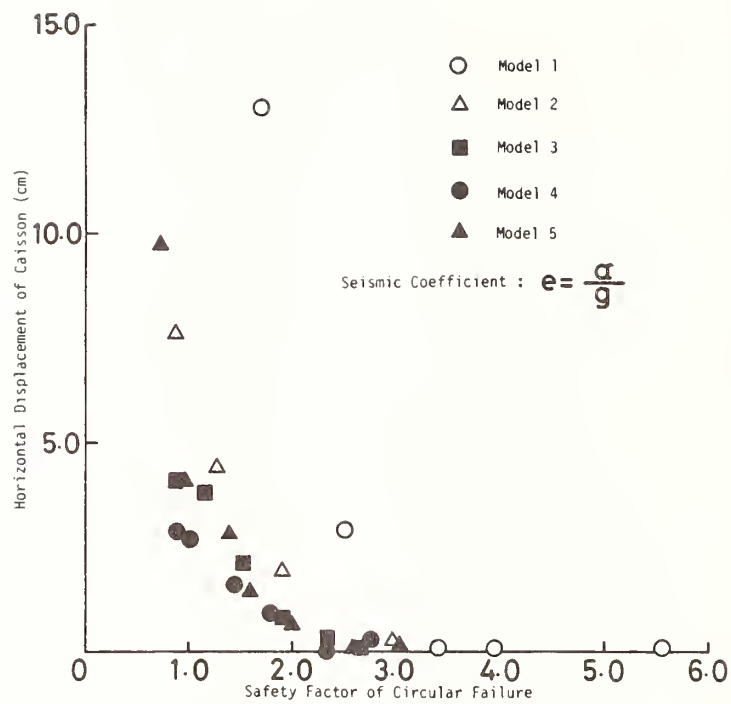
Fig.19 Horizontal Displacement of Caisson to Safety Factor of Circular Failure

FULL-SCALE EXPERIMENTAL STUDY ON THE ASEISMIC PERFORMANCE OF MEDIUM-RISE REINFORCED CONCRETE WALL STRUCTURES

by

M. Hirosawa

T. Goto

H. Hiraishi

M. Yoshimura

ABSTRACT

This study reports on an investigation of the seismic safety of medium-rise apartment houses of RC wall construction through a full scale testing program. In Japan more than 700,000 apartment houses, mainly within five stories, have been constructed. Their seismic safety, through structural experiments and studies of earthquake damage, has been confirmed primarily because of their strength in lateral resistance which compensates for an insufficient deformation capacity.

Recently, demand for eight story construction of this type has increased due to factors such as the increased cost of building sites, and the advantages of such structures in regard to urban planning. Accordingly, in 1979 an outline of a new design Code for RC wall structures was written.

In the new design Code the adopted principle is to keep ductile deformation capacity to compensate for less strength compared to that of past RC wall structure within five stories. To this purpose, the following several regulations to improve structural design deformation capacity were provided: to have shear walls with uniform stiffness, to restrict the number of members which could be anticipated to fail from brittleness, and to set a minimum value for the shear reinforcing ratio.

Tests of a model structure, designed using the new Code, were conducted. From these tests, it was found that the ultimate strength of the building was more than 50 percent of its total weight, and that the deformation capacity was sufficient.

OBJECTIVE OF TESTING

Japanese apartment houses of RC wall structure are designed according to the 1952 A.I.J. Building Code. This Code prescribes that cracks may not occur in specimens subjected to a lateral force corresponding to a design base shear, k, of 0.2. To obtain such strength, a required area, a width of shear wall, and a required shear reinforcing ratio to prevent the progress of cracks were specified. Large-scale seismic tests on RC wall structures were carried out. The tests showed such structures to have a sufficient lateral strength which is equivalent to the vertical weight, even though they were inclined to fail due to brittleness. Apartment houses of this type have hardly suffered significant damage from the several earthquakes they have experienced.

The new Building Code for medium-rise RC wall structures aims at a structure with increased ductile deformation capacity to compensate for the lowered strength from the lesser area of shear walls.

The following fundamental criteria involving assurance of seismic safety against severe earthquakes are adopted by the new Building Code: (see Figure 1 and Figure 2)

(1) To control stress to any part of the structure caused by frequently-occuring medium strength earthquakes within permissible stress levels;

(2) To prevent failure to the structure from the rare, severe earthquakes.

The provisions for achieving these purposes are:

(1) Lateral resistant strength should be more than 50 percent of the total weight of the structure.

In evaluating ultimate strength, the effect of transverse members such as slabs and transverse walls, which cause increased flexure, and the shear strength of the longitudinal members, may be included.

(2) The structure should be strong enough to not lose its strength under the compulsory displacement of more than twice the yielding displacement.

For this purpose, the following is prescribed:

(a) The cross-sectional area of shear walls in each frame should be equalized, and the structure should be designed to be as ductile as possible.

(b) Restrict the number of members which are prone to fail in nonductile manner, i.e., deep beams, members with non-structural walls, and members with openings.

(c) To design members using the criteria that flexure failure should occur prior to shear failure, and shear reinforcement ratio exceeds the specified value.

The test specimen reported here was designed to satisfy the above new regulations. The following questions summarize what should be confirmed through testing:

(1) Regarding ultimate strength,

(a) Does ultimate strength exceed 50 percent of its own weight?

(b) To what extent are transverse members more effective than longitudinal ones?

(c) Can the resulting ultimate strength be explained theoretically?

(2) Regarding the hysteretic loop,

(a) Is strength reduced when the displacement range goes beyond maximum strength?

(b) Is there any which can be expected to fail from excessive brittleness? If there is, does it not have a bad influence upon the total behavior of the structure?

(c) Do members with non-structural walls, and with openings, have stable behavior?

(d) How is the aseismic performance of the test structure estimated, on the basis of ultimate strength and deformation capacity, through testing?

TEST SPECIMEN

The Choice of a Model Test Specimen

The main objective of this testing was to investigate the properties of the provisions for seismic safety given in the newly established design Code outline. The most essential factor to seismic safety in a wall structure is thought to be the shear wall ratio, the total shear wall cross-sectional area divided by the floor area. Therefore, a structure having a shear wall ratio just beyond the regulated minimum values was chosen for the test structure.

As for loading, it was limited in one horizontal direction because of the restricted capacity of the full-scale testing facilities. The question of whether a longitudinal or transverse direction should be chosen was examined. In the transverse direction, the

structure was composed mainly of rather slender shear walls, with an average shear stress due to lateral force, 50 percent of its weight, of 15 kg/cm^2, which was less than 10 percent of the concrete compressive strength. This implied that in the transverse direction, the structure would fail in flexure prior to shear, which suggests that sufficient seismic safety will be obtained. In the longitudinal direction, there was a mixture of several shear wall types with different stiffness, so that the structure would not fail in flexure.

Accordingly, the longitudinal direction of the structure was chosen as a testing objective.

Further, the restricted funds and the necessity of maintaining the specimen in non-optimum advantageous condition forced in other design changes as follows:

(1) Test specimen reduced to first five stories from the original eight story structure.

(2) Test specimen reduced to two apartment houses, a smaller part of the original model structure.

(3) The dimensions of the transverse direction were reduced to 80 percent.

(4) Main bars in the beams of the sixth to eighth stories of the original structure were moved to the beams of the fourth and fifth floor of the specimen to make the lateral capacity of the specimen equal to that of the eight story structure.

(5) Slab reinforcement in the longitudinal direction, and shear reinforcement in the transverse wall, remain the same as the original eight story structure.

(6) The effects of deep beams, small openings [7], and a spandrel wall [8] which the original structure did not include, were added to the investigation.

(7) The effect of a shortened main bar anchoring length in the beams going into the shear walls, which differs from the plans for the original structure, was also added to investigation.

Outline of the Test Specimen

The plan and sections of the test specimen are shown in Figure 3. Figure 4 shows one example of reinforcement. Steel used in the specimen were all deformed bars, SD30, having a nominal yielding stress of 3.0 t/cm^2. The concrete was a normal one with design strength of 240 kg/cm^2, having a tested compressive strength of 240-280 kg/cm^2.

190

LOADING AND MEASURING PROGRAM

The test specimen was fabricated on the floor of the full-scale testing facilities in the Building Research Institute, Ministry of Construction. Testing lasted about one month in November, 1979.

Prior to lateral loading, a vertical load of 840 ton, the equivalent of the weight of the top three stories of the original eight story structure was applied with 16 oil jacks, and was kept constant during the lateral loading. Lateral loading was conducted by 10, 6, and 2 oil jacks at the roof, fifth and fourth floor levels, respectively. The overturning moment at the first floor caused by this lateral load was equivalent to that of the model eight story structure subjected to the uniform distribution of lateral load. Thirteen times loading reversals were conducted under the control of rotational angle, R, mainly of 1/400, 1/200 and 1/100 ratios.

The following test data were measured automatically: lateral and vertical displacements of 140, steel strain of 328, strain on the concrete surface of 135, and rotational angle at nodal points of 18.

Additionally, cracks were observed in all members including transverse walls and slabs. Significantly developed cracks were measured at each loading step. The loading and measurement conditions, and the loading program are shown in Figure 5 and 6, respectively.

EXPERIMENTAL RESULTS

Outline of Testing Results

Table 1 shows the maximum value of loads and associated displacements at each loading cycle. The relationship between load and absolute lateral displacement at roof floor is shown in Figure 7.

As is shown in Table 1, the maximum load was about four times the design load, and the associated displacement at the top floor was 1/100 of the structure's total height which was 27 times the elastic displacement of the design load. In subsequent loading, when displacement reached 1/50 of the total height of structure, the maximum load was 490 tons less than the previous maximum load.

Behavior of Specimen

Specimen behavior prior to obtaining maximum strength is summarized as follows:

(1) First cycle with half the design load showed hardly any cracks.

(2) Second cycle with the design load showed a few flexural cracks in the beams, diagonal shear cracks at the end of openings, and flexural cracks in the slabs, but no stiffness deterioration.

(3) At the rotational angle, R, of 1/800, besides progressive flexural and flexural-shear cracks in the beams and walls, horizontal cracks occurred to the transverse wall and shear cracks to short-span beams and small-depth walls in the Y2 frame. The maximum load was twice the design load and the associated displacement was 3.5 times the design displacement.

(4) At the rotational angle, R, of 1/400, (fourth cycle to sixth cycle), shear cracks in the beams and walls and horizontal cracks to the slabs and transverse wall were progressed noticeably, while diagonal cracks occurred in the beam-column connections. Yielding in the beam and wall barely occurred. The maximum load and the associated displacement were, respectively, 2.5 and 7 times the design values. Deterioration of maximum load due to loading reversals was not observed.

(5) At R = 1/200 (seventh to ninth cycle), a yielding of the beams and walls began, while shear failure of short-span beams and small-depth walls in Y2 frame became obvious. The maximum load and the associated displacement were 3.5 times and 1.5 times the design values. No deterioration of the maximum strength in loading reversals was observed.

(6) At R = 1/100 (tenth cycle), load reached its maximum. Yielding hinges were seen in almost all the member ends, the short-span beams failed in shear. This implies pronounced deterioration of the maximum strength. Figure 8 shows the development of cracks in the Y2 frame at each loading level.

Maximum Strength

The maximum strength was 1,608 tons in tenth cycle (R = 1/100). This corresponds to 86 percent of the total weight of the original eight story structure. The maximum strength of the negative direction loading was reduced to 1,529 tons which is equal to 95 percent of the 1,608 ton load. This indicates that the different width of the transverse walls under the tensile stress due to lateral load does had some influence.

Failure Mechanism and Strength Reduction

Judging from strain gages attached to the longitudinal reinforcement and from the developing crack widths on beam and wall ends, flexural yielding at the ends and the bottom of first floor walls occurred at the rotational angle, R, of 1/400. At R = 1/200, ninety-one joints, that is, more than 65 percent of all joints, yielded by flexure. Until this stage, only two walls and two beams of Y2 frame had failed in shear. At the maximum strength (R = 1/100), joint yielding increased. Shear failure, mainly that of short beams with 1.0 m span-length, also developed.

These test results indicate that it is appropriate to consider the failure mode of this specimen as a flexural failure prior to a shear failure. Existing conditions when hinging occurred were obtained by steel strain measurements and are given in Figure 9.

When the specimen was subjected to loading reversals three times under the control of the same displacement after the maximum strength, 1608 tons, the maximum capacity was reduced to 1,460 tons; and in the negative loading, the maximum strength was -1529 tons at the same, tenth, cycle as positive loading. Load capacities for the twelfth and thirteenth cycles were -1,368 tons and -1,347 tons, respectively. As shown above, strength reduction was not pronounced and the displacement limitation for ductile behavior could be thought to be 1/50.

The mean shearing stress, calculated by dividing the maximum strength, 1,608 tons, by the totaled cross-sectional wall area is 23 kg/cm^2, which corresponds to 1/10 of the compressive strength of the concrete test cylinders. This value of 23 kg/cm^2 remains in the region were satisfactorily repairable conditions are expected to occur when appropriate reinforcement is in place.

Other Test Results

(1) Effects of transverse members

(a) Judging from the reinforcement strain and from the developing cracks in the slab, it seems that the slab reinforcements are effective in increasing the flexural strength of the beams at the stage of maximum strength.

(b) Slab concrete has some effect on the shear strength of beams because some beams which failed in shear were associated with shear fracture of the slab.

193

(c) As for the effect of the transverse wall on the flexural strength of the wall, it seems from the strain gage data that all the reinforcement in the transverse wall is effective, where the transverse wall is attached to the edge of the longitudinal wall. It is also recognized, judging from the horizontal tensile cracks in the transverse wall, that attaching the transverse wall to the center of the wall increases the strength of the longitudinal wall.

(d) As for the effect of the transverse wall on wall shear strength, judging from vertical tensile cracks occurring at the transverse wall from high compression under large displacement loading, it seems that a part of the transverse wall transferred shear and increased wall shear strength.

(2) Small wall openings

Some of the walls have small openings which may be ignored in the design Code if the reinforcement is properly arranged. At four corners of these openings, diagonal shear cracks occurred in an earlier stage of loading when the mean shearing stress was about 2.5 kg/cm^2. These cracks developed as the load was increased, but the widths did not expand even in subsequent loading. In addition, crushing did not occur. Of twelve reinforced openings which had strain gages attached, only two yielded. These results indicate that there is no problem for reinforcement at small openings.

(3) Behaviors of beams with thin spandrel wall

Outer beams for the first and fifth floors of the Y2 frame had a thin spandrel wall separated from an adjacent wall by a slit, which was deemed to be structurally negligible according to the design Code outline.

Testing shows, the spandrel wall had flexural cracks near the slit at a lower load about equal to 1/3 of the maximum load, which progressed to mid-span in subsequent loading, but almost no shear cracks. Crushing at the top of the slit began near the maximum load, and concrete in the circumference exfoliated at the maximum load. Beams with spandrel wall and the walls that the spandrel wall joined did not show brittleness failure, which indicates that the spandrel wall would not adversely influence surrounding members.

(4) Short-span beam behavior

Among ten beams of 1.0 m span-length and ten beams of 1.6 m span-length in the Y2 frame, eight beams on the second, third, and roof floors obviously failed in shear

after flexure yielding. Seven of eight beams having a wider cross-sectional area on the fourth and fifth floor had slight damage. As a whole, this specimen was considered as a flexure-failure frame except for a few beams and walls, while strength capacity did not markedly deteriorate after exposure to maximum load.

(5) Failure of short-span walls in Y2 frame

Fourth and fifth floor Y2 frame short-span walls failed in shear. While these fourth and fifth floor walls developed shear cracks at low levels of load, those of first, second, and third floor had few shear cracks, and they did not notably progress. The fourth and fifth floor walls had extended shear cracks at the rotational angle, R, of 1/200, and the concrete began to exfoliate at 1/100 R. Finally, at R of 1/50, exfoliation of concrete was so extensive that the other side could be seen through the shear reinforcement.

The reason for failure is thought to be that these short-span walls had a "column" deformation condition, and the adjacent walls with high stiffness had a "canti-lever" deformation, with the result that shear forces were concentrated on the short-span walls in the upper stories.

ANALYTICAL STUDIES ON TESTING RESULTS

Elastic Analysis

The general-purpose program for elastic analysis, TABS, by the University of California, was used to investigate the behavior of structural members in the elastic range subjected to the maximum test load, 1,608 tons.

The following assumptions were introduced:

(1) Structural members were treated as line members. Columns with rigid end zones, including flexural, shear and axial deformation, and beams with rigid end zones, including flexural and shear deformation, were considered.

(2) No torsion was thought to occur under the assumption of a rigid floor.

(3) With interaction between transverse wall and column, and slab to beam having the flange width up to the mid-span in the transverse direction, all cross-sectional areas of the transverse members could be estimated in calculating the stiffness of the structure in the longitudinal direction.

(4) Despite assumption (3) above, shear area was considered as a cross-sectional area of the longitudinal members.

(5) The column rigid zone length was estimated from the nodal point to the face of the connecting beam, while the beam (rigid zone length) was from the nodal point to the face of the connecting column.

(6) Story height was measured from floor to floor.

Detailed results for the elastic analysis were abbreviated in order to be shown. Except that the calculated specimen stiffness was considerably higher than the measured one, in general, the analytical results for stress distribution of each member suffi-ciently explain the conditions of cracking and yielding of each member in the test observations.

Bearing Capacity

For the six cases shown in Table 2, the maximum specimen strength was analyzed using the principle of virtual work. The test structures failed in flexure, i.e., the beams of all floors yielded in flexure, and the walls yielded in flexure at the base of the first floor. The calculated results of each case are shown in Figure 10 as well as the shear force at the first floor.

The following can be observed from the figure.

(1) The calculated results are in good agreement with the test results in both the positive and negative loading direction. However, it should be noted carefully that the test and calculated results include the additional capacity due to the axial forces in the beams.

(2) The calculated results, which take into consideration the effect of all the members being perpendicular to the beams and walls in the loading direction, agree well with the test results. The ratios of the calculated strengths, considering no effect of the perpendicular members, and then considering the effect of only half of the perpendicu-lar members, to the above-mentioned calculated strength were 57 percent and 83 percent, respectively. Accordingly, the effect of the perpendicular members to the bearing capacity of the specimen was found to be remarkable.

(3) The result calculated using the nominal strength as the material strength (3.0 t/cm^2) for the yield strength of steel and 210 kg/cm^2 for concrete compressive

strength) was 84 percent of the calculated strength using the test results as the material strength (around 3.6 t/cm^2 and 240 kg/cm^2). This ratio almost corresponds to the ratio of the nominal yield strength of steel to the actual yield strength.

(4) The additional strength due to the axial force in beam was determined to be 240 tons. This value corresponds to about 24 percent of the measured maximum strength.

(5) The calculated result, based on design Code regulations was 87 percent of the test result.

Statistical Non-Linear Analysis

The method used for static non-linear analysis is as follows:

(1) Estimate the deteriorated stiffness of each member due to the occurrence of cracking and yielding under an increasing horizontal load, based on the elasto-plastic behavior of each member.

(2) Assemble each time the determined stiffness matrix of each member to the total stiffness matrix of the structure.

(3) Calculate the increment of displacement under the increment of the external force.

Fundamentally, since no change in stiffness is assumed during an increment of force, this method may be said to be a repetition of the ordinary elastic direct stiffness method. Horizontal displacement at each story and rotational angle at each nodal point are considered as unknown factors, and axial displacements of walls and beams are neglected. The Degrading Tri-linear model, which agrees with the hysteretic loop of reinforced concrete members failing in flexure, is used as the hysteresis characteristic of the members. Further, shear deformation is included as a flexural one under the assumption that shear rigidity deterioriates proportionally to flexure rigidity. Hence, shear collapse of the members is not considered in the analysis. The calculated load-deflection relationship at the roof and the second floor obtained by this method is shown in Figure 11, accompanied by the experimental results. As shown in the figure, the calculated results agree fairly well with the test results.

Non-Linear Dynamic Response Analysis of the Model Building

Non-Linear dynamic analysis was carried out on the eight-story building, which is considered to be the original model for the test specimen using the following assumptions:

(1) The yield capacity of each story in the model building is calculated with the conditions that the external force distribution is inverse-triangle, and that the overturning moment at the base of the first story due to the external force is equal to that of the experimental results.

(2) The total weight of the model building is assumed to be the same as the test specimen, 1,879 tons. Weight of each story is uniform.

(3) The cross-sectional area of each member of the model building is assumed to be the same as the member on the first story of the test specimen. Member stiffness is estimated taking into consideration the full extent of the transverse members.

(4) The stiffness reduction coefficient after cracking is assumed to be 5 percent of the calculated elastic story stiffness, refering to the test results. The story cracking strength is assumed to be 50 percent of the calculated story yielding strength.

(5) Damping is estimated at about 7 percent for the fundamental period within the elastic range.

The results of the response analysis for the N-S component of the El-Centro Earthquake (max. acceleration: 300, 500 and 700 gal) are shown in Figure 12. The figure shows that response displacements in all cases are within a permissible range, and that the eight-story model building exhibits excellent seismic performance.

CONCLUSIONS

A full-scale test on the first five stories of the original eight story apartment house of reinforced concrete wall construction was carried out. From the experimental and analytical results, the following was concluded.

(1) Bearing Capacity

The obtained maximum horizontal capacity of the specimen was 1,608 tons at the base floor. This value corresponds to 86 percent of the total weight of the model building. However, neglecting the additional strength due to axial stress in the beams, this value is reduced to 1,365 tons or 73 percent of the total weight.

The calculated maximum strength, using the assumption that the failure mechanism is a beam-yield type and that wall and floor slabs perpendicular to the walls and beams in the loading direction are effective over the entire length, coincided closely with the test results.

(2) Deformation Capacity

Strength reduction was not significant even under a large displacement which corresponds to a rotational angle of 1/50: excellent deformation capacity was recognized.

The elastic and plastic characteristics of the structure could be analyzed using the postulated assumptions.

(3) Synthetic Estimation of Seismic Performance of the Model Building

The foregoing results on bearing capacity and deformation capacity satisfy the regulations of the design Code. Consequently, the seismic performance of the model building test specimen is considered excellent. This is also shown by the results of dynamic response analysis using several strong earthquake motions.

(4) Notes on the Structural Design

(a) The extensive width of the perpendicular members was effective in providing flexural strength over the entire length of this specimen.

(b) The reinforcing used around the small openings in the wall was recognized to be sufficient.

(c) Thin spandrel walls, which were not considered in the structural calculation, did not unfavorably effect the beams and walls connected to them.

(d) Brittleness failure was significantly recognized in several short-span beams. However, since the number of members failing due to brittleness was small, the influence of a partial brittleness failure on the whole structure was found to be negligible.

Table 1 A List of Max. Total Load and Measured Horizontal Displacement at each Story in each Loading Cycle

(Unit: Load-ton, Displacement-mm)

Loading Cycle		Total Load	Horizontal Displacement (Y_0 Plane)						Note
			6F	5F	4F	3F	2F	1F	Scheduled Story Deflection Angle
1	+	198	2.61	2.24	1.81	1.12	0.39	0.05	1/2 times Design
	−	198	3.07	2.64	1.41	0.63	0.41	0.01	Load (k=0.2)
2	+	396	4.79	3.96	3.49	2.45	1.13	0.19	1 time Design
	−	396	5.78	5.02	4.23	2.10	1.06	0.05	Load
3	+	779.4	16.98	14.09	11.47	7.69	3.59	0.49	(1/800)
	−	759.0	16.85	14.69	11.14	6.01	2.49	0.09	
4	+	1112.4	35.16	29.90	25.30	16.85	8.19	1.17	No.1 Cycle at
	−	1054.0	33.93	28.94	22.55	11.95	4.32	0.29	1/400
5	+	1048.4	35.60	30.64	26.30	17.61	8.64	1.27	No.2 Cycle at
	−	994.6	33.87	29.50	22.61	11.88	4.19	0.34	1/400
6	+	1035.0	35.23	31.07	26.50	17.96	8.77	1.42	No.3 Cycle at
	−	960.2	33.83	29.17	22.28	11.46	3.67	0.43	1/400
7	+	1444.0	71.23	61.54	53.01	37.07	18.39	3.41	No.1 Cycle at
	−	1322.0	66.00	56.94	44.42	22.58	8.06	1.26	1/400
8	+	1209.6	71.73	63.17	52.89	36.07	18.60	3.73	No.2 Cycle at
	−	1291.4	66.03	56.94	44.35	22.65	8.12	1.27	1/400
9	+	1203.0	71.53	63.00	53.41	36.49	18.81	3.88	No.3 Cycle at
	−	1251.0	66.33	57.04	43.88	22.37	7.96	1.30	1/400
10	+	1608.0	132.50	116.75	97.29	66.40	35.86	10.54	No.1 Cycle at
	−	1528.6	133.33	111.89	82.73	39.35	16.43	5.66	1/100
11	+	1488.2	139.93	123.74	101.99	71.02	38.80	12.14	No.2 Cycle at
	−	1430.6	133.23	111.82	84.28	44.60	16.55	6.28	1/100
12	+	1460.2	144.36	127.31	98.10	68.15	37.53	12.49	No.3 Cycle at
	−	1368.4	132.80	111.42	84.41	44.74	16.53	8.26	1/100
13	+	1548.2	211.29	186.38	155.81	107.72	56.33	19.47	Last Cycle at
	−	1347.0	179.75	148.95	116.69	64.17	28.48	17.36	1/50

Table 2 A List of Structural Conditions Assumed in the Cases
of Maximum Capacity Calculation

Case	Loading Direction*1	Considered Extention of Perpendicular Wall	Material Strength*2	Axial Force in Beams*3
1	Positive	Zero	Test Result	Neglected
2	Positive	All	Test Result	Neglected
3	Positive	All	Test Result	Considered
4	Positive	Half	Nominal	Neglected
5	Positive	All	Test Result	Neglected
6	Negative	All	Nominal	Neglected

Note)

* 1 : Thick (thin) perpendicular wall is in tention side
in case of positive (negative) loading.

* 2 : Nominal yield stress for reinforcing steel is 3.0 t/cm² (SD30)
Design concrete compressive strength is 210 kg/cm² at 4 weeks.

*3 : Axial forced in the R 5 and 4th floor beams due to
concentrated loading applied in the test.
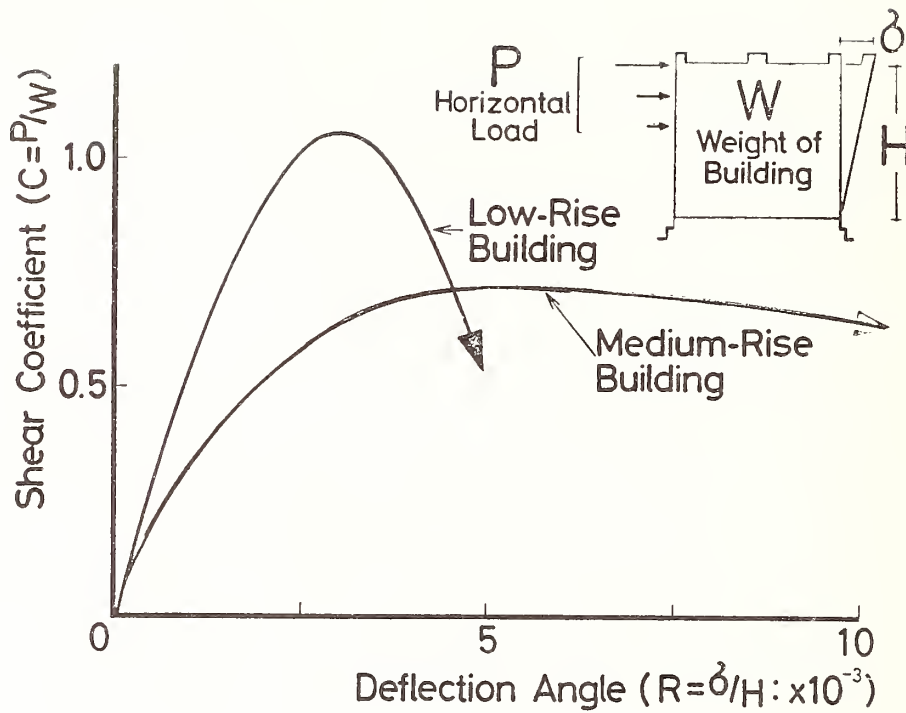
Fig. 1 Idealized Horizontal Load Vs. Deflection Relationship of Low- and
Medium-Rise Reinforced Concrete Wall Structures

a) Example of North-Side
   Section in case of
   5-Storied Building

b) North-Side Section
   of Test Specimen
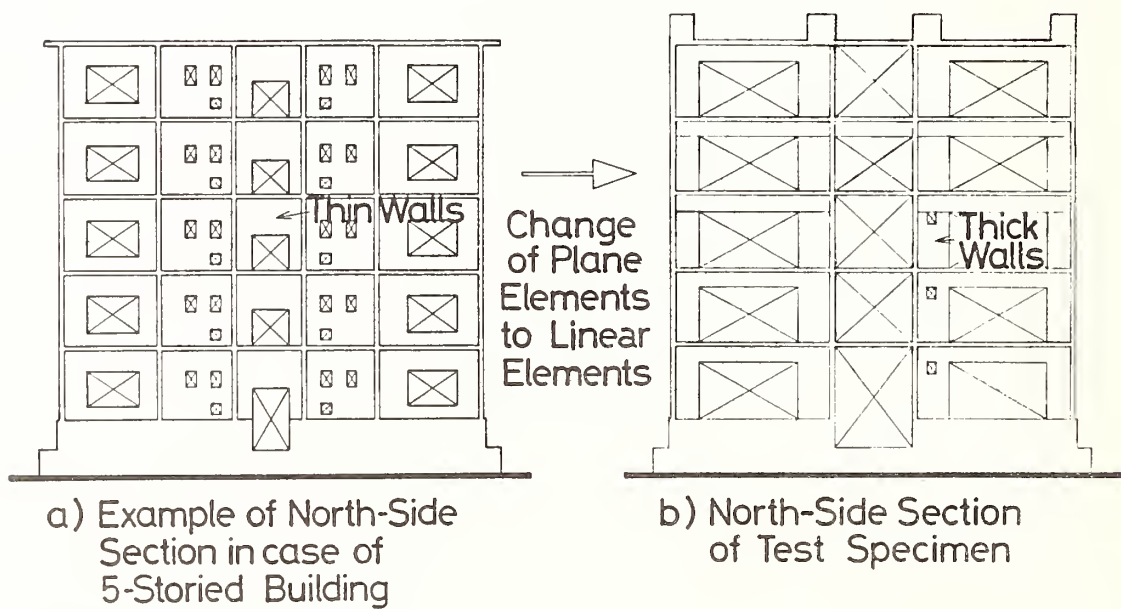
Fig. 2 Change of Structural Systems in Low- and Medium-Rise Reinforced Concrete
Wall Structures

Fig. 3 Plan and Structural Planes in the Loading Direction of the Specimen
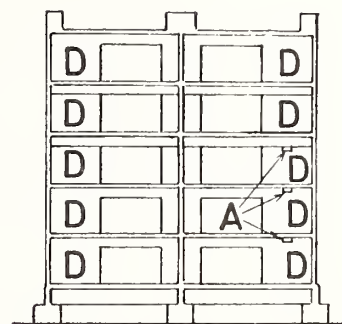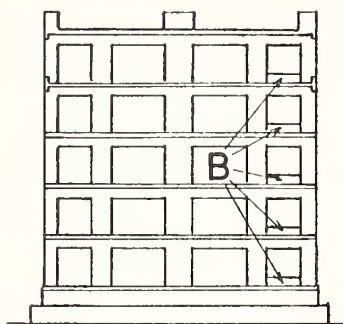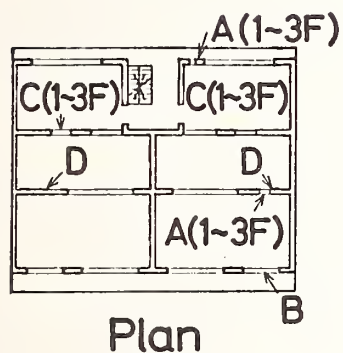
A : Shear Wall with Opening

B : Beams with Non-structur-
al Wall

C : Opening with Door

D : Wall with Finishing
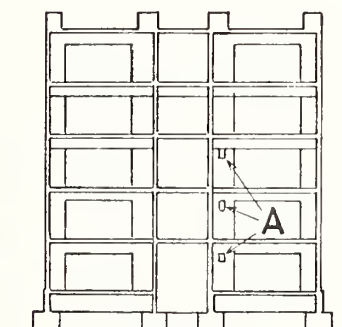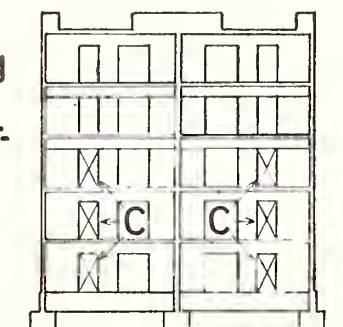
FIG.4   REINFORCEMENT DETAILS OF THE Y₂ PLANE
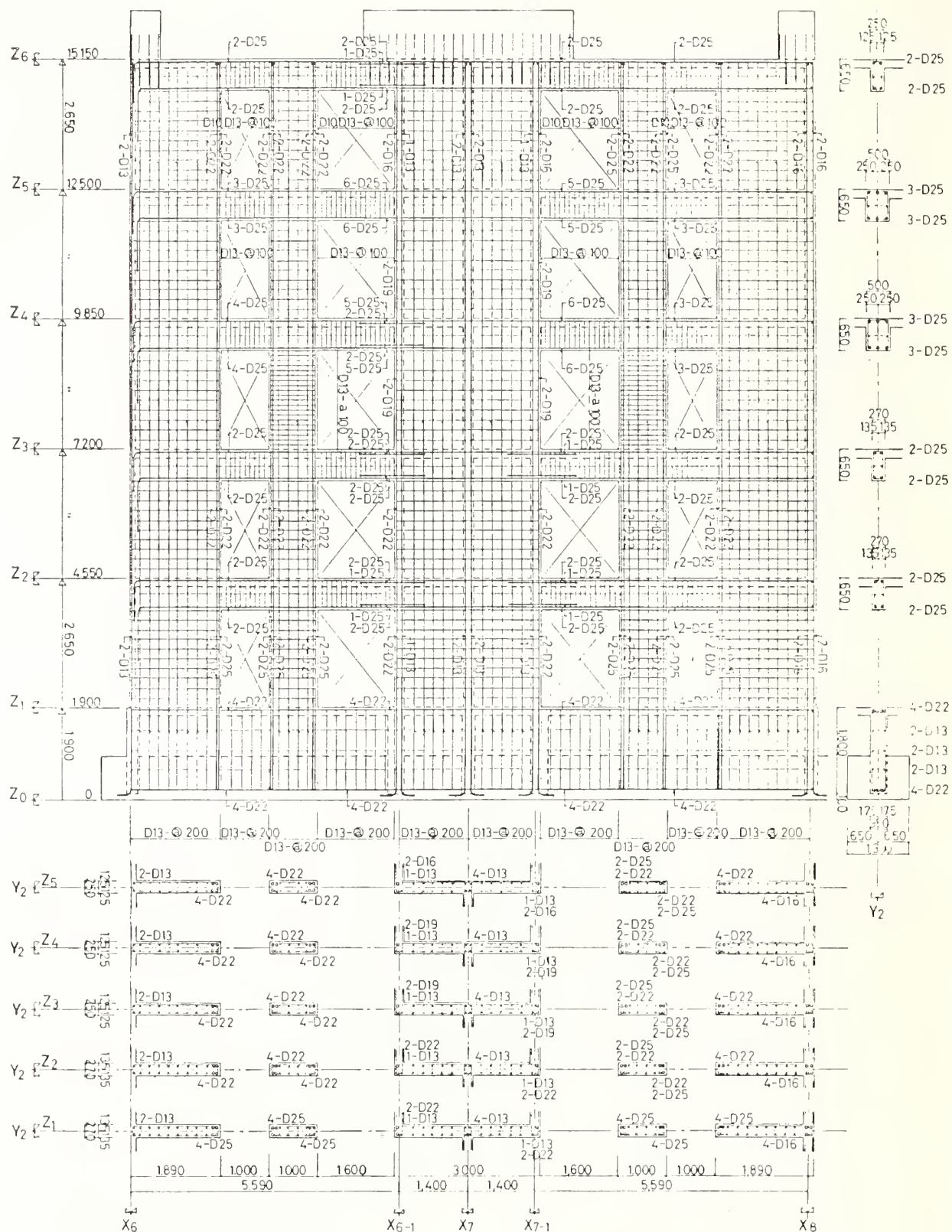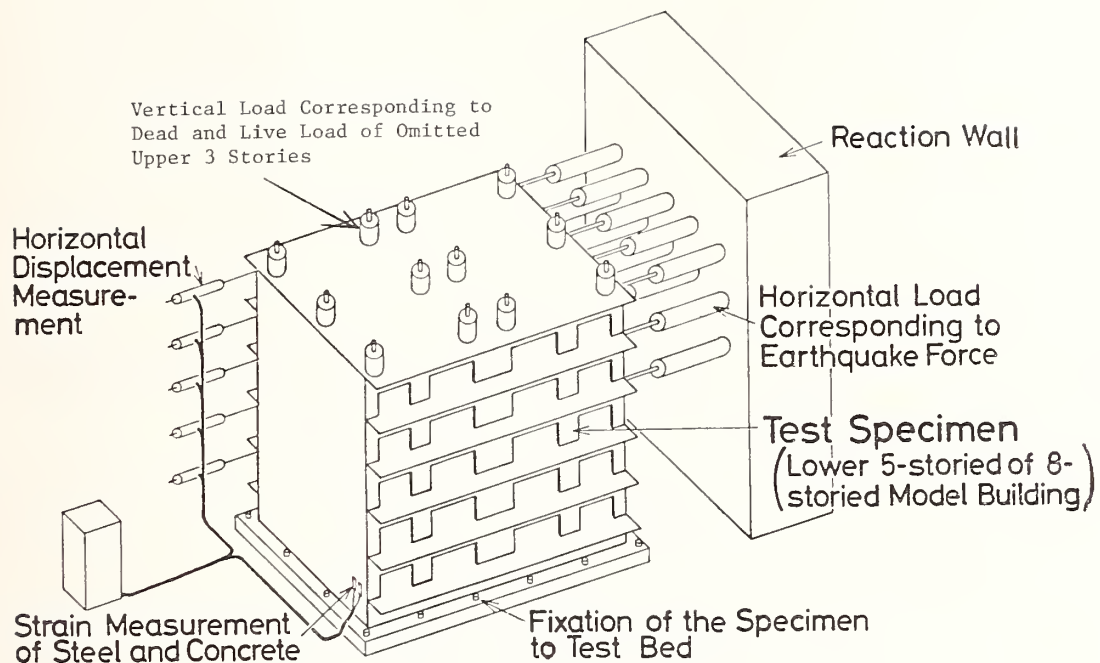
FIG.5 LOADING AND MEASURING SYSTEMS APPLIED TO THE TEST
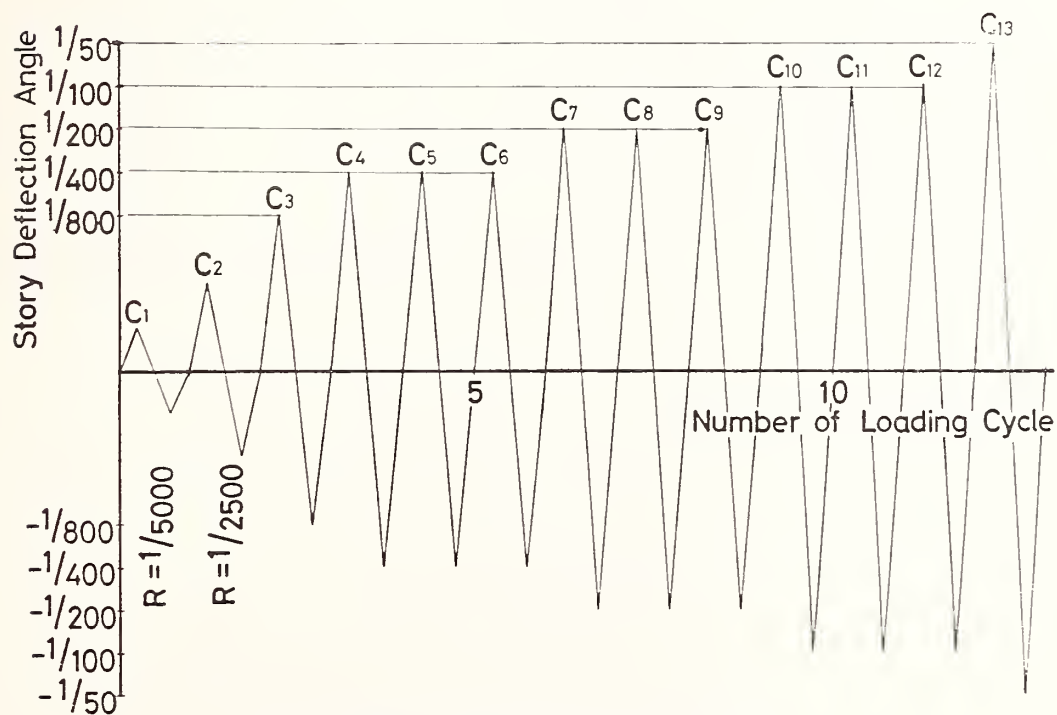
FIG.6 LOADING EXCURSION APPLIED TO THE TEST

Fig. 7 Base Shear Vs. Top-Story Displacement Relationship
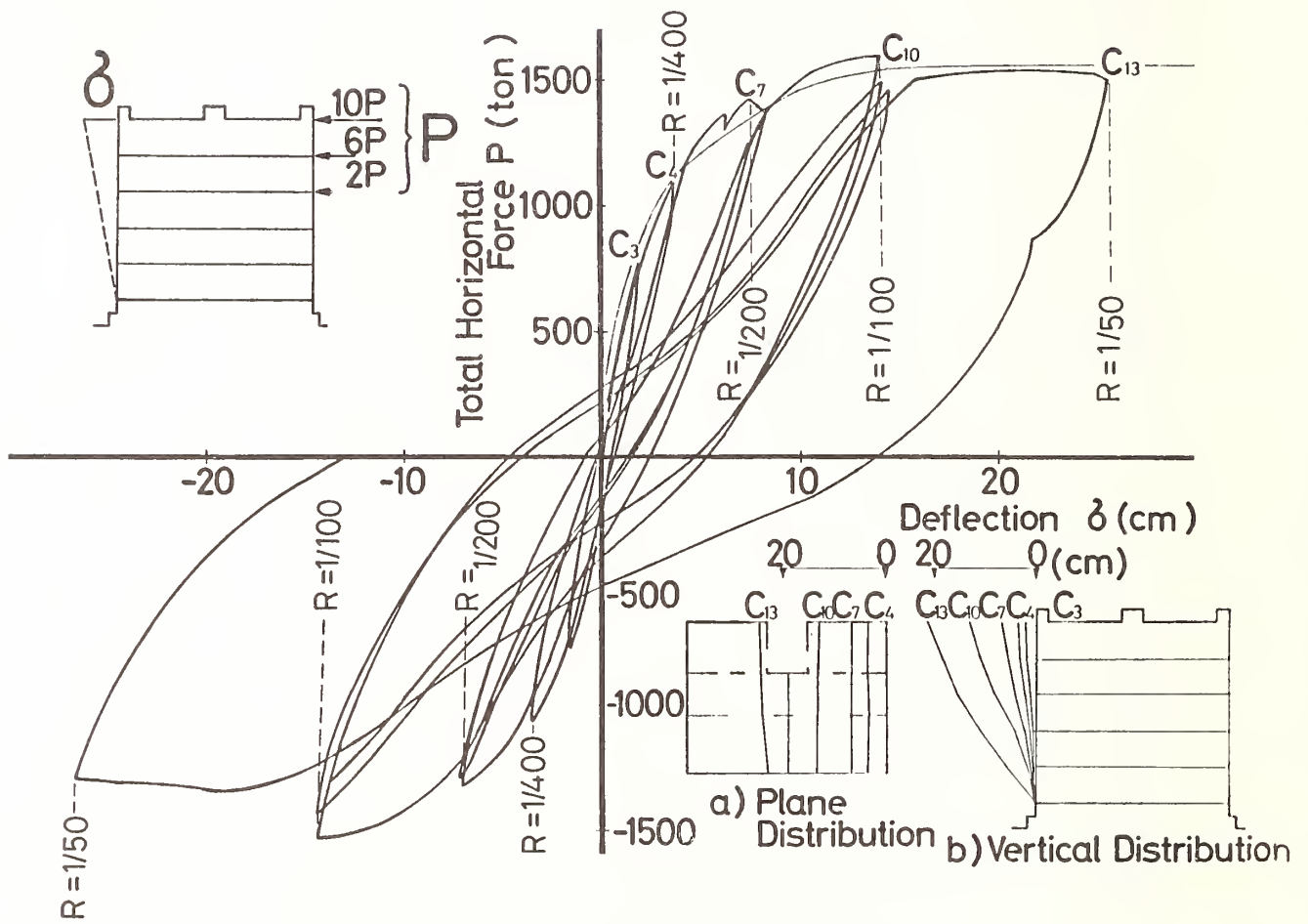
a) After No.2 Cycle
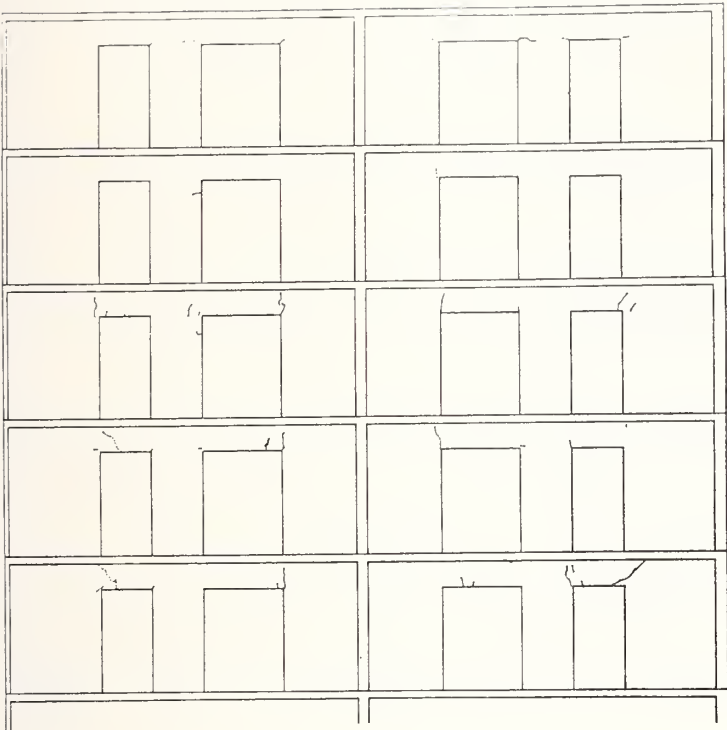
b) After No.3 Cycle
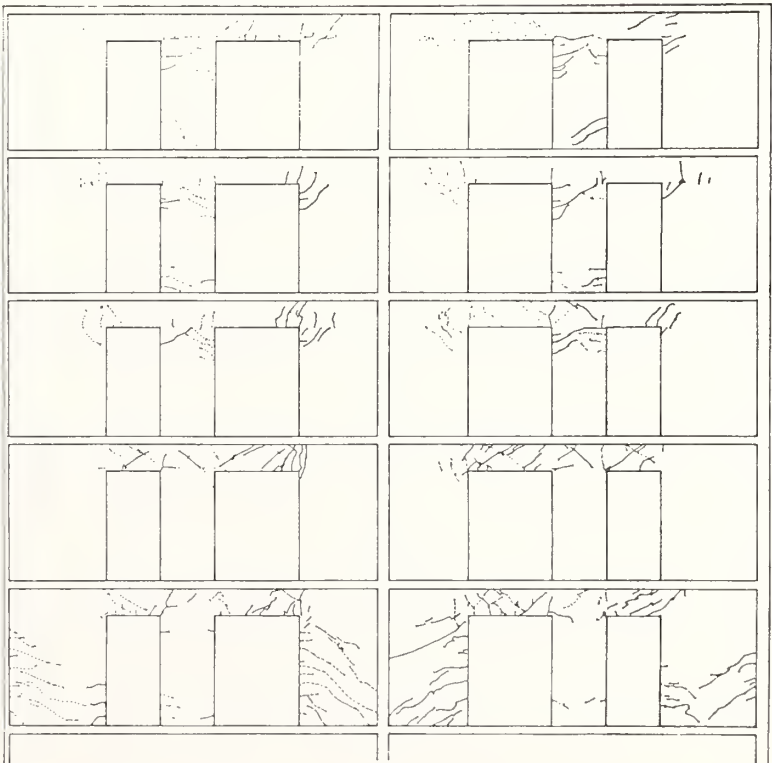
Fig. 8a. Observed Crack Pattern (No. 1)

c) After No.4 Cycle
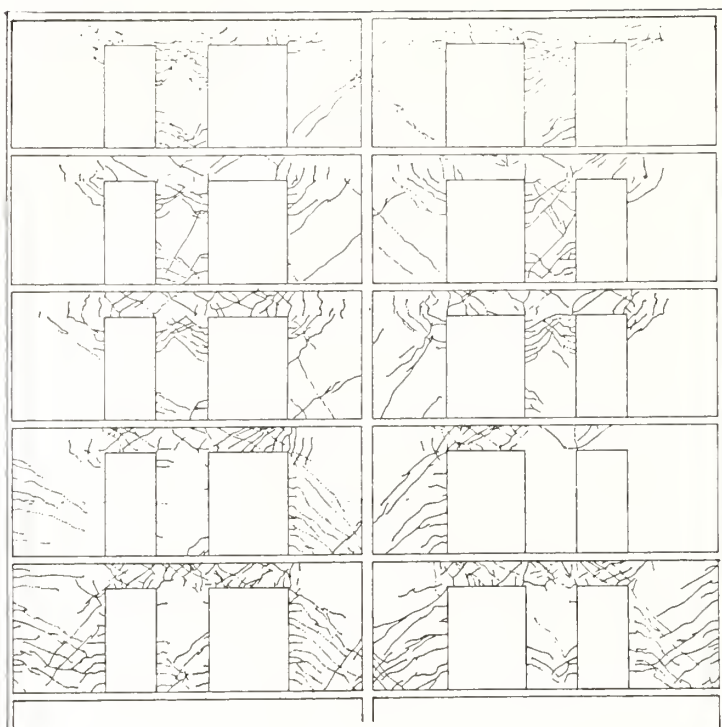
d) After No.7 Cycle
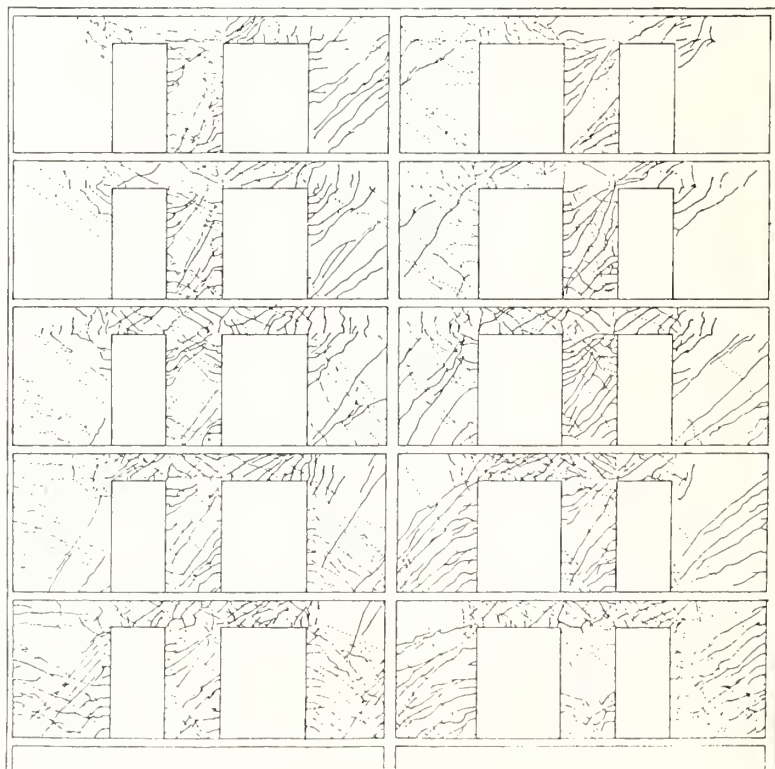
Fig. 8b. Observed Crack Pattern (No. 2)

208

e) After No.10 Cycle
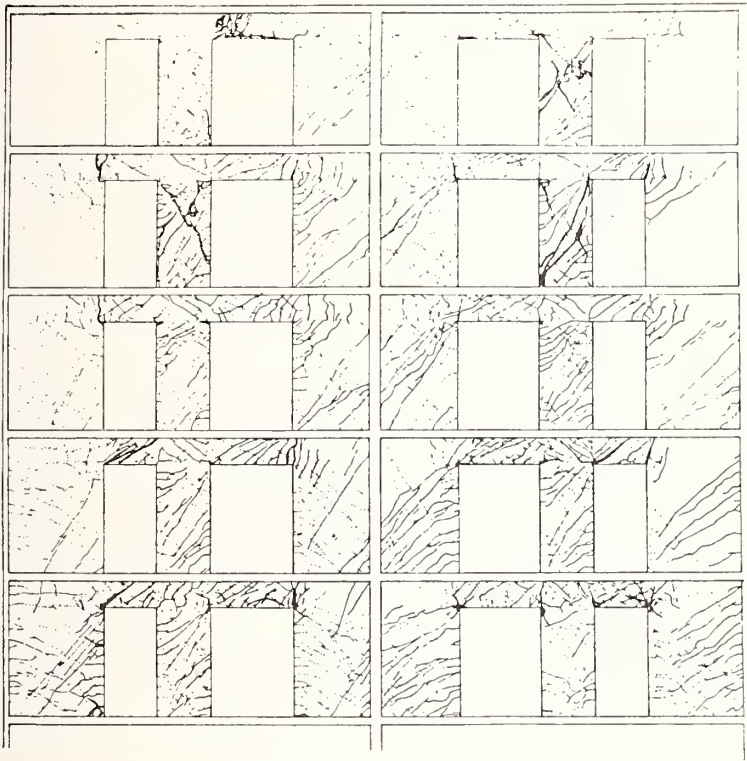
f) After No.13 Cycle
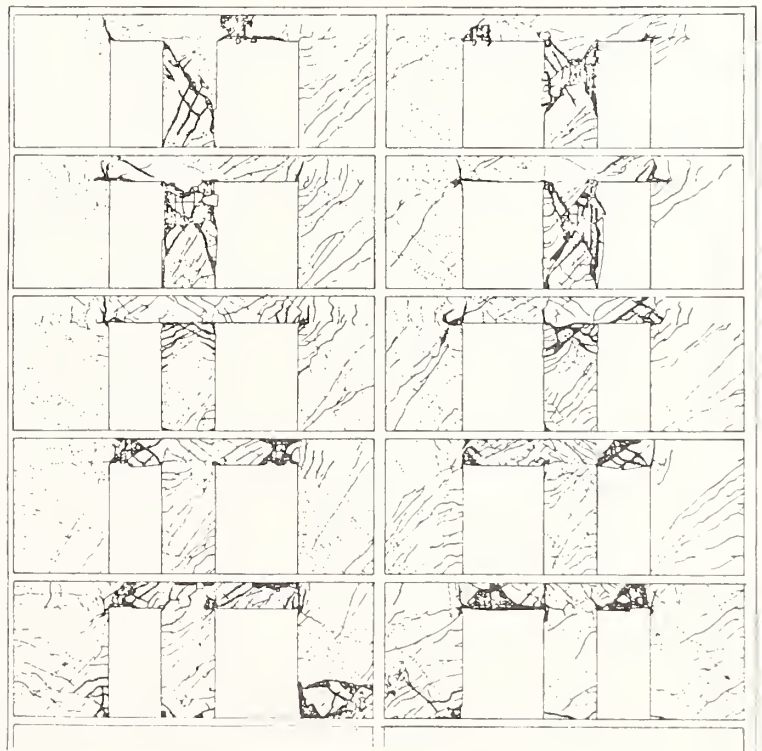
Fig. 8c. Observed Crack Pattern (No. 3)

209

Y₀ - Plane   Y₂ - Plane

○ Flexure Yield
   at R = 1/400
● Flexure Yield
   at R = 1/200
× Shear Yield
   at R = 1/200

Y₁ - Plane   Y₃ - Plane

FIG. 9a   FAILURE MECHANISM DUE TO POSITIVE LOADING
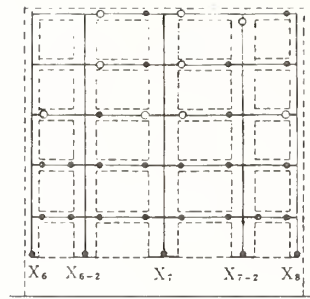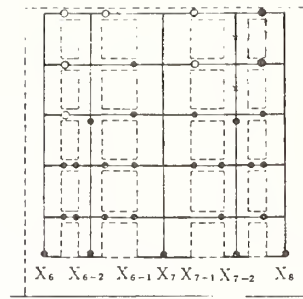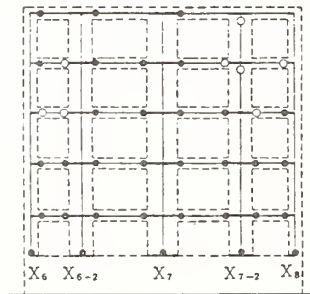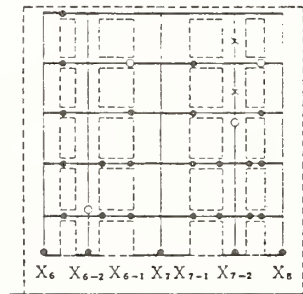
Y₀ - Plane   Y₂ - Plane
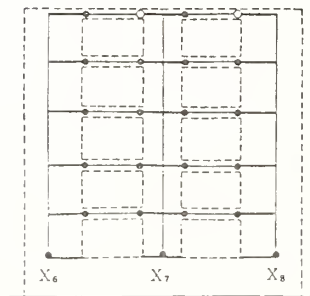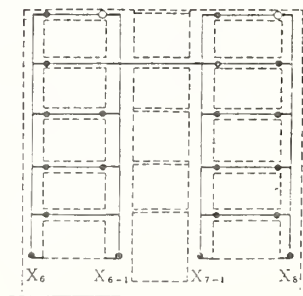
Y₁ - Plane   Y₃ - Plane

FIG. 9b   FAILURE MECHANISM DUE TO NEGATIVE LOADING

Calculated additional capacity due to axial force in beams

a) Considered Width of Perpendicular Wall   **b)** Material Strength

c) Thickness of Perpendicular Wall on Tension Side   **d)** Axial Force in Beams
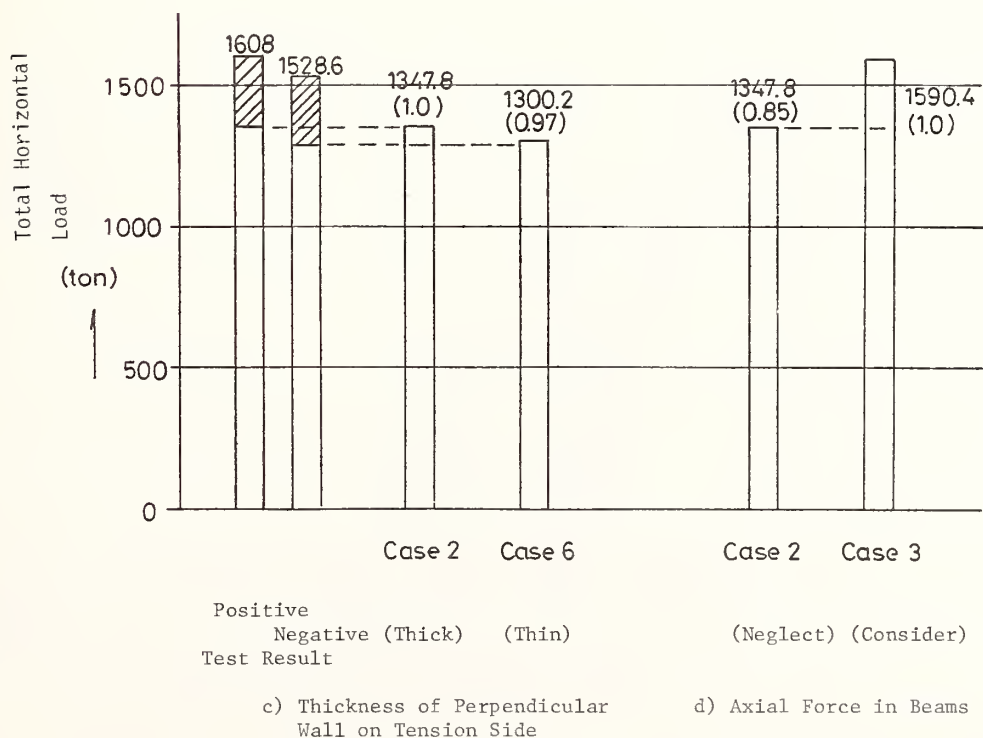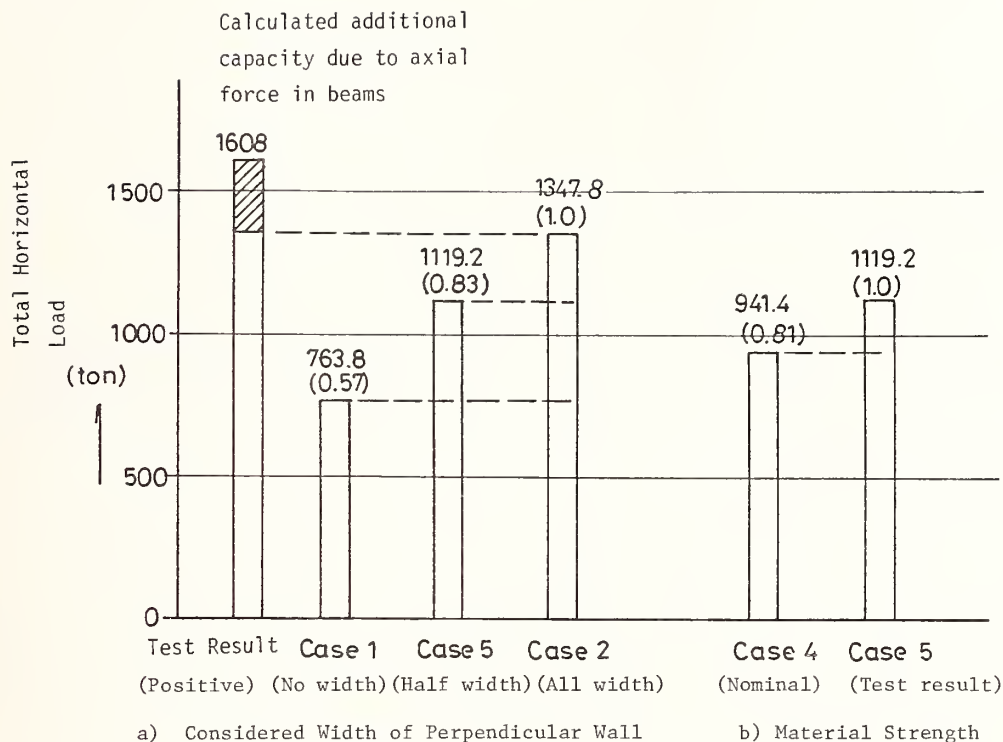
Fig. 10 Influence of Several Factors on Calculated Maximum Strength

211
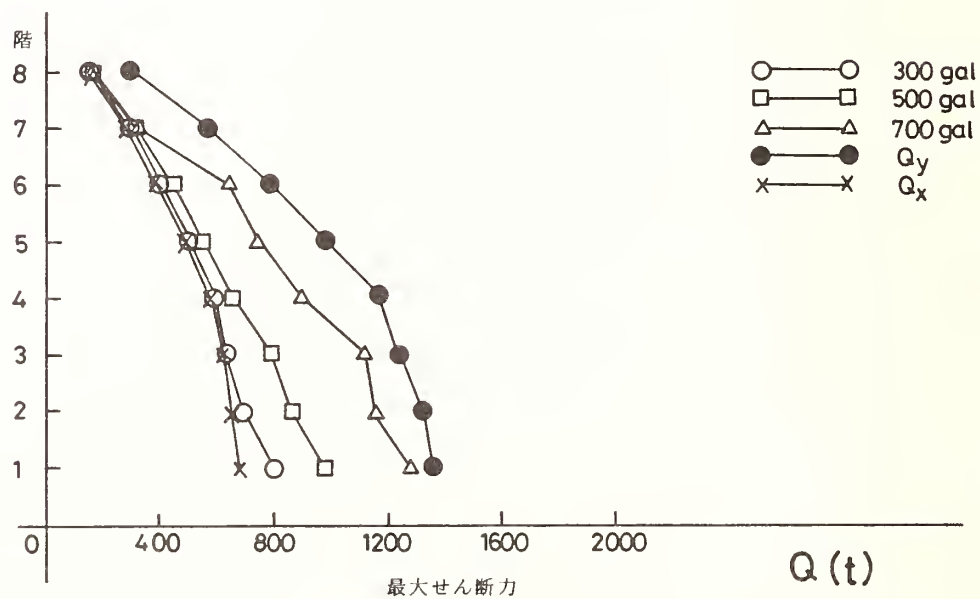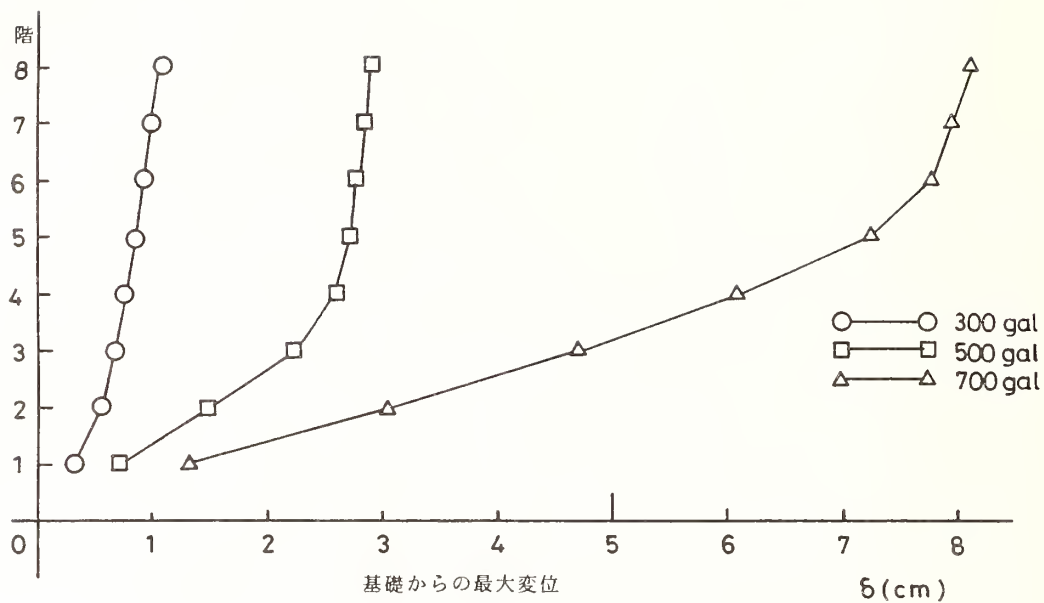
図12 弾塑性応答解析(EL CENTRO NS)

SOIL DYNAMICS - STATE OF THE ART, 1980

by

W. F. Marcuson III

A. G. Franklin

P. F. Hadala

ABSTRACT

This paper describes and evaluates important modern developments in geotechnical earthquake engineering. The current state of knowledge allows for the safe design and construction of critical structures subjected to earthquake loadings, although we generally do not know precisely the margin of safety that has been incorporated in the design. For evaluation of the seismic stability of existing critical structures, our state of knowledge is sometimes inadequate. In the analysis of existing structures we can define conditions which are clearly safe, and conditions which are clearly unsafe. Between these two limits there are many practical cases that fall into a grey area which will only be narrowed by further research and new full-scale response data.

The objective of this paper is to describe and evaluate important developments in soil dynamics, particularly those of the last fifteen years. Primary emphasis will be given to earthquake engineering, for three reasons: first, because earthquake engineering involves the same fundamental issues and problems that affect the whole field of soil dynamics; second, because of all areas of soil dynamics, earthquake engineering has seen the greatest intensity of research and development effort in the past 15 years (for example, in 1975 approximately 30 million dollars was spent on earthquake-related research, on a world-wide basis, as reported by Lee et al., (1978); and third, because the interests and experience is primarily in the United States, this paper primarily reflects the state-of-the-art of practice on the North American continent.

The categories into which soil dynamics problems are conventionally placed are often based primarily on the nature of the loading function. Major categories of dynamic loading include earthquakes, machine vibrations, pile driving, blasting vibrations, shock waves, projectile impacts, and vehicular loadings. The differences among the various categories of dynamic loading lie primarily in the frequency content or rate of loading that is characteristic of each one, and to a lesser extent on the stress levels or accelerations. We consider soil response to machine vibrations to be essentially a solved problem, and other state-of-the-art reports (Whitman and Richart, 1967; McNeill, 1969; Yoshimi, et al., 1977; Richart, 1978) cover much of this work. We will generally omit specific reference to all types of dynamic loading other than those associated with earthquakes. We also will omit reference to the prediction of ground motions, since this falls in the field of engineering seismology rather than that of soil dynamics.

From a practical point of view, there are currently two approaches to obtaining engineering solutions to geotechnical earthquake engineering problems: (1) an empirical approach, and (2) a tuned analytical approach. Conceptually, the empirical approach consists of a systematic gathering of data on past performance and the organization of the data in such a way that we have coherent patterns of behavior that can be used to predict future performance. The method is essentially correlative but takes advantage of the degree of understanding of cause and effect relationships that presently exists. By "tuned analytical approach" we mean a method of predicting performance based on an

analytical model, where the results of past analyses with the model have been compared to field case histories and correction factors have been developed to adjust the predicted values to agree with those that were observed. The use of such an approach requires the formulation of a workable theoretical model, and thus some understanding of the mechanisms and processes involved. Imperfections of the model and/or systematic errors in the input data are compensated for by correction factors. In the past 10-15 years extensive efforts have been devoted to the development of analytical or tuned analytical approaches to solving geotechnical earthquake engineering problems, but there has been a recent shift toward a more equal balance between the empirical and analytical approaches.

MAJOR ISSUES IN SOIL DYNAMICS

We can identify as major issues in soil dynamics several areas that are of concern because they constrain our ability to solve problems, or are areas of controversy, or are particular foci of effort or attention. They are not all of equal importance, and indeed we can see that the concentration of effort and progress in dealing with these issues has been very uneven. These areas are treated in the following sections.

LIQUEFACTION

The fundamentals of the liquefaction mechanism are, at the present time, not adequately understood, in the sense that we can not now formulate a model of material behavior that adequately describes liquefaction response and is amenable to numerical analysis (Hardin, 1978). In the present state-of-the-art, we are analyzing liquefaction problems using a mixture of theoretical concepts, empirical procedures, and hybrid procedures based on tuned numerical analyses. The issue is a highly controversial one; far from having general agreement on the mechanisms of liquefaction, the profession sometimes cannot even discuss the issue using a set of generally agreed upon definitions of terms (Marcuson 1978). We use the term "liquefaction" here in an inclusive sense to denote any of various phenomena that involve high pore pressures, loss of shear strength, and excessive deformation in saturated cohesionless soils. Included are phenomena which have been variously referred to in the literature as liquefaction, limited liquefaction, and cyclic mobility (Castro 1975; Casagrande, 1976; Seed, 1979a).

At the present time we have available an abundance of laboratory data on the liquefaction behavior of saturated clean sands and a limited number of well documented case histories. Current effort is focused on the seismic performance of medium dense sands, as the performance at the extremes of the density scale is easily predicted. However, our ability to predict the response of silty sands or gravelly sands is deficient. This is partly due to a lack of understanding of the fundamentals of liquefaction and partly because of limitations in our ability to perform adequate laboratory tests.

STRESS-STRAIN-TIME LAWS

These "laws" express mathematically whatever we know or hypothesize about the behavior of a material. The stress-strain-time laws that we are presently able to make use of in dynamic analyses are physically imperfect, but we do not find these imperfections to be serious constraints on our ability to use analysis to obtain useful insights into engineering problems. The various mathematical models available in the present state-of-the-art do not describe all aspects of soil behavior equally well (Hardin, 1978). Therefore, obtaining a workable engineering solution to a problem depends on the selection of a mathematical model that best describes that aspect of behavior in which we are interested, and selection of laboratory tests best suited to measuring the parameters of that model. For instance, we must at the present time use different models in the solution of wave propagation problems and the solution of dynamic strength problems.

Assuming that an appropriate model is used, a greater degree of uncertainty is produced in the results by imperfect knowledge of the input paramaters than by defects in the models themselves, so that the importance of model defects is relatively minor. The input parameter values are obtained through field exploration and laboratory testing programs. To put the matter into perspective consider that most of the computer codes and mathematical models that represent the current state-of-the-art were developed in the 1970's (Lysmer, 1978); state-of-the-art laboratory tests were developed in the 1960's (Woods, 1978), and state-of-the-art methods of obtaining undisturbed samples were developed in the 1940's (See State of the Art on Current Practice of Soil Sampling, 1979).

ANALYTICAL PROCEDURES

The development of analytical procedures is relatively far advanced, so that the degree of sophistication that has been achieved is ahead of our present ability to provide input data good enough to make full use of it. The late 1960's and the 1970's have seen the development of one-dimensional, two-dimensional, and three-dimensional methods of analysis of dynamic stress wave propagation, using both linear and nonlinear stress-strain-time laws as well as the equivalent linear approach, which involves some features of both. These methods all involve the solution of the wave equation and their common objective is to obtain time variation of shear stress within earth materials. The solution is accomplished by closed form, characteristic, finite element or finite difference methods. The latter offers an advantage of greater flexibility in the use of sophisticated material stress-strain laws (Lysmer, 1978).

Probably the most keenly felt limitation in current methods of analysis is that none of them are capable of reliably predicting deformations, using either simple or complex mathematical models. The shortcomings lie partly in the stress-strain-time laws, partly in the problems of adequately determining moduli for tests on so called undisturbed samples, and partly in the analytical procedures themselves. Computation of dynamic displacements and deformations involves integration of accelerations, and progressive amplification of relatively small errors in those values. On the other hand, stresses and accelerations can be computed with fair reliability so long as relative stiffnesses and masses are known, because these calculations rely primarily on a balance of forces, including inertial forces.

DETERMINATION OF SOIL PROPERTIES

Field Methods

In practice, field measurement of dynamic properties of soils means the measurement of compression wave and shear wave velocities, from which dynamic modulus values (applicable to a particular range of stress and strain levels) can be computed, using seismic exploration technique (Ballard & McLean, 1975). The past decade has seen considerable development in geophysical instrumentation and field techniques, including seismic sources and detectors for use in boreholes, improvements in shear wave sources, improvements in

interpretation methods, and the use of "signal enhancement" which involves the use of a series of impulses and the algebraic summing of the successive signals received at the detector in order to improve the signal to noise ratio (Woods, 1978). These methods involve the response of soils at very low strain levels (of the order of 10^{-4} percent) so that the modulus values obtained approximate the initial tangent moduli. Some work has been done in recent years on large-strain seismic velocity tests (Shannon & Wilson and Agbabian & Associates, 1979), but this has not developed yet to the point where such tests are in routine use. Figure 1 summarizes the shear strain amplitude capabilities of field technique. The determination of variations in moduli with strain level now routinely relies on supplementary tests performed in the laboratory. An additional limitation is that there is at the present time no method for the measurement of material damping values in the field, and this parameter is particularly critical in the analysis of soil-structure interaction.

A sometimes worrisome problem is that seismic wave velocities measured by different investigators show greater variations than one would expect in an apparently simple physical measurement. These inconsistencies are not easily explained, but most of the common errors involve such things as unaccounted for detonator delays or borehole deviations, and too much distance between source and receiver resulting in a travel path less direct than the one assumed (i.e. refracted through adjacent high-velocity zones), so that the reported velocity values are too high. Generally, refinements in wave velocity measurement techniques result in lower velocities being measured.

Table 1 summarizes the current techniques for measuring in situ dynamic soil properties.

With regard to evaluation of liquefaction potential, field testing methods are generally not applicable to the direct determination of soil parameters, other than density, related to liquefaction behavior. The Standard Penetration Test (SPT) is used in empirical evaluation of liquefaction potential, and other field tests such as the cone penetrometer test have the potential for being used in the same way. The difficulties that we encounter in evaluating liquefaction potential through laboratory tests tempt us to look to in situ testing methods for a remedy. However, a general limitation in this approach is our inability to control or even to know the in situ state of stress, the

drainage condition, and the volume or mass of material involved. Consequently, most in situ tests are usable for this purpose only as index tests and will rely on correlation with laboratory response and/or field observations of earthquake effects.

Laboratory Methods

In the current state-of-the-art, production testing uses the stress-controlled cyclic triaxial test as a liquefaction test and the strain controlled cyclic triaxial test or the resonant column test to measure modulus and damping. It is generally recognized that the stress-controlled cyclic triaxial test has serious shortcomings in that (a) it does not correctly represent the state of stress that we believe or assume to exist in the field and (b) it involves reversals of the principal stresses that we do not believe occur in the field. Other possiblities have been and are being explored, such as large-scale shake table tests, hollow cylinder torsional tests, and simple shear box tests. All of these alternatives have problems that have not yet been overcome, such as difficulties in preparing specimens, difficulties in applying shearing forces at the specimen boundaries, and nonuniformity of strain distribution.

One of the most troublesome problems in laboratory testing of soils is that of sample disturbance, particularly in sands. Relatively recent research has shown that structure is much more important in the behavior of sands than had previously been thought, and that sand samples compacted to a given density in the laboratory can have very different structures and very different cyclic strength response, depending on the method of sample preparation (Ladd, 1974; Mulilis, Chan and Seed, 1975; Marcuson and Townsend, 1976; Mori, Seed and Chan, 1978). These circumstances make the use of undisturbed samples imperative, but the field sampling technology with which we are presently working represents the state-of-the-art of the 1940's (Hvorslev, 1949; American Society of Civil Engineers; 1978; Marcuson and Franklin, 1979; Horn, 1979).

On a more fundamental level, we may observe that the very design of a laboratory test reflects current concepts and practice in the formulation of stress-strain-time laws, since the tests are designed to measure the parameters contained in these laws. The ideal laboratory soil tests should (1) impose the stresses anticipated in the field on the test specimen, (2) have uniform and known stresses throughout the specimen and (3) be conducted on test specimens truly representative of the material in situ. The tests that come closest

to imposing the expected field stress conditions, e.g., the simple shear box, the hollow cylinder torsional test, and the shake table test, are not well suited to the use of undisturbed samples and do not stress the specimen uniformly throughout. We now use the cyclic triaxial test in practice despite its nonuniformity of stresses and the occurrence of stress reversals which we think are not representations of actual field conditions, because of an overriding need to get on with the job and its convenience for use with undisturbed samples.

Table 2 summarizes the current laboratory techniques for measurement of dynamic soil properties and the properties obtained from each test. The shear strain amplitude capabilities of the various tests are summarized in Figure 2.

PREDICTION/CHARACTERIZATION OF LOAD FUNCTIONS

In seismic response problems, the load function is the earthquake ground motion, and its prediction properly belongs to the sphere of seismology. However, the ground motions are usually the most critical part of the input to a dynamic analysis, and it is necessary to specify the input motion in such a way as to have a well-posed problem for the dynamic analysis (Idriss, 1978). In order to insure that the specified loading function (the design earthquake) is realistic in view of the site geology and the regional seismicity, and in addition that it is specified in a way that is appropriate for the structure involved, the selection of the design earthquake should be a team effort, involving interaction of seismologists, geologists, and geotechnical and/or structural engineers. The choice of a design earthquake conventionally involves the choice of such parameters of the ground motion as the maximum acceleration, maximum velocity, and the duration of strong motion (usually motion equal to or greater than 0.05 g). But it is generally recognized that the specification of these parameters is not sufficient to define the characteristics of the loading function, so one or more recorded accelerations versus time records from some sites of similar geology, from earthquakes of about the same magnitude and epicentral distance, and scaled to give the same peak motion parameters, are chosen as loading functions. Some of the more important issues involved in the specification of the loading function are discussed in the following paragraphs.

220

Data Base

The United States, and the world, has experienced in the last decade a tremendous expansion in systems of strong-motion instrumentation, and will see in the next decade or two concomitant expansion in the available inventory of strong motion records. At the present time, however, there are some noticeable gaps in our strong-motion data base. A very large portion of the United States strong-motion data base consists of records obtained during the San Fernando Earthquake of 1971. Our inventory is totally lacking in close-in strong-motion data from earthquakes of magnitudes 7 and greater. In addition, most of the available data represent surface motions, while it would be very desirable to have documentation of motions occurring in the subsurface. An additional, and acutely felt, hiatus is in strong-motion records that can be closely correlated with records of performance of dams and other structures during past earthquakes. Such case histories would be highly desirable for the purpose of validating our analytical methods.

Location of Input Motion

A serious question in dynamic analysis is that of where to apply the input loading function. Commonly, the input motion is applied at the surface of the bedrock, but it is clearly inappropriate to apply in this manner a record obtained at the ground surface. The soil or overburden layer acts as a filter in the propagation of ground motions upward from the bedrock. A weak layer can filter out important parts of the ground-motion, as we have seen in strong-motion records from Niigata, Japan, where very weak motions were measured at the surface in areas where liquefaction occurred (Seed and Idriss, 1967). Conventional practice is to obtain transfer functions for the relations between ground motion at different levels by means of convolution through a one-dimensional wave propagation analysis. However, one-dimensional convolution ignores lateral homogenities in the soil as well as the decay of surface waves with depth.

Frequency Content

The input motions will not adequately test a structure if they are deficient in frequencies in the neighborhood of the fundamental frequency of the structure, unless that fundamental frequency is either a very high or very low one that does not normally occur in earthquakes. Spectral representations of the ground motions such as response spectra,

Fourier spectra, power spectral densities, etc., while not generally used directly in geotechnical analyses, are useful descriptors of the character of the ground-motion that should be considered in selecting the design earthquake (Christian, 1980). Spectral representations may also be used as the starting point in the generation of synthetic earthquakes (Jennings, et al., 1968, Liu, 1970), which may be used as an alternative to a natural earthquake record. A disadvantage of this is that such records are derived from smooth spectra while the spectra of natural earthquakes are irregular, so that the synthetic record represents too severe a motion.

<div align="center">SIGNIFICANT MODERN DEVELOPMENTS OR EVENTS</div>

The Good Friday (1964) Earthquake in Alaska

The Good Friday earthquake produced spectacular damage and occurrences of ground failures, but little useful ground motion data (Seed and Wilson, 1967). However, it produced a heightening of awareness of earthquake problems in the United States, and instigated appropriations and research to deal with earthquake problems.

The 16 June 1964 Niigata, Japan Earthquake

The Niigata earthquake is noteworthy especially for the spectacular effects produced by liquefaction-type ground failure. Modern structures in Niigata were seismically designed and had adequate strength to resist shaking. However, because they were not designed to float, a number of buildings overturned when the ground liquefied under them (Kishida, 1966). Other evidences of liquefaction, such as sand boils, were widespread. After the earthquake, the airport lay under a foot of water. Post-earthquake investigations in Niigata revealed useful correlations between SPT blowcounts and occrrences or nonoccurrences of liquefaction (Koizumi, 1966, Ohsaki, 1966, 1969), gave impetus to earthquake engineering research internationally, and were the basis for liquefaction research during the next decade.

The San Fernando Earthquake of 9 February 1971

Damage and loss of life during this earthquake were a source of widespread concern. The slide in the Lower San Fernando dam during this earthquake narrowly missed becoming the largest single disaster in United States history, since an estimated 80,000 people

were asleep downstream and an overtopping failure of the dam did not occur only because the
water level was below maximum pool (Seed et al., 1975). This earthquake doubled our cata-
log of strong-motion data, offering opportunities for the study of effects of site condi-
tions on ground motions and empirical correlations of ground motions with performance of
structures. It is notable that there were five hydraulic-fill dams that were subjected to
accelerations of approximately 0.2 g without incurring serious damage (Seed, Makdisi and
De Alba, 1978). On the other side of the coin, the fact that so large a part of the exist-
ing data base represents a single earthquake introduces an unknown bias into the statisti-
cal characteristics of ground motions and empirical correlations. The strong-motion record
obtained at Pacoima Dam during this earthquake represented the first time that
accelerations in excess of 1.0 g have been instrumentally recorded.

Advances in Numerical Methods

The development of computer codes for one-dimensional and two-dimensional dynamic
analyses have had a far reaching influence in earthquake engineering. Studies made with
the use of these tools have provided us a better understanding of the effects of site condi-
tions on ground motions and the relative importance of various geotechnical parameters in
influencing ground motions and soil-structure interaction (Lysmer, 1978). They have also
allowed us to exercise more realistic and sophisticated models of material and structural
behavior.

Development of Cyclic Laboratory Tests

The cyclic triaxial, resonant column, simple shear, and shake table tests have had a
major influence on the practice of geotechnical earthquake engineering. They have given
quantitative indices of the influence of void ratio and stress level on pore pressure
development and liquefaction potential in cohesionless soils and on the influence of strain
levels on stiffness and damping (Woods, 1978). Cyclic testing methods are an indispensable
part of a rational approach to the evaluation of liquefaction problems.

Development of a Coherent Approach to Liquefaction Problems

During the 1960's and 1970's, an approach to seismic analysis of liquefaction problems
was evolved, primarily through work at the University of California at Berkeley with
Professor H. B. Seed playing the leading role. The so-called "Seed approach" has been used

223

for the dynamic analysis for a number of major dams, and has been applied in a back calculation mode to the sides in the Upper and Lower San Fernando dams and to the failure in Sheffield Dam (Seed et al., 1969; Seed et al., 1973; Seed et al., 1975).

Analysis of Post-Earthquake Pore Pressure Redistribution

Analysis of seismoscope records from the Lower San Fernando Dam indicated that the slide actually occurred a short time after the earthquake shaking had ceased, and it was inferred that this was due to redistribution of earthquake-induced pore pressures. Computer codes for the analysis of post-earthquake pore pressure redistribution have since been developed (Seed, 1979b). Generally, the permeability variation within the embankment and foundation materials are not known accurately enough to permit a high level of quantitative accuracy. However, recognition of the importance of post-earthquake pore pressure redistribution phenomena and possible resulting instability at a later time is important as an identification of a possible failure mechanism that had not been previously recognized. One effect this may have on the practice of seismic analysis is to place more importance on the analysis of the effects of strong aftershocks.

Permanent Displacement Analysis

A method of analysis which treats a slide in an embankment at a rigid block on inclined plane, subjected to earthquake accelerations, was proposed by Newmark (1965), and a coherent analytical procedure has evolved on the basis of this concept (Goodman and Seed, 1966; Ambraseys and Sarma, 1967; Sarma, 1975; Franklin and Chang, 1977; Makdisi and Seed, 1977; and Sarma, 1979). This procedure offers a rational basis for the analysis and design of earth and rockfill dams that do not involve materials which might be susceptible to liquefaction. The somewhat limited experience with this procedure up to the present time indicates that in earth dams of cohesive materials and in rockfill dams with highly permeable shells which are not susceptible to liquefaction, if there is a satisfactory static factor of safety, direct damage, even from major earthquakes, should be limited to relatively minor cracking or sliding.

Development of In Situ Testing and Sampling

There is at the present time a discernible trend toward greater emphasis on in situ testing and improvement of sampling methods. There has been a great deal of study on the

reliability and causes of variability in the SPT test (see Geotechnical Division, Proceedings, Specialty Conference on In Situ Measurement of Soil Properties, Raleigh, N.C., 1975), and greater efforts to standardize the test. One notable development is the piezometer probe which measures induced pore pressures while being pushed into the soil, and which may be useful as an indicator of liquefaction susceptibility in cohesionless soils through indication of collapsing or dilatant behavior by the induced pore pressures (Thorstensson, 1975; Wissa et al., 1975; Schmertmann, 1978). Another tool under development is the dynamic pressuremeter (Mori, 1979). This equipment appears capable of measuring the in situ shear modulus over a range of strain levels and may offer the potential for obtaining in situ values of damping over a similar range of strains. A great deal of effort is going into refinement of geophysical testing methods, particularly in measurement of shear wave velocity. In the field of sampling of soils, we have an increasing need for high quality undisturbed samples of cohesionless soils for laboratory tests of liquefaction susceptibility. Until the 1970's, the significance of structure in influencing the mechanical behavior of sands was not recognized, and it was merely assumed that a sample of sand recompacted to in situ density in the laboratory was adequately representative of its in situ behavior. Recent research has shown that this assumption is unjustified; and that, moreover, the effects of disturbance caused by even the most careful conventional sampling practice are very serious (Mulilis, et al., 1977; Mori, Seed and Chan, 1978; Marcuson and Franklin, 1979). A breakthrough of considerable potential importance is the experimental proof that sands may be frozen without discernible effects on their structure, provided that free drainage is permitted away from the freezing front and the effective stress state is maintained during freezing (Yoshimi, et al., 1977, 1978; Walberg, 1978; Singh, et al., 1979). Freezing was used to aid in sampling by the Corps of Engineers at Fort Peck Dam in 1939 (Middlebrooks, 1942) but has been little used since. Yoshimi, et al., (1977, 1978) report the use of radial freezing to obtain undisturbed field samples of saturated sand, but the technique they used appears to be limited to shallow (~ 10 m) exploration. Development of a reasonably economical field technique that can be used to moderate depths (~ 50 m) remains to be accomplished.

Solution of the Machine Vibration Problem

The conquest of this problem in the 1960's contributed a great deal to the current state-of-the-art in analysis of soil-structure interaction problems in earthquake engineering. Of special importance is the understanding that was gained on the importance of material and radiation damping in such problems.

Strong-Motion Instrumentation

The past decade and a half has seen a vast expansion in the number of strong-motion instrumentation arrays throughout much of the world. The first major payoff was seen in the United States at the time of the 1971 San Fernando earthquake when more than 100 stations produced useful strong-motion records. It is to be expected that future large earthquakes, particularly in California, will produce so many new records that they will have to be used quite selectively (Iwan, 1978). The emphasis will likely be on filling gaps in the data base, particularly the lack of records of nearby earthquakes of Magnitude 7 and above, and on securing records that will document the response of particular structures to earthquakes. El Infiernillo Dam, in Mexico, was shaken by a strong earthquake (Magnitude = 7.7) in 1979, suffering minor damage, and strong-motion records were obtained at three levels in the embankment. Study of records of this type, together with observations of performance, will be invaluable in validating analytical methods.

CURRENT TRENDS

From an examination of the discussions above, several trends in the development of soil dynamics emerge. As mentioned earlier, there is a trend toward a better balance between analytical and empirical approaches to soil dynamics problems, and particularly in efforts to assemble and evaluate more empirical data on past performance of structures. Advances in the various aspects of soil dynamics have been very uneven. In particular, the development of analytical approaches, and computer codes to implement them, have reached a level of sophistication such that the input data, rather than the analytical models, now govern the accuracy of the analysis. Additionally, the analytical methods need empirical validation and we are now beginning to feel the lack of well-documented case histories. Thus, there is now a trend toward closer studies of past failures or past performance of structures that have undergone earthquakes (Seed, et al., 1978).

226

Laboratory research to attempt to explain the cyclic mobility of medium dense sands via exploration of differences in response during extensive and compression stress paths is underway. This limited research done to date indicates that reversal of principal stress directions tends to erase the beneficial effects of stress history (Tatsuoka and Ishihara, 1974).

An effective stress approach is being used for one-dimensional analysis of earthquake-induced pore pressure development (Finn, et al., 1977, 1978). Input data are obtained from constant volume, drained, cyclic simple shear tests. This is a step in the right direction. If the method is validated against field behavior it can circumvent the host of problems we associate with the cyclic triaxial test and offers the potential for computing seismically induced settlements.

The implementation of strong-motion instrumentation continues. Strong-motion instruments have themselves been improved in recent years and we now have a better understanding of where and how to place them in order to obtain the most meaningful strong-motion data. While there are only a few major earthquake events worldwide each year, we are now in a much improved position to learn as much as possible from most of them, and it is to be expected that the inventory of strong-motion records will increase rapidly in the next decade.

We are beginning to see an increased concentration of effort in the area of field exploration, particularly the development of improved sampling methods and methods of in situ testing of liquefaction potential and other dynamic properties of soils. Such efforts at the present time include the refinement of the Standard Penetration Test, study and more widespread use of the cone penetration test, the use of piezometer probes, dynamic pressuremeters, and geophysical methods, including nuclear and electrical methods directed at measurement of the in situ density. The measurement of in situ properties by means of seismic test methods has already seen a great deal of development and has long since attained the status of routine test methods.

There are two areas where there is apparently little significant work in progress in soil dynamics. One is the development of laboratory tests that meet the requirements of an ideal test as stated earlier in Laboratory Methods section of this report. The other is in

the development of better undisturbed sampling methods. With the exception of in situ one-dimensional freezing, we are essentially using 1940's technology.

SUMMARY

During the last two decades remarkable progress has been made in the field of Soil Dynamics. We consider soil response to machine vibrations to be, for all practical purposes, a solved problem. In earthquake engineering, the current state of knowledge allows for the safe design and construction of critical structures that may be subjected to earthquake loadings; however, we are unable to evaluate the margin of safety which has been incorporated in our current procedures. For the evaluation of the seismic stability of existing critical structures, such as some dams and nuclear power plants, our state of knowledge is sometimes inadequate. In the analysis of existing structures we can define conditions which are clearly safe and conditions which are clearly unsafe. Between these two limits lie many practical cases that fall into a grey area which will only be narrowed by further research and new full-scale response data.

Current seismic design methodology does not rigorously account for all cause and effect relationships. However, correction factors and compensating errors allow us to "predict" past experience, and in this way calculational techniques have been calibrated. More case histories are needed to further develop and refine our current approaches.

It is recognized that our numerical dynamic stress analysis capabilities are much more advanced than our ability to obtain representative undisturbed soil samples and to test them under the correct stress-strain conditions in the laboratory. Ongoing research in the area of in situ testing offers us hope of being able to obtain in the future more reliable soil properties and parameters, thus circumventing our sampling and laboratory shortcomings.

Finally, it is believed that the strong motion instrumentation arrays which are in place and being expanded will provide the data which will fill the present gaps existing in our present data base. This includes close-in records from earthquakes of Magnitude 7 and greater.

In the final analysis it should be realized that laboratory tests and analytical calculations are done not for the sake of the numbers obtained, but for the purpose of understanding and extending a limited field data base so that sound engineering judgments can be made regarding the safety of structures.

ACKNOWLEDGMENTS

REFERENCES

Ambraseys, N. N. and Sarma, S. K. (1967), "The Response of Earth Dams to Strong Earthquakes," Geotechnique, Vol. 17, No. 3, pp. 181-213.

American Society of Civil Engineers (1978), Soil Sampling and Its Importance to Dynamic Laboratory Testing, Preprint 3440, ASCE National Convention, Chicago, IL.

Ballard, R. F., and McLean, F. G. (1975), "Seismic Field Methods for In Situ Moduli," Proceedings ASCE Conference on In Situ Measurement of Soil Properties, North Carolina State University, Raleigh, N.C., Vol. 1, pp. 121-150.

Casagrande, A. (1976), "Liquefaction and Cyclic Deformation of Sands, A Critical Review," Harvard Soil Mechanics Series No. 88, Pierce Hall, Cambridge, Mass.

Castro, G. (1975), "Liquefaction and Cyclic Mobility of Saturated Sands," Journal of the Geotechnical Engineering Division, ASCE, Vol. 101, GT6, pp. 551-569.

Christian, J. T. (1980), "Probabilistic Soil Dynamics: State of the Art," Journal of the Geotechnical Engineering Division, ASCE, Vol. 106, No. GT4, pp. 395-397.

Finn, W. D. L., Lee, K. W., and Martin, G. R. (1977), "An Effective Stress Model for Liquefaction," Journal of the Geotechnical Engineering Division, ASCE, Vol. 103, No. GT6, pp. 517-533.

Finn, W. D. L., Martin, G. R., and Lee, M. K. W. (1978), "Application of Effective Stress Methods for Offshore Seismic Design in Cohesionless Seafloor Soils." Proceedings, 10th Offshore Technology Conference, Houston, Texas, OTC 3112, pp. 521-528.

Franklin, A. G., and Chang, F. K. (1977), "Permanent Displacements of Earth Embankments by Newmark Sliding Block Analysis," Miscellaneous Paper S-71-17, Report 5, U.S. Army Engineer Waterways Experiment Station, Vicksburg, Miss.

Geotechnical Division, Proceedings, Specialty Conference on In Situ Measurement of Soil Properties (1975), ASCE, Vols. 1, 2, North Carolina State University, Raleigh, N.C.

Goodman, R. E. and Seed, H. B. (1966), "Earthquake-Induced Displacements in Sand Embankment," Journal of the Soil Mechanics and Foundations Division, ASCE, Vol. 92, No. SM2, pp. 125-146.

Hardin, B. O. (1978), "The Nature of Stress-Strain Behavior of Soils," Proceedings, ASCE Conference on Earthquake Engineering and Soil Dynamics, Vol. 1, Pasadena, CA, pp. 3-90.

Horn, H. M. (1979), "North American Experience in Sampling and Laboratory Dynamic Testing," Geotechnical Testing Journal, ASTM, Vol. 2, No. 2, pp. 84-97.

Hvorslev, M. J. (1949), "Subsurface Exploration and Sampling of Soils for Civil Engineering Purpose," Report of Committee on Sampling and Testing, Soil Mechanics and Foundation Division, ASCE.

Idriss, I. M. (1978), "Characteristics of Earthquake Ground Motions," ASCE Conference on Earthquake Engineering and Soil Dynamics, Vol. 3, Pasadena, CA, pp. 1151-1266.

Iwan, W. D., editor (1978), "Strong-Motion Earthquake Instrument Arrays," Proceedings of the International Workshop on Strong-Motion Earthquake Instrument Arrays, Honolulu, Hawaii.

Jennings, P. C., Housner, G. W., Tsai, N. C. (1968), "Simulated Earthquake Motions," Earthquake Engineering Research Laboratory Report, California Institute of Technology, Pasadena, CA.

Kishida, H. (1966), "Damage to Reinforced Concrete Buildings in Niigata City with Special Reference to Foundation Engineering," Soils and Foundations, Tokyo, Japan, Vol. VI, No. 1, pp. 71-88.

Koizumi, Y. (1966), "Change in Density of Sand Subsoil Caused by Niigata Earthquake," Soils and Foundations, Tokyo, Japan, Vol. VIII, No. 2, pp. 38-44.

Ladd, R. S. (1974), "Specimen Preparation and Liquefaction of Sands," Journal of the Geotechnical Engineering Division, ASCE, Vol. 100, No. GT10, pp. 1180-1184.

Lee, K. L., Marcuson, W. F., III, Stokoe, K. H., II, Yokel, F. Y., editors (1978), "Research Needs and Priorities for Geotechnical Earthquake Engineering Applications," Report prepared for the National Science Foundation by the University of Texas, Austin, Texas.

Liu, S. C. (1970), "Dynamics of Correlated Random Pulse Trains," Journal of the Engineering Mechanics Division, ASCE, Vol. 96, No. EM4, pp. 455-470.

Lysmer, J. (1978), "Analytical Procedures in Soil Dynamics," ASCE Conference on Earthquake Engineering and Soil Dynamics, Pasadena, CA, Vol. 3, pp. 1267-1317.

Makdisi, F. I. and Seed, H. B. (1977), "A Simplified Procedure for Estimating Earthquake-Induced Deformations in Dams and Embankments," Earthquake Engineering Research Center Report No. UCB/EERC-77/19, University of California, Berkeley.

Marcuson, W. F., III, Chmn (1978), "Definition of Terms Related to Liquefaction," Journal of the Geotechnical Engineering Division, ASCE, Vol. 104, No. GT9, pp. 1197-1200.

Marcuson, W. F., III and Franklin, A. G. (1979), "State of the Art of Undisturbed Sampling of Cohesionless Soils," Miscellaneous Paper GL-79-16, U.S. Army Engineer, Waterways Experiment Station, Vicksburg, MS.

Marcuson, W. F., III and Townsend, F. C. (1976), "Effects of Specimen Reconstitution on Cyclic Triaxial Results," Miscellaneous paper S-76-5, U.S. Army Engineering Waterways Experiment Station, CE, Vicksburg, MS.

McNeill, R. L. (1969), "Machine Foundations: The State of the Art," Proceedings, 7th International Conference on Soil Mechanics and Foundation Engineering, Specialty Session No. 2, Soil Dynamics, Mexico City, Mexico, pp. 67-118.

Middlebrooks, T. A. (1942), "Fort Peck Slide," Transactions, American Society of Civil Engineers, Vol. 107, Paper No. 2144, pp. 723-764.

Mori, H. (1979), "A Method of Bore-Hole Tests to Obtain Dynamic Parameters of Soils," Proceedings, International Symposium on In Situ Testing of Soils and Rocks and Performance of Structures, Roorkee, India, December 1979.

Mori, K., Seed, H. B. and Chan, C. K. (1978), "Influence of Sample Disturbance on Sand Liquefaction Characterstics," Journal of the Geotechnical Engineering Division, ASCE, Vol. 104, No. GT3, pp. 323-339.

Mulilis, J. P., Chan, C. K. and Seed, H. B. (1975), "The Effects of Method of Preparation on the Cyclic Stress-Strain Behavior of Sands," Report No. EERC 75-180, University of California, Berkely, California.

Mulilis, J. P., Mori, K., Seed, H. B., and Chan, C. K. (1977), "Resistance to Liquefaction Due to Sustained Pressure," Journal of the Geotechnical Engineering Division, ASCE, Vol. 103, No. GT7, pp. 793-797.

Newmark, N. M. (1965), "Effects of Earthquakes on Dams and Embankments," Geotechnique, Vol. 15, No. 2, pp. 139-160.

Ohsaki, Y. (1966), "Niigata Earthquakes, 1964, Building Damage and Soil Conditions," Soils and Foundations, Vol. VI, No. 2, pp. 14-37.

Ohsaki, Y. (1969), "Effects of Local Soil Conditions Upon Earthquake Damage," Proceedings Specialty Session No. 2, 7th International Conference on Soil Mechanics and Foundation Engineering, Mexico City, Mexico, pp. 3-32.

Richart, F. E., Jr. (1978), "Foundations for Dynamic Machine Loadings," International Symposium on Foundations for Equipment and Machinery, 1978 Fall Convention, American Concrete Institute, Houston, Texas.

Sarma, S. K. (1979), "Response and Stability of Earth Dams During Strong Earthquakes," Miscellaneous Paper GS-79-13, U.S. Army Engineering Waterways Experiment Station, CE, Vicksburg, Miss.

Sarma, S. K. (1975), "Seismic Stability of Earth Dams and Embankments," Geotechnique, Vol. 25, No. 4, pp. 743-761.

Schmertmann, J. H. (1978), "Study of Feasibility of Using Wissa-Type Piezometer Probe to Identify Liquefaction Potential of Saturated Fine Sands," Technical Report S-78-2, U.S. Army, Waterways Experiment Station, Vicksburg, Mississippi.

Seed, H. B. (1979a), "Soil Liquefaction and Cyclic Mobility Evaluation for Level Ground During Earthquakes," Journal of the Geotechnical Engineering Division, ASCE, Vol. 105, No. GT2, pp. 201-256.

Seed, H. B. (1979b), "Considerations in the Earthquake-Resistance Design of Earth and Rock-Fill Dams," Geotechnique, Vol. 29, No. 3, pp. 215-263.

Seed, H. B., and Idriss, I. M. (1967), "Analysis of Soil Liequefaction: Niigata Earthquake," Journal of Soil Mechanics and Foundations Division, ASCE, Vol. 93, No. SM3, pp. 83-108.

Seed, H. B. and Wilson, S. D. (1967), "The Turnagain Heights Landslide, Anchorage, Alaska," Journal of the Soil Mechanics and Foundation Division, ASCE, Vol. 93, No. SM4, pp. 325-353.

Seed, H. B., Lee, K. L. and Idriss, I. M. (1969), "Analysis of the Sheffield Dam Failure," Journal of the Soil Mechanics and Foundations Division, ASCE, Vol. 95, No. SM6, pp. 1453-1490.

Seed, H. B., Lee, K. L., Idriss, I. M. and Makdisi, F. I. (1973), "Analysis of the Slides in the San Fernando Dams During the Earthquake of 9 February 1971," Report No. EERC 73-2, Earthquake Engineering Research Center, University of California, Berkeley, California.

Seed, H. B., Lee, K. L., Idriss, I. M. and Makdisi, F. I. (1975), "The Slides in the San Fernando Dams During the Earthquake of February 9, 1971," Journal of Geotechnical Engineering Division, ASCE, Vol. 101, No. GT7, pp. 651-688.

Seed, H. B., Makdisi, F. I. and DeAlba, P. (1978), "Performance of Dams During Earthquakes," Journal of the Geotechnical Engineering Division, ASCE, Vol. 104, No. GT7, pp. 967-994.

Shannon & Wilson and Agbabian & Associates (1974), "Soil Behavior Under Earthquake Loading Conditions, In Situ Impluse Tests," Progress Report Contract No. AT(04-3)-954, U.S. Atomic Energy Commission.

Shannon & Wilson and Agbabian & Associates (1979), "Technical Manual Operation and Equipment Instructions for In Situ Impulse Test," Report No. NUREG/CR-0998, U.S. Nuclear Regulatory Commission, Washington, D.C.

Singh, S., Seed, H. B. and Chan, C. K. (1979), "Undisturbed Sampling and Cyclic Load Testing of Sands," Report No. EERC-79-33, University of California, Berkeley.

State of the Art on Current Practice on Soil Sampling (1979), Proceedings International Symposium of Soil Sampling, Singapore. Japanese Society of Soil Mechanics and Foundation Engineering, Tokyo, Japan.

Tatsuoka, F. and Ishihara, K. (1974), "Drained Deformation of Sand Under Cyclic Stresses Reversing Direction," Soils and Foundations, Japanese Society of Soil Mechanics and Foundation Engineering, Vol. 14, No. 3, pp. 52-65.

Torstensson, B. A. (1975), "Pore Pressure Sounding Instrument," Proceedings ASCE Conference on In Situ Measurement of Soil Properties, North Carolina State University, Raleigh, N.C., Vol. 2, pp. 48-54.

Walberg, F. C. (1978), "Freezing and Cyclic Triaxial Behavior of Sands," Journal of the Geotechnical Engineering Division, ASCE, Vol. 104, No. GT5, pp. 667-671.

Whitman, R. V. and Richart, F. E., Jr. (1967), "Design Procedures for Dynamically Loaded Foundations," Journal Soil Mechanics and Foundations Division, Proceedings, ASCE, Vol. 93, No. SM6, pp. 169-193.

Wissa, A. E. Z., Martin, R. T. and Garlanger, J. E. (1975), "The Piezometer Probe," Proceedings ASCE Conference on In Situ Measurement of Soil Properties, North Carolina State University, Raleigh, N.C., Vol. 1, pp. 536-545.

Woods, R. D. (1978), "Measurement of Dynamic Soil Properties," ASCE Conference on Earthquake Engineering and Soil Dynamics, Vol. 1, Pasadena, CA, pp. 91-180.

Yoshimi, Y., Hatanaka, M. and Oh-Oka, H. (1977), "A Simple Method for Undisturbed Sand Sampling by Freezing," Proceedings of Specialty Session 2, Ninth International Conference on Soil Mechanics and Foundation Engineering, Tokyo, pp. 23-25.

Yoshimi, Y., Hatanaka, M., and Oh-Oka, H. (1978), "Undisturbed Sampling of Saturated Sands by Freezing," Soils and Foundations, Vol. 18, No. 3, pp. 59-73.

Yoshimi, Y., Richart, F. E., Jr., Prakash, S., Barkan, D. D., Ilyichev, V. A. (1977), "Soil Dynamics and Its Application to Foundation Engineering," Proceedings of the Ninth International Conference on Soil Mechanics and Foundation Engineering, Vol. 2, Tokyo, Japan, pp. 605-650.
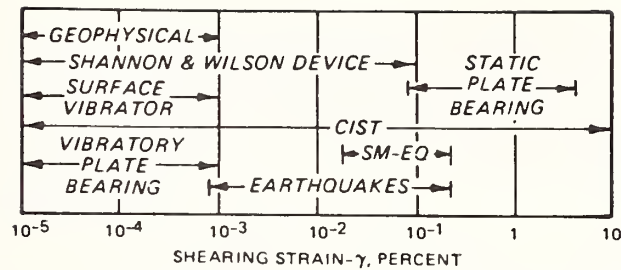
Fig 1 - Shearing strain amplitude capabilities
of field techniques (after Shannon &
Wilson and Agbabian & Associates, 1974).

TABLE 1

FIELD TECHNIQUES FOR MEASURING DYNAMIC SOIL PROPERTIES (After Woods, 1978)

Field technique	P-wave velocity	S-wave velocity	Other measurements	Advantages	Disadvantages
Refraction	X	X	Depths and slopes of layers	Reversible polarity with SH-wave* Work from surface Samples large zone Preliminary studies	Miss low velocity zones Low strain amplitudes Properties measured are for thin zones near boundaries
Cross-Hole	X	X		Reversible polarity	Need 2 or more holes Holes must be surveyed for verticality
(In Situ impulse test)	X	X	Velocity as function of strain amplitude	Works in limited space Finds low velocity	Needs short time interval resolution
Down-hole (Up-hole)	X	X		One hole Reversible polarity Finds low velocity Works in limited space	Measure average velocities Ambient noise near surface Low strain amplitude
Surface		X	Attenuation of Rayleigh wave	Work from surface	Uncertain about effective depth Needs large vibrator
SPT			Empirical correlation with liquefaction	Widely available Widely used in past	Needs "Standardization"
Resonant footing			Modulus of near surface soils	Work from surface	Limited depth of influence
Water cannon			Dynamic stiffness of support	Work from surface	Apparatus and analysis very elaborate
CIST	X	X	Constitutive Eq.	Wide amplitude range	Very elaborate

* Horizontally polarized shear wave.

```
| RESONANT COLUMN (SOLID SAMPLES)                    |
|      RESONANT COLUMN (HOLLOW SAMPLES)              |
|         TORSIONAL SHEAR (HOLLOW SAMPLES)           |
| PULSE METHODS          CYCLIC TRIAXIAL             |
|                        CYCLIC SIMPLE SHEAR         |
|                             SHAKE TABLE            |
```

TYPICAL MOTION CHARACTERISTICS

PROPERLY DESIGNED   STRONG GROUND   CLOSE-IN
MACHINE FOUNDATION   SHAKING FROM   NUCLEAR
                           EARTHQUAKE   EXPLOSION

10^{-4} 10^{-3} 10^{-2} 10^{-1} 1

SHEARING STRAIN AMPLITUDE (%)
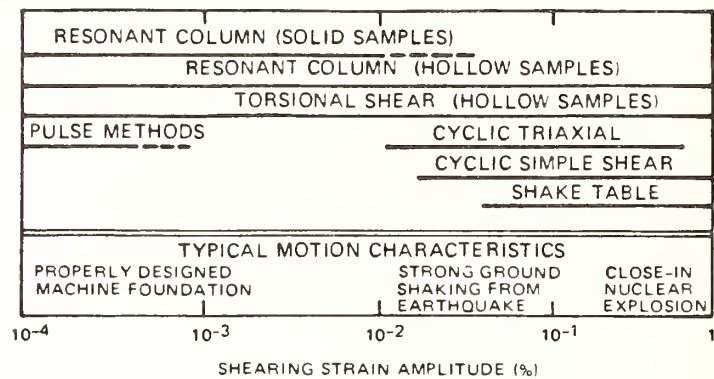
Figure 2.   Shearing strain amplitude capabilities of
            laboratory apparatus (after Woods, 1978).

TABLE 2

LABORATORY TECHNIQUES FOR MEASURING DYNAMIC

SOIL PROPERTIES (After Woods, 1978)

	Shear modulus	Young's modulus	Material damping	Cyclic Stress behavior	Attenuation
Resonant column	X	X	X		
with adaptation					X
Ultrasonic pulse	X	X			X
Cyclic triaxial		X	X	X	
Cyclic simple shear	X		X	X	
Cyclic torsional shear	X		X	X	
Shake table	X			X	

234

DYNAMIC ANALYSIS OF SHEET PILE FOUNDATIONS

by

Tatsuo Asama

Yukitake Shioi

Michio Okahara

Yasuo Mitsuie

ABSTRACT

The sheet pile foundation is a new type foundation with steel pipe sheet piles placed in the form of a circular, or oval well to produce behavior intermediate to that of a caisson and a pile.

For a reasonable design of this foundation type, it is necessary to fully consider the effect of shearing deformation of the joints between the sheet piles. From a past investigation, a program for stability calculation using a seismic coefficient method makes possible the consideration of the joint effect. By utilizing this program, a dynamic analysis program permitting time hysteresis response calculation was developed.

Using such a dynamic analysis program, a case study which examines the dynamic behavior of a sheet pile foundation was completed.

INTRODUCTION

The sheet pile foundation is a new type foundation with steel pipe sheet piles in the form of a circular, or oval well to produce behavior similar to that of a caisson from the bonding effect of joints between the sheet piles, and the restraining effect of the footing at the head of the piles. The outline was reported at the 7th meeting of the UJNR Wind and Seismic Effects Panel. [1] The authors continued to examine an earthquake resistant design calculation method which would permit evaluation of the structural characteristics of this foundation. They were able to obtain good results with respect to a static design calculation method by using a seismic coefficient method. [2]

Then, from the results of the static design calculation method investigation, the authors developed a calculation program which would permit the time-hysteresis response calculation of the sheet pile foundation. They examined the dynamic response characteristics of the sheet pile foundation, and the result of this examination is reported here.

SEISMIC RESPONSE CALCULATION PROGRAM

To examine the seismic response of a structure embedded in the ground such as a sheet pile foundation, it is necessary to consider not only the effect of the seismic movement of the bearing layer at the tip end of the foundation, but also the vibration of the subsoil on the sides of the foundation.

To incorporate the so-called interaction of the foundation and the subsoil, it is a general practice to represent the foundation and subsoil by models using the finite element method, or to replace it with a concentrated mass point - spring system. In this program, the latter method was employed in order that a solution with a relatively small number of degrees of freedom would be obtained.

The vibration model is shown in Figure 1. It is composed of a foundation model and a subsoil model. These are connected to each other using horizontal springs, vertical friction springs, and rotary springs.

In the foundation model, the element cut crosswise in the direction of depth of the sheet pile foundation was substituted by the mass points, and it was assumed that the mass

points were connected with one another across the springs and dash pots. To calculate the stiffness matrix in the vibration system of the foundation, the model was designed to permit consideration of the shearing deformation of the joints between the sheet piles.

In the response calculation, the response of the subsoil only was first calculated from an earthquake input to the bearing layer, then the response of the foundation model was calculated with the subsoil vibration thus obtained then taken as an input seismic wave to the foundation model, and the response values of displacement, acceleration, moment, and axial force were obtained.

Figure 2 shows a flow chart of the program.

<div align="center">RESPONSE CALCULATION</div>

The structural characteristics of sheet pile foundations are next examined using the dynamic analysis program.

Calculation Conditions

Through a series of examinations using a static program which employs the seismic coefficient method, the parameters which have a large influence on the response are extracted, rigidity G_J to the shearing deformation of the joints between the sheet piles, and the ratio of the frictional spring constant K_f between pile and subsoil to the horizontal spring constant K_H or K_f/K_H. The following case study will examine the effects of these parameters.

In calculations, the following conditions are assumed.

Sheet pile foundation: Diameter, 15 m, Single sheet structure

Sheet pile: Diameter, 1000 mm; Thickness, 15 m; Steel pipe pile

Joint: Diameter, 165 mm; Thickness, 11 mm; Steel pipe

Embedded depth: 60 m, 30 m, and 20 m

Subsoil conditions: Tip end (2.5 m) N value 50

                       Peripheral surface, N value 5

Calculation cases are shown in Table 1. In the table, G_{J0} represents the joint rigidity obtained by experiment [1], and is taken as 120,000 t/m^2.

<div align="center">237</div>

The values of the horizontal spring constant, K_H, and the bottom spring constant, K_V, were calculated by conversion from the N values following the Specifications for Highway Bridges.

For handling the subsoil the circular form sheet piles, all the soil was considered as added mass.

For the input seismic wave, an artifical seismic wave having as flat a frequency characteristic as practicable was provided so that the frequency characteristics of the vibration system would least affect the response. It was input at a time interval of 0.02 second with a maximum acceleration at 100 gal (Figure 3).

Calculation Conditions

As an example of response, a stress distribution in the direction of depth with $K_f/K_H = 0.5$ is shown in Figure 4. This is calculated using the pile producing the maximum stresses in the direction of vibration. As seen, a very great stress is produced close to the pile head. A similar phenomenon is observed in the static analysis; but, in the dynamic analysis, a fluctuation of the stress close to the pile head is characteristically very sharp. The stress close to the pile head is due mainly to the pile head moment. However, as the joint rigidity G_J increases, the pile head moment decreases, resulting in a decrease of the stresses. Such effect of G_J is similarly produced in the static analysis.

The G_J effect was examined as to displacement, acceleration, and cross-sectional force as shown in Figure 5. The response values at the pile head of acceleration, axial force, and bending moment, but not displacement, decrease with increasing G_J. Further, such decrease is appreciable at the stage of $G_J/G_{J0} = 0.1$. Thus, the importance of including the effect of G_J in design calculations is confirmed. Additionally, that the pile end axial force increases with increasing G_J indicates that the sheet pile foundation changes its behavior from that of the pile foundation to that of the caisson. Thus, if G_J is not taken into consideration, the design is apt to be on the unsafe side.

Such trends were also confirmed in the static analysis.

Figure 6 shows the result of an examination of the effects of the frictional spring K_f which was changed by 0, 0.2, 0.5 and 1.0 times of the horizontal spring K_H with G_J fixed at $0.1\ G_{J0}$.

The sheet pile foundation is executed as piles so that the proportion of the circumferential frictional force to the total bearing force is considered to be fairly great. In this case, it is confirmed from the result of calculations according to the method of calculation of the cirmcumferential frictional force of pile foundation that Kf = 0.5 K_H is a reasonable value.

With increasing K_f, pile head displacement, acceleration, and axial force decreases, while the bending moment tended to increase. That the pile end axial force can be reduced by considering K_f is a very advantageous trend for the design.

SUMMARY

As the result of time hysteresis response analysis of the sheet pile foundations by input of artificial seismic waves, the following is confirmed.

(1) A great stress concentration occurs close to the pile head.

(2) As joint rigidity, G_J, between the sheet piles increases, the pile head response decrease, but the pile tip axial force increases.

(3) As the frictional spring, K_f, increases, the pile head bending moment increases, but the pile tip axial force decreases.

(4) The foregoing results agree well with the results confirmed by the static analysis.

REFERENCES

[1] Kawakami, K., et al., "Sheet Pile Foundation and its Structural Characteristics Against Horizontal Loads," 7th Joint Meeting, U.S.-Japan Panel on Wind and Seismic Effects, May 20-23, 1975.

[2] Shioi, Y., et al., "Structural Analysis of Sheet Pile Foundation," Preprint of 25th Symposium on Structural Engineering, February 1979.

Fig. 1 Vibration model

Table 1 Calculation cases

	A				B				C			
D/L	15/60=0.25				15/30=0.50				15/20=0.75			
K_f/K_H ⟍ G_J/G_{Jo}	0.	0.1	0.5	1.0	0.	0.1	0.5	1.0	0.	0.1	0.5	1.0
0.	o	o	o	o	o	o	o	o	o	o	o	o
0.2		o				o				o		
0.5	o	o	o	o	o	o	o	o	o	o	o	o
1.0		o				o				o		
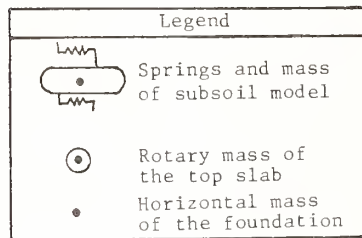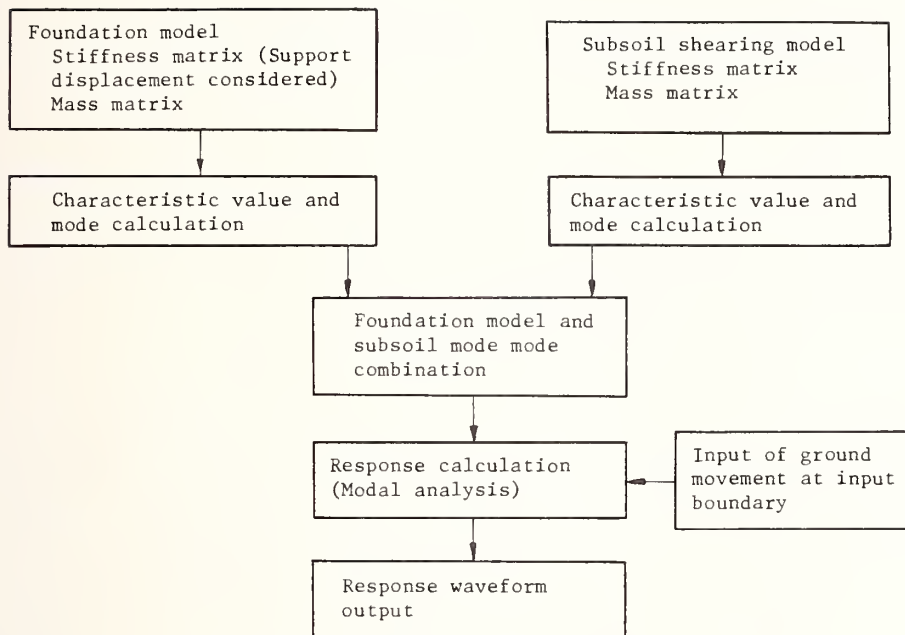
Fig. 2 Flow chart of dynamic program
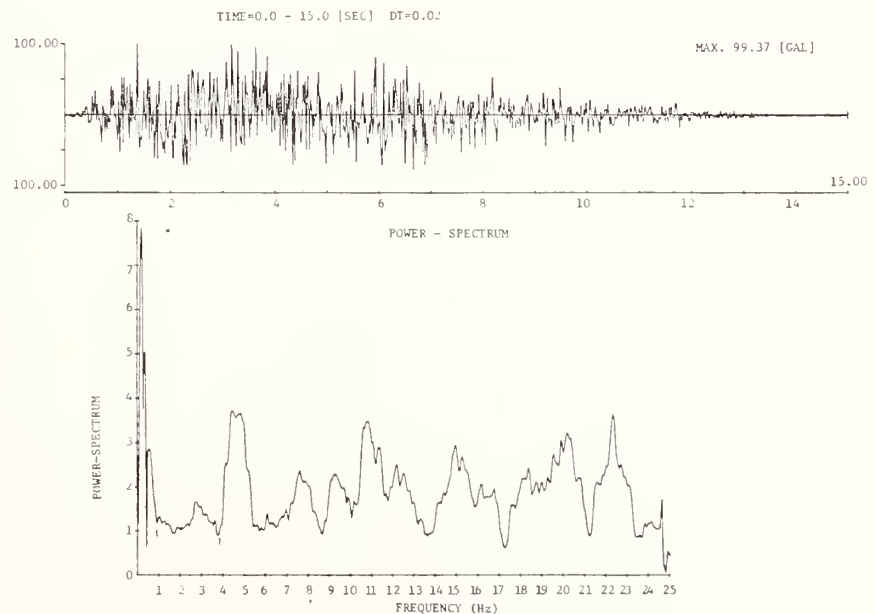
Fig. 3 Artificial earthquake waveform
and power spectrum
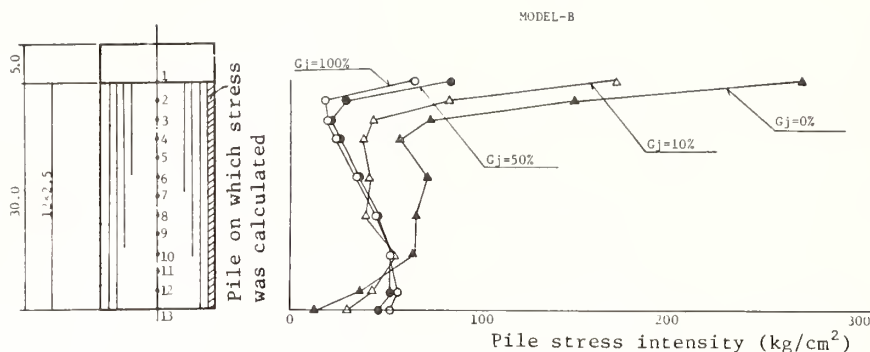
Fig. 4   Distribution of the maximum pile stress intensity
in the direction of depth (K_f/K_H=0.5, W=100%)
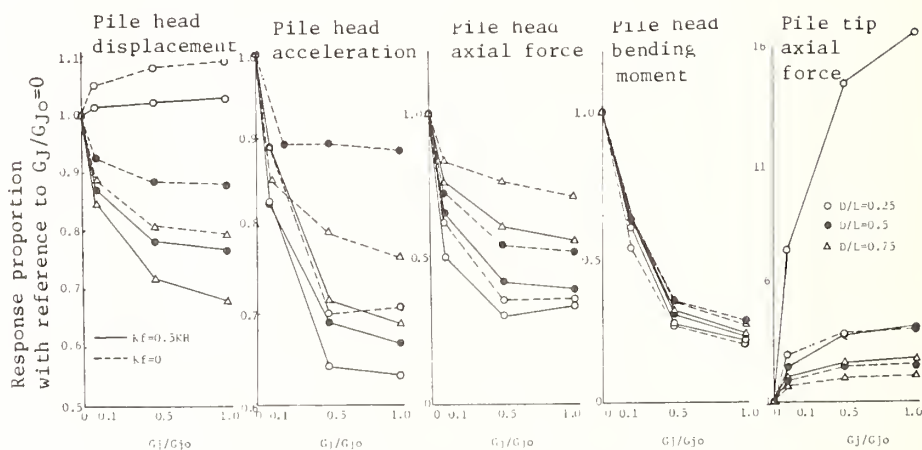
Fig. 5   Effects of joint pipe shearing rigidity (K_f, $0.5K_H$
and 0; inside soil weight, 100%)
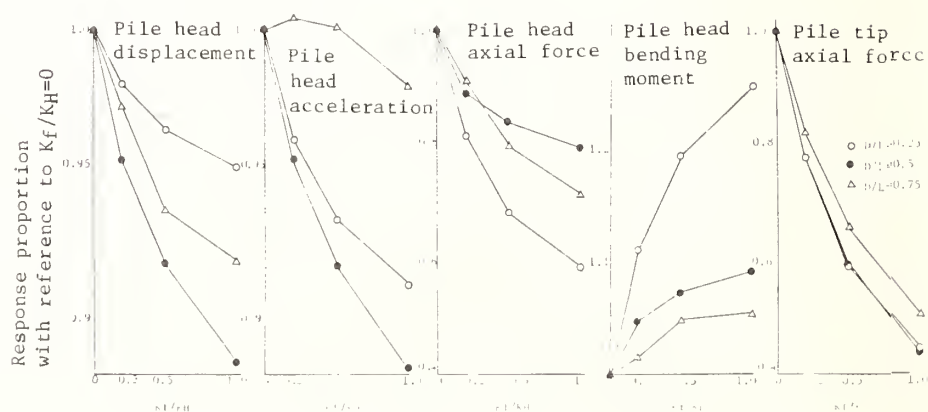
Fig. 6   Effects of Frictional spring (G_J=12,000t/m^2; inside
soil weight, 100%)

DYNAMIC BEHAVIOR OF MULTI-COLUMN FOUNDATIONS

WITH INCLINED PILES DURING EARTHQUAKES

by

Tatsuo Asama

Yukitake Shioi

Tasuo Mitsuie

ABSTRACT

To construct a pile foundation in a lake or sea, a novel method of placing piles from the water surface without coffering and constructing footings in air has been used recently. Here, the piles work as columns and is thus called the multi-column foundation.

This multi-column foundation is distinguished in workability but is lacking in rigidity to resist horizontal external forces. Particularly, the conventional multi-column foundations are composed of only vertical piles so that with an increasing free length of columns, a greater number of piles are required in order to keep the horizontal displacement below the allowable value.

In such a case, the joint use of inclined piles in a multi-column foundation is desirable. However, the multi-column foundation with inclined piles has no precedent, and its structural characteristics required that many points be resolved. In this paper, the dynamic behavior of the multi-column foundation using inclined piles is examined by calculating the time hysteresis responses.

INTRODUCTION

The multi-column foundation is a type of foundation developed for improving the workability of pile foundations in a lake or sea, and its use is increasing.

However, where the free length of pile is long and the subsoil is relatively soft, the pile has its horizontal resistance reduced, and in order to keep the displacement of the footing within allowable values, numerous piles are required.

Thus, in order to enhance the rigidity of the foundation, the use of inclined piles may be considered. However, the structural characteristic of the multi-column foundation has many points which need clarification.

This investigation is intended to clarify the structural characteristic of a multi-column foundation comprising of inclined piles, and thus the effects of inclined piles introduced upon the response displacement, acceleration, and cross-section force through calculation of the time hysteresis responses of the pier by using actual seismic records as input data both with and without the inclined piles.

METHOD OF INVESTIGATION

Vibration Model

(1) Foundation Model

A multi-column foundation of the following dimensions is assumed.

Number of piles: Longitudinal direction, 7 rows;

Transversal direction, 9 rows; a total of 63 piles.

Where inclined piles are included, the piles along the outermost row are inclined at $\theta = 15°$.

Piles: Steel pipe pile, ϕ 2500 mm, t 40 mm;

Cross-sectional secondary moment $I = 0.234$ m^4;

Area $A = 0.309$ m^2; Free length $h = 38$ m; Embedded depth $D_f = 37$ m

Footing: Pile interval, 2.0 ϕ

LG direction 35 m x TR direction 45 m x thickness 3.5 m

LG direction $I = 20.7$ m^4, $A = 20.3$ m^2

TR direction $I = 16.1$ m^4, $A = 15.8$ m^2

$E_c = 2.7 \times 10^6$ t/m^2

Body of pier   Height, 22.8 m

         LG direction, $I = 5.40 \text{ m}^4$, $A = 3.28 \text{ m}^2$

         TR direction, $I = 139 \text{ m}^4$, $A = 3.28 \text{ m}^2$

         $E_c = 2.7 \times 10^6 \text{ t/m}^2$

  The multi-column foundation having such dimensions is replaced by a plane rigid frame. In this case, the cross-sectional dimensions are so taken that in the rigid frame of the LG direction they are respectively a multiple of the number of rows in the TR direction, and in the TR direction they are a multiple of the number of rows in LG direction. As concentrated masses, a plane rigid frame structure supported by concentrated springs is assumed, as shown in Figure 1.

  (2) Subsoil Model

  It is assumed that the subsoil is composed of three layers, with the modulus of deformation of the respective layers taken as shown below.

  Upper layer (Ground surface ~ -10 m) 10 kg/cm^2

  Middle layer (-10 m ~ -20 m) 50 kg/cm^2

  Lower layer (-20 m ~) 100 kg/cm^2

  From these values of the modulus of deformation, the horizontal subsoil reaction coefficients were obtained according to the Specifications for Highway Bridges, and thus the subsoil was modeled as concentrated springs.

Method of Response Calculation

  The time hysteresis responses, using actual seismic records as input data, were calculated.

  As an input seismic wave, the records of the Izu Peninsula South Coast Earthquake (May 1974) and the Hachijo Island East Sea Earthquake (December 1972) observed in Ukishima, reclaimed land in the Tokyo Bay, were used. The records include acceleration observed at depths of 0 m, -27 m and -67 m. Figure 2 shows the records at ground surface. It will be seen that the waveform of the Izu Peninsula South Coast Earthquake is predominantly in the long frequency component, more so than the Hachijo Island East Sea Earthquake.

  In the response calculations, the record at 0 m was used as input simultaneously to the joint at the ground surface, the record at -27 m to the joint at -19 m, and the record

at −67 m to the joint at −37 m. The response calculation was executed with the maximum acceleration taken as 100 gal (at ground surface), time interval at 0.02 sec, and duration at 25 sec ~ 30 sec.

For the damping constants, 10 percent was taken for the piles in the ground and 2 percent of the piles on the ground surface, the footing, and the body of the pier.

RESULT OF INVESTIGATION

Modes of Vibration

Table 2 shows the natural periods of the respective modes in the case of both straight and inclined piles. Figures 3 through 6 show the primary to the fourth modes of vibration.

In both cases of straight and inclined piles, the foundation is a structure of very long period. However, in the example of the primary mode, it will be seen that the natural period is reduced considerably by the use of inclined piles. In the secondary and subsequent modes, partial vibration is prevailing so that it seems that there is little effect from the introduction of the inclined piles.

Response Displacement

Figure 7 shows the time hysteresis responses of the footing displacement using the Izu Peninsula South Coast Earthquake input. In the case of the straight piles, the response displacement is very great, and a gradual increase of the response amplitude is noted. Where the inclined piles are used, however, the maximum displacement is smaller by about the order of one, and the displacement peaks at about 15 sec and decreases thereafter.

Table 3 lists the maximum displacements at the respective joints. The maximum displacement of the footing is different by about an order of one due to the characteristics of the seismic waves. It is also seen that the displacement decreases considerably when using the inclined piles.

Axial Force

Figures 8 and 9 show the maximum axial forces produced in the respective members.

It will be seen that where an inclined pile is included, a great axial force is produced in the inclined pile. However, the axial force produced in the inclined pile is by

no means of a great value when compared with the maximum axial force of the straight pile in the case of straight piles only. This seems to be due to a decreasing maximum response displacement when using the inclined piles.

Bending Moment

Figures 10 and 11 show the maximum bending moments in the respective members. It will be noted that the bending moment at the pile head or at the lower end of the body of the pier is reduced greatly by use of the inclined piles.

SUMMARY

Table 4 lists the maximum values of the response.

The results of the investigation are summarized below.

(1) By introducing the inclined piles, the natural period in the primary mode of vibration is reduced considerably.

(2) Using only straight piles a phenomenon of the response increasing gradually depending on the input seismic wave was observed.

(3) The response values as displacements, axial forces, and bending moments are reduced considerably by introducing the inclined piles.

From the foregoing, it is confirmed using dynamic analysis that inclined piles are very effective in the case of soft structure foundation types, such as the multi-column foundation.

Thus, in the case of a multi-column foundation with great free length, it is necessary that the foundation itself be given a rigidity to some extent, and for such purpose, the introduction of inclined piles is desirable where the work conditions permit.

Table 1   Cross-sectional dimensions

Table 1   Cross-sectional dimensions

(1) Straight piles only, longitudinal direction

Member	A(m²)	I(m⁴)	E(t/m²)	Damping Ratio	Member, Joint, No. Connection
1	278	2.11	$2.1 \cdot 10^7$	0.10	1-8 -15-22-29-36-43-50 2-9 -16-23-30-37-44-51 3-10-17-24-31-38-45-52 4-11-18-25-32-39-46-53 5-12-19-26-33-40-47-54 6-13-20-27-34-41-48-55 7-14-21-28-35-42-49-56
2	2.78	2.11	$2.1 \cdot 10^7$	0.02	50-57-64-71-78 51-58-65-72-79 52-59-66-73-80 53-60-67-74-81 54-61-68-75-82 55-62-69-76-83 56-63-70-77-84
3	20.3	20.7	$2.1 \cdot 10^7$	0.02	78-79-80-81-82-83-84
4	3.28	5.40	$2.1 \cdot 10^7$	0.02	84-85-86

(2) Straight piles only, transversal direction

Member	A(m²)	I(m⁴)	E(t/m²)	Damping Ratio	Member, Joint, No. Connection
1	216	1.64	$2.1 \cdot 10^7$	0.10	1-10-19-28-37-46-55-64 2-11-20-29-38-47-56-65 3-12-21-30-39-48-57-66 4-13-22-31-40-49-58-67 5-14-23-32-41-50-59-68 6-15-24-33-42-51-60-69 7-16-25-34-43-52-61-70 8-17-26-35-44-53-62-71 9-18-27-36-45-54-63-72
2	2.16	1.64	$2.1 \cdot 10^7$	0.02	64-73-82-91-100 65-74-83-92-101 66-75-84-93-102 67-76-85-94-103 68-77-86-95-104 69-78-87-96-105 70-79-88-97-106 71-80-89-98-107 72-81-90-99-108
3	15.8	16.1	$2.1 \cdot 10^7$	0.02	100-101-102-103-104-105-106-107-108
4	3.28	1.19	$2.1 \cdot 10^7$	0.02	104-109-110

(3) Inclined piles included, longitudinal direction

Member	A(m²)	I(m⁴)	E(t/m²)	Damping Ratio	Member, Joint, No. Connection
1	278	2.11	$2.1 \cdot 10^7$	0.10	1-8 -15- 2-29-36-43-50 2-9 -16-23-30-37-44-51 3-10-17-24-31-38-45-52 4-11-18-25-32-39-46-53 5-12-19-26-33-40-47-54 6-13-20-27-34-41-48-55 7-14-21-28-35-42-49-56
2	2.78	2.11	$2.1 \cdot 10^7$	0.02	50-57-64-71-78 51-58-65-72-79 52-59-66-73-80 53-60-67-74-81 54-61-68-75-82 55-62-69-76-83 56-63-70-77-84
3	20.3	20.7	$2.1 \cdot 10^7$	0.02	78-79-80-81-82-83-84
4	3.28	5.40	$2.1 \cdot 10^7$	0.02	84-85-86

(4) Inclined piles included, transversal direction

Member	A(m²)	I(m⁴)	E(t/m²)	Damping Ratio	Member, Joint, No. Connection
1	216	1.64	$2.1 \cdot 10^7$	0.10	1-10-19-28-37-46-55-64 2-11-20-29-38-47-56-65 3-12-21-30-39-48-57-66 4-13-22-31-40-49-58-67 5-14-23-32-41-50-59-68 6-15-24-33-42-51-60-69 7-16-25-34-43-52-61-70 8-17-26-35-44-53-62-71 9-18-27-36-45-54-63-72
2	2.16	1.64	$2.1 \cdot 10^7$	0.02	64-73-82-91-100 65-74-83-92-101 66-75-84-93-102 67-76-85-94-103 68-77-86-95-104 69-78-87-96-105 70-79-88-97-106 71-80-89-98-107 72-81-90-99-108
3	15.8	16.1	$2.1 \cdot 10^7$	0.02	100-101-102-103-104-105-106-107-108
4	3.28	1.19	$2.1 \cdot 10^7$	0.02	104-109-110

Table 2 Natural periods of the modes (second)

Models / Mode orders	Straight piles only		Inclined piles included	
	Longitudinal direction	Transversal direction	Longitudinal direction	Transversal direction
1	2.44	2.38	1.40	1.40
2	0.90	0.39	0.90	0.39
3	0.38	0.38	0.39	0.39
4	0.37	0.37	0.38	0.38
5	0.36	0.36	0.36	0.37
6	0.36	0.36	0.36	0.36
7	0.36	0.36	0.36	0.36
8	0.36	0.36	0.36	0.36
9	0.33	0.36	0.32	0.36
10	0.19	0.36	0.18	0.35

Table 3 Maximum displacements (cm)

Location	Seismic wave	Longitudinal direction		Transversal direction	
		Straight piles only	With inclined piles	Straight piles only	With inclined piles
Footing	Hachijo Island	9.22	1.78	9.45	2.35
	Izu Peninsula South	61.22	6.74	89.33	8.90
Midpoint of piles on the ground surface	Hachijo Island	5.74	1.31	5.96	1.70
	Izu Peninsula South	38.51	4.92	56.89	7.00
Piles at groundd surface	Hachijo Island	1.52	0.41	1.60	0.52
	Izu Peninsula South	10.28	1.45	15.31	1.87
Midpoint of piles in the ground	Hachijo Island	0.03	0.02	0.03	0.02
	Izu Peninsula South	0.15	0.04	0.24	0.05

Table 4 List of responses

Shown dotted is the cross-section in transversal direction	Noted point	Input wave	Acceleration (gal)				Horizontal displacement (cm)			
			Longitudinal		Transversal		Longitudinal		Transversal	
			Straight piles only	Inclined piles included	Straight piles only	Inclined piles included	Straight piles only	Inclined piles included	Straight piles only	Inclined piles included
	Footing	Hachijo Island	77	56	123	65	9.22	1.78	9.45	2.35
		Izu Peninsula	406	145	696	186	61.22	6.74	89.33	8.90
	Midpoint of piles on the ground surface	Hachijo Island	69	69	110	84	5.74	1.31	5.96	1.70
		Izu Peninsula	249	126	444	168	38.51	4.92	56.89	7.00
	Piles at ground surface	Hachijo Island	50	52	57	48	1.52	0.41	1.60	0.52
		Izu Peninsula	76	55	121	64	10.28	1.45	15.31	1.87
	Midpoint of piles in the ground	Hachijo Island	16	18	8	8	0.03	0.02	0.03	0.02
		Izu Peninsula	19	20	5	5	0.15	0.04	0.24	0.05

Noted point	Input wave	Axial force (t) Per pile				Bending moment (t.m) Per pile				Shearing force (t) Per pile			
		Longitudinal		Transversal		Longitudinal		Transversal		Longitudinal		Transversal	
		Straight piles only	Inclined piles included	Straight piles only	Inclined piles included	Straight piles only	Inclined piles included	Straight piles only	Inclined piles included	Straight piles only	Inclined piles included	Straight piles only	Inclined piles included
Footing	Hachijo Island	·143	·180	·1.7	·241	778	230	810	264	25	8	28	9
	Izu Peninsula	941	666	1140	913	4878	761	7229	984	154	14	223	18
Midpoint of piles on the ground surface	Hachijo Island	143	181	127	241	156	107	179	133	32	10	34	12
	Izu Peninsula	742	668	1141	916	9711	320	1543	409	204	35	304	46
Piles at ground surface	Hachijo Island	144	181	128	241	472	111	490	144	32	13	36	17
	Izu Peninsula	943	669	1143	917	804	403	4471	537	214	40	323	53
Midpoint of piles in the ground	Hachijo Island	144	149	128	211	111	96	133	128	31	9	33	12
	Izu Peninsula	943	587	1143	804	20	324	3029	431	201	30	297	41
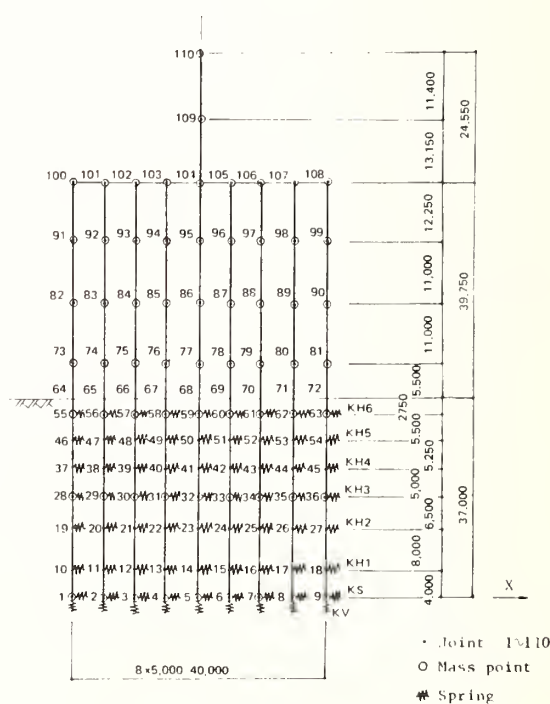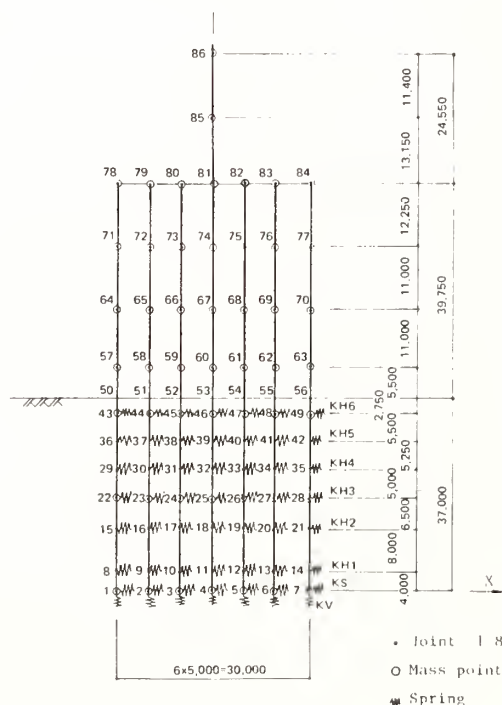
(1) Straight piles only, longitudinal direction   (2) Straight piles only, transversal direction

Fig. 1 Dynamic models

Fig. 1 Dynamic models
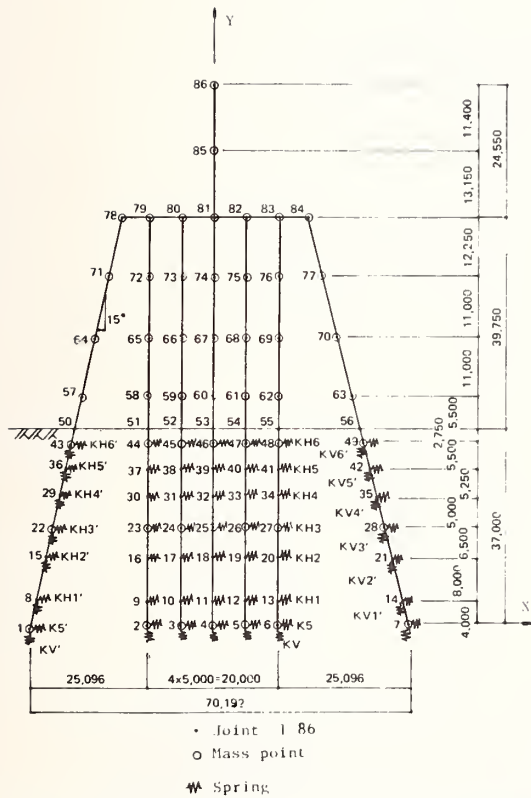
(3)   Inclined piles included, longitudinal direction

(4)   Inclined piles included, transversal direction

251

Input seismic waveforms

Ukishima, Kawasaki, Kanagawa (NScomponent)

(1) GR. UKISHIMA   N-S

Ukishima, Kawasaki, Kanagawa (NS component)
Seismic center - Izu peninsula south coast
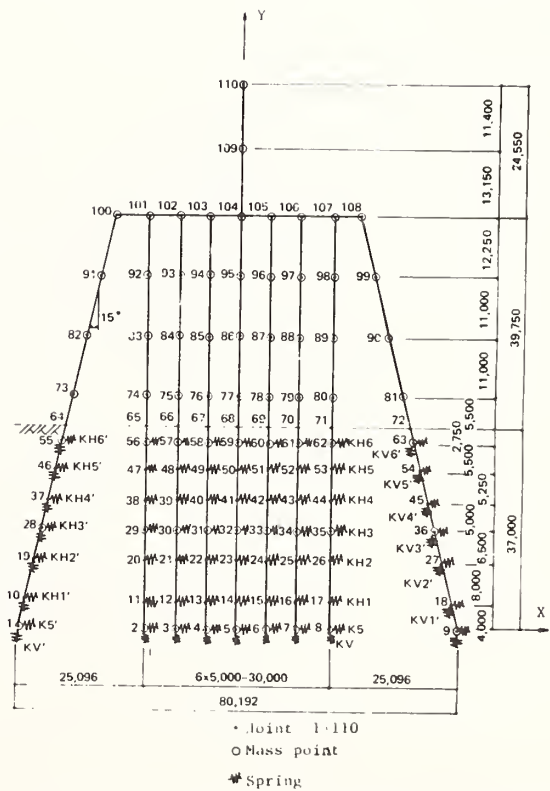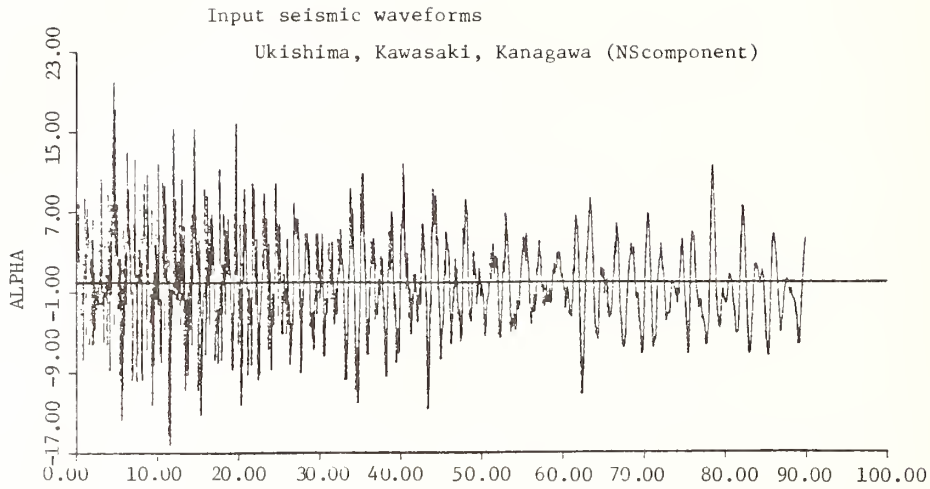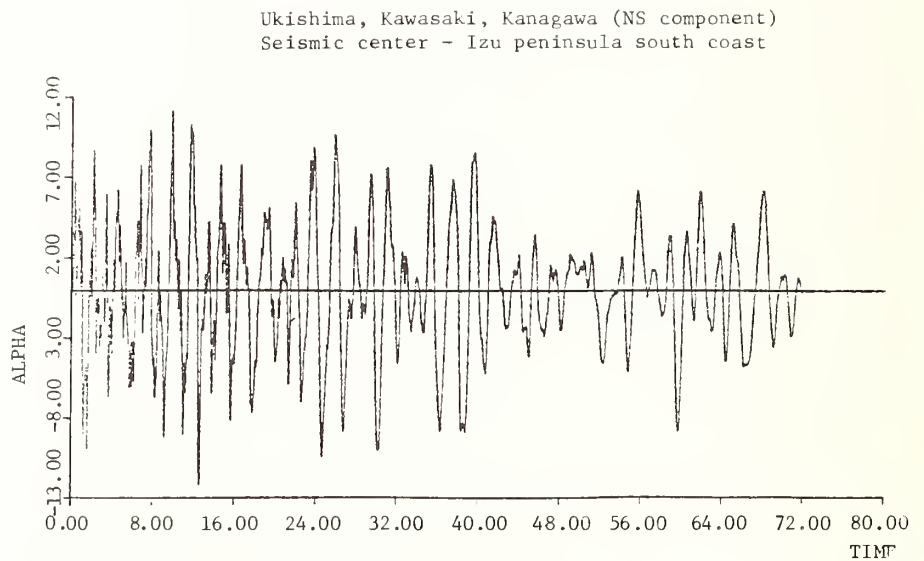
(2) GR. UKISHIMA   N-S

Fig. 2 Seismic waves used in analysis
(Records of acceleration on the ground surface)
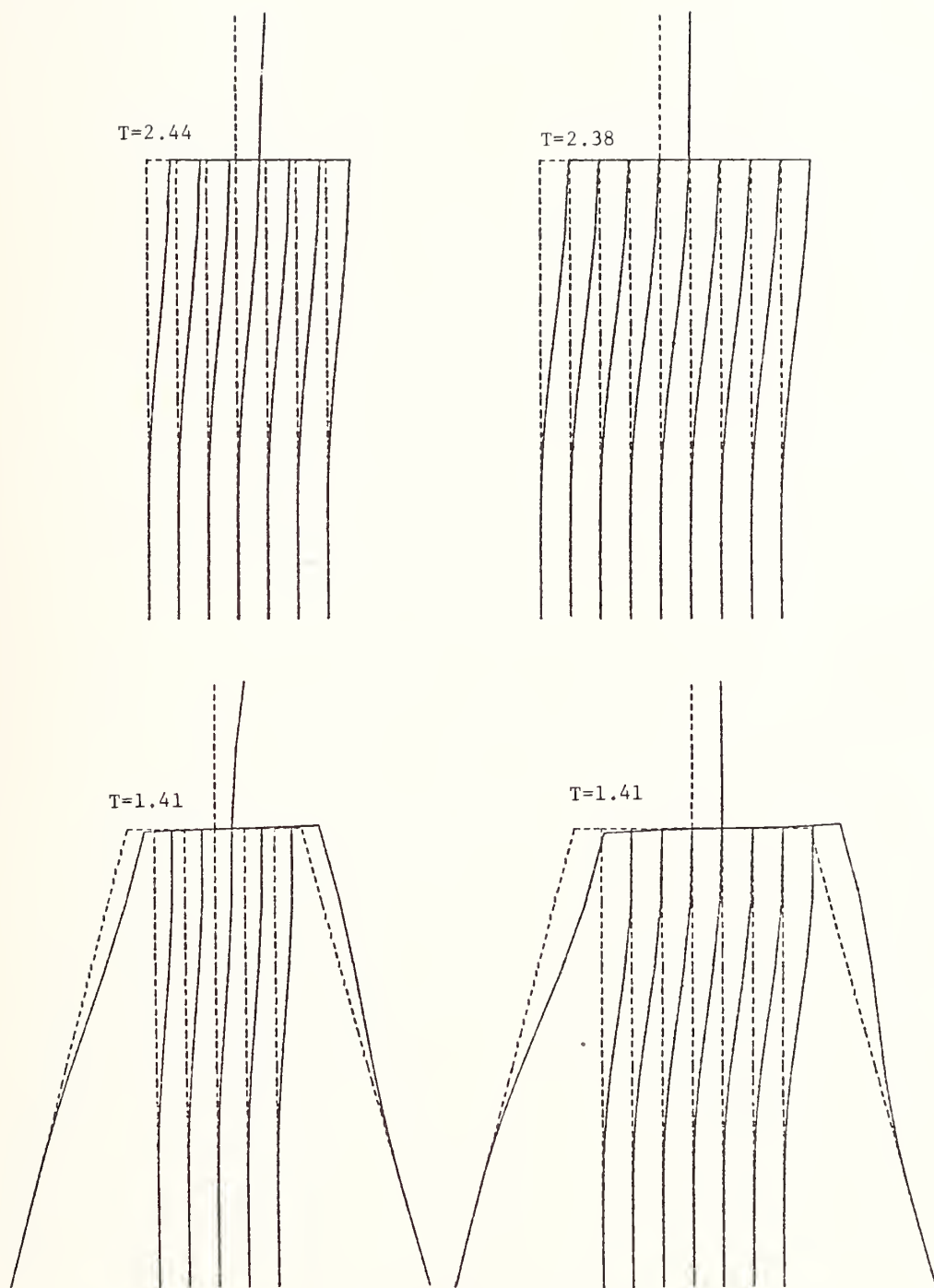
Fig. 3 Mode diagrams (Primary)
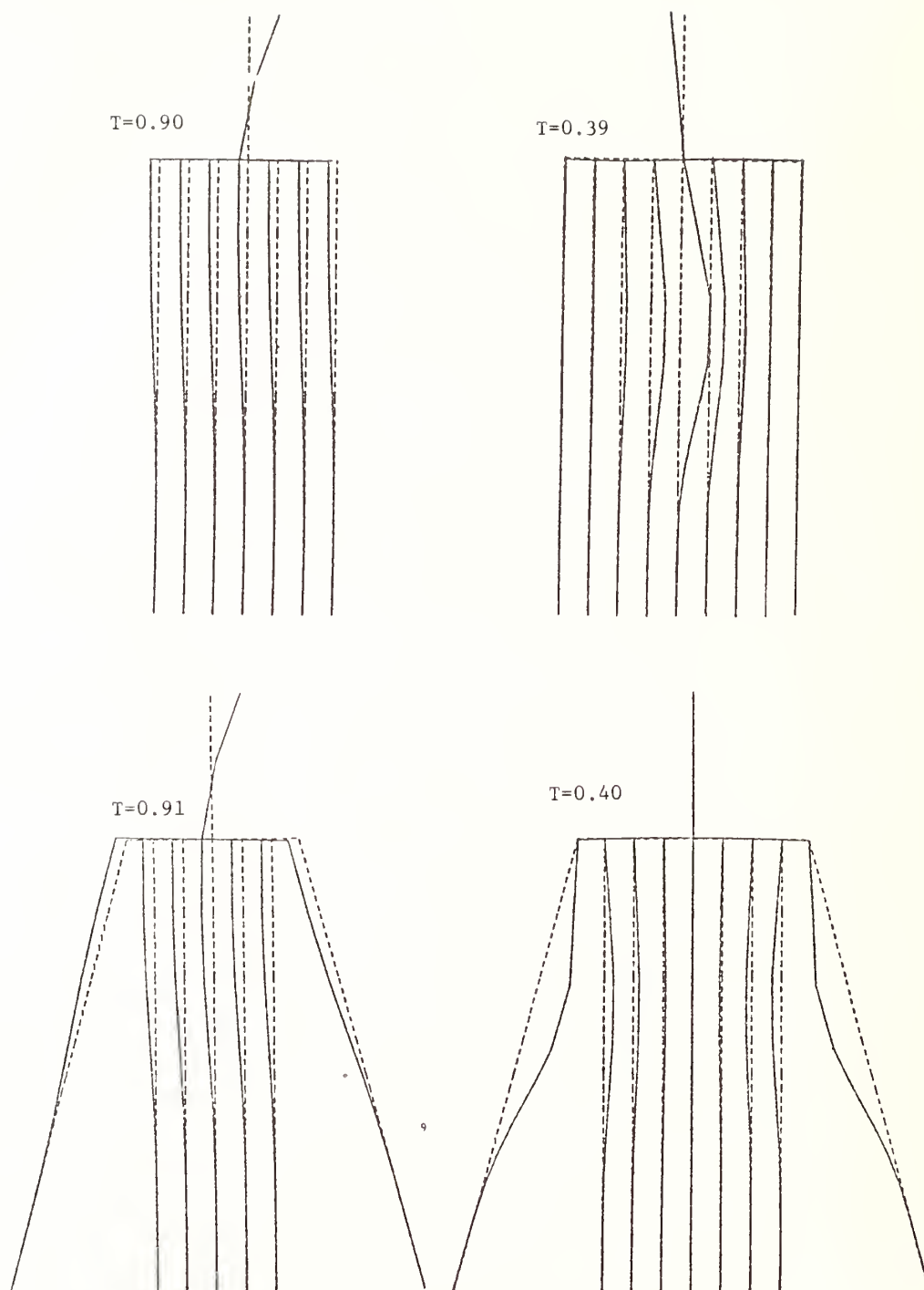
Fig. 4 Mode diagrams (Secondary)
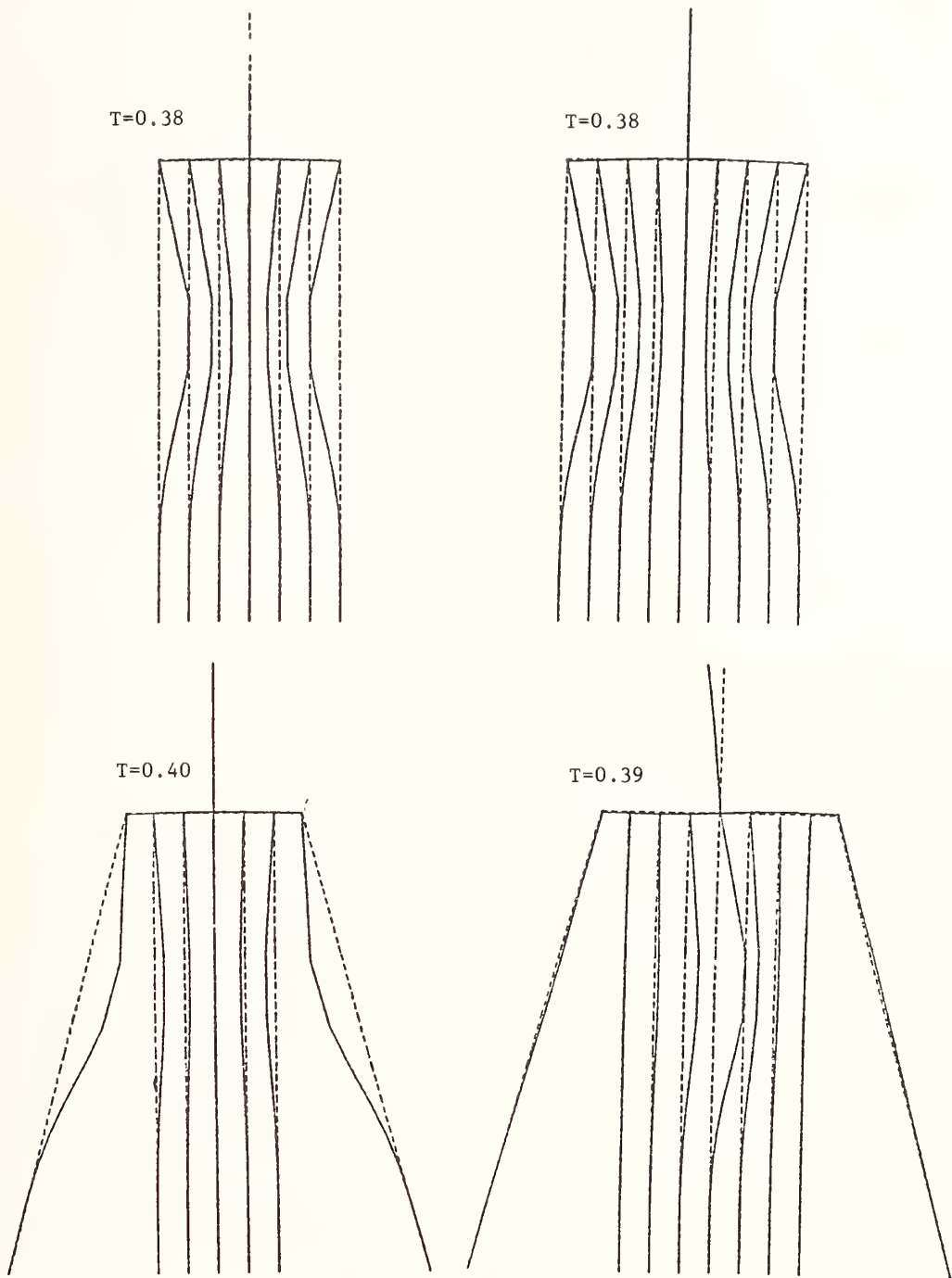
Fig. 5 Mode diagrams (Third)
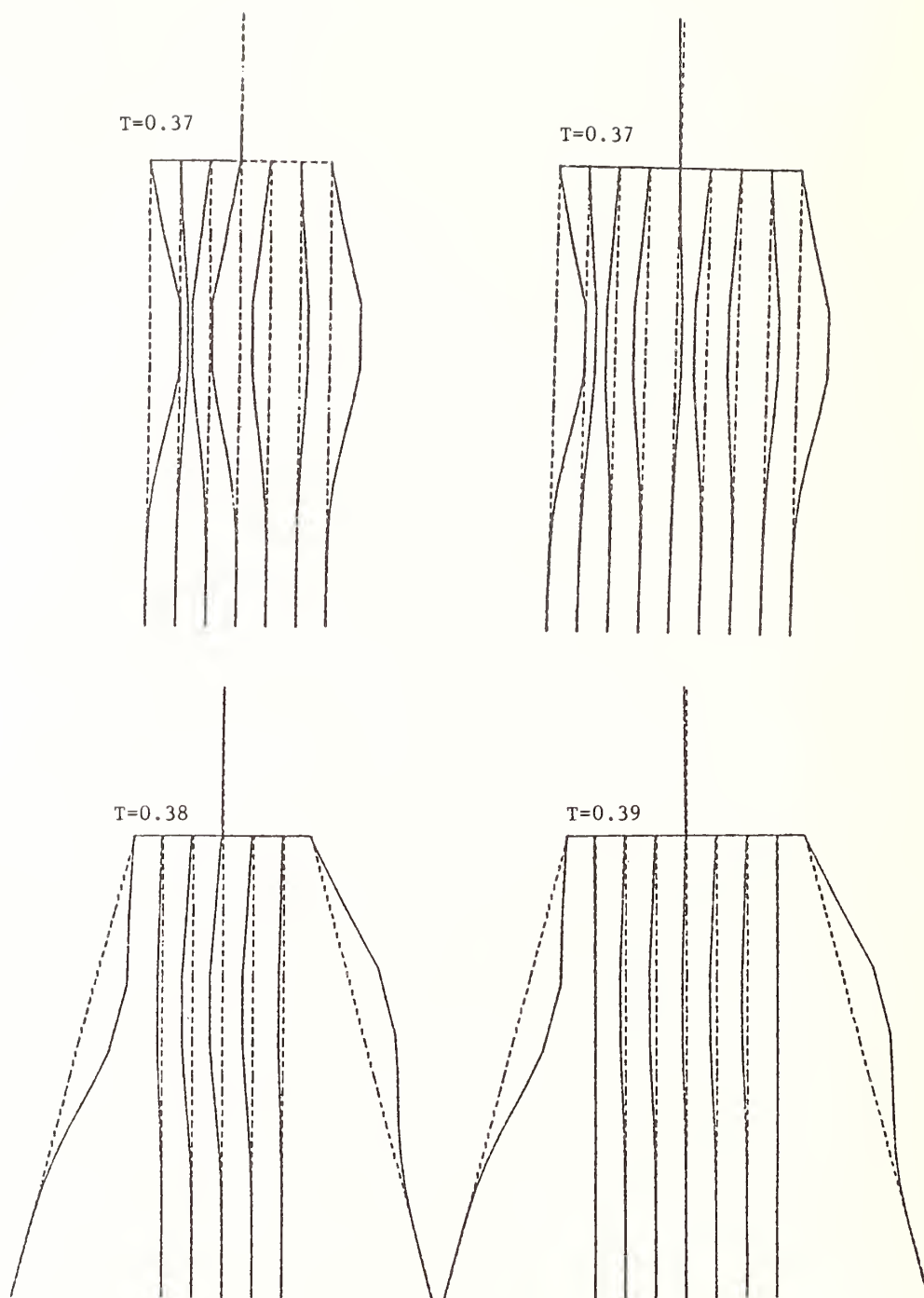
Fig. 6 Mode diagrams (Forth)

(a) Straight piles only

(b) Inclined piles included
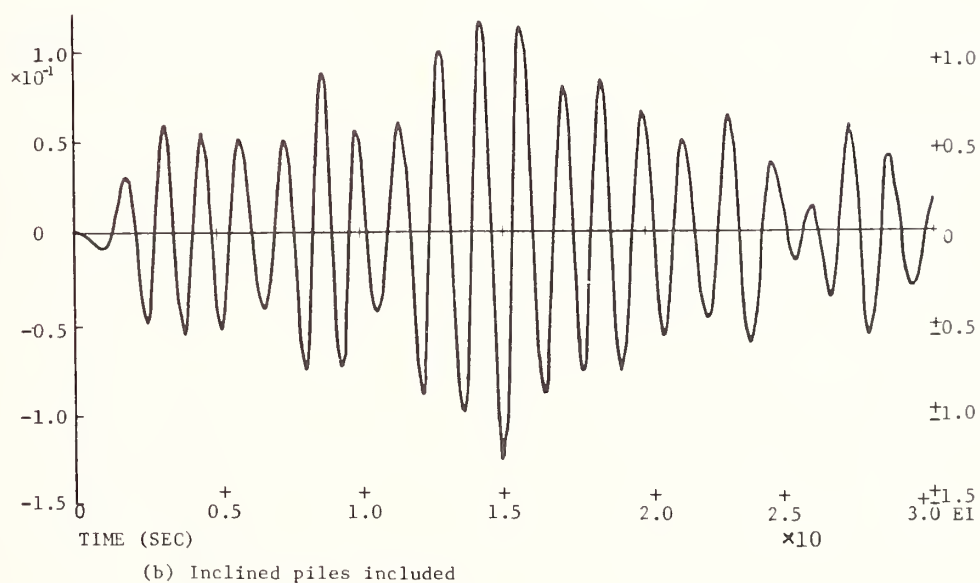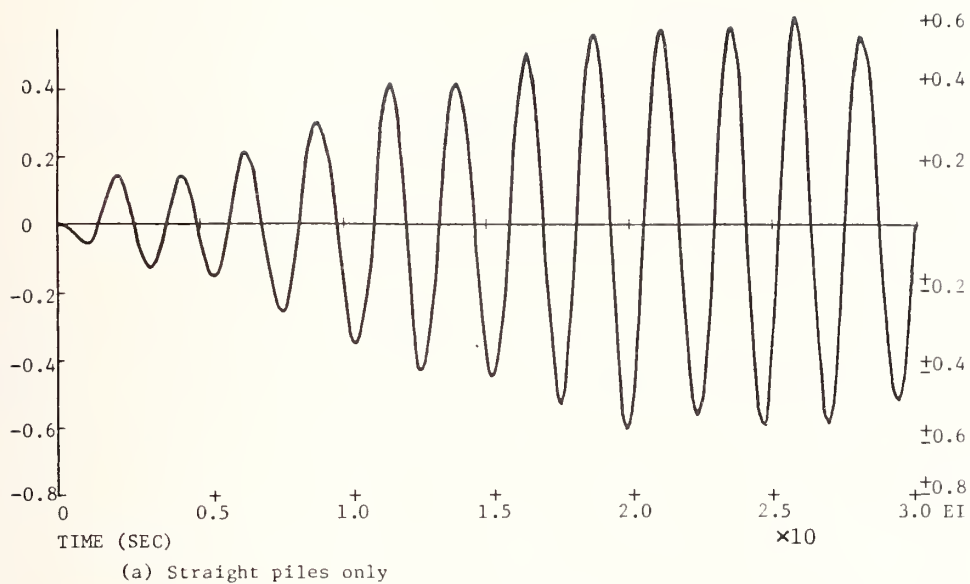
Fig. 7   Seismic responses
        (Footing; Izu peninsula south coast earthquake)

257
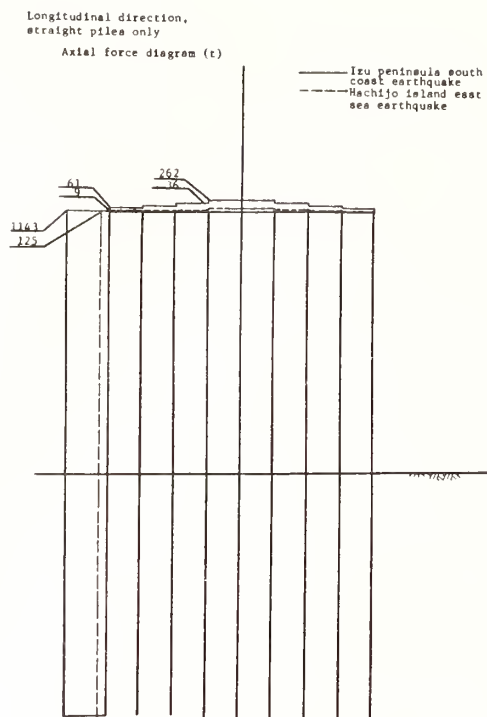
Fig. 8 Axial force distribution diagram

Fig. 9 Axial force distribution diagram

258

Fig. 10 Bending moment
distribution diagram
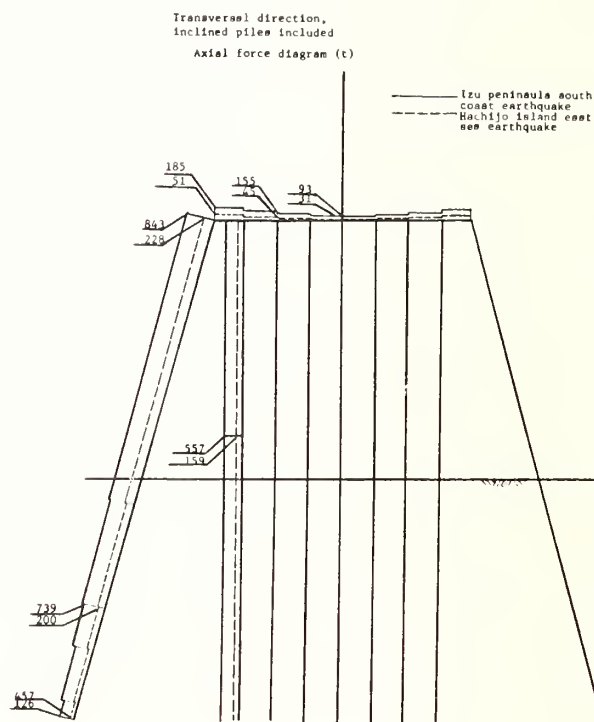
Fig. 11 Bending moment
distribution diagram

ANALYSIS OF LIQUEFACTION POTENTIAL OF SANDS ON LEVEL GROUND
DURING EARTHQUAKES USING CYCLIC STRAIN CONTROLLED TESTS

by

Felix Y. Yokel

Riley M. Chung

Ricardo Dobry

Richard S. Ladd

INTRODUCTION

The current state-of-the-art method of predicting liquefaction potential of saturated level sandy sites during earthquakes was recently summarized by Seed (1979 [1]). In this method, the cyclic stress ratio $(\tau/\sigma_v')_e$ is compared with the cyclic strength ratio $(\tau/\sigma_v')_{cs}$ where:

$$\tau \qquad = \text{cyclic shear stress}$$

$$\sigma_v' \qquad = \text{effective vertical overburden pressure}$$

$$(\tau/\sigma_v)_e = \text{cyclic stress ratio caused by the earthquake}$$

$$(\tau/\sigma_v')_{cs} = \text{cyclic stress ratio needed to cause liquefaction}$$

$$\text{(cyclic strength ratio)}$$

Whenever $(\tau/\sigma_v')_e \geq (\tau/\sigma_v')_{cs}$ liquefaction is predicted.

Two procedures have evolved for obtaining the cyclic strength ratio $(\tau/\sigma_v')_{cs}$. The first procedures relies on empirical correlations between the Standard Penetration Test (SPT) results and liquefaction potential derived from information from sites where liquefaction occurred in previous earthquakes. In the second procedure the cyclic strength ratio is determined by stress-controlled cyclic triaxial tests. Both procedures have problems as discussed by Seed (1979 [1]), Peck (1979 [2]) and Dobry et al. (1982 [3]). Some of the problems are discussed below:

While it has been demonstrated that there is a correlation between the SPT blow count and the liquefaction potential of saturated sands, this correlation has considerable scatter and provides definite answers only for extreme situations. The SPT test itself is not sufficiently standardized and the results obtained vary with the equipment and procedures

used to perform the test [i.e., see Kovacs (1979 [4])]. This variation raises serious questions about the interpretation of historical SPT data for which there is no record of equipment and procedures used.

The laboratory determination of the cyclic strength ratio is the more unreliable of the two methods. The parameters which affect the cyclic strength ratio, such as soil fabric, overconsolidation, geological age, and seismic history, cannot usually be determined for the site of interest and thus are not simulated in the laboratory. Neither is it possible to retrieve truly undisturbed samples of sand for laboratory testing. Peck (1979 [2]) discussed the laboratory procedures and concluded that they lead to decisions which are unnecessarily conservative and expensive.

The approach recommended in this paper is to predict liquefaction potential on the basis of predicted cyclic strain, rather than cyclic stress, and is designed to eliminate some of the difficulties encountered in the previously discussed state-of-the-art methods.

EFFECT OF SOIL FABRIC ON PORE PRESSURE BUILDUP

The effect of sample fabric on the cyclic strength ratio is illustrated by the cyclic triaxial test results in Figure 1. In this figure the cyclic stress ratio is defined by as τ/σ_3' where σ_3' is the effective confining pressure prior to application of the cyclic load. The circles represent data from tests performed by Park and Silver (1975 [5]) and discussed later by Yokel et al., (1980 [6]). Note that at a given stress ratio, specimens prepared by wet rodding will resist 15 to 20 times the number of stress cycles producing failure in specimens of the same relative density prepared by dry vibration. Figure 2 shows the buildup of pore pressures as a function of the cyclic stress ratio and the number of stress cycles for the same stress-controlled tests shown in Figure 1. It can be seen from Figure 2 that in this type of test the effect of sample fabric on pore pressure buildup is more important than the effect of the number of test cycles applied. This is an important (and discouraging) conclusion. The number of stress cycles is related to the duration of the ground motion and can be estimated. However, soil fabric cannot be presently (1980) measured in situ and thus its effect cannot be evaluated in an engineering study.

261

RELATIONSHIP BETWEEN CYCLIC SHEAR STRAIN AND PORE PRESSURE BUILDUP

General Trend

Figure 3 shows a curve originally proposed by Dobry and Ladd (1980 [7]) for the pore pressure buildup, Δu, during strain-controlled cyclic triaxial tests on sands having a relative density (D_r) of approximately 60 percent. Figure 3 is for 10 cycles of strain; shear strain was taken as 1.5 times the cyclic axial strain. The first three sands identified were tested by Park and Silver (1975 [5]). The other two sands are from test data obtained by Dobry and Ladd (1980 [7]). More recent tests performed by the authors on Monterey #0 sand also closely follow the solid curve in the figure which shows the trend of the test data.

It can be seen that the curve in Figure 3 very well represents data from different sands (crystal silica #20 sands, pit-run sands, and Monterey #0 sands), three methods of sample preparation (fabric) and a considerable range of confining pressures (σ_c'). Also, the data in Figure 3 were obtained independently at two different laboratories. This evidence strongly suggests that the curve in Figure 3 is generally applicable to most sands with a relative density of about 60 percent.

One of the most significant features of Figure 3 is that up to a shear strain of approximately 10^{-2} percent there is essentially no pore pressure buildup.

The trends shown in Figure 3 were further investigated in a program of cyclic triaxial strain-controlled tests, conducted by the authors on saturated Monterey #0 sand. Some of the results of these tests are discussed hereafter. More detailed information is presented in the final report on this investigation by Dobry et al., (1980, issued July 1982 [3]).

Threshold Strain

Figure 4 shows a plot of residual excess pore pressure, u, versus cyclic shear strain, γ, up to $3 \cdot 10^{-2}$ percent. These results are discussed in some detail by Yokel et al. (1980 [6]). The vertical scale which shows the residual pore pressure ratio is deliberately magnified to show even a minor increase of pore pressure. Note that below the cyclic shear strain of approximately 10^{-2} percent there is no pore pressure buildup. This confirms the observation made in Figure 3 and suggests the existence of a threshold strain, $\gamma_t \approx 10^{-2}$ percent. Figure 5 shows the effect of confining pressure on γ_t for the range 500 psf

(24 kPa) $\le \sigma_c' \le$ 4000 psf (192 kPa). Figures 4 and 5 indicate that the value of γ_t is quite insensitive to both, relative density (D_r) and confining pressure (σ_c'). These figures also show that up to a cyclic shear strain $\gamma \simeq 3 \cdot 10^{-2}$ percent the pore pressure builtup after 10 cycles is very small and is essentially a unique function of γ.

The lack of pore pressure buildup for $\gamma \le \gamma_t$ can be explained by the loading deformation behavior at the sand grain contacts at very small cyclic strains. This load-deformation behavior was originally investigated by Mindlin and Deresiewicz (1952 [8]) who studied two elastic spheres in contact pressed together by a normal static load and subjected to a tangential cyclic load. These authors derived an expression for the tangential displacement which can be taken as a measure of strain. Dobry and Swiger (1979 [9]) applied this solution to calculate threshold strain (γ_t) as a function of confining pressure (σ_c') for a cubic array of quartz spheres using the elastic constants and friction coefficient typical for quartz. Threshold strain was taken as the strain at which gross sliding between the spheres is imminent. Below this strain the sliding between spheres and the resultant volume change are frictionally blocked. The result of this work is shown in Figure 6. Note that within the range of confining pressures which is of more practical interest [500 psf (20 kPa) to 4000 psf (200 kPa)] the threshold strain does not vary significantly and is reasonably consistent with the experimentally-observed threshold strain.

The existence of the threshold strain and its practically constant value are of great practical significance, since sites which are subjected to seismic loads and experience strains smaller than the threshold strain will not liquefy, regardless of the number of applied load cycles. For small strains comparable to γ_t the anticipated shear strain can be calculated if the maximum shear modulus of sand is known. The maximum shear modulus, in turn, can be reliably determined in the field by geophysical measurements. Therefore, a design criterion based on γ_t can be developed. Such a criterion is suggested by Dobry et al. (1980 [10]). It is especially useful when considering a stiff sand site subjected to earthquake accelerations up to 0.3 g.

Effect of Number of Strain Cycles on the Pore Pressure Ratio

The effect of cyclic strain and of the number of strain cycles on Δu is shown in Figure 7 for a wide range of cyclic strains. It can be seen from this figure that up to 100 strain cycles there is no pore pressure buildup below the threshold strain. It is

also of interest to note that $\Delta u/\sigma'_3$ is below 0.2 up to a strain of $3 \cdot 10^{-2}$ percent even after 100 cycles. Thus it is reasonable to conclude that at the strain of $3 \cdot 10^{-2}$ the pore pressure ratio during an earthquake would not exceed 20 percent.

Effect of Relative Density on the Pore Pressure Ratio

The effect of relative density (D_r) is shown in Figure 8. In the tests shown in this figure the confining pressure is held constant at 2000 psf (95.8 kPa) and the number of cycles at 10. The range of relative densities is from 45 to 80 percent. Figure 8 shows that D_r is a significant variable in determining pore pressure buildup for cyclic shear strain $\gamma > 3 \cdot 1^{-2}$ percent and that the importance of D_r increases as γ increases.

CONCLUSIONS

Several important conclusions can be drawn from the data presented in this paper:

(1) Saturated sands will not experience pore pressure buildup when subjected to a cyclic strain smaller than 10^{-2} percent, regardless of the type of sand involved, its relative density, its fabric, and the number of strain cycles.

(2) When subjected to up to 100 cycles of strain smaller than $3 \cdot 10^{-2}$ percent, the pore pressure ratio in saturated sands will probably not exceed 20 percent, regardless of the relative density of the soil.

(3) There is strong evidence indicating that the effects of soil fabric on pore pressure buildup and cyclic strength reported by various authors is significantly reduced or eliminated if pore pressures are compared for the same cyclic strain, rather than for the same cyclic stress.

It appears from the results of this study that it will be possible to reasonably predict pore pressure buildup and liquefaction potential of level saturated sandy sites during earthquakes by means of a cyclic strain approach. This approach would be an alternative to the present state-of-the-art cyclic stress approach.

NOTE: The cyclic strain approach to liquefaction described in this paper was originally proposed by R. Dobry from R.P.I. and was developed in References [3] and [9]. Further work was performed in the Summer of 1979 as part of the earthquake engineering program of the Geotechnical Engineering Group of the National Bureau of Standards. This work involved the participation of R. Dobry (RPI), F. Yokel (NBS) and R. Ladd (Woodward-Clyde

Consultants), as well as other staff members of the three institutions. The tests on Monterey #0 sand presented herein were conducted at the soil dynamics laboratory of Woodward-Clyde Consultants. The final report on this research effort [7] has been published.

REFERENCES

[1] Seed, H. B., Soil Liquefaction and Cyclic Mobility Evaluation for Level Ground During Earthquakes, Journal of the Geotechnical Engineering Division, ASCE, Vol. 105, GT2, February 1979, pp. 201-255.

[2] Peck, R. B., Liquefaction Potential, Science Versus Practice, Journal of the Geotechnical Engineering Division, ASCE, Vol. 105, GT3, March 1979, pp. 393-398.

[3] Dobry, R., Ladd, R. S., Yokel, F. Y., Chung, R. M., and Powell, D. T., Prediction of Pore Pressure Buildup and Liquefaction of Sands During Earthquakes by the Cyclic Strain Method, Building Science Series Report 138, National Bureau of Standards, Washington, D.C., July 1982, 168 pp.

[4] Kovacs, W. D., Velocity Measurement of Free Fall SPT Hammer, Journal of the Geotechnical Engineering Division, ASCE, Vol. 105, GT1, January 1979, pp. 1-10.

[5] Park, T. and Silver, M. L., Dynamic Soil Properties Required to Predict the Dynamic Behavior of Elevated Transportation Structures, U.S. Department of Transportation Report DOT-TST-75-44, May 1975.

[6] Yokel, F. Y., Dobry, R., Powell, D. T., and Ladd, R. S., Liquefaction of Sands During Earthquakes - The Cyclic Strain Approach, Proc., International Symposium on Soils Under Cyclic & Transient Loading, Swansea, U.K., January 1980, A. Backema, Rotterdam, Vol. 2, pp. 571-580.

[7] Dobry, R. and Ladd, R., (1980) Discussion to Soil Liquefaction and Cyclic Mobility Evaluation for Level Ground During Earthquakes, by H. B. Seed and Liquefaction Potential: Science Versus Practice by R. B. Peck, Journal of the Geotechnical Engineering Division, ASCE, Vol. 106, No. GT6, pp. 720-724.

[8] Mindlin, R. D. and Deresiewicz, H., Elastic Spheres in Contact Under Varying Oblique Forces, Journal of the Applied Mechanics Division, ASME, Paper No. 53, November 1952.

[9] Dobry, R. and Swiger, W. F., Threshold Strain and Cyclic Behavior of Cohesionless Soils, Proceedings, Third ASCE/EMDE Specialty Conference, Austin, Texas, September 1979, pp. 521-525.

[10] Dobry, R., Powell, D. J., Yokel, F. Y., and Ladd, R. S., Liquefaction Potential of Saturated Sand - The Stiffness Method, Proceedings of the Seventh World Conference on Earthquake Engineering, Istanbul, Turkey, September 8-13, 1980, Vol. 3, pp. 25-32.
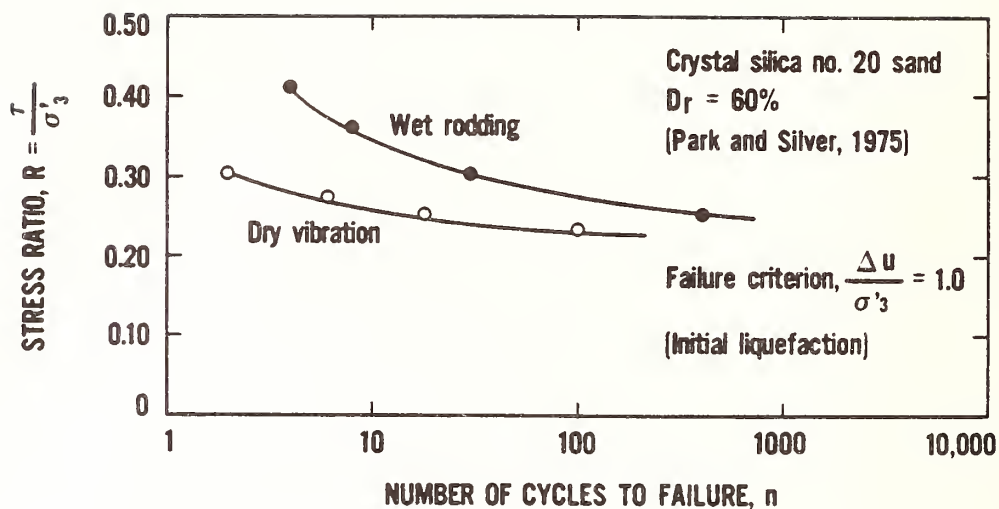
Figure 1 Effect of fabric on cyclic strength in stress–controlled cyclic
tests (based on data from Park and Silver, 1975)
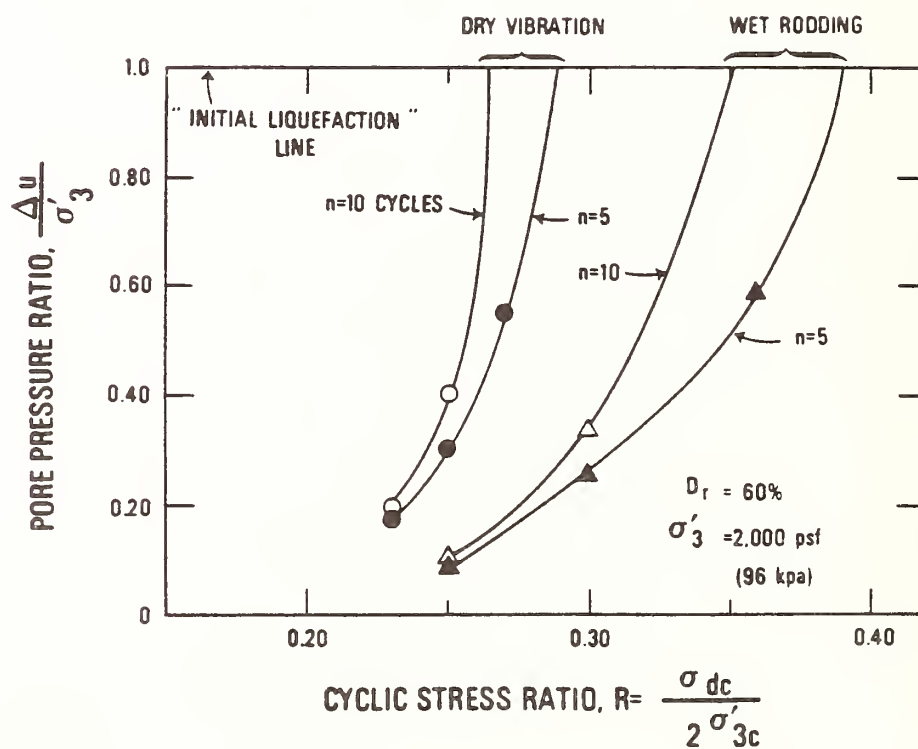
Figure 2 Effect of fabric and number of cycles on pore pressure buildup
in stress–controlled triaxial tests (based on data by Park and
Silver, 1975)
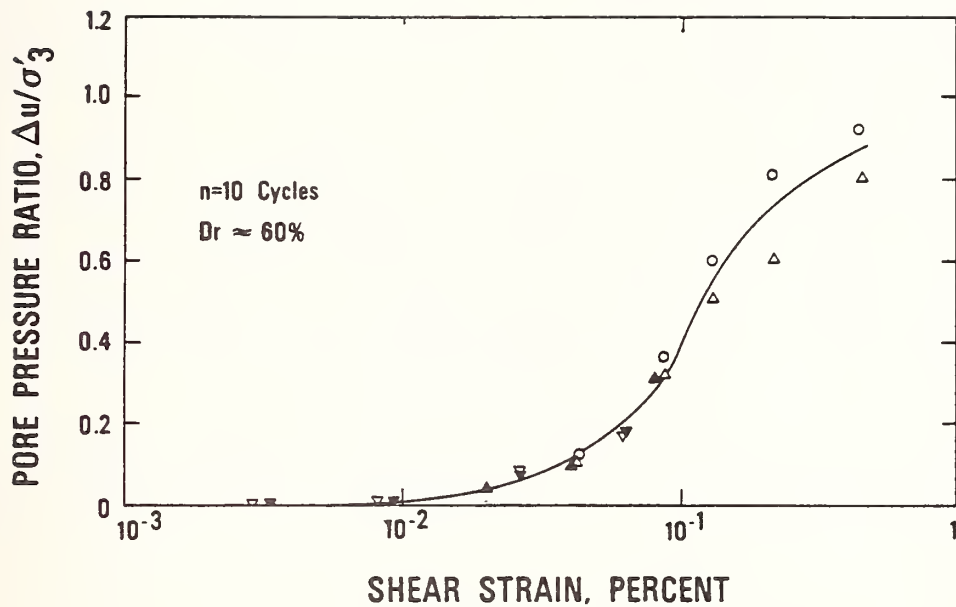
LEGEND

○	Crystal silica sand	$\sigma_3' = 14$ psi	Fresh samples, dry vibration
△	Crystal silica sand	$\sigma_3' = 14$ psi	Fresh samples, wet rodding
▲	Crystal silica sand	$\sigma_3' = 14$ psi	Staged testing, dry vibration
▼	Sand #1	$\sigma_3' = 20$ psi	Staged testing, moist tamping
▽	Sand #1	$\sigma_3' = 10$ psi	Staged testing, moist tamping

Figure 3 Measured pore pressure buildup in saturated sands after ten load
cycles (N = 10) of strain-controlled cyclic triaxial tests (Dobry
and Ladd, 1980)
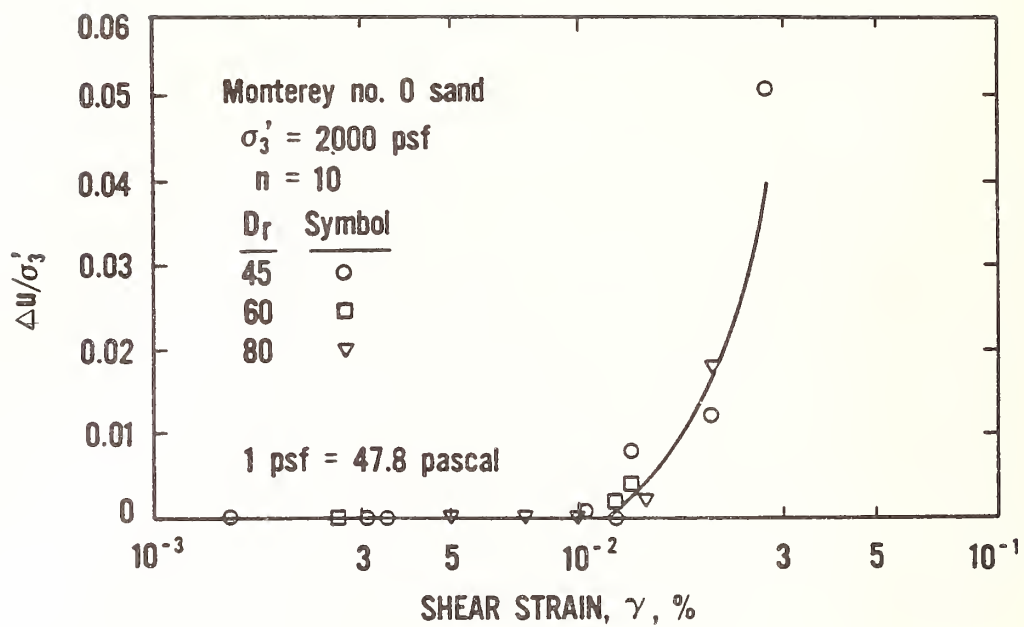
Figure 4 Residual pore pressure buildup after ten loading cycles, strain-controlled cyclic triaxial tests (see also Yokel et al., 1980)
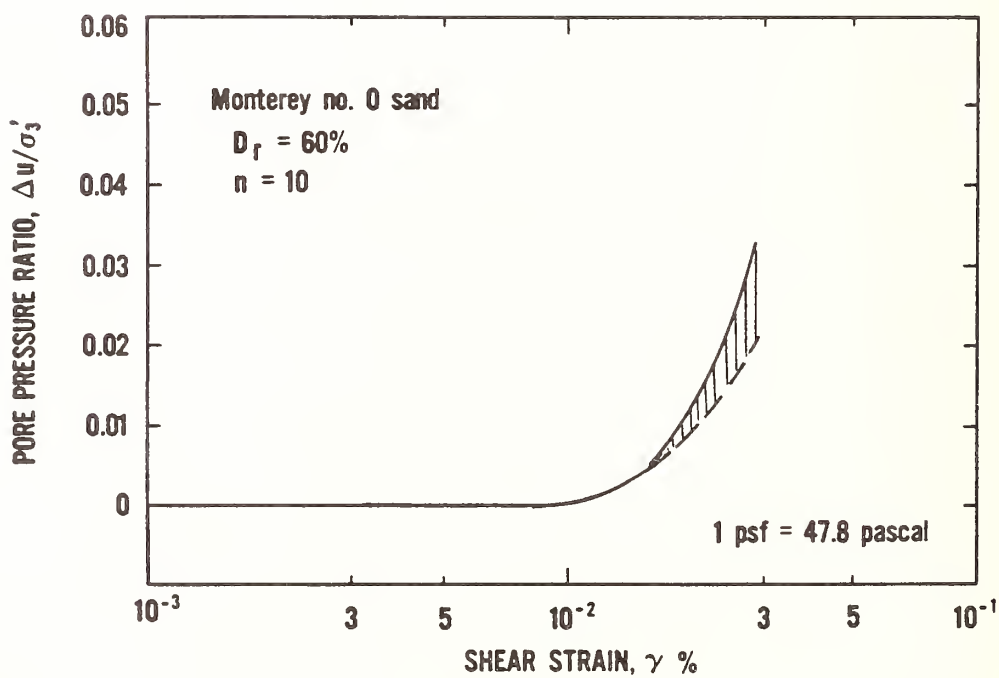
Figure 5 Effect of confining pressure, 533 psf $<\sigma_3' \leqslant$ 4000 psf
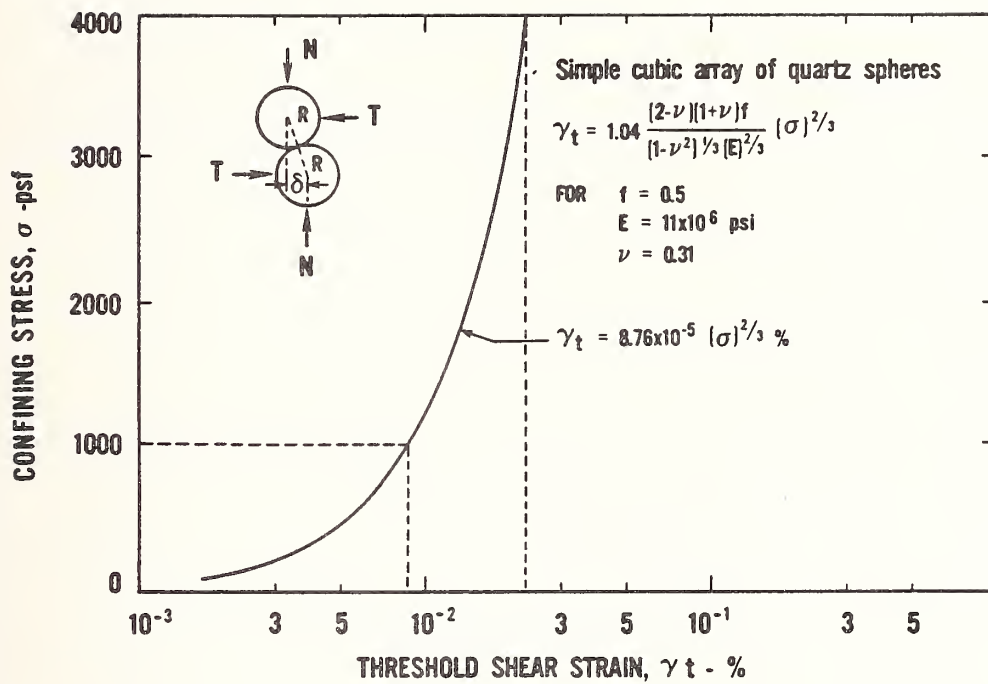
Figure 6 Calculated threshold shear strain as a function of confining pressure for a simple cubic array of quartz spheres (Dobry and Swiger, 1979)
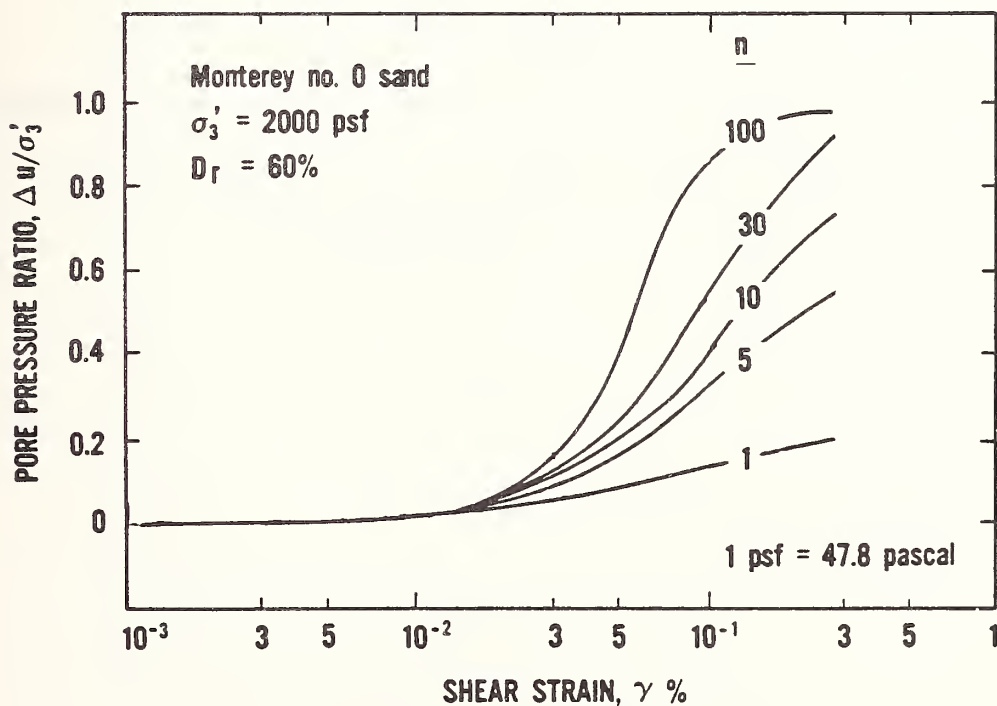
Figure 7 Effect of number of strain cycles
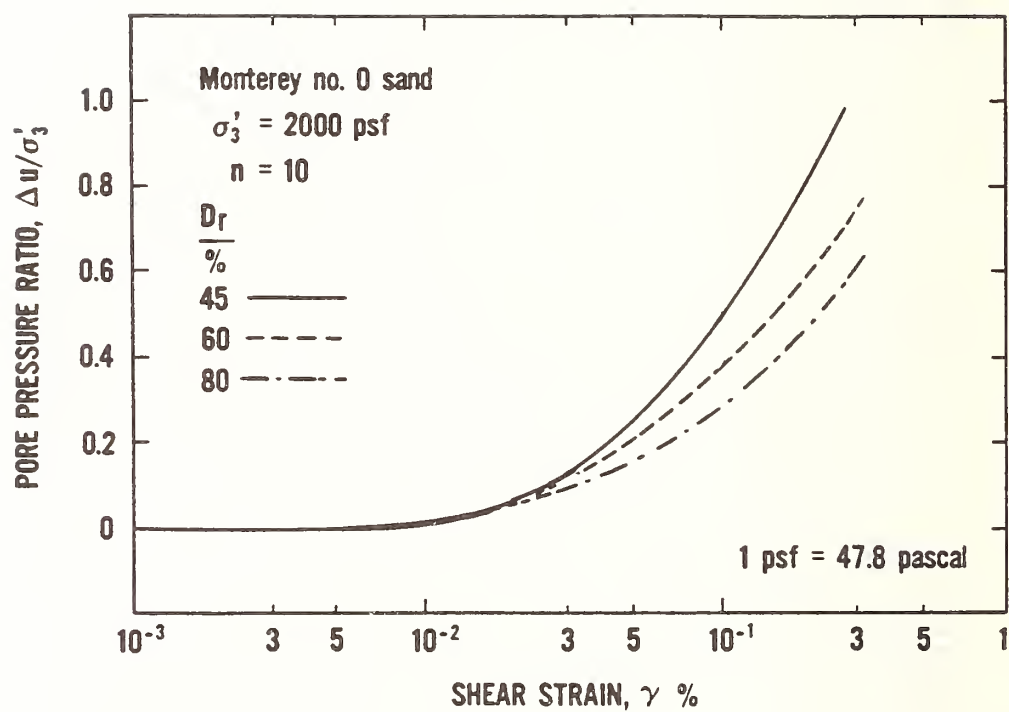
Figure 8 Effect of relative density

THE PARTICIPATION FACTOR OF HORIZONTAL FORCE APPLIED TO PILE FOUNDATIONS

by

Yoshihiro Sugimura

Makoto Watabe

ABSTRACT

The participation factor of horizontal force applied to piles is discussed for the purpose of rational seismic design of structures supported by pile foundations. Discussion topics are collected from various sources, viz., seismic damage investigation of piles by the June 12, 1978 Off-Miyagi Prefecture earthquake, response analysis of an example of a damaged pile foundation, earthquake observation data of fourteen story residential buildings supported on long piles and vibration tests for a model ground-pile-building system. A fundamental idea on the design of pile foundations is proposed as a first step for a static method in which seismic effects are introduced.

INTRODUCTION

Present methods of evaluating earthquake loads on piles and the design concept itself should be reconsidered because of the damage by the June 12, 1978 Off-Miyagi Prefecture earthquake. Several examples of completely collapsed piles were found in Sendai City since the earthquakes. This situation was the first full scale testing experience of buildings supported on piles which extend through horizontal soil deposits in Japan. More research on detailed on-site conditions through excavation will take place in the future as it will produce valuable research data to improve the earthquake resistant design of pile foundations. Of course, a few examples of damaged piles were already recorded on the occasions of the Niigata earthquake in 1964 [1,2] and the Tokachi-oki earthquake in 1968 [3,4], but these are, more or less, due to differing causes such as liquefaction of sandy soil deposits, or landslides on artificial fill ground.

Thus, research work has been initiated on topics such as the structural performance of pile members, the effects of execution of work on characteristics of pile member, the effects of horizontal loads on piles, the earthquake response of the ground-pile-structure system, the earthquake-proof design method of piles, and the excavation and research on the site mentioned above. The present paper is a preliminary report on these works and introduces the findings to date.

ACTUAL STATE OF DESIGN OF PILE FOUNDATION TO HORIZONTAL FORCES

The most customary design process to consider horizontal forces on pile foundations for buildings is summarized in Figure 1. Horizontal forces at all floors are calculated first under the condition of a fixed base. Secondly, by summing them and the moment forces to the base, respectively, the so called base shear force, Q, and the overturning moment force, M, are determined. After this procedure, the superstructure is removed and effect of the foundation (footing and beam) is considered. Finally, the two types of forces, divided by the numbers of piles, are obtained; i.e., the first is shear force minus reaction force at the part of foundation from the base shear force, and the second is the axial force which results from the foundation beam design which bears the overturning moment force. The effect of the axial force is generally considered in checking

for stresses in the pile members. This process may necessitate, at the least, resolving the following questions

(1) Is it enough to consider only the inertia force of the superstructure as a seismic design force on the pile foundation? Is it possible for the force of inertia to be replaced by static force?

(2) Is it enough to consider just the component of horizontal force as a design force at the pile cap?

(3) What percentage of base shear should be considered as a horizontal force component at the pile cap? In other words, how large is the participation factor of the horizontal force of the piles?

On the first question, it is necessary to consider the characteristics of ground and superstructure in the frequency domain. The natural vibration modes of both can be treated individually because both natural frequencies frequently disagree with each other. From this fact, it is easy to estimate as follows: the vibrational characteristics of the ground mainly control the behavior of the piles at and near the natural frequencies of the ground. On the other hand, the vibrational characteristics of the superstructure mainly control the behavior of the piles at and near the natural frequencies of the super-structure. The effects of the inertial force of the superstructure, therefore, predominant at and near the natural frequencies of the superstructure.

Regarding the second question, it should be noted that the combined mode of horizontal and rotational vibration is transmitted to the piles from the superstructure, and produces a combined changed of shear stresses, bending moments, and axial stresses. In a strict sense, therefore, it is necessary to take into account the effect of interaction between factors such as axial stress and bending moment, axial stress and shear stress, and so on.

As for the third question, there are three types of resistance elements in foundations, including basements if any exist, i.e., (1) subgrade reaction on front and back, (2) friction on sides and (3) friction on base. It is reasonable to take account of elements (1) and (2), excluding (3), generally, due to lack of contact surface because of ground settlement.

PILE DAMAGE IN THE 1978 OFF-MIYAGI PREFECTURE EARTHQUAKE

Since the June 12, 1978 earthquake (Off-Miyagi Prefecture), several examples of damaged pile foundations have been discovered in Sendai City. Table 1 shows the latest confirmed pile collapses. The possibility of this type of failure was not apparent to some researchers just after the earthquake. Gradually, suspicion increased as the effects of differential settlement of the superstructures appeared, and it was finally confirmed by excavation surveys of researchers such as the Sendai City authorities, Assistant Professor Kishida, Tokyo Institute of Technology, and others including one of the authors. More research work on the actual conditions by excavation is planned from now on, because many other examples are believed to lie concealed in this area.

This aspect of pile damage may be regarded, in a sense, as a historical event in Japan. For this is probably the first time buildings supported by piles which extend through horizontal soil deposits sustained damage from the vibrational effects of earthquake ground motion. The cases in Table 1, excluding case 5, all correspond to this situation. The typical failure mode is regarded as bending, or bending-shear failure, under axial load in the proximity of pile caps with and without final crushing. One case is followed by complete collapse of superstructure, but others are followed by slight or no damage to superstructures. These facts suggest the existence of a general tendency that the stronger the damage to the piles, the slighter the damage to the superstructure. The examples of damaged piles are shown in Figure 2 thru Figure 5.

The following factors should be considered at least a minimum list of the causes of damage to the pile foundations.

(1) All the piles shown in Table 1 are concrete piles or prestressed concrete piles, so that, it seems likely that decrements of strength to the pile members would be produced in the process of execution of work completion, such as pile driving, or cutting off the pile caps. As a matter of fact, many examples of small cracks, which suggest the after effects of such work, were observed in other pile groups of a similar building which was saved from final crushing. From this fact, particular notice in the designing process should be taken of the difference between the piles as manufactured goods and the piles after execution of work, especially prestressed concrete piles.

(2) The bearing capacity of a pile is designed considerably greater than the usual design capacity as shown in Table 1. The safety factor of the piles might be smaller, as the result of this fact. Also, a lack of consideration is recognized for pile member characteristics when combined stresses due to vertical and horizontal forces are applied, because the design calculation for horizontal force is not performed in other cases, excluding case 3 and case 4.

(3) There is an indication that those buildings in Table 1 would be vibrated by a larger earthquake ground motion than the design earthquake load of the standing code. According to existing strong motion accelerograph records in Sendai City, the maximum accelerations at the ground surface are within a range of 250 to 300 gals, varying of course within each region. These values easily lead to the supposition that earthquake loads larger than the design seismic coefficient $K = 0.2$ of the current code would act on those buildings.

It is difficult and possibly meaningless to try to judge which factor is the principal cause of pile collapse. Or rather, the hypothesis will examine the actual condition sufficiently so that the safety factor designed at the first step would be exhausted, because of overlapping of these disadvantageous factors to each other, and then, collapse of piles would be produced finally.

ANALYTICAL EXAMPLE OF DAMAGED PILE FOUNDATION

An earthquake response analysis by the method shown in previous papers [5,6,7] was performed for the building of case 3 in Table 1. The analytical models of the building, the piles, and the ground are shown in Figure 6a to Figure 6c. One frame section in the span direction (N-S) of the building, including the heavily damaged piles, was selected as an analytical example and simulated by the model of 25 degrees of freedom, i.e., 11 masses in superstructure corresponding to each floor with single degree of freedom in horizontal direction, 1 mass corresponding to foundation which has two degrees of freedom in horizontal and rotational directions, and 12 masses in total in piles with single degree of freedom in horizontal direction. It is necessary to divide the piles into two groups because the extent of damage is clearly different between the heavily damaged south side and the slightly damaged north side causing a building inclination of about 1/100. Six masses, therefore, are used per each group as shown in Figure 6b.

The input earthquake ground motion at the level of the pile tips was determined as follows: the N-S component of the acceleration records observed in the basement of a building located near the center of Sendai City was computed once to the tertiary bedrock by the shear wave multiple reflection theory. By using that figure as the bedrock motion of the site under consideration (GL-49.65 m in Figure 6c), the response at each level of the soil deposits was computed by the lumped mass system. The maximum acceleration at the ground surface and at the pile tip level using this approach to analysis are obtained as approximately 430 and 370 gals, respectively. Then, the acceleration response at the pile tip level is used again as the input earthquake ground motion for the analytical models of the ground and the pile-structure system. Two cases, with and without rocking of foundation, are analyzed.

All analytical model parameters are assumed to be linear elastic, in order to check the point where stress failure is first produced. In a strict sense, a more detailed investigation of the analytical models including the input earthquake ground motion will be required in order to follow closely the failure phenomenon of the piles. Therefore, discussions of responses such as acceleration and displacement at each mass are not included here. Figures 7 and 8 show the time histories of the shearing forces and the bending moments of the pile members at each level of the cases with and without rocking. The number I corresponds to each number of the pile member shown in Figure 6b, so the group from I = 1 to I = 7 shows the south-side piles, and the group from I = 8 to I = 14 shows the north-side piles. The arrow marks in these figures show the times when responses first agree with the values of the failure shear stress and the failure bending moment of a pile multiplied by the number of piles, i.e., four in the south-side pile group and five in the north-side pile group.

It is recognized from these figures that the earliest point at which the responses agree with the failure stresses is at the uppermost pile member of the south side (I = 7), and earlier in the case of the bending moment than in the case of the shear stress. As for the cases with and without rocking, the case with rocking is earlier than the case without rocking. From this fact, it may be possible to suppose that the progressive failure would be produced at the earliest failure point by the concentration of energy, and finally, the crushing of the pile would appear around that place, while other points, where the responses reach the failure stresses later, would be damaged only slightly and

escape the final crushing. It should be noted, however, that: (1) the failure stresses used here are estimated from the test results for the similar pile member not under the axial load, so that the real failure stresses may be changing; and (2) in order to check the real time of the failure and the behavior of the pile members after that time, the analytical models should be more highly detailed and accurate.

EARTHQUAKE SPECTRAL RATIO BETWEEN PILE CAP AND PILE TIP

Figure 9 shows an example of the spectral ratio between the pile cap and the pile tip of a building located in Tokyo, based on the seismic records from the past ten earthquakes. Figure 9b shows the spectral ratio between the ground surface and the pile tip, based on computed response at the ground surface using the seismic records at the pile tip as input earthquake motions. Details concerning the earthquakes, the building, and the ground condition were introduced in the previous paper [7]. The figures have been drawn by changing the abscissa from frequency to period in the original figures in order to clarify the differences of pile behavior between the natural periods of two ground and of the building. Although these earthquakes belong to the category of destructive earth-quakes, these figures explain the behavior of piles in the period domain very well. The two spectral ratio peaks agree completely with the natural ground periods, i.e, the first and the second shear vibration modes. Contrary to this, one of the valleys in the spec-tral ratio corresponds to the first natural period of the building. This fact suggests strongly the possibility that the effect of the ground motion on pile behavior is much larger than that of the superstructure.

VIBRATIONAL TESTS OF THE MODEL GROUND-PILE-STRUCTURE SYSTEM

Various tests using static horizontal force, free vibration, and the shaking table were performed on structures (1 span - 1 story) with and without piles by the Committee on the Horizontal Reaction of Piles. The Committee is headed by Professor Koizumi of Tokyo Metropolitan University and includes one of the authors [8]. The main purpose of the testing is to check the participation factors of the footing and of the piles under dynamic conditions.

All model parameters, excluding the damping ratio, are adjusted by the similitude law to the equivalent coefficients of the first vibration mode of a typical residential

building in Tokyo as shown in Table 2. The scale of length is selected as 1/30. Model size and materials are as follows:

(1) ground (3.7 m x 1.8 m x 0.8 m, chemical materials with bentonite)

(2) pile (2 plates of 5 cm x 0.57 cm x 71.7 cm, steel)

(3) footing (box of 27.8 cm x 17.3 cm x 8.3 cm of 7.5 kg weight, steel)

(4) structure (2 columns of 5 cm x 0.2 cm x 17 cm of 12.4 kg weight, steel)

The layout of the test observation system is outlined in Figure 10a and 10b. Figure 11a and 11b show a panoramic view of the model and its detail on the shaking table. These show the model with 8.3 cm of earth from the surface, which corresponds to the height of the footing. It is covered by a vinylon protection membrane.

Figure 12 shows an example of test results for the case of embedded footings. Figure 13 shows the distribution of the bending moment of the pile and the vibration modes of the pile and the ground, and Figure 14 shows the earth pressure measurements at the footing. The two clear peaks observed at the top of structure (B-11) in Figure 12, correspond to the natural frequencies of ground around 4 Hz and of the structure around 8 Hz, respectively. Noted, however, that the natural ground frequency would be changed to the small frequency around 4 Hz from the first frequency near 5 Hz of the simple shear ground vibration mode from the effect of the wholly rotational vibration mode of the ground block, and so on.

Location (G-10) is at ground surface removed from the model structure and not affected by it. Response differences between footings (F-11) and ground (G-10) reveals the sway of the building so that one may divide the total base shear force into two categories as follows:

$$V_T = V_G + V_B \tag{1}$$

in which,

$$V_T = \sum_{i=0}^{nn} m_i \ddot{X}_i \tag{2}$$

$$V_G = \sum_{i=0}^{nn} m_i \ddot{X}_G \tag{3}$$

$$V_B = \sum_{i=0}^{nn} m_i(\ddot{X}_i - \ddot{X}_G) \qquad (4)$$

in which,

V_T = total base shear

V_G = base shear component corresponding to ground response

V_B = base shear component corresponding to relative response

m_i = mass of each floor of building including foundation (i = 0)

$\ddot{X}_G$ = acceleration response of free ground surface

nn = number of floors of building

Component V_B can be regarded as the inertia force on the superstructure due to the excitation $\ddot{X}_G$. Component V_G is assumed to correspond approximately to the total result of the interaction between ground and piles at each level. Results calculated using this procedure and the ratio of each component to the total base shear force are shown in Figure 15a and Figure 15b, respectively. These figures lead to the conclusion that the ratio of inertia component of superstructure V_B becomes, approximately, 0.8 and 0.2 in the range of natural frequencies of superstructure and ground, respectively, and vice versa for the ratio V_G. Figure 15c shows the ratio of the horizontal reaction at the footing denoted by E to the base shear force component V_B, and vice versa for the shear force of piles denoted by P, because the friction on the sides and bottom of the footing is neglected. The horizontal reaction at the footing is determined by the following algebraical difference equation, based on the measurement by the earth pressure gages as shown in Figure 14,

$$E = \Delta P_1 - \Delta P_2 \qquad (5)$$

in which,

ΔP_1 = earth pressure increment at front of footing with positive sign

ΔP_2 = earth pressure decrement at back of footing with negative sign

According to the vibration mode and the bending moment distribution observed on 3 accelerometers and 6 strain gages installed on the pile plane, as shown in Figure 13, shapes similar to those obtained by static and free vibration tests of horizontal force at the pile cap appear in the frequency domain around 8 Hz. However, the aspect in the

frequency domain around 4 Hz is quite different and strongly affected by ground motion which is composed of the simple shear motion and the wholly rotational motion of the model ground block. From this effect, the earth pressures measured at the front and back of the footing include sizable components in the same phase with each other in the range around 4 Hz, and a correction of removing these components is made in order to obtain Figure 15c. It is necessary, therefore, to note that the result around 4 Hz does not have the same degree of accuracy the one around 8 Hz. It is also necessary to note the possibility that the earth pressure at the footing is acting as a kind of input force rather than as a reaction in the range of about 6 to 7 Hz in Figure 15b or Figure 15c.

TENTATIVE DESIGN OF PILE FOUNDATION TO HORIZONTAL FORCE

From the above discussion, a simplified draft procedure for the design of pile foundation to horizontal force is proposed as shown in Figure 16. The principle of this procedure consists of dividing the external design force into two categories, i.e., (1) the usual concentrated horizontal force at the pile cap which is determined by the inertia force of the superstructure minus the reaction at the foundation, (2) the distributed horizontal force over the total length of the pile which is determined by distributing V_G, for instance, into a triangular shape. The inertia force of the superstructure can be determined by assuming some available distribution shape of the horizontal force on each floor, and, of course, the sway component at the foundation if necessary. As for the case of total inertia force, it is considered to already include the effects of the underground part, and dividing it into two forces using the relation shown in Figure 15b is recommended. The design participation factor of the foundation reaction should be taken at an appropriate value from the relation shown in Figure 15c, and a value of not more than 0.3 is recommended here. Regarding the distribution of V_G, the most fitting shape, triangular or other, should be used to represent the effects of the natural ground vibration modes. The effects of grouping piles also should be taken into account as required. Finally, it is necessary to take the sum of the pile stresses from both branches to design the pile section and footing. At least two cases must be checked, i.e., at the first natural frequency of the superstructure and the ground; then design for the most disadvantageous case.

CONCLUSION

A reconsideration of the current static design method which conceptualizes the horizontal force being concentrated at the pile caps is strongly suggested by the observed aspects of earthquake damage to piles, and results from the model vibration tests discussed in this paper. The more desirable method is the dynamic response analysis of the total system of ground, pile and superstructure to earthquake ground motion. However it would be very convenient in the earthquake-resistant design of buildings supported by piles to have an appropriate static design method for piles which pays due regard to the seismic behavior of the ground. A tentative draft of such a method is proposed in this paper which includes the participation factor of horizontal force of piles. More detailed research on the design method for piles will be continued, however, based on the topics mentioned in the first sections of this paper because the problem of how to deal with the distribution of external force over the pile length, the effect of earth pressure in the input force state, the effect of pile grouping, and so on, still remains.

REFERENCES

[1] Kishida, H. (1966), "Damage to Reinforced Concrete Building in Niigata City with
     Special Reference to Foundation Engineering," Soils and Foundations, Vol. 6, No. 1,
     pp. 71-88.

[2] Fukuoka, M. (1966), "Damage to Civil Engineering Structures," Soils and Foundations,
     Vol. 6, No. 2, pp. 45-52.

[3] Tamura, K., Fujiwara, T. and Morishige, R. (1973), "Damage of Rigid Frame Bridges in
     the Off-Tokachi Earthquake 1968," Japan Earthquake Engineering Symposium 1973, in
     Commemoration of of the 50th Anniversary of The Kwanto Earthquake, Tokyo, Japan,
     pp. 147-154 (in Japanese).

[4] Building Research Institute (1974), "Report of Aseismic Diagnosis on the Reinforced
     Concrete Building of Aomori Prefectural Business High School," Report No. 206 (in
     Japanese).

[5] Sugimura, Y. (1973), "Estimation of Dynamic Behavior of Soil Layer-Pile Foundation
     Interaction System During an Earthquake," Japan Earthquake Engineering Symposium 1973,
     in Commemoration of the 50th Anniversary of The Kwanto Earthquake, Tokyo, Japan,
     pp. 133-140.

[6] Sugimura, Y. (1975), "Earthquake Observation and Dynamic Analysis of Pile-Supported
     Buildings," 4th Japan Earthquake Engineering Symposium, pp. 463-470.

[7] Sugimura, Y. (1976), "Earthquake Observation and Dynamic Analysis of a Building
     Supported on Long Piles," 6th WCEE, Vol. 2, pp. 1570-1575.

[8] The Committee on the Horizontal Reaction of Piles (1979), "Report of Study on Seismic
     Passive Earth Pressure to Foundation and Beams of a Tall Residential Building," (in
     Japanese).

Table 1 Damaged Piles by 1978 Off-Miyagi Prefecture Earthquake

No.	Type of Building	Pile	L (m)	D (cm)	Design Bearing Capacity (t/pile)	Failure Type	Damage of Structure	Geographical Condition	Main Soil Type
1	Box-RC 3FL	RC	5	25	20	BB	CO	Plain	Peat, Clay
2	Box-RC 4FL	PC	5	35	70	CR	NY	Plain	Clay, Sand
3	SRC 11FL	AC	12	60	150	CR	SY	Plain	Silt, Sand
4	SRC 14FL	AC	24	60,50	160	CR	SY	Plain	Peat, Sand
5	RC 4FL	PC	10	30	30	BS	SY	Slope	Loam

Notation: RC=reinforced concrete pile PC=prestressed concrete pile AC=autoclaved
prestressed concrete pile L=average length of pile D=diameter of pile
BB=bending cracks without crush BS=bending-shear cracks without crush
CR=crush with bending-shear cracks CO=collapse NY=no damage with
differential settlement SY=slight damage with differential settlement

Table 2   Properties of Prototype Structure and Model Structure
under Rules of Similitude

	Unit	Prototype	Model
Weight of Structure	kg	446700	12.4
Period of Structure	sec	0.63	0.12
Weight of Footing	kg	2.7×10^6	7.5
Size of Footing	cm	835x520	27.8x17.3
Depth of Footing	cm	250	8.3
Diameter of Pile	cm	150	5x0.57[1]
Geometrical Moment of Inertia of Pile	cm^4	2.5×10^7	0.0769
Depth of Ground	cm	2400	80
Period of Ground	sec	1.10	0.21
Shear Wave Velocity	m/sec	91	16.75

[1] Model of pile is replaced by rectangular shape section.

283

$$Q = \sum F_i \qquad\qquad Q_p = (Q - Q_f) / n$$

$$M = \sum F_i H_i$$

(Sustained by Foundation Beam)

$F_i = m_i \ddot{x}_i$

H_i

M

Q

Q_f

Q_p

N : Considered at Final Check of Pile Stress

N

Numbers of Pile = n
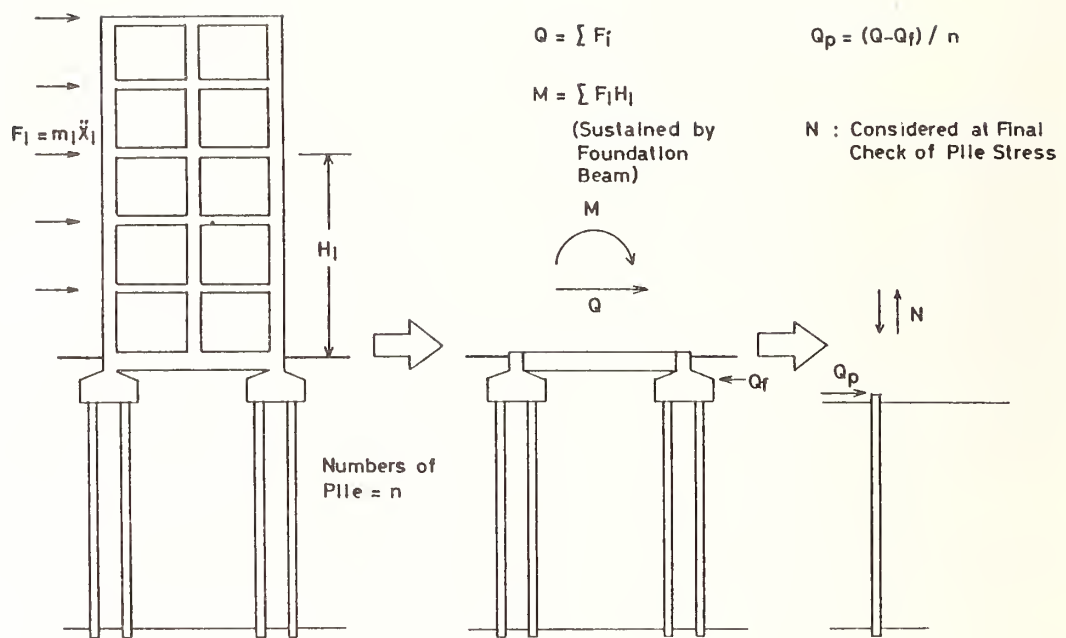
Fig. 1 Actual State of Design of Pile Foundation to Horizontal Force

Fig. 2a) Damage of Pile (Case 1)

Fig. 2b) Damage of Pile (Case 1)

Fig. 3a) Damage of Pile (Case 2)

Fig. 3b) Damage of Pile (Case 2)
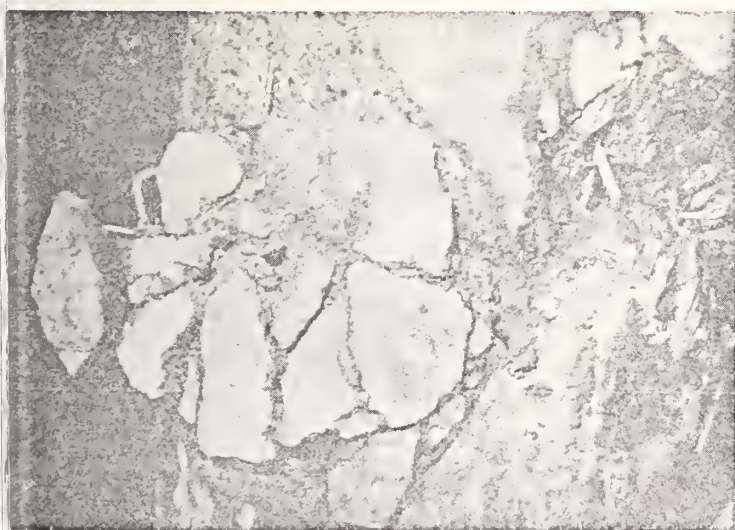
Fig. 4b) Damage of Pile (Case 3)

Fig. 4a) Damage of Pile (Case 3)

Fig. 5a) Damage of Pile (Case 5)

Fig. 5b) Damage of Pile (Case 5)
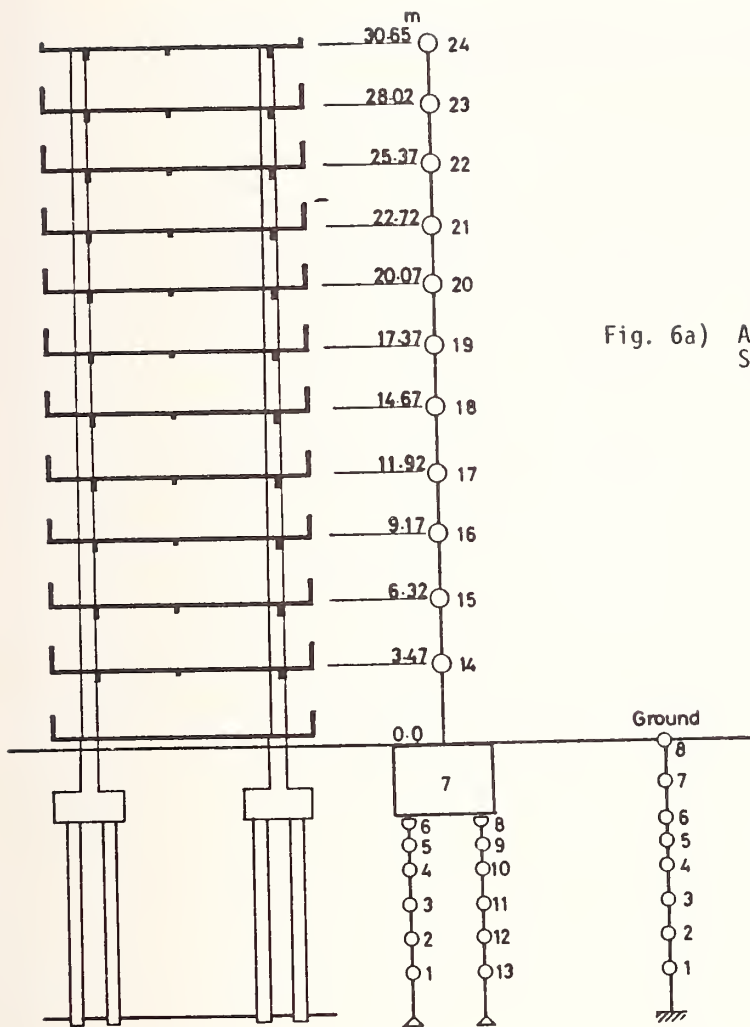
Fig. 6a) Analytical Model of Ground and Pile-Structure System (Case 3)

Fig. 6b) Details of Model of Piles and Ground (Case 3)
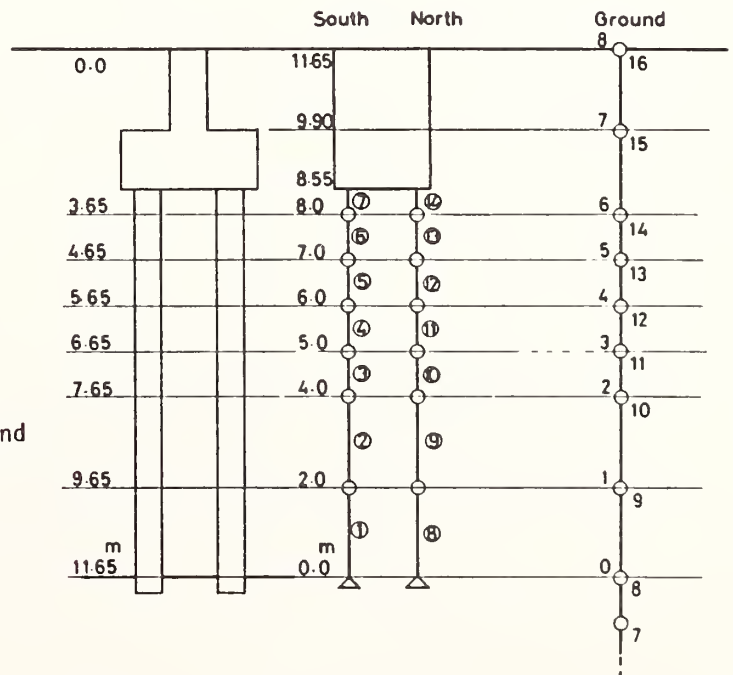
	Thickness (m)	Soil Type	Unit Weight (t/m³)	N Value	Shear Modulus (t/m²)	Shear Wave Velocity (m/sec)
	3.65	CC	1.50	4	3637.0	154.2
	1.0	SS	1.85	9	6959.5	192.0
	1.0	SG	1.97	31	15718.4	305.2
	1.0	"	"	52	28312.9	375.3
	1.0	"	"	83	41157.0	458.5
	4.0	"	"	44	24770.0	351.3
	1.0	"	"	99	47390.3	485.5
	4.0	"	"	49	26998.4	366.5
	3.0	"	"	77	38760.0	439.5
	7.0	"	"	79	39560.0	444.0
	19.0	"	"	96	46240.0	480.0
	2.0	"	"	19	12650.0	251.0
	2.0	"	"	94	45470.0	476.0
		RR	2.20	200	83177.4	608.7

Depth markers (m):
0.0 — 16
1.75 — 15
3.65 — 14
4.65 — 13
5.65 — 12
6.65 — 11
7.65 — 10
9.65 — 9
11.65 — 8
12.65 — 7
16.65 — 6
19.65 — 5
26.65 — 4
36.15 — 3
45.65 — 2
47.65 — 1
49.65

Fig. 6c) Ground Condition at the Site of Case 3

Fig. 7 Time Histories of Shear Stress and Bending Moment of Piles
(Case with Rocking)
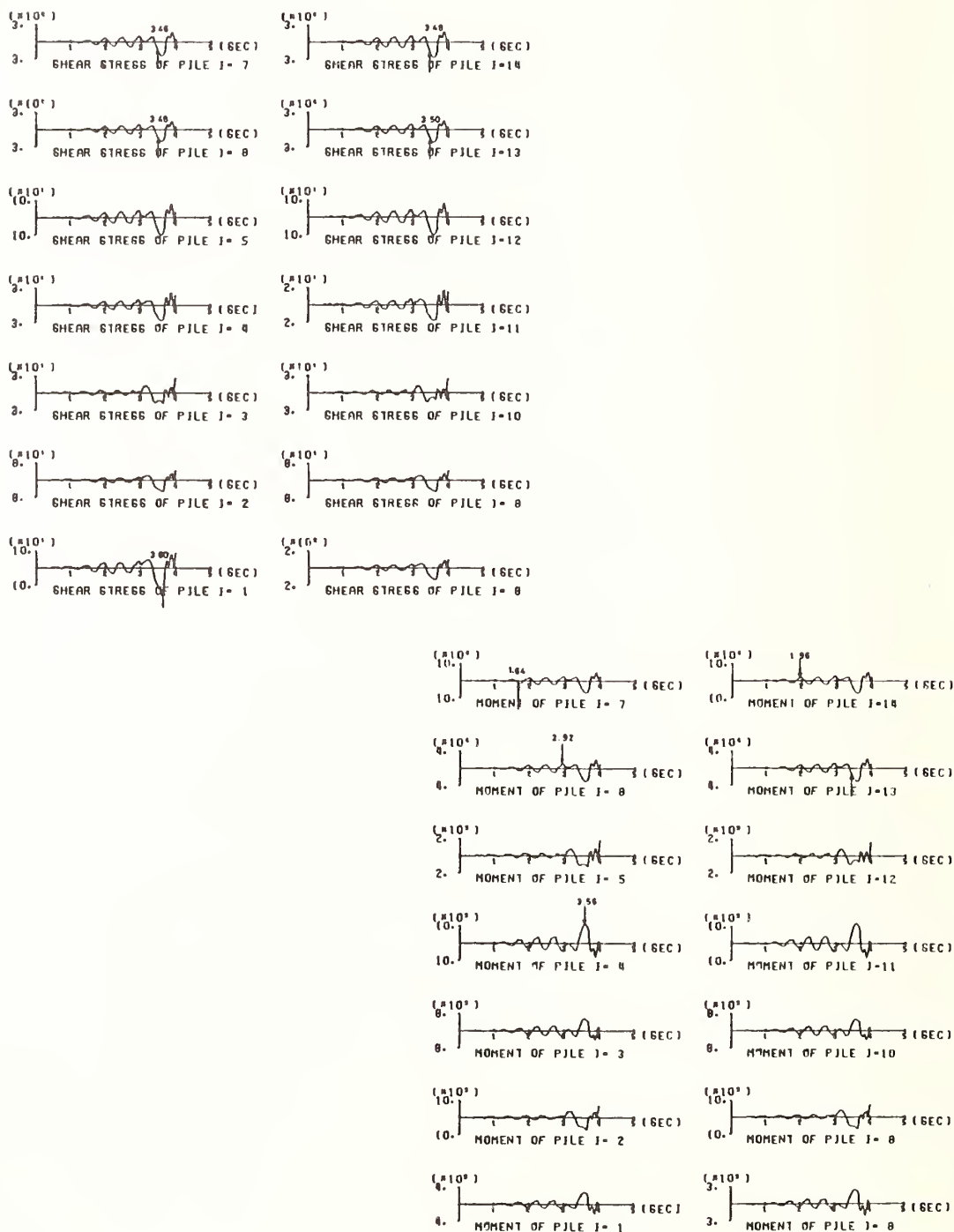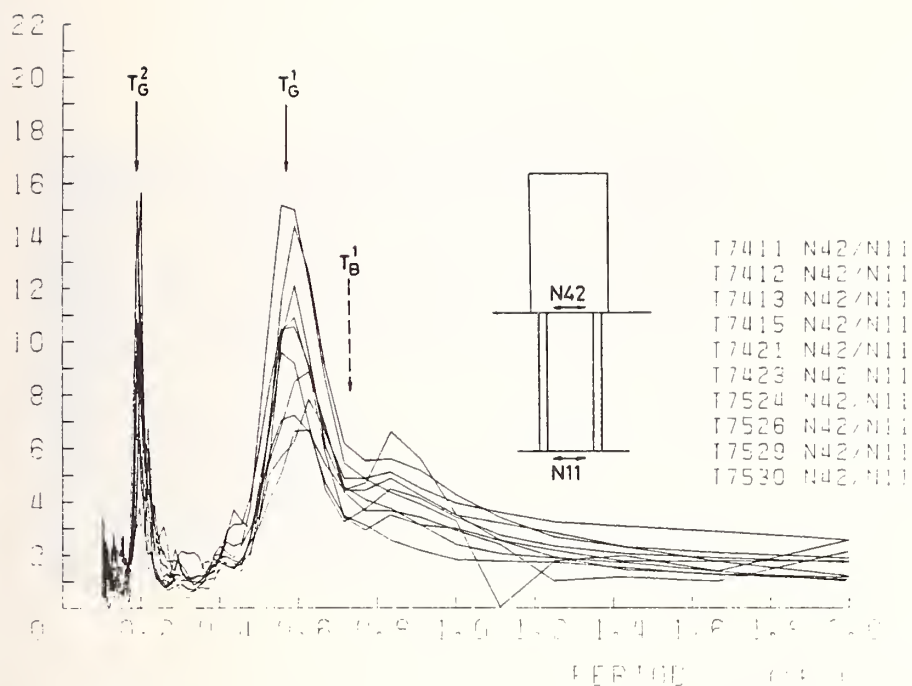
Fig. 9a) Spectral Ratio Between Pile Cap and Pile Tip
Based on Seismic Records
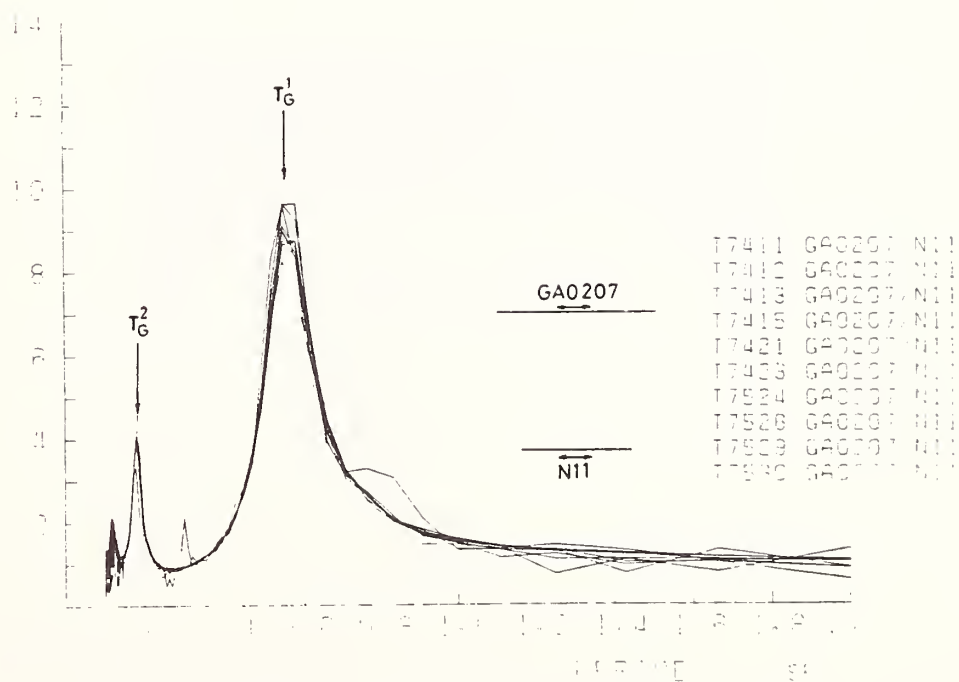
Fig. 9b) Spectral Ratio Between Ground Surface and
Pile Tip Based on Analytical Results
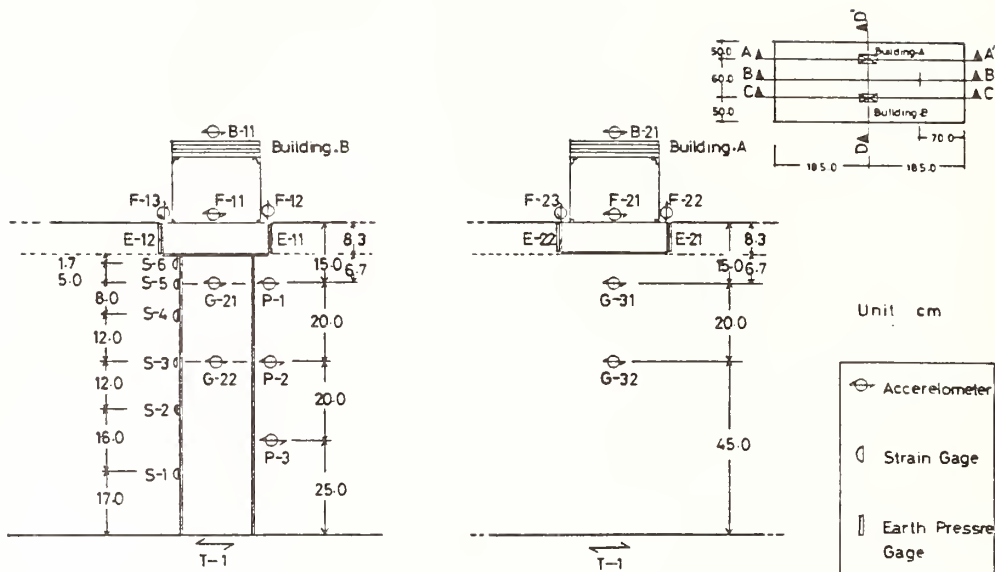
Fig. 10a) Layout of Accelerometers, Strain Gages and
Earth Pressure Gages
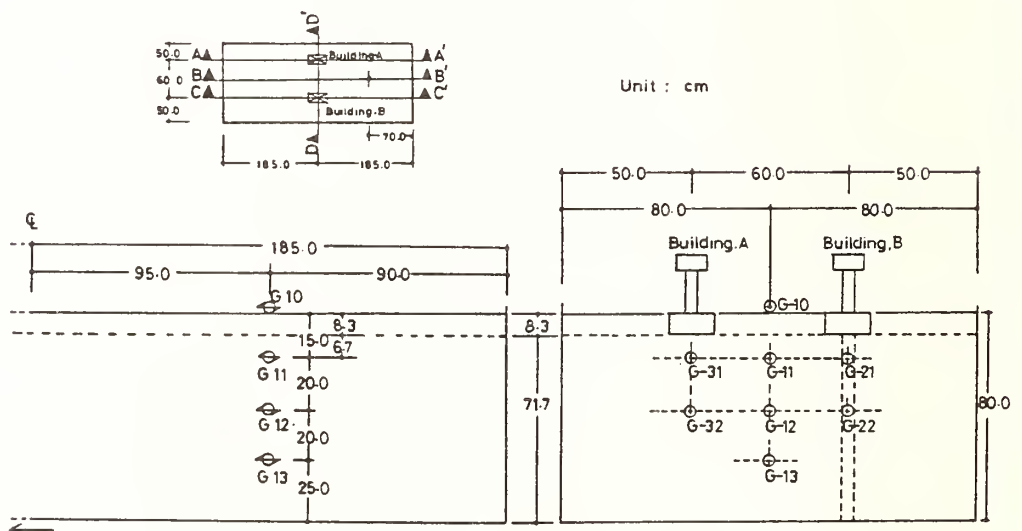
Fig. 10b) Outline of Location of Model Structure
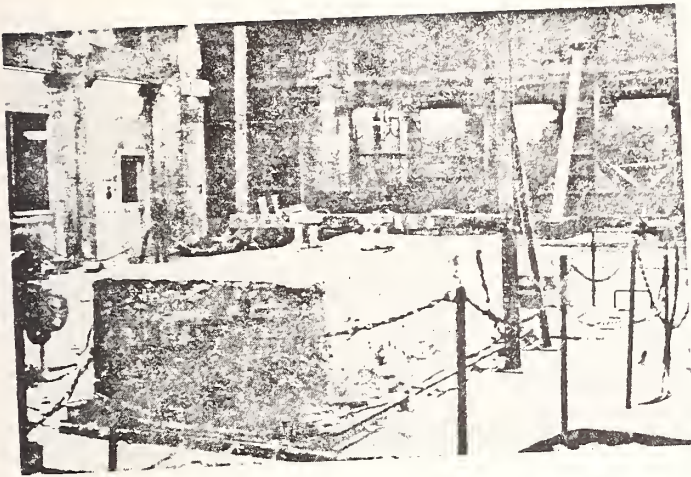
Fig. 11a) Panoramic View of Model

Fig. 11b) Models of Structures
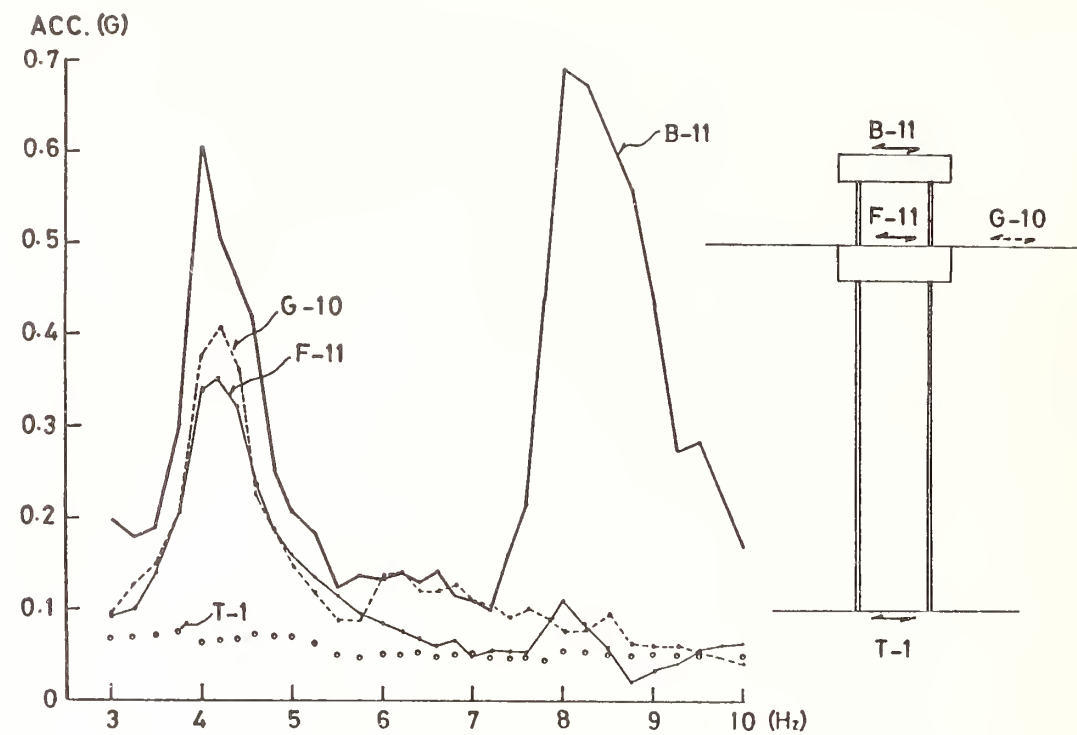
Fig. 12
Acceleration Respon
of Shaking Table Te
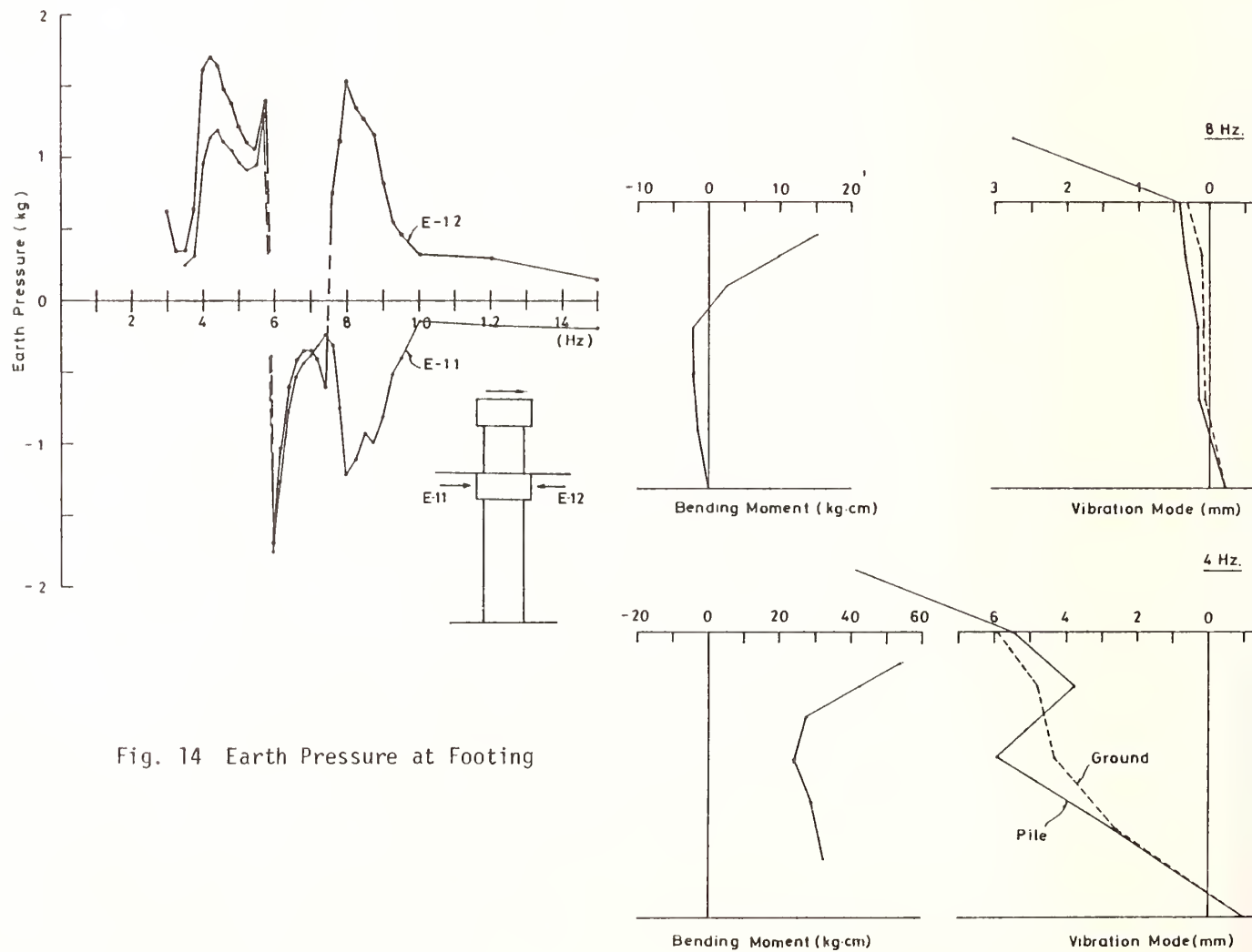
Fig. 14 Earth Pressure at Footing

Bending Moment (kg·cm)

Vibration Mode (mm)

Bending Moment (kg·cm)

Vibration Mode (mm)

Fig. 13 Bending Moment of Pile, and Vibrational
Mode of Pile and Ground

Fig. 15 Base Shear Force Component and Participation Factor
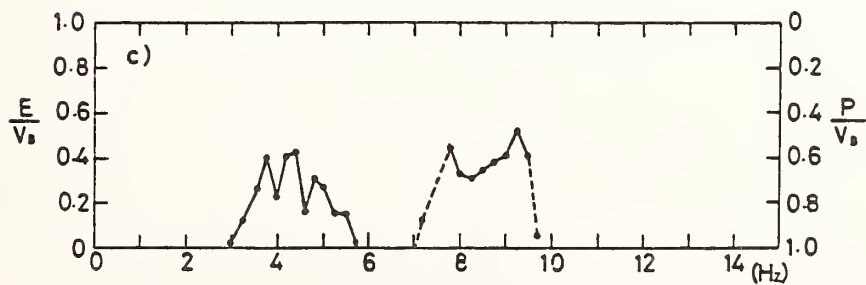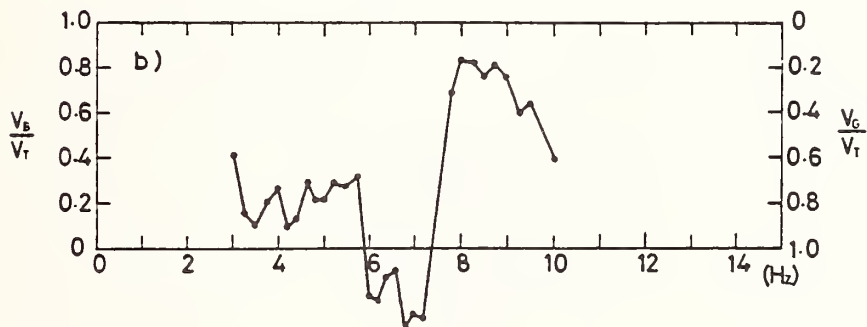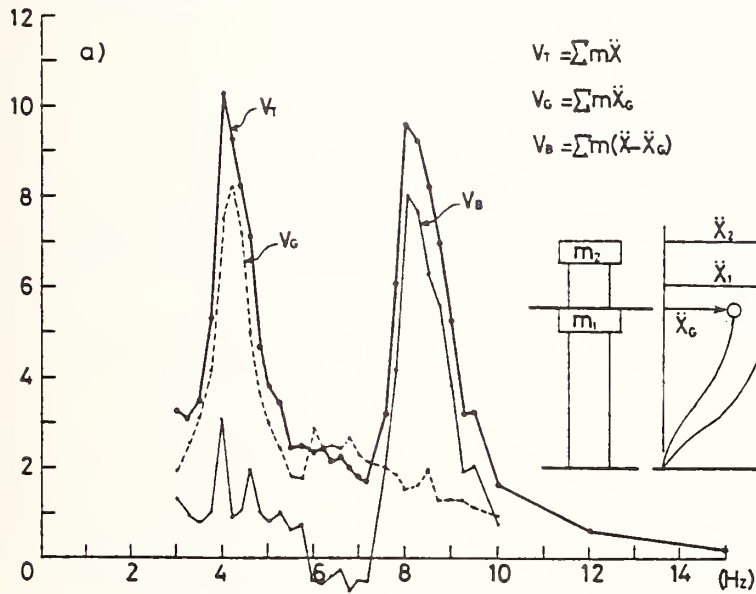
Fig. 16 Draft Design of Piles
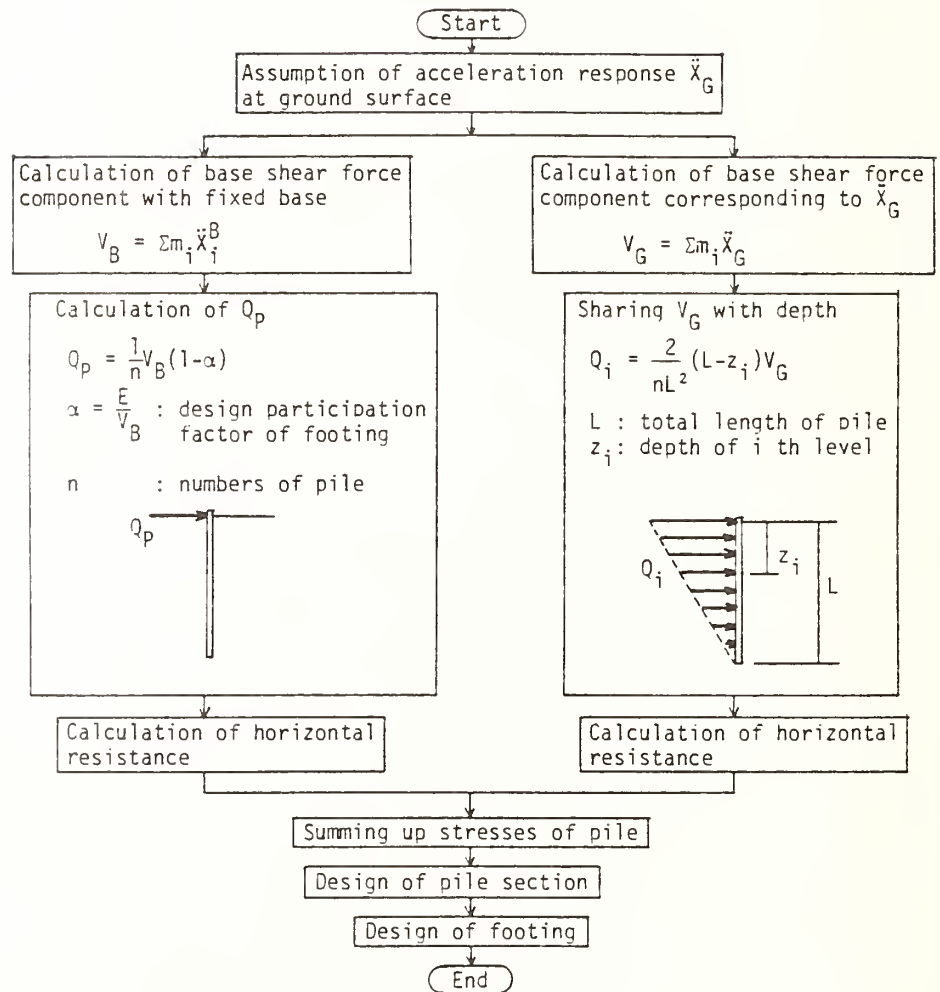
OPERATIONAL MODELS FOR FORECASTING STORM SURGES IN NOAA

by

Celso S. Barrientos

The National Weather Service of the National Oceanic and Atmospheric Administration (NOAA) is responsible for forecasting in the air and water environment. Operational models are those that are available for use at regular and scheduled basis. For example, the operational 7-level primitive equation model of the atmosphere is run twice a day everyday. There are many models in NOAA and among these are operational models. This paper is concerned only with the operational models for forecasting storm surges in NOAA. These are other storm surge models both inside and outside NOAA but they are not operational. Storm surge is the abnormal rise (or fall-negative surge) of water level due to meteorological forcings. The regular fluctuations of sea level (tides) are not included in storm surge. There are three areas in the United States where storm-generated water level fluctuations (storm surges) can cause serious problems. There are: (1) in the Great Lakes, particularly Lake Erie; (2) in the East coast of the U.S.--winter storms in the northeast portion, and tropical cyclones or hurricanes throughout the coast; and (3) in the Gulf of Mexico coast due to tropical cyclones or hurricanes.

Storm surge can cause considerable damage so that timely and accurate forecasting is essential. In Lake Erie, flooding and shoreline erosion occur when positive surges are superimposed on high lake levels. During times of low lake levels, negative surges can be hazardous to navigation and disturb hydroelectric power generation. Similarly, low water level is also a problem in Baltimore Harbor, Maryland, because it causes the ships to scrape the bottom. Storm surges in the Gulf and East coasts of the U.S. cause considerable damage every year. Storm surge episodes along the coasts always leave phenomenal amounts of property damage and a frequent loss of lives. In recent years, timely warnings have helped decrease the losses and have saved lives.

Storm surge is generated mainly by two atmospheric forces--wind and pressure. Wind acts on the water with a drag force (stress) and low pressure causes the water to bulge (increase elevation). The low pressure force is also termed the inverted barometer effect. These two forces act in a dynamically coupled way and must be considered together. Storm surge forecasting therefore, must begin with forecasting atmospheric forces. Different for-

297

mulations of atmospheric forcings are used with the different storm surge models. Success or failure of a storm surge model depends very strongly on formulation of the meteorological forces.

In the Great Lakes, we will focus our discussion on Lake Erie. There are other locations in the Great Lakes where storm surges do occur; however, the frequency and magnitude are comparatively small. On the average, major surge (3 ft or higher) occurs in Lake Erie about five times a year.

Lake Erie storm surges are generally associated with the passage of extratropical storms through the Great Lakes area. Winter storms that approach the Great Lakes from the central part of the United States can cause strong winds over Lake Erie. When these strong winds blow along the main axis of the lake, storm surges are generated. Strong southwest winds blowing over the lake cause a tilted lake surface, i.e., the water level is elevated in the eastern portion of the lake (Buffalo, N.Y. end) and lowered at the western portion (Toledo, Ohio end). Occasionally a storm will pass south of Lake Erie causing northeast winds over the lake. When this happens, the slope of the water surface is reversed with elevated water levels at the Toledo end of the lake.

Storm surges on Lake Erie are caused primarily by wind stress on the lake surface. The effect of atmospheric pressure, which causes higher water levels in areas of low pressure (bulging effect) is less important. The reason is the lake is relatively small compared to the size of the storm. Storm surges in Lake Erie are pronounced because of the shallow depth and the geographic orientation.

The National Weather Service of NOAA is responsible for predicting storm surges in Lake Erie and warning all those who may be affected to take necessary action. The first operational model was implemented in 1969 and it is based on equations derived by statistical techniques. Regression equations were derived from historical sea level pressure data around the Great Lakes. The predictand used is the actual measured lake levels or storm surges. The statistical model has worked with a high degree of success for ten years.

Objective methods to forecast winds over the Great Lakes became available in 1972. With the wind forecasts, a dynamic model to forecast storm surges in Lake Erie was developed. It uses impulse response functions to calculate the storm surge height. The surge height at a given time is calculated as the weighted sum of forcing terms during some period before the specified time.

Using two years of data (1977 and 1978), the statistical and dynamical storm surge models for Lake Erie were compared and verified. Results of the study showed that the dynamical model is better than the statistical model. Therefore, the operational statistical model was replaced by the dynamic model in 1979.

In the East and Gulf coasts of the United States, storm surge generation is further enlarged by additional factors. These are water transport by waves and swell, the Earth's rotation, rainfall, and coastline configuration and bathymetric conditions. Theory and laboratory experiments indicate that waves breaking near the shore contribute to the storm surge. Wave setup is also affected by wave refraction—that is, wave setup is higher in areas of wave convergence and smaller in areas of wave divergence. The Coriolis effect (earth's rotation) will increase the surge height on the coast when current is parallel to the coast and the coast is to the right of the direction of the current; the reversed effect is true for current moving in the opposite direction. Hurricanes and extra-tropical storms may produce a great deal of rain over extensive areas, resulting in floods that can increase the surge height near the mouths of rivers and tidal estuaries. The bottom topography near the shore has an extremely important effect on the height of the storm surge. Gently sloping topography on the continental shelf, as in the Mississippi river delta, supports the generation of higher storm surges than does a steep continental shelf. The configuration of the shore also affects the storm surge. For example, storm surge height increases in a bay with converging shorelines but decreases in a wide bay with only a narrow connection to the sea.

The path of extratropical cyclones is along the eastern coastline of the United States. This path is favorable to surge generation in coastal states from Georgia to Maine. The National Weather Service Forecast Offices are responsible for issuing storm surge warnings. Operational computerized statistical forecasts are used as guidance at these forecast offices. This automated forecast technique, which became operational in 1971, is a statistical model based on actual November through April storm surge data, from 1956 through 1969, using storms that produced surges of 2 ft (0.6 m) or more. Separate forecast equations were determined by the statistical screening procedure for each of the forecast locations so that local effects were considered.

In actual operational use, sea level pressure forecasts at the appropriate grid points are inserted in the storm surge equations. Pressure forecasts are made twice daily from

numerical weather models in the Weather Service's National Meteorological Center. This model will continuously be improved by including recent extra-tropical storm surge data beyond the original 14-year development information. More forecast locations will be added to the system, which is strongly dependent on the atmospheric models forecasts. However, during the nine years of use it has performed satisfactorily.

Hurricane storm surge produced considerable damage in the U.S. coastal areas. NOAA has two operational models to forecast hurricane storm surges--a model for the outer coast only and a model for bay and estuary for overland flooding. These models are dynamic. The storm surge dynamic equations are solved numerically. The storm models include an atmospheric model. Simple variables to define storms are forecast and used as input to the models. These variables include the central pressure of the storm, the size of the storm, the direction, and speed of motion. The outer coast model uses a curvilinear coordinate system following the coastline and a variable grid toward the sea, which is a function of depth. The bay model employs a polar coordinate system, with a smaller grid for bays which expands towards the ocean. The bay model is dynamically coupled with the ocean model, thus no input boundary is required. It is operational in five areas and will be implemented in 20 important bay and estuary systems in the Gulf and East coasts. The hurricane storm surge model mechanisms are run only when a storm is threatening the U.S. coast. These models threatening the U.S. coast. These models provide valuable information to forecasters in the preparation of the storm warnings, and are also used in evacuation planning.

STORM SURGE PREVENTION AROUND RIVER MOUTHS IN JAPAN

by

H. Hashimoto

ABSTRACT

To prevent storm surge damage, defense work has been carried out since the Isewan Typhoon caused heavy damage in 1959. Around river mouths, dikes have been constructed for the protection of densely populated areas. The dimension of dikes were determined with considerations of storm surges and high waves. Prediction models for surges and hydraulic models for waves provided necessary information. However, the effect of dikes was weakened by land subsidence caused by ground water pumping. The stability of structures against earthquakes is another problem. Efforts continue to develop new methods for the improvement of structures.

INTRODUCTION

Japan is located on the western side of the Pacific Ocean where typhoons strike about seven times a year between July and September. In a bay, plains are low flat deltas formed by the deposit of sand and silts transported by rivers. Population and structures are concentrated in plains such as Tokyo in the Kanto plain.

Once storm surges causes flooding in a delta area, damage to life and property can become enormous. As one countermeasure, dikes have been constructed along the coasts and river mouths. This report describes the design method for those structures and newly arising problems.

BACKGROUND

When a typhoon hits a bay with a mouth opening to the south, storm surges occur. Figure 1 shows frequently hit bays, and tracks of typhoons which caused large surges. In the delta area of these bays, land subsides from ground water pumping. Figure 1 also shows areas where the ground is lower than the mean sea level. These areas are protected by coastal and river dikes from flooding. Once storm surge breaks a dike, drainage of the accumulated sea water is very difficult.

In 1959, Isewan Typhoon hit Ise Bay and caused heavy damage in Nagoya. Five thousand lives were lost and property loss was estimated at five hundred billion yen. At that time, prevention measures against storm surges were reconsidered and a new technique was developed. For storm surge defense works, dikes were constructed along the coast and river mouth in Tokyo Bay, Ise Bay and Osaka Bay.

DESIGN METHOD

Dikes or breakwaters prevent flooding from surges and high waves. Because a flood from the upper river must flow easily, it is not desirable to construct structures which totally obstruct the stream. Therefore, dikes are used with gates and pumps which drain the low land.

In harbor areas, because high dikes hinder the use of quays, the flooding is prevented by breakwaters. At Nagoya harbor, 8.2 km long breakwaters were constructed to protect the

harbor area from storm surges and high waves. The breakwater has two openings, 350 m and 50 m which decrease the surge from 3.5 m to 3.0 m.

The dike was designed using the following procedure [1]:

(1) establish a design typhoon

(2) estimate the height of storm surges and wind waves at the mouth of the river

(3) analyze the deformation of the surges and waves in the river

(4) estimate the wave run-up height on the dike

(5) decide on the type and the dimensions of the dike

Storm surge and wave height are estimated from numerical computation. Deformation and run-up of waves are analysed using hydraulic models. The dike is designed to be higher than the wave run-up height. In this case, the water level is determined by the surge height and the mean high water of spring tides. The dike is covered using concrete or asphalt for stability from attack by waves and tides.

The storm surge defense work began in 1957. In 1959 the Isewan Typhoon caused heavy damage. Then the design typhoon was determined to have the magnitude of the Isewan Typhoon. The lowest pressure at the center of the typhoon and the maximum wind speed show that the Isewan Typhoon is one of the largest typhoons that we have experienced.

The analysis of construction cost and benefits based on statistical data can be used to determine the dimension of the dikes. However, this method was not applied because of a lack of adequate data. At Nagoya, the anomaly of storm surges was analysed from a total of 20 years data [2]. The return period of the anomaly caused by the Isewan Typhoon ranges from 40 years to 70 years.

<div align="center">STORM SURGE COMPUTATION</div>

In estimating surge height, the design typhoon moves on a track which produces the highest surge at the place where it is to be examined. The track is selected to be similar to the ones of the past. When the surges were estimated at the mouth of the Ibi River, Nagara River and Kiso river at the bottom of Ise Bay, five tracks were selected [3]. Figure 2 shows three of the five main tracks. Track A is a simplification of the Isewan Typhoon, and B is moved 20 km to the west and parallel to A.

Storm surges are computed by two-dimensional long-water wave equations which consist of momentum and mass conservation equations [4]. The pressure distribution in a typhoon is

derived from observed data. The wind on the sea surface is assumed to be the vector sum of the velocity derived from the atmospheric pressure gradient, and the velocity proportional to the typhoon speed. The design typhoon produces the wind distribution as shown in Figure 3. The tangential force on the sea surface caused by the wind drives the water and generates the surges. The computation is carried out on a grid of several kilometers with about one-minute intervals. In the case of Ise Bay, a wide grid of 3.2 km and a narrow grid of 0.8 km were used. The deformation of surges in a river are also computed by one-dimensional long-water wave equations.

As an example, the time history of sea levels at Nagoya, Kuwana, and the mouth of the Ibi River is shown in Figure 4. (The location is also shown in Figure 5.) A comparison between observed and predicted levels are also made, as is the highest level at each station produced by the different tracks shown in Figure 3. At the mouth of the Ibi River, the sea level reaches 4.8 m above mean sea level.

<center>WAVE RUN-UP ESTIMATION</center>

Because storm surges accompany high waves, we need to estimate the wave run-up on dikes. The wind waves generated by the typhoon are computed by Wilson's moving fetch method [5] based on the SMB method. In shallow water, energy dissipation from bottom friction is also considered by Bretchneider's equation [6].

At the mouth of the Ibi River, five fetch lines were selected. Waves from each direction were calculated at 5 km intervals [7]. Figure 6 shows the time history of significant wave heights and periods from each direction in front of the river delta. The maximum wave is 5.5 m high and of a 7.9 sec period. At the river mouth, it decreases from bottom friction to 3.0 m and 7.5 sec.

Waves which reach the river mouth deform by refraction, reflection, dissipation, and run-up on the dike. The deformation is investigated using hydraulic scale models to which the Froude similarity law is applied.

The model scale is usually from 1/30 to 1/60. The bottom friction coefficient in the prototype is estimated to be f = 0.01, but in the model, the coefficient is about 0.04. From the scale law, they should be the same. Therefore, some corrections are required to the experimental data. A distorted model is also applied; and, though the correction is small, sometimes wave generation by wind on the river is considered.

<center>304</center>

At the mouth of the river, waves deform according to bottom profiles. Because dredging and reclamation is active in the delta, we need to assess the influence of the modifications on the bottom profiles. A gradual change of the bottom profile from a deep center of the river to a shallow bank is preferable because the wave refracts to the banks and does not enter the upper reaches.

In the model experiment, wave height in a river and run-up height on a dike are measured to estimate the required dike height. As an example, Figure 6 shows the change of run-up height in the Ibi River [8]. The experiment was carried out in a horizontal scale of 1/65 and a vertical scale of 1/32.5 to analyze several methods to dissipate wave energy. In the figure, a comparison is made between the present dike and the dike with a berm. Waves break on the berm and both wave run-up and transmitted waves to the upper river decrease. For the prevention of storm surge disasters, the dikes have been designed as outlined above and constructed in three major bays.

ADDITIONAL PROBLEMS

As measures for the prevention from flooding coastal and river dikes were taken, however, a few new problems arose. They are:

- land subsidance caused by ground water pumping
- instability of structures on weak soil against earthquakes.

In Nagoya, the land subsides 3 to 10 cm a year and the area under the mean sea level gradually increased from 180 km^2 in 1959 to 250 km^2 in 1977 as shown in Figure 5. The dike also sinks from land subsidance and from a consolidation of the subsoil. The latter becomes inactive as time advances.

The pumped water is used for industry and agriculture. At the Ibi River, tide influences areas over 30 km from the mouth and salt wedges interfere with the use of river water. Deep wells supply water to rice field in the delta area. There are five layers at the mouth of the Ibi River and they are: upper gravel, upper clay, lower gravel, lower clay, and the tertiary from the surface to the bottom. The pressure depression in the lower gravel caused by the pumping causes a consolidation of the upper clay by the excess pore pressure.

At the Ibi River the dike was reconstructed because of the land subsidance. The river bed also sinks and waves become higher than before. Several measures were investigated

305

experimentally to reduce waves [9]. Figure 8 shows the effect of berm width on wave run-up. As the berm becomes wider, the run-up decreases because of the wave breaking on the berm. However, a berm wider than 15 m is not effective. Figure 9 shows the actual design of dikes on the Ibi River.

The stability of vertical walls which were constructed in densely populated areas is the other problem. Once the wall is broken by an earthquake, inundation on low land causes heavy damage. Efforts are continuing to make the structure stable. In Tokyo there is a plan to raise the land higher than mean sea level, and to make a wide dike as shown in Figure 10. Dikes covered with green grass or natural stones are preferred to high concrete walls.

SUMMARY

After heavy damage caused by Isewan Typhoon, dikes have been constructed around river mouths in delta areas. The dimensions of the dikes are designed to withstand storm surges and waves generated by a design typhoon which has the same magnitude of Isewan Typhoon. To estimate the height of surges and wave run-up, computational and hydraulic models have been used. In Tokyo Bay, Ise Bay, and Osaka Bay the defense works were completed. However, the effect of the dikes was weakened by land subsidance caused by ground water pumping. The stability of structures against earthquake is another problem. Efforts are continuing to develop new methods to improve these structures.

REFERENCES

[1] Design Manual for Coastal Protection, Association of Coastal Engineers in Japan, 1972.

[2] Report on the Analysis of Storm Surges in the Three Rivers of Kiso, Kisokaryu
     Construction Office, Ministry of Construction, 1971.

[3] Ibid, [2].

[4] Miyazaki, M., S. Unoki and T. Ueno, "Computation of Storm Surges Caused by the Isewan
     Typhoon," 7th Coastal Eng. Conf. in Japan 1960.

[5] Wilson, B. W., "Graphic Approach to the Forecasting of Waves in Moving Petches," BEB.
     Tech. Memo., No. 73, 1955.

[6] Bretchneider, C. L. and R. O. Reid, "Modification of Wave Height Due to Bottom
     Friction, Percolation, and Refraction," BEB. Tech. Memo., No. 45, 1954.

[7] Ibid [2].

[8] Model Experiments of the Storm Surge Prevention Structures in the Three Rivers of Kiso,
     Tech. Memo., PWRI, 1973.

[9] Hydraulic Model Experiments of Dikes in the Three Rivers of Kiso, Kisokaryu
     Construction Office, Ministry of Construction, 1979.
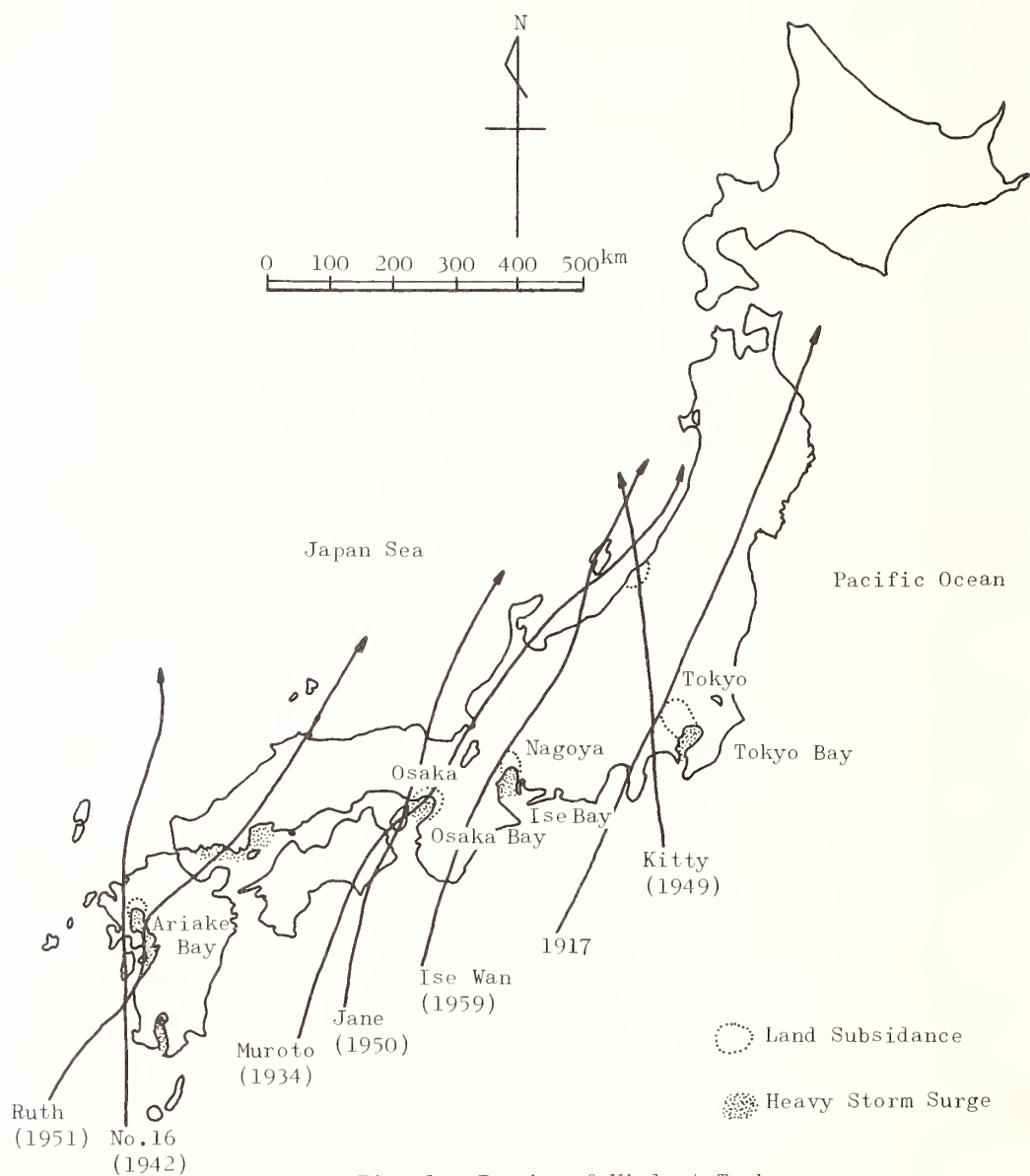
Fig. 1   Tracks of Violent Typhoons
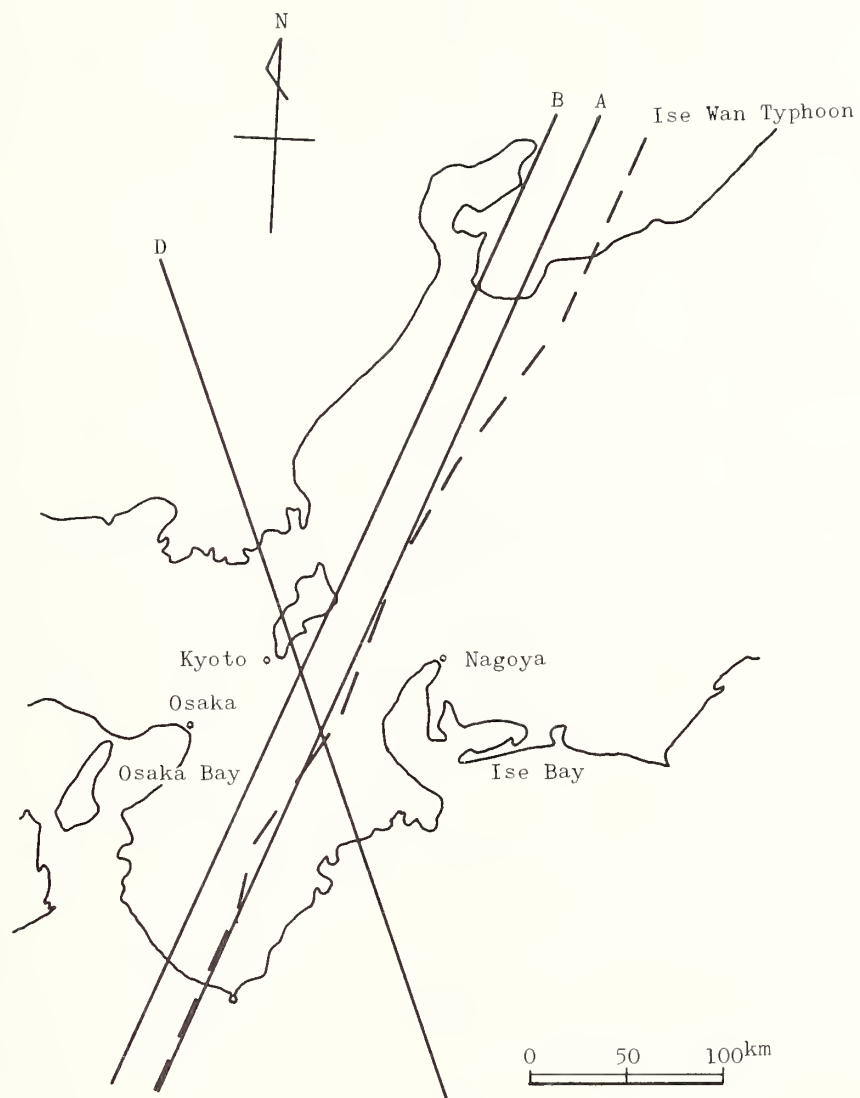
Fig. 2   Tracks of Typhoons in Storm Surge Computation
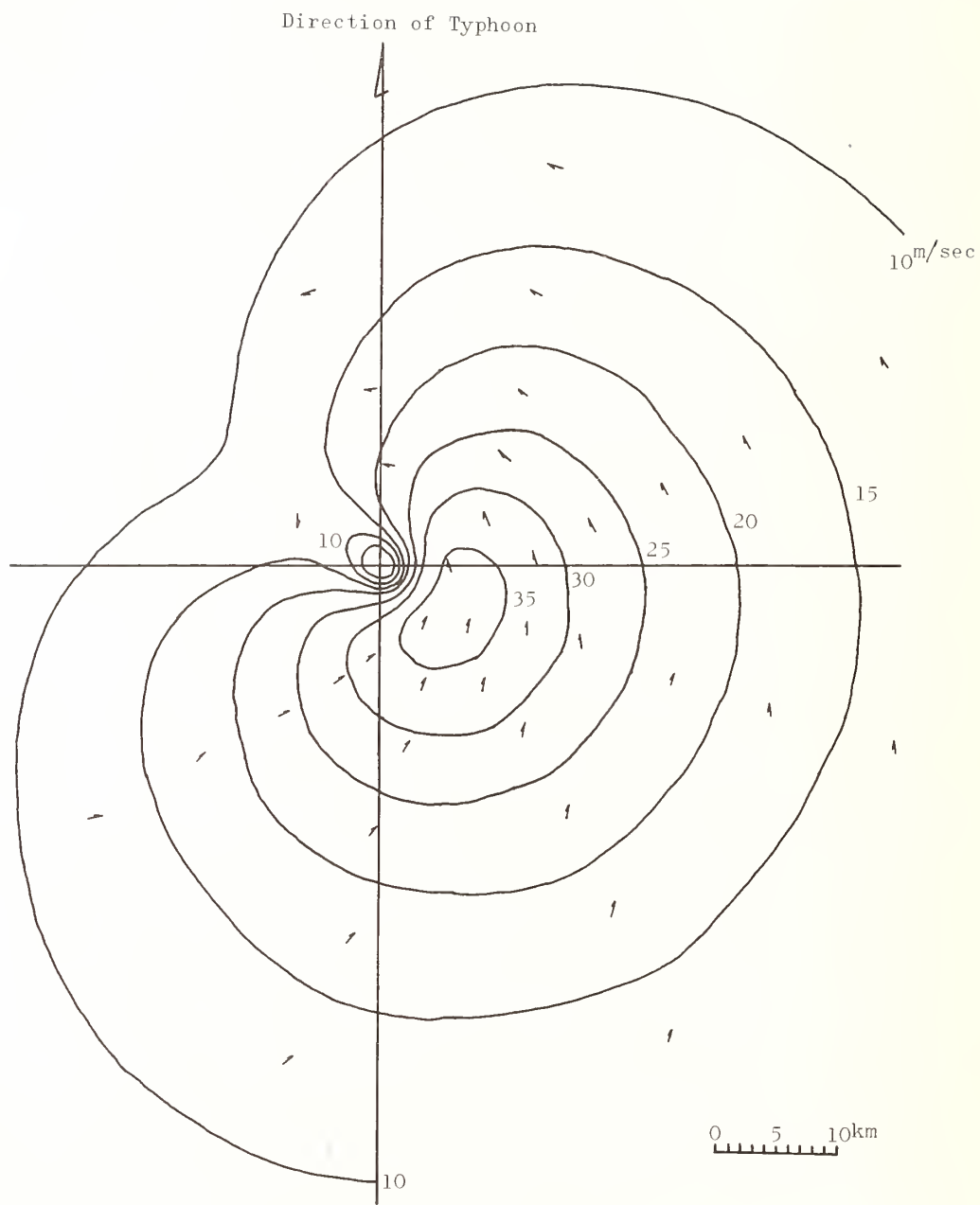
Fig. 3   Distribution of Speed and Direction
in the Design Typhoon
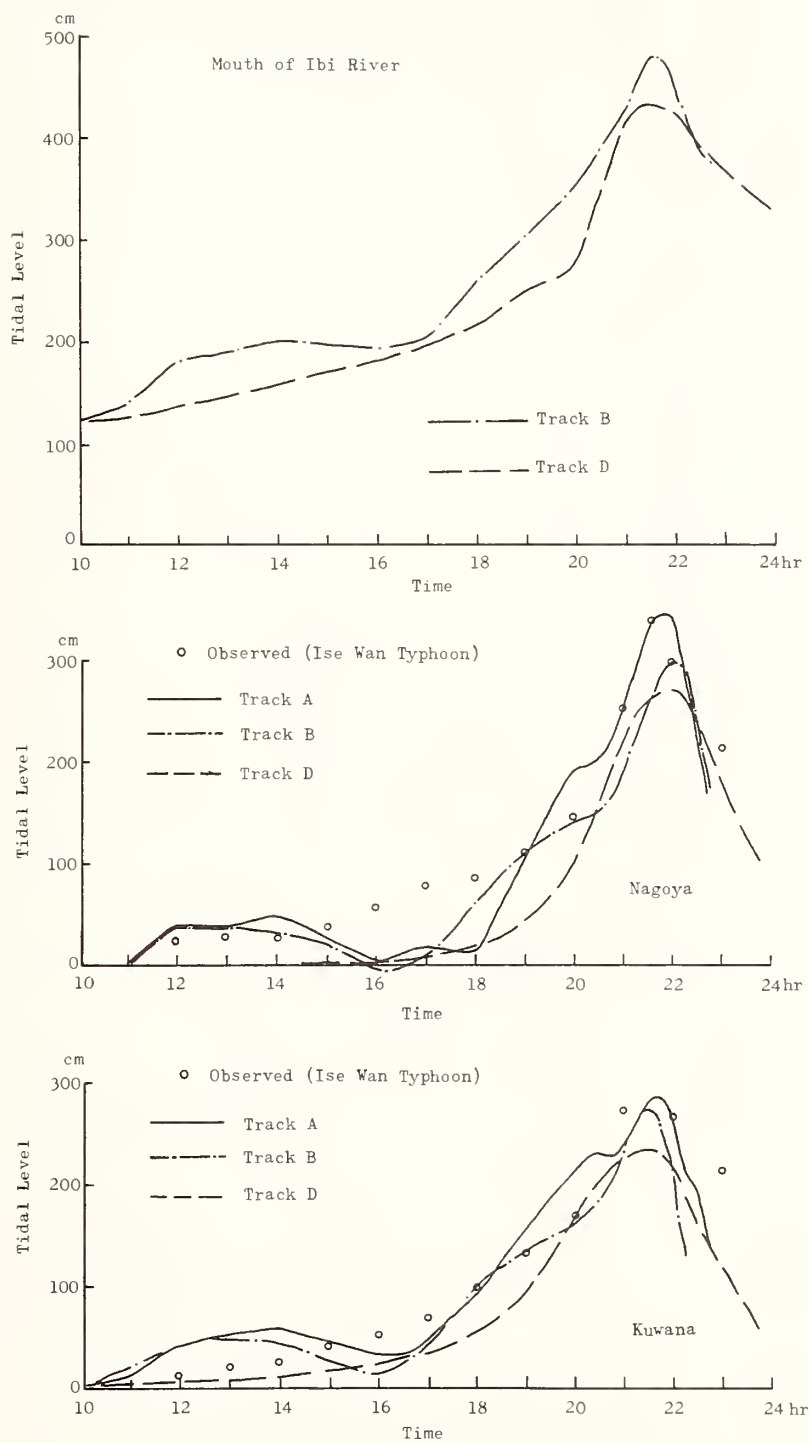
Fig. 4   Storm Surge caused by Design Typhoon

Ibi River

Nagara River

Kiso River

Syonai River

Nagoya

Nikko River

Kuwana

Yokkaichi

Nagoya Port

Storm Surge Breakwaters

below the sea level in 1959

below the sea level in 1976

0   5   10 km

II   III   IV

Fig. 5   Map of Ise Bay

312
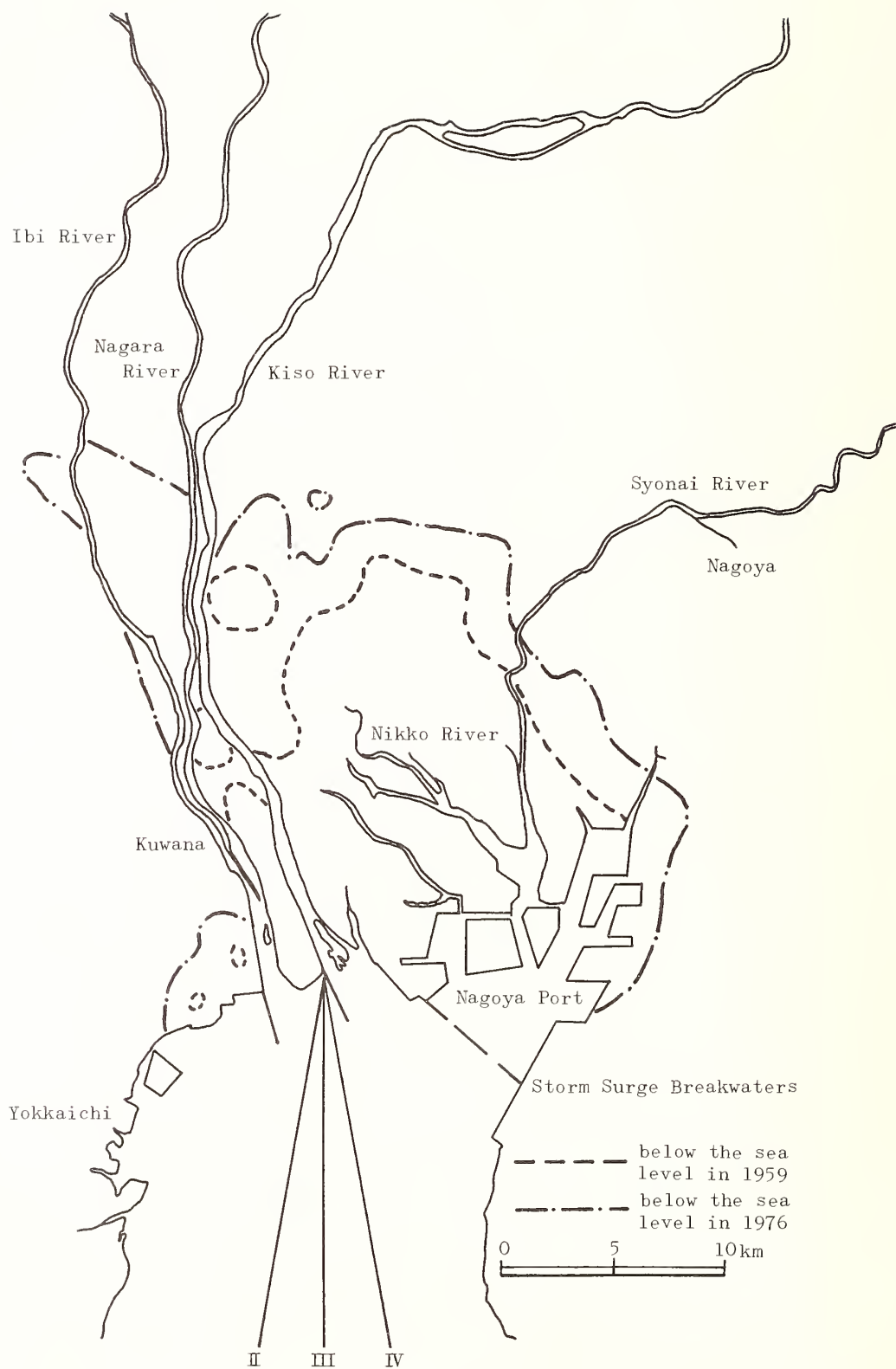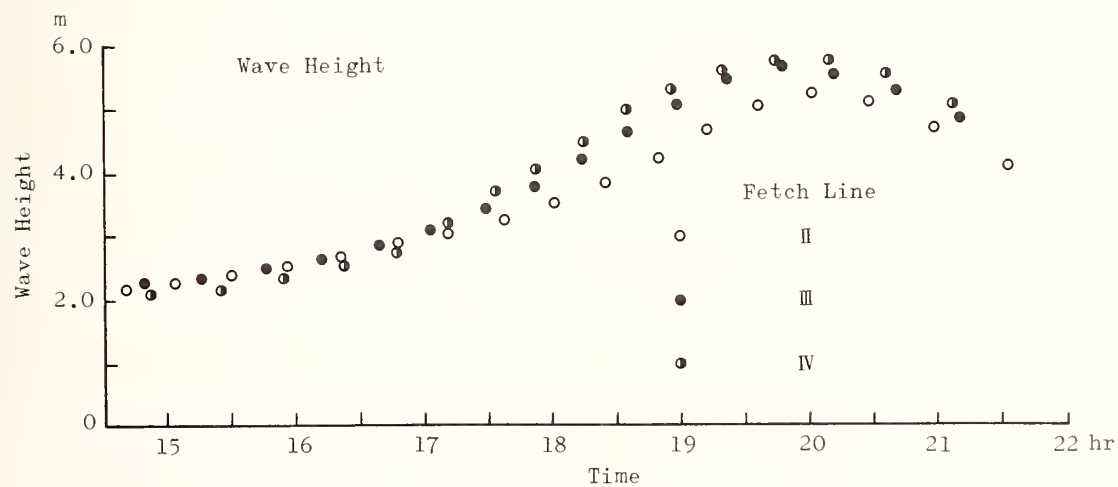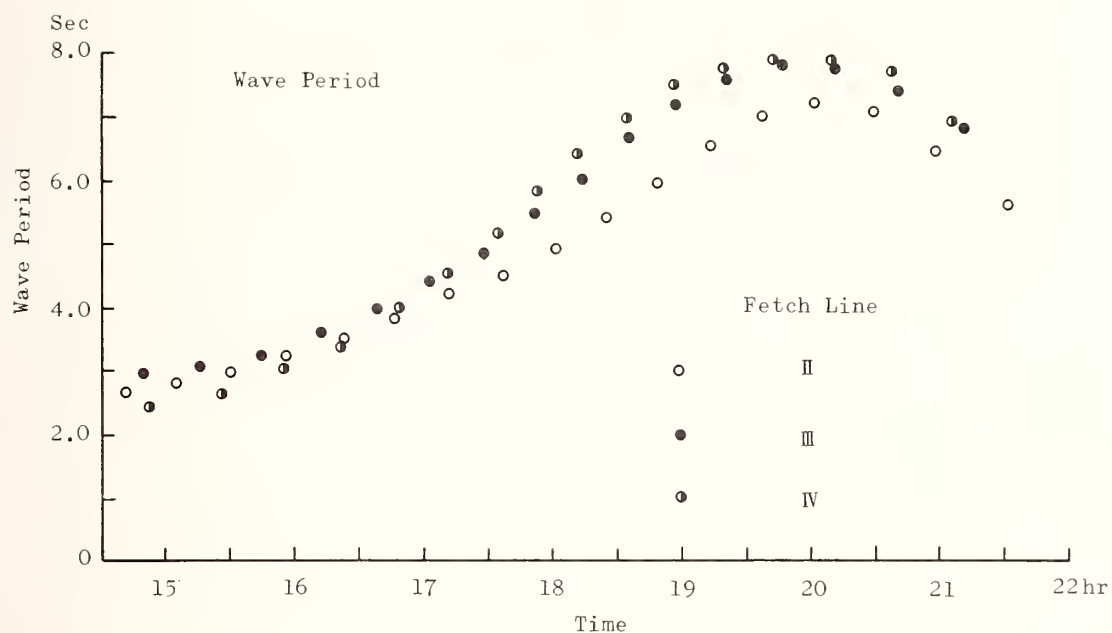
Fig. 6   Change of Wave Height and Period
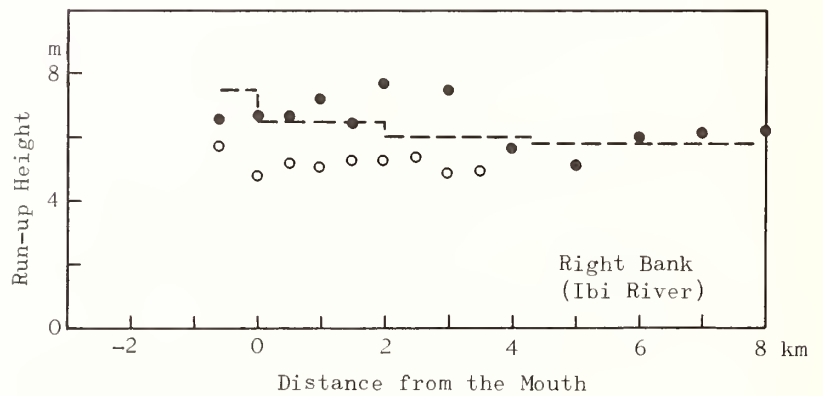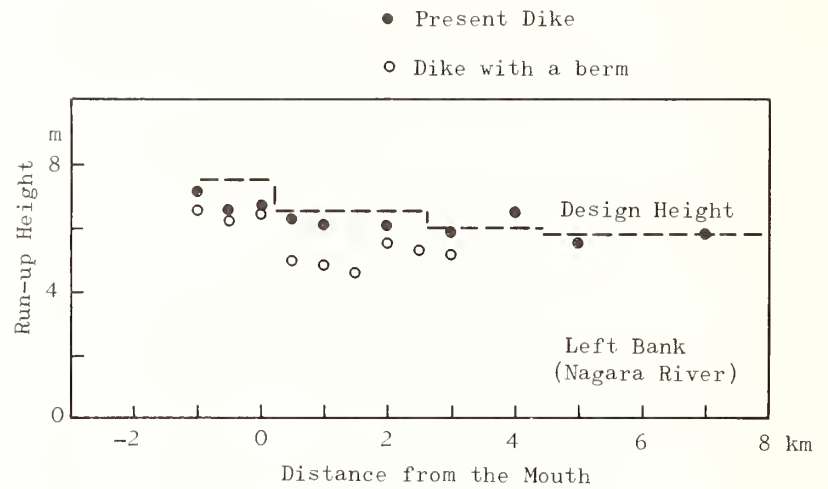
Fig. 7   Run-up Height along the Ibi and Nagara Rivers
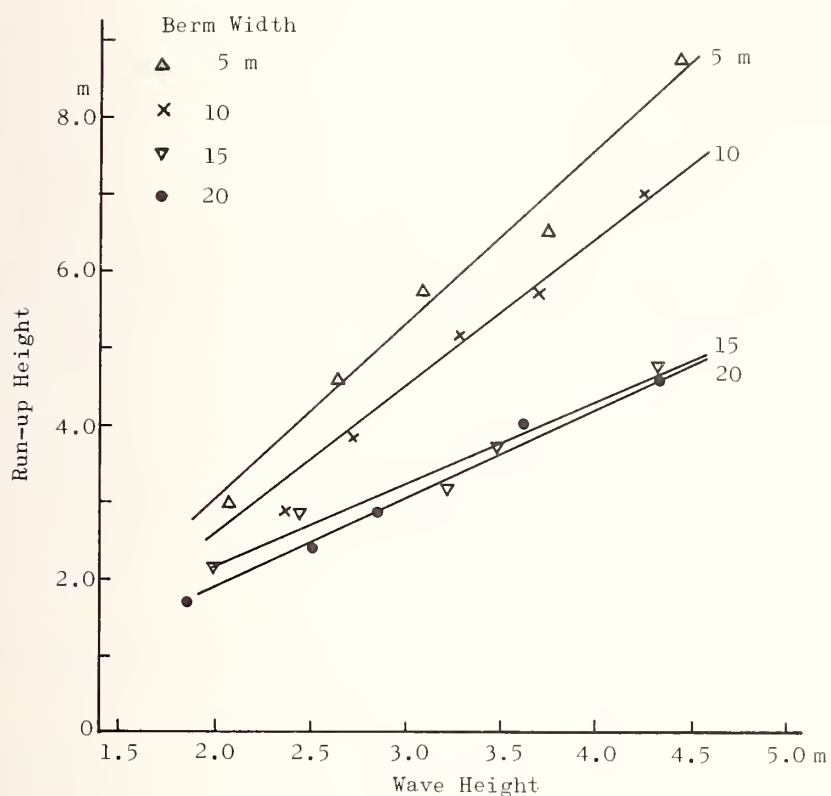
Fig. 8   Effect of Berm Width on Run-up
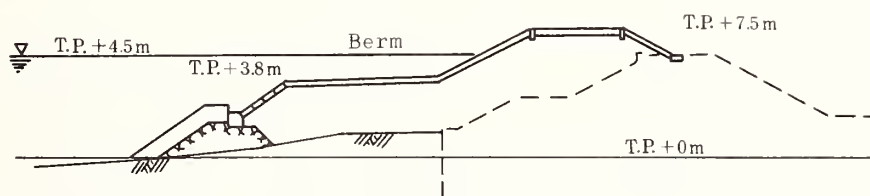
Fig. 9   Cross Section of a Dike at the Mouth of the Ibi River
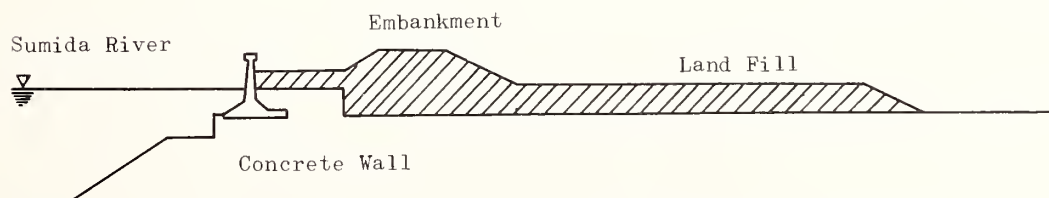
Fig. 10   Cross Section of an Improved Dike at the Sumida River in Tokyo

315

NEW STRUCTURAL DESIGN ENFORCEMENT FOR BUILDING STRUCTURES

by

Kiyoshi Nakano

Makoto Watabe

Yuji Ishiyama

ABSTRACT

This paper summarizes the draft of a new aseismic design method for the Building Standard Law Enforcement Order and related regulations which will be amended in the near future. This aseismic design method aims at two targets: (i) the buildings shall withstand almost no damage subjected to the moderate earthquake motions which would occur several times during the expected life of the buildings; (ii) the building shall not collapse nor harm human lifes from severe earthquake motions which would occur less than once during the expected life of the building.

1. GENERAL

1.1 Purpose

The purpose of this aseismic design method is to ensure that buildings shall withstand moderate earthquake motions with almost no damage which might occur several times during the expected life of the buildings, and shall not collapse nor harm human lives by severe earthquake motions which might occur less than once during the expected life of the buildings.

1.2 Scope

This aseismic design method shall apply to buildings smaller than 60 meters.

2. DESIGN PROCEDURE

2.1 Design for Moderate Earthquake Motions

(i) The stresses caused by lateral seismic shear prescribed in 3.1, 3.2 and 3.3 shall not exceed the allowable stresses for temporary loads.

(ii) Each story drift of the building caused by the lateral seismic shear prescribed in 3.1 shall not exceed 1/200 of the story height. This value can be increased to 1/120 in cases where non-structural members shall not experience severe damage under the increased story drift.

2.2 Design for Severe Earthquake Motions

The ultimate lateral shear strength of each story shall not be less than the required lateral shear, Q_R, determined in accordance with the following formula.

$$Q_R = D_S \cdot F_{ES} \cdot Q \tag{1}$$

where, D_S = the structural coefficient which can be determined by the ductility and and the damping, and shall be not less than 0.3. (See A-1)

        F_{ES} = the shape factor which shall be the product of F_E and F_S. Where, F_E and F_S shall be the factors which can be determined by the eccentricity of the center of stiffness from the center of gravity and by the variation of the lateral stiffness from the mean lateral stiffness, respectively, and both shall be not less than 1.0. (See A-2)

        Q = the lateral seismic shear for severe earthquake motions prescribed in 3.1.

317

2.3 Exceptions

    (i) The design procedure of 2.1 (ii) and 2.2 do not apply to buildings listed in Table 1.

    (ii) The design procedure of 2.2 do not apply to buildings listed in Table 2.

3.   LATERAL SEISMIC SHEAR

3.1   Lateral Seismic Shear Above Ground Level

The lateral seismic shear, Q of each story above ground level shall be determined using the following formula.

$$Q = C_I \cdot W_I \tag{2}$$

where, C_I = the lateral seismic coefficient of the I-th story as determined using Formula (3).

       W_I = the weight of the building above the I-th story.

The weight of the building shall be the sum of the dead load and the applicable portion of the live load. In heavy snow districts, the effect of snow loads shall be considered.

The lateral seismic shear coefficient of the I-th story, C_I, shall be determined using the following formula.

$$C_I = Z \cdot R_T \cdot A_I \cdot C_0 \tag{3}$$

where, Z = the seismic hazard zoning coefficient as shown in Figure 1.

       R_T = the design spectral coefficient, which shall be determined by the type of soil profile and the fundamental natural period of the buildings, as illustrated in Figure 2.

       A_I = the lateral shear distribution factor, which shall be determined by the fundamental natural period and the weight distribution of the buildings, as shown in Figure 3.

       C_0 = the standard shear coefficient, which shall be not less than 0.2 for moderate earthquake motions and 1.0 for severe earthquake motions.

The fundamental period of the building, T, to determine the design spectral coefficient and the lateral shear distribution factor, shall be determined using one of the following formulae.

313

$$T = 0.028 \, H \qquad \text{for steel frame buildings.} \tag{4}$$

$$T = 0.020 \, H \qquad \text{for other buildings.} \tag{5}$$

where, T = the fundamental natural period of the building in seconds.

H = the height of the building in meters.

3.2 Lateral Seismic Shear of Appendages

The lateral seismic shear of the penthouses, chimneys, towers, cisterns, parapets and other appendages on buildings, q, shall be determined using the following formula.

$$q = k \cdot w \tag{6}$$

where, q = the lateral seismic shear of the appendage.

k = the seismic design coefficient of appendages and shall be 1.0, but the value can be minimized to 0.5 when no harm will occur.

w = the weight of the appendage.

3.3 Lateral Seismic Shear of the Basement

The lateral seismic shear of basement, Q_B, shall be determined using the following formula.

$$Q_B = Q_P + K \cdot W_B \tag{7}$$

where, Q_p = the portion of the lateral seismic shear of the first story that will act to the basement.

K = the seismic design coefficient of the basement as determined using Formula (8).

W_B = the weight of the basement.

The seismic design coefficient of a basement, K, shall be determined using the following formula.

$$K = 0.5(1 - \frac{H}{40})Z \cdot C_o \tag{8}$$

where, H = the depth of the basement in meters and 20 meters in cases where the depth exceeds 20 meters.

Z and C_o are the same as defined in 3.1.

A-1   THE STRUCTURAL COEFFICIENT, D_S

1. The structural coefficient, D_S, can be determined using the following formula, in cases where the damping ratio and the ductility factor is available from structural experiments and analyses.

$$D_S = \frac{\beta}{\sqrt{2\mu - 1}} \qquad (A-1.1)$$

where, $\beta = \dfrac{1.5}{1 + 10h}$

μ = the ductility factor

h = the damping ratio, and the standsrd value is 0.05 for reinforced concrete buildings and 0.10 for steel encased reinforced and prestressed concrete buildings.

2. In case the damping ratio and the ductility factor are not available, the structural coefficient, D_S, can be determined based on standard values in the following table.

The value of D_S	Types of Structures
0.3 - 0.4	Moment frame structures with excellent ductility
0.4 - 0.5	Structures with ductile shear walls or braces
0.5 - 0.75	Structures with shear walls or braces with poor ductility
0.75 - 1.0	Structures with very poor ductility

A-2   SHAPE FACTOR, F_{ES}

The shape factor, F_{ES}, of each story can be determined using the following formula.

$$F_{ES} = F_E \, F_S \qquad\qquad (A\text{-}2.1)$$

where, F_E can be given by the following table as a function of eccentricity of stiffness, R_E, given by the following formula.

$$R_E = \frac{e}{r_e} \qquad\qquad (A\text{-}2.2)$$

where, e = the eccentricity of the center of the stiffness from the center of gravity

r_e = the elastic radius which can be defined as the square root of the torsional stiffness divided by the lateral stiffness.

Table A-2.1   Shape Factor, F_E, by Eccentricity of Stiffness, R_E

R_E	F_E
less than 0.15	1.0
$0.15 \leq R_E \leq 0.3$	linear interpolation
more than 0.3	1.5

And F_S can be given by the following table as a function of variation of lateral stiffness, R_S, given by the following formula.

$$R_S = \frac{r}{\bar{r}} \qquad\qquad (A\text{-}2.3)$$

where, r = the lateral stiffness which shall be defined as the value of the story height divided by the story drift caused by the lateral seismic shear for moderate earthquake motions prescribed in 3.1.

$\bar{r}$ = the mean lateral stiffness which shall be defined as the arithmetic mean of r's above ground level.

321

Table A-2.2 Shape Factor, F_S, by Variation of Lateral Stiffness, R_S

R_S	F_S
more than 0.6	1.0
$0.3 \leq R_S \leq 0.6$	linear interpolation
less than 0.3	1.5

Table 1.   Buildings Which Need Not Execute Design Procedure 2.1(ii) and 2.2

1	Buildings of conventional wooden construction, reinforced concrete block construction, or reinforced concrete panel construction that shall meet the structural requirements stipulated to the relevant regulations.
2	Buildings not exceeding five stories of reinforced concrete wall construction, or reinforced concrete precast wall construction that shall meet the structural requirements stipulated by the relevant regulations.
3	Buildings not exceeding 20 meters in height of reinforced concrete construction, prestressed concrete construction, or steel encased reinforced concrete construction. Each story shall meet the following formula $$25 \cdot A_w + 7 \cdot A_c > Z \cdot W_I \qquad\qquad (T-1.1)$$ where, A_w = the sum of the horizontal cross-sectional areas in square centimeters of reinforced concrete shear walls in the direction concerned. A_c = the sum of horizontal cross-sectional areas in square centimeters of columns. Z = the seismic hazard zoning coefficient as shown in Figure 1. W_I = the weight in kilograms of the building above the story concerned. For steel encased reinforced concrete buildings, the coefficient 7, for A_c in the above formula should be increased up to 10.

Table 2.   Buildings Which Need Not Execute Design Procedure 2.2

Buildings not exceeding 31 meters in height of reinforced concrete construction, steel encased reinforced concrete construction, or steel construction that shall meet all of the following requirements.

1	Each story above the ground level shall meet the following formula. $$\frac{r}{\bar{r}} \geq 0.6 \qquad\qquad\text{(T-2.1)}$$ where, r = the lateral stiffness which shall be defined as the value of the story height divided by the story drift caused by lateral seismic shear of moderate earthquake motions prescribed in 3.1. $\bar{r}$ = the mean lateral stiffness which shall be defined as the arithmetic mean of r's above ground level.
2	Eccentricity of the center of the stiffness from the center of gravity shall be less than 0.15 of the elastic radius at each story. Where the elastic radius shall be the square root of the torsional stiffness divided by the lateral stiffness.
3a	Each story shall meet the following formula in cases of reinforced concrete construction, or steel encased reinforced concrete construction. $$25(A_w + A_c) > A_I\ Z\ W_I \qquad\qquad\text{(T-2.2)}$$ where, A_w = the sum of horizontal cross-sectional areas in square centimeters of reinforced concrete shear walls in the direction concerned. A_c = the sum of horizontal cross-sectional areas in square centimeters of columns. A_I = the lateral shear distribution factor. Z = the seismic hazard zoning coefficient as shown in Figure 1. W_I = the weight in kilograms of the building above the story concerned.
3b	Each story which has braces shall meet the following formulae. $$\sigma_a \geq (1 + 0.7\ \beta)\sigma_B \qquad\qquad\text{(T-2.3)}$$ where, σ_a = the allowable stress for temporary loads. β = the ratio of the lateral shear of braces to the total lateral seismic shear of the story. σ_B = the stress of braces caused by the lateral seismic shear of moderate earthquake motions prescribed in 3.1. $$J^P u \geq 1.2\ M^P y \qquad\qquad\text{(T-2.4)}$$ where, $J^P u$ = the ultimate strength of the joint of the brace. $M^P y$ = the yield strength of the brace.

Fig. 1 Seismic Hazard Zoning Coefficient, Z

325
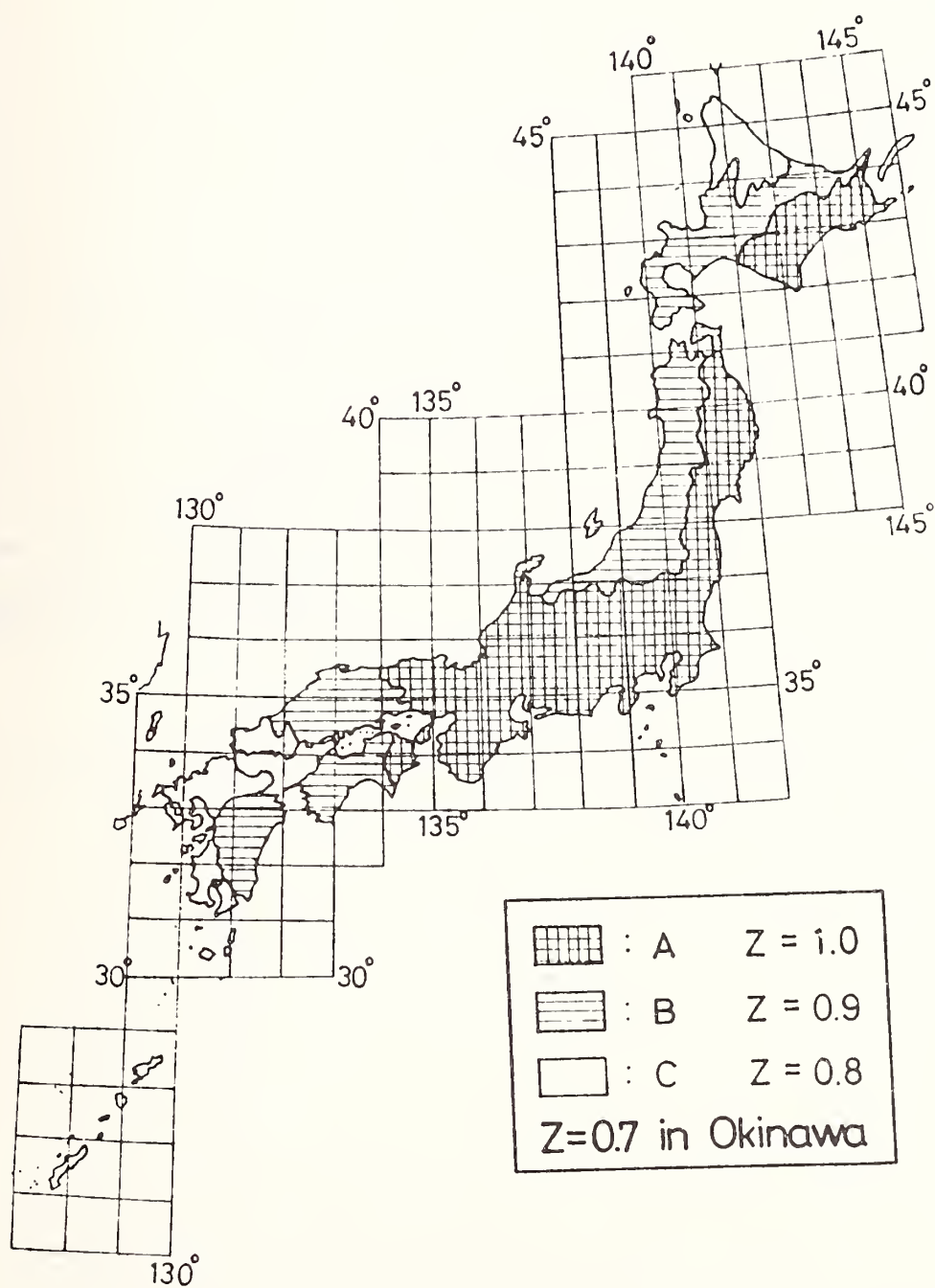
Fig. 2 Design Spectral Coefficient, R_T
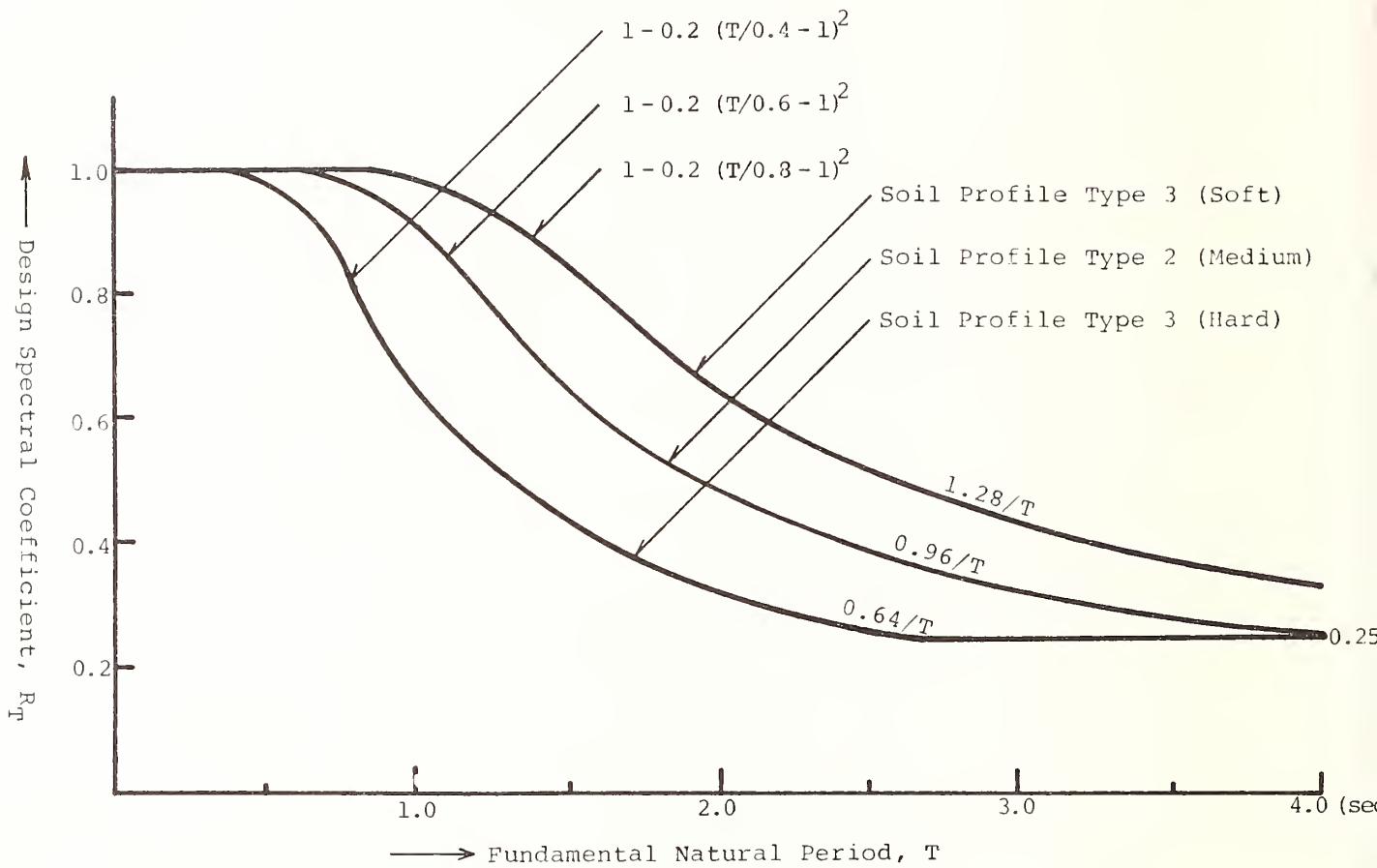
Fig. 3 Lateral Shear Distribution Factor, A_I

$$A_I = 1 + (\frac{1}{\sqrt{\alpha_I}} - \alpha_I)\frac{2T}{1 + 3T}$$

$\alpha_I = W_I/W_N$

W_I = Weight above I-th story

W_N = Weight above ground level

T = Fundamental natural period (sec)
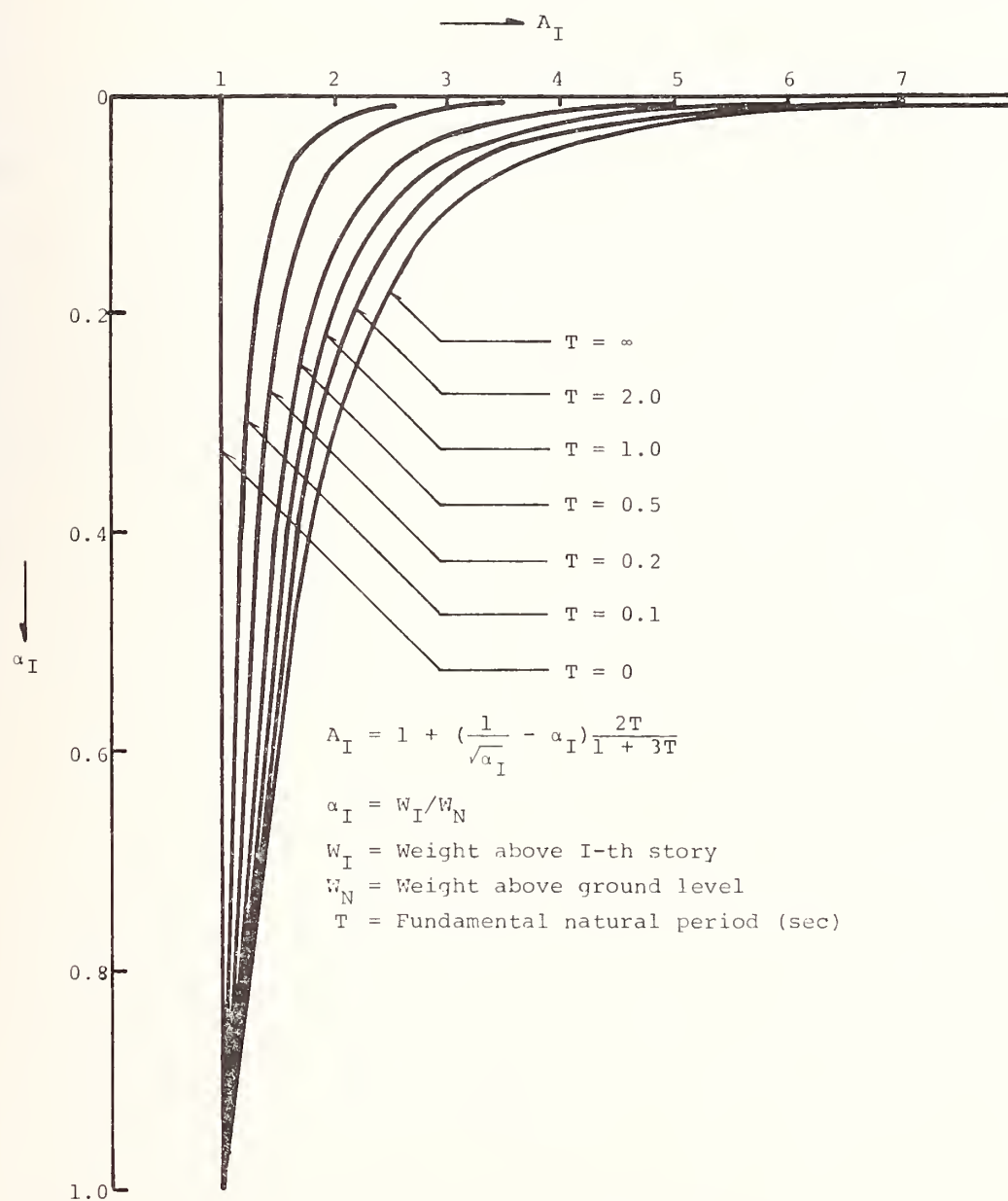
IMPACT OF DRAFT HIGHWAY BRIDGE SEISMIC DESIGN GUIDELINES

by

James D. Cooper

Ronald L. Mayes

Roland L. Sharpe

ABSTRACT

A comprehensive set of draft seismic design guidelines for highway bridges has been under development since 1977. The draft guidelines were completed in 1979 and have been the center of a concerted evaluation effort by consulting engineering firms and State departments of transportation. This paper presents the general philosophy behind the guidelines and describes the evaluation and redesign phase of the endeavor. Twenty-one bridges, which were redesigned using the draft guidelines, are documented. Economic impact and general viability of the draft guidelines along with recommendations for revisions to them are presented.

INTRODUCTION

The 1971 San Fernando earthquake presented a major turning point in the development of seismic design criteria for bridges in the United States. Prior to 1971 the American Association of State Highway Transportation Officials (AASHTO) specifications for the seismic design of bridges were based in part on the lateral force requirements for buildings developed by the Structural Engineers Association of California. [1] In 1973 the California Department of Transportation [2] (CalTrans) introduced new seismic design criteria for bridges that included the relationship of the site to active faults, the seismic response of the soils at the site and the dynamic response characteristics of the bridge. In 1975 AASHTO adopted Interim Specifications which were a slightly modified version of the 1973 CalTrans provisions and made them applicable to all regions of the United States. In addition to these code changes the 1971 San Fernando earthquake also stimulated research activity on the seismic problems related to bridges. By 1977, significant earthquake engineering research studies relating to highway bridges had been completed and the Federal Highway Administration (FHWA) funded a program with the Applied Technology Council (ATC) to develop recommended new and improved bridge seismic design guidelines and then evaluate the impact of these guidelines on the basis of design, construction, and cost implications. "Draft Seismic Design Guidelines for Highway Bridges" [3] were completed in 1979 and based on the evaluation phase of the study, final recommended guidelines will be prepared.

APPLICABILITY OF GUIDELINES TO THE UNITED STATES

A basic premise in developing the bridge seismic design guidelines was that they be applicable to all parts of the United States. The seismic risk varies from very small to rather high across the country. Therefore, for purposes of design, criteria were developed for four seismic performance categories to which bridges would be assigned based on the seismicity of the area in which the site is located and the bridge importance classification (IC).

Bridges are classified according to their relative importance--either as an essential bridge or not. An IC coefficient of II is assigned for essential bridges and I for all others. Essential bridges are determined based on their social/survival and security/defense classification. Essential bridges are those that must keep functioning during and after an

earthquake. Another aspect of classification covers the differing degrees of complexity and sophistication of seismic analysis and design which are specified. This is called Seismic Performance Category (SPC). SPC-D bridges include those designed for the highest level of seismic performance with particular attention to methods of analysis, design and quality assurance. SPC-C bridges include those where a slightly lower level of seismic performance is required but the potential for damage is slightly greater than SPC-D. SPC-B bridges include those where a lesser level of seismic performance is required and a minimum level of analysis and specific attention to support design details are provided. SPC-A bridges include those where no seismic analysis is required but attention to certain design details for superstructure support is provided.

DESIGN PHILOSOPHY

The primary basis for development of the seismic design guidelines for bridges is to minimize the hazard to life and provide the capability for bridges to survive during and after an earthquake with essential bridges to remain functional. To meet this philosophy, certain principles were followed:

Small-to-moderate earthquakes should be resisted within the elastic range of the structural components without damage. Realistic seismic ground motion intensities should be used in the design procedure. Exposure to shaking from large earthquakes should not cause collapse of all or part of the bridge. Where possible, damage that does occur should be readily detectable and accessible for evaluation and repair.

Conceptually there are two different approaches that are currently in use to satisfy the above principles. These are mainly "force design" approaches and are the current New Zealand [4] and CalTrans [5] approaches.

In assessing bridge failures of past earthquakes in Alaska, California, and Japan many of the "loss of span" type failures are attributed in part to relative displacement effects. Relative displacements arise from out of phase motion of different parts of a bridge, from lateral displacement and/or rotation of the foundations and differential displacements of abutments. Therefore in developing the draft guidelines the design displacements were considered to be just as important as design forces and for SPC-C and -D bridges, requirements

330

for ties between non-continuous segments of a bridge are specified in addition to minimum bearing support lengths at abutments, columns and hinge seats.

The methodology used in the draft guidelines is in part a combination of the CalTrans and New Zealand "force design" approaches but it also addresses the relative displacement problem. The methodology varies in complexity as the SPC increases from A to D. Three additional concepts are included in the draft guidelines that are not included in either the New Zealand or CalTrans approach. First, minimum requirements are specified for bearing support lengths of girders at abutments, columns, and hinge seats to account for some of the important relative displacement effects that cannot be calculated by current state-of-the-art methods. A somewhat similar requirement is included in the latest Japanese bridge code. Second, member design forces are calculated to account for the directional uncertainty of earthquake motions and the simultaneous occurrence of earthquake forces in two perpendicular horizontal directions. Third, design requirements and forces for foundations are intended to minimize damage since most damage that might occur will not be readily detectable.

For SPC-A bridges the only design requirement is one of providing minimal bearing support lengths for girders at abutments, columns, and expansion joints. Even though the level of seismic risk of these bridges is very small, prevention of superstructure collapse was deemed necessary and hence the requirement. Design for the level of seismic force in these regions was not considered necessary.

For SPC-B bridges the elastic member forces are determined by a single mode spectral approach. Design forces for each component are obtained by dividing these elastic forces by a reduction factor (R). For connections at abutments, columns and expansion joints, the R-factor is either 0.8 or 1.0 and they are therefore designed for the expected or greater than the expected elastic forces. Foundations are also designed for the elastic forces. For columns and piers the R-factor varies between 2 and 6 and they are therefore designed for forces lower than expected from an elastic analysis and are expected to yield when subjected to the forces of the design earthquake. Design requirements to ensure reasonable ductility capacity of columns in SPC-B are not specified whereas they are for SPC-C and -D bridges.

For SPC-C and -D bridges the general approach is similar to SPC-B; however several additional requirements are included. For columns, additional requirements are included to

331

ensure that they are capable of developing reasonable ductility capacity. For connections and foundations alternate design forces to those determined by the procedures of SPC-B are also permitted. These are based on the maximum shears and moments that can be developed by column yielding when the bridge is subjected to the design earthquake forces. Horizontal linkage and tie down requirements at connections are also provided. For SPC-D bridges, settlement slabs are required to reduce the chance of abutment backfill settlement.

SEISMIC GROUND MOTION INTENSITIES

The selection of ground motion intensities to be used with the seismic design provisions was carefully reviewed. Considerable study and effort had recently been made to develop seismic risk maps and associated design spectra for the "Tentative Provisions for the Development of Seismic Regulations for Buildings" (ATC-3-06) [6]. The ATC-3-06 maps are based on (1) a realistic appraisal of expected ground motion intensities, (2) the probability that the design ground shaking will be exceeded is approximately the same in all parts of the United States, and (3) frequency of occurrence of earthquakes in various regions of the country. It is possible that the design earthquake ground shaking might be exceeded, although the probability of this happening is quite small.

Ground motion is characterized by the use of two parameters - Effective Peak Acceleration (EPA), A_a and Effective Peak Velocity-Related Acceleration (EPV), A_v. Although these parameters do not at present have precise definitions in physical terms, they should be considered as normalizing factors for the construction of smoothed elastic response spectra [7] for ground motions of normal duration. The EPA is proportional to spectral ordinates for periods in the range of 0.1 to 0.5 seconds, while the EPV is proportional to spectral ordinates at a period of about 1 second. [8] The constant of proportionality (for a 5 percent damped spectrum) is set at a standard value of 2.5. Thus when the ordinates of a smoothed spectrum between the periods mentioned above are divided by 2.5, the EPA and EPV are obtained. The EPA and EPV thus obtained are related to peak ground acceleration and peak ground velocity but are not necessarily the same or even proportional to peak acceleration and velocity.

METHODS OF ANALYSIS

The draft guidelines provide for 3 methods of analysis which vary according to the refinement in the mathematical idealization. They are the seismic coefficient method, the single mode spectral method, and the multimode spectral method. All methods assume simultaneous ground motion at all supports.

Simple Seismic Coefficient Approach – Method 1

This method does not require a calculation of the period of the bridge. In effect, the method is designed to specify a lateral (i.e., longitudinal or transverse) force equal to some fraction of the bridge weight. The bridge, or bridge section, is designed to resist the lateral seismic load applied along the center of mass of the superstructure.

Single Mode Spectral Approach – Method 2

This method requires a calculation of a period. The method is based on the premise that the mode shape of the vibrating structure can be assumed and represented by a shape function which can be expressed mathematically in terms of a single generalized coordinate taken as the amplitude at the point of maximum displacement. It is designed to approximate the dynamic character of the bridge. The method consists basically of the following steps:

(1) Determine the period for the assumed mode.

(2) Determine the corresponding seismic coefficient as a function of A_v, structure period, and soil type.

(3) Determine the maximum displacement due to the seismic loading.

(4) Determine the component forces corresponding to the maximum displacement.

Multimode Spectral Approach – Method 3

Bridges having complex geometry due to horizontal and vertical alignments and/or skew support conditions have coupling in the three coordinate directions within each mode of vibration. These coupling effects make it difficult to categorize the modes into simple longitudinal or transverse modes of vibration. In addition, several modes of vibration will in general contribute to the total response of the structure. These complex coupling effects and multimodal contributions to the final response necessitate the use of computer programs with space frame analysis capabilities for this method. Support motions applied in

any one of the two horizontal directions will generally yield forces about both principal axes of the individual members due to these coupling effects.

BRIDGE REDESIGNS

Five State departments of transportation (California, Idaho, New York, Oklahoma, and Washington) and four design consultants participated in the redesign and evaluation of the "Draft Seismic Design Guidelines for Highway Bridges" [2] developed by the ATC Project Engineering Panel. A total of 21 bridges were seismically redesigned using the draft guidelines. All bridge loadings remained the same for the redesigns except for the seismic loads. The States redesigned their bridges based on the actual location of the structure. Thus the SPC and analysis method was fixed by the guidelines. The consultants redesigned actual bridges for all Seismic Performance Categories and related methods of analysis. A description of the bridges along with parameters used in the redesigns are presented in Table 1.

IMPACT OF DRAFT SEISMIC DESIGN GUIDELINES

Evaluation and impact of the draft seismic design guidelines is based on comments received from the bridge designers who redesigned the 21 bridges listed in Table 1. It is noted that the experience of the designers varied from those having little or no seismic design time to those who routinely design bridges to resist earthquake imposed loading. Some designers, particularly those who have little experience, tended to make the most conservative interpretation of the guidelines, thus significantly increasing costs. The first 5 bridges in Table 1 were redesigned by State bridge designers. The bridges were originally designed using CalTrans criteria. The designers assumed that the value of A_a may be as high as 0.7 in some parts of the State and thus used that value. In areas where A_a exceeds 0.4, the draft guidelines recommend a maximum value of 0.4 be used in analyses. The impact on total cost is seen to be minimal, varying from no change to an increase of 4.3 percent in structure cost. The designer for the fifth bridge assumed an A_a of 0.4 which actually resulted in a 0.6 percent decrease in structural cost.

Bridges 6, 7, 8, 9, 14, and 15 were redesigned by several consulting engineering firms. The respective bridges were redesigned as though they were sited in each of the SPC locations (A through D) and then those new details required by the guidelines were compared to the actual design details. The fact that many of the bridges had no seismic design

provisions, coupled with conservative interpretations of the guidelines account for cost increases of up to 55 percent. Typically, most of the increase was due to assuring that foundation uplift did not occur. The cost increases would have been greatly reduced had designers used ultimate capacities for piles and soils.

Bridges 7 and 8 probably give a more reasonable indication of the impact of imposing more stringent design requirements in seismic areas of the country. Costs increased by 12 percent and 25 percent respectively when increasing design requirements for structures in SPC-B to SPC-D. Increased foundation requirements account for most of the increased costs. However, once again, utilizing ultimate capacities of piles and soil to resist earthquake imposed loads would reduce these cost increases.

The remaining structures were redesigned by individual State departments of transportation. Cost impact varies from no increase to 19 percent, again somewhat misleading because of foundation overdesign.

REVISIONS TO DRAFT SEISMIC DESIGN GUIDELINES

The draft guidelines represent a radical departure from previous earthquake design guidelines used in the United States. The redesign phase of the guideline development effort has been beneficial in providing input which can be used as the basis for making some apparent needed revisions to the guidelines. Most designers found the format of the guidelines to be cumbersome. Consequently, it was recommended the format be changed.

Technical changes include the following:

(1) Add requirements for steel bridges. Specifically add a section to determine the plastic forces for yielding of steel columns and add a section to assure that the columns develop the required ductility capacity.

(2) Reduce the gap requirement (D^1) at expansion joints. Redesigners indicated that the gaps required by the guidelines were excessive. It seems reasonable to provide adequate bearing support lengths to avoid loss of span and decrease the gap requirement and accept some damage due to slamming.

(3) Recommend that bridges designed in SPC-B use Analysis Method 2 instead of 1. Analysis Method 1 produces overly conservative design forces. The redesign results indicate that seismic forces determined from Analysis Method 1 are greater than wind forces.

335

(4) Response Modification Factors have not been specified for pile bent requirements. Specify factors for incorporation into the final guidelines.

(5) Specify to what force level column connections to bent caps should be designed.

(6) Clarify that the ultimate capacity of soils and piles should be used with the foundation design forces. Give guidelines or references to determine the ultimate capacities. For SPC-B recommend a simplified method consistent with the design philosophy to reduce the foundation design forces from the elastic forces.

(7) Consider if and when uplift of foundations can be permitted in the design of foundations.

In general, the guidelines were found to be realistic and workable. Most designers stated that the guidelines represent a significant improvement over current criteria used in the United States. Further, the guidelines are sufficiently general. Rail, mass transit, as well as highway, organizations are reviewing the guidelines for possible use in the earthquake design of their respective structures.

CONCLUSION

The draft seismic design guidelines developed by the Applied Technology Council for the Federal Highway Administration represent a national earthquake design criteria for highway bridges. Use of the guidelines, when modified to incorporate designer's recommendations made during the bridge redesign phase of the study, will assure improved seismic resistance for new bridges. Further, the increased seismic protection can be achieved for relatively modest cost increase in parts of the United States where seismic design is not normally considered.

ACKNOWLEDGMENTS

(ATC Board Representative and Senior Vice President, URS/Blume Engineers), J. Penzien
(Professor, University of California, Berkeley), W. Podolny (Federal Highway Administration),
R. H. Scanlan (Professor, Princeton University), J. D. Cooper (Project Manager, Federal
Highway Administration), R. L. Mayes (ATC Project Technical Director), and R. L. Sharpe
(ATC Project Director). Two project consultants have also made material contributions:
R. A. Imbsen (Engineering Computer Corporation) and D. Elms (Professor, University of
Canterbury, New Zealand).

The 21 bridge redesigns discussed in this paper were performed by the following
consulting engineering firms and State departments of transportation: Modjeski and Masters;
DeLeuw Cather; Howard, Needles, Tammen and Bergendorf; Moffat and Nichol, Idaho, Oklahoma,
New York, Washington, and California.

REFERENCES

[1] Structural Engineers Association of California, "Recommended Lateral Force Requirements and Commentary," Second Edition 1966.

[2] Gates, J. H., "California's Seismic Design Criteria for Bridges," Journal ASCE Structural Division, December 1976.

[3] Cooper, J. D., Scheffey, C. F., Sharpe, R. L., and Mayes, R. L., "Draft Seismic Design Guidelines for Highway Bridges," Eleventh Joint Conference of the United States-Japan Cooperative Program in Natural Resources, Panel on Wind and Seismic Effects, Tokyo, Japan, September 1979.

[4] Chapman, H., "An Overview of the State of Practice in Earthquake Resistant Design of Bridges in New Zealand," Proceedings of a Workshop on the Earthquake Resistance of Highway Bridges, Applied Technology Council, Palo Alto, California, January 1979.

[5] Gates, J. H., "Factors Considered in the Development of the California Seismic Design Criteria for Bridges," Proceedings of a Workshop of the Earthquake Resistance of Highway Bridges, Applied Technology Council, Palo Alto, California, January 1979.

[6] Applied Technology Council, "Tentative Provisions for the Development of Seismic Regulations for Buildings," prepared for the National Bureau of Standards/National Science Foundation, ATC Report No. 3-06, Palo Alto, California, June 1978.

[7] Newmark, N. M., and Hall, W. J., "Seismic Design Criteria for Nuclear Reactor Facilities," Proc. 4th WCEE, Santiago, Chile, 1969.

[8] McGuire, R. K., "Seismic Structural Response Risk Analysis, Incorporating Peak Response Progressions on Earthquake Magnitude and Distance," Report R74-51, Dept. of Civil Engineering, Mass. Institute of Technology, Cambridge, Mass., 1975.

Table 1

Summary of Bridge Redesigns Using Draft Seismic Design Guidelines for Highways Bridges

Bridge Name & Location	Length Meters	No. of Spans	A_a*	SPC	Analysis Method	Superstructure	Substructure	Foundation	Abutments	Comments
1. Kern River California	123	3	0.7 / <u>0.2</u>	C / C	CalTrans 1	Composite concrete slab on steel plate girders 19m width	Wall Piers	Spread foundation	Cantilever seat type abutment	3.3% increase in pier costs 0.03% increase in foundation costs 0.25% increase in superstructure/pier connection Increases based on going from CalTrans method to ATC-6 with A_a=0.7.
2. Route 80 on Ramp California	212	7	0.7 / <u>0.2</u>	C / C	2	2Frames-CIP/PS Box Girder and RC Box Girder 12m wide	Single cantilever columns	Concrete cast in drilled holes	Expansion type with end diaphragm on piles	1.5% increase in column costs 1.0% increase in foundation 0.3% increase in restrainers 1.5% increase in hinges Increases based on going from CalTrans method to ATC-6 with A_a=0.7.
3. Milliken Ave. California	139	7	0.4 / 0.2	C / C	2 / 2	Reinforced concrete box girders 13m wide	2 column bents	Concrete footings on CIDH piles	Cantilever type with back-wall	Redesign not completed. Designer states that results from method 2 of analysis may be on conservative side.
4. Verdugo Blvd. California	160	5	0.7 / Av=0.4	C / C	3 / 3	CIP reinforced box girders 16m wide	Multi-column bents	Spread footings and short steel H piles	Diaphragm type on spread footings	No changes required compared to original design.
5. Camden Ave. California	69	2	0.4 / 0.3	C / C	1 / 1	Composite concrete slab on steel box girders 21m wide	2 column bent	Spread footings	Monolithic abutment on spread footing	0.3% increase in column costs 0.5% increase in footing costs 1.4% decrease in abutment costs Decrease of 0.6% based on going from CalTrans method to ATC-6 with A_a=0.4.
6. Hudson River Valley New York	109	5	0.05 / 0.1 / <u>0.2</u> / 0.3 / 0.4	A / B / C / C / D	- / 1 / 1 / 1 / 2	Continuous rolled beam - concrete structure 11m wide	3 Column Reinf. Conc. Bents Squ. Columns w/pier caps	Pile Supported Concrete Slabs	Stub Abutments w/wind walls supported by piles	Cost increases were incurred in columns, footings, and abutments as the force level increased. Designed by 1957 AASHTO.
7. Humbolt River Nevada	88	3	<u>0.05</u> / 0.1 / 0.2 / 0.3 / 0.4	A / B / C / C / D	- / 1 / 2 / 2 / 2	Cast in place conc. box girder 17m wide w/396m radius of curvature	Four Column Bents. Skew varies between 30 to 40 degrees	Pile footing	Open end seat with spread footings	Costs varied by 12% between SPC-B and SPC-D designs with 70% in the abutment. Designed by 1977 AASHTO.
8. Durham Road California	62	2	0.05 / 0.1 / 0.2 / 0.3 / 0.4	A / B / C / C / D	- / 1 / 2 / 2 / 2	Cast in place conc. box girder 26m wide	Four Column bent	Pile footing	Monolithic w/ deck on pile footings	Costs varied by 25% between SPC-B and SPC-D designs with 70% in the foundation. Designed by 1977 AASHTO & CalTrans criteria.
9. Menomonee Riv. Wisconsin	73	2	0.1 / 0.2 / 0.3 / 0.4	B / C / C / D	1 / 2 / 2 / 2	Continuous welded steel composite plate girder 9m wide	12m wide x 6m long pier with 11 degree skew	Pile footing	1-Free Standing full retaining. 1-Free Standing cellular. Both pile supported	Significant cost increases in foundations as force level increases. Total cost increased by 9-43%. Designed by 1976 AASHTO.
10. Lewiston Idaho	77	3	<u>0.05</u>	A	N/A	Cast in place conc. box girder 24m wide	3 columns per bent	Spread footings	Concrete cap supported on piles	No change in the design or related costs. No seismic design.

* Underlined values indicate approximate initial design values used.

Table 1 (Continued)

Bridge Name & Location	Length Meters	No. of Spans	A_a *	SPC	Analysis Method	Superstructure	Substructure	Foundation	Abutments	Comments
11. Heyburn Idaho	400	32	0.10 A_v= 0.15	C	1	Prestressed T-beams w/concrete deck 13m wide	Steel shell pile bents filled with concrete with 35° skew	Piles and columns are continuous	Beam type supported by piles	A 19% increase in total cost due to additional pile requirements. Designed by 1975 AASHTO.
12. Verdigris Riv. Oklahoma	137	5	0.10	B	1	Prestressed conc. I beam 11m wide	2 columns w/pier cap and web wall	Spread footing on piles with wing walls	Cantilever type	Slight increase (≃2% of total) in cost on one pier. Designed by 1976 AASHTO.
13. Poteau River Oklahoma	174	5	0.1	B	1	Reinforced concrete girders on approach spans. Haunched steel plate girder center 3 spans. 11m wide.	2 Columns per bent w/a web wall and tie beam between columns.	Two footing conditions were included. A drilled shaft and a spread footing	Cellular type abutments.The approach spans form the top part of the abutment.	≈ 3.6% (of total cost) increase in cost of each foundation. Designed by 1976 AASHTO.
14. Michelson Dr. California	107	4	0.05 0.10 0.2 0.3 0.4	A B C C D	- 1 2 modified 2 modified 2 modified	Precast-prestressed concrete girders w/reinforced concrete deck. 13m wide	Solid reinforced concrete walls 13m long 51cm thick 7m high	45 ton pre-stressed conc. piles	Open end seat type, free standing with back wall	Additional construction cost increased by 2% for SPC-A to 47% for SPC-D with 2/3 of the cost increase in the piers. Designed by 1973 AASHTO and CalTrans.
15. South E. Street California	195	8	0.05 0.10 0.20 0.3 0.4	A B C C D	- 3 3 3 3	Cast in place R.C. T beams. 2 inter-mediate hinges and expansion joints at ea. abutment. 12m wide	Solid reinforced concrete piers 13m long 11m high 51cm inches thick 20° skew	50 ton driven steel H piles	Open end seat type free standing with back wall	Construction cost increased by 1% for SPC-A to 55% for SPC-D with 80% of the cost occuring in the pier foun-dation. Designed by 1973 AASHTO and CalTrans.
16. Battenkill New York	55	1	0.1	B	1	Prestressed post tensioned concrete beams with 10cm. concrete slab 14 m wide	------	-------	Open end seat type on spread foundations	An increase in the cost of the abutment bearings. In the calcs a reduction of 2.5 was not used but is permitted. Designed by NYDOT spec.
17. Rt. 225 New York	71	2	0.1	B	1 and 2	Steel plate girders w/concrete slab 19m wide	3 column bent	Spread footing	Open end seat type on spread foundations	Major redesign of bearings. Foundation size increased. Designed by NYDOT spec.
18. Hulett Street New York	192	3	0.1	B	1 and 2	Steel plate girders w/concrete slab 13m wide	Two column bent	35 ton cast in place con-crete piles	Open end abutments supported on piles	Large expense in increasing the gap separation. Bearings require redesigning. No change in column design. Designed by NYDOT spec.
19. Rt. 28A New York	145	2	0.1	B	1 and 2	Steel plate girders w/composite slab 11m wide	Two column bent	Spread foot-ing	Open seat abutment on spread foun-dations	No change in footing and column design. Large gap separation at joint. Designed by NYDOT spec.
20. Midway Avenue Washington	73	2	0.2	C	1	Precast girders, continuous for live load. 13m wide	Single column 7m high	Spread foot-ings	Cantilever bearing wall w/spread footings	Small cost increase (1%) in footings and increasing gap width. Designed by 1977 W DOT spec. for E.Q.
21. Yakima River Washington	174	6	0.10 A_v= 0.15	C	2	Prestressed girder 16m wide.	Two column bents	Spread foot-ing.	Stub wall	An 8% increase in total cost compared to original struc-ture. Designed by 1977 W DOT spec. for earthquake.

* Underlined values indicate approximate initial design values used.

NEW SPECIFICATIONS FOR EARTHQUAKE-RESISTANT

DESIGN OF JAPANESE HIGHWAY BRIDGES

by

Eiichi Kuribayashi

Toshio Iwasaki

Osamu Ueda

ABSTRACT

This paper briefly discusses the history of seismic design provisions for highway bridges in Japan, and introduces the new specifications (Japan Road Association, 1980) for earthquake-resistant highway bridge design.

INTRODUCTION

Since the Kanto Earthquake of 1923 Japan has experienced a number of severe earthquakes, and the incidence of damage to highway bridges is considerable. Stemming from the damage caused by the Kanto Earthquake, seismic forces were first taken into account in highway bridges design in 1926. The seismic coefficient method in the practical design of structures was developed and introduced at that time. After experiencing severe damage during consecutive strong earthquakes, seismic regulations were reviewed and amended several times. In view of the damage caused by the Niigata Earthquake of 1964 the amended specifications for earthquake-resistant design of highway bridges were issued in 1971 by the Japan Road Association. Much work has been done to establish more rational seismic criteria for highway bridges. This includes recent advancements in earthquake engineering associated with bridges, the damage experience due to the Miyagi-ken-oki Earthquake of 1978, and the new specifications which were completed in March, 1980. This paper briefly describes the history of highway bridge seismic design codes in Japan, and introduces the new specifications (JRA, 1980) for highway bridge seismic design.

HISTORY OF EARTHQUAKE RESISTANT DESIGN PROVISIONS FOR HIGHWAY BRIDGES IN JAPAN

The Ministry of Home Affairs stipulated, in 1926, the "Specifications for Design of Road," which are parts of the "Road Laws." In the specifications, seismic forces were first taken into account in the design of highway bridges, since several highway bridges sustained substantial damage during the 1923 Kanto Earthquake. The specifications provided that highway bridges be designed using the seismic coefficient method, in which horizontal seismic coefficients were taken from 0.1 to 0.4. The values of the coefficients were dependent on areas and ground conditions. For bridges to be constructed in Tokyo and Yokohama, seismic coefficients of 0.3 or more were recommended. This seems due to the substantial damage to bridge structures in the areas during the Kanto Earthquake.

The Ministry of Home Affairs issued, in 1939, "Specifications for Design of Steel Highways," which took place of the earlier specifications. The new ones stipulated both a horizontal coefficient of 0.2 and a vertical coefficient of 0.1.

The specifications were revised again in 1964 by the Japan Road Association, with a commission from the Ministry of Construction. The revised specifications specified that

both a horizontal coefficient of 0.1 to 0.35 depending on areas and ground conditions, and a vertical coefficient of 0.1 shall be considered in the aseismic design.

In view of extensive damage to bridge structures from the 1964 Niigata Earthquake, the Japan Road Association, also with a commission from the Ministry of Construction, drew up in January 1971, comprehensive specifications [1,2] exclusively for earthquake-resistant design of highway bridges. In the 1971 specifications, two methods are provided for a seismic design. One is the conventional seismic coefficient method for rigid structures, where the horizontal coefficient ranges between 0.1 and 0.24 depending on areas, ground conditions, and importance. The other is the modified seismic coefficient which considers structural responses for comparatively flexible structures, where horizontal seismic coefficients vary from 0.05 to 0.3 depending on fundamental natural periods in addition to the three factors above.

During these years after the 1971 specifications were issued, technological advancements in bridge engineering and earthquake engineering have been remarkable. Especially comprehensive research works were executed in the New Aseismic Technology Development Project of the Ministry of Construction from 1972 through 1976. The results of the investigations achieved in this project were put into a unified form of provisions on earthquake resistant design for civil engineering structures and building structures, and "A Proposal for Earthquake Resistant Design Methods," was issued by the Ministry of Construction in March, 1977 [3,4]. Also, the Miyagi-ken-oki Earthquake of June 12, 1978 caused extensive damage to numerous bridges [5]. In view of the results of the above investigations and the damage features, the Japan Road Association amended the 1971 specifications and stipulated, in March 1980, new specifications for earthquake resistant design of highway bridges [6]. The new specifications became a part of "Specifications of Highway Bridges," which consist of five parts, Part I General Specifications (1972), Part II Steel Bridges (1972), Part III Concrete Bridges (1977), Part IV Substructures (1980), and Part V Earthquake Resistant Design. The new specifications (Part V Earthquake Resistant Design) will be outlined below. [6,7,8]

Further, characteristic criteria was proposed, between 1966 and 1968, tentatively for the aseismic design of highway bridges relating to specific projects administered by the Japan Highway Public Corporation (JHPC), the Metropolitan Expressway Public Corporation (MEPC), the Hanshin Expressway Public Corporation (HEPC) and the Honsyu Shikoku Bridge

Authority (HSBA). The Japanese National Railways (JNR) stipulated in 1968, and revised in 1979, its own criteria for aseismic design of railway bridges.

Table 1 lists briefly this history of design loads (primarily seismic loads) for highway bridges in Japan. [9]

NEW SPECIFICATIONS (JRA-1980)

Outline

Efforts to revise the 1971 specifications into the form of Part V. of the Specifications for Highway Bridges have been underway by the Earthquake Resistant Design Subcommittee from 1977 to 1980, and the new specifications were issued in April, 1980. The contents of the new specifications are presented in Table 2. They apply to the design of highway bridges with span lengths not longer than 200 meters.

The specifications basically stipulate using seismic coefficient methods and provide two methods in determining design seismic coefficients. One is the conventional seismic coefficient method that applies to the design of relatively rigid structures. The other is the modified seismic coefficient method which considers structural responses that apply to the design of relatively flexible structures. Provisions on seismic motions in dynamic analysis, and seismic coefficient in ductility analysis, were newly introduced.

The principal features and improvements of the design methodology in the new specifications are described as follows:

Seismic Coefficient Method

(1) In the seismic coefficient method for relatively rigid structures, the horizontal design seismic coefficient (kh) shall be determined by

$$k_h = \nu_1 \cdot \nu_2 \cdot \nu_3 \cdot k_0 \tag{1}$$

where k_h = horizontal design seismic coefficient,

k_0 = standard horizontal design seismic coefficient (= 0.2),

ν_1 = seismic zone factor,

ν_2 = ground condition factor,

ν_3 = importance factor.

344

The values of ν_1, ν_2, and ν_3 are shown in Tables 3, 4 and 5, respectively. The minimum values of k_h shall be taken as 0.1.

(2) The vertical design seismic coefficient may generally be considered as zero, except for special portions, such as bearing supports.

(3) The horizontal design seismic coefficient for structural parts, soils, and water below the ground surface may be considered as zero.

(4) Hydrodynamic pressures and earth pressures during earthquakes are specified in the specifications.

(5) Special attention is paid to very soft soil layers and soil layers vulnerable to liquefaction during earthquakes. The bearing capacities of these layers were either decreased or neglected in the design, in order to assure high earthquake-resistance for structures that are built in these layers.

(6) Special attention is also paid to the design of structural details, because of damage previously experienced on bridge structures. Provisions are specified for bearing supports and devices to prevent bridge girders from falling.

(7) Increases in allowable stresses of materials may be considered in the earthquake-resistant design, magnitudes of increases for various materials are specified in several related specifications.
The increasing rates are as follows:

concrete in reinforced concrete structures:	50%
reinforcements in reinforced concrete structures:	50%
structural steel for superstructures:	70%
structural steel for substructures:	50%
concrete in prestressed concrete structures subjected to compressive forces:	65%
foundation soils:	50%

Seismic Zoning Map

The newly developed seismic zoning map illustrated in Figure 1 was adopted. The map is based on the Proposal for Earthquake Resistant Design Methods [3,4] is intended to unify seismic zoning maps currently applied to civil engineering structures and buildings. Slight modifications were introduced to the proposed original map out of administrative considera-

tions. The values of ν_1, are 1.0, 0.85 and 0.7 for A, B, and C zones, respectively, as shown in Table 3.

Classification of Ground Conditions

In the previous specifications, the classification of ground conditions was determined in accordance with geological conditions. However, since subsurface ground responses during earthquakes would generally be more largely affected by the predominant period of the ground, it is considered more reasonable to classify grounds into groups in terms of the period of the ground. Consequently in the new specifications, the ground conditions are classified into four groups according to Table 4, in which the characteristic value of ground, T_g, is stipulated to be principally calculated by the following equation:

$$T_g = \sum_i \frac{4Hi}{V_{si}} \tag{2}$$

where T_g = Characteristic value of ground (second)

Hi = Thickness of i-th subsoil layer (m)

V_{si} = Shear wave velocity of i-th subsoil layer at low strain (around 10^{-4} percent)

As for shear wave velocities, it is recommended that it be directly measured through site investigation. Shear wave velocities may be assumed from N-values of standard penetration tests by

$$V_s = \begin{cases} 100 \ N^{1/3} \ (1 \leqslant N \leqslant 25) \text{ for cohesive soils} \\ 80 \ N^{1/3} \ (1 \leqslant N \leqslant 50) \text{ for sandy soils} \end{cases} \tag{3}$$

The baserock for calculation of Eq. (2) is stipulated to take on the soil layer that has a shear wave velocity at low strain equal to 280 m/sec or higher and is not underlaid by materials having significantly lower shear wave velocities.

The characteristic value T_g implies a natural period of subsurface ground at low strain levels. The classification of T_g shown in Table 3 was proposed from numerical seismic analyses of various types of subsurface grounds. Such analyses revealed that the natural period T_s of subsurface ground at high strain levels which would be expected to occur during strong earthquakes can be approximately obtained by the following equation.

$$T_s = 1.25 \ T_g \tag{4}$$

It was also found that ground conditions could be adequately classified into four groups by taking T_s as $T_s < 0.25$ seconds, $0.25 \leqslant T_s < 0.5$ seconds, $0.5 \leqslant T_s < 0.75$ seconds and $T_s \geqslant 0.75$ seconds. The characteristic values T_g presented in Table 4 were thus obtained by substituting the above mentioned T_s into Eq. (4).

Figure 2 is one of representative results of analyses showing a relationship between the characteristic values T_g and the thickness of soil deposits. It is apparent from the result that the classification of ground conditions determined by the characteristic value T_g as shown in Table 4 can also be approximately estimated by the thicknesses of alluvial and diluvial layers. It is therefore recommended to use this relation to classify the ground condition when T_g cannot be obtained.

Figure 3 shows a comparison of the ground classifications which were provided in the 1971 specifications and in the new specifications. It is understood from the results that some ground areas which are evaluated as Groups 1 and 2 in the current specifications turn into Groups 2 and 3, respectively, in the new specifications.

Liquefaction of Sandy Soil Layers

In the 1971 specifications, it was stipulated that saturated sandy soil layers that are within 10 meters of the actual ground surface, and that have a standard penetration test N-value less than 10, a coefficient of uniformity less than 6, and also a D_{20}-value on the grain size accumulation curve between 0.04 mm and 0.5 mm, shall have a high potential for liquefaction during earthquakes, and that bearing capacities of these layers shall be neglected in design.

After the Niigata Earthquake, comprehensive studies were conducted to assess the vulnerability of saturated sandy soils. Based on these studies, the provisions for lique-faction are improved in the new specifications as follows:

(1) <u>Sandy Soil Layers Needed to be Checked for Liquefaction</u> -- Saturated alluvial sandy layers which have a water table within 10 meters from the ground surface, and have D_{50}-values on the grain size accumulation curve between 0.02 and 2.0 mm, are vulnerable to liquefaction for the depth between 0 and 20 m, and liquefaction potential of these layers shall be estimated according to item (2).

(2) <u>Estimation of Liquefaction</u> -- For those soil layers which are judged to be vulnerable for liquefaction, liquefaction potential shall be checked based on liquefaction resistance factor, F_L, defined by the following equation.

$$F_L = \frac{R}{L} \tag{5}$$

where F_L = liquefaction resistance factor

R = resistance of soil elements to dynamic loads, and

$$R = R_1 + R_2 \tag{6}$$

R_1 and R_2 shall be determined in accordance with Figures 6 and 7, respectively.

L = dynamic loads to soil elements induced by earthquake motion

$$L = r_d k_s \frac{\sigma_v}{\sigma_v'} \tag{7}$$

$$r_d = 1.0 - 0.015z \tag{8}$$

z = depth from the actual ground surface (m)

k_s = seismic coefficient for evaluation of liquefaction, and shall be determined by the following equation:

$$k_s = \nu_1 \cdot \nu_2 \cdot \nu_3 \cdot k_{so} \tag{9}$$

ν_1, ν_2, ν_3 = seismic zone factor, ground condition factor, and importance factor, provided in Tables 3, 4 and 5, respectively.

k_{so} = 0.15

σ_v = total overburden pressure (kg/cm^2)

σ_v' = effective overburden pressure at the static condition (kg/cm^2)

Soil layers having a liquefaction resistance factor F_L smaller than 1.0 shall be judged to liquefy during earthquakes. Figures 4 and 5 are graphic illustrations of the first term R_1 and the second term R_2 represented in the following equations, which were proposed based upon the results of laboratory dynamic triaxial tests on soil specimens taken from several sites in Japan [10,11].

348

$$R = \begin{cases} 0.0882 \sqrt{\dfrac{N}{\sigma'_v + 0.7}} + 0.19 & (0.02 \text{ mm} \leqslant D_{50} \leqslant 0.05 \text{ mm}) \\[3ex] 0.0882 \sqrt{\dfrac{N}{\sigma'_v + 0.7}} + 0.225 \log_{10}(\dfrac{0.35}{D_{50}}) & (0.05 \text{ mm} < D_{50} \leqslant 0.6 \text{ mm}) \\[3ex] 0.0882 \sqrt{\dfrac{N}{\sigma'_v + 0.7}} - 0.05 & (0.6 \text{ mm} < D_{50} \leqslant 2.0 \text{ mm}) \end{cases}$$

(3)   Treatment of Soil Layers which were Judged to Liquefy -- For those soil layers which are judged to liquefy by the above estimation and are within 20 meters of the actual ground surface, bearing capacities and other soil constants shall be either neglected or reduced in the seismic design by multiplying the original bearing capacities by reduction factors D_E which are determined in accordance with F_L-values and tabulated in Table 6.

Modified Seismic Coefficient Method

In the 1971 specifications, the modified seismic coefficient method was provided to apply to bridges which have flexible piers and fundamental periods longer than 0.5 seconds, such as those with piers taller than 25 meters above the ground surface. Accounting for seismic responses, magnification factors (β) for the modified seismic coefficient method were stipulated. However, it has been pointed out that fundamental natural periods sometimes exceed 0.5 seconds even for those bridges with piers lower than 25 meters above the ground surface. Using experimental data on the relationship between fundamental natural periods and pier heights, it is modified in the new specifications so that the modified seismic coefficient method shall apply to bridges which have flexible piers and long fundamental periods, such as those with piers higher than 15 meters above the ground surface.

In addition to the above change, the following two modifications were also introduced:

(1)   The magnification factors (β) are modified as shown in Table 7 and Figure 6 so as to avoid a sudden change of β-value at a period of 0.5 seconds.

(2)   In the 1971 specifications, the effects of subsoil conditions were not considered in estimating fundamental natural periods. Since the effects of subsoils would be predominant in calculating fundamental natural periods, especially for bridges with short piers, it is stipulated in the new specifications that the effects of subsoils shall be taken into account for those bridges which are constructed in the soft ground. It is recommended that the fundamental natural period for the individual system consisting of each substructure

and the part of superstructures supported by it be estimated using the following equation.

$$T = 2.01 \sqrt{\delta} \tag{11}$$

where T = Fundamental natural period in seconds of the system consisting of a substructure and the section of the superstructures supported by it.

δ = Maximum horizontal displacement (in meters) of the pier when subjected to the dead weight of the section of superstructure supported by the substructure and also to 80 percent of the dead weight of the substructure above the ground surface assumed in earthquake resistant design.

Seismic Motions in Dynamic Analysis

In the 1971 specifications, it is stipulated that dynamic earthquake response analyses shall be adopted for those bridges for which detailed investigations are required. In the new specifications, an article is introduced concerning the seismic motions to be utilized in dynamic response analyses. The principal provisions are as follows:

(1) Dynamic response analyses may apply to those bridges which are designed either by the seismic coefficient method or the modified seismic coefficient method, in order to investigate precisely the earthquake resistivity of bridges in terms of ductilities and maximum bearing capabilities. Dynamic analyses are needed for those bridges having structural systems which are significantly different from those assumed in the seismic coefficient method or the modified seismic coefficient method, those bridges having new structural types for which the experience of damage accumulated from past earthquakes cannot be adequately extended, those bridges which are constructed on extremely soft soil deposits and are expected to deform considerably during earthquakes, and those bridges for which detailed investigations on requirements of ductility of structures are needed.

(2) Two types of dynamic earthquake response analyses, i.e., response spectrum analyses and time history analyses can be used.

(3) Input motions used for the time history analyses shall be selected from strong-motion acceleration records which consider the dynamic characteristics of bridges and the characteristics of the records.

In determining input seismic motions, two procedures are proposed. One is to estimate expected intensities at the side based on the life-time of the bridge and the recurrence period of earthquake events. Another procedure is to estimate the expected ground motions by assuming the locations and the magnitudes of specific earthquakes around the site. In the second, ground motions can be evaluated either by the theory of seismic gaps or the statistics of the past historical earthquakes. It is also recommended that the input seismic motions be selected according to the objectives of the earthquake response analyses. It states that bridges shall maintain their functions for those motions which are expected to occur two or three times during the bridge lifetime, and they shall survive those motions which are expected to occur once, or rarely, at the site.

(4) In utilizing seismic ground motions recorded on soft soil deposits which have appreciably different ground conditions compared to those at a planned construction site, it is recommended such effects be taken into account in the analyses. For such purposes, earthquake response analyses based on the baserock motions are recommended.

(5) Input earthquake response spectra used for the response spectrum analyses shall be determined using the response spectra calculated from strong-motion accelerations. In an appendix to the new specifications, the results of statistical analyses of strong-motion acceleration records are presented. Some of the representative earthquake response spectra and relations between maximum horizontal accelerations and epicentral distances are presented in Figures 7 and 8, respectively [12].

Seismic Coefficient in Ductility Analysis

In order to avoid brittle failure during earthquakes, it is extremely important that reinforced concrete structures have adequate ductility. A provision that stipulates the seismic coefficient used for the design of reinforced concrete piers with ductility is introduced. It stipulates that the seismic coefficient in ductility analysis shall be determined using the following equation.

$$k_{hd} = \nu_4 \cdot k_h \tag{12}$$

where k_{hd} = seismic coefficient in ductility analysis

ν_4 = structural characteristics factor (greater than 1.3)

k_h = horizontal design seismic coefficient provided in Eq. (1).

Table 8 shows maximum ductilities of ordinary RC bridge piers which were analytically determined to account for deformation due to bending of piers and deformation of reinforcement pulled out from footings, in which the critical strains of concrete were assumed as 0.35 percent. It can be recognized from these results that the maximum ductilities of bridge piers normally designed by the seismic coefficient method can be taken as approximately 6. However, since values for maximum ductilities are derived from analytical calculations for a half cycle loading, it is considered desirable to take maximum design ductilities to be smaller than 6. Considering the fact that concrete pier ductility decreases significantly under alternatingly repeated loading conditions [13], one third of the values tabulated in Table 8, which lead to about 2, is recommended as the ductility factor for design purposes.

CONCLUSIONS

Earthquake resistant highway bridge design criteria in Japan is briefly described with emphasis given to improvements and modifications in the new specifications (JRA-1980). In view of the history of the earthquake resistant design of highway bridges, it is considered necessary to concentrate a comprehensive investigation on the following subjects in the future.

(1) Analysis of the Effects of Soil-Structure Interactions

Bridge construction on deep, soft soil deposits has increased recently. From the evidence of past, extensive earthquake damage, it is well recognized that the influence of surrounding subsurface soils are very important for the seismic responses of substructures, especially for substructures which are embedded in deep soft ground. Consequently, considerable interest has been focused on the soil-structure interaction effects on such structures by model experiments and theoretical analyses. However, very limited research has been undertaken to investigate the seismic response of actual substructures during strong seismic excitations. Investigations of the effects of soil-structure interaction which utilize strong-motion records obtained at actual bridges are encouraged. For this purpose, it is recommended that strong motion observations, especially simultaneous observations of both the bridges and the surrounding subsurface grounds, be extended.

(2) Analysis of Seismic Behavior of Substructures in Liquefied Soil Layers

Due to the comprehensive research conducted after the 1964 Niigata Earthquake, determining the vulnerability of saturated sandy deposits and judging in situ liquefaction potential became both possible and practical. However, further investigation of the seismic behavior of substructures in liquefied layers is needed, as is the development of suitable earthquake resistant design procedures for bridges under such conditions.

(3) Experiments on Ductilities of Bridge Piers

Seismic damage to bridges were most commonly caused by pier and foundation failures. It is, therefore, extremely important to prevent brittle failure to substructures. Up to the present, only very limited experimental studies have been conducted on the hysteretic behavior of bridge piers under cyclic loading. Such a lack of data on the hysteretic response of piers is one of the major obstacles to introducing limit design to bridges to account for the ductility of members. It is recommended that extensive efforts be devoted to accumulating such experimental data.

(4) Design Details of Bearing Supports and Connections

For providing highway bridges with adequate resistance to seismic disturbances, it is very important to give special attention to the design details of connections between super-structures and substructures, to preventing girder fall, and to avoid severe damage which is caused by bearing support failures.

REFERENCES

[1] Japan Road Association, "Specifications for Earthquake Resistant Design of Highway Bridges," 1971.

[2] Kawakami, K., Kuribayashi, E., Iwasaki, T. and Iida, Y., "On Specifications for Earthquake Resistant Design of Highway Bridges," (January, 1971), 7th Joint Meeting, U.S.-Japan Panel of Wind and Seismic Effects, UJNR, Tokyo, 1975.

[3] Ministry of Construction, "A Proposal for Earthquake Resistant Design Methods," 1977 (In Japanese).

[4] Nakano, K. and Ohashi, M., "A Proposal for Earthquake Resistant Design Methods," 9th Joint Meeting, U.S.-Japan Panel on Wind and Seismic Effects, UJNR, Tokyo, 1977.

[5] Okubo, T. and Iwasaki, T., "Summary of Experimental and Analytical Seismic Research Recently Performed on Highway Bridges," Workshop on Research Needs of Seismic Problems Related to Bridges, Palo Alto, California, USA, 1979.

[6] Japan Road Association, "Specifications for Highway Bridges," Part V, Earthquake Resistant Design, 1980 (In Japanese).

[7] Ohashi, M., Kuribayashi, E., Iwasaki, T., and Kawashima, K., "An Overview of the State of the Practice in Earthquake Resistant Design of Highway Bridges in Japan," Workshop on Research Needs on Seismic Problems Related to Bridges, Palo Alto, California, USA, 1979.

[8] Kuribayashi, E., Iwasaki, T., "Progress Report on Research Work in Bridge Earthquake Engineering at the Public Works Research Institute, Japan," Seventh World Conference on Earthquake Conference, Istanbul, Turkey, 1980 (to be presented).

[9] Iwasaki, T., Penzien, J., and Clough, R. W., "Literature Survey - Seismic Effects on Highway Bridges," EERC Report No. 72-11, University of California, Berkeley, 1972.

[10] Ohashi, M., Iwasaki, T., Tatsuoka, F. and Tokida, K., "A Practical Procedure for Assessing Earthquake-Induced Liquefaction of Sandy Deposits," 10th Joint Meeting, U.S.-Japan Panel on Wind and Seismic Effects, UJNR, Washington, D.C., 1978.

[11] Iwasaki, T., Tatsuoka, F., Tokida, K. and Yasuda, S., "A Practical Method for Assessing Soil Liquefaction Potential Based on Case Studies at Various Sites in Japan," Second International Conference on Microzonation for Safer Construction Research and Application, San Francisco, 1978.

[12] Iwasaki, T., Katayama, T., Kawashima, K. and Saeki, M., "Statistical Analysis of Strong-Motion Acceleration Records Obtained in Japan," 2nd International Conference on Microzonation for Safer Construction Research and Application, San Francisco, 1978.

[13] Osaka, Y. and Ohta, M., "Experimental Study on the Behavior of Reinforced Concrete Bridge Piers under Seismic Alternating Load," A.I.C.A.P.-C.E.P. Symposium on Structural Concrete under Seismic Actions, Rome, 1979.

Table 1 History of Design Loads for Highway Bridges in Japan
(Primarily Seismic Loads)

Year	Name of Regulations	Design Live Loads				Impact Loads	Seismic Loads k: Horizontal Seismic Coefficient	Other Seismic Regulations (k: seismic coef.)	Major Earthquake
		Class	Truck Roller Loads Streetcar	Uniform Loads	Line Loads				
1) 1886	Order No. 13 Ministry of Home Affairs (MHA)			U-454 kg/m	–	not consi- dered	not considered		(M>7) after Rika Nenpyo (1971)
2) 1906	Order MHA		R-13.6 t S-12.7	U-400 600 kg/m (carriage way) U-270 400 kg/m (footway)		not consi- dered	not considered		
3) 1919	Road Laws MHA		R-13.6 t T-11.2 t S-30 t	Same as 2)	–	not consi- dered	not considered	1924 Building Law (k≥0.1) 1950. Kawasumi's Seismic Map.	1923 Kanto (M=7.9)
4) 1926	Specifications for Design of Roads, Road Laws, MHA	1st 2nd 3rd	T-12 t T-8 t T-6 t	U-600 kg/m U-500 kg/m U-500 kg/m	–	consi- dered	Seismic Coefficient Method k=0.15∿0.4 depending on location and ground condition (k≥0.3 advised in Tokyo, Yokohama)		
5) 1939	Specifications for Design of Steel High- way Bridges, MHA	1st 2nd	T-13 t T-9 t	U-500 kg/m U-400 kg/m		consi- dered	Seismic Coefficient Method k_h=0.2, k_v=0.1	1950. New Building Law (k=0.2, H≤16m increase 0.01 per an increase of 4m above 16(m))	1946.Nankai (M=8.1) 1948. Fukui (M=7.3) 1952. Tokachi- oki.(M=8.2)
6) 1956 (and 1964)	Revision of Specifica- tions for Design of Steel HIGHWAY Bridges, JRA	1st 2nd	T-20 t T-14 t	– –	L-20(5t/m) L-14(3.5t/m)	consi- dered	Seismic Coefficient Method k=0.1∿0.35 depending on location and ground conditions		
7) 1964 to 1971	Specifications for Design of Substructures of Highway Bridges, JRA	Same as 6)					same k as (6) Detailed calculation methods	1964. High- Rise Building (H≥45m) h=(0.18∿0.36) /T(T:period) (0.05≤k≤0.2) 1965. Report of JSCE on Civil ERD of Engineering Structures.	1964. Niigata (M=7.5)
8) 1966* (and 1970)	Design Standards, JHPC	Same as 6)					Design Code for High- Rise Bridges, (Increase in k with the height of the piers)		
9) 1967*	Specifications for Earthquake Resistant Design of Honshu-Shikoku Bridges, JSCE	Special Live Loads and Impact Loads for Suspension Bridges are Considered					Modified Seismic Co- efficient Method (Basic Coef. k=0.2)		1968. Tokachi- oki(M=7.9)
10) 1967*	Specifications for Earthquake-Resistant Design of Metropolitan Expressway Public Corporation, MEPC	Same as 6)					Seismic Coef. Method k=0.2∿0.3	1968. Report of JSCE on Earthquake- Resistant Design of Substructures of Railway Bridges.	
11) 1968*	Aseismic Design Standards, HEPC	Same as 6)					Seismic Coef. Method k=0.2∿0.28		
12) 1971	Specifications for Earthquake-Resistant Design of Highway Bridges, JRA	same as 6)					Seismic Coef. Method k=0.1∿0.24 (Rigid) Modified SCM. k=0.05∿0.3 (Flexible)	1977. A Proposal for Earthquake Resistant Design Methods (MDC) 1979. New Specifi- cations for Earth- quake-Resistant Design of Railway Facilities	1978. Miyagiken- Oki(M=7.4)
13) 1980	Part V Earthquake Resistant Design, Specifications for Highway Bridges (New Specifications), JRA	same as 6)					Seismic Coef. Method k=0.1∿0.24 (Rigid) Modified SCM. k=0.05∿0.3 (Flexible) Earthquake Response Analysis (Very Flexible Bridges)		

* Specifications from 8) to 11) are for highway bridges related to special large projects.

Table 2 Contents of Part V Earthquake Resistant Design, Specifications for Highway Bridges [Japan Road Association, 1980]

Contents		Same As the Previous Spec.(1971)	Modified		Newly Introduced
			Slightly	Completely	
Chapter 1	General 1.1 Scope	○			
	1.2 Definitions of Terms	○			
Chapter 2	Basic Principles for Earthquake Resistant Design		○		
Chapter 3	Loads and Conditions in Earthquake Resistant Design 3.1 General	○			
	3.2 Seismic Effects	○			
	3.3 Seismic Forces Transmitted from Superstructures to Substructures		○		
	3.4 Earth Pressures during Earthquakes		○		
	3.5 Hydrodynamic Pressures during Earthquakes	○			
	3.6 Classification of Ground Conditions in Earthquake Resistant Design		○		
	3.7 Soil Layers Whose Bearing Capacities are Reduced in Earthquake Resistant Design			○	
	3.8 Ground Surface Assumed in Earthquake Resistant Design			○	
Chapter 4	Design Seismic Coefficient 4.1 General		○		
	4.2 Design Seismic Coefficient in the Seismic Coefficient Method	○			
	4.3 Factors for Modifying the Standard Horizontal Design Seismic Coefficient		○		
	4.4 Design Seismic Coefficient in the Modified Seismic Coefficient Method Considering Structural Response			○	
	4.5 Earthquake Motions in the Earthquake Response Analyses				○
	4.6 Design Seismic Coefficient Accounting of Ductilities				○
Chapter 5	General Provisions for Design of Structural Details 5.1 General		○		
	5.2 Devices for Preventing Superstructures from Falling		○		
	5.3 Vertical Seismic Forces for Design of Connections between Superstructures and Substructures	○			
	5.4 Methods for Transmitting Seismic Forces at Connections between Superstructures and Substructures		○		
	5.5 Devices Expected for Decreasing Seismic Forces	○			
Appendices I.	References on Liquefaction			○	
II.	Examples of Classification of Ground Conditions			○	
III.	Example of Estimation of Design Horizontal Seismic Coefficient	○			
IV.	References on Earthquake Motions in the Earthquake Response Analyses			○	
V.	Example of Calculating Natural Periods Utilized in the Modified Seismic Coefficient Method			○	
VI.	Example of Calculating Ductilities				○
VII.	Major Related Provisions Concerning Earthquake Resistant Design		○		
VIII.	Detailed Practices			○	
IX.	References			○	

Table 3 Seismic Zone Factor ν_1 for Highway Bridges

Zone[1]	Value of ν_1
A	1.00
B	0.85
C	0.70

Note: 1) Zones A, B and C are illustrated in Fig. 1.

Table 4 Classification of Ground Conditions and Value of ν_2

Group	Characteristic Value T_g (second)	Value of ν_2
1	$T_g < 0.2$	0.9
2	$0.2 \leqq T_g < 0.4$	1.0
3	$0.4 \leqq T_g < 0.6$	1.1
4	$0.6 \leqq T_g$	1.2

Table 5 Importance Factor ν_3 for General Highway Bridges

Group	Definitions	Value of ν_3
1	Bridges on expressway (limited-access highways), general national highways and principal prefectural highways. Important Bridges on general prefectural highways and municipal highways.	1.0
2	Other than the above	0.8

Note: The value of ν_3 may be increased up to 1.10 for special cases in Group 1.

Table 6 F_L-D_E Relation

F_L	Depth, Z(m)	Reduction Factor, D_E
$F_L \leqq 0.6$	$Z \leqq 10$	0
	$10 < Z \leqq 20$	1/3
$0.6 < F_L \leqq 0.8$	$Z \leqq 10$	1/3
	$10 < Z \leqq 20$	2/3
$0.8 < F_L \leqq 1.0$	$Z \leqq 10$	2/3
	$10 < Z \leqq 20$	1
$1.0 < F_L$	–	1

Table 7 Magnification Factor β for Modified Seismic Coefficient Method

G. C.	β-value			
Group 1	$\beta = 2T$ $0.5 \leqq T \leqq 0.625$	$\beta = 1.25$ $0.625 \leqq T \leqq 1.12$	$\beta = 1.40/T$ $1.12 \leqq T \leqq 2.8$	$\beta = 0.50$ $T \geqq 2.8$
Group 2	$\beta = 2T$ $0.5 \leqq T \leqq 0.625$	$\beta = 1.25$ $0.625 \leqq T \leqq 1.4$	$\beta = 1.75/T$ $1.4 \leqq T \leqq 3.5$	$\beta = 0.50$ $T \geqq 3.5$
Group 3	$\beta = 2T$ $0.5 \leqq T \leqq 0.625$	$\beta = 1.25$ $0.625 \leqq T \leqq 1.68$	$\beta = 2.10/T$ $1.68 \leqq T \leqq 4.2$	$\beta = 0.50$ $T \geqq 4.2$
Group 4	$\beta = 2T$ $0.5 \leqq T \leqq 0.625$	$\beta = 1.25$ $0.625 \leqq T \leqq 2.0$	$\beta = 2.50/T$ $2.0 \leqq T \leqq 5.0$	$\beta = 0.50$ $T \geqq 5.0$

Table 8 Maximum Ductilities from the Analyses of RC Bridge Piers

Section		Maximum Ductility	Number of Piers Examined
Circle-Shaped Column		$6.4 \sim 8.1$	6 Specimens
Hollowed-Circle Shaped Column		$5.8 \sim 6.8$	6 Specimens
2-Rectangular Column	Longitudinal	$5.6 \sim 10.5$	6 Specimens
	Transverse	$5.7 \sim 8.6$	4 Specimens
Oval-Shaped Column	Longitudinal	$5.3 \sim 7.3$	3 Specimens

Note: Ogasawara Islands:Zone C

A :
B :
C :
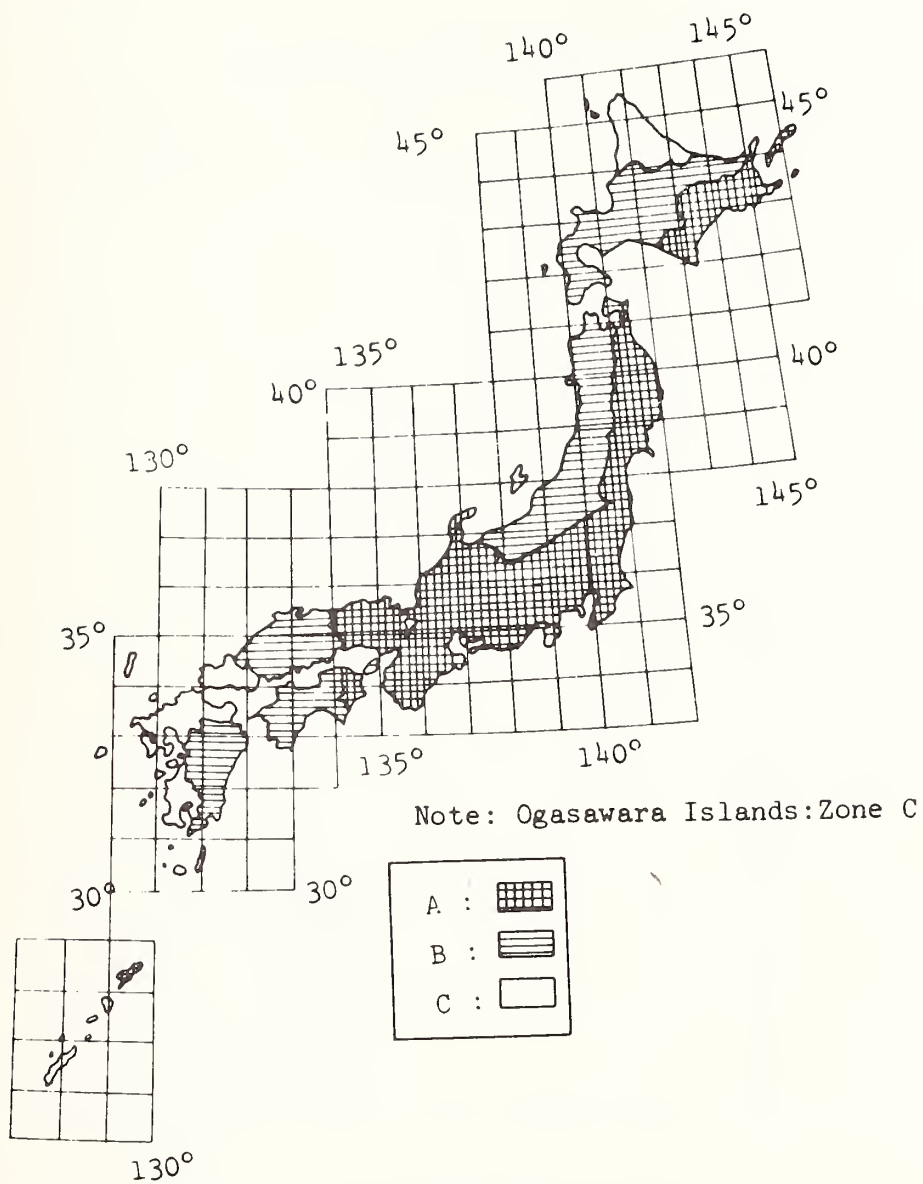
Fig. 1 Seismic Zoning Map
(New Specifications)
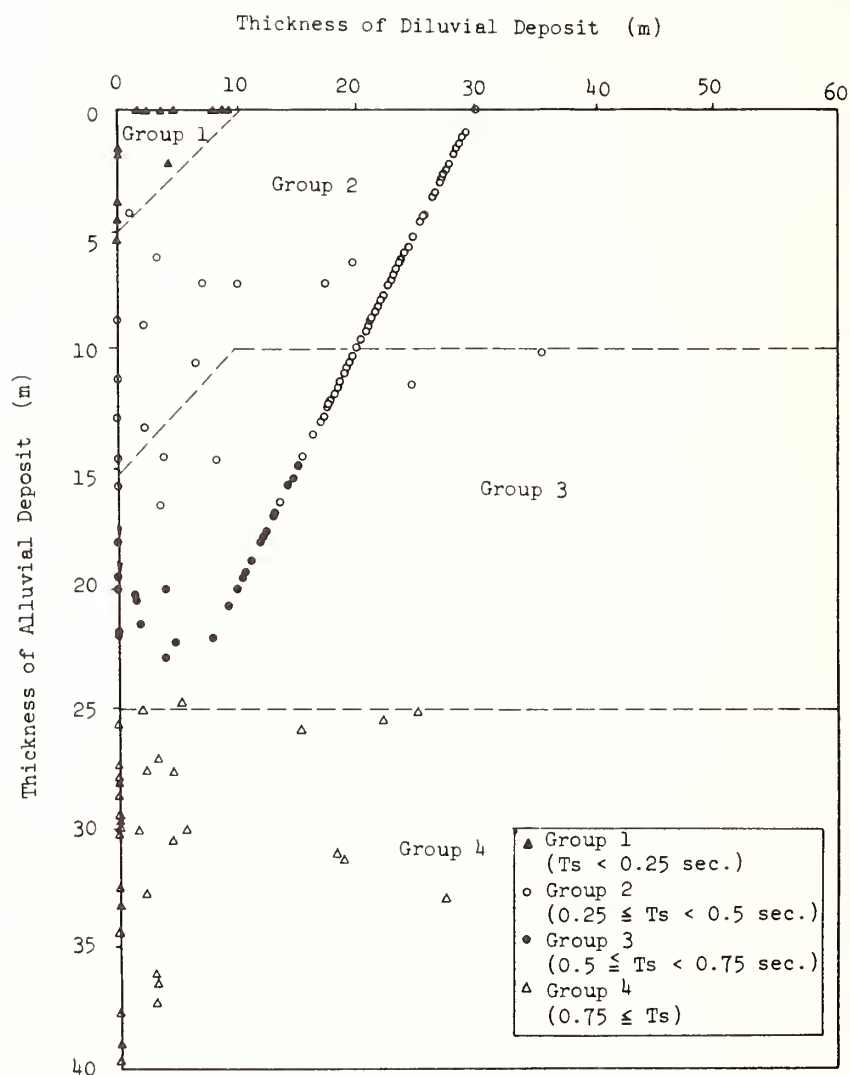
Fig. 2 Classification of Ground Conditions in Terms of Thicknesses of
Alluvial and Diluvial Soil Layers

Thickness of Diluvial Deposit (m)
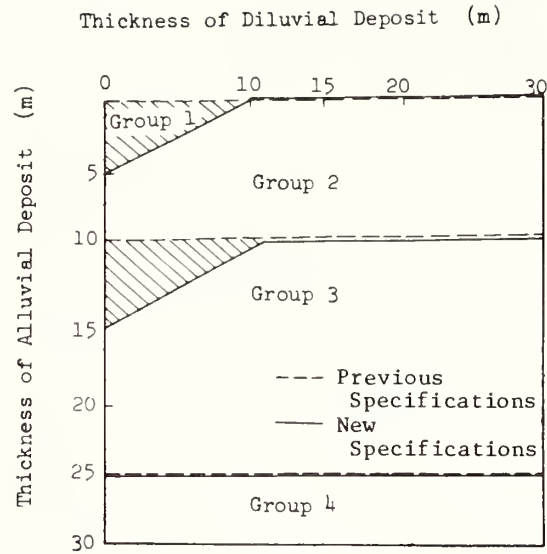
Fig. 3 Comparison of Ground Conditions Provided
in Previous and New Specifications

N-Value by the Standard Penetration Test
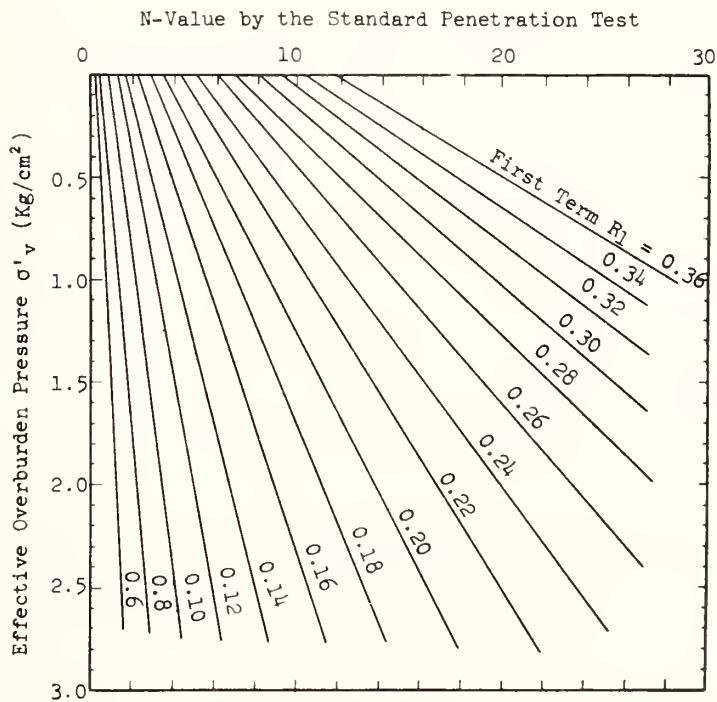
Fig. 4 R_1-Value (First Term of Resistance R)
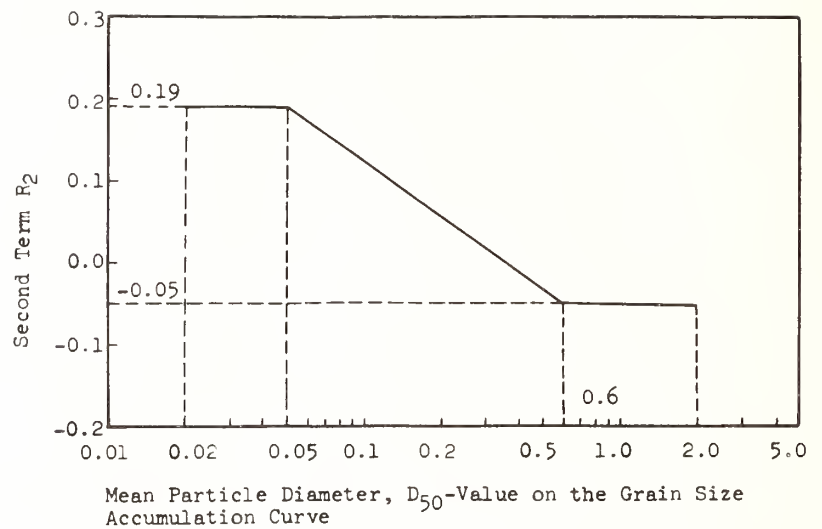
Fig. 5 R_2-Value (Second Term of Resistance R)
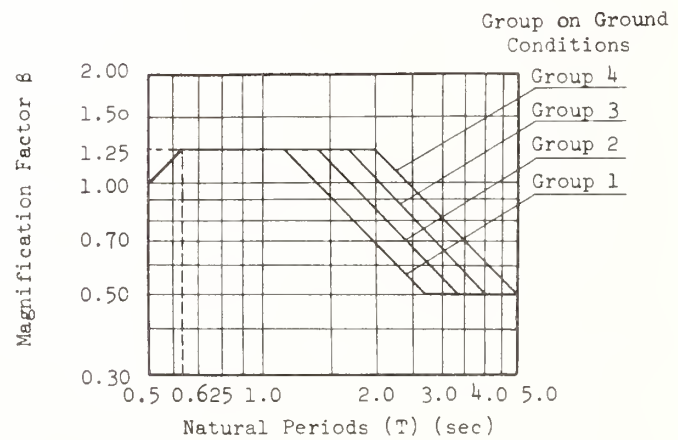
Fig. 6   Magnification Factor for the Modified
Seismic Coefficient Method (New Specifications)

Fig. 7　Response Spectrum Curves β in case of 7.5 ≦ M ≦ 7.9
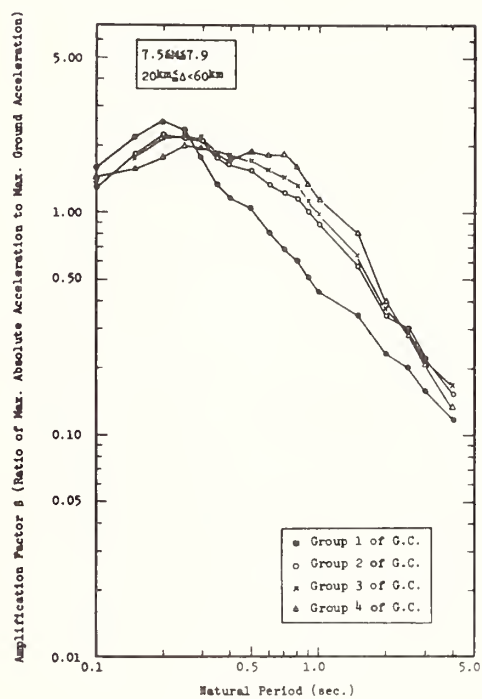
(a)　20km ≦ Epicentral Distance Δ < 60km
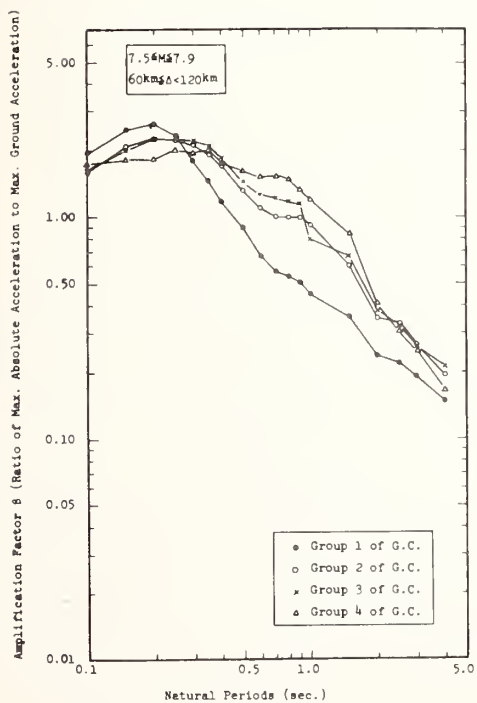
(b)　60 km ≦ Epicentral Distance Δ < 120km
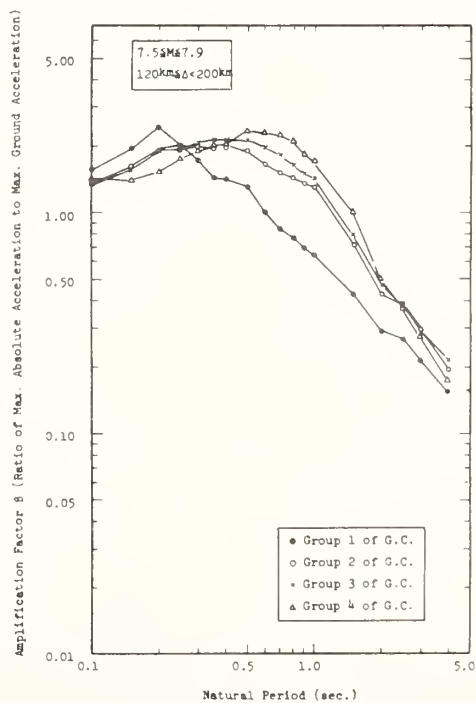
(c)　120km ≦ Epicentral Distance Δ < 200km

Fig. 8   Relationship Between Maximum Horizontal Acceleration (Amax) and
Epicentral Distance (Δ) Obtained by Statistical Analyses of
Strong-Motion Acceleration Records
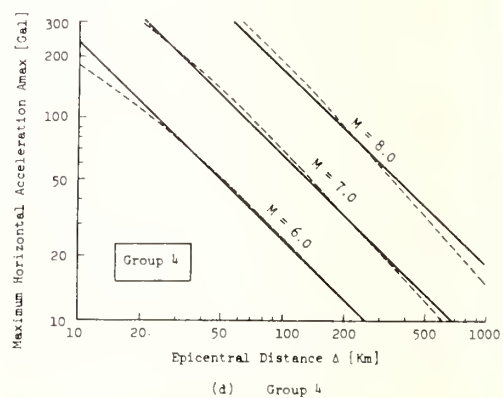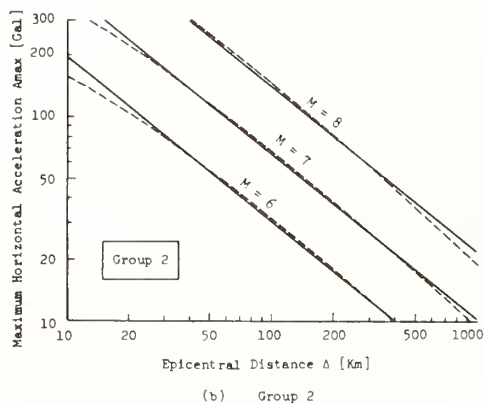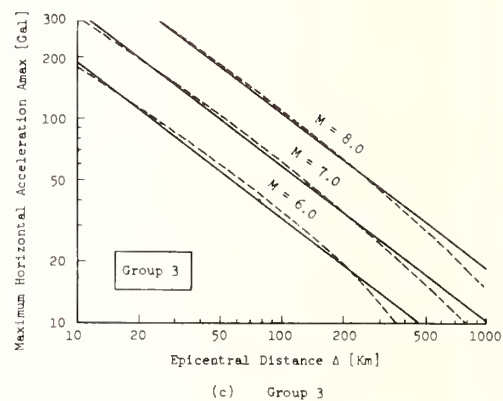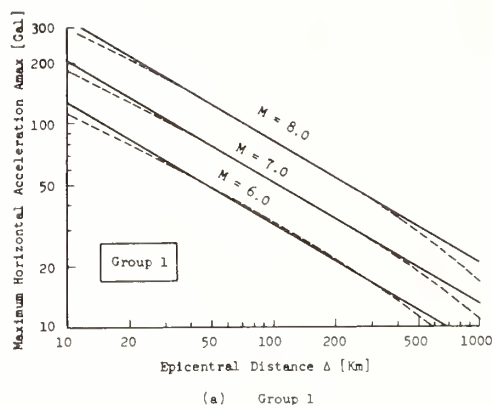
(a)   Group 1

(b)   Group 2

(c)   Group 3

(d)   Group 4

SINGLE-STORY RESIDENTIAL MASONRY CONSTRUCTION IN UNIFORM

BUILDING CODE SEISMIC ZONE - TENTATIVE RECOMMENDATIONS

by

Ronald J. Morony

ABSTRACT

The U.S. Department of Housing and Urban Development's (HUD) Minimum Property Standards (MPS) currently require that all masonry construction in the Uniform Building Code (UBC) Seismic Zone 2 have partial reinforcement.

The housing industry objected that there was not a good basis for this requirement and it was needlessly adding cost. HUD therefore contracted with the University of California at Berkeley to establish the behavior of typical single story dwellings under seismic loads using full scale specimens. This paper is a summary of the four shaking table tests and timber connection tests previously reported. The form and substance of the tentative results which were prepared for HUD by the Applied Technology Council of Berkeley are given. A future fifth shaking test is also discussed.

Upon completion of the contract in middle 1981, a separate report will be presented to the UJNR Panel.

In 1979, Mr. G. Robert Fuller of HUD presented the testing program on single-story masonry houses in Seismic Zone 2. This report will give a brief summary of that testing program and then discuss the tentative conclusions and the method of using them. Historically, the research project was caused by complaints from builders in the Phoenix, Arizona area. In order for houses to be accepted under any of HUD's many programs the construction must conform to HUD's Minimum Property Standards [1] (MPS). Seismic design requirements are specified by referring to the Uniform Building Code (UBC) [2]. So in 1973 when UBC changed their seismic risk map and Phoenix was now in Zone 2 instead of Zone 1 there was a conflict between the local building code and the MPS. To help clarify the problem a Local Acceptable Standard (LAS) was issued in August 1974. This LAS did not permit unreinforced masonry and masonry walls of single-story residences in Seismic Zone 2. The LAS would require at least the following amounts of vertical reinforcement:

(1) Number 4 bars at all building corners, at wall ends, at all door and window openings, and in wall sections 2'-0" (0.6 m) wide or less. Openings larger than 12'-0" (3.7 m) in width require special analysis.

(2) Number 4 bars spaced at not over 12'-0" (3.7 m) on center.

(3) All reinforcement to be matched with dowels embedded in foundation walls or slabs.

Local builders questioned the above requirements which are considered to be "partial reinforcement." The construction contractor's contention was that this reinforcement was unnecessary and therefore was increasing the construction cost needlessly. The Department undertook the following research program in order to experimentally determine the actual minimum requirements.

RESEARCH PROGRAM

There are three parties to the research program. The first is HUD who is sponsoring the program. Second is the Earthquake Engineering Research Center (EERC) who has performed the physical testing and is responsible for recommendations to the specific reinforcing needed. The third party is the Applied Technology Council (ATC). ATC has two tasks, the

first is to establish a four man Advisory Panel to assist in monitoring the testing program and to advise on the preparation of the Guidelines.

The Guidelines will specify and illustrate the method of satisfying the requirements. It is anticipated that the Guidelines will be referenced in the MPS or the Manual of Acceptable Practices (MAP) as one acceptable method of satisfying the Seismic requirements. ATC is also responsible for developing the Guidelines.

The Advisory Panel consists of three consulting structural engineers from three different geographical areas all of which is Seismic Zone 2 and a representative of the home building industry in Arizona. [3] The Guidelines are being written by subcontractor of ATC, Benson and Gerdin Consulting Engineers.

Both the Earthquake Engineering Research Center and the Applied Technology Council are under contract to HUD.

The EERC ran a series of four tests on their shaking table, Figure 1 [4] is typical configurations of the specimens used on the shaking table. Note that the shaking table is capable of one horizontal motion only. It does have the capability of a vertical motion in conjunction with the horizontal motion.

The single horizontal motion resulted in walls that are either in the plane of the motion (parallel to the motion) or walls that are out of the plane of the motion (perpendicular to the motion). The walls were 16'-0" (4.9 m) long and 8'-8" (2.6 m) high. The walls were connected at the top by a timber truss roof diaphram with trusses arranged sometimes parallel and sometimes perpendicular to the horizontal motion of the shaking table. Concrete slabs were bolted to the roof to account for the reduction in mass from the scaled down floor plan. Additionally nineteen joint connections were tested.

After three sets of shaking table tests it was determined that the house would not collapse under the simulated earthquakes. Therefore, the researchers requested that HUD establish what constituted structural failure since it was a policy decision. Structural failure was defined as a permanent displacement of 1/4" (5.8 mm) or greater. This limit was chosen because it was considered that smaller displacements could be economically repaired whereas the cost of repair of larger displacements would be relatively expensive. All of the EERC's recommendations are based upon this failure criterion.

The problem of making recommendations become more complex because during the course of testing a new seismic risk map was published. This is contained in the "Tentative Provisions for the Development of Seismic Regulations for Buildings" [5] (ATC). It was decided to use the accelerations from ATC-3 and apply this criteria to the areas shown in the UBC 1973 Seismic Zone 2. This overlay is shown in Figure 2. The ATC-3 document speaks to Effective Peak Accelerations (EPA) which are related to the seismic spectrum. The shaking table motion having a peak acceleration of 1 g (acceleration of gravity) is assumed to have an EPA of 0.82 g. The maximum EPA of 0.2 g indicated by the ATC-3 for UBC Zone 2 is represented by a peak shaking table acceleration of 0.24 g [6]. Because of the large range of accelerations in Seismic Zone 2, Seismic Zone 2 was subdivided into Zone 2A with a range of EPA = 0.1 g or less and Zone 2B with a range of EPA = 0.2 g. The zones are shown on Figure 3.

The recommendation for Zone 2A is very simple. No reinforcement in single-story residential buildings of standard clay brick or concrete block construction is required for earthquake resistance [6].

Zone 2B will require some partial reinforcement in masonry walls. The requirements will be specified in the Guidelines. The Guidelines are meant to be used by home builders and therefore are a "how-to-do-it" manual. The use of the manual will be restricted to houses that are "regular" in plan and meet the following requirements:

(1)   The area under roof must not be greater than 3,400 square feet (315 m).

(2)   The total weight of roofing, ceiling, insulation and other materials supported directly by the roof trusses or rafters must not exceed 20 pounds per square foot (100 kg/m^2).

(3)   All masonry walls must be constructed with a concrete or masonry stem wall on a concrete footing.

(4)   The unsupported height of any wall above the floor must be no greater than 8'-4" (2.5 m) and the height of any parapet above the roof must be no greater than 3'-0" (0.9 m).

(5)   The roof must be plywood and mailed to the wood framing members (trusses or rafters).

(6) Roof trusses bearing on the top of the unit masonry unit must not have a clean span greater than 40'-0" (12.2 m).

(7) The roof rafters, joists, and trusses which are supported from a ledger bolted to the face of the masonry wall must not have a clean span greater than 20'-0" (6.1 m).

If the house does not fall within these limitations, the Guideline is not applicable and the house should be reviewed by a registered structural engineer for earthquake resistance. [7]

The Guidelines would illustrate the response of houses to earthquakes such as Figure 4. It will show how to resist these forces such as Figure 5. It will also illustrate how to make connections between the timber members and the masonry such as is shown in Figure 6. This general approach is taken so that the homebuilder may readily use the Guidelines. For clarity the Guidelines will be printed in two colors so that the non-conventional construction will be readily apparent. The requirements and location of shear panels is shown in Figure 7.

The Guidelines have not been finalized because there are some critical issues that could not be resolved by the Project Advisory Panel. Because of the physical limitations of the shaking table there was data on walls in-plane and walls out-of-plane. In a real earthquake all walls will be both in-plane and out-of-plane at the same time. Another problem was that using accepted analytical methods the number 3 bars should have broken but they did not. This fact raised a concern that the entire research program could be seriously questioned on this account. And finally, a concensus could not be reached as to the required length of shear panel and the effects of tension on placement of shear panels. It appeared that the vast majority of these issues could be resolved if an additional test were performed. This test would subject the walls to a combination of in-plane and out-of-plane forces simultaneously.

ADDITIONAL RESEARCH

The testing program has significantly increased the state-of-the-art and has provided for the first time, quantitative as well as qualitative data on the response of typical single-story masonry houses to earthquakes. It is the opinion of the researchers, the Project Advisory Panel and the HUD representatives that most aspects of the behavior of real houses during actual earthquakes have been adequately simulated during the research

program. To quote from the final report by the EERC "... this report has emphasized that one important feature of the real earthquake situation has not been included in these tests: biaxial horizontal excitation. No shaking table in the United States has the capacity of testing structures of the size of these house models with biaxial horizontal motions, so it is not possible this biaxial effect with complete similitude ... if a test structure ... were positioned on the shaking table with one of its axes rotated 30 degrees relative to the excitation axis, then the single horizontal earthquake component would induce both in-plane and out-of-plane forces in all walls." [8]

The possibility of the additional test was discussed with the Project Advisory Panel in February 1980. The panel was of the opinion that this additional test could resolve the problem of combining the in-plane and out-of-plane effects, the apparent over stressing of the number 3 bar and the attendant determination of the minimum length of shear panels. The Advisory Panel suggested that a 40 degree orientation might be more advantageous since a cursory review of accellometer readings indicated that the minor axis accelerations were approximately 80 percent of the major axis accelerations. It was also suggested that the reinforcement be instrumented with strain gages to determine actual stresses in the reinforcement.

<center>CONCLUSIONS</center>

It is the explicit goal of the Department to set standards at the lowest reasonable level. Therefore every effort is being made to either sponsor or obtain funds to perform the fifth test described. It is anticipated that this test will be performed in the last part of 1980 or in early 1981. Copies of the first two volumes are currently available from the National Technical Information Service (NTIS) Springfield, Virginia 22161 USA. The third volume "Summary, Conclusions and Recommendations" should be available through NTIS shortly.

Films of the first four tests and the fifth shaking table will be edited into a concise presentation and should be available for future UJNR Panel meetings.

The Guidelines will be published as a two color document by HUD's Office of Policy Development and Research. It is anticipated that the Guidelines will be referenced in either HUD's Minimum Property Standards (MPS) or in the Manual of Acceptable Practice (MAP).

REFERENCES

[1] U.S. Department of Housing and Urban Development, "Minimum Property Standards, One-
     and Two-Family Dwellings," HUD 4900.1, 1973 Edition, Washington, D.C.

[2] International Conference of Building Officials (ICBO), Uniform Building Code, Vol. 1,
     1973 Edition, Whittier, CA.

[3] The three consulting engineers are O. Clarke Mann, Memphis, Tennessee, James P. Kesler,
     Pasadena, California, and Joseph A. Gervasio, Phoenix, Arizona. The home building is
     Lenn Pritchard, a masonry contractor.

[4] Ray W. Clough, Ronald L. Mayes and Polat Gulkan, "Shaking Table Study of Single-Story
     Masonry Houses; Volume 3: Summary, Conclusions and Recommendations," Report No.
     UCB/EERC 79/25 September 1979.

[5] Applied Technology Council Publication ATC 3-06, "Tentative Provisions for the
     Development of Seismic Regulations for Buildings," (NSF Publication 78-8, NBS Special
     Publication 510) U.S. Government Printing Office, June 1978.

[6] Ray W. Clough, Ronald L. Mayes and Polat Gulkan, "Shaking Table Study of Single-Story
     Masonry Houses, Volume 3, Summary, Conclusions and Recommendations," Report No.
     UCB/EERC 79125, September 1979.

[7] Benson and Gerdin, Consulting Engineers for the Applied Technology Council,
     "Guidelines for One-Story Houses in Seismic Zone 2" (Draft) January 15, 1980
     unpublished.

[8] Ray W. Clough, Ronald L. Mayes and Polat Gulkan, "Shaking Table Study of Single-Story
     Masonry Houses; Volume 3: Summary, Conclusions and Recommendations," Report No.
     UCB/EERC 79125, September 1979.

Figure 1 House 2

PLAN

EXTERIOR ELEVATIONS

372
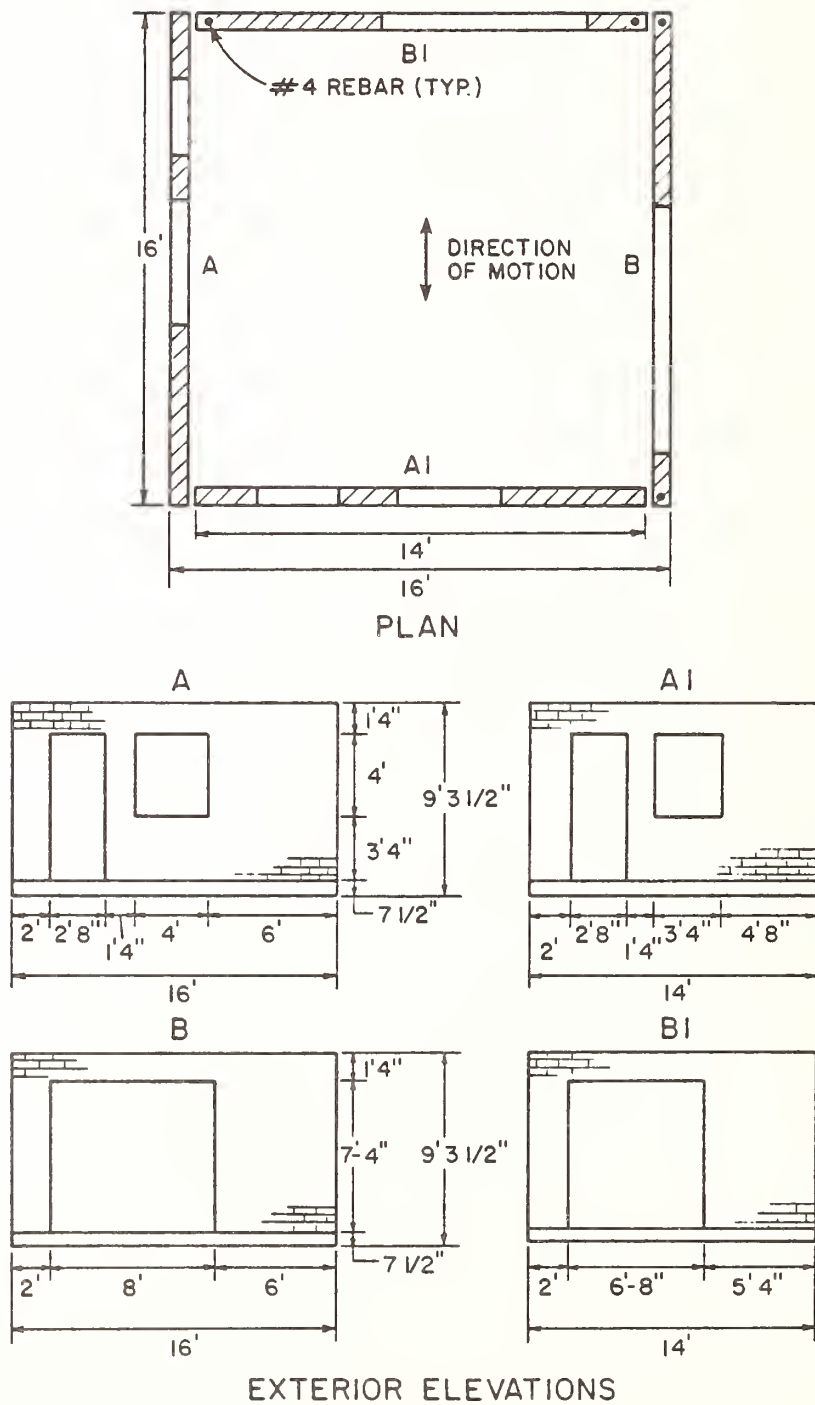
Figure 2   COMPARISON OF UBC SEISMIC ZONE 2 AND THE CONTOUR MAP OF EFFECTIVE
             PEAK ACCELERATIONS

UBC SEISMIC ZONE 2

EPA CONTOURS IN UNITS OF
ACCELERATION OF GRAVITY
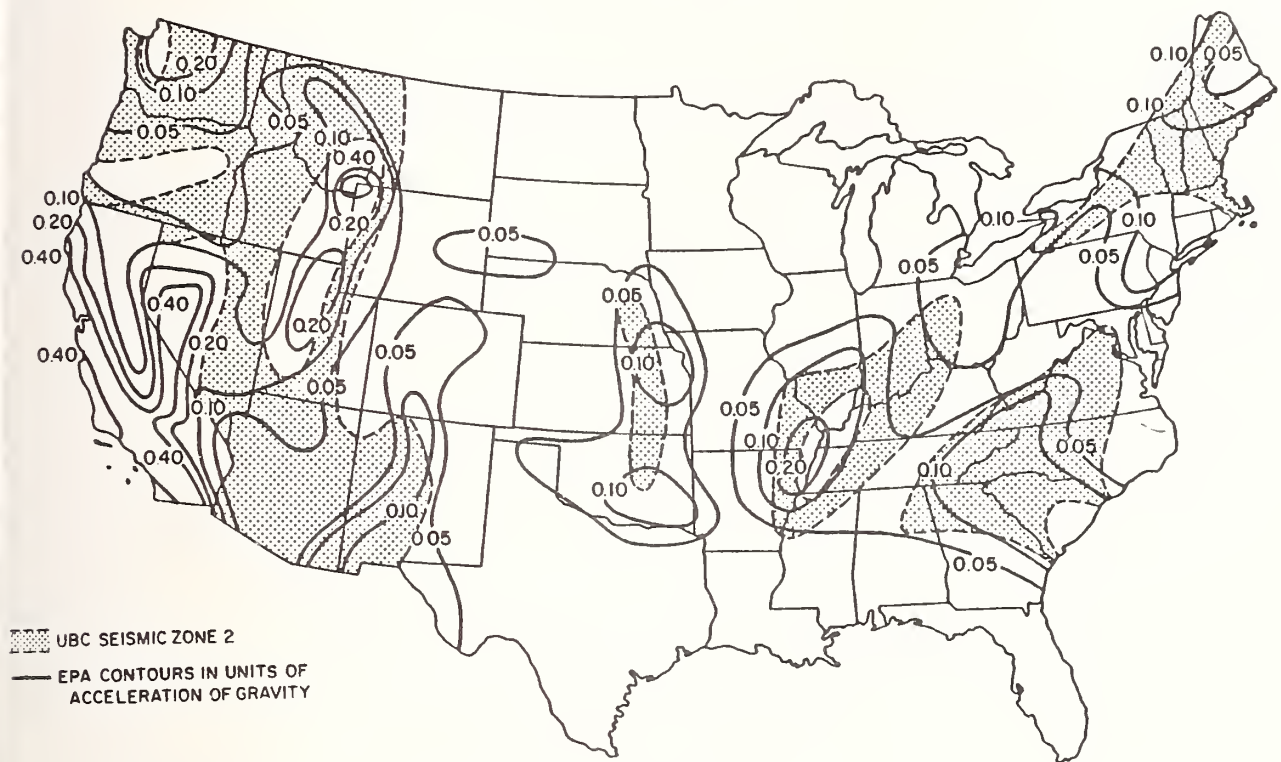
Figure 3   Seismic Zone 2A And 2B Of The United States

Legend
Zone 2A
Zone 2B
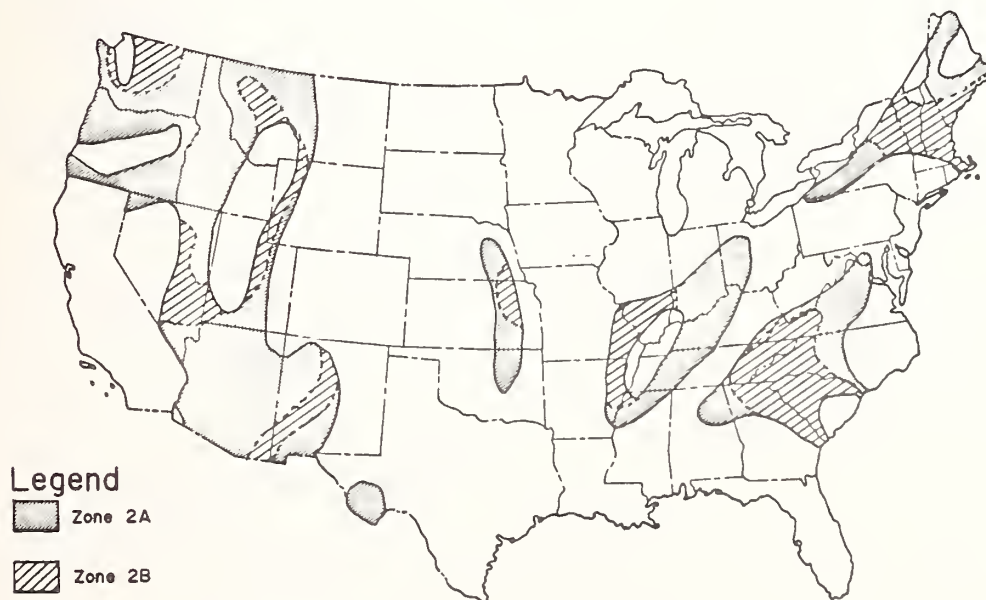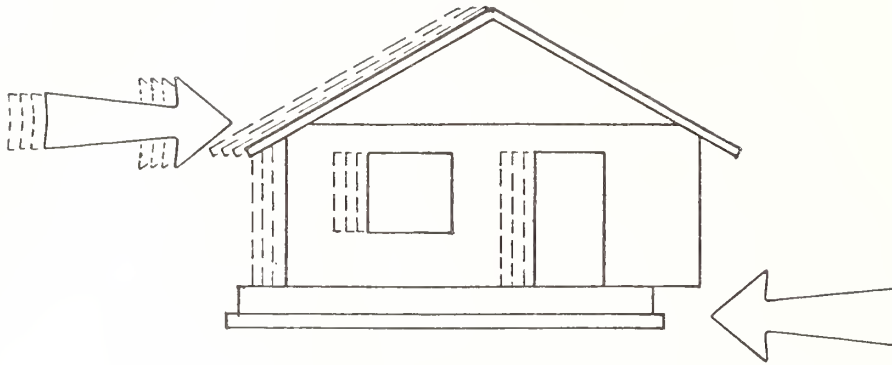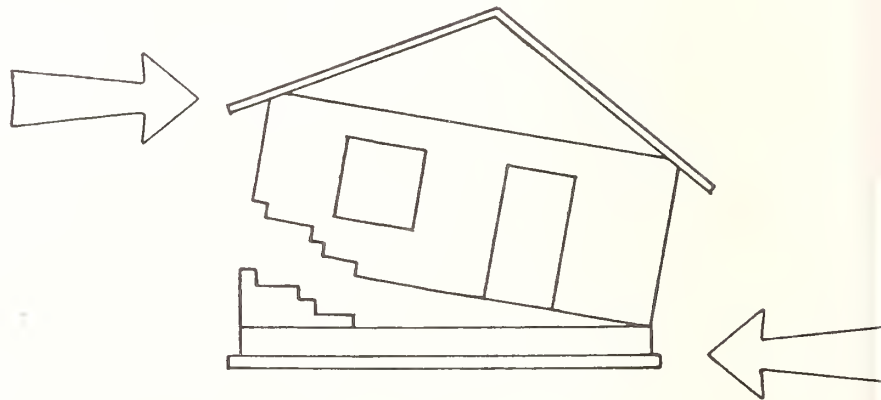
Sliding Effect

Overturning Effect

FIGURE 4

FIGURE 5 **Earthquake Resistance System**

ROOF SYSTEM

GABLE
END
TRUSS

PLYWOOD

SHEAR
PANEL
"A"

SHEAR
PANEL
"B"

SHEAR
PANEL
"B"

SHEAR
PANEL
"A"

STUD
PARTITIONS

FOUNDATION

"B"   "A"

"A"   "B"

FIGURE 6

2x4 WALL TIES @ 6'-0" O.C. ALONG
WALL W/ 2x4 BLOCKING, EXTENDING
TO SECOND INTERIOR TRUSS

2x6 BLOCKING CONT.
BTWN. ANCHOR
BOLTS W/ 4-12d BOX NAILS
MIN. @ BLOCK TO ₽; W/ FRAM-
ING ANCHOR @ BLK. TO
TRUSS @ 48" O.C.

2x6 TOP ₽ W/
1/2" ∅ ANCHOR
BOLTS @ 48" O.C.

9 GA. HORIZ.
JOINT REINF.

6" MASONRY WALL

3-16d BOX TOE NAILS
@ BLOCKING TO BLOCK

BOTTOM
CHORD OF
GABLE TRUSS

3-16d
BOX NAILS

2-16d
BOX NAILS

BOTTOM CHORD
OF 1ST TWO
INTERIOR TRUSSES

GYPSUM BOARD
CEILING W/ 5d-
COOLER NAILS @
7" O.C. TO BOTTOM
OF BLOCKING

Roof To Masonry Non-Bearing Wall

2x4 BLOCKING @ 2'-0' O.C.
W/ 2-16d TOE NAILS
EA. END TRUSS TO
BLOCKING W/ TRUSS
CLIP, 1-EA. SIDE BLOCKING
TO TOP ₽

2x6 TOP ₽ W/
1/2" ∅ ANCHOR
BOLTS @ 48" O.C.

9 GA. HORIZ.
JOINT REINF.

BOTTOM CHORD OF
ROOF TRUSS

GYPSUM BOARD
CEILING W/ 5d-
COOLER NAILS @
4" O.C. TO BOTTOM
OF BLOCKING
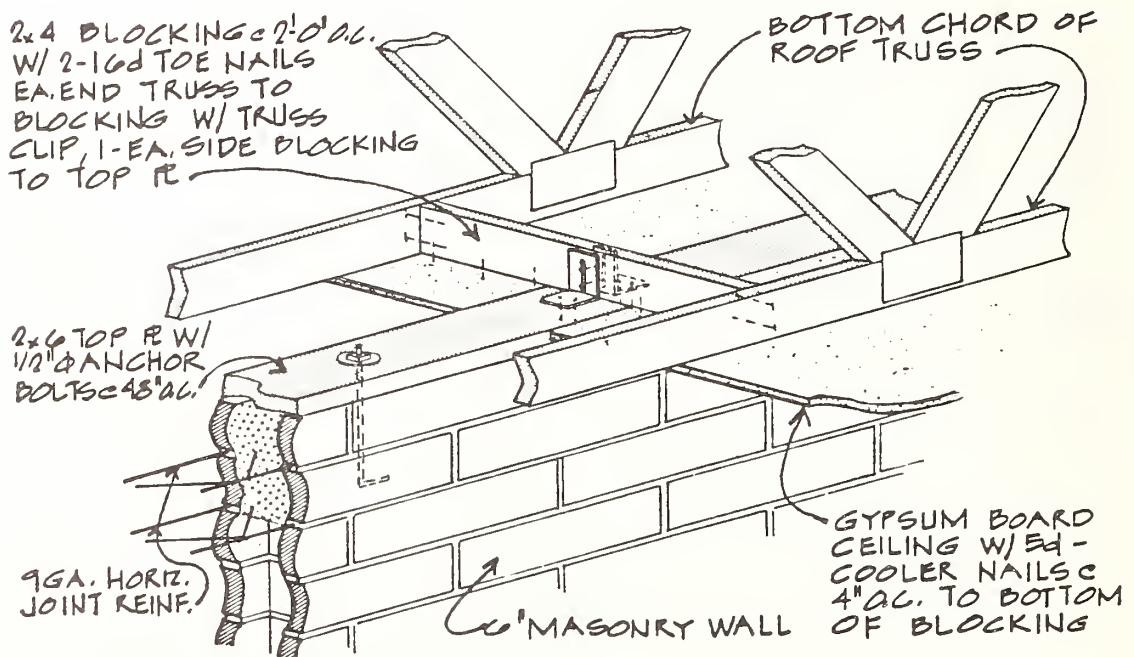
6' MASONRY WALL

Masonry Wall Brace(Truss Parallel To Wall)

FIGURE   7

6'-0" MIN. TYP.
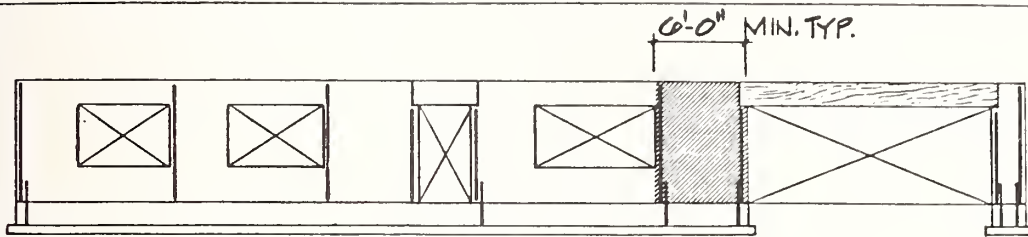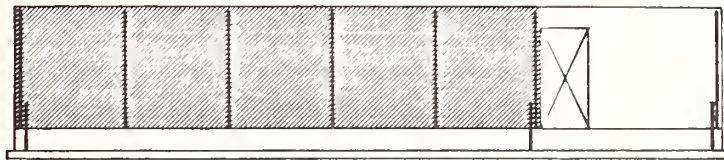
Front   Elevation

Right   Elevation
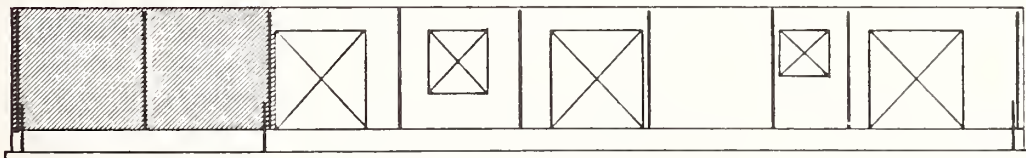
Rear   Elevation
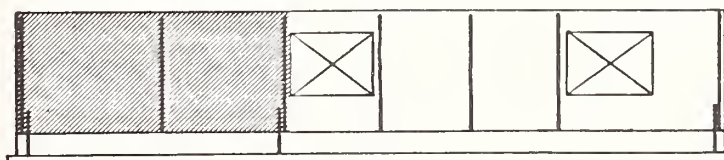
Left   Elevation

Zone 2B- Plan 1- Exterior Elevations

EARTHQUAKE DISASTER PREPAREDNESS PROGRAM FOR THE LIMA, PERU METROPOLITAN AREA

by

Masamitsu Ohashi

Makoto Watabe

Yoshio Kumagai

Yoshihisa Hoshino

INTRODUCTION

Disaster prevention in major earthquakes is a most important national project in earthquake-prone countries. Though some minor differences can be observed in seismological conditions between Peru and Japan, both countries are quite similar. Based on this fact, our technical cooperation will be quite fruitful for disaster prevention projects in both countries.

In spite of great advances in the technology of predicting major earthquakes, prediction at present still is not completely dependable. Therefore, the best method to prevent earthquake hazards is to prepare all possible countermeasures against major earthquakes, namely, disaster prevention projects.

By establishing disaster prevention systems, earthquake hazards will be reduced drastically even for the great earthquake expected in the future.

Twice, our technical cooperation mission from Japan has been to Peru. The first mission was sent to Peru in 1979. It consisted of three members, Mr. Masamitsu Ohashi, the leader of the mission, Mr. T. Matsui, and Mr. Y. Kitani. The mission stayed in Peru about ten days to investigate the types of technical cooperation that might be most effective for disaster prevention in the Lima Metropolitan Area.

Based upon the report of the first mission, the second technical mission was sent to Peru in late 1980. The second mission stayed in Peru about three weeks and was mainly devoted to the collection of information, meeting with persons concerning disaster prevention for major earthquakes. These visits benefitted from the courtesy and kindness of the Civil Defense which played the role of the counterpart organization in Peru.

Names and specialized fields of the members of the second mission, as well as their schedule in Peru are as follows:

(1) Makoto Watabe, Mission Leader,   Earthquake engineer, Dr. of Engineering

(2) Yoshio Kumagai   Urban plan specialist, Dr. of Engineering

(3) Yoshihisa Hoshino   Geologist

(4) Kazuhiko Kawashima   Civil Engineer

SCHEDULE

November

22   Arrived at Lima

23   Courtesy call on Minister of Interior and Director of Civil Defense

26   Meeting at Civil Defense

28   Meeting at Geophysical Institute

29   Meeting at Geological Institute

30   Meeting at La Molina University

December

3   Meeting at UNI

4   Meeting at Catholic University

5   Meeting at Ministry of Housing and Construction

6   Evaluation at Civil Defense

7   Visiting Arequipa to meet with the engineer

8   Visiting Cusco, courtesy call on the mayor

10   Preparation of report

11   Lecture to staff of Ministry of Housing and Construction, and lecture to staff of
     Civil Defense later in the day

12   Discussion at Catholic University

13   Discussion at UNI

14   Submitting report to the Minister of Interior.

The report contents include the following items: (1) City planning for disaster prevention, (2) Geological works, (3) Earthquake ground motions, (4) Microzonation, (5) Civil Engineering structures, (6) Housing and buildings, (7) Civil Defense.

Here, all members of the mission would like to express the hearty gratitude to Colonel EP Heraclio Fernandez Pendola, Director Superior del Comite National de Defensa

Civil for his warm hospitality and cooperation, and to Colonel PIP Guillermo Castillo Rivadeneyra, Jefe del Comité de Asesoramiento del Comite National de Defensa Civil; Ingeniero Julio Kuroiwa Horiuchi, Presidente del Comité Cientifico de la Secretaria Ejecutiva de Defensa Civil; Ingeniero Guillermo Chamorro Rodriguez; and all the staff of the Comité National de Defensa Civil for their cooperation.

CITY PLANNING FOR DISASTER PREVENTION

One aim of this project, Disaster Prevention in Lima Metropolitan Area, is the formulation of a basic plan for disaster prevention. The first year, 1979, objectives of this technical cooperation are as follows:

° Develop comprehensive planning system for the regional and city plan in Peru and in the Lima Metropolitan Area,

° Provide suggestions for earthquake disaster countermeasures and earthquake disaster prevention plans in the Lima Metropolitan Area,

° Present the contents and schedule for this technical cooperation in the future.

For these purposes, we held discussions with members of the National Committee of Civil Defense, Ministry of Housing and Construction, National University of Engineering, and others. The suggestions to these groups were as follows.

To the National Committee of Civil Defense

° Estimate the degree of danger of a large scale earthquake in the Lima Metropolitan Area

° Establish a public relations system for earthquake disasters

° Coordinate and arrange a earthquake disaster prevention plan for each ministry

° Establish a radio communication network system for the ministry

° Provide planning provisions for emergency support from abroad

° Designate emergency evacuation sites.

To the Ministry of Housing and Construction

° Establish a new type of zoning system for building structure control

° Initiate model planning for a small plaza in a concentrated block of "adobe" construction

380

     °   Designate reconstruction sites for post large-scale earthquake activities.

To other ministries

     °   The intensification of the official car check system

     °   Designate a traffic control zone for post large-scale earthquake activities

     °   Establish a fail safe system for public facilities

     °   Concentration of governmental office buildings

These suggestions are further detailed in Table 1.

Other suggestions are shown in Figures 1 and 2. Regarding a new type of zoning system for building structure control, we discussed the four following types:

(1) Aspects of important zones

    (a) Around emergency facilities

      °   Obligation to build earthquake resistant buildings within 10 or 15 years

      °   The necessity to subsidize people for reconstruction.

    (b) Important zones in relation to urban activities

      °   Control of the building structure in new construction, reconstruction, and remodeling

(2) Aspects of microzonation

    (a) Urban activities and microzonation

      °   Control of building structure in new construction, reconstruction, remodeling, and after a large scale earthquake

    (b) Zones estimated to experience huge damage in large scale earthquakes

      °   Prohibition of new construction after large scale earthquakes

      °   Preparation and designation of reconstruction sites

      °   Prohibition of new construction in designated reconstruction sites before large scale earthquakes

GEOLOGICAL WORK

The geological data, including the geomorphological and geodesical, are important for microzonation. We recommended three works on the geology. They are the Landform Classification Map, the Superficial Geological Map, and the Neotectonic (Quaternary Tectonics) research.

Landform Classification Map

From our surveys in Japan, we are able to recognize interrelationships between earthquake damage patterns and landforms. This derives from the fact that some coincidence can be seen between landforms and ground conditions, since each landform, either erosional or depositional, has an individual internal structure which depends on the forming process.

This interrelation can be used in reverse, and geologically high-risk areas can be disclosed qualitatively.

A Landform Classification Map should be planned using a scale of 1:50,000 or larger. The scale of 1:25,000 is better.

Superficial Geological Map

In addition to the Landform Classification Map, the Superficial Geological Map is suggested. Useful information about the superficial ground condition can be obtained by making a Superficial Geological Map.

Boring data is needed to develop the Superficial Geological Map. Therefore, boring data in and around Lima should be collected and compiled as soon as possible.

Neotectonics (Quaternary Tectonics)

For microzonation, information about crustal movements of recent time is important. Recent crustal movement has continued to present time since the early Quaternary period. Therefore, research on Quaternary Tectonics should be carried out. The crustal movements of past and present time can be investigated using the three methods: the geological method, the geomorphological, and the geodesical. The geological method can make clear the crustal movement before 10^{5-6} years B.P. The geomorphological method is effective in learning of crustal movements during $10^{5-6} - 10^3$ B.P. While, the geodesical method is indispensable to get data about the crustal movement after 10^2 years B.P.

The crustal movement as revealed by the geological method is only the old structure in general which has not always succeeded to the Quaternary period. Therefore, the geological method is sometimes not useful to study Quaternary Tectonics. Instead, the geomorphological method is effective for such purposes.

The geodesical method is fundamental in deciphering present crustal movement. A survey of trig stations and bench marks will be recommended as a beginning point, not for making maps but to get data about present crustal movement. However, the geodesical method covers

382

the tendency of crustal movement for only 100 years at most, despite the fact that the crustal movement sometimes has a periodicity of more than 100 years.

Therefore, the geomorphological method and geodesical method should be coordinated to develop the recent tectonic situation. The research of geomorphology in general, and the geodesic survey in and around Lima will be recommended for the long term efforts.

EARTHQUAKE GROUND MOTIONS

(1) According to several accelerograms obtained here in Peru, the characteristics of earthquake ground motions, such as peak accelerations and shapes, are quite different from those observed in Japan and the United States. Therefore, an extensive collection of strong motion accelerograms in Peru is urged, so that Peruvian characteristics of earthquake ground motions may be established.

(2) In view of very high peak accelerations in Peru, studies of earthquake ground motions which correlate observed physical values (such as effective peak accelerations) and those estimated through investigation of damaged structures may be important for the interpretation of observed accelerograms. Also, re-evaluation of peak accelerations of original accelerogram records is suggested.

(3) In order to collect as many strong motion accelerograms as possible, an instrumentation plan for strong motion accelerographs on the ground as well as on specific structures will be necessary: this instrumentation plan should cover a short, intermediate, and long term scheme with an order of priorities.

(4) Strong motion accelerograph arrays are recommended for instrumentation in such a place as La Molina, where some heavier damage has been reported in past earthquakes, and where detailed study on response behavior of soil-deposits due to earthquake excitations appears necessary.

(5) Positive establishment of systems for faster digitization and analyses of accelerograms obtained as well as faster supply procedures for these results to concerned practical researchers and engineers is strongly recommended.

MICROZONATION

<u>General</u>

Through past experience with earthquake damage, it is known that there are clear differences between severely damaged areas and slightly-damaged areas even within a relatively small area. Such evidence is clear in the La Molina district of the Lima Metropolitan Area since the MM intensity in the district has been two to three grades stronger in the 1904, 1932, 1940, 1966 and 1974 earthquakes. It is considered important to define the area where damage is expected in the future earthquake using the microzonation technique. From an earthquake disaster prevention point of view, the following microzonation might be effective.

(1) Subsurface ground condition

(2) Distribution of SH-wave velocity

(3) Amplification factor of subsurface ground

(4) Liquefaction

(5) Land slide

(6) Slope failure

(7) Water table

(8) Distribution of building construction zone maps

(9) Tsunami

For the above purposes, two approaches are proposed for microzonation, i.e., an approach based on investigations of past earthquake damage, and the theoretical approach.

<u>Recommended Approach for Microzonation in Lima Metropolitan Area</u>

In order to conduct microzonation in the Lima Metropolitan Area, the theoretical approach based on the calculations of subsurface ground motions is recommended, and then to re-check and improve the calculated results from the knowledge obtained by the investigations of past earthquake damage features. The following subjects are recommended for investigation using the theoretical approach:

(1) Research on the dynamic characteristics of subsoils

Improved test procedures and the results concerning dynamic properties of subsoils have been developed in recent years. Also recommended is the acquisition of test

apparatus and study of the test procedures in order to investigate the following subjects:

(a)   Dynamic shear moduli

(b)   Damping characteristics

(c)   Dynamic shear strength

(d)   Sampling technique to get undisturbed soil specimens

The introduction of the resonant column apparatus and the dynamic triaxial test unit are suggested to pursue these investigations.

CIVIL ENGINEERING STRUCTURES

Transporation Facilities

Roads

It is suggested that roads be classified into several groups in accordance with their functions after the earthquake hazard. The important functions, indispensable for post-earthquake activities, might be as follows:

(1)   Roads for refuge

(2)   Roads for rescue

(3)   Roads for fire emergencies

(4)   Roads for transportation needed for restoration

(5)   Roads for transportation of food and water

For such functions, it is suggested the following points be examined:

(a)   Check earthquake resistance of road facilities, including traffic control
      equipment

(b)   Survey for possible bottleneck points

(c)   Reinforcement and retrofitting procedures to upgrade marginal roads

(d)   Preparation of duplicate roads for important highways

Bridges

Certain types of bridges are quite susceptible to earthquake damage. Seismic damage is most commonly caused by foundation failures resulting from excessive ground deformation and/or loss of stability and bearing capacity of the foundation soils. As a

385

direct result, substructures often tilt, settle, slide, or even overturn. Severe cracking, or complete failure, does occur.

A survey of present bridge design and construction practice is suggested, paying special attention to earthquake resistance of foundations and foundation soils.

The establishment of earthquake resistant design methods for bridges, and the investigation of retrofitting methods is recommended.

Ports and Harbors

A survey of present design and construction practice of ports and harbors is suggested.

The establishment of earthquake resistant design methods for ports and harbors is recommended.

Dams and Reservoirs

A survey of present design and construction practice for dams and reservoirs, which are used for irrigation purposes, generation of electricity, and water supply is suggested.

The establishment of earthquake resistant design methods for dams and reservoirs is recommended.

River and Coast Dykes

A survey of the present condition of river and coast dykes, especially where floods or Tsunamis may occur, is suggested.

Underground Structures

Underground structures such as conduits and pipe-lines are widely used for the supply of electricity, water, petroleum, the distribution of telecommunications, etc. From past earthquake damage, it is often observed that the damage to underground structures takes place where the structural or geological conditions change discontinuously.

A survey of present design and construction practice for underground structures is suggested. The establishment of earthquake resistant design methods for underground structures important to post-earthquake activities is recommended.

Tunnels

From past earthquake damage, it is often seen that the interruption of traffic in tunnels is not caused by damage to the tunnels themselves but by slope-failures at the

ends of the tunnels. A check of the present condition of tunnels paying special attention
to slope-stability at the end of tunnels is suggested.

HOUSING AND BUILDINGS

(1) It surprised us to see that many adobe structures have survived with little damage
the various strong motion earthquakes of the past 200 years. In view of this, it is sug-
gested that simple local materials such as adobe or brick blocks be used for low-cost
housing, if such materials are used properly.

(2) Extensive research and development projects on low-cost housing are underway;
from what we gathered in visiting two major Lima universities, the philosophy and orienta-
tion of the projects are quite satisfactory. Most possible methodologies for strengthening
adobe walls and their connections have been explored. It is, however, also true that with
some moderate increase in experimental instruments at these facilities, the efficiency and
accuracy of research work might be dramatically improved.

(3) Essential experimental equipment and facilities such as microtremor measurement
instruments, hydraulic actuators, dynamic strain-meters, and shaking tables should be
quickly supplied.

(4) Development of a low-cost house with one very strong room against earthquakes,
research on the connections between walls, and shear connections between adobe walls and
wooden braced frames, may be a useful focus.

(5) Public dissemination of research results on developments mentioned above are
vital to improve the low-cost housing. Various investigations of possibilities such as
tax-reductions, economical structure investigations, land-use advantages, or training
projects for builders and engineers should be studied to encourage people to adopt the
recommendations.

(6) Retrofitting buildings and housing against possible strong motion earthquakes is
urged, especially for governmental office buildings. For this purpose, evaluation criteria
of the aseismic capacities of buildings and reinforcing procedures for these buildings
should be investigated. It is also important to educate engineers in the evaluation of the
degree of diminished safety in damaged buildings after earthquakes.

(7) In order to coordinate practical and precise earthquake resistant regulations for
buildings, the following back-up research work is needed:

(a) Micro-tremor measurement of natural periods and damping characteristics of building structures

(b) Behavior of infill-wall structures

(c) Effects of shape factors of structures such as the torsional and discontinuity effects

(d) Research on the behavior of non-structural elements

(e) Research on the ductility of various structural types

CIVIL DEFENSE

In Japan, we have no permanent and independent organization for disaster prevention. The National Land Agency does include a Disaster Prevention Policy Planning Division, and the division manages the Central Disaster Prevention Council. The council is established by law, the Disaster Countermeasure Basic Act. Based on the act, local governments establish local disaster prevention councils. When a big disaster, such as storm, flood, or severe earthquake occurs in a region, the national and local governments cooperatively establish disaster prevention headquarters based on the disaster prevention plan.

In Peru on the other hand, there is a permanent and independent organization for disaster prevention. Few countries in the world have an organization such as Defensa Civil, so there is good reason to be proud of it. We do recommend several items to reinforcing its function.

The first point relates to budget and scope. Individual items for disaster prevention, such as adobe construction, observations of strong motion etc., are pursued in the universities and institutes. These are of high level importance, but there are few comprehensive projects for disaster prevention such as the estimation of dangerous degrees, damage estimations, and designation of evacuation sites, etc. So, the Civil Defense should take a leading role in such comprehensive work in cooperation with the universities and institutes. For this purpose, we recommend budget increases for such disaster prevention activities and to increase the number of full-time technical staff members.

The second point relates to earthquake preparedness in the other Civil Defense Headquarters itself. Defensa Civil has an exclusive building which will be effective in countermeasures for a severe earthquake. However, if the building itself is damaged by such an earthquake, the abilities of the Civil Defense to lead will suffer. So, we

388

recommend the reinforcement of the building structure, securing antennas and other important instruments, such as radio apparatus, attaching heavy furniture -- such as bookshelves, and steel lockers -- to walls to prevent their overturning and destruction.

CONCLUDING REMARKS

Comments and recommendations on basic concepts of disaster prevention against major earthquake hazards in the Lima Metropolitan Area, are introduced in previous section. As indicated in section summaries, research needs, tasks, projects and works are classified in short term (approximately one year), intermediate (approximately three years), and long term (approximately more than three years).

Although all of these items are essential for a project of disaster prevention in the Lima Metropolitan Area, the following items should be strongly emphasized for the short term;

(1) Designation of model districts, such as Callao City and the Lima District, for degree of danger estimates

(2) Division of model districts into several zones according to state-of-art microzonation procedures

(3) Collection of urban statistical data in each zone

(4) Develop a Landform Classification Map for microzonation in and around the Lima Metropolitan Area

(5) Collect boring data in specific districts such as Callao, La Molina and Lima

(6) Establish a shared publication system of accelerograms and analytical results for research and practical engineers

(7) Develop installation plans for accelerographs on the ground and in structures with a priority order for engineering purposes

(8) Survey subsurface ground conditions, including the measurement of SH-wave velocity in the specific districts such as Callao, La Molina and Lima

(9) Initiate research on the dynamic properties of subsoils

(10) Begin organization of post-earthquake transportation systems and survey for bottleneck points in the total transportation system

(11) Survey the present design and construction practices in the civil engineering of structures

(12) Establish a research center for earthquake disaster prevention in Peru.

(13) Establish an evaluation system for aseismic capacity of R.C., masonry, and adobe structures

(14) Retain at least three full-time engineers in the Comite National of the civil Defense

In order to implement the above, a personnel exchange not only from Japan to Peru, but from Peru to Japan in as early a stage as possible is strongly emphasized.

Table 1. CITY PLANNING RESEARCH, TASKS AND PROJECTS FOR DISASTER PREVENTION

	Short Term	Intermediate Term	Long Term
esearch	1. Study on designation of evacuation sites 2. Study on designation of model district and division into zones to estimate degree of danger 3. Study to estimate degree of danger 4. Study of public relation system for earthquake disaster 5. Study of new zoning system for control of building structures	Continue 3 Continue 4	Continue 3
Tasks	6. Designate evacuation sites in Lima Metropolitan Area 7. Establish radio communication network system among ministries 8. Intensification of offical car check system 9. Designation of traffic control zones after large scale earthquakes 10. Collecting statistical data in each model district zone 11. Estimation of degree of danger in model district 12. Designation of new building structure control zone	Planning in concentration of governmental office buildings Continue 8 Collection of statistical data in the whole of Lima Metropolitan Area Estimation of degree of danger in the whole of Lima Metropolitan Area Continue 12	
Projects or Works	13. Model planning of a small plaza in an "adobe" - construction-concentrated zone 14. Establish fail-safe system for public facilities 15. Preparation of reconstruction sites 16. Planning provisions for emergency support from abroad 17. Establish public relation system for earthquake disaster 18. Formulating earthquake disaster prevention plans in each ministry	Carrying out 13 Continue 14 Designation of reconstruction sites Arrangement of 16 Continue 17 Continue 18	Concentration of governmental office buildings Continue 15 Continue 17

	Short Term	Intermediate Term	Long Term
Research	Data processing procedures for accelerograms Effective peak acc. E.P.A. concept	Correlation study, observed and estimated	Risk analysis in view of E.P.A. and spectra The same as item at left
Tasks	Publication of strong motion accelerograms (digitized and spectra obtained in Peru Instrumentation plan with priority, ground, and structure	Strong motion acc. arrays observation	The same as item at left
Projects or Work	Establishment of faster digitization, analyses, and publication systems Installation of strong motion accelerographs	Strong motion acc. array installations in La Molina The same as item at left	Collection of strong motion accelerograms The same as item at left

	Short Term	Intermediate Term	Long Term
Research	Investigation of earthquake damage, liquefaction, land slide, slope failure, Tsunami, etc.	Calculation of subsoil deposits for strain dependency of shear moduli and damping characteristics Effects of ground condition Classification of ground condition	Effects of topographical condition Evaluation of liquefaction potential Evaluation of land slide potential
Tasks	Collection of boring data Measure of SH-wave velocity Distribution of building construction maps Collection of literature and information concerning earthquake damages Preparation of questionnaires and forms on damage ground motion	Same as left	Sampling of undisturbed soil Classification of ground condition
Projects		Experimental work concerning dynamic shear moduli and damping characteristics of subsoil using resonance column apparatus	Collection of data concerning dynamic strength of subsoils using dynamic triaxial test apparatus

393

RESEARCH, TASKS, AND PROJECTS FOR CIVIL ENGINEERING STRUCTURES

	Short Term	Intermediate Term	Long Term
Research	Survey of earthquake resistant design methods	Seismic response characteristics of facilities such as dams, bridges, high embankments, retaining walls, port, harbor, and underground structures	Research on earthquake resistant design procedures Research on retrofitting methods
Tasks	Definition and selection of important transportation roads Checking facilities and present design and construction practice Listing bottle neck points on roads vital to total transportation system	Determination of design forces Collection strong motion earthquake records for each structure Research foundation structure design procedures	
Projects			Establish earthquake resistant design methods Establish retrofitting methods

	Short Term	Intermediate Term	Long Term
Research	Microtremor analyses Shape factor research on low-cost housing Evaluation method for aseismic capacities of adobe, masonry and R.C.	Methodology for masonry and R.C. structure repair work Infill-wall structure	Non-structural element equipment Ductility of R.C. and masonry structures
Tasks	Communication plans for developed low-cost housing	Development of low-cost prefabricated house Aseismic capacity evaluation of important buildings Collecting building code research results	Building code development
Project or Work	Plan for Peru Earthquake Engineering Research Center	Retrofitting important buildings Establish Earthquake Research Center with basic equipment	Continue at left Continue at left

Fig. 1 Flow Chart Estimate of Danger Degrees in the Lima Metropolitan Area

```
┌──────────────────────────┐      ┌──────────────────────────┐      ┌──────────────────────────┐
│ • Population and          │      │  Designation of          │      │  Example                 │
│   number of households    │      │    model districts       │══════│    Lima District         │
│                           │      │                          │      │    Callao City           │
│ • Microzonation           │      └──────────────────────────┘      └──────────────────────────┘
│                           │                   │
│ • Building structure      │─────▶┌──────────────────────────┐
│   and Building use        │      │  Division to small zones │
│                           │      │    in model districts    │
│ • Distribution of         │      └──────────────────────────┘      ┌──────────────────────────┐
│   public facilities       │                   │                    │ • Trend of population    │
└──────────────────────────┘      ┌──────────────────────────┐      │                          │
         │                         │  Collection of statistical│     │ • Composition of         │
         │                         │    data in each zone      │═════│   population and         │
         │                         └──────────────────────────┘      │         households       │
         │                                    │                       │                          │
         │                         ┌──────────────────────────┐      │ • Dangerous              │
         │                         │  Estimation of degree of │      │         facilities       │
         │                         │  danger in model districts│     │ • Disaster Prevention    │
         │                         └──────────────────────────┘      │         facilities       │
         │                                    │                       └──────────────────────────┘
         │                         ┌──────────────────────────┐                   │
         └────────────────────────▶│  Division to small zones │                   │
                                   │    in the whole of Lima  │                   │
                                   │    Metropolitan Area     │                   │
                                   └──────────────────────────┘                   │
                                              │                                   │
                                   ┌──────────────────────────┐                   │
                                   │  Collection of statistical│                  │
                                   │  data in each zone in the │══════════════════┘
                                   │  whole of Lima Metropolitan│
                                   │            Area           │
                                   └──────────────────────────┘
                                              │
                                   ┌──────────────────────────┐
                                   │  Estimation of degree of │
                                   │  danger in the whole of Lima│
                                   │  Metropolitan Area        │
                                   └──────────────────────────┘
                                              │
                                   ┌──────────────────────────┐
                                   │  Execution of map of degree│
                                   │  of danger in the whole of │
                                   │  Lima Metropolitan Area   │
                                   └──────────────────────────┘
                                              │
                                   ┌──────────────────────────┐
                                   │  Formulation of earthquake│
                                   │  disaster prevention plan in│
                                   │  Lima Metropolitan Area   │
                                   └──────────────────────────┘
```

Fig. 2 Technical Cooperation Schedule on Disaster Prevention City Planning

1978, Pre-survey Committee

* Dispatch of experts
* Acceptance of counterparts

* Request of Technical
    Cooperation
* Preparation of Technical
    Cooperation

1979, Technical Cooperation

* Necessary of estimation of degree
    of danger
* Data for the estimation

* Designation of model district
* Division to small zones in
    model district
* Collection of statistical data

1980, Technical Cooperation

* Method of estimation of degree
    of danger
* Estimation of degree of danger
    in model district

* Division to small zone in the
    whole of Lima Metropolitan Area
* Collection of statistical data
    in each zone

1981, Technical Cooperation

* Estimation of degree of danger
    in Lima Metropolitan Area
* Disaster prevention basic plan

* Execution of map of degree of
    danger in Lima Metropolitan
                        Area
* Collection of data in relation
    to disaster prevention plan

1982, Technical Cooperation

* Formulation of disaster preven-
    tion basic plan in Lima
            Metropolitan Area

Japanese Team   Peruvian Team

397

FUNDAMENTAL FACTORS IN OPTIMIZING EARTHQUAKE

DISASTER MITIGATION INVESTMENTS

by

Yoshijiro Sakagami

Eiichi Kuribayashi

Osamu Ueda

Tadayuki Tazaki

INTRODUCTION

Earthquake disaster mitigation investment become more reasonable by comparing invested resources to expected effects. Unlimited investment is not possible, for one reason, because severe earthquakes occur so infrequently that the new resources do not yield sufficient expected effect. Moreover, there are limited resources to invest.

Earthquakes are unusual phenomena, so disaster mitigation investment plans should not be alien to the usual regional plans. Inconvenience and inefficiency may not always be prime factors in considering disaster mitigation investments. This paper discusses a number of the fundamental factors in choosing earthquake disaster mitigation investments.

For the purposes above, it is necessary to estimate damage amounts and probability. Damage is classified as follows:

    (1) Physical loss

    (2) Economic loss

    (3) Social damage

Social damage is difficult to estimate because it is complicated by political, sociological, and psychological implications. Therefore, this paper deals mostly with physical and economic losses, and decision making procedures.

ESTIMATION OF PHYSICAL LOSS

Property Loss

Property loss is defined as the reduced value of property due to earthquakes. Estimating methods of property loss are classified in two ways: First, the loss is correlated with earthquake dimensions and ground conditions by using data from past, damaging earthquakes to estimate the loss from future earthquakes by using the correlation. Second,

the mechanical fracture of a structure and the ultimate seismic loading is defined, and the probability of the occurrence of an ultimate loading is estimated. The index of property loss is defined as the damage ratio to an individual facility or as the loss ratio valued in money. The damage ratio of an individual facility is used to assess the effectiveness of strengthening and retrofitting the vulnerable aspects. However, this is not adequate to assess regional disaster resistivity, because it does not represent the total damage of the region. Neither can it be compared with that of other individual facilities. To establish regional resistivity, the loss ratio which is the ratio of the loss to existing assets, both valued in money, is more useful. [1] This ratio can be used to compare the resistivity of different facilities, to calculate the ratio for total facilities, and for application in evaluating economic loss.

In evaluating the loss ratio of past earthquakes, property loss, which has two definitions, should be used. One is the replacement cost. The second is the value in current prices which takes depreciation into consideration. The former is mostly applied to public facilities, and the latter mostly to private property. Both methods have not yet been standardized in a official manner, and the data might contain a certain range of error.

Functional Loss

Lifeline facilities -- such as road, railroad, electric power, telecommunication, water supply, sewerage, and natural gas supply -- are infrastructures which supply goods, energy, and information to the society. If they are damaged, the functional loss is more important than the property loss. Functional loss delays the social and economic activities which are supported by lifeline facilities. One delay causes another delay in growing repetition.

The relationships between recovery time of lifelines as an index of the functional loss and severity of a disaster have been studied in several natural disasters. [2,3] Recovery time is determined not only by the property loss, but it also is affected by the difficulty of recovery which depends on topographical and geological conditions, equipment, material, and labor forces for recovery. High density of lifeline activities due to urbanization may further slow recovery.

Tables 1 and 2 summarize the recovery time for electric power and natural gas supply facilities in past Japanese earthquakes. Taking as examples the Niigata and Miyagiken-oki earthquakes, the magnitude and the size of the quake-hit cities of Niigata and Sendai -- population as of the year of the earthquake was 360,000 and 620,000 respectively -- of the two earthquakes are roughly equivalent. Epicentral distances to the two cities were 50 km and 110 km respectively. Recovery time in Sendai is much shorter than in Niigata. The reason is that redundancy in electric lines and the inter-gas company emergency cooperation system had been improved after the Niigata earthquake.

ECONOMIC LOSS

Property and functional loss affect the regional economy by causing damage to the machinery of industry and reducing productivity. As an example of the biggest consequence, Kato refers to the aftermath of the Kanto earthquake when a recession was accelerated and the government faced difficulty in finance and international trade. [4] However, in recent earthquakes we have not had a national-scale consequence. In many cases the economic consequence was hard to recognize statistically even at the prefectural level. One reason is that the recent earthquakes were not as big when compared to the Kanto earthquake. Another reason is that an earthquake has a positive influence in the economy as well as the negative one. An earthquake generates additional demand of material, equipment, and labor for recovery and reconstruction. If a surplus of labor force and equipment exists, the impact of an earthquake may absorb them.

In the Alaska earthquake of 1964 it is reported that the earthquake damage generated new demand for reconstruction which absorbed surplus labor force and also the renewal of aging equipment in the reconstruction improved productivity.

External aid also alleviates economic loss. The region which provides the aid suffers opportunity loss. Owing to the foregoing positive effects, it is possible that no recognizable consequence follows after an earthquake as far as economic statistics are concerned.

Figure 1 shows the trend of industry output before and after the Kanto earthquake of 1923. There was a clear reduction of the output. Figure 2 shows the index of industrial products in the Miyagiken-oki earthquake of 1978. The consequence of the earthquake did not last as long as in the case of Figure 1. Although the magnitude of the latter is not as big as the Kanto earthquake, industrial and commercial facilities in the Sendai and

400

adjacent areas suffered considerable damage. Outages of electricity, water, and natural gas supplies also affected industry and commerce to some extent. The reason that the consequences of the earthquake were minor is the prosperity in Sendai due to the opening of the Tohoku expressway and the construction of the New Tohoku railroad line which generated new demand and external aid.

Figure 3 shows a schematic tendency of an economic index before and after an earthquake. Curve (C) is the tendency without earthquake effects. Curve (A) shows the tendency assuming that the economic structure after the earthquake would not change compared to that before the earthquake. The drop in curve (A) can be named the loss potential, which is determined by earthquake dimensions, structural resistance, and economic structure. On the other hand, the actual economic index may follow curve (B) when the consequences of the earthquake are mitigated. The difference between curves (A) and (B) can be called the economic resistance, since it is the difference between the anticipated and actual economic loss. The economic resistance is determined by the following factors:

(1) Conditions of national and regional economy,

(2) Surplus productivity before the earthquake (labor force, equipment, and inventory),

(3) Recovery and reconstruction, and

(4) External aid.

The damaged economy returns to the original trend after a certain period, this is called the restoration period. The restoration periods of curves (A) and (B) are not always the same.

Economic loss is evaluated by using the loss potential, economic resistance, and the restoration period. The loss with no resistance is expressed by the area enclosed by curves (A) and (C). It is determined by the loss potential and the restoration period. It is considered to be the possible maximum loss, since it expects no surplus productivity or external aid. It is determined by the earthquake dimensions, structural resistance, and economic conditions within the damaged region. The economic resistance has the effect of alleviating the maximum. It is determined by economic conditions in and outside the damaged region. The economic loss is expressed, in other words, by the possible maximum loss and the economic resistance.

401

DECISION MAKING IN OPTIMIZING EARTHQUAKE DISASTER MITIGATION INVESTMENT

Decision making in earthquake hazard mitigation involves selecting the most effective means to alleviate the losses expected to the society. To do this the decision maker compares the resources invested and the effect of the alternative policies proposed. The resources invested involve the cost of strengthening structures, land use management, research, and inconvenience to the society. The effect includes the reduced physical and economic loss, and social damage.

It is much easier to compare cost and effect quantitatively when the alternatives have a certain similarity. Comparing the strengthening of high-rise buildings to single family dwellings is possible by figuring the cost of material, labor, and the reduced damage in both alternatives. However, comparing land use restrictions from the hazardous area to increasing hydrants for fighting fires quantitatively is almost impossible, or maybe senseless. In earthquake disaster we have many cases of the latter type.

The most popular method of comparing invested resources to effects is the cost-benefit analysis. The cost is relatively easy to define, except for the inconvenience to the society. It is defined as the expected expense of investment. As for the inconvenience to the society, one example is the unwilling relocation of residents enforced by a land use program. Some parts can be quantified while most, such as an increase in human comfort, are hard to quantify. Benefits are rather hard to define. Most narrowly, they are defined as reduced damage. However, more widely, they involve reduced casualties, increased comfort, and reduced need for disaster investment, which may be difficult to evaluate.

In cost-benefit analysis, investments whose C/B (ratio of cost to benefit) is greater than 1.0 are usually not adopted. In earthquake disaster mitigation, many alternatives may have a greater ratio than 1.0. However Oppenheim [6] suggested those are not always rejected. In his "risk aversion" theory the utility to be saved by an earthquake engineering investment is sometimes not proportional to the value in money to be saved. For instance the utility of the saved money of $10,000 is not necessarily ten times that of $1,000. Following this theory the investment with greater C/B may be adopted, because it may have greater utility compared to the cost.

It is possible to use this procedure as a tool for decision making. The problem is the difficulty in determining the utility function. Utility is a subjective matter which is difficult to translate in a quantitative manner.

Final decisions are not always based on quantitative data. Rather, many decisions are made using the qualitative information. It is vain or impossible to quantitize all factors and to compare their values.

How can the logical decision be reached considering all quantitative and qualitative information? In earthquake disaster mitigation investment, a decision maker has to consider many factors in multi-dimensional planes. It is not appropriate to translate them into one dimension. Taking property loss, economic loss, and social damage as an example, they have independent influences on a decision maker (see Figure 4). For example, social damage is not willingly accepted in order to reduce economic loss. Each dimension of the information has to be examined independently. The decision maker synthesizes independent factors and reaches a final decision. The procedures of selecting appropriate dimensions and of examining them accurately should be further studied.

CONCLUSIONS

(1) In earthquake disaster mitigation planning, it is recommended that earthquake damage be examined using the following three items, (a) physical loss, (b) economic loss, and (c) social damage.

(2) The loss ratio is one of the convenient indexes to evaluate the property loss.

(3) The economic loss is evaluated by the possible maximum loss and the economic resistance.

(4) In making earthquake disaster mitigation investment decisions, physical, economic, and social factors should be examined multi-laterally.

REFERENCES

[1]   Kuribayashi, E. and Tazaki, T., "An Evaluation Study on the Distribution Character-
      istics of Property Losses Caused by Historical Earthquakes," 10th Joint Meeting of
      UJNR, May, 1978.

[2]   Haas, J. E., et al., "Reconstruction Following Disaster," Cambridge, MA, MIT Press,
      1977.

[3]   Friesema, H. P., et al., "Aftermath," Sage Publications, 1979.

[4]   Kato, T., "Earthquake and Economy," Earthquake, University of Tokyo Press, 1976 (in
      Japanese).

[5]   National Academy of Sciences, "The Great Alaska Earthquake of 1964," Human Ecology
      Edition, Washington, D.C., 1970.

[6]   Oppenheim, I. J., "Economic Analysis of Earthquake Engineering Investment," 2nd
      National Conference on Earthquake Engineering, Stanford, 1979.

Table 1   RESTORATION OF ELECTRIC POWER

Earthquake	Date	M	Damaged Area	50% Restored	80% Restored	100% Restored
Kanto	1923.9.1	7.9	Tokyo, Yokohama	10 days	1 month	2 months
Niigata	1964.6.16	7.5	The area with V or more in JMA* intensity scale (excluding Niigata City)	3 hours	12 hours	1 day
"	"	"	Niigata City	1 day	3 days	24 days
Tokachi-oki	1968.5.16	7.9	The area with V in JMA intensity scale	5 hours	1 day	2 days
Miyagiken-oki	1978.6.12	7.4	Miyagi Pref.	8 hours	16 hours	1 day and 13 hours

* JMA : Japan Meteorological Agency

Table 2   RESTORATION OF GAS SUPPLY

Earthquake	Date	M	Gas Co.	Number of Customers	50% Restored	80% Restored	100% Restored
Kanto	1923.9.1	7.9	Tokyo Gas Co.	251,500	—	—	2 months (Unburned Area) 6 months (Burned Area)
Niigata	1964.6.16	7.5	Hokuriku Gas Co.	45,000	3 months	5 months	6 months
"	"	"	Aomori Gas Co.	4,000	—	—	6 days
Tokachi-oki	1968.5.16	7.9	Hachinohe Gas Co.	4,600	2 days	5 days	20 days
"	"	"	Towada Gas Co.	1,400	12 days	20 days	1 month
Miyagiken-oki	1978.6.12	7.4	Sendai Municipal Gas Bureau	135,863	12 days	15 days	27 days

Fig. 1　Impact of Kanto Earthquake of 1923 on Industries

Source: Statistics of Industries, Ministry of Trade and
　　　　　Industry, Japan

Number of Factories

Turnout
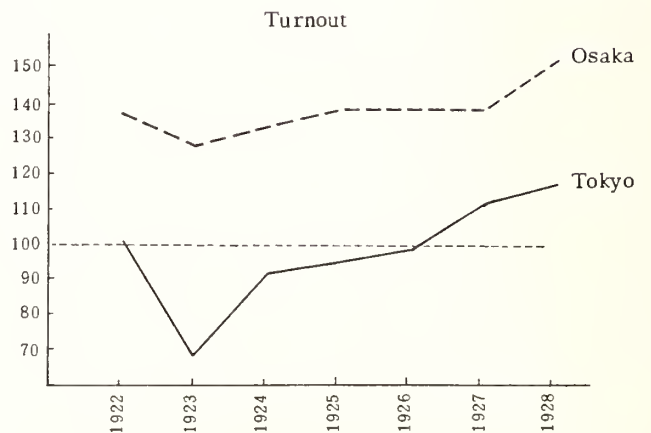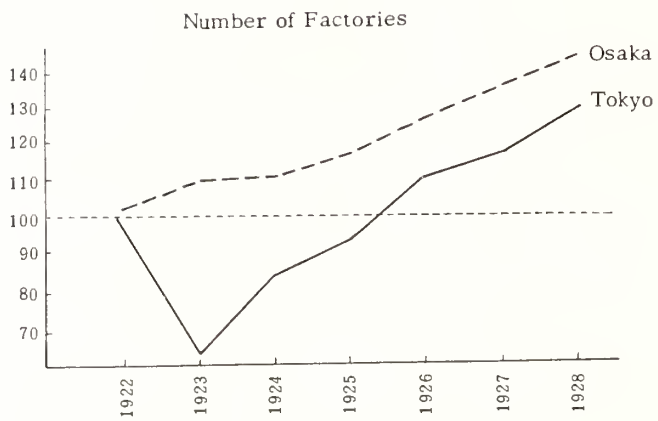
* Tokyo (1922) = 100
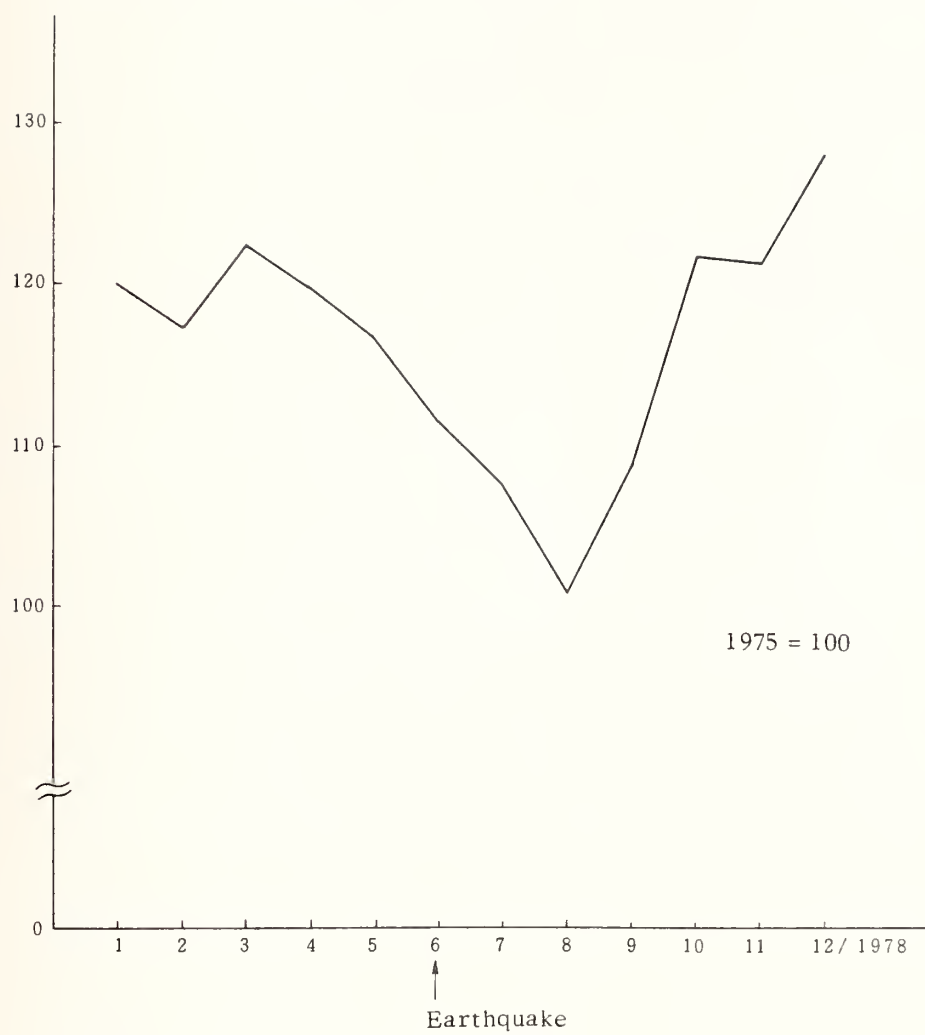
Fig. 2   Index of Industrial Product in Miyagi Prefecture
before and after the Earthquake
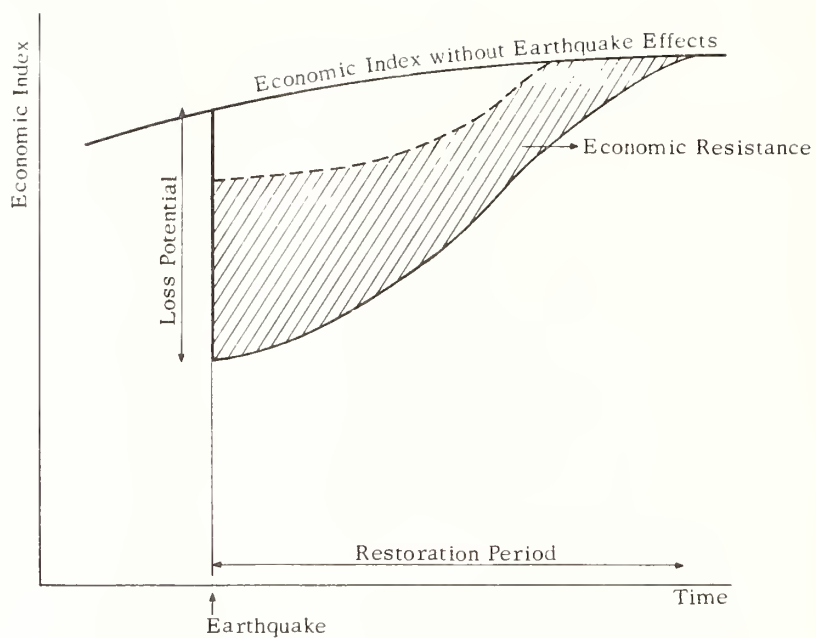
Fig. 3   Economic Resistance in Economic Loss due to Earthquake
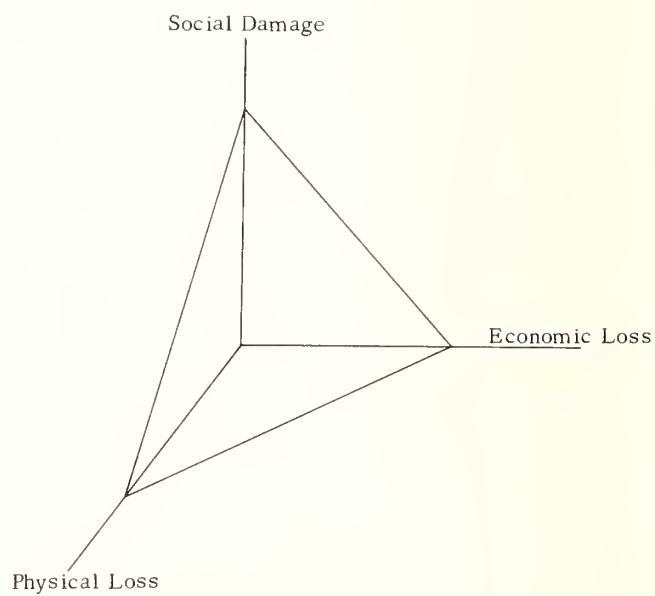
Fig. 4   An Example of Factors to be Considered in Earthquake
          Disaster Mitigation Investment

WOOD SHEATHED DIAPHRAGMS AS LATERAL FORCE RESISTING ELEMENTS

by

Edwin G. Zacher

INTRODUCTION

Wood sheathed diaphragms have been used in the design of lateral force resisting systems for less than fifty years in the United States. The performance of some masonry walled structures with diagonally sheathed wood floors and/or roofs during the 1933 Long Beach, California earthquake, encouraged some engineers to explore the possibility of using these building subsystems for resisting seismic forces. Tests were conducted using actual floor or roof systems of buildings being demolished. The tests led to proposed methods of analysis for diagonally sheathed diaphragms and acceptance of allowable values for the capacities of them. The draft of the Applied Technology Council project ATC-7, "Guidelines for the Design of Wood Sheathed Diaphragms" will have an extensive bibliography listing papers on these and other diaphragm tests. The "Guidelines" is due to be published in four to six months and it would be inappropriate to include this information in this short paper.

Since these initial tests there have been a number of tests conducted on diaphragms having dimensions of 16 to 20 feet by 48 to 60 feet. The early tests were made on diaphragms sheathed with one inch and two inch thick boards laid at an angle of 45 degrees or 90 degrees to the supporting framing. There was also one test made on a system with 3 inch decking. There were different fastening devices and different details for end posts and "chords" used in the tests to establish criteria for design of these systems.

The advent of plywood for the construction of floor and roof systems, and the labor savings made possible with this material, supplanted lumber (board) sheathing in wood frame construction. The plywood manufacturers association recognized the need to establish the acceptability of plywood sheathed floor and roof systems as diaphragms. They conducted a series of tests of plywood sheathed diaphragms of the same size as previously described. The results of these tests have been used to establish allowable diaphragm capacities and design procedures for these systems.

Plywood sheathed diaphragms can be conveniently analyzed by the girder analogy shown graphically on Plate 2.1 taken from the "Guidelines".

The "flange", often termed "chord" of the diaphragm can be the double top plate of a wood frame wall. The "flange" can also be a continuous wood ledger attached to a concrete or masonry wall. Steel ledgers, usually angles, have also been used. The reinforcement in the concrete or masonry wall is often used as the "flange".

The flanges of the diaphragms are typically considered in design to provide all of the resistance to the flexural stresses in the diaphragm. Based on this assumption the force on the flanges of the diaphragm can be determined by dividing the moment due to the loading by the distance between the center-lines of the flanges.

The flanges of most diaphragms, due to the length of these systems and the limitation on the length of available flange material, will have to be spliced. Splices should be located as far from the position of maximum moment as the length of available flange material will permit. Metal splice plates are often used with wood flange members. An oversight in the design of these splice plates which has often been noted is the failure to check the compression capacity of the plates.

The plywood sheathing is the analogous web of the diaphragm and is assumed to resist the shears due to the forces acting on the diaphragm. The diaphragms being considered in this paper are classified as "blocked". Unblocked diaphragms have low capacities and are not analogous to girders. A major feature of the diaphragm web is the number of splices required due to the limitation on the dimensions of the plywood panels in relation to the total dimensions of the system. There are a number of panel arrangements that can be used. Two of these arrangements are shown on Plate 2.2. The splice in the direction of the applied forces can be continuous or interrupted. The splices are made to occur over the framing members or "blocking". The blocking is in effect a splice plate and may take several forms. The arrangement at the top of Plate 2.2 shows interrupted splices and the connections (nails) required to effect the shear transfer are less than are required for the arrangement at the bottom of the plate. The codes recognize this by requiring that the nailing along the panel edges for the continuous splices conform to the nailing required for the "boundary" edges at the diaphragm reactions.

410

Most diaphragms have openings for various purposes, such as duct openings, skylights and stairways. Small openings which do not interrupt a full panel of plywood are not a concern in design. Larger openings which eliminate a number of plywood panels are considered in design. The analogous girder is again used for the analysis. Steel girders have been extensively studied for the effect of openings in their webs. There have been rules of thumb established for aspect ratios of openings with respect to depth of beam which indicate whether or not reinforcement of the opening is required. The tests on diaphragms with openings has been limited and similar rules have not been established for diaphragms.

The Vierendeel truss approach has been used to analyze steel girders with web openings and is appropriate for diaphragms with web openings. When the opening in the web is centered on the width of the diaphragm the distribution of the shear at the opening is one half to each portion of the diaphragm remaining. When the opening is not centered the distribution is made on the basis of the relative widths of the diaphragm remaining on each side of the opening. Plate 2.6 illustrates the two conditions.

The segments of the diaphragm at each side (ahead of and beyond the opening in the direction of the applied forces) are analyzed as separate diaphragms for the local forces acting on them. The forces in the main flanges due to the action of the diaphragm segment are then combined with the forces due to the action of the total diaphragm. The forces on the flanges at the edges of the opening are those due to the action of the diaphragm segment only. These forces must be distributed into the body of the diaphragm and requires that the framing member acting as the interior flange be extended beyond the opening. The detail for accomplishing the transfer of the flange force will vary depending on the framing arrangement. Metal splice plates are often used with blocking to extend the discontinuous header joists at these locations.

PERFORMANCE OF DIAPHRAGMS

Buildings utilizing wood sheathed diaphragms have had a variable record of performance in past earthquakes and wind storms. The performance can generally be associated with the degree of detail that went into the construction. Where diaphragms have been well detailed and the details have been followed in construction the buildings have had a good record of performance. The bad performance record is attributable to poor details for connections or lack of compliance with the design drawings.

411

The 1971 San Fernando earthquake provided a good test of the detailing and construction practices for connecting wood sheathed diaphragms. There were a good number of one story warehouse, manufacturing and commercial buildings in the area built during the preceeding twenty years. The change in construction practice during that period was evident in the differences in damage to the buildings. There were several older buildings with diagonally sheathed roofs and standard roof joist framing. These had anchorages connecting the walls to the joists at four foot centers. No damage was observed in connection with these buildings. A majority of the buildings were constructed with "panelized" roof systems and the wall anchorages were made through ledgers bolted to the walls. Many of these systems had failures when the connection of the main roof framing was inadequate to transfer the forces from the walls into the diaphragm.

High winds have resulted in similar performance records for buildings using wood sheathed diaphragms. The wind forces create a local effect at eaves, ridges, corners and similar surface discontinuities which causes uplift on the diaphragm sheathing. This local effect can reduce the effectiveness of the diaphragm although it is not involved in the diaphragm action. There are fastening devices now available which are capable of resisting these uplift forces, and thus permit the diaphragm to act as was intended.

DESIGN OF CONNECTIONS

Wood sheathed diaphragms can be designed and constructed to perform more reliably if care is taken with the connection details. In order to design connection details it is necessary to understand how these forces are applied. Plates 1.1 and 1.2 illustrate the forces acting on the various elements of the building. Wind forces acting on the diaphragm will be those due to the wind on the wall elements tributary to the roof and the horizontal component of the wind on the roof. The wind forces for which connection details have been found to be critical are those acting on the walls. Seismic forces are contributed by the portion of the wall elements tributary to the roof and by the roof itself. In this case, also, the forces for which the connections have been found to be critical are those from the walls.

Plates 3.1 and 3.3 illustrate some of the conditions that are encountered in buildings with diaphragms. The force from the wall in Detail 3.1 A is delivered to the diaphragm through the sheet metal framing anchor to the blocking, and thence to the diaphragm by the

412

nails through the sheathing to the blocking. The number of nails required to transmit the force from the blocking to the sheathing can be calculated. The number of nails may be more than can be safely and prudently installed in one piece of blocking, in which case additional blocks are installed in adjacent joist spaces and continuity is provided by sheet metal splice straps. This will extend the distance available to transfer the force into the body of the diaphragm. A block in a single joist space is not advisable except for very small tributary forces. Detail 3.1 B illustrates the method of transfer when the wall is structurally discontinuous, such as at gable ends of roofs. The force from the wall is transmitted through the sheet metal framing clip to the 2 x - brace, which is nailed to the blocking, and the force is then transferred to the sheathing as in Detail 3.1 A. The framing devices used in both details are capable of resisting uplift forces and would thus provide for vertical and lateral force components due to wind. Detail 3.1 C illustrates the simplest and most direct method of transferring the forces from the wall to the diaphragm.

Details 3.3 A and 3.3 B illustrate two different framing arrangements used in this country for multiple story wood frame construction. "Baloon" framing is illustrated in Detail 3.3 A. This type of framing arrangement was more prevalent some years ago than it is today. The "platform" framing arrangement shown in Detail 3.3 B is more common today. The force from the wall in Detail 3.3 A is that due to the contribution from the wall above and below the diaphragm. The force is transferred from the wall to the blocking by the sheet metal twist strap, and from the blocking to the diaphragm by nails through the sheathing to the blocking. The forces from the wall elements above and below the dia-phragms are delivered through separate paths in Detail 3.3 B. The force from the wall above the diaphragm is transferred by the nails through the sole plate to the blocking. These nails also penetrate the sheathing, thus affecting the transfer. The force from the wall below the diaphragm is transferred through the sheet metal shear angle to the block and is similar to Detail 3.1 A for the remainder of the transfer. Detail 3.3 C is similar to Detail 3.3 B except that the wall below the diaphragm is concrete or masonry. For this detail the anchor bolt transfers the force from the wall to the sill. A sheet metal framing clip is used for transmitting the force from the sill to the block in lieu of the shear angle used in Detail 3.3 B. This was done to prevent creating a transverse tension condition in the sill. This condition is prohibited for seismic force resistance.

413

There are often other loads which must be delivered into the diaphragm, such as concentrated loads from a large sign structure acted on by winds or a heavy piece of building equipment acted on by seismic motions. Plate 2.10 illustrates the sign condition in the upper portion. The lower portion of the plate illustrates another condition where large concentrated loads may be delivered to the diaphragm. The forces due to wind or seismic in the second story portion must be delivered through the second story wall at the break to the diaphragm, which must transmit this force to the end walls since there is no interior wall in the first story at the break. The small segment of exterior wall at this location is inadequate to act as a support. Plate 5.20 illustrates two special loads being transmitted to the diaphragm. One load is a line load from the penthouse walls and other loads are concentrated point loads from the tank supports. Adequate vertical support for these loads must, of course, be provided and, in addition, the lateral forces resulting from seismic motion must be distributed into the diaphragm. The details at the bottom of the plate indicate the methods used for this purpose.

The connections discussed to this point were provided to deliver the forces to the diaphragm. As in all structural systems there is a requirement that reactions by provided to resist the forces that have been introduced. The reaction components of the lateral force resisting system usually employed with buildings having diaphragms are shear walls. The connection details for transferring the reaction from the diaphragm to the shear wall are as critical to the performance of the building as the connections for transferring the forces to the diaphragm. Plates 3.5 and 3.6 show various details for accomplishing this transfer.

Details 3.5 A and 3.5 B show the method of transfer involved with two different joist support arrangements in balloon framed wood wall construction. The force is transferred from the sheathing in Detail 3.5 A to the header-joist ledger and from the ledger to the blocking and thence to the wall sheathing. The transfer in Detail 3.5 B is from the diaphragm sheathing to the horizontal blocking, from the horizontal blocking to the vertical blocking, and from the vertical blocking to the wall sheathing.

Detail 3.5 C indicates a condition where two diaphragms abut to a shear wall at different levels. The transfer at the upper level is accomplished by the nailing to the header-joist through the diaphragm sheathing, then to the double top plate by means of the sheet metal shear angle and finally to the wall sheathing by the nailing of the sheathing

414

to the plate. The force from the lower diaphragm sheathing is transmitted to the header-joist ledger, from the ledger to the top plate by nailing through the ledger to the plate and finally to the wall sheathing.

The transfer details on Plate 3.6 are for use with concrete or masonry walls. Detail 3.6 A has a framing arrangement with the framing members parallel to the wall. The ledger in this detail is the common member for attachment to the sheathing and the wall. The nailing of the sheathing transmits the force to the ledger and the bolts transmit the force on to the wall. The ledger bolts are also subjected to vertical loads and the combination of the loads must be resisted.

Detail 3.6 B is a more involved detail having a steel angle ledger. This might be employed when there are large vertical loads being supported by the ledger. Wood in cross grain bearing has limited capacity well below the capacity of the bolt in the concrete. The force from the sheathing is transmitted to the blocking, then from the blocking to the ledger angle by bearing against the welded plates. The bolts from the ledger angle to the wall complete the transfer. The number of pieces involved and the need for close dimensional coordination between the framing layout, the ledger angle fabrication and the bolt spacing in the concrete relegate this detail to use only when other considerations override the problems enumerated. The alternate solution shown dashed on the same detail eliminates a number of the problems but creates another problem; the transfer of forces to the diaphragm for the normal direction requires additional devices.

Detail 3.6 C shows a typical "panelized" roof construction with the wall stopping at the roof line. The transfer here is from the sheathing to the sill, and from the sill to the wall by means of nailing and bolting, respectively. There are an unlimited number of different conditions that can occur and there are additional details in the "Guidelines" including design examples with numerical results.

There is one additional type of force transfer from the diaphragm to the vertical resisting element which needs to be discussed. The details shown thus far had the vertical resisting element at the location of the boundary of the diaphragm but there are many occasions where this condition is not provided. Plate 5.7 illustrates one condition where the vertical resisting element extends over only a portion of the width of the diaphragm. In this case it becomes necessary to introduce a member to "drag" the forces from the diaphragm to the vertical element, a "drag strut."

Plate 2.9 show two other configurations of buildings where drag struts must be introduced to effect the transfer of lateral forces from the diaphragm to the vertical resisting elements. The top portion of the Plate shows a type of residence that experienced considerable damage in the San Fernando earthquake. The failure to provide drag struts and vertical transfer members resulted in essentially total loss of some of these buildings. The building at the bottom of the Plate illustrates a more complex version of the conditions shown at the top of the Plate. The problems created by site and architectural arrangement conditions often tax the ingenuity of the design engineer to provide a structural system that will provide the required resistance to lateral forces.

There are a number of additional configurations and conditions which are encountered in buildings with diaphragms but this short paper cannot include illustrations and discussions on all of these. Diaphragm stiffness has an important effect on the performance of buildings. Procedures have been developed for calculating the stiffness of plywood sheathed diaphragms which have been shown to be somewhat reasonable by test measurements. Diagonally sheathed diaphragm deflections are not as well known. The period of the diaphragm may govern the response of the building to seismic motions and, since the period of the diaphragm is related to its stiffness, it is important to be able to reasonably determine the stiffness of this element. Recent strong motion instrumental records will assist in determining the effects of diaphragm action. Diaphragms are often irregular in shape, as was shown on Plate 2.10, and special detailing is necessary to resist the stresses created by the discontinuities. Diaphragms may also be continuous over a number of spans. The distribution of the forces to the various reactions should be determined on the basis of the relative rigidities of the diaphragm and the vertical elements of the lateral force resisting system providing the support.

Wood sheathed diaphragms can be used as parts of lateral force resisting systems. Buildings utilizing wood sheathed diaphragms will perform well when they are properly detailed and constructed. The importance of providing continuous paths for transmitting lateral forces from their point of origin to the final point of resistance at the foundation level can not be overemphasized.

Wind pressures in
pounds per square
foot, psf

psf

psf

psf

psf

psf

Assumed wind
direction
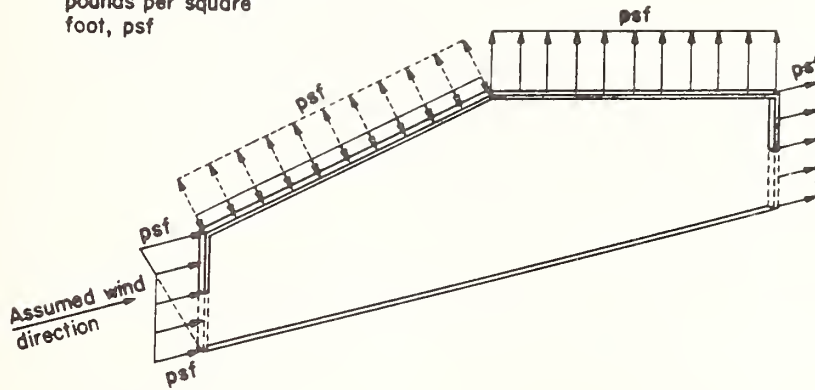
I FOOT SEGMENT OF BUILDING

Wind forces in pounds
per lineal foot, plf

Reaction

Forces contributed by leeward roof

Forces contributed by
leeward wall

plf

plf

plf

plf

Forces contributed by windward roof

Assumed wind
direction

Forces contributed by
windward wall

Reaction
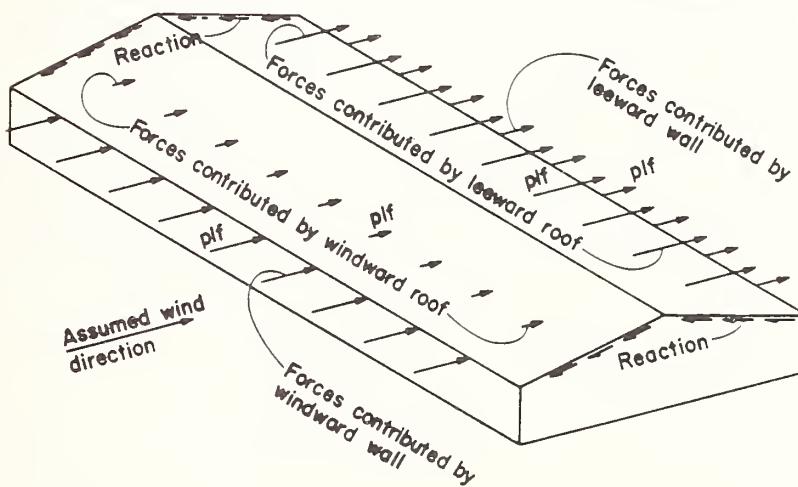
ONE STORY BUILDING

WIND FORCES

PLATE I.I

Seismic "pressures" in pounds per square foot, psf

psf

Assumed seismic force direction

psf

Portion tributary to roof level

psf
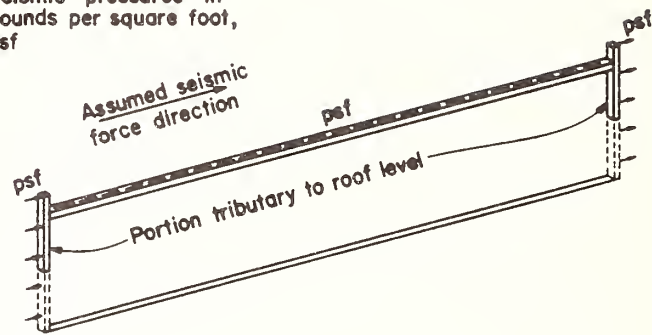
I FOOT SEGMENT OF BUILDING

Seismic forces in pounds per lineal foot, plf

Reaction

Forces contributed by roof

Forces contributed by right hand wall

plf

plf

plf

Assumed seismic force direction

Forces contributed by left hand wall

Reaction
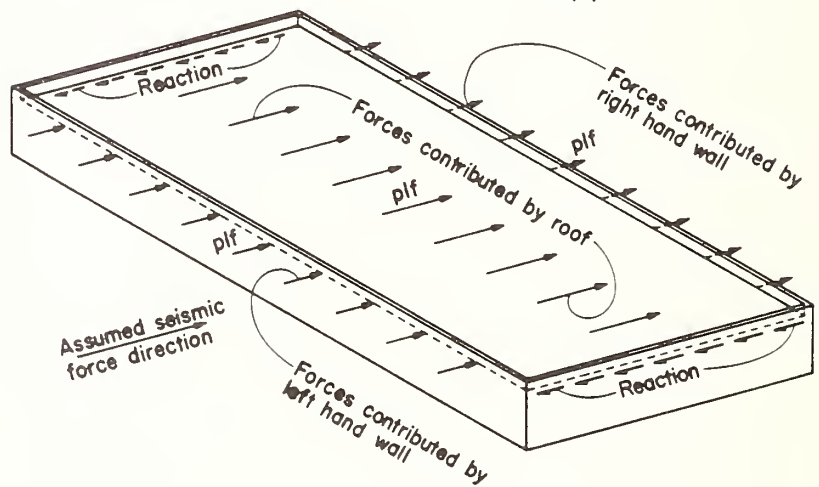
ONE STORY BUILDING

SEISMIC FORCES   PLATE 1.2

418

Sym. about ℄

Web splice

Flange - web shear transfer

Forces

Flange splice

Reaction

Web

Flange

BUILT UP STEEL GIRDER

*Continuous rim joist often used instead - preferable

Sym. about ℄

Web splice

*Blocking (typical)

Blocking

Forces

Joist or rafter

Wall sheathing

Flange splice

Flange - web shear transfer

Reaction

Web

Flange
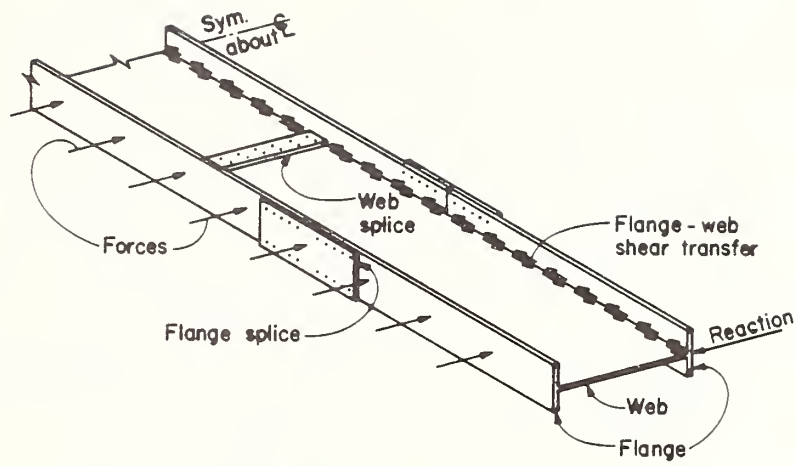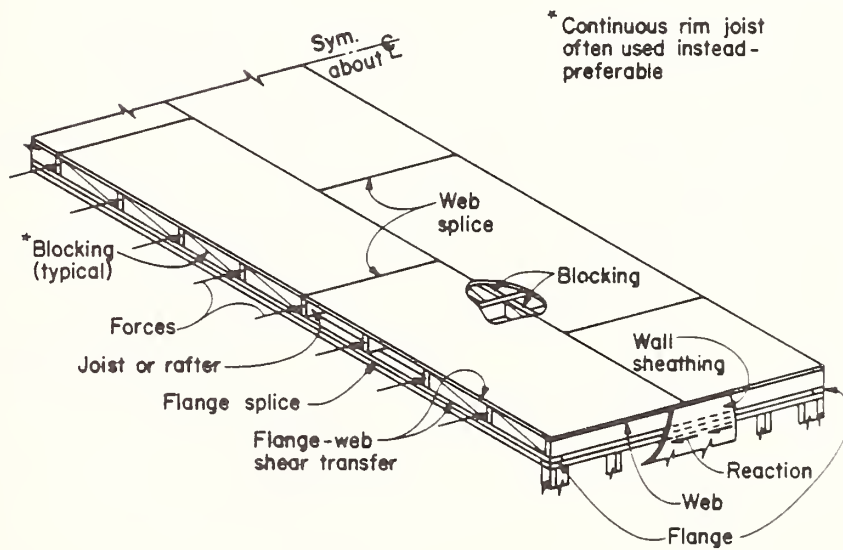
PLYWOOD SHEATHED DIAPHRAGM

GIRDER ANALOGY   PLATE 2.1

Direction of assumed forces

Panel edges

Joists

Blocking

Panel edges not continuous in direction of force

Diaphragm boundary

CASE 1

Direction of assumed forces

Panel edges

Joists

Blocking

Panel edges continuous in direction of force

Diaphragm boundary
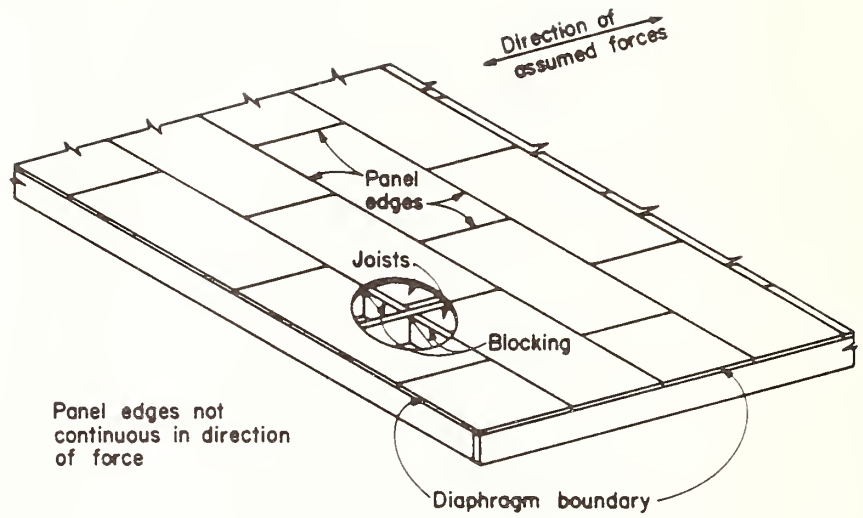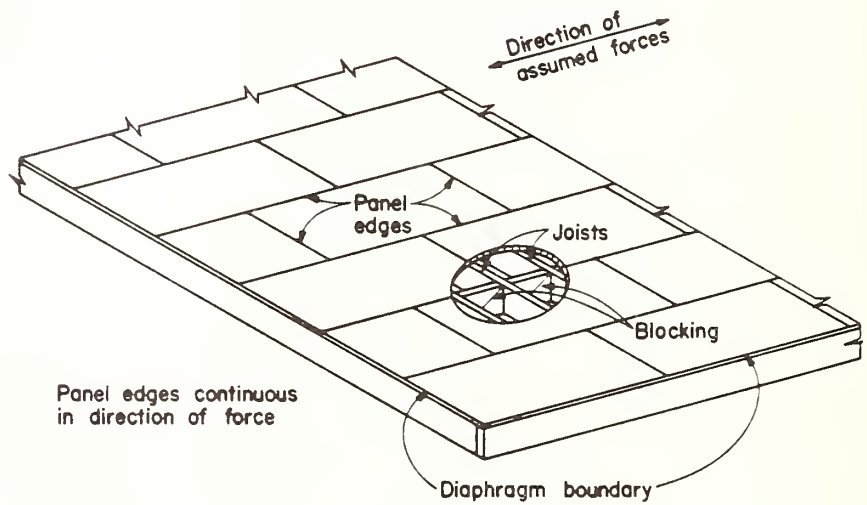
CASE 2

PLYWOOD PANEL ARRANGEMENTS   PLATE 2.2

SEGMENT OF BUILDING

SEGMENT OF BUILDING

DIAPHRAGMS WITH OPENINGS   PLATE 2.6

421

Forces contributed by leeward roof

Sign

Forces contributed by leeward wall

Force on sign

Forces contributed by windward roof

Assumed wind direction

Forces contributed by windward wall

SIGN ON ROOF

Forces contributed by wall

Forces contributed by upper roof

Forces contributed by wall

Forces contributed by wall

Forces contributed by wall reaction

Forces contributed by floor

Forces contributed by lower roof

Assumed seismic force direction

Forces contributed by wall

ONE AND TWO STORY BUILDING

SPECIAL LOADING CONDITIONS   PLATE 2.10

422

Diaphragm sheathing

2 x - blocking

Boundary nailing

Nails to blocking

Typical nailing

Wall sheathing

Joist

Double plate

Force

Sheet metal framing anchor at each block

Stud wall

DETAIL 3.1 A

Diaphragm sheathing

16^d nails

Gable end stud wall

2 x - brace

Force

Blocking

Anchor bolt

Sheet metal framing clip

Sill

DETAIL 3.1 B

Boundary nailing

Diaphragm sheathing

Roof joist

Force

Joist hanger

Blocking

Stud wall

DETAIL 3.1 C

CONNECTION DETAILS FOR
TRANSFER OF FORCES TO DIAPHRAGM   PLATE 3.1

423
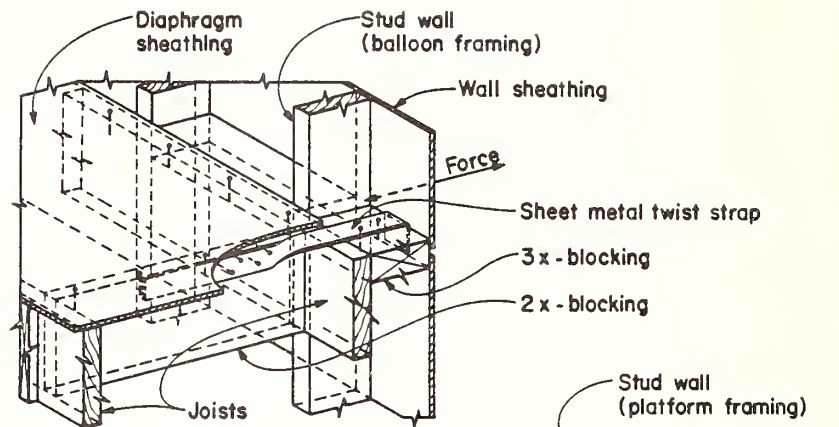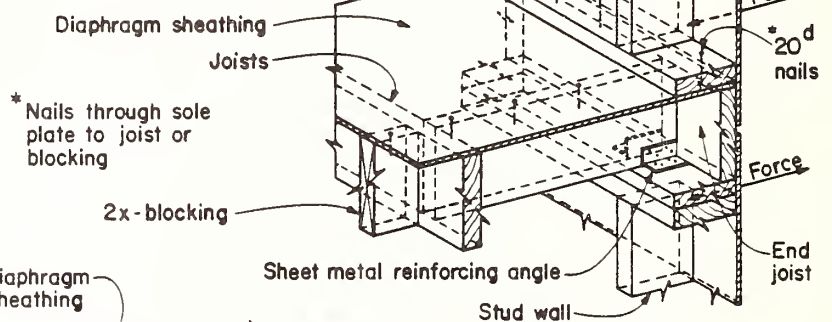
DETAIL 3.3 A
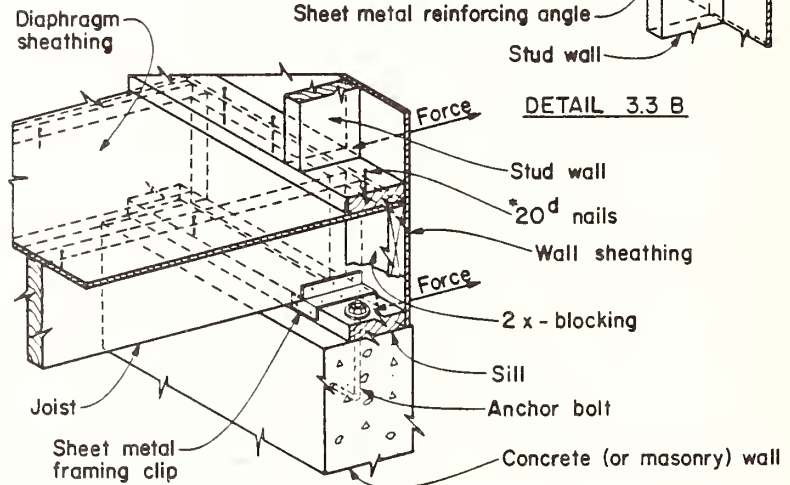
DETAIL 3.3 B

DETAIL 3.3 C

CONNECTION DETAILS FOR
TRANSFER OF FORCES TO DIAPHRAGM   PLATE 3.3

Stud wall
(balloon framing)

Wall sheathing

Typical nailing

Blocking

Diaphragm
sheathing

Boundary nailing

Reaction

Force

Joist

Joist hanger

Header joist - ledger

16^d nails

DETAIL 3.5 A

Boundary nailing

Stud wall (balloon framing)

Diaphragm sheathing

16^d nails·

Typical nailing

Force

Reaction

Wall sheathing

Joist

Joist

1x - ribbon

Blocking

DETAIL 3.5 B

Boundary nailing

Diaphragm sheathing

Sheet metal shear transfer angle

Joist hanger

Typical nailing

Joist

Stud wall

Header joist - ledger

Force

Reaction

Force

DETAIL 3.5 C

CONNECTION DETAILS FOR
TRANSFER OF FORCES FROM DIAPHRAGM   PLATE 3.5

Boundary nailing

Diaphragm sheathing

Concrete (or masonry) wall

Joist

Anchor bolt

4 x – ledger

Reaction

Force

DETAIL 3.6 A

Diaphragm sheathing

Typical nailing

Concrete (or masonry) wall

Boundary nailing

Alternate – 3 x – ledger bolted to wall and joists bevel cut

Reaction

Force

Joist

2 x – blocking

Plate welded to angle and bolted to joist

Angle ledger with anchor bolts

DETAIL 3.6 B

Diaphragm sheathing

Boundary nailing

Joist hanger

Sub – purlin

Force

Reaction

Purlin

Joist hanger

Concrete (or masonry) wall

Sill with anchor bolts

DETAIL 3.6 C

CONNECTION DETAILS FOR
TRANSFER OF FORCES FROM DIAPHRAGM   PLATE 3.6

426

Wind pressures in pounds per lineal foot, plf

Open

133 plf

125 ft

8 ft

Shear wall

36 plf

5.7A

Reaction

Roof rake overhang

5.7B

126 plf

186 plf

Open

100 ft

PARTIAL BUILDING

Joist

Diaphragm sheathing

Blocking

Splice plate with
$4-1\frac{1}{8}$ in. x 12 in. lag bolts
to beam and
$4-1\frac{1}{8}$ in. machine bolts
to plate

$1\frac{1}{2}$ in.

3 at $4\frac{1}{2}$ in.

8 in.

8 in.

3 at $4\frac{1}{2}$ in.

$1\frac{1}{2}$ in.

2-3x6 plate

Wall sheathing

DETAIL 5.7 A

Diaphragm sheathing

Joist

Blocking

Splice plate with
$8-1\frac{1}{8}$ in. x 12 in. lag
bolts to beam

Beam

$1\frac{1}{2}$ in.

3 at $4\frac{1}{2}$ in.

8 in.

Symmetrical

Column

DETAIL 5.7 B

**WIND FORCES
DESIGN EXAMPLE 5.3**

PLATE 5.7

SPLIT LEVEL RESIDENCE
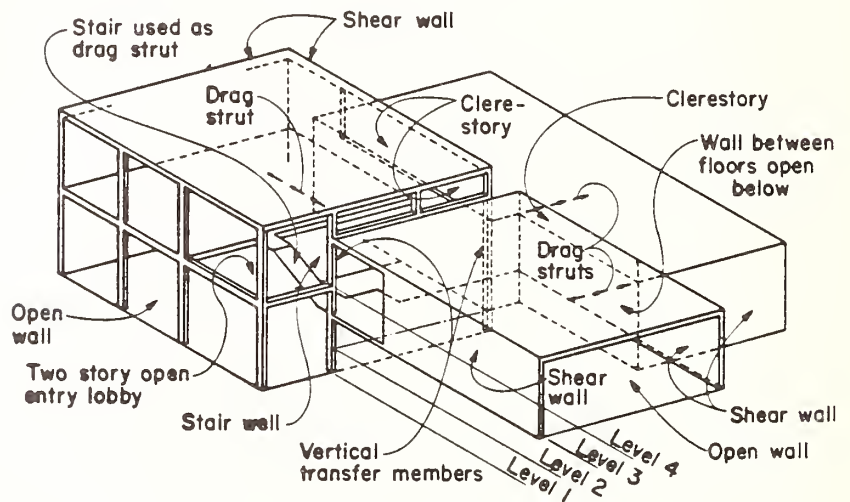
MULTI LEVEL OFFICE

SPECIAL CONFIGURATIONS   PLATE 2.9

A PROPOSED METHOD FOR THE EVALUATION OF ASEISMIC
PERFORMANCE OF EXISTING TIMBER DWELLINGS

by

T. Murota

H. Okada

ABSTRACT

In response to strong social concerns about aseismic performance of existing buildings in Japan, the Ministry of Construction and the Japanese Building Disaster Prevention Association proposed, in 1979, an evaluation method for aseismic performance of existing timber dwellings. This was in addition to the earlier proposals of similar evaluation methods for existing reinforced concrete and steel construction buildings of 1977 and 1978. The evaluation method for timber dwellings differs from the preceding two methods in that aseismic performance can be evaluated not by structural engineers but by owners themselves.

In this paper an outline of the aseismic performance evaluation method for timber dwellings and some applications are described.

INTRODUCTION

In recent years severe earthquakes such as the Izu-Penninsula Earthquake, the Izuohshima Earthquake, and the Off-Miyage Earthquake have continued to occur. It is predicted that a big earthquake may occur in the near future at a point offshore from the Tokai area. Under these circumstances a general concern about the aseismic performance of buildings has been itensified.

Corresponding to this concern, the Ministry of Construction and the Japanese Building Disaster Prevention Association proposed aseismic performance evaluation methods for existing reinforced concrete buildings, and for steel buildings in 1977 and 1978, respectively. However, most Japanese buildings are timber constructed dwellings and therefore the above methods were not enough to satisfy the general concerns. The Ministry of Construction and the Japanese Building Disaster Prevention Association then began to develop a similar method for timber construction dwellings in 1978. A committee, which consists of the members named below, was organized and along with the Japanese Building Disaster Prevention Association undertook the development and completed the work in 1979. An outline and some applications of the aseismic performance evaluation method for timber dwellings developed by the committee are described in the following sections.

COMMITTEE MEMBER LIST

Hideo Sugiyama	Chairman, Professor, Department of Agriculture, Tokyo University
Yukihiro Kamiyama	Professor, Department of Engineering, Waseda University
Isao Sakamoto	Assistant Professor, Department of Engineering, Tokyo University
Tatsuo Murota	Building Research Institute, Ministry of Construction
Hisashi Okada	Building Research Institute, Ministry of Construction
Koji Ueda	Housing Bureau, Ministry of Construction
Haruhisa Kato	Housing Bureau, Ministry of Construction
Kyoichi Kobayashi	Housing Bureau, Ministry of Construction
Toshibumi Fukuda	Housing Bureau, Ministry of Construction
Tamio Oba	Urban Planning Bureau, Tokyo Metropolis Administration

Kuniaki Shimazaki   Urban Planning Bureau, Tokyo Metropolis Administration

Tatsuo Watanabe   Urban Planning and Housing Department, Shizuoka Prefecture

Atsushi Maseki   Building Safety Association of Aichi Prefecture

Hiroshi Nakajima   Japanese Architecture Association

Mikio Maeoka   Japanese Building Disaster Prevention Association

ASEISMIC PERFORMANCE EVALUATION METHOD

The purpose of this aseismic performance evaluation method is to provide residents with safety measures for their houses. Using this method, residents may easily find conclusions to the problem of whether their houses can better resist strong earthquake motions.

In the method, residents are asked to judge the following six items:

(a) soil condition and type of foundation

(b) weight of roof and number of stories

(c) arrangement of walls

(d) existence of diagonal members

(e) length of walls

(f) extent of aging

Residents can make the judgment easily by drawing a first floor plan of their houses (Figure 1), making observations at several places in their houses, and by then making simple calculations.

Drawing the First Floor Plan

As the first step residents are requested to draw the first floor plan on graph paper. The first floor plan is necessary to calculate floor area, wall length, and to determine wall arrangements. An example is shown in Figure 1. The length unit for the drawing is the "ken" which is a traditional Japanese unit of about 1.8 m.

Calculation of Floor Area

The calculation of floor area is to be made in a Japanese unit called the "Tsubo" (= 1 ken x 1 ken = 3.3 m^2).

<u>Completing the Mark (or Ranking) Sheet</u>

Following Table 1, as the next step, residents are to select appropriate marks for each items from a to f described below which correspond to results of observations or calculations requested.

In cases where more than two marks may be selected for an item, the smaller values are to be selected.

Procedures for making the judgments or calculations and the background for the ranking scheme shown in Table 1 are as follows:

(a) Soil Condition and Type of Foundation

Soil condition is closely related to the acceleration level put into houses during an earthquake. Footings of timber houses are generally embedded into very shallow ground, and this often leads to differential settlement of the surface ground. Damage is observed more in the case of separated footings than in the case of continous footings. These facts are reflected in the marks for item a.

Classification of soil condition is generally very difficult for nonprofessionals and therefore the following suggestions are provided for reference:

hard ground -- rock, sand gravel, gravelly soil

soft ground -- marsh, reclaimed land, artificial fill ground, top of slopes

(b) Weight of Roof and Number of Stories

This item is related to the input lateral force caused by earthquakes. In general, the shear force which acts on houses is roughly proportional to the dead weight of houses, which consist, mainly of roof weight and number of stories. Marks for this item are decided by these facts.

Roof weight is to be judged by referring to examples below:

heavy roof -- clay-tile roofing, cement-tile roofing

light roof -- iron-sheet roofing, asbesto-cement roofing

The number of stories is confined to two cases. This is because timber construction of more than 3 stories are prohibited as a rule and basements are very rare in Japan.

(c) Arrangement of Walls

Observing the earthquake damage to timber dwellings, it is noted that the arrangement of walls and openings on the exterior wall planes has a great effect on

432

the extent of damage. In this evaluation, wall-opening arrangements are classified into six types as shown in Figure 2.

(d) Existence of diagonal members

Earthquake resistant structural elements in Japanese houses of timber construction are mainly plaster walls, walls of board siding, and diagonal bracings. In the Japanese building code, a relative bearing capacity for these elements is provided, i.e., bearing capacities of board siding walls and diagonal bracings (30 mm x 90 mm cross-section) are 1.5 times that of plaster walls.

The object of this item is to estimate the bearing capacity of the walls. In cases where diagonal bracings are adopted, the corresponding mark for this item is 1.5 and in other cases 1.0. The mark for board siding walls can be estimated as 1.5 according to the Japanese code but in this evaluation method 1.0 is adopted because the value 1.5 seems to be over-estimated considering the test results.

Usually the existence of diagonal members can not be determined from external appearance, therefore, except when the existence is confirmed by design documents or memory it must be judged that diagonals do not exist.

(e) Length of Walls

Referring to the first floor plan drawn before, the length of walls are to be summed up for two perpendicular directions, respectively. The lesser of the two values divided by the first floor area previously calculated determines the mark for this item according to Table 1.

In the Japanese building code, a minimum requirement of wall length/floor area is provided. According to this provision, in cases where a one-story timber house is constructed on continuous footings and plaster walls are adopted as earthquake resistant structure elements, the total sum of the plaster wall length in a direction must be more than 15 cm per unit floor area 1 m^2. Reducing the unit into "ken/tsubo" which is used in this evaluation method, it becomes 0.275 ken/tsubo.

From this fact a mark of 1.0 is taken as a standard for this item when the wall length/floor area is in the range of 0.275 ± 0.025. Therefore a mark of 1.0 for this item is considered to be legal concerning the wall length requirement for earthquakes.

(f) Extent of Aging

This item is provided to estimate the decrease in bearing capacity which may have been caused by aging. Marks for this item are based on the assumption that when things like deformation to structural frames or foundation, cracks in footings, remarkable decay in timbers, nesting of white ants, etc. are seen, aseismic performance may have decreased.

Total Marks and Judgment

The total mark is obtained by multiplying all the marks for items a to f. According to the value of the total mark, residents can arrive at one of four judgments as shown in Table 2.

For a house with a total mark less than 0.7, the house is judged to have a possibility of collapse, and it is recommended the owner consult with structural engineers about retrofitting. Houses whose mark is 0.7 to 1.0 are judged not to have enough aseismic performance and a more detailed inspection is recommended. When the mark is more than 1.0, it is judged that the house will be safe in earthquakes but when the mark does not exceed 1.5 it is still thought to be better to ask a structural engineer to make an inspection. This is due to the calculation of wall length where all walls are considered effective when some walls may, in fact, be ineffective as structural members.

APPLICATION

Results of the application of this evaluation method to existing timber houses are shown in Table 3. Sixty-two houses were selected as objects of application. No. 1 to 50 are houses in Kodaira City, Tokyo; No. 51 to 53 are those in Shizuoka Prefecture; No. 54 to 60 are those which appeared in the magazine "New Housing;" and No. 61 and 62 are those of "daikoku-bashira" construction, which is a traditional Japanese construction.

The distribution of total marks for these 62 evaluations is shown in Figure 3. Mean and standard deviation of total marks were 1.56 and 0.51 respectively. Only one house (1.6 percent) scored less than 0.7 and was judged liable to collapse. Five houses (8.1 percent) scored 0.7 to 1.0 and were judged to need a more detailed inspection. Fifty-six houses (90.3 percent) scored more than 1.0. Thirty-four houses (54.8 percent) ranked higher than 1.5, and they were judged to have sufficient aseismic performance.

434

CONCLUDING REMARKS

In this paper the aseismic performance evaluation method for timber dwellings proposed by the Ministry of Construction and the Japanese Building Disaster Prevention Association is described. Many problems concerning the accuracy of results obtained using this method can be seen. The purpose of this evaluation, however, is to provide large numbers of residents with a rough measure of the aseismic performance of their dwellings', and it is considered almost inevitable that accuracy will be sacrificed to some extent.

There is much interest in the predictive accuracy of this evaluation method. However, no data has been collected as yet, but as earthquakes occur it is expected that detailed comparisons will be made.

Table 1 Marks for item a to f (Ranking Criteria)

Mark for item a soil condition and type of foundation

type of foundation	soil condition		
	hard	medium	soft
continuous concrete footing	1.2	1.0	0.7
others	0.7	0.6	0.5

Mark for item b weight of roof and number of story

number of story	weight of roof	
	heavy	light
1	1.3	1.0
2	0.7	0.6

Mark for item c arrangement of walls

type of wall arrangement	mark
A	1.2
B	1.0
C	0.9
D	0.8
E	0.7
F	0.8

* Types of wall arrangement are shown in Fig.2.

Mark for item d existence of diagonal members

diagonal members	mark
exist	1.5
none	1.0

Table 1 continued

Mark for item e length of walls

total wall length / first floor area	mark
L/A < 0.08	0.2
0.08 ≤ L/A < 0.14	0.4
0.14 ≤ L/A < 0.19	0.6
0.19 ≤ L/A < 0.25	0.8
0.25 ≤ L/A < 0.30	1.0
0.30 ≤ L/A < 0.35	1.2
0.35 ≤ L/A < 0.41	1.4
0.41 ≤ L/A < 0.46	1.6
0.46 ≤ L/A < 0.52	1.8
0.52 ≤ L/A < 0.57	2.0
0.57 ≤ L/A < 0.63	2.2
0.63 ≤ L/A < 0.68	2.4
0.68 ≤ L/A < 0.74	2.6
0.74 ≤ L/A < 0.79	2.8
0.79 ≤ L/A	3.0

Mark for item f extent of aging

extent of aging	mark
not decayed	1.0
decayed	0.9
cracks in foundation	0.9
eaten by white ants	0.8

Total mark P

$$P = a \times b \times c \times d \times e \times f$$

Table 2 Judgement of results

total mark	judgement	comment
P < 0.7	may possibly be collapsed	should consult with structural engineers about retrofitting
0.7 ≤ P < 1.0	necessary to make more detailed inspection	ask structural engineers to make an inspection on site
1.0 ≤ P < 1.5	safe	better to ask structural engineers to make an inspection
1.5 ≤ P	safe	

Table 3 Result of application

No.	number of story	first floor area (m^2)	marks of each item						total mark
			a	b	c	d	e	f	
1	2	11.6	1.0	0.7	1.2	1.5	2.0	1.0	3.02
2	2	14.0	1.0	0.6	0.8	1.5	1.6	1.0	1.38
3	2	27.4	1.2	0.6	0.8	1.5	1.0	1.0	0.86
4	2	15.8	1.0	0.6	1.0	1.5	1.8	1.0	1.94
5	2	15.4	1.0	0.6	1.0	1.5	1.8	1.0	1.94
6	2	13.4	1.0	0.6	1.2	1.5	1.8	1.0	2.33
7	2	20.8	1.0	0.6	1.0	1.5	1.6	1.0	1.73
8	2	14.2	1.0	0.6	1.0	1.5	1.8	1.0	1.94
9	2	12.7	1.0	0.6	0.9	1.5	1.6	1.0	1.56
10	2	8.8	1.0	0.7	0.9	1.5	1.0	1.0	1.14
11	2	8.7	1.0	0.7	0.9	1.5	1.4	1.0	1.58
12	2	10.6	1.0	0.7	1.0	1.5	1.2	1.0	1.51
13	2	12.5	1.0	0.6	0.8	1.5	1.8	1.0	1.56
14	2	35.9	1.0	0.6	0.8	1.5	1.2	1.0	1.03
15	2	11.1	1.0	0.6	0.9	1.5	1.0	1.0	0.97
16	2	26.2	1.0	0.6	0.8	1.5	1.4	1.0	1.21
17	2	23.8	1.0	0.6	0.8	1.5	1.2	1.0	1.03
18	2	11.5	1.0	0.7	0.8	1.5	1.8	1.0	1.81
19	2	20.0	1.0	0.6	0.8	1.5	0.8	1.0	0.70
20	2	8.7	1.0	0.7	1.0	1.5	1.8	1.0	2.26
21	2	11.0	1.0	0.7	1.2	1.5	1.8	1.0	2.72
22	2	10.3	1.0	0.7	0.8	1.5	1.6	1.0	1.61
23	2	10.5	1.0	0.7	1.0	1.5	1.6	1.0	2.02
24	2	18.2	1.0	0.6	0.8	1.5	1.2	1.0	1.03
25	2	9.5	1.0	0.6	0.9	1.5	1.4	1.0	1.36
26	2	7.7	1.0	0.7	0.8	1.5	1.4	1.0	1.40
27	2	11.0	1.0	0.6	1.0	1.5	1.6	1.0	1.73
28	2	11.0	1.0	0.6	1.0	1.5	1.6	1.0	1.73
29	2	10.1	1.0	0.6	0.8	1.5	1.4	1.0	1.21
30	2	12.1	1.0	0.6	0.9	1.5	1.6	1.0	1.55
31	2	11.3	1.0	0.6	0.8	1.5	1.6	1.0	1.38

Table 3 continued

No.	number of story	first floor area (m²)	marks of each item						total mark
			a	b	c	d	e	f	
32	2	11.6	1.0	0.6	0.8	1.5	1.8	1.0	1.56
33	2	11.3	1.0	0,6	1.0	1.5	1.8	1.0	1.94
34	2	12.1	1.0	0.6	1.0	1.5	1.8	1.0	1.94
35	2	11.5	1.0	0.6	0.8	1.5	1.6	1.0	1.38
36	2	14.4	1.0	0.6	1.0	1.5	1.4	1.0	1.51
37	2	16.5	1.0	0.7	1.0	1.5	1.2	1.0	1.51
38	2	9.5	1.0	0.7	1.0	1.5	1.6	1.0	2.02
39	2	11.2	1.0	0.6	1.0	1.5	1.6	1.0	1.73
40	2	11.3	1.0	0.7	1.0	1.5	2.0	1.0	2.52
41	2	9.0	1.0	0.7	0.9	1.5	1.8	1.0	2.04
42	2	9.4	1.0	0.6	0.8	1.5	1.4	1.0	1.21
43	2	42.4	1.0	0.6	0.8	1.5	1.2	1.0	1.03
44	2	13.5	1.0	0.6	1.0	1.5	2.0	1.0	2.16
45	2	11.2	1.0	0.6	1,0	1.5	2.0	1.0	2.16
46	2	13.7	1.0	0.6	0.8	1.5	1.8	1.0	1.56
47	2	6.8	1.0	0.7	0.9	1.5	2.2	1.0	2.50
48	2	10.2	1.0	0.6	0.8	1.5	1.2	1.0	1.03
49	2	10.0	1,0	0.6	1.0	1.5	1.2	1.0	1.30
50	2	13.1	1.0	0.6	1.0	1.5	1.8	1.0	1.94
51	1	23.6	1.0	0.6	1.0	1.5	1.4	1.0	1.26
52	1	27.8	1.0	1.0	0.8	1.5	1.6	1.0	1.92
53	1	25.9	0.7	0.7	0.8	1.5	1.4	1.0	0.82
54	2	11.4	1.0	0.6	1.0	1.5	1.8	1.0	1.62
55	2	14.7	1.0	0.6	0.9	1.5	1.8	1.0	1.46
56	2	20.0	1.0	0.6	1.0	1.5	1.6	1.0	1.44
57	2	23.7	1.0	0,6	1.0	1.5	1.4	1.0	1.26
58	2	15.3	1.0	0.6	0.8	1.5	1.4	1.0	1.01
59	2	19.0	1.0	0.6	0.9	1.5	1.4	1.0	1.13
60	2	10.5	1.0	0.6	1.0	1.5	1.4	1.0	1.26
61	1	14.0	0.6	1.0	0.8	1.0	1.6	1.0	0.77
62	1	22.4	0.6	1.0	0.8	1.0	0.8	1.0	0.38
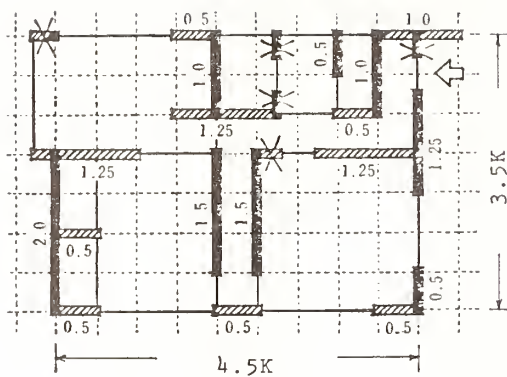
Fig. 1 Drawing example of first floor
plan.

1K=180cm
X shows invalid walls
of less than 0.5K
in length.
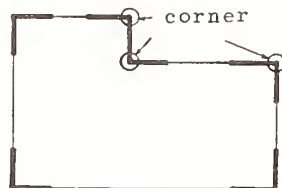
(A)L-shaped pair of walls
are arranged on every
corner of first floor
plan.

(B)L-shaped pair of walls
and single walls are
arranged on every corner
of first floor plan.
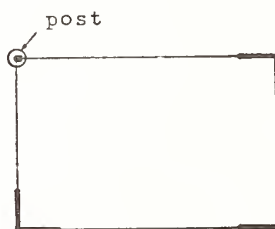
(C)More than a corner are
not stiffened by walls.
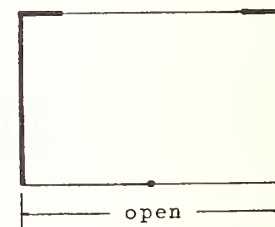
(D)One side is opened
clearly.
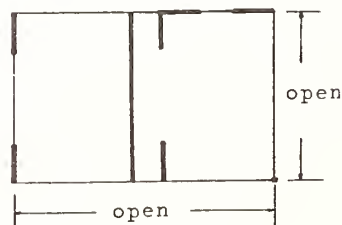
(E)Two sides are opened
clearly.
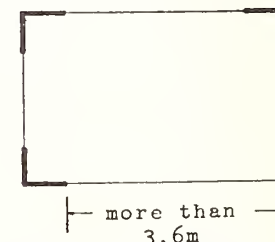
(F)Openings continue more
than 3.6m in length.

Fig. 2 Types of wall arrangement

440
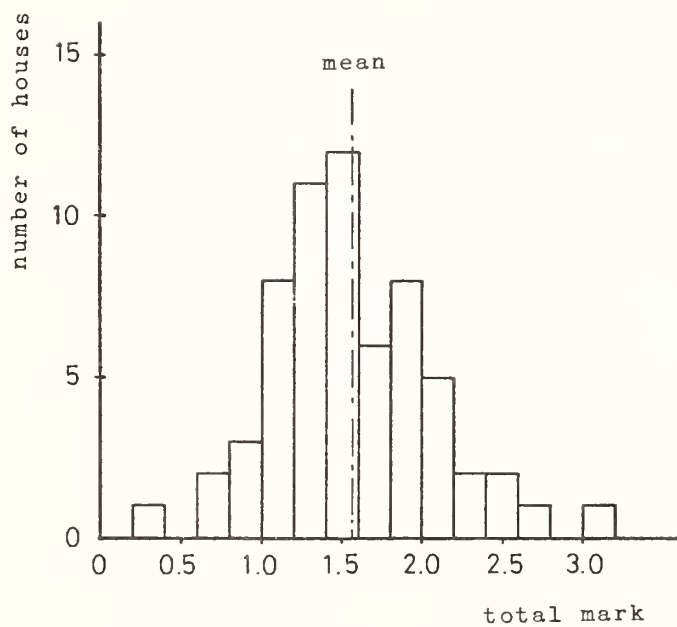
Fig. 3 Frequency distribution of total marks

AN EVALUATION METHOD ON THE ASEISMICITY OF EARTH STRUCTURES (ROAD EMBANKMENTS)

by

Tatsuya Fujii

Yasushi Sasaki

ABSTRACT

This paper describes a simple method of aseismatic evaluation of earth structures (road embankments).

With the exception of large scale structures, few earth-filled structures have been constructed so far taking aseismicity into consideration.

However, in view of the anticipated occurrence of large-scale earthquakes, it has become necessary in some parts of Japan to conduct surveys on the aseismicity of existing earth-filled roads to reduce the danger to road traffic as well as to maintain transport functions after the earthquakes have occurred.

Though this survey is necessary for other road structures, such as bridges, tunnels, etc. as well, this paper confines itself to earth-filled roads and presents a method of aseismatic evaluation based on analysis of damage to earth structures from past earthquakes.

INTRODUCTION

There are many examples of disasters and damage involving Japanese earth-filled structures, such as road embankments, river dykes, and filled railroad beds which were caused by large-scale earthquakes which have occurred in the past.

Up to the present, most earth-filled structures have been constructed without any estimating and testing in advance of their seismic strength or their earthquake-resistant abilities, except for the important large-scale structures such as earth-fill dams. The reason for this is that functional recovery after damage to such structures made of filled earth is considered to be relatively easy, since the earth itself is used as reconstruction material. In addition, appropriate earthquake-resistant designs have not been established.

To establish an appropriate earthquake-resistant design, it is necessary to clarify forecasting methods for the magnitude of seismic force taken as the design force, the deformation and strength characteristics of soil due to external dynamic forces, the pattern of failure, and the amount of deformation to earth structures. Many researchers have been exploring these questions.

It has also become necessary to evaluate the earthquake-resistant strength not only of proposed earth structures, but also of existing earth structures. In Japan, additional measures to prepare for earthquake disasters are increasingly expected by the citizenry-at-large, as seen in the establishment of new laws requiring more preparation for a large-scale earthquake in the Tokai District which is expected to occur in the near future.

To meet society's demands, it has become necessary to develop methods for examining the earthquake-resistant strength of earth structures, primarily, that of existing earth-filled roads. However, to investigate the aseismicity of existing earth structures, the soil characteristics of underlying subsoil and the earth fill must be known in some detail. In reality, such detail has not been collected in most instances.

Thus, it has become necessary to develop a simple method of examination which enables judgments to be made on the probability of damage. The method described in this paper is based on information currently available, though it may be extremely limited in quantity and kind.

It is also based on results selected from cases of damage to earth-filled structures which were caused by relatively large-scale earthquakes in the past.

443

OUTLINE OF DAMAGE TO EARTH STRUCTURES FROM PAST EARTHQUAKES

In the 1964 Niigata Earthquake, damage to river embankments and earth-filled roads resulted from the liquefaction of saturated sandy soil. In the 1968 Tokachi-Oki Earthquake, damage to road embankments was intensified because of the reduced strength of soil caused by rainfall which occurred immediately before the earthquake. Many newly constructed earth-filled railroad beds were also damaged. In the 1975 Ohita-Chubu Earthquake and the 1978 Izu-Ohshima-Kinkai Earthquake, damage to earth-filled roads in mountainous regions was severe. In the Miyagi-Ken-Oki Earthquake which occurred in June, 1978, much damage took place along road embankments and river dykes constructed on soft ground. Damage also occurred to earth-filled structures for roads which were constructed in mountainous regions.

Among earth structures damaged by these earthquakes, the structures for which data on ground conditions and cross sections before and after the earthquakes were available have been collected and are shown in Tables 1 and 2. Most of these damaged earth structures are located in regions where the Japan Meteorological Agency seismic intensity is equal to or greater than V. These damage cases include not only roads but also river dykes and railroad beds which are similar in type and size to the earth structures for the roads.

In the same manner, selected examples of damage to earth structures constructed on slopes, such as mountain roads, are shown in Table 2.

Damage patterns to earth structures on flat lands due to earthquakes, as set forth in Table 1, can be generally classified into the five damage patterns shown in Figure 1.

Type-I damage is a collapse of the slope of embankment. In the case of roads, this is mostly limited to the slope, without causing damage to traffic lanes on the road surfaces.

Type-II damage is a collapse that has almost reached the center of the top of the structure. This represents an increase in the scale of failure.

Type-III damage is a collapse of an earth structure in which the structure is destroyed to such an extent that the original shape of the structure cannot be recognized. This includes the collapse of underlying subsoil. This kind of damage frequently occurs where the subsoil has liquefied.

Type-IV damage is a deformation where the original shape of a structure is maintained to a certain degree as the result of uniform settlement.

Results of the classification of damage set forth in Table 1 are shown in Figure 2 as a frequency distribution diagram for each damage pattern.

This figure shows that earth-filled structures without pavement on top, such as most river dykes and railroad beds, fit type-II or type-III damage patterns while earth-filled road structures topped with pavement fit type-I or type-II damage patterns.

Next, the grade of damage to embankments is classified by the following three ranks, which depend on the degree of hazard to road traffic functions caused by the embankment damage.

Damage rank α: Serious damage to the whole top portion (the road surface) of the earth structure. Motor vehicle traffic is almost impossible.

Damage rank β: Degree of damage is slightly less than α. Ordinary traffic functions on the roads are not possible, but partial functions, such as single-lane traffic remains.

Damage rank γ: No damage, or minor damage. Traffic functions are virtually maintained.

Collected damage examples include not only roads but river dykes and railroad beds of the earth-filled type. Naturally, traffic function impairments do not occur to dykes. Also, the degree of actual impairment of some traffic functions immediately after earthquakes is not recorded for such earth structures.

Therefore, it was decided to rank the state of deformation to earth structures so they correspond to the traffic function defects in the three ranks just cited, based on crack widths and the amount of structural settlement. The standards for such determination are indicated in Table 3. The standards for judgment are given for each damage pattern to earth structures on flat land. Damage patterns have not been determined separately for embankments on a slope.

The degree of damage determined by using this table is shown in Tables 1 and 2.

Figure 3 shows the width of cracks and the amount of settlement damage to earth structures on flat land for each damage pattern. In this figure, river dykes whose tops are used as roads are classified in the road category.

This figure shows that the amount of settlement of embankment top for heavily damaged earth structures such as in type-III is greater than 1 meter, and that more than one-half of the type-I and type-II structures settled more than 0.5 meter.

445

APPROACHES TO THE ASEISMATIC EVALUATION OF EARTH STRUCTURES

The cases of damage to earth structures constructed on flat land shown in Table 1, cases where ground conditions and fill patterns are known, have been analyzed. It was found that damage of rank γ occurred only to earth structures of less than 6 meters in height, and structures of more than 6 meters in height suffered damage of rank α or rank γ (Figure 4).

Thus, it may be stated that the degree of damage from earthquakes tends to increase as the embankment height increases. It is known that factors other than the embankment height affect the degree of damage, since even earth structures less than 6 meters high and other structures with gentle slopes suffered damage of rank α or rank β.

Among factors other than embankment height, underlying subsoil characteristics are considered the most important.

Figures 5 and 6 show the distribution of damage degree in relation to fill height on the vertical axis and the mean N value (blow count of the standard penetration test) of ground on the horizontal axis for underlying subsoils with sandy soil and clay soil, respectively.

On sandy soil, it was found that severe damage, equivalent to damage rank α, frequently occurred at places where N values were less than 10.

Even where the embankment height was relatively low, ground where the N value was less than 6 sometimes suffered rank α or β damage.

With clayey soil, the distribution of damage ranks begins to change near the N value of 4 (Figure 6). That is, if the N value is less than 4, the degree of damage tends to increase even though embankment height is low. Most rank α damage occurred at locations with N values of less than 4. Damage on cohesive soil where mean N values exceed 8 is not included in Table 1.

Earth structure damage cases on slopes shown in Table 2, only those caused by the Miyagi-Ken-Oki Earthquake were compiled. The results are shown in Figure 7. Only two cases fit rank α. The distribution of damage in rank β and rank γ shows that damage tends to increase as embankment height increases, and as ground slope steepness increases.

Figure 8 contains the cases classified and compiled for each mean slope of the earth structures shown in Figure 7. It shows the height of earth structures, with mean slopes

steeper than 1/1.2, to be at most about 15 meters; this occurs because the bottom portions of filled earth slopes are confined by retaining walls in such structures. In these cases, rank β damage occurs even when the embankment height is about 5 meters.

With respect to earth structures having a mean slope less than 1/1.5, rank β damage occurs even when the embankment height is relatively low and the ground slope is gentle. However, if the data for ground slopes of less than 15 degrees are excluded, the damage distribution indicates that the degree of damage to structures with mean embankment slopes gentler than 1/1.5 is almost the same as that of structures with mean embankment slopes greater than 1/1.2.

For earth structures constructed on ground sloped less than about 15°, it might be suitable to treat them as the earth structures constructed on flat ground. That is, the failure surface in such an earth structure is considered to be governed only by failure in the filled earth, rather than by the boundary surface between the earth fill and the ground.

The following can be concluded from the above analysis:

(1) Embankment height is an important factor in determining the degree of damage.

(2) In case of earth structures on flat ground, the degree of damage begins to change at a point where the N value is about 6 for ground of sandy soil, and at a point where the N value is about 4 for ground of cohesive soil.

(3) For earth structures constructed on sloped ground, the factors which determine the degree of damage are ground slope and embankment height.

(4) With respect to earth fill accompanied by retaining walls, damage of rank β may occur, even though the embankment height may be low. Extra precautions will be necessary when concrete block retaining walls are used, as in the case shown in Figure 8.

(5) If the grade of sloped ground is gentle, the embankment can be treated as if it were constructed on flat ground.

Based on the facts above, Table 4 shows the method for evaluating the earthquake-resistant strength of existing earth structures which has been proposed.

According to the test methods used in this evaluation, each earth structure will first be checked to determine whether the embankment is constructed on sloped or flat ground. Then, ground and fill conditions of each structure will be judged separately to determine the particular factor, a, b, c, or d, into which each condition fits. An overall

447

rank, A, B, or C, will be established after considering the multiplied effect of such conditions.

Also, adjustments will be made to the overall ranks, A, B, and C, for embankments with continuously high water content due to drainage topography, as well as for embankments that have been disturbed in the past.

The adjusted ranks are defined as follows:

Adjusted rank A: Degree of anticipated damage is high.

      B: Degree of anticipated damage is relatively high.

      C: Degree of anticipated damage is relatively low.

The standard slope of embankment shown in the Table 4 survey sheet equals these values as listed in Table 5. Boring data should be used whenever possible in evaluating ground conditions for embankments constructed on flat lands.

REVIEW OF THE SUITABILITY OF EVALUATION METHODS

This evaluation method has been applied to the actual damage cases listed in Tables 1 and 2. The results indicate that for 54 percent of the cases, ranks evaluated in accordance with the evaluation method correspond exactly to the degree of actual damage caused. This is shown in Table 6. When those actual damage cases which have degrees of damage one rank lower than the ranks determined using the evaluation method are included, the rate becomes 75 percent (Rate II shown in Table 6). If only earth structures with pavement are considered, rates become 59 percent and 83 percent, respectively. As indicated in Table 7, the rate of cases for actual damage greater than that evaluated was 19 percent, and the rate of actual damage less than that evaluated was 27 percent.

Though the above evaluation method is very simple, it is based upon a number of assumptions; but as indicated by the attached tables, predictions made on the basis of fill and ground conditions will quite satisfactorily express the degree of damage caused by previous earthquakes. However, many technical points still remain to be solved; for instance, the after-shocks which follow the main shock frequently occur in actual earthquakes, but the chance of increased damage from such after-shocks is unclear; and the possibility of increased damage from post-rainfall earthquakes also is unknown. These points must be studied further and reviewed again in the future.

ACKNOWLEDGMENT

Table 1 List of Damage Cases of Earth Structures on Flat Ground

Identifi-cation No.	Embankment type	Ground type	Soil type	Blow count of S.P.T.	Embankment height (cm)	Mean Grade of Embankment (cotangent)	Filling material	Damage pattern	Width of crack (cm)	Settlement (cm)	Damage rank
NG- 1	River dyke	III	Cohesive soil	2	3.2	1.9	Sand	II	20	70	α
NG- 2	"	IV	"	2	2.7	2.5	"	II	30	50	α
NG- 3	"				2.6	2.2	"	V	—	—	γ
NG- 4	"	IV	Sandy silt	5	5.8	2.7	"	V	—	—	γ
NG- 5	"				3.2	2.1	"	V	—	—	γ
NG- 6	"	IV	Silt	3	3.4	1.9	"	III	100	40	α
NG- 7	"	IV	"	2	3.1	1.8	"	I	20	20	β
NG- 8	"	IV	Clay, sand	2	4.0	1.5	"	V	—	—	γ
NG- 9	"	IV	Sandy soil	8	5.2	1.9	"	II	7	30	β
NG- 10	"	IV	Cohesive soil	5	6.1	1.9	"	III	—	200	α
NG- 11	"	III	Sandy soil	10	3.5	1.9	"	II	40	60	α
NG- 12	"	IV	Silty sand	5	3.7	1.8	"	II	20	—	β
NG- 13	Railroad Embankment	IV	Sand	5 - 6			"	III	—	300	α
NG- 14	"				8.0		"	III	—	200	α
TK- 1	Road Embankment	IV	Clay, sand	3	9.0	1.7	Volcanic ash	II	—	100	α
TK- 2	"	II	Sand	3	3.8	1.2	Kuroboku	II	—	250	α
TK- 3	"	IV			3.8	1.7		I	—	300	α
TK- 4	"				5.0	1.7		III	—	150	α
TK- 5	"	IV	Sand, silt	2	2.5	1.3	Sand	III	—	120	α
TK- 6	"	IV	Sand, clay	2 - 3	3.0	1.7	Loam	IV	5	30	γ
TK- 7	Railroad Embankment	IV			3.0			III	—	200	α
TK- 8	"	IV	Clay, sand	2 - 3	3.5	3.6	Loam	III	—	—	α
TK- 9	"				5.5			II	25	15	β
TK- 10	"				4.1		Sand mixed with pumice	II	—	200	α
TK- 11	Railroad Embankment	IV	Clay, sand	2 - 6	3.8	1.7	Volcanic ash	III	50	—	α
TK- 12	"				4.5			III	100	300	α
TK- 13	"							I	7	30	β
TK- 14	"	IV	Peat				Sandy soil	II	—	50	α
TK- 15	"				10.0		Volcanic ash, sand	II	—	600	α
TK- 16	"	IV	Peat					II	—	200	α
TK- 17	"	IV	Clay, sand	2 - 3	9.5	1.5	Sand	II	—	200	α
TK- 18	"								—	—	
TK- 19	"	IV			12.0	1.8		II	—	100	α
TK- 20	"	IV					Sandy soil	II	—	100	α
TK- 21	"	IV	Peat		7.0			II	—	400	α
TK- 22	"	IV	Peat		5.5	1.4		I	—	300	β
TK- 23	"	IV	Peat		15.0	1.5		II	—	500	α
TK- 24								I	—	100	β
MY- 1	River dyke	III	Sandy soil	20	3.4	2.1	Sand	II	5	10	β
MY- 2	"	III	"	10	3.2	2.2	"	II	20	30	β
MY- 3	"	IV	"	8	4.8	2.7	"	II	50	25	β
MY- 4	"	III	"	10	4.2	2.6	"	II	15	5	β
MY- 5	"	III	"	9	6.4	2.9	"	II	30	10	β
MY- 6	"	III	Cohesive soil	6	5.2	3.8	Clay, silt	II	10	25	β
MY- 7	"	IV	Sandy soil	5	5.2	3.1	Sand	I	60	75	β
MY- 8	"	IV	"	5	5.0	2.5	"	I	20	35	β
MY- 9	"	IV	"	10	3.9	1.6	"	I	3	5	γ
MY- 10	"	IV	"	12	3.4	3.8	"	II	10	5	β
MY- 11	"	IV	"	3	2.8	2.1	"	II	30	30	β
MY- 12	"	IV	"	10	4.6	1.7	"	II	30	50	α
MY- 13	"	IV	Cohesive soil	5	8.0	2.8	"	IV	—	100	β
MY- 14	"	IV	"	4	8.4	2.6	"	I	50	50	β
MY- 15	"	III	"	5	8.0	3.1	"	IV	15	100	β
MY- 16	"	IV	"	3	5.6	3.4	"	III	—	—	α
MY- 17	"	IV	"	3	4.0	2.5	"	III	—	—	α
MY- 18	"	IV	"	3	5.4	3.5	"	V	—	—	γ
MY- 19	"	IV	"	0	3.2	2.6	"	III	—	—	α
MY- 20	"	III	Sandy soil	9	2.8	1.8	"	II	—	—	β
MY- 21	"	III	Cohesive soil	3	4.8	2.4	Clay, silt	II	7	—	β

Table 1 (Continued)

MY- 22	"	III	"	7	5.0	2.9	"	II	100	100	α
MY- 23	"	III	"	3	4.0	2.5	"	II	5	5	β
MY- 24	River dyke	III	Sandy soil	12	4.8	3.2	Sand	I	7	0	γ
MY- 25	"	IV	Cohesive soil	4	5.9	2.3	"	III	—	—	α
MY- 26	"	IV	"	4	3.9	1.6	"	II	3	1	β
MY- 27	"	III	Sandy soil	20	2.8	2.1	"	III	—	—	α
MY- 28	"	IV	Cohesive soil	4	8.0	2.8	"	IV	—	60	β
MY- 29	"	IV	"	3	5.4	3.5	"	IV	—	—	β
MY- 30	"	IV	"	4	5.4	3.3	"	IV	—	—	β
MY- 31	Road embankment	IV	—	—	6 - 7	1.5 - 1.8	—	I	—	50	δ

Table 2 List of Damage Cases of Earth Structures on Sloped Ground

Identification No.	Embankment type	Ground type	Soil type	Ground slope (degrees)	Embankment height (cm)	Embankment grade (cotangent)	Filling material	Damage pattern	Width of crack	Settlement (cm)	Damage rank
NG- 15	Road Embankment	I		34.0	40.0	1.2	Sand		5	15	β
NG- 16	"	"	Tuffacius siltstone	37.0	15.0	1.5				150	α
TK- 25	"	"		20.0	8.4	1.8				300	α
OT- 1	"	II	Loam	7.0	4.0	1.0 - 1.2			2	5	γ
OT- 2	"	"	"	16.5	4.0	1.0			20	0	δ
OT- 3	"	"	"	3.5	12.0	1.6			2	0	γ
OT- 4	"	I	Tuff breccia	32.0		1.6			20	50	α
OT- 5	"	"	Pyroclastic rocks	35.0	35.0	1.2				500	α
MY- 32	"	"		30.0	12.0	1.0			2	0	γ
MY- 33	"	"		16.0	7.0				2	0	γ
MY- 34	"	"			9.0					15	β
MY- 35	"	"		13.0	14.5	1.99			20	20	β
MY- 36	"	"		16.5	10.6	1.85			0	0	γ
MY- 37	"	"		25.0	25.6	1.89				300	α
MY- 38	"	"		17.5	26.0	1.85			2	0	δ
MY- 39	"	"		25.0	8.6	1.44			0	0	γ
MY- 40	"	"		30.0	34.8	1.53			5	0	β
MY- 41	"	"		28.5	14.1	1.32			3	0	γ
MY- 42	"	"		38.5	15.1	0.53			4	0	β
MY- 43	"	"		35.0	15.1	0.52			3	0	γ
MY- 44	"	"		32.5	35.0	1.35			2	0	β
MY- 45	"	"		30.0	15.2	0.52			0	30	β
MY- 46	"	"		31.5	27.1	1.34			2	0	β
MY- 47	"	"		25.0	22.7	1.86			1	0	γ
MY- 48	"	"		29.0	14.1	1.88			1	12	γ
MY- 49	Road Embankment	I		34.0	14.7	0.59			0	0	γ
MY- 50	"	"		34.5	28.3	2.37			1	0	δ
MY- 51	"	"		33.5	28.7	1.34			1		β
MY- 52	"	"		18.0	9.0	1.77			2	0	γ
MY- 53	"	"		22.5	25.6	1.33			1	0	β
MY- 54	"	"		37.5	16.9	2.10			5	12	β
MY- 55	"	"		25.0	21.4	1.46			5	7	β
MY- 56	"	"		23.5	10.5	1.33			3	0	γ
MY- 57	"	"		33.0	25.0	1.40			3	0	β
MY- 58	"	"		35.0	10.6	0.57			1	0	γ
MY- 59	"	"		32.0	30.0	1.32			6	4	δ
MY- 60	"	"		9.5	7.6	1.22			0	0	γ
MY- 61	"	"		33.0	10.6	0.53			0	25	δ
MY- 62	"	"		30.0	19.6	1.32			5	5	γ
MY- 63	"	"		21.0	31.5	2.09			2	0	β
MY- 64	"	"		32.5	25.4	1.33			25	10	δ
MY- 65	"	"		12.0	10.9	1.27			0	0	γ

Table 2 (Continued)

MY- 66	"	"		30.0	26.0	1.51			1	0	β
MY- 67	"	"		33.0	34.2	1.21			—	—	γ
MY- 68	"	"		43.0	18.8	1.62			5	0	β
MY- 69	"	"		15.5	14.7	1.33			5	0	γ
MY- 70	"	"		31.5	18.1	2.09			10	10	β
MY- 71	"	"		32.0	40.8	1.33			7	0	β
MY- 72	"	"		30.0	23.0	1.36			5	5	β
MY- 73	"	"		14.5	10.7	1.81			1	0	γ
MY- 74	"	"		12.5	9.1	1.79			20	20	β
MY- 75	"	"		10.5	9.0	1.78			15	25	β
MY- 76	"	"		31.5	5.0	0.80			6	0	β
MY- 77	Road" Embankment	"		32.0	34.8	1.34			30	200	α
MY- 78	"	"		17.5	16.8	2.10			0	0	γ
MY- 79	"	"		30.0	10.8	1.15			0	0	γ
MY- 80	"	"		34.0	22.9	1.35			5	25	β
MY- 81	"	"		34.0	24.2	1.80			3	5	β
MY- 82	"	"		24.5	16.8	1.76			15	10	β
MY- 83	"	"		30.0	34.1	1.30			3	5	β
MY- 84	"	"		31.5	20.8	1.24			10	20	β
MY- 85	"	"		25.0	13.0	0.66			5	3	β
MY- 86	"	"		21.0	13.0	1.81			0	0	γ
MY- 87	"	"		11.0	10.0	1.86			0	0	γ

Table 3. Damage Rank and Degree of Damage

	Damage pattern	Damage rank	
Embankment on lfat ground	I	β	Width of crack greater than 15 cm, or settlement greater than 20 cm.
		γ	Width of crack less than 15 cm, and settlement less than 20 cm.
	II	α	Width of crack exceeding 30 cm, and settlement exceeding 50 cm.
		β	Width of crack less than 30 cm, or settlement less than 50 cm.
	III	α	
	IV	β	Settlement greater than 50 cm.
		γ	Settlement less than 50 cm.
	V	γ	No damage
Embankment on sloped ground		α	Embankment completely slipped. Road surface and shoulder were lost.
		β	Cracks and settlement occurred on the road surface as a result of deformation of the filling. Or cross sectional area for restoration is greater than 2 squre meters.
		γ	No damage or hair-line cracks on road surface not damaged. Or cross sectional area for restoration is smaller than 2 square meters.

Table 4 Aseismatic Survey Sheet for Embankment

Name of office											
Survey taken by					Date of survey	Year:		Month:		Day:	
Embankment location		Name of Line ( ) Distance mark (km – km), Applicable section (km – km)									

						a	b	c	d	Factor rank
Embankment on Sloped Ground (Ground Slope > 1/4.0)	Ground condition		Ground slope 1/α = in cotangent			α<1.8	1.8≤α<3	3<α<4		
	Embankment condition		Embankment height H = m Embankment slope 1/x = in cotangent Existance of retaining wall (yes, no) Type Height m	Embankment with standard slope		H≥35m	35>H≥20	20>H≥5	5>H	
				Embankment with slopes steeper than standard slope and approach embankment to bridge abutment		H≥30m	30>H≥15	15>H≥5	5>H	
Embankment on Flat Ground (Ground Slope ≤ 1/4.0	Ground condition	Ground with Cohesive Soil	Blow count of S.P.T. N = Thickness of soft soil layer m Soil improvement (yes, no) (Work method:)	Degree of ground softness		Extremely soft	Soft	Others		
				Blow count of S.P.T.		N<4	4≤N<8	8≤N		
		Ground with Sandy Soil	Blow count of S.P.T. N = Thickness of loose sand layer m Depth of groundwater (m from ground surface) Classified with old river bed on land condition classification map (applicable) Soil improvement (yes, no) (Work method:)	Possibility of liquefaction		Extremely high	Medium	Others		
				Blow count of S.P.T.		N<6	6≤N<10	10≤N		
	Embankment condition		Embankment height H = m Embankment slope 1/x = in cotangent Embankment retaining wall (yes, no) Type Height m	Embankment with standard slope		H≥10m	10>H≥6	6>H≥3	3>H	
				Embankment with sloped ground		H≥8m	8>H≥4	4>H≥2	2>H	

Standard for Judgement of overall rank

Embankment on Flat Ground

Embankment condition / Ground condition	a	b	c	d
a	A	A	A	B
b	A	B	B	C
c	B	B	C	C

Embankment on Sloped Ground

Embankment condition / Ground condition	a	b	c	d
a	A	B	B	C
b	B	B	C	C
c	B	C	C	C

Cross section of Embankment (scale)

Overall rank (A, B, C)

Correction of rank due to notes (1), (2) & (3) shown below. (C → B, B → A, A → A)

(1) Water content in filling is always high because embankment is located on water-collection ground.

(2) Settlement or cracks on top of embankment occurred in the past due to rainfall or earthquakes.

(3) Deformation such as settlement or cracks already appeared in the embankment at its widened portion after usage began.

Corrected judgement rank (A, B, C)

Table 5. Standard Grades for Slopes Corresponding to Filling Material and Embankment Height

Filling material	Embankment height (m)	Grade	Remarks
Sand with good grading (SW), Gravel and sand mixed with gravel (GM), (GC), (GW), (GP)	less than 5 m	1:1.5 – 1:1.8	These are applicable to embankment on foundation with sufficient bearing capacity and without fear of infiltration of water. A typical soil in Japanese unified classification category is shown in ( ).
	5 – 15 m	1:1.8 – 1:2.0	
Sand with poor grading (SP)	less than 10 m	1:1.8 – 1:2.0	
Rocks (including muck)	less than 10 m	1:1.5 – 1:1.8	
	10 – 20 m	1:1.8 – 1:2.0	
Sandy soil (SM), (SC), hard cohesive soil, hard clay (such as hard cohesive soil of diluvium, clay, Kanto loam)	less than 5 m	1:1.5 – 1:1.8	
	5 – 10 m	1:1.8 – 1:2.0	
Soft cohesive soil (VH$_2$)	less than 5 m	1:1.8 – 1:2.0	

Table 6. Rate of Suitability

All earth structures surveyed (road embankments railroad beds and river dykes)

	Rate of suitability 1 (%)	Rate of suitability II (%)
Embankments on flat cohesive ground	55.2	72.4
Embankments on flat sandy ground	44.4	55.6
Embankments on sloped ground	56.6	83.0
Total	54.0	75.0

Earth structures with pavement (earth-filled roads & river embankments also treated as roads)

	Rate of suitability I (%)	Rate of suitability II (%)
Embankments on flat cohesive ground	66.7	77.8
Embankments on flat sandy ground	66.7	88.9
Embankments on sloped ground	56.6	83.0
Total	59.2	83.1

Rate of suitability:

$$\text{II} = \frac{\text{Number of survey points shown by} \quad \text{▨}}{\text{Total number of survey points}}$$

	A	B	C
α	▨		
β	▨	▨	
γ		▨	▨

Rate of suitability:

$$1 = \frac{\text{Number of survey points shown by} \quad \text{▨}}{\text{Total number of survey points}}$$

	A	B	C
α	▨		
β		▨	
γ			▨

Table 7 Rates of unsuitability

All earth structures surveyed

	Rate of having actual damage greater than those evaluated in %	Rate of having actual damage less than those evaluated in %
Embankments on flat cohesive ground	13.8	31.0
Embankments on flat sandy ground	44.4	11.1
Embankments on sloped ground	13.2	30.2
Total	19.0	27.0

Earth structures with pavement

	Rate of having actual damage greater than those evaluated in %	Rate of having actual damage less than those evaluated in %
Embankments on flat cohesive ground	11.1	22.2
Embankments on flat sandy ground	11.1	22.2
Embankments on sloped ground	13.2	30.2
Total	12.7	28.2

I: Slippage on sloped surface, failure or settlement from cracking is limited to shoulder, thus not affecting the central portion of the top of the embankment (traffic lanes, in the case of road).

II: Slip failure or settlement due to craking in the embankment, occurring at the central portion of the top of the embankment (traffic lanes, in the case of the road).

III: Collapse also occurs in the underlying subsoil. The original shape of the embankment is unnoticeable.

IV: As a result of uniform settlement of the embankment, the filling is deformed but embankment shape is maintained to a certain degree.
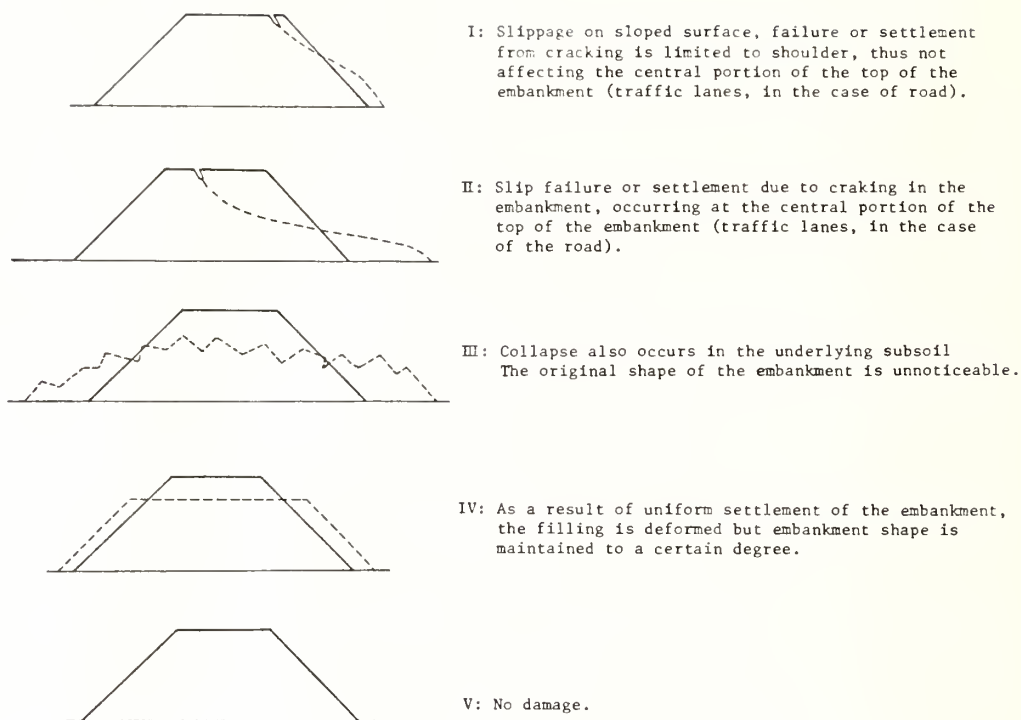
V: No damage.

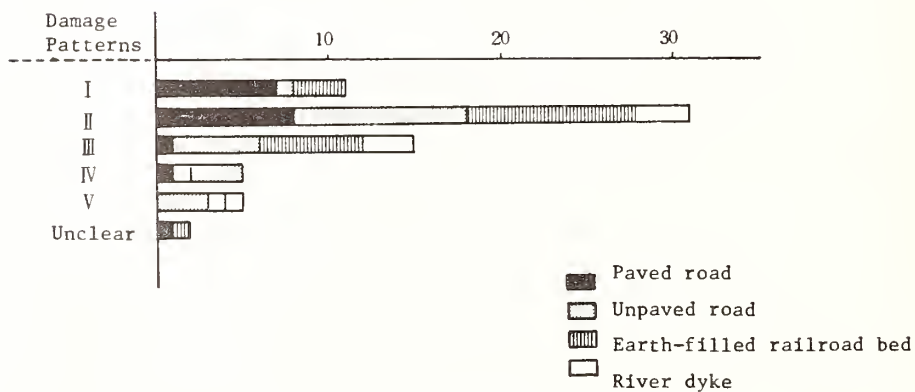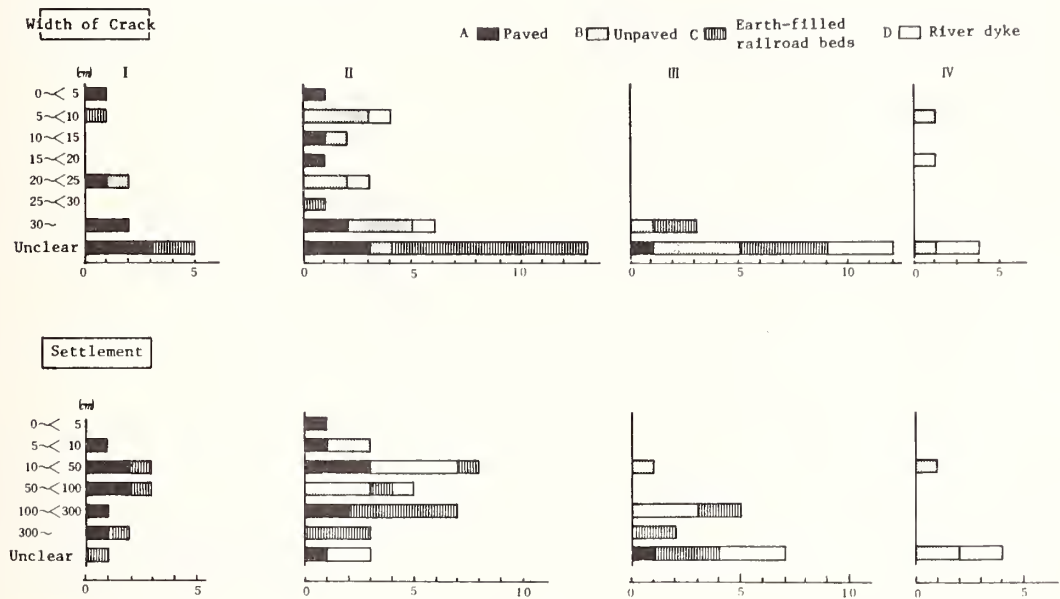Fig. 1 Classification for Damage Patterns

Fig. 2 Frequency Distribution of Damage Patterns of Embankment on Flat Ground

Fig. 3 Frequency Distribution of Crack Widths and Settlement by Damage Pattern, Embankment on Flat Ground

* River embankment used also as road is classified as either A or B.

Fig. 4 Relationship between Damage Ranks, Heights, and Slopes, Embankment on Flat Ground

457

Fig. 5 Relationship between Damage Rank,
Embankment Heights, and Blow
Count N of Ground, Embankment
on Flat Sandy Ground

Damage rank

α ● ▨
β ⊙ ▨
r ○ ▭

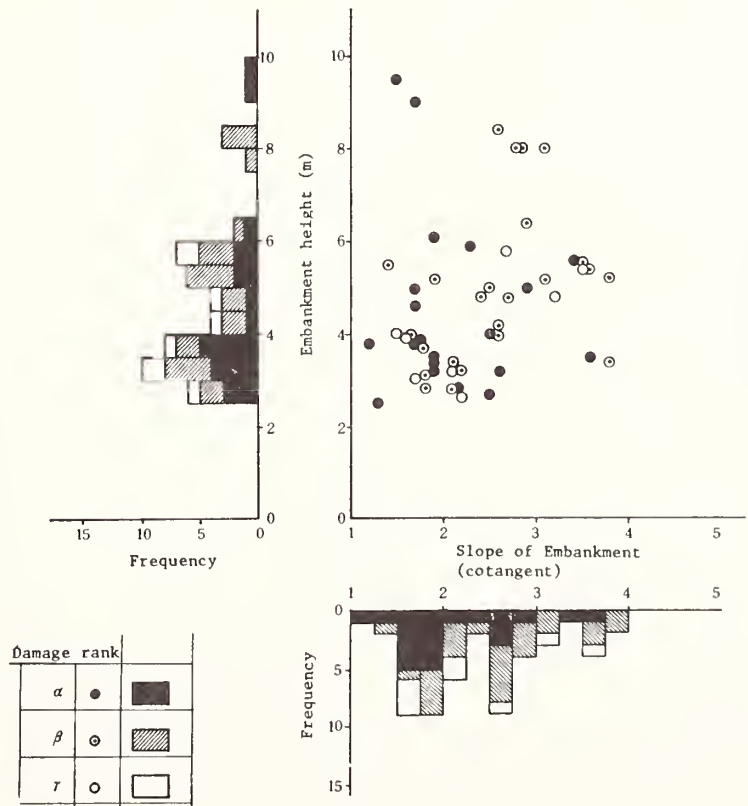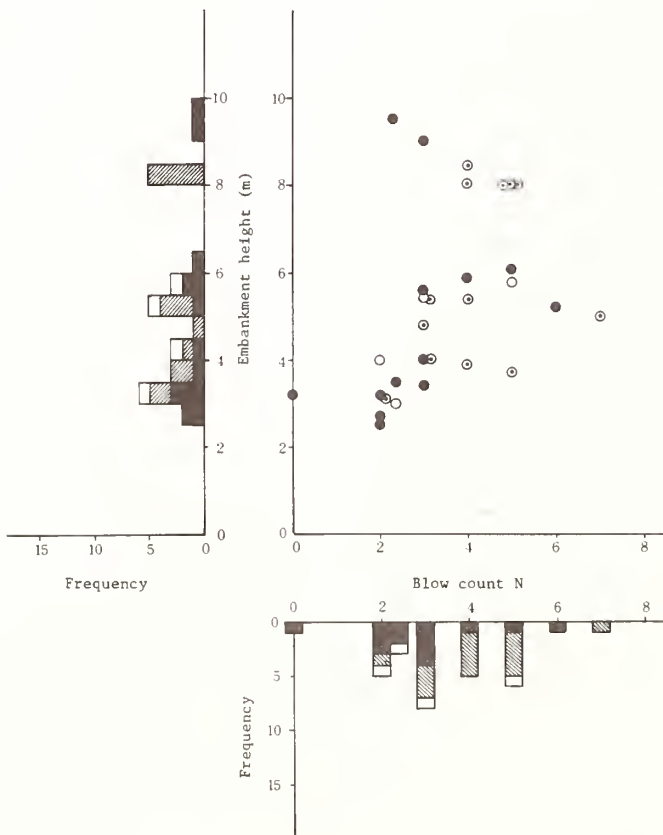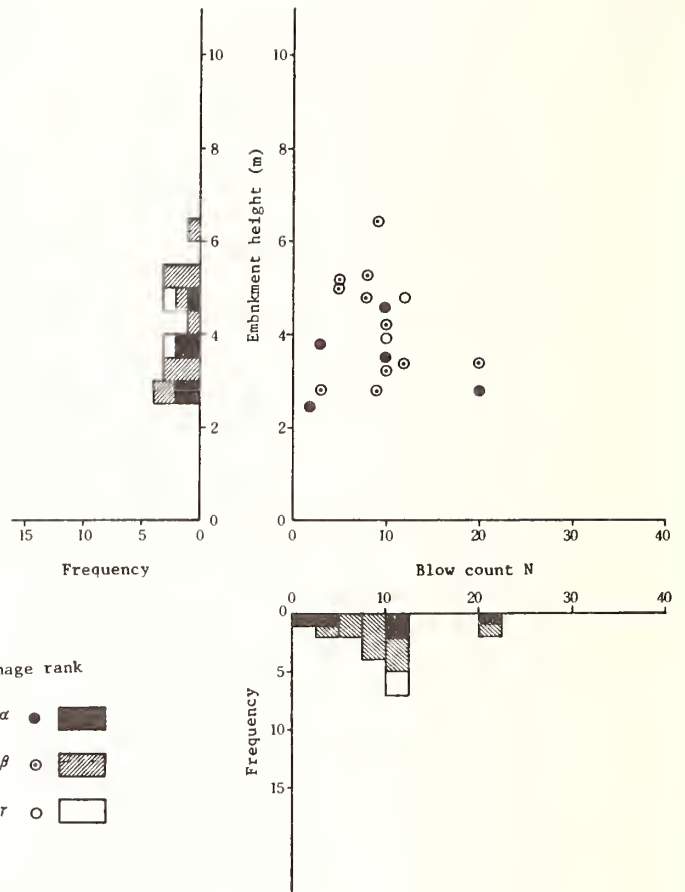Fig. 6 Relationship between Damage Rank,
Embankment Heights, and Blow
Count N of Ground, Embankment
on Flat Cohesive Ground

458

Fig. 7 Distribution of Damage to Embankment
        on Sloped Ground

Embankment height (m)

Slope of underlying
Ground (degrees)

Frequency

Damage rank

α   ●   ■

β   ⊙   ▨

γ   ○   □

Fig. 8 Relationship between Damage Ranks, Embankment Heights, and Ground Slopes, Embankment on Sloped Land

Embankment height (m)
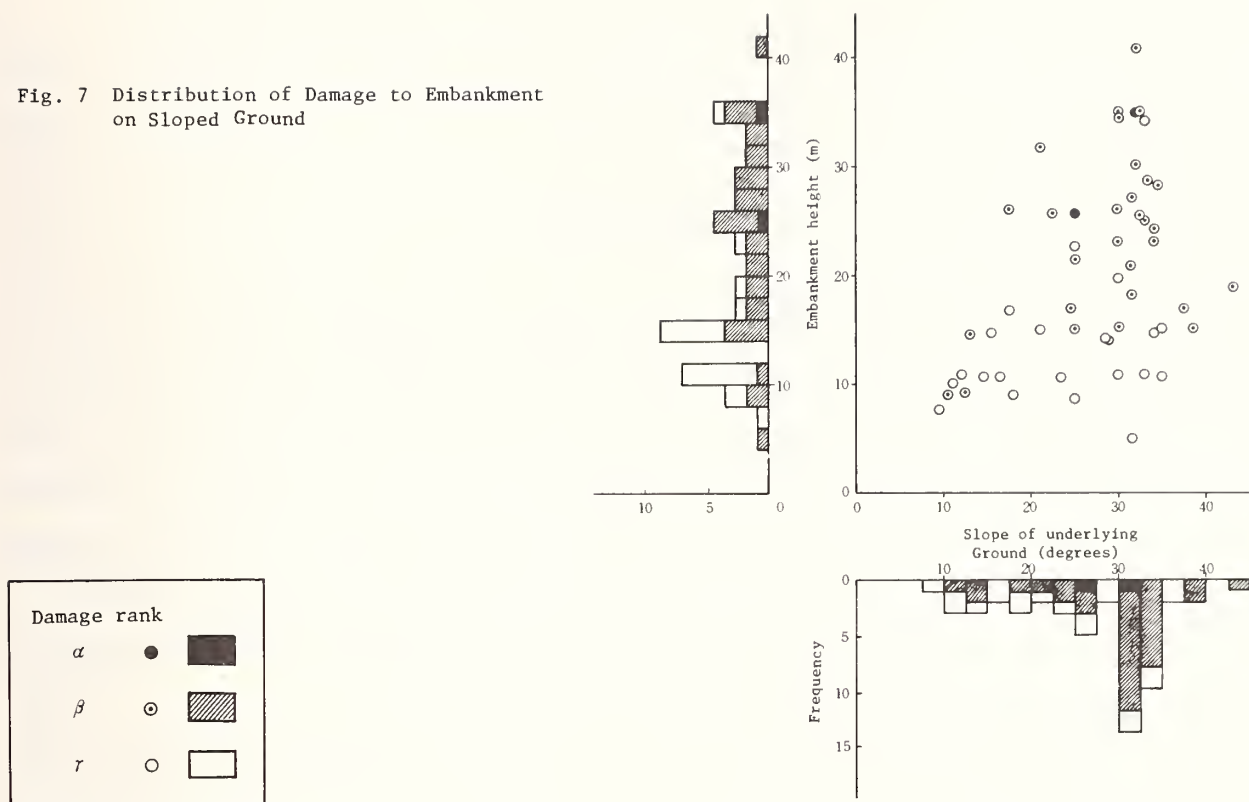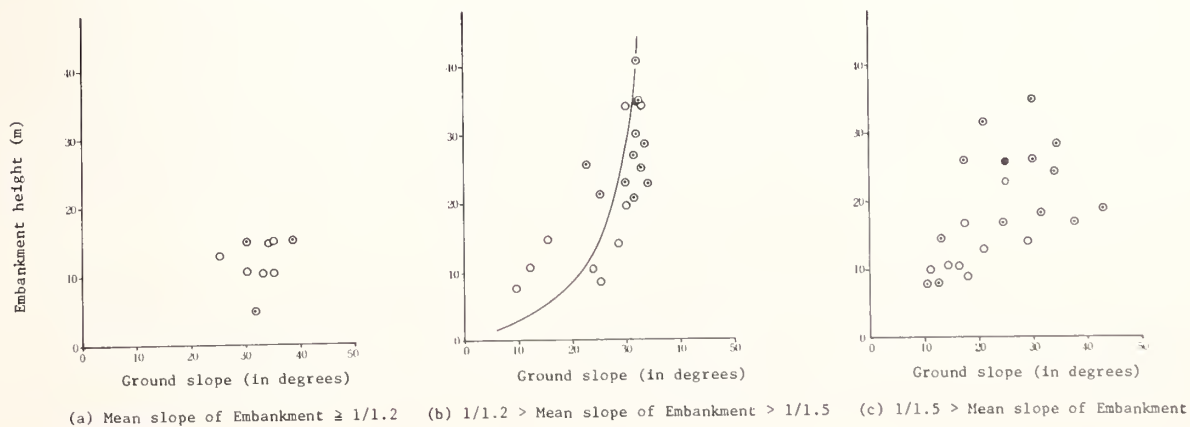
Ground slope (in degrees)

Ground slope (in degrees)

Ground slope (in degrees)

(a) Mean slope of Embankment ≥ 1/1.2   (b) 1/1.2 > Mean slope of Embankment > 1/1.5   (c) 1/1.5 > Mean slope of Embankment

459

WIND-INDUCED VIBRATION OF TRUSS MEMBERS OF THE COMMODORE BARRY BRIDGE

by

Gerald F. Fox

INTRODUCTION

The Tacony-Palmyra Bridge was constructed in 1929 and spans the Delaware River at Philadelphia, Pennsylvania. The 537-foot main span of the bridge is a steel tied arch with a trussed rib (Figure 1). Shortly after the bridge was opened to traffic, two of the longer H hangers broke at the top during a severe two-day storm. The bridge was closed to traffic and further inspection revealed that other hangers exhibited cracking, some at the top and others at the bottom. The fractures were due to fatigue resulting from wind-induced vibrations. Repairs were made and a horizontal strut added between panel points 4 and 4'. The added bracing has been entirely effective.

The Commodore Barry Bridge was constructed in 1973 and spans the Delaware River between Chester, Pennsylvania and Bridgeport, New Jersey. It is only 22 miles south of the Tacony-Palmyra Bridge. It is the longest cantilever truss bridge in the United States with a main span of 1,644 feet and anchor span lengths of 822 feet (Figure 2). The depth of trusses is 85 feet at the center of the main span and 230 feet over the piers. The distance between trusses is 72'-6". Many of the web members, diagonals and verticals are H sections and are unusually light. As is well known, long, light structural H members are susceptible to wind-induced vibrations which can eventually lead to fatigue fractures that can be catastrophic.

In March 1973, while the bridge was still being constructed, a storm with recorded gusts up to 65 miles per hour caused several of the members to vibrate violently. Upon subsequent inspection, open cracks through the flanges of the H vertical members either at their top or bottom were discovered. The contractor, Bethlehem Steel Corporation, spliced the cracked members and installed steel cables to restrain against any additional wind-induced problems. These temporary guys proved to be effective and the bridge was completed and then opened to traffic with the cables still in place.

In the 45 years between the incidents noted for the Tacony-Palmyra Bridge and the Commodore Barry Bridge there have been many similar failures. Those that have been recorded in the literature include bridges constructed in Japan, Czechoslovakia, Canada and

the United States. In view of the great number of such incidents, one is led to ask the question, "Why should they continue to occur?" Is there something radically wrong in the way that engineering information is communicated or are engineers naturally lazy and don't read the literature available? Perhaps they are not given the time or can't afford the time to adequately research a project before final design is initiated. Very appropriate is the old quotation, "He who ignores history is bound to relive it."

In April 1974, The Delaware River Port Authority (DRPA) engaged Howard Needles Tammen and Bergendoff (HNTB) to investigate the causes and suggest possible solutions for the wind problems of the Commodore Barry Bridge. Dr. Robert H. Scanlan of Princeton University served as a special consultant during the investigations.

This paper briefly summarizes the phenomenon known as von Karman vortex shedding that led to the damaging vibrations of the truss members of the Commodore Barry Bridge. In addition, the alternatives that were studied to prevent future vibrations from occurring are described. Also the estimated costs of the various schemes are given.

Von Karman Vortices

Everyone here has, at one time or another, looked down upon a flowing stream from a country bridge. If you were observant, you noticed the water flowing around the rocks that protruded above the water and that immediately downstream of and adjacent to these rocks small vortices or whirlpools formed. You really would be classified as very observant if you noticed that these vortices were not directly opposite each other on either side of an individual rock, but were rather alternately spaced. This alternate spacing of vortices given rise to periodic forces perpendicular to the stream flow. Wind acts in the same manner as flowing water. Wind, as it flows around the truss members of the Commodore Barry Bridge forms alternating vortices which give rise to forces perpendicular to the wind-flow direction. This phenomenon was discovered by Professor Theodore von Karman and is named after him (Figure 3). The frequency of the shedding vortices and therefore the resulting forces is governed by the following very simple law:

$$S = \frac{fb}{V}$$

S = Strouhal number

f = Frequency of shedding

461

b = Width of object normal to the flow

V = Velocity of wind.

Values of the Strouhal numbers used in the investigation are given in Figure 4 and were obtained from References [1-3].

All structures vibrate from the forces caused by wind vortices. It's only when the natural frequency of the structural member approaches the shedding frequency that a serious problem occurs. When these frequencies are equal, a condition of resonance occurs in which very high amplitudes are reached when low damping is present.

The velocity of wind that would allow resonance to occur can be calculated since the Strouhal number, flange width and natural frequency of the truss members (Figure 5) in bending and torsion are known or can be easily calculated. For example, the bending natural frequency for a beam which is fixed at both ends and subject to a tension force is:

$$ f = C \sqrt{\frac{EI}{m\ell^4}} \sqrt{1 + \frac{P}{P_{cr}}} $$

f   = Frequency

C   = 3.56 for fixed-fixed condition

E   = Modulus of elasticity

I   = Moment of inertia

m   = Mass per unit length

ℓ = Length of member

P   = Applied tension force

P_{cr} = Euler critical buckling load.

$$ P_{cr} = \frac{4\pi^2 EI}{\ell^2} $$

Stresses in Truss Members

The resonant wind velocities calculated for the web members of the Commodore Barry Bridge ranged as low as 32 miles per hour.

The stresses in the members resulting from the resonant wind velocity were calculated from the following approximate formula from Reference [4]:

462

$$y = \frac{W_a V^2 b}{60 W_b f^2 S}$$

y = Amplitude of vibration

W_a = Weight of air - 0.0766 lbs per cu ft at 15°C sea level

v = Velocity of wind

b = Object width normal to flow

W_b = Weight of beam per unit length

f = Natural frequency

S = Logrithmic decrement taken as 0.3 for this investigation.

The stresses associated with bending vibrations were calculated using the above amplitude displacement. For example, for member U24-L24 the calculated stresses are shown in Figure 6.

Wind Criteria

Utilizing the methods of H.C.S. Thom [5], the mean recurrence interval of wind 30 feet above the ground was plotted (Figure 7). The recurrence interval at the bridge height was also plotted in accordance with the following formula:

$$V_H = \left(\frac{H}{H_R}\right)^y \times V_R$$

where: V_H = velocity at a height H

V_R = reference velocity at height H_R

y = an exponent depending on the character and/or degree of development of the terrain. For the bridge site a value of 0.143 was used.

Historical data on the duration of extreme winds are scarce. For this investigation the plot shown in Figure 8 was assumed [4].

The design wind velocity was established at 100 miles per hour at the height of bridge which has a recurrence interval of about 50 years. All main members shall be modified if they undergo detrimental vibrations from winds below the design winds.

Alternative Methods of Performance Permanent Rectifications

There are three types of corrective measures which can be used to increase the resistance of structural members to wind-induced vibration. These are:

463

- Aerodynamic, in which the periodicity of wind-induced force is destroyed by the addition of "spoilers" to break up the flow or else the force is eliminated (by "streamlining" or perforation of the member).

- Mechanical, whereby the energy of the periodic wind forces is absorbed by mechanical devices and vibration amplitude is thus kept within safe limits.

- Structural, whereby the physical characteristics of the basic member are altered so as to raise its natural frequency of vibration. This can be done by adding material to increase elastic stiffness, or by using intermediate supports to decrease effective length.

For the wind-vibration-susceptible members of the cantilever truss spans of the Commodore Barry Bridge, the use of the aerodynamic solutions of spoilers and/or stream-lining was not considered feasible for reasons of appearance and the considerable lead time required in order to develop effective solutions by experimentation with various configurations. Also, there was no assurance that such experimentation would, in the end, provide a satisfactory solution.

Two basic variants of a structural type solution, the addition of a system of structural members (sub-struts and braces) and a system using permanent steel restraining cables, were studied (Figures 9 and 10).

In addition, another structural method which was considered is that of "boxing-in" those H-section members requiring rectification. This method consists of the welding (or bolting) on of plates so as to form closed box sections.

For the mechanical solution, a vibration absorber was considered. A tuned vibration absorber is a system consisting of a small mass attached to the individual bridge members by means of a rubber stem which provides for both the stiffness and damping required for the absorber. The natural frequency of the absorber is tuned to the natural frequency of the truss member. When the bridge member begins to oscillate it excites the absorber which provides effective damping and thus reduces the amplitude of motion of the bridge member to safe and tolerable values [6,7].

The costs of the proposed rectifications were estimated for a 100 mile per hour wind and are as follows:

| Sub-struts and braces | - $3,230,000 |
| Steel restraining cables | - 1,580,000 |

"Boxing-in" of H members   −   3,660,000

Vibration absorbers   −   1,140,000

In view of their aesthetic appeal and estimated low cost, it was recommended that a research program be initiated with the following objectives:

(1) To verify by means of laboratory and field testing the effectiveness and applicability of the mechanical absorber type of solution.

(2) To develop a satisfactory mechanical absorber for use on the structure.

(3) To develop, from the results of previous investigations and the research program, definite recommendations to DRPA for permanent rectifications.

The research program included analytical investigations, field testing, laboratory testing and wind tunnel testing. [8]

Analytical Investigations

The analytical investigations included a solution of the response of structural members equipped with one or more vibration absorbers and a study of the following parameters in regard to their effect on the vibration response of the member:

M_a/M_o =   ratio of mass of absorber to effective mass of member

ζa =   damping ratio of absorber

W_a/W_o =   tuning ratio (the ratio of vibration frequency of absorber to that of the member)

The results of these studies are shown on Figures 11, 12, and 13. On these figures the vertical scale represents the magnification ratio (x/x_{static}). This is the ratio of the maximum half applitude of the member to the deflection which would result if the force were applied as a steady load. The damping ratio of the member proper has been assumed as 0.004 throughout.

Referring to Figure 11, which is drawn for an absorber damping of 0.04, it can be noted that there is little improvement in the effectiveness of properly tuned absorbers with an increase in the mass ratio beyond about 0.005. For "de-tuned" absorbers there is little improvement for mass ratios above about 0.015.

Figure 12 shows the variation in absorber performance with a change in damping ratio. The most important conclusion to be drawn from this figure is that the absorber effectiveness is sensitive to changes in its damping ratio for low mass ratios, but that for a 0.02

465

mass ratio, varying the absorber damping ratio between 0.04 and 0.14 has little effect on the maximum response.

Figure 13, showing the effect of the tuning ratio on absorber effectiveness, shows clearly the presence of an "optimum" turning ratio for each mass ratio and again indicates that absorbers with larger mass ratios are more tolerant of variations in the other parameters.

Field Investigation

The field investigation consisted of the three phases of (1) Calibration of synthetic rubber and wire rope test absorbers; (2) Monitoring the behavior of member 24 with and without absorbers; and (3) Measuring the natural vibration frequencies of selected members without absorbers.

Stanford University, California performed the field monitoring and measuring of the natural vibration frequencies. This was accomplished by means of accelerometers mounted on the members which were connected via a coaxial cable to a Fourier analyzer computer. The differences between the field observations and theoretical results are shown in Table 1.

The results of the field investigation led to the following conclusions:

(1) The synthetic rubber exhibited consistent and desirable properties for use in mechanical absorbers but needed to be larger than 3-1/2" square.

(2) Steel cable is not a satisfactory absorber material due to the high fraction of critical damping and the inconsistent results.

(3) First mode frequencies of members requiring rectification should be measured in place.

(4) The difference in energy levels of the member and the mechanical absorber indicates probable effectiveness of the absorber. However, wind tunnel tests were needed to test the results at high wind speeds.

Wind Tunnel Testing

Wind tunnel testing was performed at the Low Speed Aerodynamics Laboratory, Canadian Research Council, Ottawa, under the direction of Dr. R. L. Wardlaw. The truss member (prototype member) selected for modeling and laboratory testing was member U24-L24 and the testing program, developed during discussions between Dr. Wardlaw, Dr. R. H. Scanlan and

HNTB, consisted of the testing of a 1:3 scale, two dimensional sectional model and a 1:7.5 scale, three-dimensional elastic model. Both models were tested without and with attached mechanical absorbers.

The results of the 1:7.5 scale elastic model tests in weak axis motion, strong axis motion and torsional motion are shown on Figures 14 to 16, respectively. A comparison of the sectional and elastic model results, in general, were satisfactory.

From the results of the experimental and analytical studies performed during the research program, it was concluded that a system of mechanical vibration absorbers would provide the necessary protection against undesirable wind-induced vibrations of the truss members of the Commodore Barry Bridge. The DRPA accepted the recommendation and gave approval for the preparation of plans and specifications.

Laboratory Testing

While the plans were being prepared, the designed vibration absorber (Figure 17) was being further tested at the General Testing Laboratories in Kansas City, Missouri. These tests provided:

(1) The variation of the natural frequency of the vibration absorber for varying lengths of rubber stem, combined with a variety of weights as anticipated for actual use on the Commodore Barry Bridge, under a temperature range of 0°F to 125°F. The plots of frequency vs. length followed the same trend as obtained by field testing at the bridge site.

(2) The variation in the absorber damping values for the conditions outlined in (1) above.

Installation

Bids were taken in May 1976 and the United States Steel Corporation was the low bidder at a price of $1,162,375. The D. S. Brown Company furnished the absorbers to United States Steel for erection. A total of 920 absorbers were installed on 166 members. The temporary cables were removed and the installation of the absorbers was completed in August 1977.

Since that time there have been no problems reported and two inspections of the absorbers have taken place. While the solution of vibration absorbers was correct for remedying an existing condition of the Commodore Barry Bridge, it does not necessarily

follow that absorbers should be used for initial design. It would appear superior to provide adequate stiffness or sufficient damping, or both, in the original design.

REFERENCES

[1] Transactions of the American Society of Civil Engineers, Vol. 126, 1961, Part II, p. 1124, "Wind Forces on Structures."

[2] Yamaguchi, T., Shiraki, K., Umemura, S. and Tanaka, H., "Vibrations Caused by Von Karman's Vortex on Bridge Members and its Counter Measure."

[3] Otsuki, Y., Washizu, K., Ohya, A., Tomizawa, H., and Fujii, K., "Experiments on the Aeroelastic Instability of Prismatic Bars with Rectangular Sections," presented at Tokyo Wind Conference, 1971.

[4] Merrison Committee Report Great Britain, "Inquiry into the Basis of Design and Method of Erection of Steel Box Girder Bridges," 1973, p. 4/23.

[5] Thom, H. C. S., "New Distributions of Extreme Winds in the United States," Journal of the Structural Division, ASCE, Vol. 94, No. ST7, July 1968, p. 1787.

[6] Timoshenko, S., "Vibration Problems in Engineering," Third Edition, D. Van Nostrand Company, Inc., 1955.

[7] Wardlaw, R. L., and Cooper, K. R., "Mechanisms and Alleviation of Wind-Induced Structural Vibrations," Proceedings - Second Symposium on Applications of Solid Mechanics, McMaster University, Hamilton, Ontario, Canada.

[8] Irwin, H. P. A. H., Cooper, K. R., Wardlaw, R. L., "Application of Vibration Absorbers to Control Wind-Induced Vibration of I-Beam Truss Members on the Commodore Barry Bridge," LTR-LA-194, National Research Council of Canada, Ottawa, January 1976.

TABLE   I

MEASURED AND COMPUTED FUNDAMENTAL
FREQUENCIES (HERTZ)

| Member	Field Observations			Theoretical Results*		
	Weak	Strong	Torsional	Weak	Strong	Torsional
Members w/o Sway Frames or Intermediate Struts						
24	3.49	4.67	3.05	3.51	5.31	3.52
28	4.18	7.10	3.10	4.15	7.77	3.86
Members with Sway Frames						
15	2.34	--	3.28	2.24	--	--
29	2.58	--	--	2.39	--	--
Members with Horizontal Strut and w/o Sway Frame						
20	--	2.58	--	--	2.80	--
20**	3.28	2.58	2.85	3.37	2.80	3.73

* Effect of bracket weight included
** 2nd mode frequencies
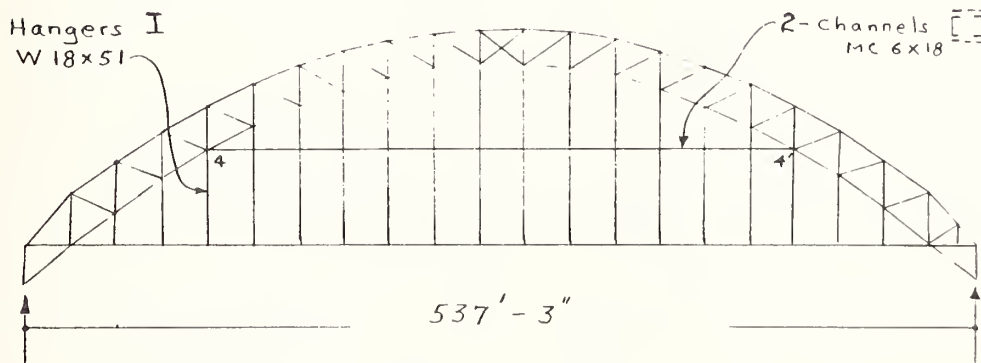
TACONY-PALMYRA BRIDGE
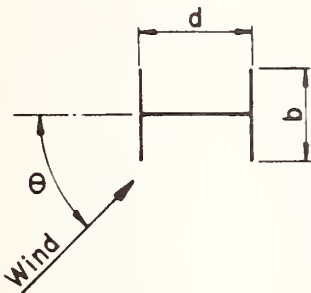
FIGURE 1

Fig. 2 Commodore Barry Bridge
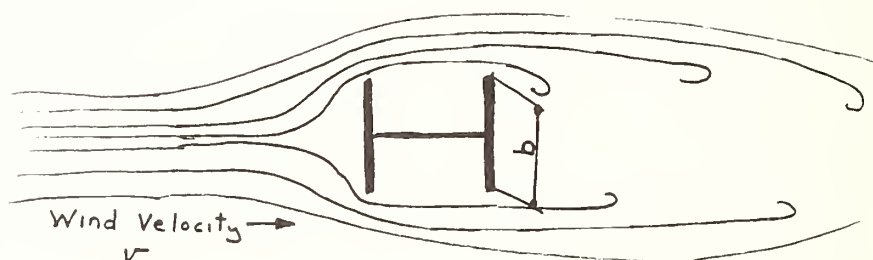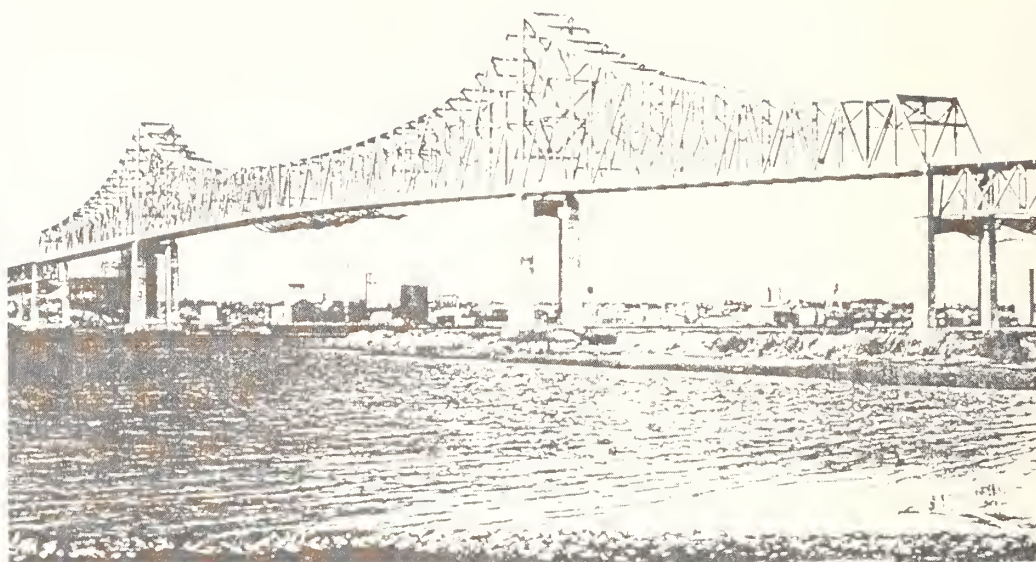
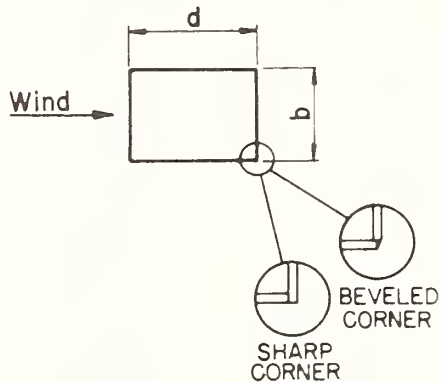KARMAN VORTEX TRAILS

$$S = \frac{fb}{v}$$

S - Strouhal Number
f - frequency of shedding
b - flange width
v - velocity of wind

FIGURE 3

H-SECTION
$(0.7 \leq b/_d \leq 1.2)$

BOX SECTION
$(0.50 \leq b/_d \leq 2.0)$

Θ(DEG.)	S
0	0.120
20	0.153
40	0.116
60	0.133
90	0.137

$b/_d$	S_{SHARP}	$S_{BEVELED}$
0.50	0.079	0.087
1.00	0.125	0.138
1.50	0.136	0.150
2.00	0.140	0.154

Source: Transactions of the American
Society of Civil Engineers,
Vol. 126, 1961, Part II, P. 1124
"Wind Forces on Structures"

Vibration caused by Von Karman's
Vortex on Bridge Members and
its Countermeasure by
T. Yamaguchi, K. Shiraki,
S. Umemura and H. Tanaka.

Source: Experiments on the aeroelastic
instability of prismatic bars
with rectangular sections by
Y. Otsuki, K. Washizu, A. Ohya,
H. Tomizawa and K. Fujii.
Presented at Tokyo Wind
Conference, 1971.

STROUHAL NUMBERS (S)

FIGURE 4

1ST MODE   2ND MODE   1ST MODE   2ND MODE

BENDING   TWISTING

SECTION A-A   SECTION B-B

MEMBER VIBRATION

FIGURE 5

472
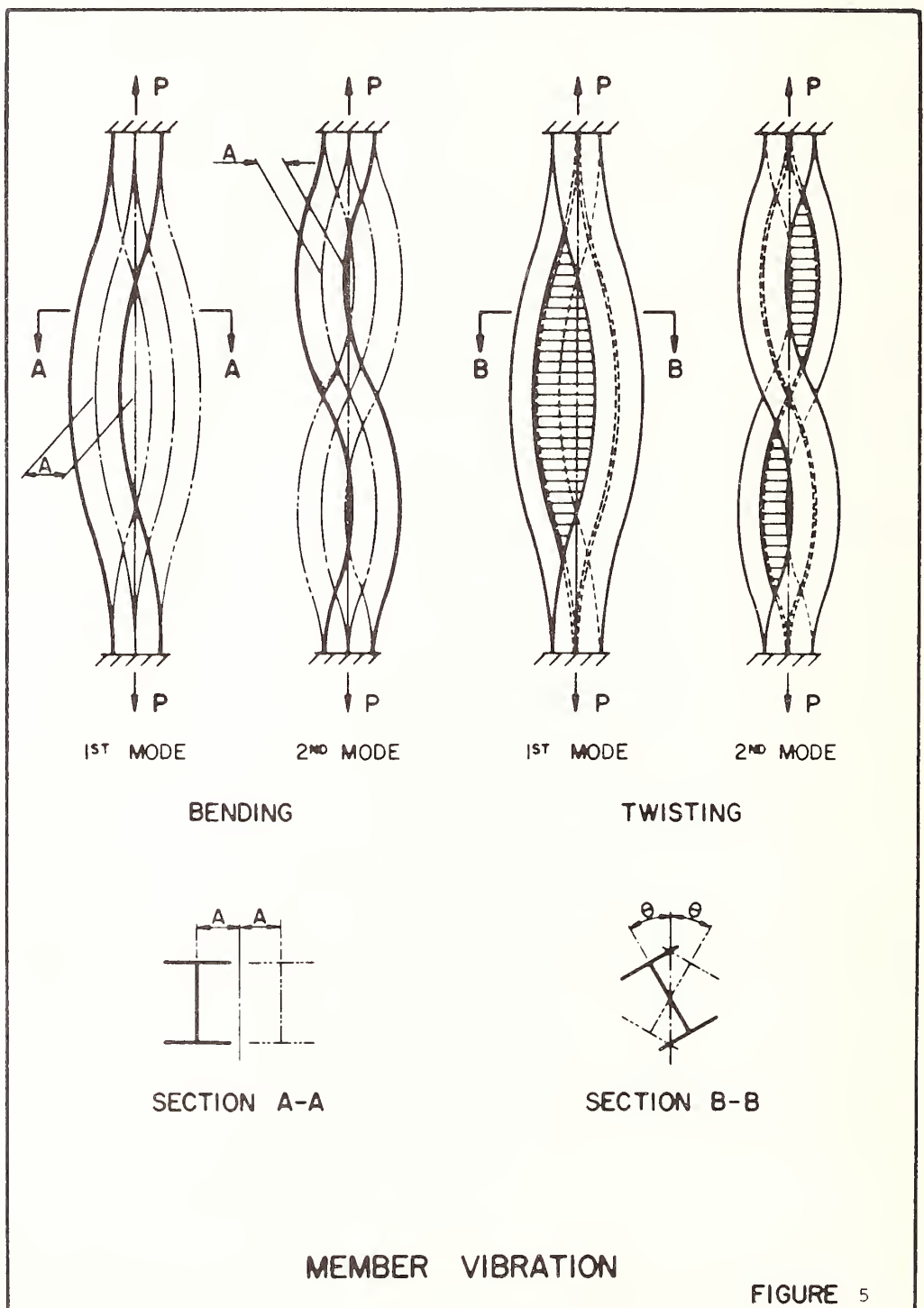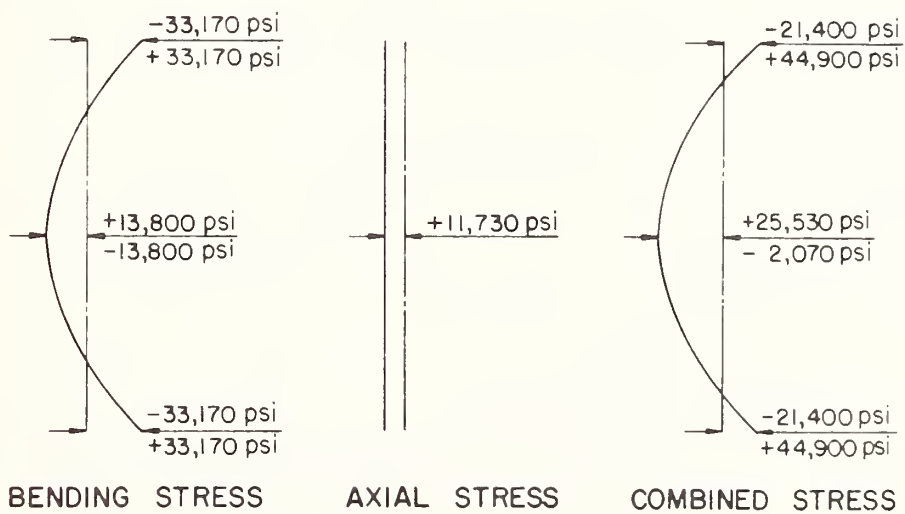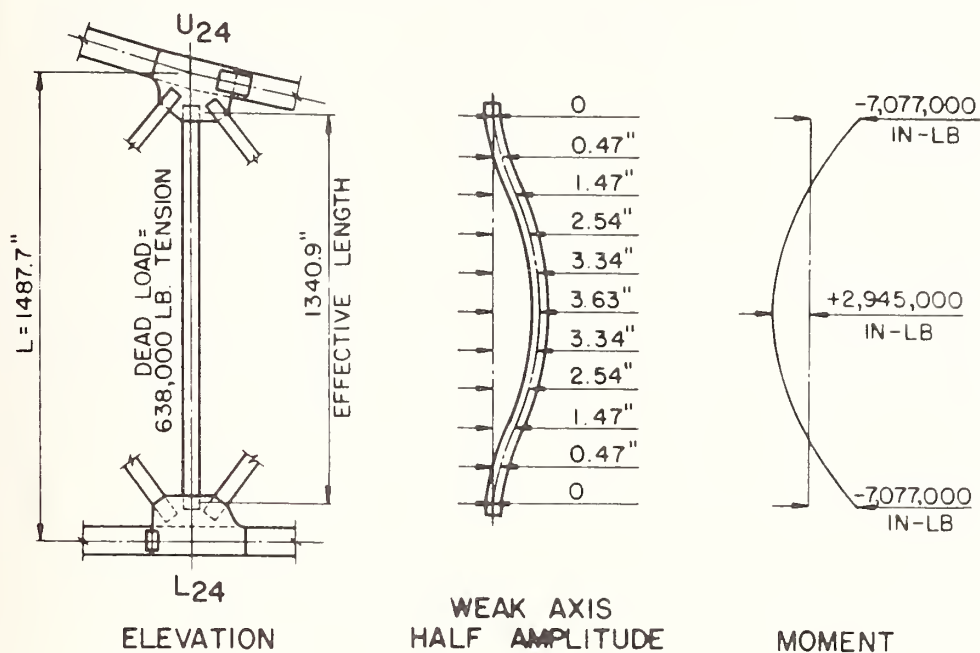
AMPLITUDE, BENDING MOMENTS AND STRESSES
FOR TYPICAL H-SECTION MEMBER

FIGURE 6
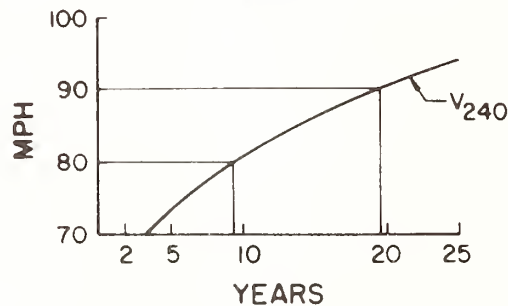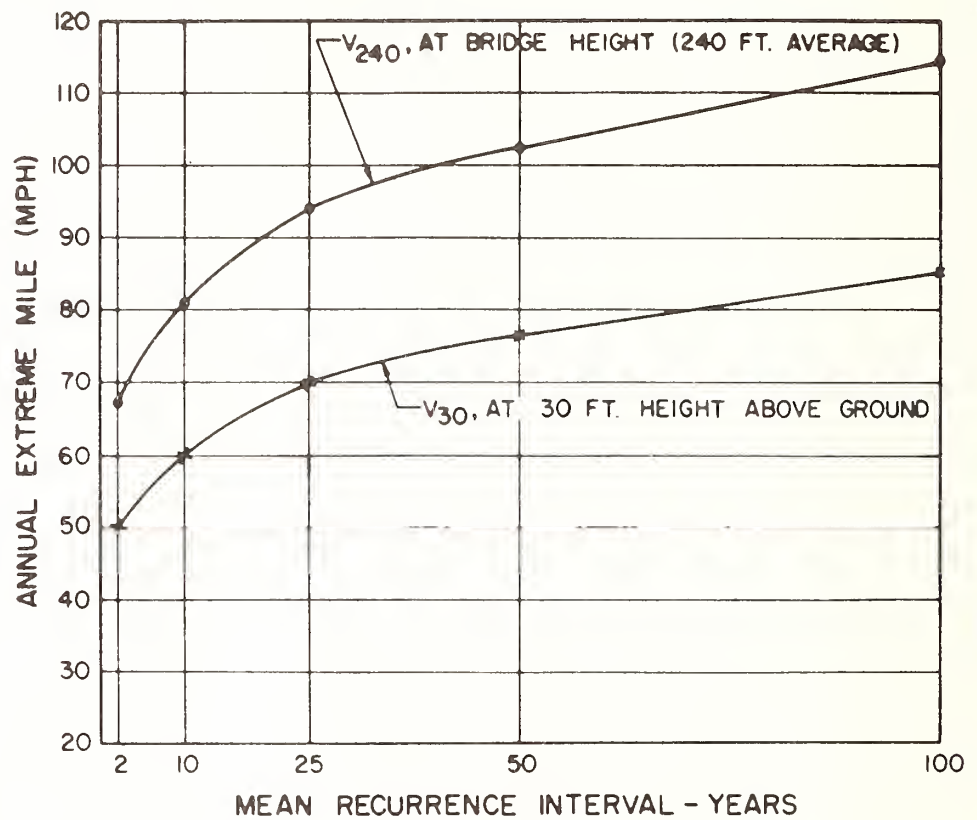
EXTREME WINDS IN
THE AREA OF PHILADELPHIA

FIGURE 7

DESIGN WIND DURATION
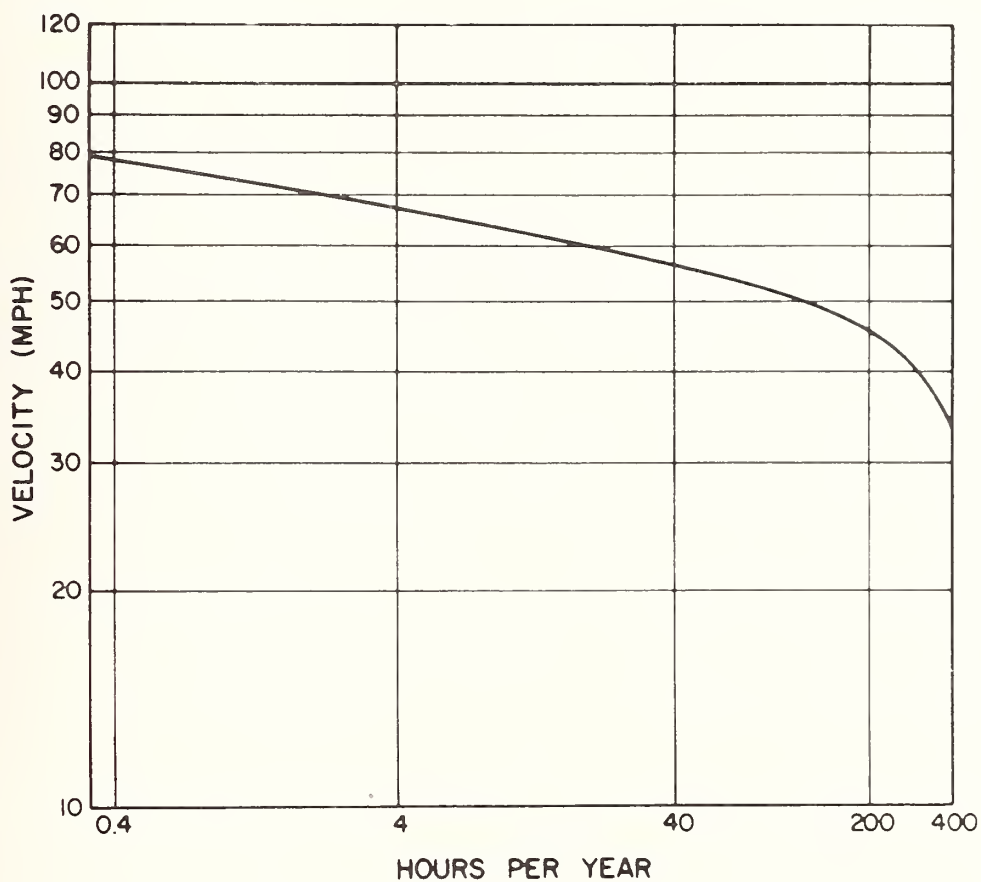
Source: Merrison Committee Report, "Inquiry Into The Basis of Design and Method of Erection of Steel Box Girder Bridges", 1973. Data taken for "Estuarial bridges or high valley crossings".

FIGURE 8

ADDITIONAL BRACING, TYPICAL

EXISTING MEMBERS, TYPICAL

HYDRAULIC DAMPER

SUB STRUT

ADDITIONAL BRACING, TYPICAL

A

A
27

ADDITIONAL BRACING (SAME SECTION AS LONG. BRACES)

U27

L27

SECTION A-A
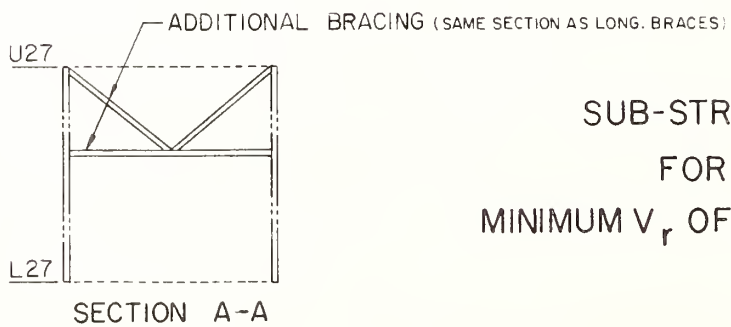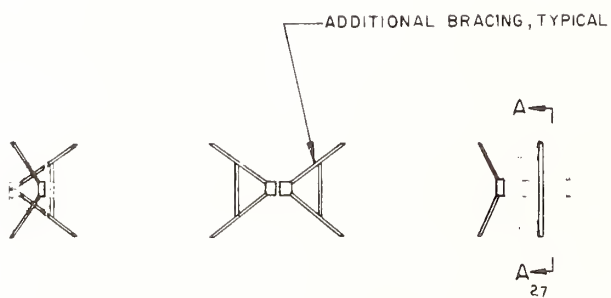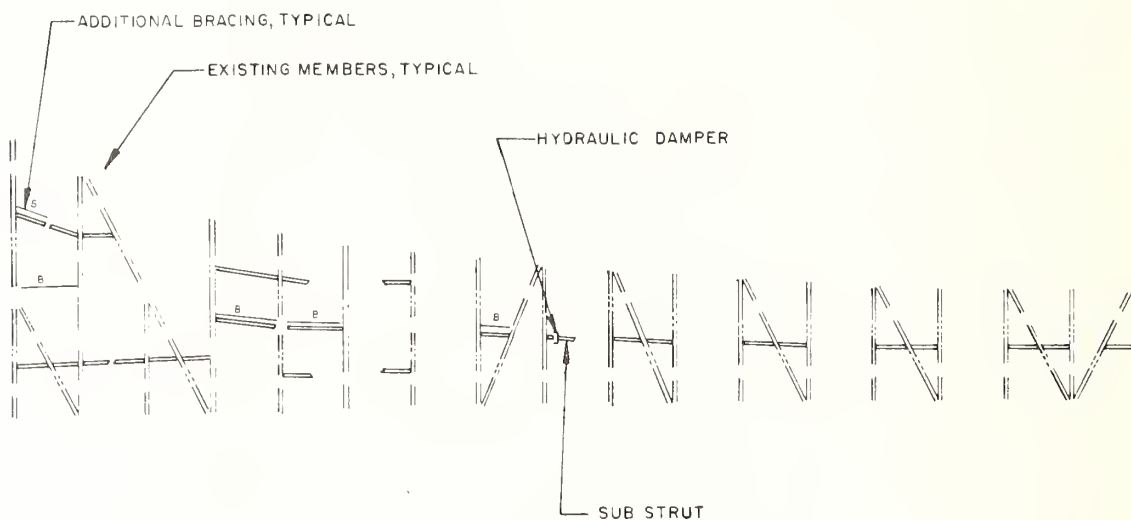
SUB-STRUTS
FOR
MINIMUM V_r OF 100 M.P.H.

FIGURE 9

ADDITIONAL BRACING, TYPICAL

EXISTING MEMBERS, TYPICAL

HYDRAULIC DAMPER

SUB STRUT

ADDITIONAL BRACING, TYPICAL

A

A

U27

ADDITIONAL BRACING

L27

SECTION A-A
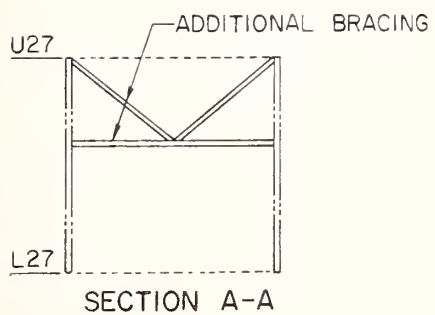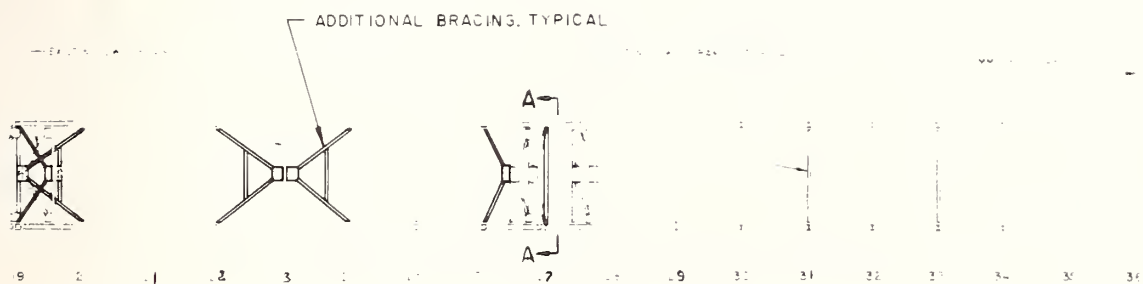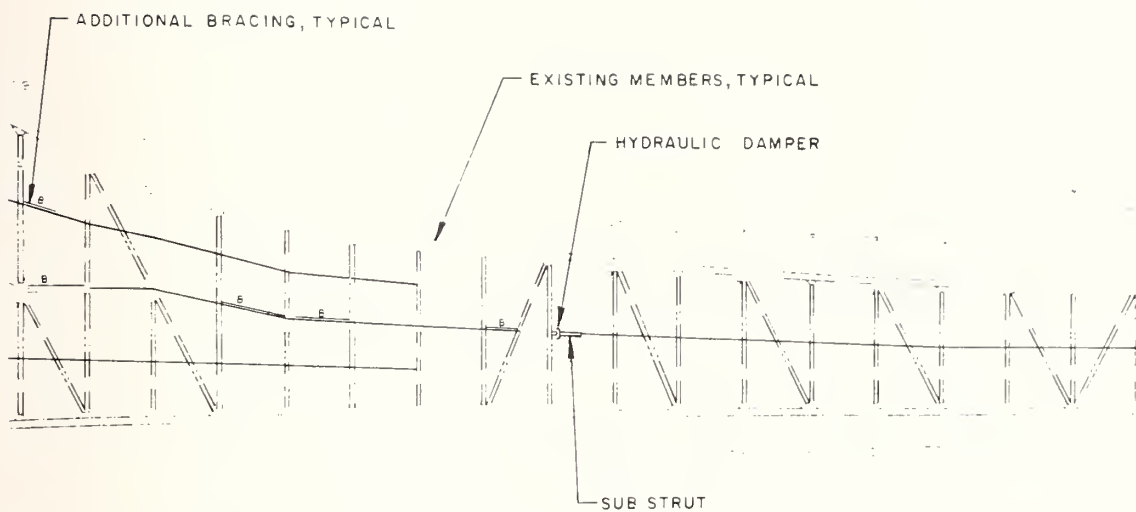
PERMANENT CABLES
FOR
MINIMUM V_r OF 100 M.P.H.

FIGURE 10

477
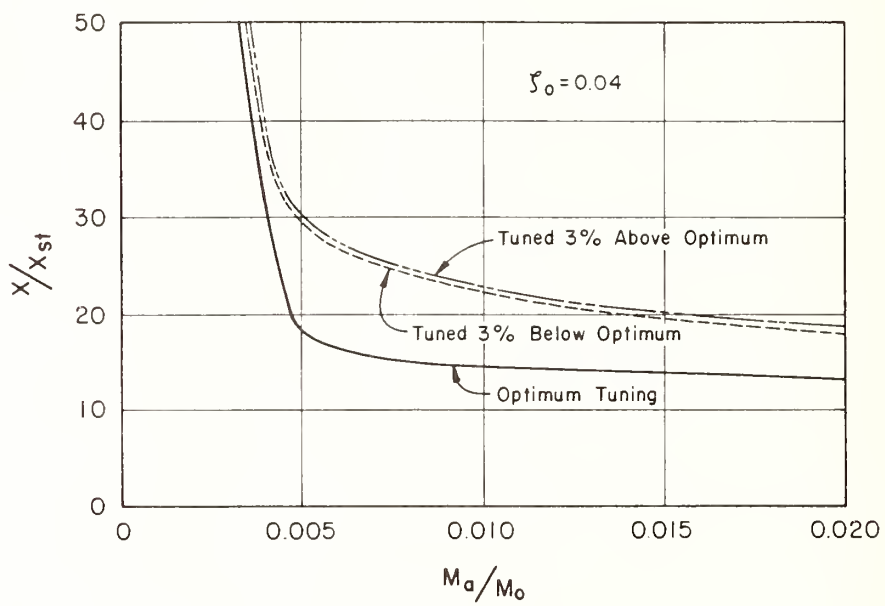
VARIATION IN ABSORBER EFFECTIVENESS
WITH MASS RATIO

FIGURE 11
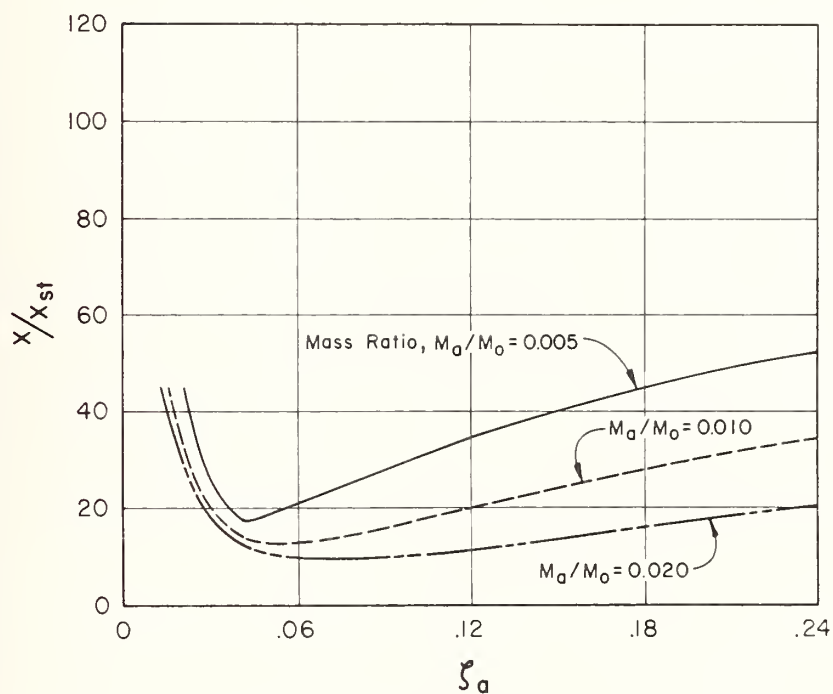
VARIATION IN ABSORBER EFFECTIVENESS
WITH ABSORBER DAMPING

FIGURE 12
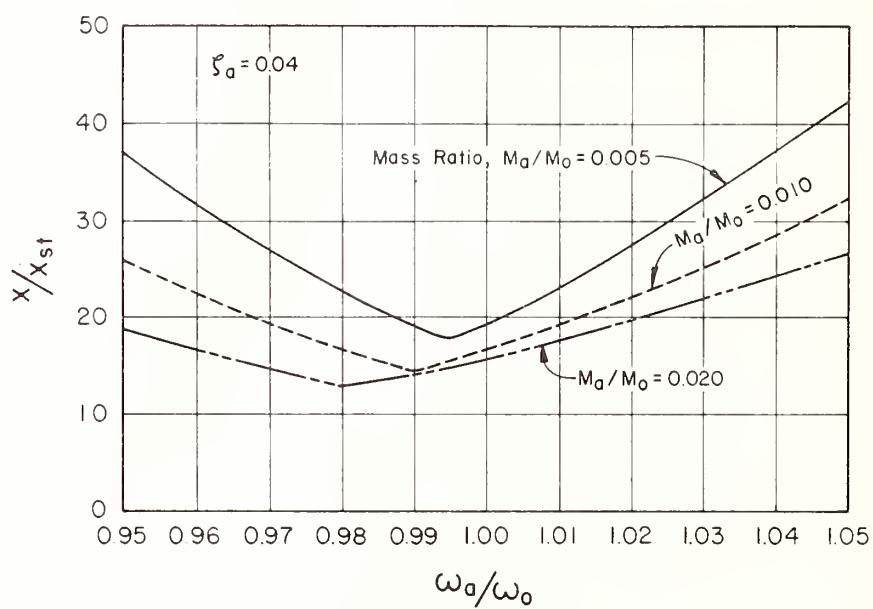
VARIATION IN ABSORBER EFFECTIVENESS
WITH ABSORBER TUNING

FIGURE 13
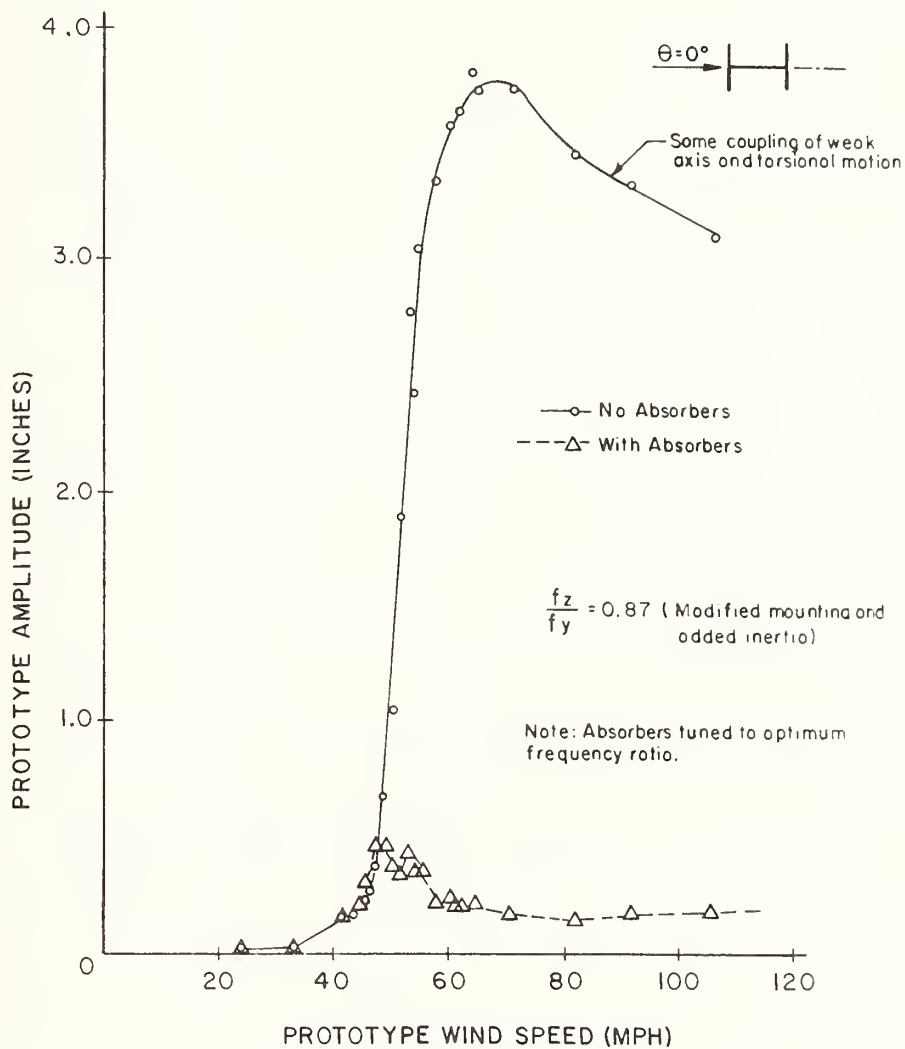
1:7.5 SCALE ELASTIC MODEL
WEAK AXIS MOTION VERSUS WIND SPEED-
WITHOUT AND WITH TWO 0.005 SYNTHETIC
RUBBER ABSORBERS.

FIGURE 14

1:7.5 SCALE ELASTIC MODEL —
STRONG AXIS MOTION VERSUS WIND SPEED — WITHOUT
AND WITH TWO 0.005 SYNTHETIC RUBBER ABSORBERS
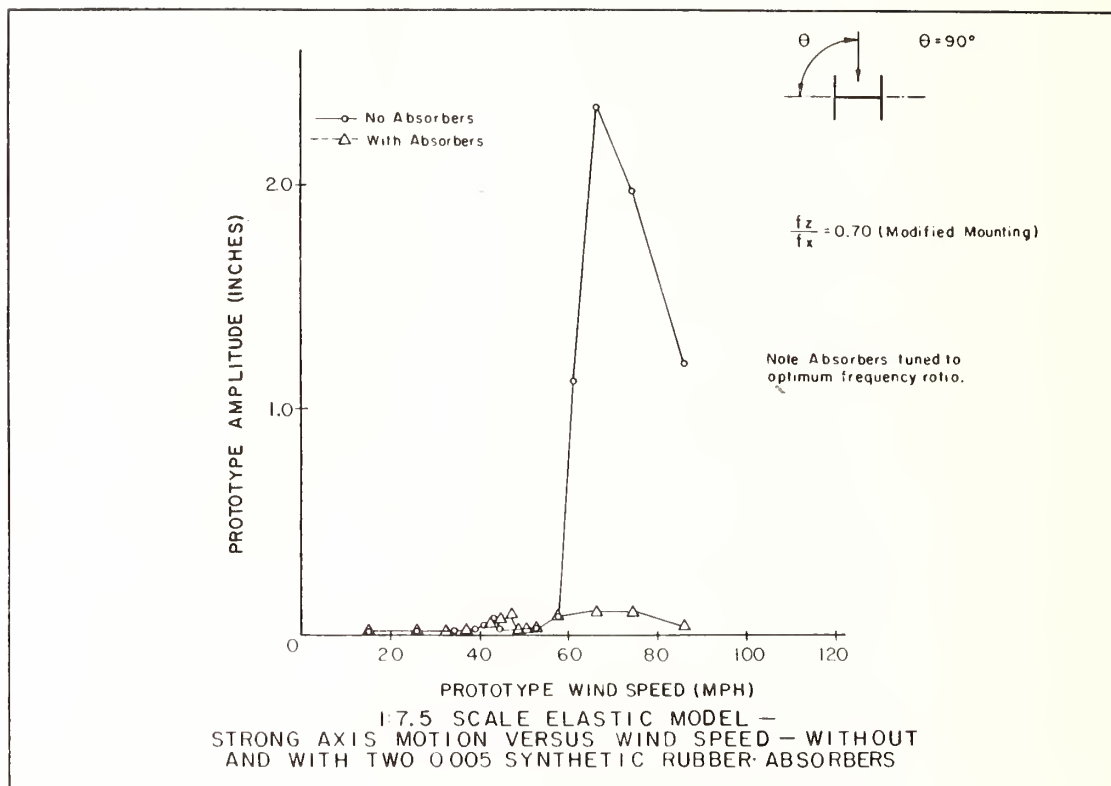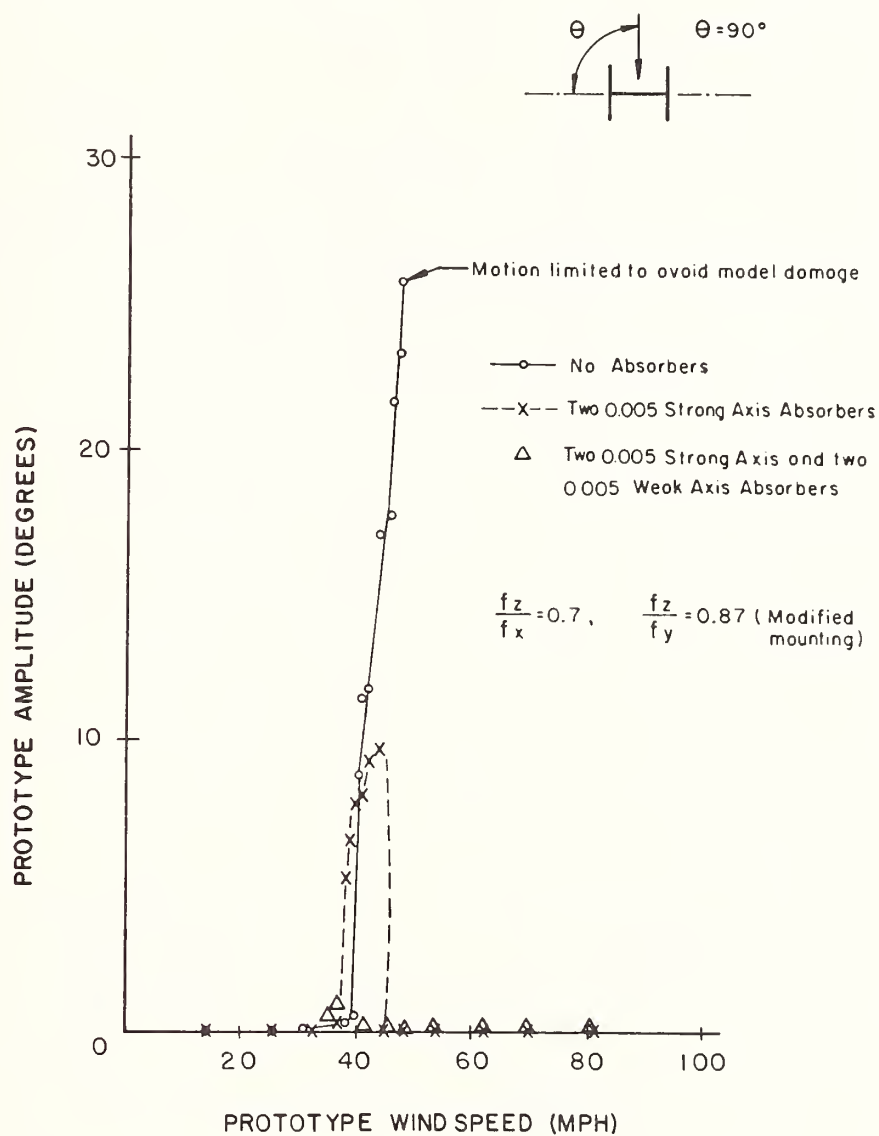
FIGURE 15

1:7.5 SCALE ELASTIC MODEL—
TORSIONAL MOTION VERSUS WIND SPEED—
WITHOUT AND WITH SYNTHETIC RUBBER
ABSORBERS

FIGURE 16

VERTICAL ABSORBER

*7" for strong axis
absorbers

15" *

$\frac{9}{16}$"X1$\frac{1}{2}$"slotted hole

4"   6"

$\frac{3}{8}$" ∅ bolt with hex head
and two nuts

5"
7"

$\frac{9}{16}$"hole

℄ $\frac{1}{2}$"∅bolt

℄ Bracket

9"

Synthetic
Rubber
stem

1'-4"

4"

Varies 6" to 18"

B

A

H-section web or
box-section flange

8$\frac{1}{2}$"

Varies
3$\frac{7}{8}$"to 9$\frac{3}{4}$"

Note: Absorbers will be
mounted in pairs.

$\frac{3}{4}$"

1"

$\frac{1}{2}$"X$\frac{3}{4}$"slot

$\frac{3}{8}$"∅ rod

Note: All plate
thicknesses are $\frac{3}{8}$"
unless noted.

ELEVATION

1'-3"

2$\frac{1}{2}$"   2$\frac{1}{2}$"

6"

℄$\frac{3}{8}$" ∅ bolt

7"

2$\frac{1}{2}$"

$\frac{3}{4}$"

4"

1'-4"

Drill & tap for
cover box
screw (typ.)

6"

Bent ℄

$\frac{1}{2}$"∅ hole

9"

SECTION B-B

℄$\frac{11}{16}$"∅ holes for $\frac{5}{8}$"∅
high strength bolts

2$\frac{1}{2}$"

SECTION A-A

Note: For box sections drill and tap
flange for $\frac{5}{8}$"∅ bolts. Absorbers to be
mounted on opposite sides of box in pairs.

ABSORBER DETAILS

FIGURE 17

CALCULATION OF THE GUST RESPONSES OF LONG-SPAN BRIDGES (II)

by

Nobuyuki Narita

Hiroshi Sato

ABSTRACT

The random responses of long-span bridges due to the turbulence of natural wind, important in the fatigue problem of structural materials and in the serviceability of public bridges are discussed. A simple formula by which the standard deviation of vertical bending gust responses can be calculated is derived. It is proposed that designers of long-span bridges can use this formula to assess gust responses, especially in the early stages of design.

INTRODUCTION

In a previous paper [1] the strict method of calculating both the vertical bending and the torsional mode of gust responses in the frequency domain and in the time domain was described. Calculated results agreed reasonably with the observed ones, and it was found that by setting more rational values for the parameters, the gust responses of long-span bridges can be assessed more precisely by using the method. This strict method, however, requires rather burdensome programming and computer operations. A simpler formula will be helpful when designers of long-span bridges want to assess gust responses in round numbers in the early stages of design. In this paper a simpler formula for calculating vertical bending gust responses is proposed, and its derivation is explained.

NOTATION

B = Width of bridge deck

C_F = Lift coefficient defined for the structural axis

f = Frequency

f_1 = Natural frequency of the first vertical bending mode

I_w = Intensity of turbulence of vertical component of wind

L = Span length of bridge

m = Mass per unit length of span

mg = Weight per unit length of span

R = Cross-correlation coefficient of wind

S = Power spectral density

U = Mean horizontal component of wind speed perpendicular to the bridge axis

u = Fluctuating horizontal component of wind speed perpendicular to the bridge axis

w = Fluctuating vertical component of wind speed

x = Spanwise coordinate of bridge

X = Aerodynamic admittance

α = Angle of attack

γ = Constant for aerodynamic damping

η_1 = Vertical bending displacement

ζ_s = Structural damping constant

ρ = Air density

σ = Standard deviation

Φ_1 = Vertical bending vibration mode of the first order

SIMPLE FORMULA FOR CALCULATING VERTICAL BENDING GUST RESPONSES

The standard deviation of vertical bending gust responses at the center of the main span of a long-span bridge, whose first symmetrical vertical bending vibration mode dominates in gust responses, can be calculated approximately with the following formula.

$$\sigma_\eta(x)\Big|_{x=L/2} = const \cdot \frac{dC_F}{d\alpha} \cdot I_w \cdot U^2 \cdot B^{1/2} \cdot f_1^{-2} \cdot L^{-1/3} \cdot (mg)^{-1} \tag{1}$$

The proper value for the constant is found to be $0.03 - 0.06$ when each value of variables in the formula is substituted in the following unit.

$$\sigma_\eta; cm, \quad U; m/s, \quad B; m, \quad f_1; H_z, \quad L; m, \quad mg; \frac{ton}{m}$$

DERIVATION OF THE FORMULA

When the above formula was derived, the factors which relate to quantities of vertical bending gust responses were taken up first, the degree of influence of each factor was investigated, then the shape of the formula was determined. Finally, the constant value was calculated using the measured data of gust responses.

Holmes' method of calculating the gust responses was referenced when examining the factors and investigating the degrees of influence. In Holmes' method, only the first vertical bending vibration mode is considered, the same aerodynamic admittance and cross-correlation coefficient is used for wind speed u and w, and the aerodynamic damping is obtained from the quasi-steady theory. Thus, Holmes' method is simpler and less strict than author's method [1], however, it can be said to be useful when it is referenced to obtain this simple and approximate formula.

Holmes' calculation method is as follows.

$$\sigma_\eta(x)^2 = \frac{\Phi_1(x)^2}{(2\pi f_1)^4 \left\{\int_0^L m\Phi_1(x)^2 dx\right\}^2} \left[S(f_1) \frac{\pi f_1}{4\zeta} + \int_0^{f_1} S(f)df \right] \tag{2}$$

$$S(f) = (\rho BU)^2 \ X(f)^2 \left[C_F^2 \ S_u(f) + (\frac{1}{2}\frac{dC_F}{d\alpha})^2 \ Sw(f) \right] \tag{3}$$

$$x \int_0^L \int_0^L \Phi_1(x) \ \Phi_1(y) \ R(x, y, f) dxdy$$

$$\zeta = \zeta_s + \frac{\dfrac{dC_F}{d\alpha} \rho UB}{8\pi m f_1} \gamma \tag{4}$$

FACTORS IN DETERMINING THE QUANTITIES OF VERTICAL BENDING GUST RESPONSES

From Eq. (2) – Eq. (4), the factors in determining the quantities of vertical bending gust responses of long-span bridges can be listed as follows.

Structure; vibration mode, natural frequency, mass per unit length of span, span length of bridge, structural damping constant, width of bridge deck

Natural wind; air density, mean horizontal component of wind speed perpendicular to the bridge axis, power spectral density of fluctuating component of wind speed, cross-correlation coefficient of wind

Aerodynamic characteristics; aerodynamic admittance, lift coefficient and lift slope defined for the structural axis, aerodynamic damping

DEGREE OF INFLUENCE OF EACH FACTOR

Most decks of long-span bridges have much smaller values for lift coefficients than those of lift curves around angle of attack of zero degree. Using this fact, the following proportional relationship can be derived approximately from Eq. (2) and Eq. (3).

$$\sigma_\eta (x) \propto \frac{dC_F}{d\alpha} \cdot I_w \cdot U^2 \cdot f_1^{-2} \cdot m^{-1} \tag{5}$$

Next, a calculation was carried out using Eq. (2) – Eq. (4) in order to investigate the degree of influence of factors whose influence cannot be obtained directly from Eq. (2) and Eq. (3), and to recognize the relationship of Eq. (5). The fundamental parameters and the calculated vertical bending gust responses using these parameters are shown in Table 1, and Table 2, respectively. The gust responses were calculated changing one factor at a time and are shown in Table 3. From Table 3, the degree of influence of each factor can be assessed as follows.

Vibration mode; Two modes were considered. One was the mode of having the bridge deck supported with hinges, and in the other mode supported rigidly. The difference of σ_η between the two modes is less than 10 percent.

Natural frequency; $\sigma_\eta \propto f_1^{-2.0 \sim -2.3}$

Mass per unit length of span; $\sigma_\eta \propto m^{-0.8 \sim -0.9}$

Span length of bridge; $\sigma_\eta \propto L^{-0.3}$

Structural damping constant; The difference between σ_η with ζ_s of 0.003 and σ_η with ζ_s of 0.03 is about 10 percent even where the aerodynamic damping has as small a value as possible for the ordinary deck of long-span bridges.

Width of bridge deck; $\sigma_\eta \propto B^{0.6}$

Air density; This can be neglected because its variation seems to be very small.

Mean horizontal component of wind speed perpendicular to the bridge axis;
$\sigma_\eta \propto V^{2.1 \sim 2.3}$

Power spectral density of wind speed fluctuating component; Instead of considering the influence of P.S.D. directly, the influence of intensity of turbulence and that of the distribution of power in the frequency domain were considered separately. As for intensity of turbulence, $\sigma_\eta \propto I_w^{10}$, when I_u and I_w change their values with a constant ratio. In order to examine the influence of distribution, three formulae of $S_w(f)$ by Panofsky and McCormick, Busch and Panofsky, and Singer, Busch and Frizzola [3] were considered. In doing this, their influence on σ_η was found to be about 10 percent.

Cross-correlation coefficient of wind and aerodynamic admittance; It is difficult to set the precise values of these two factors, and unfortunately their effect, especially of the aerodynamic admittance, cannot be neglected. Therefore, these effects were considered in determining the constant value in Eq. (1) from measured data.

Lift slope for the structural axis; $\sigma_\eta \propto \left(\dfrac{dC_F}{da}\right)^{0.8 \sim 0.9}$

Aerodynamic damping; In comparing unsteady aerodynamic coefficients of a bridge deck measured in a wind tunnel tests with Eq. (4) derived from the quasi-steady theory, almost all the experimental coefficients fall between γ of 0.5 - 1.0. When γ is varied from 0.5 to 1.0 with ζ_s of 0.003, σ_η varies about 20 percent.

By using the above indicies in round numbers and neglecting factors of small influence, the shape of the formula can be determined as in Eq. (1).

DETERMINATION OF THE CONSTANT VALUE

The constant value in Eq. (1) was calculated using the data shown in Table 4. The calculated constant values - using the data measured at the sites of the Kammon Bridge, Suehiro Bridge, Hirado Bridge, and in the wind tunnel test of the West Gate Bridge [2] - were 0.047, 0.032, 0.039 and 0.026 - 0.059, respectively. Thus, the proper value for the constant can be said to be 0.03 - 0.06. In the above calculation, the data from the Kammon Bridge and the Suehiro Bridge were used in a form of an approximated equation as derived from the data with I_w at about 0.10 under the assumption that $\sigma_\eta \propto U^2$. The data used from the Hirado Bridge have the largest U value in any of the data obtained so far.

REFERENCES

[1] Narita, N. and Sato, H., "Calculation of the Gust Responses of Long-Span Bridges," 11th Joint Meeting, Japan-U.S. Panel on Wind and Seismic Effects, UJNR, Tsukuba, September 4-7, 1979.

[2] Holmes, J. D., "Prediction of the Response of a Cable Stayed Bridge to Turbulence," Proc. 4th International Conference on Wind Effects on Buildings and Sites, 1975.

[3] Okauchi, I., Ito, M., and Miyata, T., "Structures Resistant to Wind," 1977 (in Japanese).

Table 1.   Fundamental Parameters

Vibration Mode	calculated value for West Gate Bridge
Natural Frequency	0.33Hz
Weight per Unit Length of Span	20.10 ton/m
Span Length of Bridge	336m
Structural Damping Constant	0.013
Width of Bridge Deck	37.4m
Mean Horizontal Component of Wind Speed Perpendicular to the Bridge Axis	18.5m/s, 37.0m/s, 49.3m/s
Power Spectral Density of Fluctuating Component of Wind Speed	S_u; due to Harris S_w; due to Busch & Panofsky I_u; 0.20 I_w; 0.10
Decay Factor of Cross-Correlation Coefficient of Wind	7.0
Aerodynamic Admittance	due to Holmes suggested by Vickery
Lift Slope Defined for the Structural Axis	5.10
Aerodynamic Damping	quasi-steady theory with constant of 0.60

Table 2.   Calculated Vertical Bending Gust Responses with Parameters in Table

	σ_r (L/2)
U=18.5m/s	0.028cm
37.0	0.14
49.3	0.27

Table 3. Degree of Influence of Each Factor (Calculation Result)

Vibration Mode (L=848m)

| | σ_{η} (L/2)(cm) | |
Support	Hinge	Rigid
U=18.5m/s	0.025	0.027
37.0	0.11	0.12
49.3	0.21	0.23

Natural Frequency f_1

| | σ_{η} (L/2)(cm) | | | |
f_1(Hz)	0.0825	0.165	0.330	0.660
U=18.5m/s	0.65	0.14	0.028	0.006
37.0	2.4	0.65	0.14	0.03
49.3	3.7	1.1	0.27	0.05

Weight per Unit Length of Span mg

| | σ_{η} (L/2)(cm) | | | |
mg(ton/m)	5.0	10.0	20.1	40.0
U=18.5m/s	0.099	0.053	0.028	0.015
37.0	0.43	0.24	0.14	0.08
49.3	0.79	0.46	0.27	0.16

Span Length of Bridge L (Mode for Hinge-Support)

| | σ_{η} (L/2)(cm) | | | | |
L(m)	212	424	848	1696	3392
U=18.5m/s	0.037	0.030	0.025	0.021	0.019

Structural Damping Constant ζ_s

| | σ_{η} (L/2)(cm) | | | |
ζ_s	0.0032	0.0064	0.013	0.025
U=18.5m/s	0.031	0.030	0.028	0.027
37.0	0.15	0.15	0.14	0.13
49.3	0.29	0.28	0.27	0.25

Width of Bridge Deck B

| | σ_{η} (L/2)(cm) | | | |
B(m)	12	24	37.4	48
U=18.5	0.014	0.021	0.028	0.034
37.0	0.070	0.11	0.14	0.16
49.3	0.14	0.21	0.27	0.31

Table 3. (Continued)

Intensity of Turbulence I_w ($I_u = I_w \times 2.0$)

I_w	$\sigma_\tau (L/2)$ (cm)				
	0.025	0.05	0.10	0.15	0.20
U=18.5m/s	0.007	0.014	0.028	0.042	0.056
37.0	0.04	0.07	0.14	0.21	0.28
49.3	0.07	0.14	0.27	0.41	0.54

Shape of Power Spectral Density S_w

S_w	$\sigma_\tau (L/2)$ (cm)		
	Panofsky & McCormick	Busch & Panofsky	Singer, Busch & Frizzola
U=18.5m/s	0.028	0.028	0.027
37.0	0.13	0.14	0.13
49.3	0.26	0.27	0.24

Decay Factor of Cross-Correlation Coefficient of Wind k

k	$\sigma_\tau (L/2)$ (cm)				
	1.0	3.5	7.0	14.0	28.0
U=18.5m/s	0.047	0.034	0.028	0.023	0.020
37.0	0.24	0.18	0.14	0.11	0.09
49.3	0.43	0.34	0.27	0.21	0.17

Aerodynamic Admittance X

X	$\sigma_\tau (L/2)$ (cm)		
	Liepmann	Holmes	Davenport (k=7.0)
U=18.5m/s	0.020	0.028	0.024
37.0	0.09	0.14.	0.12
49.3	0.18	0.27	0.24

Lift Slope Defined for the Structural axis $\dfrac{dC_F}{d\alpha}$

$\dfrac{dC_F}{d\alpha}$	$\sigma_\tau (L/2)$ (cm)					
	1.0	2.0	3.0	4.0	5.1	6.0
U=18.5m/s	0.007	0.012	0.018	0.023	0.028	0.033

Constant in Aerodynamic Damping τ

τ	$\sigma_\tau (L/2)$ (cm)			
	(ζ_s=0.0032) 0.5	1.0	(ζ_s=0.0047) 0.5	1.0
U=18.5m/s	0.032	0.028	0.031	0.028
37.0	0.16	0.13	0.16	0.13
49.3	0.31	0.25	0.30	0.25

Table 4. Data Used for Determination of the Constant Value in Eq. (1)

	Kammon Br.	Suehiro Br.	Hirado Br.	West Gate Br.**		
				1	2	3
$dC_F/d\alpha$	3.55	2.86	3.31	5.10	5.10	5.10
I_w	0.10	0.10	0.10*	0.10	0.10	0.06
U (m/s)	———***	———***	18.5	18.5	37.0	18.5
B (m)	29.0	18.5	14.5	37.4	37.4	37.4
f_1(Hz)	0.20	0.48	0.31	0.33	0.33	0.33
L (m)	712	250	460	336	336	336
mg(ton/m)	24.7	9.26	11.0	20.1	20.1	20.1
σ_τ(L/2) (cm)	1.0×10^{-2} xU^2	3.0×10^{-3} xU^2	2.0	2.8	16.6	1.1
const.	0.047	0.032	0.039	0.040	0.059	0.026

* estimated value

** Three experimental data were used which have maximum (2), minimum (3), and intermediate (1) values of σ_τ/U^2.

*** These data were used in the form of $\sigma_\tau = const. xU^2$.

ACTIVE TURBULENCE GENERATOR FOR AERODYNAMIC

TESTS OF BRIDGE SECTION MODELS

by

B. Bienkiewicz

J. E. Cermak

J. A. Peterka

INTRODUCTION

Turbulence in an oncoming flow has profound effects on aerodynamic behavior of suspension bridges. Even simple wind-tunnel tests with a typical section of a bridge deck (the so-called bridge section model) indicate -- at least qualitatively -- the main changes introduced by turbulence. In a typical situation turbulence usually transfers occurrence of flutter-type aerodynamic instability to higher values of the reduced velocity. At the same time random oscillations of a bridge deck (buffeting) -- not present in a smooth flow -- appear at lower values of reduced velocity. Their magnitude ordinarily increases with the wind speed, Cermak et al. [1].

Wind-tunnel tests with bridge section models are less expensive than wind-tunnel tests with full bridge models. Also they can be conducted in smaller wind tunnels. Typically, turbulence for a section-model test is introduced into the flow by placing a grid of rectangular or cylindrical rods upstream of the test section. The main characteristics of turbulence generated in such a manner, especially integral length scale, depend on the wind-tunnel size. If a wind-tunnel with a relatively small test section is considered, the attainable integral length scale is usually smaller than the width of a bridge deck scaled for the tunnel. On the other hand, full-scale measurements show that the integral length scale of the atmospheric turbulence is several times longer than the width of a typical bridge deck, Scanlan [2]. It has not been determined yet what the effects of the integral length scale of turbulence are on a bridge-deck aerodynamic response. In order to explore this question in more detail it is necessary to conduct a series of tests with bridge section models where the turbulence integral length scale could be easily changed to attain values far beyond the limits imposed by grid turbulence.

This paper describes a concept and results of initial testing of a turbulence generator which attempts to provide the desired flexibility for control of the integral length scale.

ACTIVE TURBULENCE GENERATOR

The concept for an active turbulence generator was described earlier in some detail by Cermak et al. [3]. It is proposed that a generator of the same type be constructed in the George S. Vincent Wind Tunnel shown in Figure 1. The main components of the generator are two arrays of symmetrical airfoils (A and C) oscillating 180 degrees out of phase and in phase, respectively. The array A is assumed to produce primarily longitudinal velocity fluctuations whereas array C is intended to generate primarily fluctuations of transverse velocity component. The driving mechanism of the generator contains components of a standard electro-hydraulic servo-system. The system is driven by input signals recorded on an analog magnetic tape. It is expected that in order to improve "control" of the two generated turbulent velocity components -- longitudinal and transverse -- some flow suppressors B shown in Figure 1 will be necessary.

The concept has been initially tested in the Fluid Dynamics and Diffusion Laboratory, Colorado State University, as a part of a study sponsored by the Federal Highway Administation, Department of Transportation (FHWA, DOT). The generator was placed in the open-circuit wind tunnel as shown in Figure 2. The two arrays of symmetrical airfoils NACA 0015 made of extruded aluminum were driven by hydraulic actuators controlled by a MTS Corporation servo-system. Two kinds of input driving signals were used. Initially an analog signal -- Gaussian white noise with low-pass filtering -- produced by a standard noise generator (Hewlett-Packard) was used to drive the arrays. Later a computer-simulated signal after digital-to-analog conversion was fed as input to the driving system. During a Monte Carlo computer simulation the time series of a given spectra was generated using procedure suggested by Shinozuka (4) and Wittig et al. [5]. Use of a FFT "stacked" routine, Hudspeth et al. [6], resulted in a substantial reduction of computer time required for simulation.

For most of the experiments only one array of oscillating airfoils was activated and the resulting turbulent velocity field downstream of the generator was evaluated. Some results obtained with the array of airfoils oscillating in phase will be presented in the next paragraph.

EXEMPLARY RESULTS

During initial tests with the active turbulence generator a driving input signal was obtained from an analog noise generator. An example of such a signal -- Gaussian white noise with a low pass filtering -- is shown in Figure 3. It can be seen from this spectrum that signal was filtered with a frequency cut-off equal to approximately 5 Hz. This signal was used to drive the generator. Spectra of the turbulent velocity components were taken downstream of the generator. Figure 4 shows such spectra for the case when the generator contains only one array of airfoils oscillating in phase (vertical mode). The generated turbulence is approximately isotropic (I_v = 6.5 percent = I_u = 7.6 percent and L_u = L_v), Batchelor (7), and spectra can be fitted by the von Kármán formulas -- smooth curves --, von Kármán [8]. The resulting integral scale of turbulence is relatively low (0.17 W where W is width of the wind-tunnel test section); however, it is larger than scales obtained using a typical grid to generate turbulence.

In the next step, a computer simulated signal of a given spectra was used to drive the generator. A typical spectrum of a simulated signal compared with a target spectrum is shown in Figure 5. The digital signal and its analog counterpart are presented in Figure 6. It can be seen that all the features of the digital signal are preserved during the digital-to-analog conversion. As a target spectrum for the vertical velocity component an expression proposed by Panofsky et al. [9] was chosen. The frequency cut-off of the simulated signal shown in Figure 6 was 20 Hz. The same signal was used to determine a transfer function of a control-driving system. As can be seen in Figure 7 the system has a good frequency response up to roughly 15 Hz.

Spectra of vertical velocity component generated using the mentioned signal (see Figures 5 and 6) and the array of airfoils oscillating in phase (vertical mode) is shown in Figure 8. The spectrum obtained and the target spectrum match quite well except for a spike at a reduced frequency nz/v of about 2. The corresponding integral length scale was about 1.2 ft which indicates a substantial improvement when compared with scales of turbulence generated using analog Gaussian white noise with a low-pass filtering. In order to investigate the origin of the spike in Figure 8 a series of tests was conducted. A computer simulated signal with lower frequency cut-off, shown in Figure 9, was used in turbulence generation. For this case, see Figure 10, the agreement between the generated

and target spectra of vertical velocity component was worse but at the same time the spike was less pronounced. The integral scale of turbulence was found to be 2.5 ft.

Finally the origin of the spike in the turbulent velocity spectra was fully explained. Measurements of wind-tunnel oscillations showed that the frequency at which the spike occurred coincided with the lowest natural frequency of the wind tunnel, compare Figures 8 and 11. Even small oscillations of the wind tunnel, excited by supports of the oscillating airfoils attached to the tunnel, developed pronounced effects on the turbulence spectra as was shown by the data presented.

REMARKS

The results obtained to date indicate that the turbulence integral length scale can be controlled by the input driving signal. The ratios of integral length scale to model-bridge width that appears to be realizable are similar in magnitude to those for full-scale bridges in natural winds. Even small oscillations of a wind-tunnel test section that encloses the flow (and generator) can introduce large disturbances in a turbulent velocity field developed by an active generator. Therefore, the driving system of the generator and the generator itself should be isolated from the wind tunnel. Further measurements of spectra should be made when this has been accomplished for the present system. However, this phenomena should not be a problem for active turbulence generation in an open-jet wind tunnel such as the George S. Vincent wind tunnel shown in Figure 1.

ACKNOWLEDGMENTS

REFERENCES

[1] Cermak, J. E., Bienkiewicz, B., and Peterka, J. A., "Effects of Turbulence on Aerodynamic Characteristics of Bluff Bodies and Suspension-Bridge Decks," presented at 1978 FCP Research Review Conference, College Park, Maryland, October 1978.

[2] Scanlan, R. H., "Recent Methods in the Application of Test Results to the Wind Design of Long, Suspended-Span Bridges," Report FHWA TD-75-HS, Federal Highway Administration, Washington, D.C., October 1975.

[3] Cermak, J. E., Bienkiewicz, B., Peterka, J. A., and Scanlan, R. H., "Active Turbulence Generator for Study of Bridge Aerodynamics," Proceedings Third Engineering Mechanics Division Specialty Conference, September 17-19, 1979, The University of Texas at Austin, Austin, Texas, pp. 183-186.

[4] Shinozuka, M., "Digital Simulation of Random Processes in Engineering Mechanics with the Air of FFT Technique," in Stochastic Problems in Mechanics, Waterloo Press, Waterloo, Ontario, Canada, 1974, pp. 277-286.

[5] Wittig, L. E., and Sinka, A. K., "Simulating of Multicorrelated Random Processes Using FFT Algorithm," Jl. Acoust. Soc. of America, Vol. 58, No. 3, September 1975, pp. 630-634.

[6] Hudspeth, R. T., and Borgman, L. E., "Efficient FFT Simulation of Digital Time Sequences," Jl. Engrg. Mech. Div., ASCE, Vol. 105, No. EM2, April 1979, pp. 223-234.

[7] Batchelor, G. K., "The Theory of Homogeneous Turbulence," Cambridge at the University Press, 1956.

[8] von Kaŕmań, T., "Progress in the Statistical Theory of Turbulence," Proc. Nat. Acad. Sci., Vol. 34, 1948, pp. 530-539.

[9] Panofsky, H. A., and McCormick, R. A., "The Spectrum of Vertical Velocity Near the Surface," Quart. Jl., Royal Meteorological Soc., 1960, Vol. 86, pp. 495-503.
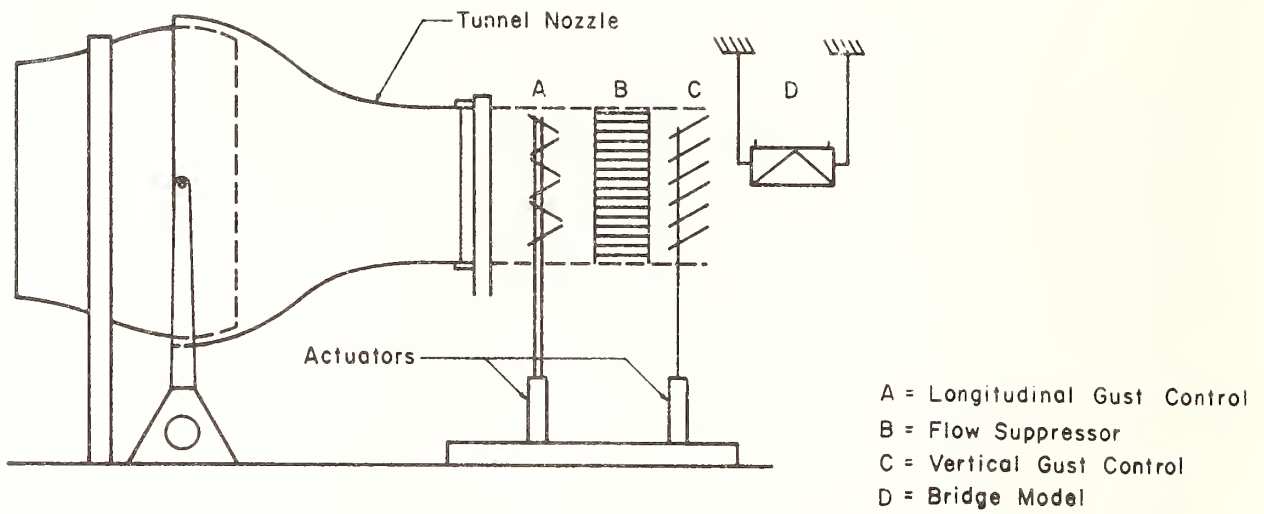
Figure 1. George S. Vincent Wind Tunnel, FHWA
Fairbank Research Laboratory, DOT

A = Longitudinal Gust Control
B = Flow Suppressor
C = Vertical Gust Control
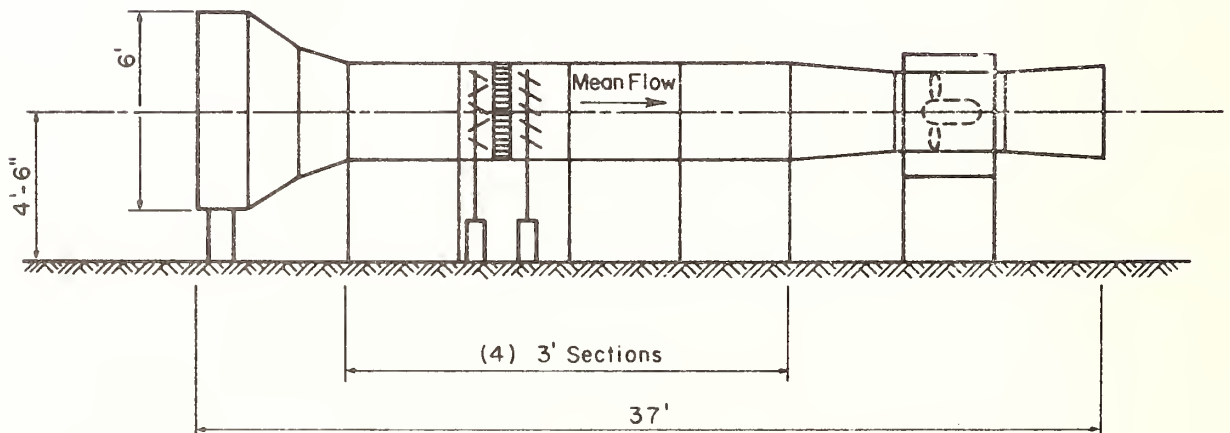D = Bridge Model

Figure 2. Structural Wind Tunnel
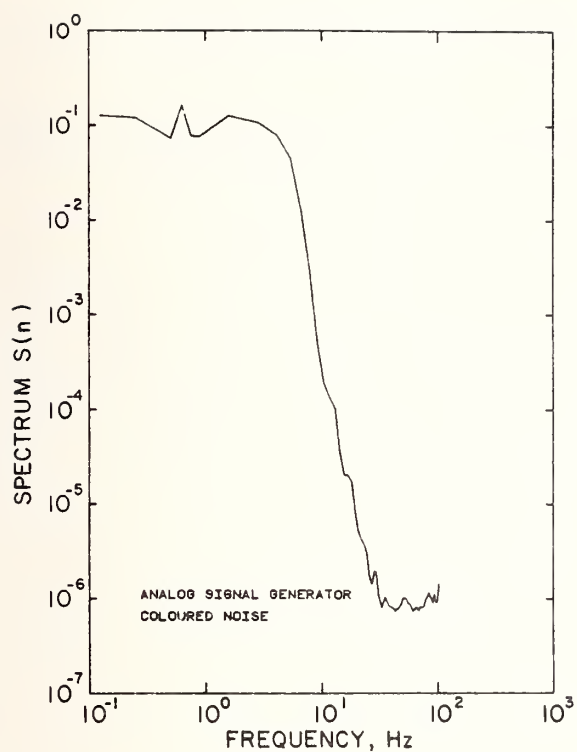
Figure 3. Analog Input Signal

Figure 4.(a) Generated Turbulence Using Analog Input Signal
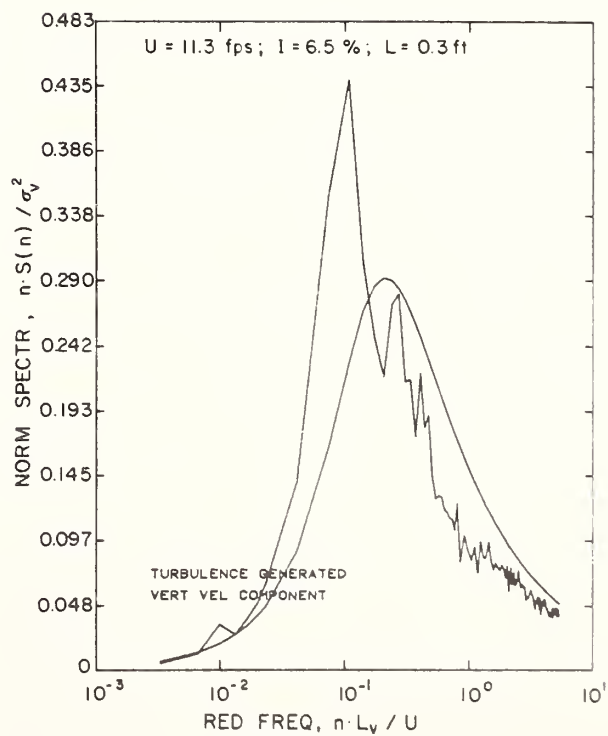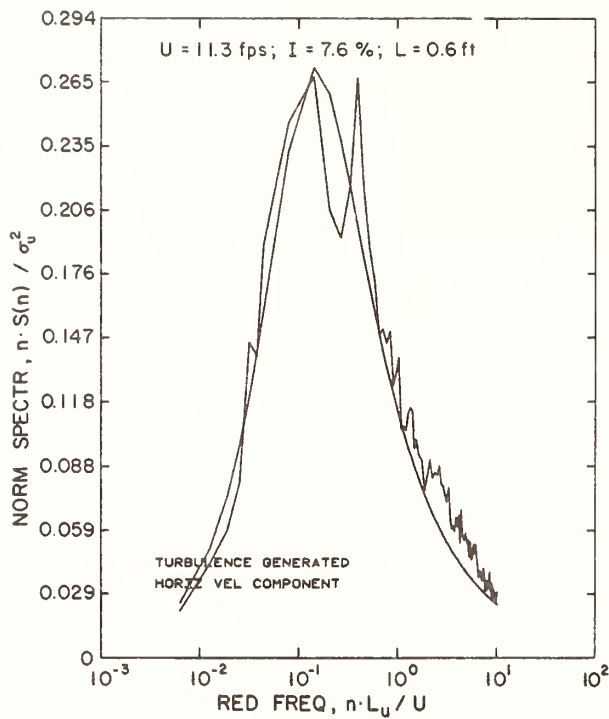
Figure 4.(b) Generated Turbulence Using Analog Input Signal

Figure 5. Spectra of Simulated Input Signal for Vertical Mode
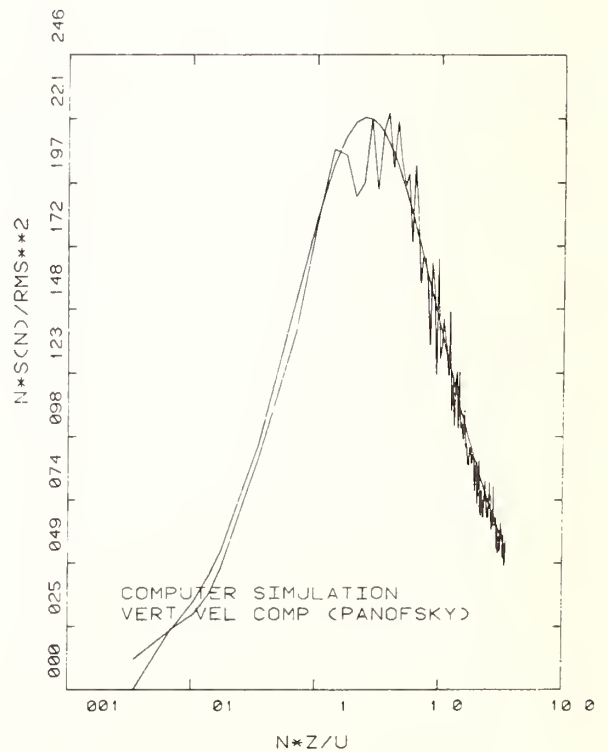
Figure 6. Digital and Analog Input Signal for Vertical Mode
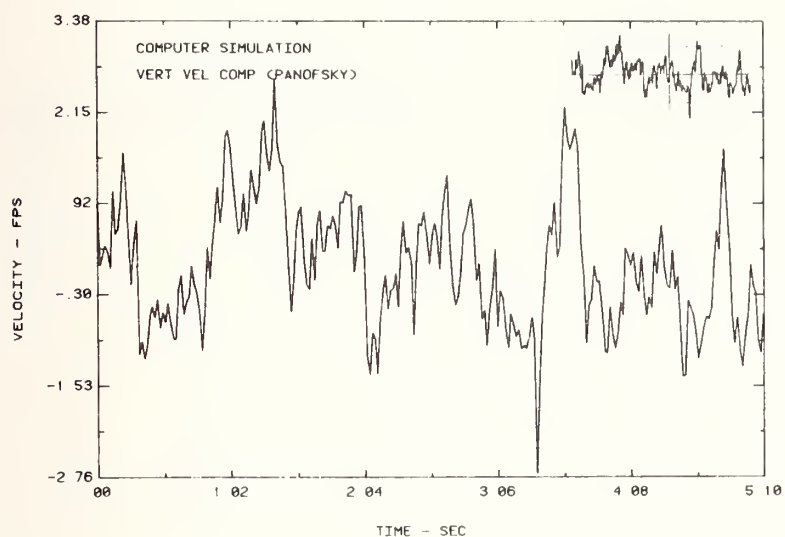
Figure 7. Transfer Function for Mechanical Driving Signal
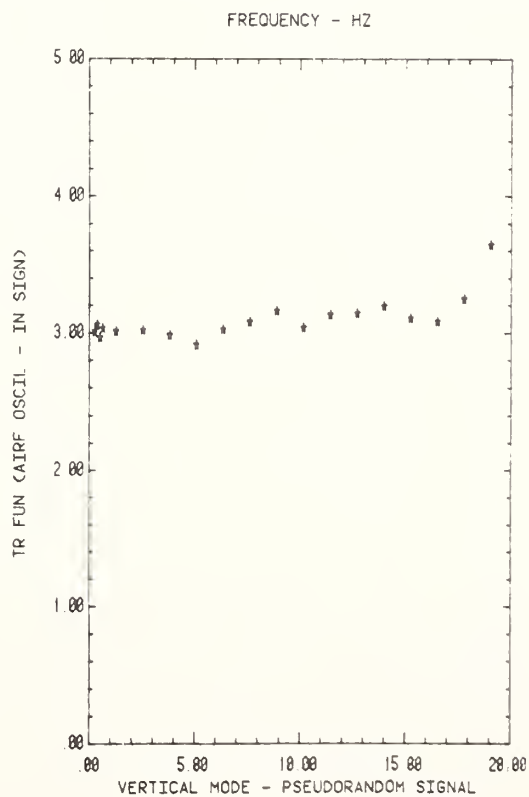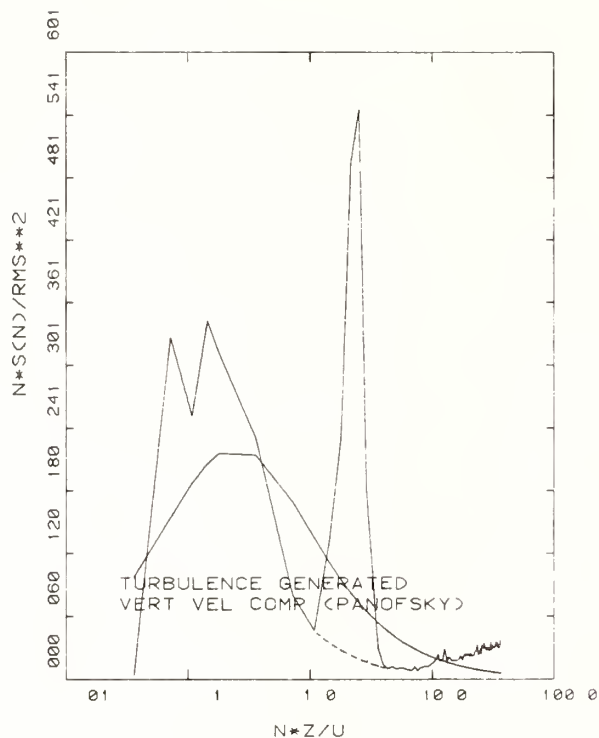
Figure 8.   Generated Turbulence Using
            Simulated Signal for Vertical Mode

Figure 9.   Spectra of Simulated Input
            Signal with Low Frequency Cut-off
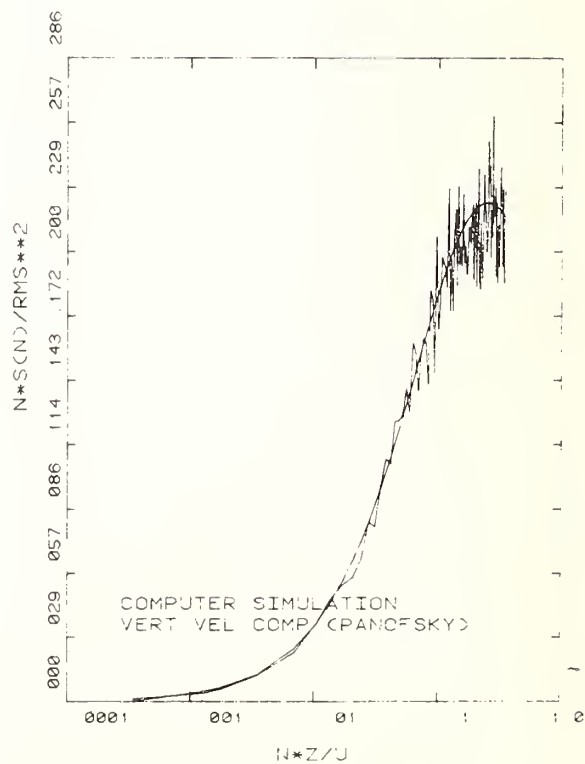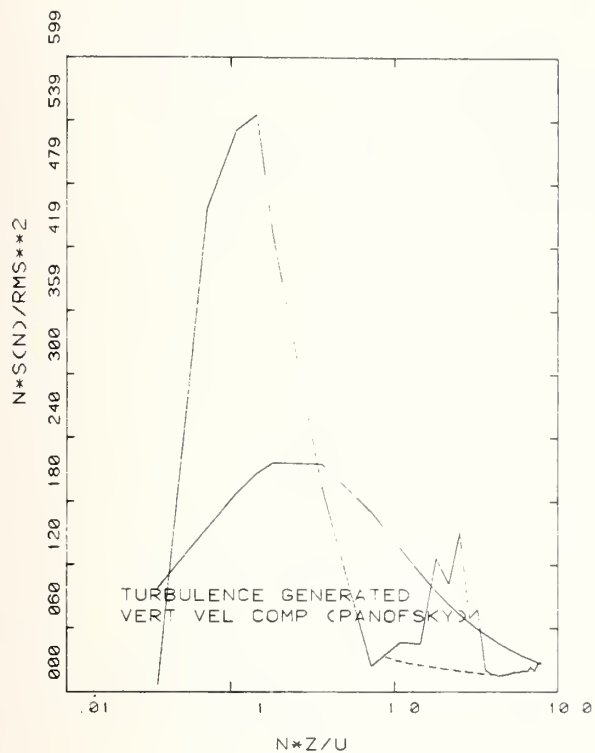
Figure 10. Generated Turbulence Using
Signal with Low Frequency Cut-off

Figure 11. Spectra of Wind Tunnel Oscillations
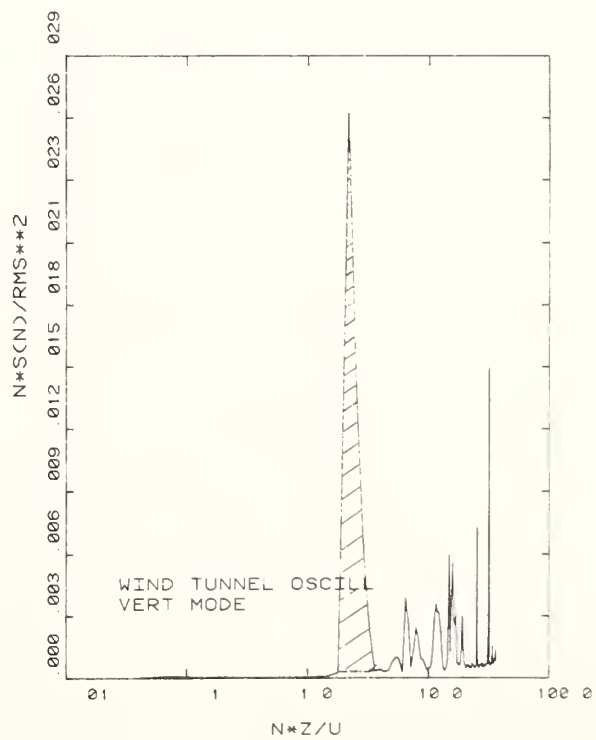
Report of the Task Committee on

(A) Strong-Motion Instrumental Arrays and Data

UJNR PANEL ON WIND AND SEISMIC EFFECTS

Date: May 20, 1980

Place: National Bureau of Standards
        Washington, D.C. U.S.A.

Task Group: U.S. Side – Gutam Bagchi (Acting Chairman)

             Japan Side – Hajime Tsuchida (Chairman)

(1) Activities and Principal Accomplishments to Date

Catalogues of strong-motion earthquake records observed both in
the United States and Japan are being exchanged. U.S. data are
published in the "Seismic Engineering Program Report," and the
Japanese data are reported in the publication, "Strong-Motion
Earthquake Records in Japan."

The Imperial Valley Earthquake of October 15, 1979, and the
Coyote Lake Earthquake of August 6, 1979, were discussed in a paper
and reports containing a catalogue of the event records were provided
for the Japanese side. One of the Japanese papers described their
Dense Instrumentation Array Program. This program promises to provide
the most elaborate data necessary to enhance the state-of-knowledge
in ground-motion propagation.

(2) Future Programs

The both sides of the Task Committee plan to continue their
respective efforts in the following eight points:

1) After an earthquake which has caused damage to structures or an earthquake during which maximum acceleration exceeding about 0.1 G has been recorded, the task committee of a country where the earthquake has taken place will provide a list of the strong-motion earthquake records for the counterpart of the task committee. The list contains maximum component acceleration of each record. If there is such a list compiled by any organization, the list mentioned above may be replaced by it.

2) Every year the task committee will exchange catalogs of the strong-motion earthquake records in the last year. The catalog contains maximum component accelerations and wave forms of major records. If there is such a catalog compiled by any organization, the catalog mentioned above may be replaced by it.

3) The task committee makes appropriate arrangements to provide digitizable copies of records when they are requested. In addition, arrangements will be made to provide information on the characteristics of the site and structures at the locations where such records are obtained.

4) When the organizations taking part in the panel publish reports on the strong-motion earthquake records, the organizations will distribute copies of the reports to the organizations of the panel interested in them. The task committee exchanges lists of the organizations which wish to receive the reports.

5) Every year at the time of the joint meeting the task committee exchanges lists of reports on the strong-motion earthquake records and on analysis of the records published in the last year. The list will cover all the reports on the above mentioned topics published by the organizations taking part in the panels and as many reports as possible published by other organizations and universities.

6) The task committee will continue to exchange lists of digitized data on all the major strong-motion earthquake records recovered in both countries. Besides the digitized records in form of lists, an exchange of digitized records in form of computer magnetic tapes, cards, and other media will be continued.

7) The task committee plans to assist and cooperate, where possible, in the following areas.

   a) Assistance and cooperation with governmental organizations in other seismic areas, in order to promote high quality strong earthquake motion observations in all seismically active areas of the world.

   b) Assistance and cooperation with any international effort to record strong ground motion close to the source of a large magnitude shock.

8) The task committee feels the UJNR Panel on Wind and Seismic Effects should play a major cooperative role in the implementation of relevant parts of the Resolution of the International Workshop on Strong-Motion Earthquake Instrument Arrays held May 2 – 5, 1978, in Honolulu, Hawaii, USA, and particularly support the recommendation to install dense arrays of strong-motion instrument (See Appendix I). The exchange of complete information on all aspects of the program, as it develops particularly in Japan and the United States, will be carried out in the manner of our standard exchange when appropriate.

Resolution of the International Workshop
                       on Strong-Motion Earthquake
                            Instrument Arrays

                    (May, 1978, Honolulu, Hawaii, U. S. A.)

        The following resolution was approved unanimously by the delegates
of the International Workshop on Strong-Motion Earthquake Instrument
Arrays during a general session on May 5, 1978.

        The protection of life and property from the devastating effects
of earthquakes is an urgent world-wide problem. An understanding of the
nature of strong earthquake motions is of crucial importance in solving
this problem. At the present time, however, there is a scarcity of
engineering data acquired near the centers of destructive earthquakes,
and existing instrument arrays are inadequate to provide the necessary
data. Yet there is a high probability of occurrence of destructive
earthquakes in different parts of the world in the next decade. The
participants in this international workshop unanimously recommend that
the earthquake-threatened countries and other concerned countries and
organizations make a concerted effort to establish a comprehensive
world-wide system of specialized strong-motion earthquake instrument
arrays capable of resolving the nature of the earthquake source
mechanism, wave propagation and local site effects. As a first step,
the following specific recommendations should be implemented.

    1. The International Association for Earthquake Engineering in
        collaboration with the International Association of
        Seismology and Physics of the Earth's Interior form an
        International Strong Motion Arrays Council to facilitate
        the establishment of strong-motion earthquake instrument
        arrays.

        Earthquake-threatened countries individually and collec-
        tively initiate the immediate installation of minimal
        arrays of 10-20 strong-motion instruments at least at
        the 28 world-wide sites identified by this workshop.

        High priority be given to the design and installation of
        more elaborate source mechanism, wave propagation and
        local effects arrays, particularly at the six critical
        sites identified.

        A mobile strong-motion instrument array capable of making
        source mechanism, wave propagation and local effects
        measurements be established and maintained for deployment
        immediately following the occurrence of a major earthquake
        for the recording of aftershocks.

Report of Task Committee on

(B) Large-Scale Testing Program

UJNR PANEL ON WIND AND SEISMIC EFFECTS

Date: May 19, 1980

Place: National Bureau of Standards
        Gaithersburg, Maryland U.S.A.

Attendees: Japan side - Keiichi Ohtani (Co-Chairman)
                          Makoto Watabe

            U. S. side - Edgar V. Leyendecker (Co-Chairman)
                         Hai Sang Lew

(1) Activities and Principal Accomplishments to Date

The status of the U.S.-Japan Joint Earthquake Research Program Utilizing Large-Scale Testing was discussed, and for the purpose of the Panel's endorsement the available U.S.-Japan Joint Research Program Plans were reviewed.

(2) Future Programs

The Task Committee adopted the following resolutions as a result of discussion:

A.   The Co-Chairmen of both sides of the UJNR Panel on Wind and Seismic Effects have received a request for endorsement of the U.S.-Japan Joint Earthquake Research Program Utilizing Large-Scale Testing in a letter signed jointly by the Science and Technology Agency and the Ministry of Construction of Japan and the National Science Foundation of the U.S., referred to herein after as the Parties. The Panel has previously expressed its support for the Large-Scale Testing Program.

B.   This Task Committee recommends that the program and its components proposed for endorsement by the Panel be submitted to the Task Committee for its review and comments. Based on this review, the Committee Co-Chairmen will prepare recommendations to the Panel Co-Chairmen at as early a date as possible. The Task Committee recommends that the Panel Co-Chairmen jointly notify the requesting Parties of those proposals receiving endorsement, along with Committee review comments.

C.   The Task Committee recommends that close liaison be maintained between the Panel and the Parties. This should include notification of proposed research direction and change in direction and should also include a periodic review of progress of the joint research program. The periodic review should include presentations to the Panel at one or more of its joint meetings.

D.   The Task Committee will review progress of the Joint Research Program and continue to reassess the need for testing of other structures and report its findings and recommendations to the Panel.

E.   Membership of the Task Committee should be expanded to include larger and more diverse membership. In particular, representation from (F) Disaster Prevention Methods for Lifeline Systems and (C) Repair and Retrofit of Existing Structures Task Committees should be included.

REPORT OF TASK COMMITTEE ON
(C) REPAIR AND RETROFIT OF EXISTING STRUCTURES

U.S.-JAPAN PANEL ON WIND AND SEISMIC EFFECTS
May 19, 1980
Gaithersburg, Maryland

PRESENT: M. Watabe   Japan
          R.D. McConnell   USA
          R.J. Morony   USA
          J.D. Cooper   USA
          J.B. Scalzi   USA

ACCOMPLISHMENTS TO DATE - DURING 1979-1980:

A grant was made to Dr. Robert D. Hanson, University of Michigan to serve as Project Manager for the U.S. Task Committee.

By correspondence with Dr. Kiyoshi Nakano, he established areas of interest to be the repair and retrofit of buildings and bridges. Buildings is interpreted as general structures.

At the 11th Joint Meeting of UJNR it was decided to hold a one day seminar and one day field trip preceding the 12th Joint Meeting. The seminar to be held in L.A. As a result, a meeting of U.S. experts was held in December of 1979 in Washington to discuss topics to be presented and speakers to be invited from the U.S. side. Correspondence with Japan listed the topics and requested speakers.

The seminar was held in Los Angeles at the offices of Dr. M. Agbabian. Many interesting papers were presented by both sides. The proceedings will be published by Dr. Hanson and distributed to the members and others. The field trip included a visit to bridge sites to view the cable restrainers which were being installed. Three bridges were inspected. A visit to a school (John Marshall) which was being restored for preservation was very interesting. The local residents wanted to preserve the school because of its architectural beauty. The cost of the repairs and new installations were a little less than building a new school.

Discussion at Los Angeles among the members present included:

1. Task Committee to confine itself to structures
2. Lifeline systems was to be include at a later date. However, a member (preferably chairman) of the ASCE TCLEE Committee is to be invited to participate.

511

3. Next meeting to be in Japan. Exact time and place to be determined by co-chairmen.
4. Research topics are to be studied and presented as areas of cooperative effort in the future.

MEETING OF MAY 1980:

Progress to date was reviewed and discussed. Topics discussed were:
1. Format (title page of seminar proceedings) to include UJNR Task Committee.
2. It is suggested that Dr. Hanson contact other people for papers to be included in the proceedings in particular James Lefter of the Veterans Administration.
3. Seminar proceedings to be distributed to all agencies, practitioners, reserachers, and NTIS.
4. Papers in native language to be translated by each side for distribution in their country.
5. Recommended that scope of Task Committee activities be reviewed in light of interest by members of Lifelines Committee.
6. Recommend that activities from U.S.- U.S.S.R. and U.S.-PRC groups be reported at next meeting.
7. Recommend that topics of economics and cost-effectiveness be delayed until technical problems have been reasonably solved.
8. Suggest that next meeting of the Task Committee be held in conjunction with UJNR meeting in May 1981, or at time of performing large scale test of reinforced concrete building.
9. Recommend that exchange of data be a continuous activity between members as well as co-chairmen.
10. Recommend that exchange of data include non-structural components, elevators, parapets, etc.
11. Recommend that discussion of single family residences be included in next seminar.

Report of Task Committee on

(D) Evaluation of Performance of Structures

UJNR PANEL ON WIND AND SEISMIC EFFECTS

Date: May 20, 1980

Place: National Bureau of Standards
Gaithersburg, Maryland U.S.A.

Attendees: U.S. Side - G. Robert Fuller (Co-Chairman)

John B. Scalzi

Richard McConnell

Japan Side - Makoto Watabe (Co-Chairman)

I. Progress 1979-1980

A considerable amount of effort has been expended in both the U.S. and Japan to develop methodologies and procedures for evaluating the seismic resistance of existing civil engineering structures. Closely related are the projects involving repair, retrofit, strengthening, and rehabilitation of structures.

A. U.S. Activities:

1. Federal Interagency Committee on Seismic Safety in Construction (ICSSC): This organization is made up of representatives of all U.S. Federal Government agencies involved in construction of buildings and lifeline structures. The Earthquake Hazards Reduction Act of 1977 charges the President with establishing and maintaining an effective earthquake hazards reduction program. ICSSC was originally organized by the Presidents' Office of Science and Technology Policy, but now is under the auspices of the Federal Emergency Management Agency (FEMA).

Ten subcommittees, under ICSSC, were established to develop seismic design and construction standards for Federal buildings, rehabilitation of existing buildings, and also buildings constructed under grant, loan, leasing and regulatory programs.

Subcommittee Three - Existing Buildings is establishing procedures for evaluating the seismic resistance and for strengthening existing buildings. This criteria will be completed later in 1980 for review and testing by Federal agencies, prior to adoption and implementation in 1981.

2. Building Seismic Safety Council (BSSC): This Council was established by private industry, under the auspices of the National Institute of Building Sciences, to develop aseismic design and construction recommendations to be adopted by model building codes, local municipalities, and the design profession. BSSC established nine technical committees to review and refine the Applied Technology Council document ATC 3-06, "Tentative Provisions for Development of Seismic Regulations for Buildings."

Technical Committee Nine (TC-9) on Regulatory Use is charged with reviewing ATC 3, Chapters 1 - "General Provisions" and Chapter 13 - "Systematic Abatement of Seismic Hazards in Existing Buildings." Chapter 13 contains provisions for identifying buildings requiring evaluation, evaluation procedures (qualitative and analytical) and hazard abatement measures.

Chapter 14 of ATC 3-06 contains guidelines for repair and strengthening of existing buildings which includes a "Checklist for Existing Building Data File."

Chapter 15 provides "Guidelines for Emergency Post-Earthquake Inspection and Evaluation of Earthquake Damage in Buildings." This includes:

    a) Selection of Inspection Personnel

    b) Training Programs

    c) Inspection Equipment

    d) Procedures for Inspection

    e) Evaluation of Structural Damage

    f) Evaluation of Nonstructural Damage

    g) Evaluation of Auxiliary Systems

    h) On-Site Soil and Foundation Conditions

    i) Tsunami and Seiche Effects

    j) Reinspection, Repairs, and Records.

3. Housing and Urban Development (HUD): The "Methodology for Seismic Evaluation of Existing Multistory Residential Buildings" was published in November 1978, and reported by Mr. Fuller at the 10th Joint Panel Meeting held in May 1978. A presentation was then made by Mr. Fuller at a Workship on Earthquake-Resistant Repair and Retrofit of Buildings, held on May 16, 1980 in Los Angeles, California.

This "Seismic Evaluation and Rehabilitation of HUD Residential Buildings" paper included the two example buildings in the Methodology plus several other buildings evaluated and strengthened using the methodology. Several structures in Los Angeles, San Francisco, Oakland, Memphis (TN), Rochester (NY), and St. Louis (MO) have been reviewed, analyzed and strengthened.

B. Japan Activities:

1. Over all investigations on reinforced concrete building structures have been conducted, especially in Tokia Districts.

2. Repair or retrofitting of steel structures has been accomplished in Sendai area.

3. An automatic computer evaluation system for reinforced concrete building structures has been completed.

4. A practical procedure to calculate ultimate shear strength of building structures in accordance with the promulgation of "New Aseismic Enforcement of Buildings," has been developed.

5. A simple aseismic capacity evaluation procedure for wood-framed houses has been drafted by the Building Disaster Prevention Association and the Ministry of Construction.

II. Resolutions

Because of the recent increase in the use of various evaluation and analysis techniques for assessing the earthquake resistance of existing structures, an attempt should be made to exchange reports of projects which have been evaluated and strengthened.

A. Establish a bibliography of evaluation methodologies and analysis techniques in cooperation with the Task Committee on Repair and Retrofit.

B. Maintain a file in each country and exchange technical data on projects analyzed for seismic resistance and strengthened.

C. Develop recommendations for evaluating structures to assess earthquake hazard potential. Include recommendations for post-earthquake evaluation of performance and damage assessment of structures.

D. Instrument existing structures that have been evaluated and strengthened and monitor performance during earthquakes. Conduct post-earthquake investigations and damage assessment of these structures.

Report of the Task Committee on

(E) Land Use Programs for Controlling Natural Hazard Effects

UJNR PANEL ON WIND AND SEISMIC EFFECTS

Date: May 21, 1980

Place: National Bureau of Standards
        Gaithersburg, Maryland U.S.A.

Attendees: U.S. side - G. Robert Fuller (Chairman, Temporary)

            Japan side - Hajime Tsuchida (Chairman, Temporary)

A. Activities

    1. It was reported that in January 1980 Mr. T. Tazaki, Public Works
        Research Institute, Ministry of Construction, completed his study
        at UCLA on socio-economic aspects of land use programs, in
        cooperation with U.S. researchers.

B. Resolutions

    1. The resolutions of this Task Committee from the 8th through 11th
        Joint Panel Meetings are still in effect and will continue.

    2. The Task Committee recognizes that methodology on the land use
        programs should be urgently developed considering the implementation
        of the Earthquake Hazards Reduction Act of 1977 (Public Law 95-124)
        in the U.S.A. and the Large Scale Earthquake Countermeasures Act,
        Law No. 73 (1978.6.7) in Japan.

    3. The exchange of papers and references on land use planning should
        be continued, especially in the following areas:

            a) Current methods of earthquake hazard risk analysis,

            b) Applications of the methods contained in the above
                earthquake hazard mitigation acts, and

            c) Hazard maps for earthquake disaster prevention planning,
                including socio-economic considerations.

    4. Cooperation and exchange of engineers, geophysicists, land use
        planners and social scientists should be encourgaed in order to
        promote more effective land use planning.

Report of the Task Committee
on
(F) Diaster Prevention Methods for Lifeline Systems

UJNR PANEL ON WIND AND SEISMIC EFFECTS

Date: May 20, 1980

Place: National Bureau of Standards, Gaithersburg, Maryland, U.S.A.

Attendees: Japan side – Keiichi Ohtani (Chairman, Temporary)
                          National Research Center for Diaster Prevention
                          Science and Technology Agency

                          Yasuyuki Koga
                          Public Works Research Institute
                          Ministry of Construction

             U.S. side – Charles F. Scheffey (Chairman)
                          Federal Highway Administration

                          James D. Cooper
                          Federal Highway Administration

                          Haaren A. Miklofsky
                          Federal Highway Administration

                          Teoman Ariman
                          Dept. of Aerospace and Mechanical Engineering
                          University of Notre Dame

(1) Activities and Principal Accomplishments to Date

     Through the exchange of letters between the chairmen of both sides, an
initiation of immediate planning, for use of the large-scale testing facilities
of both countries to resolve critical problems in the behavior of lifeline
systems, has been undertaken.

     From the U.S. side, several professors concerned visited Tsukuba Science
City and exchanged information on earthquake engineering of lifeline systems and
view of cooperative research program.

(2) (Description of discussions carried out the meeting.)

(3) Future Programs

     The Task Committee adopted the following resolutions as a result of
discussion:

     1) The present area and level of information exchange on damage studies,
research information, design standards criteria, and administrative regulations
with regard to lifeline safety should be continued, with expanded effort to
include governmental agencies not now involved which have major missions
involving lifelines and non-governmental activities. Present governmental members
on each side to propose details of such expansions in their respective countries.

2) Coordination effort of U.S.-Japan joint research program on the safety of lifeline system and its components at every level of cooperation should be initiated through the co-chairman of the Task Committee.

3) Planning of cooperative large-scale testing of lifeline systems should immediately be initiated, with details to be arranged by correspondence.

4) In preparation for items 2) and 3) mentioned above, members of the Task Committee on both sides should be expanded to the extent of covering each field of lifelines concurred by both co-chairmen as subjects of cooperative research program.

Report of Task Committee on

(G) Wind Characteristics and Structural Response

UJNR PANEL ON WIND AND SEISMIC EFFECTS

Date: May 19, 1980

Place: National Bureau of Standards
       Washington, D.C. U.S.A.

Attendees: U.S. Side - Celso S. Barrientos (Chairman)

                       Richard D. Marshall

           Japan Side - Toshio Iwasaki (Chairman, Temporary)

                        Hajime Tsuchida

                        Yasuyuki Koga

To expand the activities of the Task Committee, the name of the Task
Committee was changed to "Wind Characteristics and Structural Response,"
and two members will be added on the U.S. side.

(1) Activities and Principal Accomplishments to Date

The Task Committee notes that:

1) Strong winds frequently cause loss of life and extensive property
   damage,

2) The exchange of high wind data and information on wind effects
   can be useful for reducing loss of life and property damage,

3) Insufficient knowledge exists on the effects of strong winds upon
   structures and methods for modeling these effects, and

4) The needs for wind data for various applications and new projects
   are increasing.

(2) Future Activities

In view of the above items, the Task Committee hereby resolves to
carry out the following programs:

1) Exchange observations and records of high wind data (including remote-sensing reports, i.e., aircraft, satellite) available from the respective national meteorological services and special observation sites.

2) Encourage the exchange of actual wind observations (described in 1) in appropriate format. When necessary, the Task Committee Chairman will establish procedures to facilitate the exchange of such data.

3) Exchange available specialized high wind data sets and wind pressure sets. The information may include surface meteorological data sets and data sets at other levels. Documentation of instrument characteristics, exposure, and elevation above ground may be included.

4) Encourage the establishment of standard methods for the simulation of boundary layers in wind tunnels, the promotion of data exchange of boundary layer wind observations, and the exchange of information on methods of measurement and determination of structural response.

5) Encourage the interaction between meteorologists and engineers to identify the types of wind data required for future use; in establishing extreme wind distributions; in determining wind loadings on structures; in understanding the urban wind climate; and in considering structural design issues in the wind generation of energy.

Report of the Task Committee On
(H) Soil Behavior and Stability During Earthquakes
UJNR Panel on Wind and Seismic Effects

Date   : May 21, 1980

Place   : Bureau of Standards, Gaithersburg, Maryland, U.S.A.

Attendees: Japan side – Toshio Iwasaki (Chairman)
                         Hajime Tsuchida
                         Yasuyuki Koga

            U.S. side – H. S. Lew (Temporary Chairman)
                         Felix Y. Yokel
                         Riley M. Chung

(1) Activities and Principal Accomplishments to Date:

   1) Pursuant to the resolution of the task committee of the 11th
       Joint Meeting, the co-chairman of the task committee prepared
       mailing lists and exchanged them for the distribution of docu-
       ments.

   2) Exchanges of relevant documents, including reports on the
       recent earthquakes and guidelines for assessing soil lique-
       faction were made.

(2) Future Programs

   1) When requested, the task committee will assist in arrangements
       for visits to earth embankments and soil foundations which have
       been subjected to significant ground motions.

   2) Discussions and correspondence are being continued concerning
       soil liquefaction potential for submerged foundations, founda-
       tion settlements, and stability of soil structures due to
       earthquake motions.

   3) Efforts for comparing results of standard penetration tests
       conducted in the United States with the results from Japan
       will be continued.

   4) Guidelines for assessing soil liquefaction in the United States
       and Japan are currently being reviewed and final drafts are ex-
       pected to be published in the near future. These reports will be
       transmitted to counterpart sides when completed.

Report of Task Committee on

(I) Storm Surge and Tsunami

UJNR PANEL ON WIND AND SEISMIC EFFECTS

Date: May 21, 1980

Place: National Bureau of Standards
        Washington, D.C. U.S.A.

Attendees: U.S. side - Celso S. Barrientos (Chairman)

            Japan side - Hajime Tsuchida (Chairman, Temporary)

        This is the newest Task Committee of this Panel. The Task Committee
was formally formed during the 11th Panel Meeting in Tsukuba, Japan in
September 1979. Members of the Task Committee were appointed as follows:

        U.S. side - Celso S. Barrientos (Chairman)

                    Michael P. Gaus

        Japan side - Yoshimi Goda (Chairman)

                     Hiroshi Hasimoto

                     Akira Katayama

        It is desirable to add memberships in the Committee: U.S. side -
tsunami research and tsunami forecasting.

        Storm surges and tsunamis caused considerable damage to properties
and loss of lives in Japan and the United States and in other countries where
these geophysical phenomena occur. Storm surge and tsunami are clearly
wind and seismic effects and therefore a very logical part of this Panel.

        The Task Committee will facilitate exchange of information related to
storm surge and tsunami, such as, publications, damages, and measures to
reduce or prevent damages.

The Chairman of the Task Committee will consider the following cooperation programs:

1) Exchange information on storm surge models used for forecasting, planning, design, and disaster prevention purposes. The information include type and formulation of models, verification data, and empirical constants. Contacts between scientists working on storm surge models will also be part of the information exchange.

2) Encourage development of meteorological models that are aimed to be utilized with the storm surge models. These are atmospheric models that are designed as input initial conditions to the surge models. Since storm surge generation is primarily dependent on the atmospheric forcings, storm surge models are only as good as the atmospheric models.

NBS-114A (REV. 2-80)

U.S. DEPT. OF COMM. BIBLIOGRAPHIC DATA SHEET *(See instructions)*	1. PUBLICATION OR REPORT NO. NBS SP 655	2. Performing Organ. Report No.	3. Publication Date January 1984

4. TITLE AND SUBTITLE

Wind and Seismic Effects: Proceedings of the 12th Joint UJNR Conference

5. AUTHOR(S)

E. V. Leyendecker and R. M. Chung, editors

6. PERFORMING ORGANIZATION *(If joint or other than NBS, see instructions)* NATIONAL BUREAU OF STANDARDS DEPARTMENT OF COMMERCE WASHINGTON, D.C. 20234	7. Contract/Grant No.
	8. Type of Report & Period Covered Final

9. SPONSORING ORGANIZATION NAME AND COMPLETE ADDRESS *(Street, City, State, ZIP)*

Same as item 6.

10. SUPPLEMENTARY NOTES

Library of Congress Catalog Card Number: 83-600593

☐ Document describes a computer program; SF-185, FIPS Software Summary, is attached.

11. ABSTRACT *(A 200-word or less factual summary of most significant information. If document includes a significant bibliography or literature survey, mention it here)*

The Twelfth Joint Meeting of the U.S.-Japan Panel on Wind and Seismic Effects was held in Gaithersburg, Maryland on May 19-23, 1980. The proceedings of the Joint Meeting include the program, the formal resolutions, the Task Committee Reports, and the technical papers. The subjects covered in the papers include: (1) the characterization of seismic ground motion, (2) the characterization of natural wind and extreme wind records, (3) structural response to earthquake loading, (4) storm surge and tsunamis, (5) recent developments in seismic design criteria, (6) technical cooperation with developing countries, (7) earthquake hazard mitigation, and (8) structural response to wind loading.

12. KEY WORDS *(Six to twelve entries; alphabetical order; capitalize only proper names; and separate key words by semicolons)*

accelerograph; bridges; codes; design criteria; disaster; earthquakes; geotechnical engineering; ground failures; seismic design; seismicity; standards; structural engineering; tsunamis; and winds.

13. AVAILABILITY	14. NO. OF PRINTED PAGES
[X] Unlimited ☐ For Official Distribution. Do Not Release to NTIS [X] Order From Superintendent of Documents, U.S. Government Printing Office, Washington, D.C. 20402.	543
☐ Order From National Technical Information Service (NTIS), Springfield, VA. 22161	15. Price

NBS TECHNICAL PUBLICATIONS

PERIODICALS

JOURNAL OF RESEARCH—The Journal of Research of the National Bureau of Standards reports NBS research and development in those disciplines of the physical and engineering sciences in which the Bureau is active. These include physics, chemistry, engineering, mathematics, and computer sciences. Papers cover a broad range of subjects, with major emphasis on measurement methodology and the basic technology underlying standardization. Also included from time to time are survey articles on topics closely related to the Bureau's technical and scientific programs. As a special service to subscribers each issue contains complete citations to all recent Bureau publications in both NBS and non-NBS media. Issued six times a year. Annual subscription: domestic $18; foreign $22.50. Single copy, $5.50 domestic; $6.90 foreign.

NONPERIODICALS

Monographs—Major contributions to the technical literature on various subjects related to the Bureau's scientific and technical activities.

Handbooks—Recommended codes of engineering and industrial practice (including safety codes) developed in cooperation with interested industries, professional organizations, and regulatory bodies.

Special Publications—Include proceedings of conferences sponsored by NBS, NBS annual reports, and other special publications appropriate to this grouping such as wall charts, pocket cards, and bibliographies.

Applied Mathematics Series—Mathematical tables, manuals, and studies of special interest to physicists, engineers, chemists, biologists, mathematicians, computer programmers, and others engaged in scientific and technical work.

National Standard Reference Data Series—Provides quantitative data on the physical and chemical properties of materials, compiled from the world's literature and critically evaluated. Developed under a worldwide program coordinated by NBS under the authority of the National Standard Data Act (Public Law 90-396).

NOTE: The principal publication outlet for the foregoing data is the Journal of Physical and Chemical Reference Data (JPCRD) published quarterly for NBS by the American Chemical Society (ACS) and the American Institute of Physics (AIP). Subscriptions, reprints, and supplements available from ACS, 1155 Sixteenth St., NW, Washington, DC 20056.

Building Science Series—Disseminates technical information developed at the Bureau on building materials, components, systems, and whole structures. The series presents research results, test methods, and performance criteria related to the structural and environmental functions and the durability and safety characteristics of building elements and systems.

Technical Notes—Studies or reports which are complete in themselves but restrictive in their treatment of a subject. Analogous to monographs but not so comprehensive in scope or definitive in treatment of the subject area. Often serve as a vehicle for final reports of work performed at NBS under the sponsorship of other government agencies.

Voluntary Product Standards—Developed under procedures published by the Department of Commerce in Part 10, Title 15, of the Code of Federal Regulations. The standards establish nationally recognized requirements for products, and provide all concerned interests with a basis for common understanding of the characteristics of the products. NBS administers this program as a supplement to the activities of the private sector standardizing organizations.

Consumer Information Series—Practical information, based on NBS research and experience, covering areas of interest to the consumer. Easily understandable language and illustrations provide useful background knowledge for shopping in today's technological marketplace.

Order the above NBS publications from: Superintendent of Documents, Government Printing Office, Washington, DC 20402.
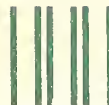
Order the following NBS publications—FIPS and NBSIR's—from the National Technical Information Service, Springfield, VA 22161.

Federal Information Processing Standards Publications (FIPS PUB)—Publications in this series collectively constitute the Federal Information Processing Standards Register. The Register serves as the official source of information in the Federal Government regarding standards issued by NBS pursuant to the Federal Property and Administrative Services Act of 1949 as amended, Public Law 89-306 (79 Stat. 1127), and as implemented by Executive Order 11717 (38 FR 12315, dated May 11, 1973) and Part 6 of Title 15 CFR (Code of Federal Regulations).

NBS Interagency Reports (NBSIR)—A special series of interim or final reports on work performed by NBS for outside sponsors (both government and non-government). In general, initial distribution is handled by the sponsor; public distribution is by the National Technical Information Service, Springfield, VA 22161, in paper copy or microfiche form.

U.S.MAIL